Refining the geochronology and paleoenvironmental significance of key tephra beds in Yukon and Alaska

by

Serhiy Dmytrovy Buryak

A thesis submitted in partial fulfillment of the requirements for the degree of

Doctor of Philosophy

Department of Earth and Atmospheric Sciences
University of Alberta

Abstract

Developing precise analytical tools for dating young volcanic deposits (under 3 million years old) is essential for constructing Quaternary chronological frameworks. This dissertation presents an improved method for determining eruption ages of volcanic ash (tephra) deposits in the ice-age sediments of unglaciated Yukon and Alaska (eastern Beringia). These regions, largely unglaciated during the Quaternary Period (last 2.6 million years), preserve a unique sedimentary record crucial for reconstructing past climate and environmental changes. Abundant tephra beds in these sediments are key to dating past climate changes, evaluating megafauna extirpation hypotheses, and understanding climate-landscape linkages.

However, radiometric dating of these relatively young tephra deposits is difficult. Some tephra can be directly dated with glass fission-track techniques, but relatively low precision of this technique has hindered progress in deciphering the sedimentary record of eastern Beringia. In the last decade, major improvements in instrumentation and other methodological advances are offering new opportunities to revisit this outstanding problem. Here a combination of U-Pb and/or U-series zircon dating via laser ablation inductively coupled plasma mass spectrometry (LA-ICP-MS) is used to resolve eruption age uncertainty for important Quaternary tephra deposits. U-Pb zircon dating is commonly used to date much older geological materials, but there is a pressing need to adapt these techniques for application to more recent periods of time that are directly relevant to issues of global environmental change.

The enhanced tephrochronological framework, combined with paleoenvironmental and paleobiological data, offers a better understanding of eastern Beringian sediment deposition over the last 3 million years. This research presents zircon ages for 14 key tephra layers providing critical temporal anchors for Marine Isotope Stages 5 to 8 and older sediments in eastern

Beringia. This includes improved dates for Old Crow, Sheep Creek - Fairbanks, HP, Gold Run, PA, Quartz Creek, Lost Chicken, GI tephra, and new chronology for Woodchopper Creek, Snag, Biederman PAL, and 80 Pup tephra. The dissertation also addresses statistical challenges in evaluating complex zircon populations and proposes refined age calculation methods. Additionally, it examines the preservation of volcanogenic zircon grains in sediment, highlighting the relationship between age, grain morphology, and recovery methods, thus improving the identification of syn-depositional grains in detrital sediments. This research revises the chronology of volcanism in Alaska and Yukon and refines methods for dating young volcanic deposits.

Preface

This dissertation consists of four original research articles that are the collective effort of several projects focused on laser ablation inductively coupled plasma mass spectrometry U-Pb and U-Th analysis of "young" zircon crystals—Plio-Pleistocene tephrochronometry—and implications for paleoenvironmental studies in eastern Beringia. All research presented in this manuscript was supervised by Dr. Alberto Reyes and Dr. Britta Jensen at the University of Alberta. For each chapter I was responsible for the project formulation, methods development, data collection, analysis, interpretation, and writing of the manuscript. My responsibilities and contributions for each chapter are as follows:

Chapter 2 has been published as: Buryak, S.D., Reyes, A.V., Jensen, B.J.L., Davies, J.H.F.L., Westgate, J.A., DuFrane, S.A., Luo, Y., Froese, D.G., Pearson, D.G., Benowitz, J.A., 2022, Laser-ablation ICP-MS zircon U-Pb ages for key Pliocene-Pleistocene tephra beds in unglaciated Yukon and Alaska, *Quaternary Geochronology* [vol.73, 101398]. I was responsible for sample preparation, methods development, collecting data, age data modeling, and data interpretation/synthesis. J. Westgate provided updated glass fission-track data and Y. Luo and S.A. DuFrane assisted with U-Pb data collection. The manuscript was written by me with contributions from all authors.

Chapter 3 is planned for submission to a short-format geoscience journal (e.g. *Geology* or *Earth and Planetary Science Letters*) as: Buryak S.D., Jensen, B.J.L., Reyes, A.V., Benowitz, J.A., Gmeinweser T., Luo Y., Pearson, D.G. "Syn-depositional volcanogenic zircons and where to find them: The challenge for detrital zircon geochronology". I was responsible for project formulation, data collection, data processing, and interpretation. I prepared the initial manuscript.

T. Gmeinweser assisted with the data collection and J. Benowitz provided updated argon-argon age data. The manuscript was written by me with contributions from all authors.

Chapter 4 has been submitted to *Quaternary Geochronology* as: Buryak S.D., Luo Y., Jensen, B.J.L., Reyes, A.V., Bolton M.S.M., Davies, J.H.F.L., Pearson, D.G. “A refined and simplified sector-field LA-ICP-MS method for combined single-grain U-Th and U-Th-Pb dating of Quaternary zircon”. I was responsible for method development, sample preparation, experimental design, data processing, and manuscript preparation. Y. Luo assisted with the method development and instrumentation. The manuscript was written by me with contributions from all authors.

Chapter 5 is planned for submission to *Quaternary Science Reviews* as: Buryak, S.D., Jensen, B.J.L., Reyes, A.V., Bolton M., Davies, J.H.F.L., Westgate, J.A., Luo, Y., Pearson, D.G., Ward, B., Turner, D. “Refining Marine Isotope Stage 5 to 7 tephrochronology in eastern Beringia: an integrated zircon geochronology, tephra geochemistry, and stratigraphy approach “. I was responsible for sample preparation, methods development, collecting data, and age data modeling. The manuscript was written by me with contributions from all authors.

Acknowledgements

Firstly, I would like to thank Dr. Alberto Reyes and Dr. Britta Jensen for their guidance, support, and patience throughout the duration of this project. Their insightful comments and suggestions were most helpful throughout the entire research period and during the writing of this thesis.

Secondly, I would like to thank Dr. Joshua Davies, Dr. Yan Luo, Dr. Andy DuFrane, Dr. Graham Pearson, Dr. Duane Froese, Dr. John Westgate, Dr. Seth Burgess, Dr. Michel Lamothe and many others for insightful comments and support during difficult months of research. I also would like to extend my thanks to Dr. Jeff Benowitz for his contributions to the study of the Grubstake tephra and Ar-Ar dating expertise.

Finally, I would like to thank my family and friends for being supportive throughout my time in a graduate program.

Table of Contents

List of Tables

List of Figures

Chapter 1: Introduction

1.1. What is Beringia?

Beringia is a large subarctic region that extends from the Lena River in Siberia to the Mackenzie River in northwest Canada. During glacial periods and low global sea level, it was a continuous landmass that connected Asia with North America (Fig. 1.1; Hoffecker and Elias, 2007). The region exposed during glaciations is known as the Bering land bridge, which established a terrestrial link between western Beringia (Siberia) and eastern Beringia (Alaska, Yukon Territory). This vast biogeographical corridor was characterized by a unique biological diversity, including large herbivores like mammoths, horses, and bison (Hopkins, 1982; Guthrie, 1990; Sher, 1999; Hoffecker and Elias, 2007; Goebel et al., 2008).

Understanding the Quaternary history of Beringia is critical for addressing many paleoenvironmental, paleobiological, paleogenomic, and archeological questions. These include the evolution of flora and fauna and Beringia's role as a hub for speciation, glacial refugia, and the exchange of biota between Eurasia and the American continent (Sher, 1999). Similarly, the paleogenomic studies of the Pleistocene-Holocene fauna in eastern Beringia are becoming increasingly important for understanding migration patterns (e.g., migration of megafauna through major climatic shifts) and evolutionary conundrums (e.g., investigation of *Equus* evolution from early Middle Pleistocene horse fossil remains) (e.g., Orlando et al., 2011; Froese et al., 2017). Moreover, the study of Beringia is important for understanding of the temporal aspects and pathways of human migration to the American continent (e.g., Morlan, 2003; Goebel et al., 2008). Beringia's sedimentary deposits are critical for identifying the timing and causes of megafauna extinction at the Pleistocene/Holocene transition, whether influenced by climate-driven factors or anthropogenic activities (Martin, 2005; Guthrie, 2006).

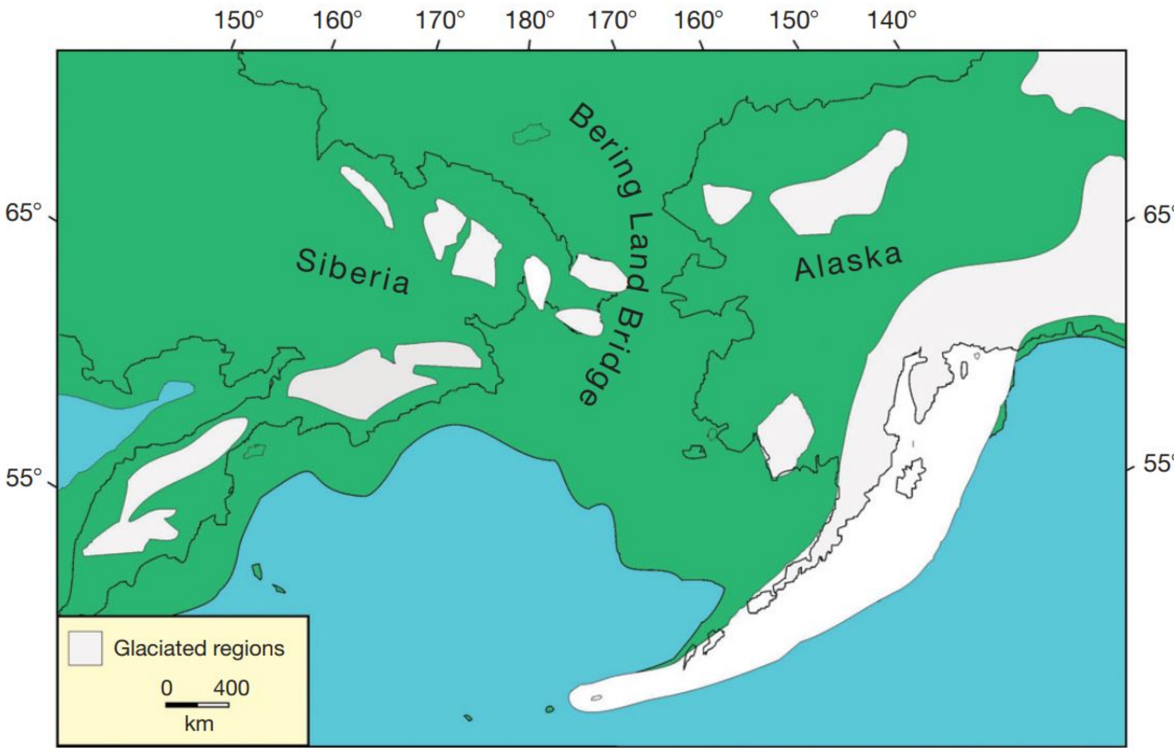

Figure 1.1. *Beringia as it is today, area shaded in green represents the extent of the region (After Elias and Brigham-Grette, 2013)*

1.2. Sediments of Beringia

Loess and reworked loess are widespread in Beringia, extensively covering Yukon and Alaska (Péwé, 1975; Froese et al., 2009). These deposits, often fragmented and interrupted by periods of erosion or non-deposition, date back to 3 million years in some regions (Westgate et al., 1990). Permafrost formation in Beringian loess facilitates exceptional preservation of organic material, including floral and faunal remains, thereby providing a valuable archive of biological and climatic information (e.g., Péwé et al., 1997; Zazula et al., 2007; Fig. 1.2.). A precise and accurate chronological framework is crucial for interpreting these records. In eastern Beringia, numerous tephra layers hosted within loess provide a means to date and correlate these deposits (e.g. Muhs et al., 2003; Beget, 2001). Robust chronologies from eastern Beringian loess also align local/regional records with global climatic events, which is critical for understanding climatic shifts (e.g., glacial-interglacial cycles) and ecological responses (e.g. Péwé et al., 1997; Froese et al., 2009).

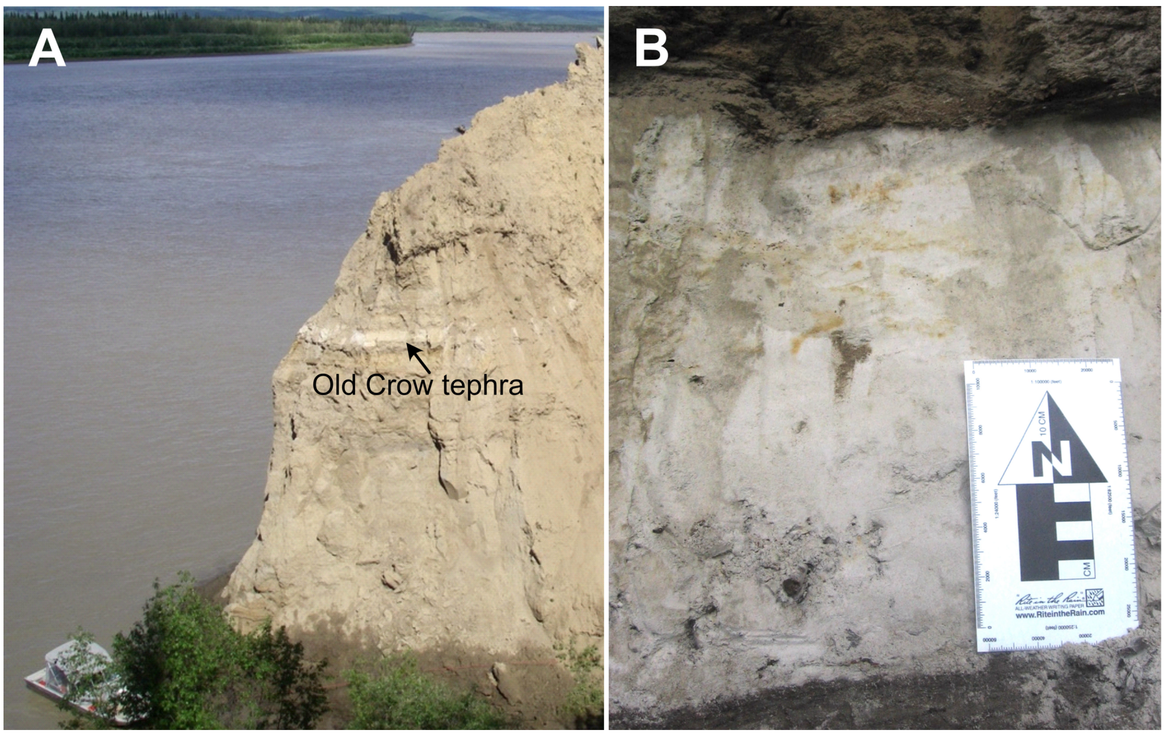

Figure 1.2. *(A) Palisades site in centra Alaska, the arrow is pointing at the Old Crow tephra layer. (B) In-situ Old Crow tephra layer at the same location (Photo credit: A.V. Reyes/ B.J.L. Jensen)*

A prime example of the importance of tephra in loess sediments in eastern Beringia is the study of the last interglacial period, Marine Isotope Stage (MIS) 5, which is based on loess exposures across that rely primarily on the presence of the ca. 160 ka Old Crow tephra (Hamilton and Brigham-Grette, 1991; Jensen et al., 2013, 2016; Reyes et al., 2023). The prevailing conditions during preceding interglacial periods (e.g., MIS 7) in eastern Beringia are less well-documented, in part due to the lack of a reliable chronostratigraphic framework for that interval, which can largely be resolved by establishing accurate and precise ages for currently undated tephra beds (e.g., PAU, P8, PAL; Jensen et al., 2013). Another example is the Late Pliocene deposits at Lost Chicken Mine in east-central Alaska, anchored by ca. 3 Ma Lost Chicken tephra that provide an important archive of the boreal forest vegetation, insect fauna, and paleoenvironmental conditions before the onset of global cooling ~ 2.7 Ma (Matthews et al., 2003; Péwé et al., 2009). The timing of the Lost Chicken tephra deposition is primarily based on the relatively low precision (30% uncertainty at 95% confidence level) glass fission-track age of 2.91 ± 0.88 Ma (Matthews et al., 2003). The chronology of this deposit can be refined by improving the precision of the absolute age constraints (e.g., via zircon U-Pb dating), which in turn will allow the paleoclimate and paleoenvironmental proxy records from Lost Chicken to be better incorporated into the emerging picture of proxy and model estimates for Pliocene global warming.

1.3. Tephrochronology: characterization and dating

Tephra is a pyroclastic product of volcanic eruption. The usefulness of tephra beds for deciphering of the sedimentary record in eastern Beringia requires robust tools for identification and characterization of distal tephra beds as isochronous stratigraphic markers. This involves the examination of mineralogy, geochemical composition, glass morphology, petrology/petrography, and grain size distribution. These characteristics are used to differentiate and correlate tephra deposits (e.g. Preece et al., 2000; Westgate et al., 2005).

The primary sources of volcanic ash in eastern Beringia are the Aleutian Arc–Alaska Peninsula and the Wrangell Volcanic Field. Historically, tephra from these areas were classified as “Type I” (Aleutian Arc) and “Type II” (Wrangell Volcanic Field). Type I tephras are dacitic to rhyolitic, characterized by bubble-wall glass shards and low crystal content, while Type II tephras are mainly rhyolitic with higher crystal content. To accommodate the growing awareness of the compositional diversity of late Cenozoic tephra beds in eastern Beringia, Preece et al. (2011) proposed a revised classification into three types: adakite, transitional, and typical arc tephra. Typical arc tephra contains flat rare earth element (REE) profiles and low Sr contents, adakite tephra is characterized by high La/Yb and Sr/Y values with steep REE profiles, and transitional tephra has intermediate characteristics. Tephras are further categorized by the presence or absence of hydrous minerals, reflecting the water content during formation (Preece et al., 2011).

The main correlation tool relied on is the major and minor element geochemical composition of the glass. In combination with other lines of evidence such as stratigraphy, petrography and glass morphology, the unique geochemical signature of each tephra bed enables the correlation and comparison of spatially distal sedimentary records (e.g., Preece et al., 2011; Jensen et al., 2016; Fig. 1.3.). If that tephra is dated, that date can be transferred to any new site it is found.

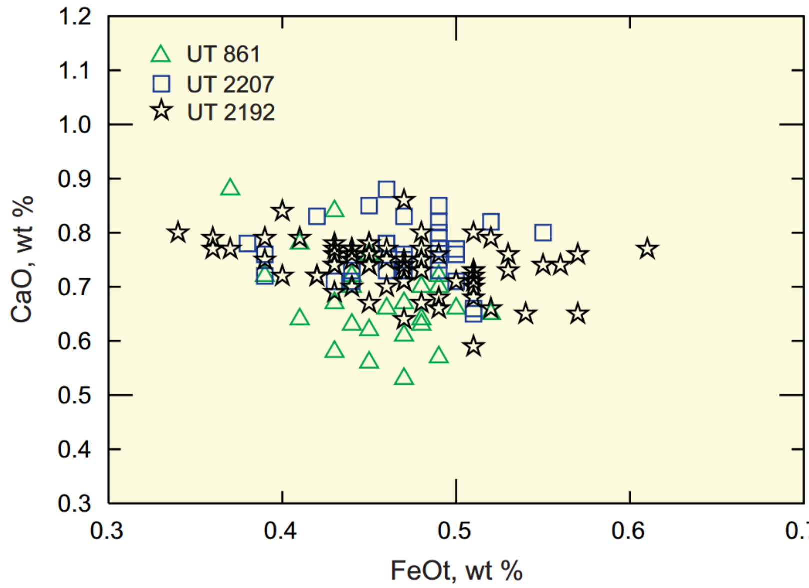

Fig. 1.3. *CaO – FeOt plot of glass shards from HP tephra at Fairbanks, Alaska (UT861) correlated to those of a tephra bed from a site in the Klondike goldfields of Yukon.*

Establishing reliable chronologies is key to addressing the main paleoenvironmental, paleobiological and paleoclimatic questions in eastern Beringian research. The use of tephra beds as chronostratigraphic markers relies on knowing their depositional age with sufficient precision and accuracy (e.g. Lowe, 2011; Buryak et al., 2022). Accurate geochemical fingerprinting necessitates an understanding of chemical properties of the tephra, whereas dating typically includes numerical determination of the age of either the tephra layer or the surrounding material, along with knowledge of the stratigraphic context. Dating volcanic eruptions serves a dual purpose, not only enabling the determination of their chronological age but also aiding in establishing the minimum or maximum ages of geological, archaeological or paleontological deposits located stratigraphically above or below the volcanic deposit. These isochronous markers play a crucial role in dating archaeological and paleontological sites (e.g., Orlando et al., 2011; Ulusoy et al., 2019), and provide invaluable temporal constraints for understanding paleoclimatic records (e.g., Shane and Sandiford, 2003; Brendryen et al., 2010; Jensen et al., 2011).

Contemporary radiometric dating methods for Quaternary tephra can be direct ($^{40}Ar/^{39}Ar$, U-based methods, fission-track,) or indirect (radiocarbon, luminescence, paleomagnetism) (e.g., Kunk, 1995; Sandhu and Westgate, 1995; Demuro et al., 2008; Burgess et al., 2019; Buryak et al., 2022). However, their applicability is often constrained by various factors such as limited minerals that can be dated, restricted timespans of individual dating methods, open-system behavior, mass-dependent kinetic isotopic fractionation, analytical sensitivity limitations, and imperfections in datable materials (Chen et al., 1996; Spell et al., 2001; Morgan et al., 2009).

Within the Quaternary Period, spanning from present day to 2.6 Ma, substantial challenges arise in dating geological materials, particularly in the younger portion of this period (50 ka to 1 Ma). This thesis places emphasis on accurate determination of the eruption age of volcanic deposits within this timeframe, highlighting the inherent complexities associated with dating materials from this time.

1.4. Direct dating of tephra

Successfully dating tephra layers directly has been accomplished using multiple techniques, for example: fission-track dating (Westgate et al., 1990); ^{40}Ar-^{39}Ar dating (e.g., Kunk, 1995; Vidal et al., 2022); luminescence dating (Berger, 1987; Auclair et al., 2007); and more recently using U-based dating methods (Burgess et al., 2019; Burgess et al., 2021; Buryak et al., 2022).

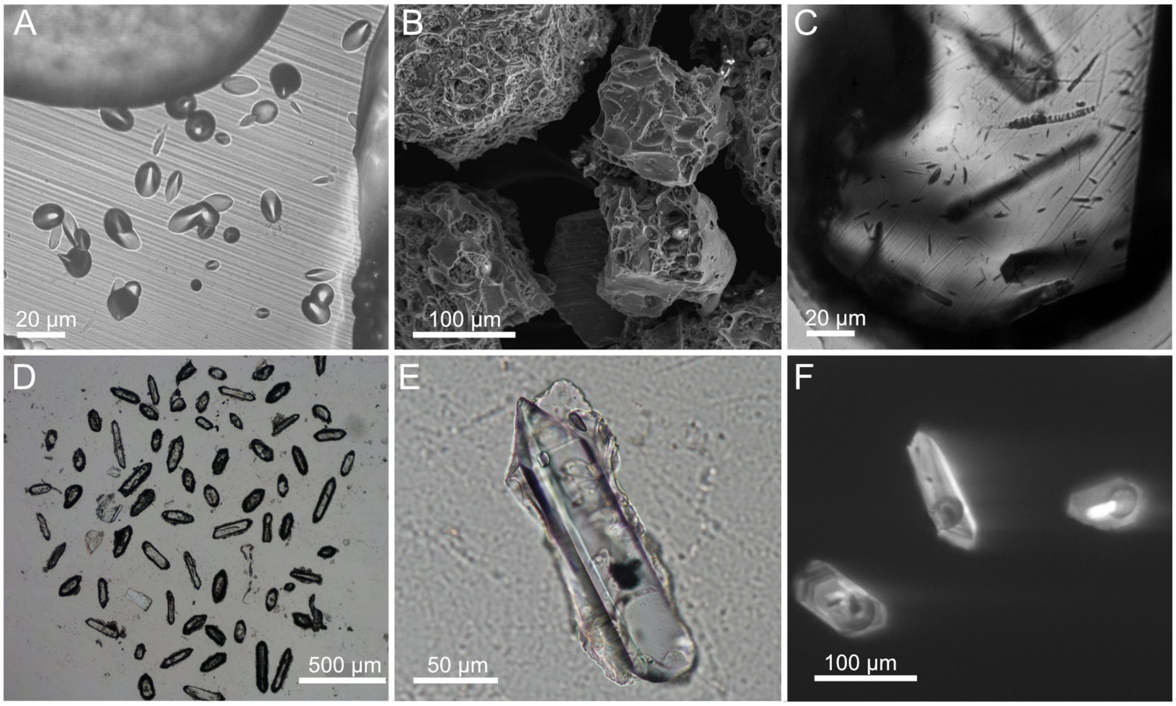

Figure 1.4. *Representative micrograph of geochronological materials and features.*

A. Image showing fission tracks in a glass shard of the Huckleberry Ridge tephra (photo credit J. Westgate). B. Gold Run tephra glass. Gold Run tephra consists of three types of pyroclasts: solid glass shards, highly pumiceous pyroclasts, and ones of low vesicularity. Only the solid glass shards and low-vascularity clasts are useful for glass fission-track dating (photo credit J. Westgate). C. Fission tracks in zircon. The short, linear features are the fission tracks (photo credit J. Westgate). D. Plane polarized image of zircon crystals from Old Crow tephra. E. Plane polarized image of zircon crystal with adhered glass rim recovered from Old Crow tephra. F. Cathodoluminescence image of zircon crystals from Gold Run tephra. Note the laser ablation pits.

Radiocarbon dating is the main technique used to establish depositional ages for deposits <50 ka. Dating of bracketing organic material can be used to constrain the timing of tephra deposition (e.g., Froese et al., 2006). Radiocarbon dating has been used extensively in Late Pleistocene Beringian research, providing highly precise and accurate age constraints for MIS 1-3 sediments. However, this technique has limitations, among which is the assumption that the organic material being dated is co-depositional with the stratigraphic unit being dated, which cannot be verified for regions with significant reworking and redeposition of material. For example, the sampling and dating of reworked organic material can introduce significant uncertainties in radiocarbon chronologies (e.g., Blong and Gillespie, 1978; Reyes et al., 2011). Additionally, radiocarbon dating has a maximum time range of ~40-50 ka (Pigati et al., 2007), so it cannot be applied to pre-MIS 3 deposits.

Until recently, distal tephra beds in eastern Beringia >50 ka were predominantly dated by fission-track methods (Westgate et al., 1990; Preece et al., 1999, 2000; Sandhu et al., 2001). Ages for various Beringian tephra beds obtained through this technique span from <100 ka to 3.5 Ma (Westgate et al., 1990, 2008; Sandhu and Westgate, 1995; Preece et al., 1999; Sandhu et al., 2001). Playing a pivotal role, these ages have contributed to determining crucial geological and paleoenvironmental events, such as the initiation of loess deposition in interior Alaska and the first advance of the Cordilleran ice sheet into the Yukon Territory (Preece et al., 1999; Westgate et al., 2005). However, the relatively low precision of fission-track dates (often >20% at 95 % confidence level) and the dating material requirements (e.g., non-pumiceous glass, defect free zircon/apatite) often restrict its application (Fig. 1.4B).

Similarly, the widespread use of potassium-argon and argon-argon dating of volcanogenic deposits (e.g., Kunk, 1995) has limitations when applied to the tephra deposits of eastern Beringia. Both techniques are unsuitable for dating distal tephra layers in eastern

Beringia characterized by fine grain sizes, low crystal content, and low potassium concentrations (Shane, 2000; Alloway et al., 2007).

Due to recent technological development, zircon U-Pb, U-Th and (U-Th)/He dating methods became critical for understanding the high-temperature cooling history of magmas and establishing the ages of young tephra beds (Schmitt, 2011). Laser ablation-inductively coupled plasma-mass spectrometry (LA-ICP-MS) has become one of the most widely used techniques for U-Pb dating in Quaternary geochronology, complemented by secondary ion mass spectrometry (SIMS) and thermal ionization mass spectrometry (TIMS) (Schaltegger et al., 2015). Obtaining accurate U-Pb ages from young zircon crystals requires correcting for initial disequilibria caused by intermediate nuclides in the ^{238}U and ^{235}U decay series, specifically ^{230}Th and ^{231}Pa (Wendt and Carl, 1985). To address this, corrections can be applied to U-Pb ages (Schärer. 1984; Sakata et al., 2013) or, alternatively, U-Th dating can be employed to measure the time-dependent disequilibrium between ^{238}U and ^{230}Th, persisting for ~350 ka (about five half-lives of ^{230}Th) after crystallization.

Additionally, when dating young zircon crystals, contributions from non-radiogenic Pb (common Pb) to the radiogenic-Pb can be substantial. Several approaches exist for common Pb correction, with the ^{207}Pb method (Williams, 1998) being the most used for young zircon dating. Notably, this method doesn't rely on the measurement of ^{204}Pb, which occurs in minor isotopic abundances and may suffer from isobaric interference from ^{204}Hg (LA-ICP-MS). The ^{207}Pb method assumes concordance between ^{238}U-^{206}Pb and ^{235}U-^{207}Pb ages. This assumption is true for Quaternary zircon crystals that are generally too young to have undergone sufficient radiation damage to cause Pb mobility (Cherniak and Watson, 2001). However, the effects of initial disequilibria on ^{230}Th and ^{231}Pa complicate the equations of ^{238}U-^{206}Pb and ^{235}U-^{207}Pb ages compared to conventional U-Pb geochronology (Wendt and Carl, 1985). In the case of young zircon dating with the ^{207}Pb method, initial disequilibria and common-Pb are interdependent, requiring an internally consistent correction.

The initial secular disequilibrium between ^{238}U and ^{230}Th initially creates an age bias that needs correction, but also offers an opportunity to date very young zircons (<350 ka). The U-Th disequilibrium zircon dating method is particularly effective for dating crystallization events of around 350,000 years or less due to the approximately 75,000-year half-life of ^{230}Th (Cheng et al., 2000). The process of U-Th disequilibrium dating involves measuring activity ratios of $^{230}Th/^{232}Th$ and $^{238}U/^{232}Th$ in zircon crystals. These activities can be used to determine how long the theoretically closed system has been at secular disequilibrium. Various techniques, including secondary ion mass spectrometry (SIMS) and laser ablation inductively coupled plasma mass spectrometry (LA-ICP-MS), are used for this measurement. Additionally, U-Th dating plays an important role in "zircon double-dating" (ZDD), a geochronological approach for dating the eruption age of extrusive volcanic products younger than approximately 350,000 years. ZDD corrects for disequilibrium effects on the (U-Th)/He systematics using the crystallization age of zircon (Schmitt et al., 2011; Danišík et al., 2017).

1.5. Scope and objectives

The main objectives of this dissertation are tied to the development and application of U-based *in-situ* dating to young tephra deposits and implications of the new chronologies to the paleoenvironmental record in eastern Beringia.

To improve chronological constraints on important tephra in eastern Beringia, and to develop analytical and statistical methods for dating of young silicic volcanic rocks, the main objectives of this dissertation are as follows:

1. To assess the applicability of LA-ICP-MS zircon U-Pb and U-Th dating of Pliocene-Pleistocene tephra and to evaluate methods for analysis of complex zircon age data.
2. To develop improved analytical techniques for LA-ICP-MS (e.g., development of single spot U-series and simultaneous U-Pb/U-series zircon dating).
3. Build an improved chronological framework for the key Pliocene-Pleistocene tephra deposits in eastern Beringia and explore implications for the paleoenvironmental and palaeobiological studies in the region.

Together, these efforts will provide a foundation for an improved chronology of tephra in eastern Beringia and an establishment of improved chronological and statistical methods for dating of Quaternary-age zircon.

1.6. References

Anderson, P.M., Lozhkin, A.V., 2001. The Stage 3 interstadial complex (Karginskii/middle Wisconsinan interval) of Beringia: variations in paleoenvironments and implications for paleoclimatic interpretations. Quaternary Science Reviews 20, 93–125.

Auclair, M., Lamothe, M., Lagroix, F., Banerjee, S.K., 2007. Luminescence investigation of loess and tephra from Halfway House section, central Alaska. Quaternary Geochronology 2, 34–38.

Begét, J., 1990. Middle Wisconsinan Climate Fluctuations Recorded in Central Alaskan Loess. Géographie physique et Quaternaire 44, 3–13.

Begét, J.E., 2001. Continuous Late Quaternary proxy climate records from loess in Beringia. Quaternary Science Reviews 20, 499–507. https://doi.org/10.1016/S0277-3791(00)00102-5

Berger, G.W., 1987. Thermoluminescence dating of the Pleistocene Old Crow tephra and adjacent loess, near Fairbanks, Alaska. Canadian Journal of Earth Sciences 24, 1975–

Blong, R.J., Gillespie, R., 1978. Fluvially transported charcoal gives erroneous 14C ages for recent deposits. Nature 271, 739–741

Brendryen, J., Haflidason, H., Sejrup, H.P., 2010. Norwegian Sea tephrostratigraphy of marine isotope stages 4 and 5: Prospects and problems for tephrochronology in the North Atlantic region. Quaternary Science Reviews 29, 847–864. https://doi.org/10.1016/j.quascirev.2009.12.004

Burgess, S.D., Coble, M.A., Vazquez, J.A., Coombs, M.L., Wallace, K.L., 2019. On the eruption age and provenance of the Old Crow tephra. Quaternary Science Reviews 207, 64–79.

Burgess, S.D.D., Vazquez, J.A.A., Waythomas, C.F.F., Wallace, K.L.L., 2021. U–Pb zircon eruption age of the Old Crow tephra and review of extant age constraints. Quaternary Geochronology 101168.

Buryak, S.D., Reyes, A.V., Jensen, B.J.L., Davies, J.H.F.L., Westgate, J.A., DuFrane, S.A., Luo, Y., Froese, D.G., Pearson, D.G., Benowitz, J.A., 2022. Laser-ablation ICP-MS zircon U-Pb ages for key Pliocene-Pleistocene tephra beds in unglaciated Yukon and Alaska. Quaternary Geochronology 101398.

Chen, Y., Smith, P.E., Evensen, N.M., York, D., Lajoie, K.R., 1996. The Edge of Time: Dating Young Volcanic Ash Layers with the 40Ar-39Ar Laser Probe. Science 274, 1176–1178.

Chen, J., Li, G., Yang, J., Rao, W., Lu, H., Balsam, W., Sun, Y., Ji, J., 2007. Nd and Sr isotopic characteristics of Chinese deserts: Implications for the provenances of Asian dust. Geochimica et Cosmochimica Acta 71, 3904–3914.

Cheng, H., Adkins, J., Edwards, R.L., Boyle, E.A., 2000. U-Th dating of deep-sea corals. Geochimica et Cosmochimica Acta 64, 2401–2416.

Cherniak, D.J., Watson, E.B., 2001. Pb diffusion in zircon. Chemical Geology 172, 5–24.

Cooper, A., Turney, C., Hughen, K.A., Brook, B.W., McDonald, H.G., Bradshaw, C.J.A., 2015. Abrupt warming events drove Late Pleistocene Holarctic megafaunal turnover. Science 349, 602–606. https://doi.org/10.1126/science.aac4315

Danišík, M., Schmitt, A.K., Stockli, D.F., Lovera, O.M., Dunkl, I., Evans, N.J., 2017. Application of combined U-Th-disequilibrium/U-Pb and (U-Th)/He zircon dating to tephrochronology. Quaternary Geochronology 40, 23–32.

Demuro, M., Roberts, R.G., Froese, D.G., Arnold, L.J., Brock, F., Bronk Ramsey, C., 2008. Optically stimulated luminescence dating of single and multiple grains of quartz from perennially frozen loess in western Yukon Territory, Canada: comparison with radiocarbon chronologies for the late Pleistocene Dawson tephra. Quaternary Geochronology 3, 346–364.

Elias, S.A., Brigham-Grette, J., 2013. GLACIATIONS | Late Pleistocene Glacial Events in Beringia, in: Encyclopedia of Quaternary Science. Elsevier, pp. 191–201.

Froese, D.G., Zazula, G.D., Reyes, A.V., 2006. Seasonality of the late Pleistocene Dawson tephra and exceptional preservation of a buried riparian surface in central Yukon Territory, Canada. Quaternary Science Reviews 25, 1542–1551.

Goebel, T., Waters, M., O'Rourke, D.H., 2008. The Late Pleistocene dispersal of modern humans in the Americas. Science 319, 1497–1502.

Guthrie, R.D., 1990. Frozen Fauna of the Mammoth Steppe: The Story of Blue Babe. University of Chicago Press, Chicago, 323 p.

Guthrie, R.D., 2006. New carbon dates link climatic change with human colonization and Pleistocene extinctions. Nature 441, 207–209.

Hamilton, T.D., Brigham-Grette, J., 1991. The last interglaciation in Alaska: stratigraphy and paleoecology of potential sites. Quaternary International 10–12, 49–71.

Hoffecker, J.F. and Elias, S.A., 2007. Human ecology of Beringia. Columbia University Press.

Hopkins, D.M., 1982. Aspects of the paleogeography of Beringia during the late Pleistocene, in: Hopkins, D. M., Matthews, J.V., Schweger, C.E., Young, S.B. (Eds.), Paleoecology of Beringia. Academic Press, pp. 3–28.

Jaffey, A.H., Flynn, K.F., Glendenin, L.E., Bentley, W.C., Essling, A.M., 1971. Precision measurement of half-lives and specific activities of U235 and U238. Physical Review C 4, 1889–1906. https://doi.org/10.1103/PhysRevC.4.1889

Jensen, B.J.L., Preece, S.J., Lamothe, M., Pearce, N.J.G., Froese, D.G., Westgate, J.A., Schaefer, J., Begét, J., 2011. The variegated (VT) tephra: A new regional marker for middle to late marine isotope stage 5 across Yukon and Alaska. Quaternary International 246, 312–323.

Jensen, B.J.L., Reyes, A.V., Froese, D.G., Stone, D.B., 2013. The Palisades is a key reference site for the middle Pleistocene of eastern Beringia: New evidence from paleomagnetics and regional tephrostratigraphy. Quaternary Science Reviews 63, 91–108. https://doi.org/10.1016/j.quascirev.2012.11.035

Jensen, B.J.L., Evans, M.E., Froese, D.G., Kravchinsky, V.A., 2016. 150,000 years of loess accumulation in central Alaska. Quaternary Science Reviews 135, 1–23.

Kunk, M.J., U.S. Dept. of the Interior, G.S., 1995. 40Ar/39Ar age-spectrum data for hornblende, plagioclase and biotite from tephras collected at Dan Creek and McCallum Creek, Alaska and in the Klondike Placer district near Dawson, Yukon Territory, Canada, Open-File Report.

Lamothe, M., Forget Brisson, L., Hardy, F., 2020. Circumvention of anomalous fading in feldspar luminescence dating using Post-Isothermal IRSL. Quaternary Geochronology 57.

Lowe, D.J., 2011. Tephrochronology and its application: A review. Quaternary Geochronology

Martin, P.S., 2005. Twightlight of the Mammoths: Ice Age Extinctions and the Rewildering of America. University of California Press, California, 250 p.

Matthews, J.V., Westgate, J.A., Ovenden, L., Carter, L.D., Fouch, T., 2003. Stratigraphy, fossils, and age of sediments at the upper pit of the Lost Chicken gold mine: New information on the late Pliocene environment of east central Alaska. Quaternary Research 60, 9–18.

Morgan, L.E., Renne, P.R., Taylor, R.E., WoldeGabriel, G., 2009. Archaeological age constraints from extrusion ages of obsidian: Examples from the Middle Awash, Ethiopia. Quaternary Geochronology 4, 193–203.

Morlan, R.E., 2003. Current perspectives on the Pleistocene archaeology of eastern Beringia. Quaternary Research 60, 123–132.

Muhs, D., 2003. Stratigraphy and palaeoclimatic significance of Late Quaternary loess–palaeosol sequences of the Last Interglacial–Glacial cycle in central Alaska. Quaternary Science Reviews 22, 1947–1986. https://doi.org/10.1016/S0277-3791(03)00167-7

Orlando, L., Ginolhac, A., Raghavan, M., Vilstrup, J., Rasmussen, M., Magnussen, K., Steinmann, K.E., Kapranov, P., Thompson, J.F., Zazula, G., Froese, D., Moltke, I., Shapiro, B., Hofreiter, M., Al-Rasheid, K.A.S., Gilbert, M.T.P., Willerslev, E., 2011. True single-molecule DNA sequencing of a Pleistocene horse bone. Genome Research 21, 1705–1719.

Pewe, T.L., 1975. Quaternary stratigraphic nomenclature in unglaciated central Alaska, Professional Paper.

Péwé, T.L., Westgate, J.A., Preece, S.J., Brown, P.M., Leavitt, S.W., 2009. Late Pliocene Dawson cut forest bed and new tephrochronological findings in the Gold Hill Loess, east-central Alaska. Bulletin of the Geological Society of America 121, 294–320.

Pigati, J.S., Quade, J., Wilson, J., Jull, A.J.T., Lifton, N.A., 2007. Development of low-background vacuum extraction and graphitization systems for 14C dating of old (40–60 ka) samples. Quaternary International 166, 4–14.

Preece, S.J., Westgate, J.A., Gorton, M.P., 1992. Compositional variation and provenance of late Cenozoic distal tephra beds, Fairbanks area, Alaska. Quaternary International 13–14, 97–101.

Preece, S.J., Westgate, J.A., Stemper, B.A., Péwé, T.L., 1999. Tephrochronology of late Cenozoic loess at Fairbanks, central Alaska. Bulletin of the Geological Society of America 111, 71–90.

Preece, S.J., Westgate, J.A., Alloway, B.V., Milner, W., 2000. Characterization, identity, distribution, and source of late Cenozoic tephra beds in the Klondike district of the Yukon, Canada. Canadian Journal of Earth Sciences 37, 983–996.

Preece, S.J., Westgate, J.A., Froese, D.G., Pearce, N.J.G., Perkins, W.T., 2011. A catalogue of late Cenozoic tephra beds in the Klondike goldfields and adjacent areas, Yukon Territory. Canadian Journal of Earth Sciences 48, 1386–1418.

Reyes, A.V., Zazula, G.D., Kuzmina, S., Ager, T.A., Froese, D.G., 2011. Identification of last interglacial deposits in eastern Beringia: a cautionary note from the Palisades, interior Alaska. Journal of Quaternary Science 26, 345–352. https://doi.org/10.1002/jqs.1464

Reyes, A.V., Jensen, B.J.L., Woudstra, S.H., Bolton, M.S.M., Buryak, S.D., Cook, M.S., Harvey, J., Westgate, J.A., 2023. Detrital glass in a Bering Sea sediment core yields a ca. 160 ka Marine Isotope Stage 6 age for Old Crow tephra. Geology 51, 106–110.

Sakata, S., Hirakawa, S., Iwano, H., Danhara, T., Hirata, T., 2013. Correction of initial disequilibrium on U-Th-Pb system for dating of young zircons. Mineralogical Magazine 77, 2116. https://doi.org/10.1180/minmag.2013.077.5.19

Sandhu, A.S., Westgate, J.A., 1995. The correlation between reduction in fission-track diameter and areal track density in volcanic glass shards and its application in dating tephra beds. Earth and Planetary Science Letters 131, 289–299.

Sandhu, A.S., Westgate, J.A., Preece, S.J., Froese, D.G., 2001. Glass-fission-track ages of late Cenozoic distal tephra beds in the Klondike district, Yukon Territory. In: Edmond, D.S., Weston, L.H. (Eds.), Yukon Exploration and Geology 2000. Exploration and Geological Services Division, Yukon, Indian and Northern Affairs Canada, pp. 247–256.

Schaltegger, U., Schmitt, A.K., Horstwood, M.S.A., 2015. U–Th–Pb zircon geochronology by ID-TIMS, SIMS, and laser ablation ICP-MS: Recipes, interpretations, and opportunities. Chemical Geology 402, 89–110.

Schärer, U., 1984. The effect of initial 230Th disequilibrium on young UPb ages: the Makalu case, Himalaya. Earth and Planetary Science Letters 67, 191–204. https://doi.org/10.1016/0012-821X(84)90114-6

Schmitt, A.K., 2011. Uranium Series Accessory Crystal Dating of Magmatic Processes. Annu. Rev. Earth Planet. Sci. 39, 321–349.

Schoene, B., 2013. U-Th-Pb Geochronology, Treatise on Geochemistry: Second Edition. https://doi.org/10.1016/B978-0-08-095975-7 .00310-7

Shane, P., 2000. Tephrochronology: a New Zealand case study. Earth-Science Reviews 49, 223–259.

Shane, P., Sandiford, A., 2003. Paleovegetation of marine isotope stages 4 and 3 in Northern New Zealand and the age of the widespread Rotoehu tephra. Quaternary Research 59, 420–429.

Sher, A., 1999. Traffic lights at the Beringian crossroads. Nature 397, 103–104.

Spell, T.L., Smith, E.I., Sanford, A., Zanetti, K.A., 2001. Systematics of xenocrystic contamination: preservation of discrete feldspar populations at McCullough Pass Caldera revealed by 40Ar/39Ar dating. Earth and Planetary Science Letters 190, 153–165. https://doi.org/10.1016/S0012-821X(01)00382-X

Ulusoy, İ., Çubukçu, H.E., Mouralis, D., Aydar, E., 2019. Nemrut Caldera and Eastern Anatolian Volcanoes: Fire in the Highlands, in: Kuzucuoğlu, C., Çiner, A., Kazancı, N. (Eds.), Landscapes and Landforms of Turkey, World Geomorphological Landscapes. Springer International Publishing, Cham, pp. 589–599.

Vidal, C.M., Lane, C.S., Asrat, A., Barfod, D.N., Mark, D.F., Tomlinson, E.L., Tadesse, A.Z., Yirgu, G., Deino, A., Hutchison, W., Mounier, A., Oppenheimer, C., 2022. Age of the oldest known Homo sapiens from eastern Africa. Nature 601, 579–583. https://doi.org/10.1038/s41586-021-04275-8

Walker, M., 2005. Quaternary Dating Methods. John Wiley & Sons Ltd, England. 286 p.

Wendt, I., Carl, C., 1985. U/Pb dating of discordant 0.1 Ma old secondary U minerals. Earth and Planetary Science Letters 73, 278–284.

Westgate, J.A., 1988. Isothermal plateau fission-track age of the late Pleistocene Old Crow tephra, Alaska. Geophysical Research Letters 15, 376–379.

Westgate, J.A., Walter, R.C., Pearce, G.W., Gorton, M.P., 1985. Distribution, stratigraphy, petrochemistry, and palaeomagnetism of the late Pleistocene Old Crow tephra in Alaska and the Yukon. Canadian Journal of Earth Sciences 22, 893–906.

Westgate, J.A., Stemper, B.A., Péwé, T.L., 1990. A 3 m.y. record of Pliocene-Pleistocene loess in, interior Alaska. Geology 18, 858–861.

Westgate, J.A., Preece, S.J., Froese, D.G., Pearce, N., Alloway, B., 2005. Late Cenozoic tephrochronology of the Klondike area. In: Froese, D.G., Westgate, J.A., Alloway, B.V. (Eds.), Field Trip Guide for International Field Conference and Workshop on Tephrochronology and Volcanism: Dawson City, Yukon Territory, Canada July 31st – August 8th, 2005 Institute of Geological & Nuclear Sciences science report 2005/26, pp. 43–51

Westgate, J.A., Preece, S.J., Froese, D.G., Pearce, N.J.G., Roberts, R.G., Demuro, M., Hart, W.K., Perkins, W., 2008. Changing ideas on the identity and stratigraphic significance of the Sheep Creek tephra beds in Alaska and the Yukon Territory, northwestern North America. Quaternary International 178, 183–209

Williams, I.S., 1998. U-Th-Pb Geochronology by Ion Microprobe, Applications of Microanalytical Techniques to Understanding Mineralizing Processes. Society of Economic Geologists.

Zazula, G.D., Froese, D.G., Elias, S.A., Kuzmina, S., Mathewes, R.W., 2007. Arctic ground squirrels of the mammoth-steppe: paleoecology of Late Pleistocene middens (~24000–29450 14C yr BP), Yukon Territory, Canada. Quaternary Science Reviews 26, 979–1003. https://doi.org/10.1016/j.quascirev.2006.12.006

Chapter 2: Laser-ablation ICP-MS zircon U-Pb ages for key Pliocene-Pleistocene tephra beds in unglaciated Yukon and Alaska

2.1. Introduction

The eastern Beringia region of Yukon and Alaska remained largely unglaciated during the Quaternary (Hultén, 1937; Hopkins et al., 1971; Brigham-Grette, 2001; Froese et al., 2009). The lack of glaciation in this region, coupled with the long-term presence of permafrost (Froese et al., 2008; Reyes et al., 2010a; Biller-Celander et al., 2021) and thick aggradational sequences of loessal sediment (e.g., Pewe, 1975; Begét, 1990; Westgate et al., 1990), has led to a rich terrestrial paleoenvironmental and paleontological record spanning the Quaternary into the latest Pleistocene (e.g., Hopkins et al., 1971; White et al., 1997; Matthews et al., 2003; Froese et al., 2009; Schweger et al., 2011; Orlando et al., 2013; Willerslev et al., 2014).

Critical to the development of these records, particularly beyond the range of ^{14}C dating, is the extensive record of tephra beds associated with two major volcanic zones at the northwest edge of North America: the Alaska Peninsula-Aleutian Arc and Wrangell Arc (Fig. 2.1.). Both zones have been active throughout the Quaternary, resulting in the preservation of hundreds of tephra beds throughout sedimentary deposits in the Yukon and Alaska that can be characterized on the basis of their unique glass and mineral geochemical signatures (e.g., Begét and Keskinen, 2003; Jensen et al., 2008; Preece et al., 1999, 2011; Davies et al., 2016). When tephra geochemical fingerprinting is combined with stratigraphic and paleoenvironmental context (Westgate and Briggs, 1980), the resulting tephra-enabled chronostratigraphic frameworks in eastern Beringia (e.g., Preece et al., 1999, 2011; Jensen et al., 2013, 2016; Davies et al., 2016) have facilitated confident correlation of sedimentary records that would otherwise be difficult or impossible to link.

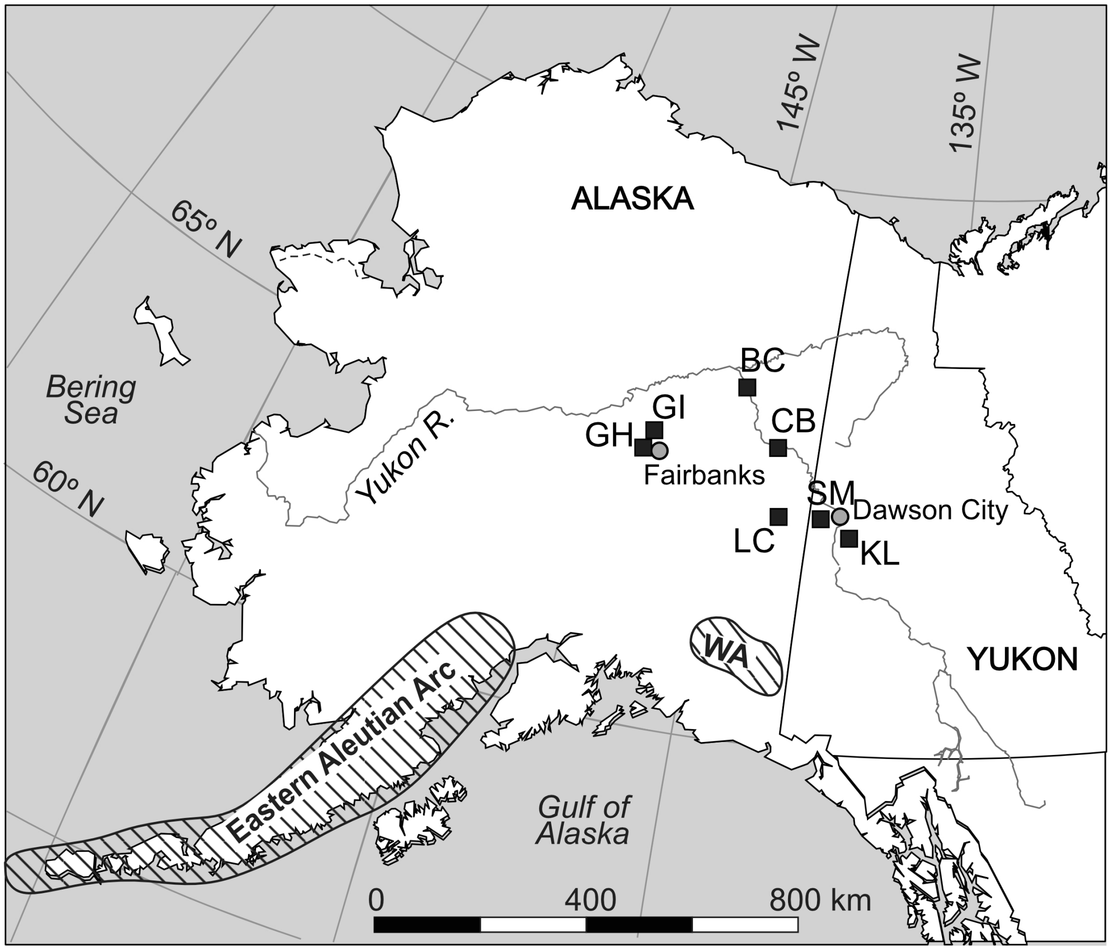

Figure 2.1. *Map of Yukon and Alaska with the locations of the sampling sites for the tephra analyzed in this study and major volcano source regions (WA, Wrangell Arc). GH (Gold Hill): HP, PA tephra; GI (Geophysical Institute): GI tephra; LC: Lost Chicken tephra; KL (Klondike): Gold Run tephra, Flat Creek tephra, Quartz Creek tephra; SM (Sixtymile River): Gold Run tephra, Flat Creek tephra; CB (Chester Bluff), BC (Birch Creek): Biederman tephra.*

Importantly for the development of temporally calibrated sedimentary records beyond the range of ^{14}C dating, it has been possible to obtain direct ages for some key tephra beds in this region (e.g., Kunk, 1995; Preece et al., 1999; Westgate et al., 2001) to supplement those based on dating of surrounding sediments (e.g., by luminescence dating, Berger, 1987, 1991; Auclair et al., 2007; Lamothe et al., 2020). For the most part, direct ages have been obtained using glass fission-track techniques (Westgate, 1988; Sandhu et al., 2000; Preece et al., 2011; Westgate et al., 2013) that are thought to record the timing of the associated volcanic eruptions. However, Burgess et al. (2019, 2021) recently questioned the accuracy of glass fission-track dating for the regionally important Old Crow tephra, previously constrained by glass fission-track and luminescence techniques to late Marine Isotope Stage (MIS) 6 (e.g., Preece et al., 2011; Lamothe et al., 2020). Burgess et al. (2019, 2021) instead proposed an older Old Crow tephra age of ca. 200 ka using U-Pb, U-series and (U-Th)/He dating techniques on zircon. These new age estimates for Old Crow tephra are contentious because they are inconsistent with existing stratigraphic, paleomagnetic, palaeoecological, and paleogenomic constraints for this tephra (e.g., Edwards and McDowell, 1991; Hamilton and Brigham-Grette, 1991; Waythomas et al., 1993; Reyes et al., 2010b; Preece et al., 2011; Jensen et al., 2013, 2016; Froese et al., 2017).

Despite the brewing controversy over the age of Old Crow tephra, which we do not address in this paper, dating of Pliocene-Pleistocene tephra in eastern Beringia by U-Pb techniques offers the potential to expand the framework of directly dated tephra in this region. Silica-rich tephra usually contains several accessory minerals that can be dated using U-based methods, including zircon, apatite, titanite and other actinide-rich phases. *In-situ* zircon U-Pb geochronology has been used in dating of Quaternary-age tephra (e.g., Bacon et al., 2000; Ito et al., 2013; Guillong et al., 2014; Ito, 2020). The application of this method is particularly promising for Alaska/Yukon tephra beds, which commonly do not contain mineral phases suitable for ^{40}K-^{40}Ar (or $^{40}Ar/^{39}Ar$) dating methods and are outside the practical limit of ^{14}C and luminescence dating on bracketing materials. Furthermore, the use of glass fission-track dating is limited to samples with pristine, non-pumiceous glass shards with sufficient surface area to accurately measure the track densities (Westgate, 2015). Hence, fission-track dating cannot be used to obtain ages on tephra with glass morphology that does not fit these criteria, such as the many pumiceous tephra originating from the Wrangell Arc (Preece et al., 1999, 2000).

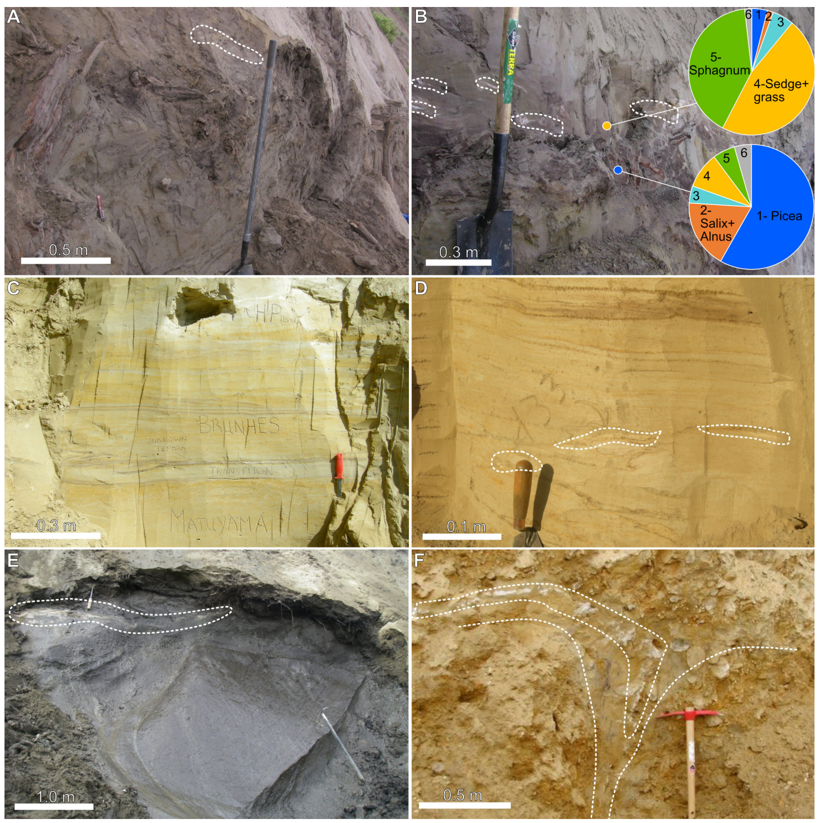

Figure 2.2. *Photos of selected tephra dated in this study. Dashed polygons mark the location of tephra beds/laminae. Scales are approximate, particularly for (A) and (B). (A) Biederman tephra at Birch Creek lies directly above a thaw unconformity that contained large woody debris and spruce cones. (B) Biederman tephra at its reference section at Chester Bluff (Jensen et al., 2008) lies above an organic-rich silt that collapses into an ice wedge cast. Pollen from the organic bed suggest deposition during an interglacial; 3 – Graminaceae; 6 – herbs and woody shrubs (C)*

HP tephra (after collection from the excavated silt block at top of photo) at Gold Hill IV, with the Brunhes-Matuyama boundary etched into the silt to left of the knife for scale (Evans et al., 2011). (D) GI tephra at Gold Hill IV is a diffuse pinkish unit that is difficult to spot in the orange-tinged loess. This tephra is often associated with silts interpreted to represent one or more paleosol(s) (e.g., Jensen et al., 2008). (E) Gold Run tephra deposited above a relict ice wedge (Froese et al., 2008) at its reference section on Dominion Creek. (F) Quartz Creek tephra collapsed into an ice wedge cast at its reference section at the Quartz Creek site.

Nevertheless, there are substantial challenges in applying LA-ICP-MS U-Pb zircon geochronology to Pleistocene tephra. The closure temperature for Pb diffusion in zircon is in excess of 900 °C; as a result, U-Pb ages record the timing of zircon crystallization in a magma rather than the time the erupted magma cooled below a certain temperature as would be the case with ^{40}K/^{40}Ar (^{40}Ar/^{39}Ar) or (U-Th)/He dating techniques (McDougall and Harrison, 1999; Cherniak and Watson, 2001; Danišík et al., 2017). There are multiple studies comparing eruption ages determined by the ^{40}Ar/^{39}Ar method to zircon U-series or U-Pb ages. Some of these studies yield results that are in agreement (e.g., Matthews et al., 2015; Stelten et al., 2015; Coble et al., 2017; Till et al., 2019), while others yield U-Pb zircon ages that are older than ^{40}Ar/^{39}Ar ages (e.g., Simon et al., 2008; Zimmerer et al., 2016; Krautz et al., 2018., Sisson et al., 2019). Hence, the U-Pb zircon technique does not always directly age the timing of eruption, potentially biasing the deposition age of the tephra toward an older estimate.

Further complications for U-Pb dating of Pleistocene zircon are the extreme ratios of common- to radiogenic-Pb (routinely exceeding 75% common-Pb), as well as initial ^{230}Th (and possibly ^{231}Pa) disequilibrium which can substantially bias the age of a sample given the magnitude of required adjustments (e.g., Sakata, 2018). Low abundances of radiogenic-Pb make it challenging to apply accurate common-Pb corrections. Similarly, disequilibrium in ^{230}Th (an intermediate product in the ^{238}U decay series) due to melt-mineral U-Th partitioning can bias U-Pb ages up to ~110 ka too young and requires correction to obtain an accurate age (Ludwig, 1977; Schärer, 1984). In addition, the small Pb ion signals produced from small diameter laser ablation spots require careful evaluation of instrumental backgrounds across the Pb mass spectrum.

Furthermore, post-depositional reworking of distal tephra beds can lead to contamination from admixed detrital zircon crystals which results in a long tail of old ages usually pre-dating the eruption by millions of years. Post-deposition detrital zircon admixing, coupled with presence of xenocrystic/antecrystic zircon crystals in the primary tephra deposit, makes it difficult to ascertain which ages constitute the autocrystic zircon population. Thus, the age data require careful evaluation to ensure that the ages most representative of the timing of eruption are selected for depositional age calculation.

In this paper, we assess the utility of LA-ICP-MS zircon U-Pb techniques for direct dating of Pliocene-Pleistocene tephra via application to tephra deposits from eastern Beringia. We obtained U-Pb zircon ages for Biederman, HP, Gold Run, Flat Creek, PA, Quartz Creek, Lost Chicken and GI tephra — eight important regional marker tephra deposits, spanning latest Pliocene to Middle Pleistocene time, collected at various sites in Yukon and Alaska (Preece et al., 1999; Froese, 2001; Westgate et al., 2001; Matthews et al., 2003; Jensen et al., 2008; Jensen et al., 2013; Fig. 2.1.; Fig. 2.2; Table 2.1.). We chose these specific tephra because they have published glass fission-track and ^{40}Ar/^{39}Ar data and/or have stratigraphic and paleomagnetic constraints that allow us to evaluate our new U-Pb ages and propose the most probable age ranges for tephra deposition.

Table 2.1. Accession ID numbers, sampling locations and the most recent age estimates for dated tephra beds. GFT = glass fission-track. Uncertainties are displayed at 2σ level.

Tephra	ID	Sample Location	Coordinates	Magnetic Polarity	Existing Age Estimates
Biederman[1]	UT1884	Site C, Chester Bluff	65° 22' 48" N 142° 40' 12" W	Normal	-
HP[2]	UA2841	Gold Hill IV	64° 51' 12" N 147° 55' 44" W	Normal	590 ± 200 ka (GFT)
Gold Run[3]	UA1001	Gold Run Creek type section	63° 41' 20" N 138° 36' 22" W	Normal	690 ± 100 ka (GFT)
Flat Creek[4]	UA1012	Flat Creek type section	63° 56' 23" N 139° 33' 47" W	Normal	-
PA[5]	UA1327	Gold Hill II	64° 51' 18" N 147° 55' 55" W	Reversed	2.02 ± 0.28 Ma (GFT)
Quartz Creek[6]	UA1004	Quartz Creek type section	63° 48' 50" N 139° 3' 29" W	Normal	2.82 ± 0.24 Ma (GFT); 2.64 ± 0.48 Ma ($^{40}Ar/^{39}Ar$)
Lost Chicken[7]	UA1013	Lost Chicken Mine	64° 4' 12" N 141° 54' 22" W	Reversed	2.91 ± 0.88 Ma (GFT)
GI[8]	UA1668 & UA2838	Type section near Geophysical Institute, UAF	64° 51' 34" N 147° 50' 58" W	Normal	500 ± 200 ka (GFT)

[1]Jensen et al., 2008; Jensen et al., 2013. [2]Preece et al., 1999; Preece et al., 2011. [3]Bond, 1997; Westgate et al., 2011. [4]Westgate et al., 2011. [5]Preece et al., 1999; Westgate et al., 2001. [6]Froese, 2001. [7]Kunk, 1995; Matthews et al., 2003; Preece et al., 2011. [8]Preece et al., 1999; Preece et al., 2011.

2.2. Methods

Zircon crystals were extracted from bulk tephra samples from the University of Alberta Tephra Collection (accession numbers UA1001, UA1012, UA1004, UA1327, UA1013, UA1668, UA2838, UT1884; Fig. 2.3.). The samples were sieved to isolate the < 250 μm fraction and zircon crystals were separated using standard heavy-liquid density separation methods (e.g., Strong and Driscoll, 2016). Zircon crystals were hand-picked from the heavy mineral separates under stereoscopic microscope and mounted in epoxy for analysis. All grains were inspected for inherited cores, inclusions, physical defects, and zonation patterns using cathodoluminescence, backscatter electron imaging, and reflected and transmitted light microscopy. Primary/secondary reference materials and instrumental parameters are summarized in Supplemental Tables A.3 and A.6, respectively.

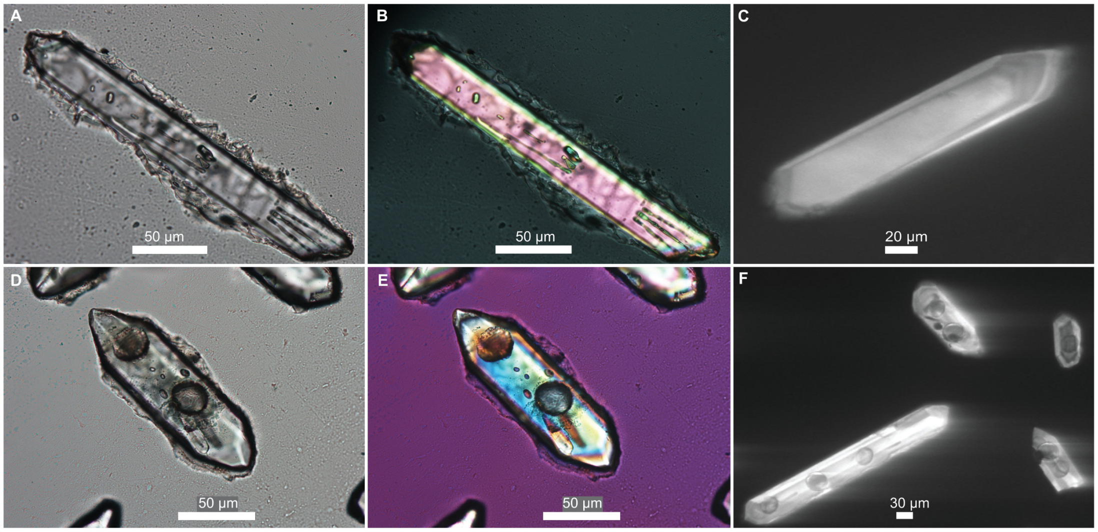

Figure 2.3. *Micrographs of representative zircon crystals from samples analyzed in this study. (A, B) Plane (A) and cross-polarized (B) light micrographs of euhedral, prismatic zircon from Biederman tephra (grain BT002) with adhered glass rim. (C) SEM-cathodoluminescence micrograph of zircon from Biederman tephra (grain BT44P2) displaying weak oscillatory zoning. (D, E) Plane (D) and cross-polarized (E) micrographs of euhedral zircon from Flat Creek tephra (grain UA1012-11) with adhered glass rim and ablation pits. (F) SEM-cathodoluminescence micrograph of zircon crystals from Gold Run tephra (clockwise from top left, grains are UA1001-11, UA1001-12, UA1001-25, and UA1001-1; analyzed using MC-ICP-MS setup).*

2.2.1. Zircon U-Pb

2.2.1.1. Multi-collector (MC)-ICP-MS

Zircon crystals from Gold Run (UA1001), Flat Creek (UA1012), Quartz Creek (UA1004), PA (UA1327), Lost Chicken (UA1013) and GI (UA1668 and UA2838) tephra were analyzed using a New Wave UP-213 nm laser ablation system coupled to a NuPlasma I multi-collector (MC)-ICP-MS, using an ESI/New Wave Research cell. The analytical procedure is described in detail by Simonetti et al. (2005). Zircon crystals were spot ablated for 40 seconds using a 30 μm beam at a 5 Hz repetition rate and laser energy at the sample surface ~3 J/cm^2 producing well-defined, flat-bottomed near-cylindrical pits 30 μm in diameter and ~10-15 μm deep. The ablations were conducted in a He atmosphere at a flow rate of 1 L/min through the cell with output from the cell joined to the output from a standard Nu plasma desolvating nebulizer. On peak gas and acid blanks were measured for 30 seconds prior to a set of 10-20 analyses. Data were collected statically, consisting of 30 one-second integrations. The primary standard reference sample GJ-1 (608.5 ± 0.4 Ma; Jackson et al., 2004; Heaman, unpublished data) and secondary zircon reference materials Plešovice (337.1 ± 0.4 Ma; Sláma et al., 2008) and Bishop Tuff (0.767 ± 0.001 Ma; Crowley et al., 2007; Chamberlain et al., 2014; Ickert et al., 2015) were analyzed before and after each set of 10-20 unknowns to monitor U–Pb fractionation, reproducibility, and instrument drift. The Plešovice and Bishop Tuff yielded weighted mean ^{206}Pb-^{238}U ages of 336.0 ± 1.9 Ma (MSWD = 0.3, n = 13) and 0.773 ± 0.005 Ma (MSWD = 1.6, n = 13), respectively, over three days of analytical sessions (Supplemental Table A.3). The ^{206}Pb-^{238}U ages for reference materials are within 2σ uncertainty of the literature values: values for the entire suite of analyses are within the permissible range at 95% confidence level for the single population of replicated analyses (Mahon, 1996). The $^{206}Pb/^{238}U$ average precision of these reference materials is ~2% (2σ) for individual spot analyses. All data were reduced offline using an in-house Microsoft Excel spreadsheet with unknowns normalized to the GJ-1 zircon primary reference standard. Mass bias for Pb isotopes was corrected using an exponential law and assuming $^{205}Tl/^{203}Tl$ of 2.3871; U/Pb fractionation and instrument drift were corrected using a sample-standard bracketing technique. The uncertainties of measured isotopic ratios are a quadratic combination of the standard error of the measured isotope ratio and the long-term excess scatter of the GJ-1 means.

2.2.1.2. iCAP quadrupole (Q)-ICP-MS

Zircon crystals from HP (UA2841) and GI (UA2838) tephra were analyzed using a New Wave UP-213 nm laser ablation system coupled to a Thermo Scientific iCAP quadrupole (Q)-ICP-MS, using an ESI/New Wave Research cell. The iCAP setup was also used to obtain Th/U_{zircon} data on the tephra zircons that were U-Pb dated using (MC)-ICP-MS. Zircon crystals were spot ablated for 40 seconds using a 30 µm beam at a 5 Hz repetition rate and laser energy at the sample surface ~3 J/cm^2, producing well-defined, flat-bottomed cylindrical pits 30 µm in diameter and ~10-15 µm deep. Ablated aerosol particles were carried in a He atmosphere at a flow rate of 0.5 L/min through the ablation cell. Output from the cell was joined to an Ar (0.55 L/min) makeup gas line and an N_2 line (0.004 L/min) before entering the injector. The instrument was auto-tuned by ablating NIST 612 and then manually adjusting the Ar makeup gas to achieve ThO/Th < 0.5%. Data were collected in time resolved mode including a 25 second gas blank and a 30-45 second washout between analyses. Dwell times were 20 ms (masses 238, 232), 30 ms (masses 235, 208-206), and 40 ms (mass 204). The primary standard reference sample GJ-1 (608.5 ± 0.4 Ma; Jackson et al., 2004; Heaman, unpublished data) and secondary zircon reference materials 94-35 (56.4 ± 1.2 Ma; Chang et al., 2006) and Plešovice (337.1 ± 0.4 Ma; Sláma et al., 2008) were analyzed before and after each set of 10–20 unknowns to monitor U–Pb fractionation, reproducibility, and instrument drift. The GJ-1, Plešovice, and 94-35 zircons yielded weighted mean ^{206}Pb-^{238}U ages of 605.5 ± 2.6 Ma (MSWD = 0.8, n = 11), 338.0 ± 2.6 Ma (MSWD = 0.9, n =7), and 54.8 ± 1.2 Ma (MSWD = 0.5, n =11) respectively, over two days of analytical sessions

(Supplemental Table A.3). The ^{206}Pb-^{238}U ages for reference materials are within 2σ uncertainty of the literature values: values for the entire suite of analyses are within the permissible range at 95% confidence level for the single population of replicated analyses (Mahon, 1996). The ^{206}Pb/^{238}U average precision of secondary reference materials is ~4% (2σ) for individual spot analyses. All data were processed using the Iolite v.3 (Paton et al., 2010, 2011) "VisualAge" data reduction scheme (Petrus and Kamber, 2012). For consistency, external uncertainties were propagated manually in an excel spreadsheet in the same manner as with the multi-collector ICP-MS data.

2.2.1.3. Sector-field (SF)-ICP-MS

Zircon crystals from Biederman (UT1884) and an additional sample of Gold Run (UA1001) tephra were analyzed using a RESOlution ArF Excimer 193 nm laser ablation system coupled to a Thermo Scientific Element XR magnetic sector-field (SF)-ICP-MS, using a Laurin-Technic S-155 cell. Samples were spot ablated for 40 seconds using a 33 µm (Gold Run tephra) or 40 µm (Biederman tephra) beam at a 5 Hz repetition rate and laser energy at the sample surface ~3 J/cm^2. The resulting ablation pits are flat-bottomed with near-vertical sides and ~10-15 µm deep. The mass spectrometer was operated in low mass resolution mode (M/ΔM= ~300). An analysis comprised 30 seconds of background gas collection followed by 40 seconds of ablation. Ablated aerosols were entrained in a He cell gas flow (0.350 L/min) and subsequently mixed with N_2 (0.002 L/min) and Ar (0.85 L/min) prior to entering the ICP-MS torch. The instrument was optimized by ablating NIST 612. Argon and helium gas flow, torch position, and focusing potentials were tuned to achieve optimal signals on Pb and U, and ThO/Th < 0.2%. Data were collected for ^{202}Hg, ^{204}Pb, ^{206}Pb, ^{207}Pb, ^{208}Pb, ^{235}U using the ion counting modes of the

SEM detector, for ^{232}Th using triple detection mode, and for ^{238}U using analog mode. Dwell times were 10 ms (masses 202, 204), 20 ms (masses 208, 232, 235, 238), 40 ms (mass 206) and 50 ms (mass 207). The primary standard reference sample 91500 (1062.4 ± 0.4 Ma; Wiedenbeck et al., 1995) and secondary zircon reference materials GJ-1 (608.5 ± 0.4 Ma; Jackson et al., 2004), Plešovice (337.1 ± 0.4 Ma; Sláma et al., 2008) and Bishop Tuff (0.767 ± 0.001 Ma; Crowley et al., 2007; Chamberlain et al., 2014; Ickert et al., 2015) were analyzed before and after each set of 10–20 unknowns to monitor U–Pb fractionation, reproducibility, and instrument drift. The 91500, GJ-1, Plešovice, and Bishop Tuff yielded weighted mean ^{206}Pb-^{238}U ages of 1059.8 ± 3.6 Ma (MSWD = 0.8, n = 15), 609.1 ± 2.1 Ma (MSWD = 0.6, n =9), 339.6 ± 1.9 Ma (MSWD = 0.5, n = 9), and 0.756 ± 0.010 Ma (MSWD = 1.3, n = 6) respectively, over three days of analytical sessions (Supplemental Table A.3). The ^{206}Pb-^{238}U ages for reference materials are within 2σ uncertainty of the literature values: values for the entire suite of analyses within the permissible range at 95% confidence level for the single population of replicated analyses (Mahon, 1996). The $^{206}Pb/^{238}U$ average precision of secondary reference materials is ~1.5% (2σ) for individual spot analyses. Data were reduced off-line using Iolite software (v.4.1) following the method described by Paton et al. (2010, 2011) for subtraction of gas blanks and U-Pb downhole fractionation correction. The uncertainties of measured isotopic ratios are a quadratic combination of the standard error of the measured isotope ratio and reproducibility of the reference material.

2.2.2. Data processing and maximum deposition age calculation methods

The correction for common-Pb followed the "^{207}Pb-method" (Williams, 1998), with initial-Pb composition estimated from the Stacey and Kramers (1975) lead evolution model for all tephra except for PA (Supplemental Fig. A.1). For PA tephra, the initial common-Pb composition is instead based on the upper intercept from free regression through the youngest eight analyses in Tera-Wasserburg Concordia space (Tera and Wasserburg, 1972), yielding $^{207}Pb/^{206}Pb_i = 0.981 \pm 0.055$ (Supplemental Fig. A.4), which is distinct from the 0.835 value obtained using the Stacey and Kramers (1975) Pb evolution model. This alternative approach has been successfully applied to young zircon samples where the regression line lies at a high angle to the Concordia curve (e.g., Kirkland et al., 2020). Data with <75% of common-^{206}Pb (f_{206} (%)) contamination were used to calculate the final tephra ages. Data with large $^{206}Pb/^{238}U$ analytical uncertainties of >45% (2σ) were not further considered, except for GI tephra, which had a limited number of non-detrital grains <1 Ma (n=3).

Pleistocene-age zircon U-Pb ages need to be corrected for ^{230}Th disequilibrium because melt-mineral U-Th partitioning induces a ^{230}Th deficit in zircons, resulting in erroneously young apparent ages (Ludwig, 1977; Schärer, 1984). We estimated the melt-zircon fractionation factor ($f_{Th/U}$) using $f_{Th/U} = (Th/U)_{zircon}/(Th/U)_{melt}$, where $(Th/U)_{zircon}$ was determined during LA-ICP-MS U-Pb analysis, and tephra glass Th/U was used as a direct proxy for $(Th/U)_{melt}$. Individual U-Pb ages in this study were corrected for ^{230}Th disequilibrium following Schärer (1984) (Eq. 1) for ages >350 ka:

$$\text{(Eq. 1)}\ ^{206}Pb/^{238}U = (\exp(\lambda_{238}t) - 1) + \lambda_{238}/\ \lambda_{230}(f_{Th/U} - 1)$$

For ages <350 ka, individual U-Pb ages were corrected for ^{230}Th disequilibrium following Sakata et al. (2013) and Sakata (2018). Sakata et al. (2013) demonstrated that for very young zircon samples, that still have ^{230}Th in disequilibrium (<350 ka), the Schärer (1984) correction approach leads to "under corrected" ages. Instead, they proposed a correction that accounts for both ^{230}Th ingrowth and decay (Eq. 2):

$$(\text{Eq. 2})\ {}^{206}Pb/{}^{238}U = (\exp(\lambda_{238}t) - 1) + \lambda_{238}/\lambda_{230}(f_{Th/U} - 1)(1 - \exp(-\lambda_{230}t))\exp(\lambda_{238}t)$$

The parent melt was assumed to be in secular equilibrium at the time of zircon crystallization with an initial activity ratio $^{230}Th/^{238}U_{melt}$ equal to one (e.g., Charlier et al., 2005; Crowley et al., 2007). The uncertainty from $f_{Th/U}$ was propagated quadratically following the approach outlined by Ickert et al. (2015). The influence from the uncertainty of $f_{Th/U}$ is small (typically <5% contribution to the overall uncertainty for ages <1 Ma and <1% for ages >1 Ma) in comparison to the analytical uncertainty of measured $^{206}Pb/^{238}U$. All U-Pb ages in this paper are reported with 2σ uncertainty; we use σ to represents the combined uncertainty of the standard error of the measured isotope ratio, reproducibility of the reference materials, and $f_{Th/U}$.

We identified zircon xenocrysts and antecrysts using a two-step method. First, we visually inspected the age distribution in each sample and qualitatively identified grains that significantly predate (typically by hundreds of thousands to millions of years) the youngest coherent grain cluster and are incompatible with stratigraphic constraints on the age of the sample. After this procedure, we verified the normality of the data using Q-Q plots and Shapiro-Wilk tests, followed by quantitative outlier identification based on the modified 2σ criteria used by Isoplot v.4.15 to identify the remaining non-reproducible, outlier analyses (Ludwig, 2012). We also tested outlier detection using the modified Chauvenet's criterion implemented in IsoplotR v.3.8 (Vermeesch, 2018) and the double median absolute deviation outlier detection tests. The differences between the three techniques of outlier detection were negligible. The maximum crystallization age cut-off boundary was set to include only ages deemed to best represent the eruptive/autocrystic zircon population (Supplemental Table A.1).

Alpha particle release in zircon during the decay of ^{238}U, ^{235}U, ^{232}Th, and their daughter products, damages the crystal lattice and can lead to faster laser ablation rates during analyses.

The degree of radiation damage (i.e., the amount of alpha particle dose) in older reference materials used during analyses of very young zircon samples might lead to a small difference in ablation behavior between reference materials and the samples, in turn biasing the downhole fractionation correction (e.g., Sliwinski et al., 2017). To evaluate the degree of potential bias in the U-Pb downhole fractionation correction, we used the two youngest available reference material samples Bishop Tuff (0.767 ± 0.001 Ma; Crowley et al., 2007) and 94-35 (56.4 ± 1.2 Ma; Chang et al., 2006). Analyses of these reference materials yielded $^{206}Pb/^{238}U$ ages that agree with reported literature values, suggesting that influence of downhole fractionation correction on the final ages is likely negligible (Supplemental Table A.6). Downhole fractionation may also be exacerbated by uneven energy distribution across the laser beam and variability in the geometry of the ablation pit (Horn et al., 2001). However, the laser ablation systems used in this study have a homogenous energy profile ("flat top") that produce well-defined, flat-bottomed pits with near-vertical sides. These characteristics reduce the degree of differential vaporization and melting between the center and the margin of the ablation pit, which mitigates the effects of depth-dependent fractionation.

Compared to secondary ion mass spectrometry (SIMS), which removes only the outermost few microns from zircon surfaces, LA-ICP-MS requires more volume of material (ablation pit depth ~10-15 µm). This makes it challenging to interpret LA-ICP-MS U-Pb age data when individual zircon crystals might have a prolonged duration of growth or contain inherited cores within young overgrowth (e.g., Guillong et al., 2014; Ito, 2020). Hence, in cases when zircon interiors are temporally heterogenous, the U-Pb data from inner crystal zones can reflect the timing of pre-eruptive crystallization or contamination from older inherited cores (e.g., Matsu'ura et al., 2020). Although the zircon crystals in this study were lightly polished to remove the adhered glass mantling many of the grains and to expose the rims at the surface of the mount, the zircon surface remained largely unpolished. We estimate that in most cases only the uppermost few microns of the zircon exterior were removed, thus largely preserving the last stages of zircon growth. The integration intervals for data reduction were selected from time resolved data to mitigate the effect of temporal heterogeneities, inclusions, and inherited cores. In addition, all zircon grains were inspected for the inherited cores and inclusions prior to the analysis.

Apart from analytical and isotope systematic difficulties, a critical challenge is estimating a tephra deposition age from a pool of single-crystal ^{206}Pb-^{238}U ages. We use five different methods to calculate a tephra maximum depositional age from the U-Pb ages: (1) the weighted mean age, (2) the maximum likelihood age, (3) an iterative-MSWD approach, (4) Bayesian age modeling, and (5) using the youngest zircon age as the age of deposition.

(1) The weighted mean age was calculated from the youngest group of at least three zircon ages that have overlapping 2σ uncertainties following the approach outlined by Sharman et al. (2018). The weighted mean, uncertainty and the MSWD were calculated using IsoplotR v.3.8 software (Vermeesch, 2018; Supplemental Fig. A.2). The MSWD value was used to assess the degree to which the weighted mean and uncertainty represent a single population.

(2) A maximum likelihood algorithm was used to calculate the minimum age from the pool of zircon ^{206}Pb-^{238}U ages, as outlined by (Vermeesch, 2021). IsoplotR v.3.8 radial plots were used to calculate the minimum age and the uncertainty (Vermeesch, 2018; Supplemental Fig. A.3).

(3) The iterative-MSWD age was calculated following Popa et al. (2020), where the rate of change in MSWD is used to identify the youngest zircon population. Briefly, after pairing the two youngest grains, older crystals are progressively added to the age pool and MSWD is calculated each time. The youngest zircon population is identified once MSWD starts to increase steeply with addition of older crystals, and a weighted mean of the youngest crystals is then calculated.

(4) We used the Chron.jl Bayesian age modelling software framework (Keller et al., 2018) which makes a probabilistic estimate of maximum depositional age based on the dated population of zircon in each tephra sample. For priors, we used uniform, triangular, and MELTS zircon crystallization distributions. The uniform distribution is a probability distribution in which the probability of the ages recording zircon crystallization is uniform across minimum and maximum age bounds (i.e., the probability density function is a flat line). The triangular distribution is a probability distribution with a probability density function of triangular form defined by minimum and maximum age bounds and the peak age value or mode. The MELTS zircon crystallization distribution is derived from kinetic and thermodynamic models for a single, steadily cooling magma batch and estimates the relative proportions of datable grains formed throughout mineral growth (Keller et al., 2018).

(5) The youngest zircon grain method simply selects the youngest grain in a sorted list (e.g., Dickinson and Gehrels, 2009; Vermeesch, 2021). For some samples a slightly older, more precise analysis was selected instead of a younger, less precise analysis if the two ages are indistinguishable within analytical uncertainty.

2.2.3. Glass fission track methods

We recalculated previously published glass fission-track ages for the tephra beds studied here using the most recent and precise Moldavite tektite age of 14.808 ± 0.021 Ma ($^{40}Ar/^{39}Ar$, Schmieder et al., 2018). Following expected reporting requirements (Schaen et al., 2021), Schmieder et al. (2018) applied a $^{40}Ar/^{36}Ar$ atmospheric ratio of 298.6 ± 0.3 Ma (Lee et al., 2006), an age of 99.738 ± 0.104 Ma for the flux monitor GA1550 biotite age (Renne et al., 2011), and the K decay constants from Renne et al. (2010) during age determination. The fission-track method used to determine the eruption age of natural glasses is the zeta calibration method (Hurford and Green, 1983), with the Moldavite tektite as the reference material. Previous age determinations for the Moldavite tektite have varied from 15.1 ± 0.7 Ma (K-Ar, Gentner et al., 1967) to 15.21 ± 0.15 Ma ($^{40}Ar/^{39}Ar$, Staudacher et al., 1982) to 14.34 ± 0.08 Ma ($^{40}Ar/^{39}Ar$, Laurenzi et al., 2007) to 14.68 ± 0.055 Ma ($^{40}Ar/^{39}Ar$, Di Vincenzo and Skála, 2009). More detailed descriptions of glass fission-track age calculation are available in Westgate (1989) and Sandhu and Westgate (1995). Individual recalculated glass fission-track age determinations for a given tephra were combined as inverse-variance weighted means (Supplemental Table A.2). The averaging of age determinations on different field tephra samples, either at the same site or at different sites, is justified by tephra correlations based on glass geochemistry supplemented by mineralogy, morphology, and stratigraphy. All reported glass fission-track ages in this paper are reported with 2σ uncertainty.

2.2.4. $^{40}Ar/^{39}Ar$ methods

We recalculated the previously published $^{40}Ar/^{39}Ar$ ages for the Quartz Creek tephra bed (Kunk, 1995) studied here using the currently accepted age for Fish Canyon Tuff (28.294 ±

0.036 Ma; Renne et al., 2011) and updated K decay constants (Renne et al., 2010) using the recalculation software ArAR (Mercer and Hodges, 2016). All reported $^{40}Ar/^{39}Ar$ ages in this paper are reported with 2σ uncertainty. We do not account for changes in the mass discrimination correction that would result from changes in the accepted Ar isotopic abundance values given there is no practical way to revise legacy data for changes in mass discrimination correction (Mercier and Hodges, 2016). However, these corrections if made would not affect the age determination significantly (Renne, 2009). Following expected reporting requirements (Schaen et al., 2021), Kunk (1995) applied a $^{40}Ar/^{36}Ar$ atmospheric ratio of 295.5 ± 0 Ma (Dalrymple, 1969) during age determination.

2.3. Results

The single grain U-Pb data are summarized in Supplemental Table A.1. Bayesian model results in this application are relatively insensitive to the choice of the prior. We prefer the triangular prior in each sample and report those ages in the following sections based on the following criteria: first, since no closed-system zircon ages should post-date the eruption (except within analytical uncertainty) we expect a sharply truncated relative distribution of ages at the time of tephra deposition and second, empirical observation of the age distributions in each sample tends to take an approximately triangular form. The simple triangular distribution effectively encapsulates both criteria for the relative distribution of zircon ages in each sample (e.g., Deino et al., 2021). Results for the various methods of calculating maximum depositional ages for each tephra are summarized in Table 2.2.

Table 2.2. Comparison of maximum deposition age methods used in this study. MLA: maximum likelihood algorithm; YSG: youngest single grain. All ages reported at 2σ uncertainties.

Tephra	Bayesian Age	Weighted Mean	MLA	YSG	Iterative-MSWD	Revised glass fission-track
Biederman	178 ± 17 ka	184 ± 10 ka	188 ± 18 ka	156 ± 36 ka	185 ± 11 ka	-
HP	680 ± 47 ka	719 ± 22 ka	698 ± 73 ka	624 ± 87 ka	631 ± 76 ka	706 ± 68 ka
Gold Run	688 ± 44 ka	723 ± 22 ka	719 ± 23 ka	683 ± 87 ka	700 ± 38 ka	717 ± 108 ka
Flat Creek	708 ± 43 ka	759 ± 18 ka	736 ± 35 ka	715 ± 61 ka	714 ± 45 ka	-
PA	1.92 ± 0.06 Ma	1.94 ± 0.04 Ma	1.94 ± 0.04 Ma	1.79 ± 0.16 Ma	1.89 ± 0.07 Ma	2.07 ± 0.5 Ma
Quartz Creek	2.62 ± 0.08 Ma	2.71 ± 0.04 Ma	2.66 ± 0.07 Ma	2.62 ± 0.09 Ma	2.62 ± 0.14 Ma	2.88 ± 0.3 Ma
Lost Chicken	3.14 ± 0.07 Ma	3.21 ± 0.03 Ma	3.21 ± 0.03 Ma	3.11± 0.09 Ma	3.21 ± 0.03 Ma	2.87 ± 0.28 Ma
GI	542 ± 64 ka	562 ± 56 ka	-	534 ± 131 ka	-	565 ± 156 ka
Chester Bluff	-	326 ± 32 ka[1]	-	-	-	255 ± 40 ka
Old Crow	-	207 ± 13 ka[2]	-	-	-	144 ± 14 ka

[1]Burgess et al., 2019. [2]Burgess et al., 2021.

2.3.1. Results for Biederman tephra

Of 98 dated grains for Biederman tephra, 40 grains satisfied the common-Pb and analytical uncertainty thresholds. The filtered U-Pb ages ranged from 152 ka to 1.11 Ma with majority of analyses being < 350 ka, suggesting only minor presence of xenocrysts and/or antecrysts in the zircon population (Fig. 2.4). The Biederman tephra Bayesian model age of 178 ± 17 ka is indistinguishable from the weighted mean (184 ± 10 ka, MSWD = 0.48), maximum likelihood algorithm (188 ± 18 ka), youngest zircon (156 ± 36 ka) and iterative-MSWD (185 ± 11 ka) age estimates at 2σ level (Fig. 2.5A). No glass fission-track age is available for Biederman tephra as its glass is too vesicular for this dating method.

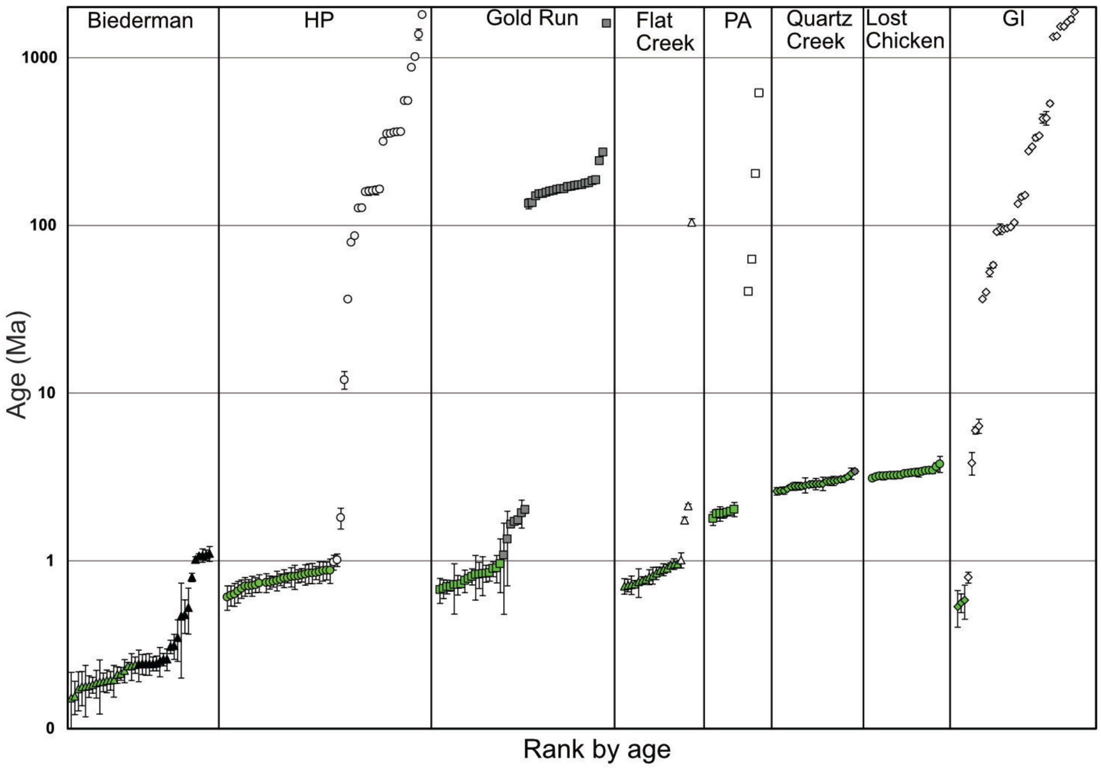

Figure 2.4. *^{206}Pb-^{238}U zircon age rank-order plot for all samples. Data points colored in green were used for Bayesian modeling. Uncertainties are displayed at 2σ level.*

2.3.2. Results for HP tephra

The full HP tephra U-Pb dataset (n = 59 dated grains) is heterotemporal with ages ranging from ca. 600 ka to ca. 1.8 Ga, suggesting either a high proportion of xenocrysts and/or antecrysts in the tephra zircon population, or a detrital component (Fig. 2.4). The HP tephra grains <1 Ma are characterized by consistently high U concentrations averaging ~1600 ppm, distinct from the majority of the >1 Ma analyses which are typically characterized by U concentration <500 ppm (Supplemental Table A.1).

The weighted mean HP tephra age of 719 ± 22 ka (MSWD = 1.54) is older than the maximum depositional ages produced by the youngest grain (624 ± 87 ka), iterative-MSWD

(631 ± 76 ka) methods, and the Bayesian model (680 ± 47 ka) (Fig. 2.5B). The recalculated weighted mean glass fission-track age of 706 ± 68 ka (n = 5) presented here is ~120 ky older than the most recent published glass fission-track age of 590 ± 200 ka (Preece et al., 2011), but overlaps within uncertainty with the HP tephra U-Pb results.

2.3.3. Results for Gold Run tephra

Of 77 grains dated for Gold Run tephra, 47 zircon crystals satisfied the common-Pb and analytical uncertainty thresholds. The Gold Run tephra filtered zircon ages range from ca. 670 ka to ca. 1.6 Ga, with 64% of the grains being > 1 Ma, suggesting a high xenocrytsic, antecrystic or detrital zircon component in the tephra (Fig. 2.4.). All five methods of calculating the maximum depositional age for Gold Run tephra overlap within 2σ uncertainty: the Bayesian model age of 688 ± 44 ka is indistinguishable from the weighted mean (723 ± 22 ka, MSWD = 1.02), maximum likelihood algorithm (719 ± 23 ka), the youngest zircon (683 ± 87 ka), and the iterative-MSWD (700 ± 38 ka) age estimate (Fig. 2.5C). The recalculated weighted mean glass fission-track age of 717 ± 104 ka (n = 3) is 27 ky older than the most recent published glass fission-track age 690 ± 100 ka (Westgate et al., 2011), and overlaps within uncertainty with the Gold Run tephra zircon U-Pb results.

2.3.4. Results for Flat Creek tephra

For Flat Creek tephra 20 of the 25 analyzed grains met the common-Pb and analytical uncertainty thresholds. The Flat Creek filtered zircon ages range between ca. 700 ka and ca. 105 Ma, with ~80% of the grains ≤ 1 Ma (Fig. 2.4.). The zircon Bayesian model yielded an age of 708 ± 43 ka which agrees with the maximum likelihood algorithm (736 ± 35 ka), the youngest grain (715 ± 61 ka) and the iterative-MSWD (714 ± 45 ka) methods (Fig. 2.5D). The weighted mean 759 ± 18 ka (MSWD = 1.64) gives a slightly older minimum depositional age estimate than the other methods. No reliable glass fission-track age has been obtained for Flat Creek tephra, due to the pumiceous nature of the glass shards.

2.3.5. Results for PA tephra

Few zircon crystals were separated from the PA tephra sample, and only eight out of 15 dated zircon grains were ≤ 2 Ma and satisfied the common-Pb and analytical uncertainty filters. The zircon weighted mean age of 1.94 ± 0.04 Ma (MSWD = 0.87) was calculated for the seven youngest ages and is in agreement with the Bayesian model age of 1.92 ± 0.06 Ma (Fig. 2.5E). The recalculated weighted mean glass fission-track age of 2.07 ± 0.50 Ma (n = 2) is 0.05 My older than the most recent published glass fission-track 2.02 ± 0.28 Ma age (Preece et al., 1999). The U-Pb ages are consistent with the recalculated glass fission-track age, but more analyses would be required to obtain a more reliable representation of the zircon population.

2.3.6. Results for Quartz Creek tephra

Of 25 zircon grains dated from Quartz Creek tephra, 23 grains satisfied the common-Pb and analytical uncertainty thresholds. The filtered zircon dataset has a tight range of ages from 2.60 Ma to 3.42 Ma (Fig. 2.4.). The Quartz Creek tephra yielded a Bayesian model age of 2.62 ± 0.08 Ma that is indistinguishable at 2σ from maximum likelihood algorithm (2.66 ± 0.07 Ma), the youngest grain (2.62 ± 0.09) and the iterative-MSWD (2.62 ± 0.14 Ma) maximum deposition age estimates (Fig. 2.5F). The weighted mean age of 2.71 ± 0.04 Ma (MSWD = 1.95) gives a slightly older maximum deposition age estimate for Quartz Creek. The recalculated weighted mean glass fission-track age of 2.88 ± 0.30 Ma (n = 2) is within uncertainty of the most recent published glass fission-track age of 2.82 ± 0.24 Ma (Preece et al., 2011), as well as the uncertainty with the Quartz Creek tephra U-Pb results.

2.3.7. Results for Lost Chicken tephra

For the Lost Chicken tephra all 20 analyzed grains satisfied the common-Pb and analytical uncertainty thresholds. The filtered zircon ages range from 3.11 Ma to 3.64 Ma (Fig. 2.4). The zircon weighted mean age of 3.21 ± 0.03 Ma (MSWD = 1.38) is in agreement with the Bayesian model (3.14 ± 0.07 Ma), maximum likelihood algorithm (3.21 ± 0.03 Ma), the youngest grain (3.11 ± 0.09 Ma) and the iterative-MSWD (3.21 ± 0.03 Ma) maximum deposition age estimates at 2σ level (Fig. 2.5G). The recalculated weighted mean glass fission-track age of 2.87 ± 0.28 Ma (n = 3) is within uncertainty of the most recent published glass fission-track age 2.91 ± 0.88 Ma (Matthews et al., 2003). The revised glass fission-track age of 2.87 ± 0.28 Ma is ~1% younger than the weighted mean, the iterative-MSWD and the maximum likelihood age estimates but overlaps with the Bayesian model and youngest grain ages within 2σ uncertainty.

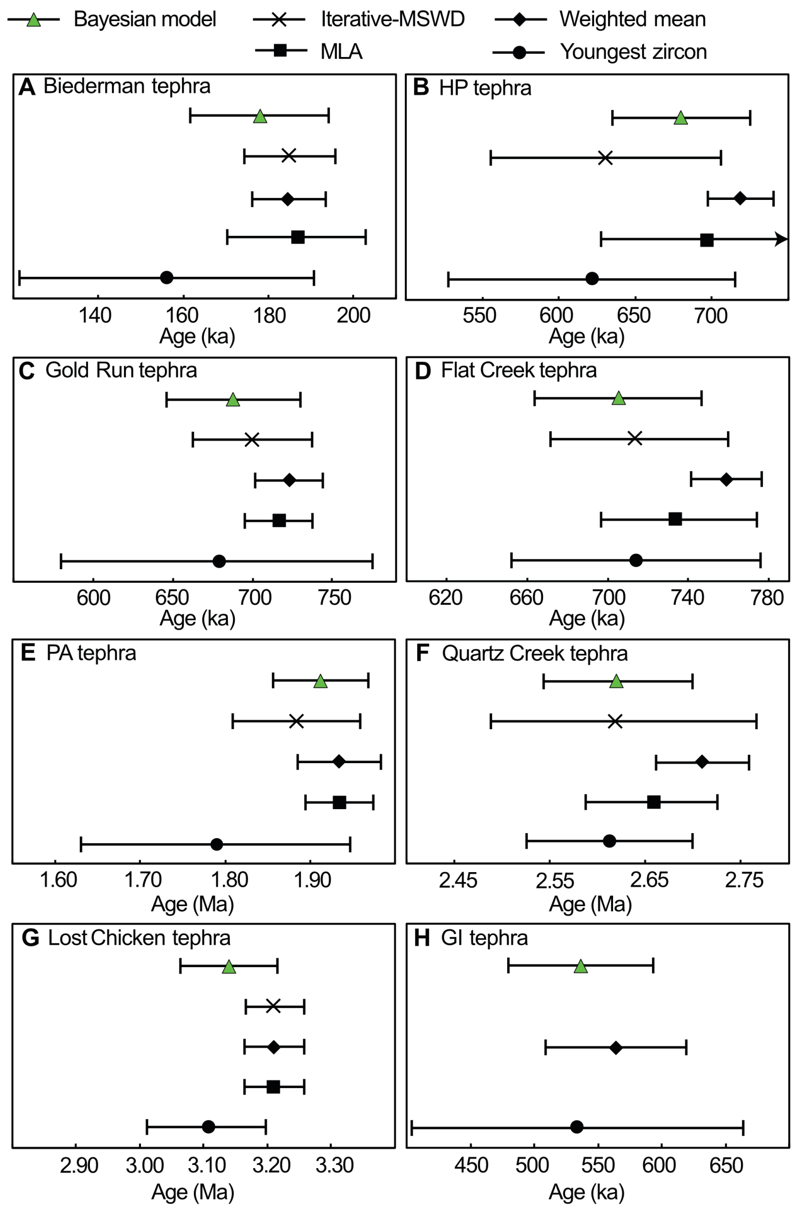

Figure 2.5. *Comparison of tephra maximum depositional age estimates using five different methods. The preferred ages based on the Bayesian modeling are highlighted in green. All uncertainties are plotted at 2σ. For GI tephra, only the Bayesian model, weighted mean, and the youngest zircon were calculated because only three grains produced meaningful ages. MLA = maximum likelihood algorithm.*

2.3.8. Results for GI tephra

The GI tephra samples, UA2838 and UA1668, contained a large proportion of xenocrystic and potentially detrital zircon crystals substantially older than 1 Ma (Fig. 2.4.). Out of 65 zircon grains analyzed only four grains were <1 Ma, yielding a weighted mean age of 562 ± 56 ka (MSWD = 0.14), a Bayesian model age of 542 ± 64 ka, and a youngest grain age of 534 ± 131 ka (Fig. 2.5H). As a maximum depositional age, the U-Pb results for GI tephra should be treated with caution due to large uncertainties and very high common-Pb component (>90%) in two of the three grains used in calculations. The revised glass fission track age of 545 ± 156 ka (n = 2) is within uncertainty of the most recently recalculated glass fission-track age of 500 ± 200 ka (Preece et al., 2011) and is consistent with U-Pb dating results.

2.4. Discussion

2.4.1. Comparison of maximum deposition age calculation methods

The Bayesian modeling, iterative-MSWD, and maximum-likelihood methods generally yielded similar estimates for tephra maximum depositional age, with comparable uncertainties. The advantage of the Bayesian modeling and the maximum-likelihood approach is that they decrease subjectivity in the age interpretation by reducing the number and impact of user decisions (Keller et al., 2018; Vermeesch, 2021). However, even Bayesian modeling and maximum-likelihood approaches are not entirely objective, as the pool of tephra zircon ages usually requires data parsing based on the presence of antecrysts/xenocrysts and user-specified thresholds for common-Pb contamination. Additionally, the Bayesian framework requires specification of the prior based on the zircon distribution, though our results suggest that the difference in modeling results is small between different priors (Supplemental Table A.5). The iterative-MSWD method relies on visual interpretation of the change in MSWD as progressively older zircons are included in the mean age and has not yet been widely tested. Nevertheless, identifying inflection points in the rate of MSWD change with the iterative-MSWD method may allow identification of different age populations in the zircon pool that otherwise would have been obscured (Popa et al., 2020).

The youngest zircon grain method may seemingly provide a more accurate maximum deposition age estimate for samples with low number of analyses and a high global MSWD. However, reliance on the single or youngest few ages obtained via *in-situ* techniques (e.g., LA-ICP-MS and SIMS) always carries a risk of underestimating the age (i.e., the true tephra age is older than the interpreted age) due to the analytical or reference material matrix effects (Marillo-Sialer et al., 2014) and absence of reproducibility. In addition, individual zircon analyses obtained by LA-ICP-MS or SIMS commonly have low precision, making it difficult to the resolve an eruption age for Pliocene-Pleistocene age deposits with adequate resolution (e.g., Burgess et al., 2021). Hence, for *in-situ* dating methods a large number of analyses is preferred to obtain a more accurate representation of the eruptive zircon population and to mitigate potential inaccuracy resulting from young outliers (e.g., Matthews et al., 2015; Burgess et al., 2021). The weighted mean is one of the most common methods for maximum deposition age calculation and its usage can be justified when the spread of zircon ages in a sample is small relative to analytical uncertainty (e.g., Bowring et al., 1993; Keller et al., 2018). However, the accuracy and precision of this method has been questioned for samples that record prolonged pre-eruptive zircon crystallization history or include detrital materials (e.g., Keller et al., 2018; Vermeesch, 2021). In these scenarios, the weighted mean tends to yield a maximum deposition age that is systematically too old and with unrealistically high precision.

Our results generally indicate agreement between different maximum deposition age calculation methods and are consistent with the biases discussed above. The weighted mean for the dated tephra zircons tends to yield a slightly older age estimate than other methods but usually produces ages consistent with revised glass fission-track age estimates. In contrast, the youngest grain method tends to produce a slightly younger estimate of the tephra maximum deposition age. The Bayesian modelling, maximum likelihood algorithm, and iterative-MSWD approaches produce comparable results that agree with revised glass fission-track ages, except for the Lost Chicken tephra where iterative-MSWD and maximum likelihood algorithm ages are slightly older than Bayesian model and revised glass fission-track ages. The cause of this offset is not directly known; several possible contributing factors include prolonged zircon residence time in the magma, uncertainty in the zircon U-Pb or glass fission-track correction schemes, or methodological differences in the maximum depositional age calculations. Henceforth, for consistency we rely on the Bayesian model age as the best estimate for the timing of zircon crystallization and the tephra maximum deposition age, although the maximum likelihood algorithm method is arguably of similar reliability.

2.4.2. Analytical constraints on U-Pb dating of zircon in Pleistocene tephra

In addition to uncertainties associated with different methods of calculating a tephra depositional age from a pool of tephra zircon ages, there are several analytical challenges that are particularly relevant to dating zircon from Pleistocene tephra. The possibilities to further improve the method include the development of young zircon reference materials (<10 Ma) to improve the accuracy of the downhole fractionation correction and implementation of alpha dose correction schemes to improve the accuracy of the age data and decrease systematic age bias (e.g., Sliwinski et al., 2017). In addition, for older zircon grains (>~1 Ma), chemical abrasion treatment prior to the analysis can be used to reduce the possible effect of Pb loss or crystal damage caused by the alpha dose (von Quadt et al., 2014). Future studies would benefit from explicit efforts to collect paired core and rim dates on zircon, to assess temporal "contamination" of eruption/deposition ages by older zircon core material. We collected three pairs of core-rim dates for Gold Run and Biederman tephra, which yielded no major variations in the age between the rim and interior of the grains within the uncertainty of the analyses (Supplemental Figure A.5).

In terms of analytical limitations, the common-Pb correction, and the accuracy/precision of $^{206}Pb/^{238}U$ and $^{207}Pb/^{206}Pb$ ratios, may be improved by obtaining better detection of ^{206}Pb and ^{207}Pb signals through increasing dwell times, repetition rate, and/or pit size. Because ablation of undetected mineral inclusions within zircon can further increase common-Pb contamination, the monitoring of additional elements (^{31}P, ^{27}Al, ^{56}Fe, ^{43}Ca) might help to recognize these inclusions (Guillong et al., 2014). Additionally, the development of simultaneous, single spot LA-ICP-MS zircon U-series and U-Pb dating for crystals <350 ka would allow for cross-verification of the age data (e.g., Ito, 2014).

2.4.3. Tephra U-Pb age discussion and comparison to existing age constraints

2.4.3.1. Biederman tephra

Biederman tephra zircon U-Pb dating yielded a Bayesian model age of 178 ± 17 ka that we interpret to be a maximum-limiting age for Biederman tephra deposition due to the lack of other direct chronological constraints. At the Chester Bluff and Birch Creek localities (Fig. 2.1), Biederman tephra sits on a peaty organic-rich bed (Fig. 2.2B; Fig. 2.6) interpreted as an interglacial unit due to the high abundance of spruce pollen, presence of large woody macrofossils, spruce cones, and other plant macrofossils (Jensen et al., 2008; Fig. 2.2B; Supplemental Table A.4). Further, the stratigraphic context of Biederman tephra relative to other tephra beds led to a preliminary correlation of that interglacial to MIS 7 (Jensen et al., 2013). Biederman is found above Chester Bluff tephra (Fig. 2.6.) which has a recalculated glass fission-track age of 255 ± 40 ka and a ^{206}Pb-^{238}U weighted mean age of 326 ± 32 ka (Burgess et al., 2019).

Furthermore, at both sites Biederman tephra is found stratigraphically below the regionally prominent Old Crow tephra (Preece et al., 2011). The most recent published glass fission-track age for Old Crow tephra is 124 ± 20 ka (Preece et al., 2011), with a recalculated glass fission-track age of 144 ± 14 ka; both glass fission-track ages are consistent with the long-standing interpretation, based on stratigraphic and paleoecological data, of a late MIS 6 age for the tephra (e.g., Reyes et al., 2010b; Preece et al., 2011). In contrast, Burgess et al. (2021) reported a weighted mean age of 207 ± 13 ka for Old Crow tephra based on the mean zircon ages derived from U-Pb, U-series, and (U-Th)/He techniques. At the Birch Creek site in east-central Alaska (Fig. 2.1.), Sheep Creek-Fairbanks (SC-F) tephra, dated by thermoluminescence to 190 ± 40 ka (Berger et al., 1996), is found directly below Old Crow tephra and above Biederman tephra. The Biederman ^{206}Pb-^{238}U age reported here suggests deposition during earliest MIS 6 which is consistent with its stratigraphic position directly above a presumably interglacial peat, and the lack of interbedded peat in the stratigraphic sequence spanning Biederman, SC-F, and Old Crow tephra.

The Biederman tephra ^{206}Pb-^{238}U age and stratigraphic position is also most consistent with a late MIS 6 age for Old Crow tephra (Preece et al., 2011). It is strictly possible to reconcile the Biederman tephra ^{206}Pb-^{238}U age with the proposed zircon-based age of 207 ± 13 ka for Old Crow tephra (Burgess et al., 2021) if the uncertainties are applied to yield the youngest possible Old Crow tephra age from Burgess et al. and the oldest possible Biederman tephra age. However, this interpretation—which mandates only ~1 kyr of sedimentation between Old Crow and the Biederman tephra beds—cannot be reconciled with stratigraphic and paleoecological constraints that clearly demonstrate the two tephra are associated with different interglacial stages. Effectively, this discrepancy suggests either that the ^{206}Pb-^{238}U Bayesian model age for Biederman tephra is too young or that the Old Crow zircon U-based ages of Burgess et al. (2019, 2021) are too old.

2.4.3.2. HP tephra

We interpret the Bayesian model age of 680 ± 47 ka to represent the last zircon crystallization stage prior to the eruption and deposition of HP tephra. The revised glass fission-track age of 706 ± 68 ka for this tephra is consistent with ^{206}Pb-^{238}U data reported here and suggests that zircon crystallization occurred during or shortly before the eruption (Fig. 2.7.). The glass fission-track and zircon U-Pb ages are also consistent with the paleomagnetic stratigraphy of loess surrounding HP tephra at the Gold Hill locality near Fairbanks (Fig. 2.1.), where HP tephra is reworked directly above sediments interpreted to represent a paleosol ~50 cm above the Brunhes-Matuyama boundary (Evans et al., 2011; ~780 ka; Fig. 2.2C; Fig. 2.6.; Fig. 2.7.). The ^{238}U-^{206}Pb age is further supported by tephrostratigraphy at Gold Hill, where HP tephra is found higher in the exposure—though not in direct stratigraphic association—with the SP tephra (Fig. 2.6.), which has an unrevised glass fission-track age of 870 ± 120 ka (Preece et al., 1999). Taken together, the Bayesian model age obtained in this study is consistent with the glass fission-track age and geomagnetic polarity of surrounding loess, indicating that HP tephra eruption and deposition occurred early in the Brunhes chron, at or close to 680 ± 47 ka.

2.4.3.3. Gold Run and Flat Creek tephra

The earliest Middle Pleistocene Gold Run tephra (Westgate et al., 2011) provides chronological context for the oldest-known relict permafrost in eastern Beringia (Froese et al., 2008), as well as one of the oldest full genome sequences from a horse fossil recovered in stratigraphic association with the tephra (Orlando et al., 2013).

The Gold Run tephra Bayesian model age of 688 ± 44 ka is consistent with the revised glass fission-track age of 717 ± 104 ka, supporting our interpretation that the zircon U-Pb age closely reflects the timing of deposition (Fig. 2.7.). At its type section at Dominion Creek in the Klondike region of central Yukon (Fig. 2.1.), Gold Run tephra has a normal remanent magnetic polarity recorded from the surrounding loess and is ~2.5 m above the transition from reversed to normal polarity (Froese et al., 2000; Fig. 2.6). The normal polarity of Gold Run tephra is compatible with its glass fission-track and ^{238}U-^{206}Pb ages, and suggests deposition during the early stages of the Brunhes Chron (Fig. 2.6.; Fig. 2.7.). This age is also consistent with the molecular clock age estimate of the Thistle Creek horse reported in Orlando et al. (2013).

Ephemeral placer mining cuts in the lower Sixtymile River area (Fig. 2.1.) contain a complex ~6-m-thick succession of tephra and reworked tephra in the following order from oldest to youngest: TA, SM3, Gold Run, reworked Gold Run, reworked Gold Run with Hollis 2 tephra, reworked Gold Run, and Flat Creek tephra (Westgate et al., 2011; Fig. 2.6.). Though TA and SM3 tephra do not have independent age constraints and cannot be used as age markers, shards of Hollis 2 tephra (unrevised glass fission-track age of 630 ± 160 ka; Westgate et al., 2011) were found intermixed within a reworked bed of Gold Run tephra glass, indicating that Hollis 2 tephra must be younger than Gold Run tephra. At the Hollis Mine type locality for Hollis 2 tephra, the Hollis (unrevised glass fission-track age of 700 ± 80 ka; Westgate et al., 2011) and Hollis 2 tephra beds are found in close stratigraphic association; their glass fission-track ages are indistinguishable at 2σ uncertainty and are stratigraphically and chronologically consistent with Gold Run tephra U-Pb and revised glass fission-track ages (Westgate et al., 2011).

The chronology of Gold Run tephra is further bolstered by the new ^{238}U-^{206}Pb age of the Flat Creek tephra, which is in normally polarity sediments above Gold Run tephra in the Sixtymile River area (Westgate et al., 2011). The Flat Creek Bayesian model age of 708 ± 43 ka is indistinguishable from the Gold Run U-Pb age at 2σ uncertainty (Fig. 2.7.), with stratigraphy in the Sixtymile River area (Fig. 2.6.) indicating that Flat Creek tephra was likely deposited shortly after the Gold Run tephra. The ^{238}U-^{206}Pb age for Flat Creek tephra, which until now had not been directly dated, provides a minimum-limiting age constraint for the Wounded Moose paleosols that developed on glaciofluvial surfaces associated with the earliest and most extensive Pleistocene glaciations at the margin of eastern Beringia (Smith et al., 1986). Stratigraphic relations between Flat Creek tephra and the Wounded Moose paleosol at the Flat Creek site in west-central Yukon, near Dawson City, indicate that the Wounded Moose Paleosol must be older than 708 ± 43 ka, a minimum age that is consistent with previous estimates based on ^{10}Be and ^{26}Al profiles (Hidy et al., 2018).

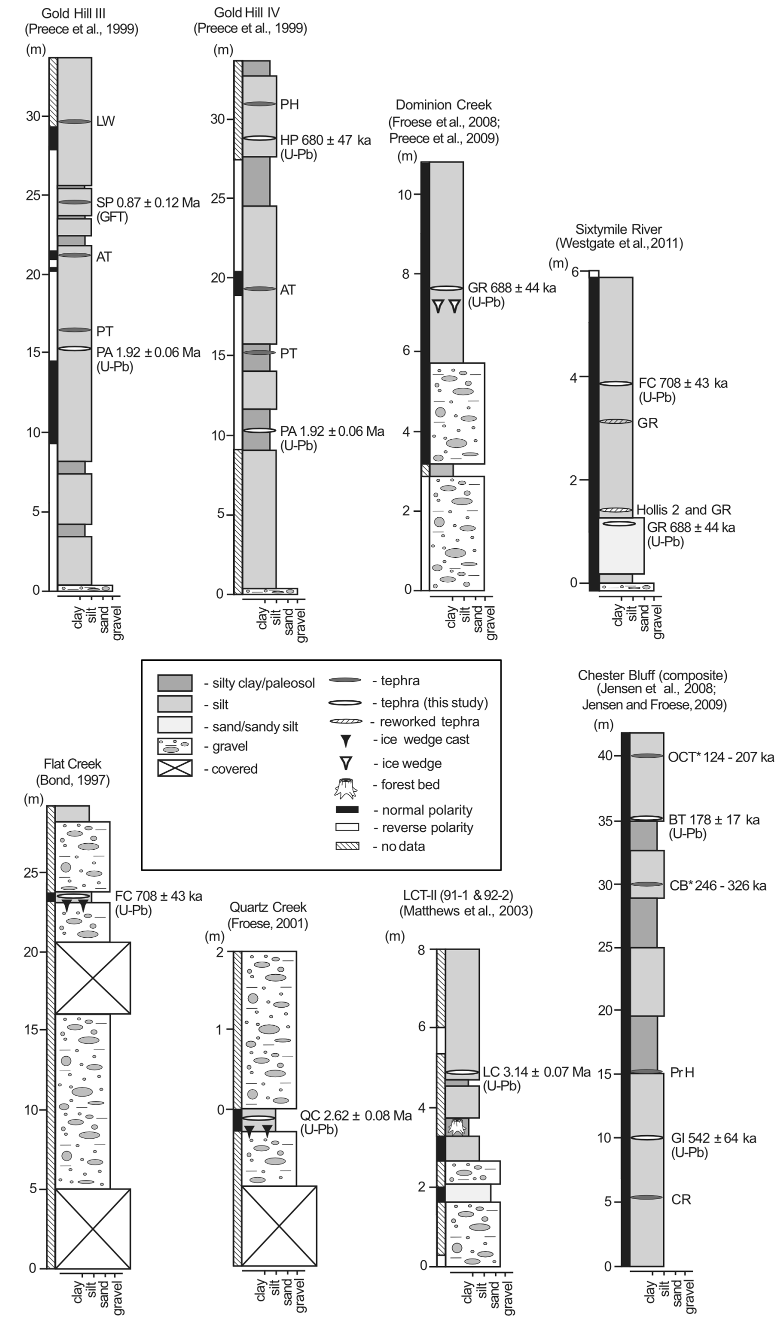

Figure 2.6. *Stratigraphic contexts of the tephra beds in this study. The Dominion Creek, LCT-II and Chester Bluff are composite stratigraphic columns. Note that vertical scale varies from one section to another. GR = Gold Run tephra; FC = Flat Creek tephra; LC = Lost Chicken tephra; QC = Quartz Creek tephra; BT = Biederman tephra; OCT = Old Crow tephra. GFT = glass fission-track.*

2.4.3.4. PA tephra

PA tephra yielded a Bayesian model age of 1.92 ± 0.06 Ma, which is consistent with the revised glass fission-track age of 2.07 ± 0.50 Ma (Fig. 2.7.). Although U-Pb data from only seven grains were used to calculate an age for PA tephra, due to a limited number of grains recovered from the tephra sample, the model age is consistent with stratigraphic constraints from other dated tephra beds. At Gold Hill (Fig. 2.1.), PA tephra is bracketed by loess with reversed remanent magnetic polarity (Preece et al., 1999), suggesting that the tephra was deposited during the C2r.1r subchron (1.945 -2.128 Ma) of the Matuyama chron (Ogg, 2020; Fig. 2.6.; Fig. 2.7.). At a mining exposure in the Cripple Sump area near Fairbanks, Alaska, PA underlies the NT tephra (Preece et al., 1999) which is correlative to the 1.45 ± 0.28 Ma (unrevised glass fission-track age; Westgate et al., 2001) Mosquito Gulch tephra in the Klondike region. Thus, the U-Pb and revised glass fission-track ages for PA tephra are consistent with its stratigraphic position relative to other dated tephra beds.

The PA tephra is the lowest and oldest directly-dated tephra layer at Gold Hill, where it is ~10-15 m above the base of the Gold Hill III section (Preece et al., 1999). Matheus et al. (2003) identified PA tephra within ice-wedge casts and solifluction deposits at the Palisades site in central Alaska, indicating the presence of permafrost in the region before 1.92 Ma. Matheus et al. (2003) also identified PA tephra directly beneath a peat/forest bed at the Palisades, Yukon River, Alaska which was in turn correlated to the Early Pleistocene interglacial Dawson Cut Forest Bed in the Fairbanks region where PA tephra is in close stratigraphic association with the forest bed deposits (Péwé et al., 2009). However, the presence of PA tephra at Palisades could not be corroborated after ~20 days of field investigation at the site (Reyes et al., 2010a; Jensen et al., 2013). If PA tephra is indeed present at the Palisades, it implies the existence of a remnant exposure of ~1.9 Ma loess within a sequence otherwise dominated by Middle Pleistocene loess and paleosols (Jensen et al., 2013).

2.4.3.5. Quartz Creek tephra

Quartz Creek tephra has a Bayesian model age of 2.62 ± 0.08 Ma, in accordance with the revised glass fission-track age of 2.88 ± 0.30 Ma (Fig. 2.7.). The recalculated Quartz Creek tephra $^{40}Ar/^{39}Ar$ data of Kunk (1995) yield an isochron age of 2.67 ± 0.49 Ma, which is indistinguishable from our U-Pb and revised glass fission-track ages at 2σ uncertainty. All radiometric age estimates are compatible with the normal remanent magnetic polarity of the surrounding sediment at the Quartz Creek type section in the Klondike region (Fig. 2.1.; Fig. 2.6.), suggesting deposition during the C2An.1n normal subchron (2.581 - 3.032 Ma) within the Gauss Chron (Froese et al., 2000, 2001; Westgate et al., 2003; Ogg, 2020). Hence, the ^{238}U-^{206}Pb age of 2.62 ± 0.08 Ma likely closely reflects the eruption timing associated with deposition of Quartz Creek.

Quartz Creek tephra is found in ice-wedge casts in central Yukon, so a direct age for the tephra provides a close minimum age for periglacial conditions in eastern Beringia. Earlier glass fission-track and $^{40}Ar/^{39}Ar$ ages for Quartz Creek tephra suggested that permafrost was established in eastern Beringia by ~3 Ma (Westgate et al., 2003). Our new U-Pb age estimate has substantially lower 2σ uncertainty and supports a somewhat younger age (~2.6 Ma) for the onset of periglacial condition in eastern Beringia.

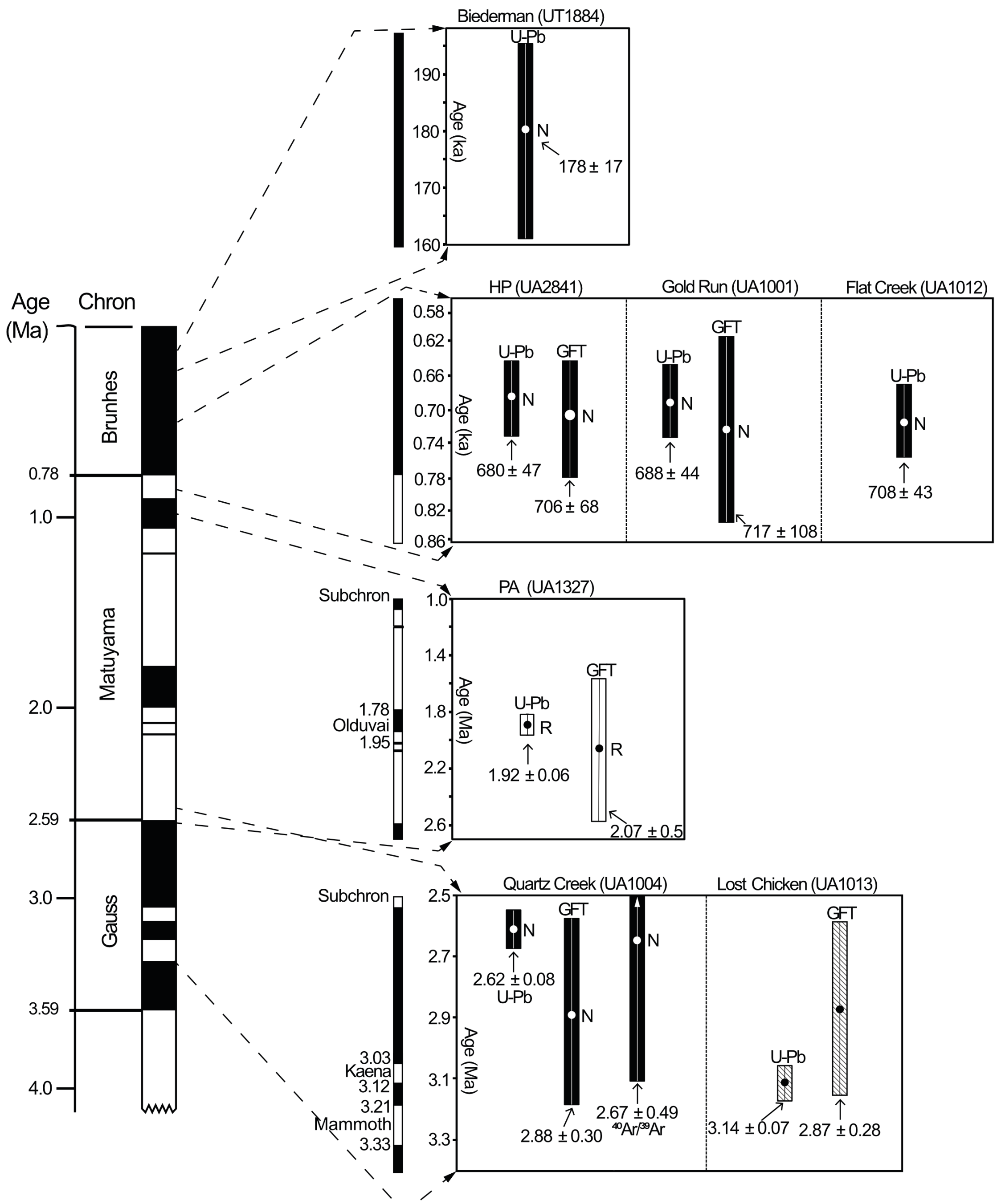

Figure 2.7. *Summary of zircon ^{206}Pb-^{238}U ages (^{230}Th corrected; Bayesian model), revised glass fission-track ages (GFT), and ^{40}Ar/^{39}Ar age (Quartz Creek tephra only) for the tephra analyzed in this paper, in the context of paleomagnetic constraints and the geomagnetic polarity time scale (Mankinen and Dalrymple, 1979; Ogg, 2020).*

2.4.3.6. Lost Chicken tephra

Lost Chicken tephra has a Bayesian model age of 3.14 ± 0.07 Ma, which is consistent with the revised glass fission-track age of 2.87 ± 0.28 Ma (Fig. 2.7.) within the 2σ bounds of both dating techniques. There are no paleomagnetic measurements on the organic-rich silts and peat that surround the tephra, although sediments directly below Lost Chicken tephra have normal remanent magnetic polarity, while sediments up to ~1 m above and ~3 m below have reversed magnetic polarity (Matthews et al., 2003; Fig. 2.6.). The revised glass fission-track age still aligns with the original interpretation by Matthews et al. (2003) that Lost Chicken tephra was deposited in the youngest normal subchron of the Gauss chron (C2An.1n; 3.032-2.581 Ma), while the underlying reversed sediments represent the Kaena (C2An.1r) subchron (3.032-3.116 Ma) and the upper reversed sediments represent the Matuyama chron (Fig. 2.7). If, instead, the zircon ^{238}U-^{206}Pb age more accurately reflects the timing of deposition, the paleomagnetic data indicate that the normal-polarity sediments directly beneath Lost Chicken tephra were likely deposited during the C2An.2n normal subchron (3.116 - 3.207 Ma) of the Gauss chron. In turn, this would suggest the reversed sediments overlying Lost Chicken tephra represent the Kaena subchron (3.032 - 3.116 Ma), while the underlying reversed sediments may be the Mammoth subchron (C2An. 2r; 3.207-3.330 Ma) (Ogg, 2020).

Regardless, the new and existing radiometric ages and paleomagnetic data support a late Pliocene age for the Lost Chicken tephra. The Lost Chicken tephra sits directly above or within Late Pliocene preglacial peat at Lost Chicken Mine in east-central Alaska (Matthews et al., 2003). This site is an important archive of the boreal forest vegetation, insect fauna, and paleoenvironmental conditions before the onset of global cooling ~ 2.7 Ma (Matthews et al., 2003; Péwé et al., 2009). Our new zircon U-Pb Lost Chicken age provides an improved chronological constraint for the Lost Chicken Mine exposure and indicates that boreal forest was present in Alaska ~3.14 ± 0.07 Ma. The tephra has also been a target of studies attempting to use δD from hydrated glass and associated clays to infer regional uplift, changes in air mass circulation, and temperature over the late Pliocene (Bill et al., 2018; Otiniano et al., 2020).

2.4.3.7. GI tephra

We discuss GI tephra last because it yielded the least reliable age estimate of the tephra beds presented here. GI tephra has a revised glass fission-track age of 545 ± 156 ka and a Bayesian model age of 542 ± 64 ka, the latter of which is based on only three zircon analyses. The large error for the GI tephra glass fission-track age is due to poor recovery of platy glass shards, resulting in low track counts and poor statistics. The high proportion of significantly older U-Pb-dated zircon crystals, which predate the eruption by 100s or 1000s of kyr, makes it difficult to interpret the U-Pb results. GI tephra must be younger than 780 ka, based on the normal remnant magnetic polarity of the host sediment (Fig. 2.6.; Preece et al., 1999), placing the deposition of GI tephra within the Brunhes Chron. GI is also present approximately 8 metres above HP (680 ± 47 ka) at Gold Hill IV (Fig. 2.2.; Supplemental Table A.7), and >10 m below Chester Bluff tephra (recalculated glass fission-track age of 255 ± 40 ka, Westgate and Pearce, 2017; zircon U-Pb age of 326 ± 32 ka, Burgess et al., 2019) at Chester Bluff (Jensen et al., 2008). These stratigraphic constraints support the revised glass fission-track and U-Pb results, collectively indicating a Middle Pleistocene age for the tephra and closely associated paleosols in Gold Hill Loess and at Chester Bluff (Froese et al., 2003; Jensen et al., 2013). The low precision of the previous age estimates means that the tephra could be associated with any interglacial between MIS 11 and MIS 17. Although still uncertain, the agreement between GI tephra U-Pb age of 542 ± 64 ka and the revised glass fission-track age suggest that paleosol horizons are more likely to be associated with MIS 13 or MIS 15. However, more zircon analyses are clearly required to obtain a reliable representation of the youngest population.

2.5. Conclusions

U-Pb LA-ICP-MS dating was performed on zircon crystals from eight major tephra deposits in Yukon and Alaska, most of which have existing age constraints based on glass fission-track dating and stratigraphic association with other dated tephra. We provide updated maximum deposition ages for these tephra by combining U-Pb data with revised glass fission-track ages and other published geochronological constraints. In all cases, tephra zircon U-Pb ages were consistent—within 2σ uncertainty—with revised glass fission-track and $^{40}Ar/^{39}Ar$ age, suggesting that eruption likely commenced during or shortly after crystallization of the youngest zircon grains. The consistency between our zircon U-Pb results and revised glass fission-track ages further suggests that glass fission-track dating can be a reliable tephra geochronology tool on the timescales evaluated in this study (>500 ka), albeit with a lower precision than zircon U-based dating techniques.

This work demonstrates that LA-ICP-MS method is well suited for rapid *in-situ* dating of very young zircon crystals. In addition, the LA-ICP-MS cost per analysis is low and it is possible to analyze hundreds of grains per day. We also show that tephra ages derived from zircon U-Pb ages are sensitive to the method used to average the pool of ages, with youngest-single-grain and weighted mean methods tending to yield the youngest and oldest age estimate, respectively. We recommend the following ^{238}U-^{206}Pb Bayesian model ages as the most reliable and precise estimates of tephra age: Biederman tephra 178 ± 17 ka, HP tephra 688 ± 47 ka, Gold Run tephra

688 ± 44 ka (and stratigraphically older than Flat Creek tephra), Flat Creek tephra 708 ± 43 ka, PA tephra 1.92 ± 0.06 Ma, Quartz Creek Tephra 2.62 ± 0.08 Ma, Lost Chicken tephra 3.14 ± 0.07 Ma, and GI tephra 542 ± 64 ka. These results highlight the potential of LA-ICP-MS U-Pb zircon dating to refine the chronology of Pliocene-Pleistocene tephra beds, although stratigraphy and palaeoecological context always play a significant role in determining the reliability of any age determined by this or any other method.

2.6. Supplemental Figures

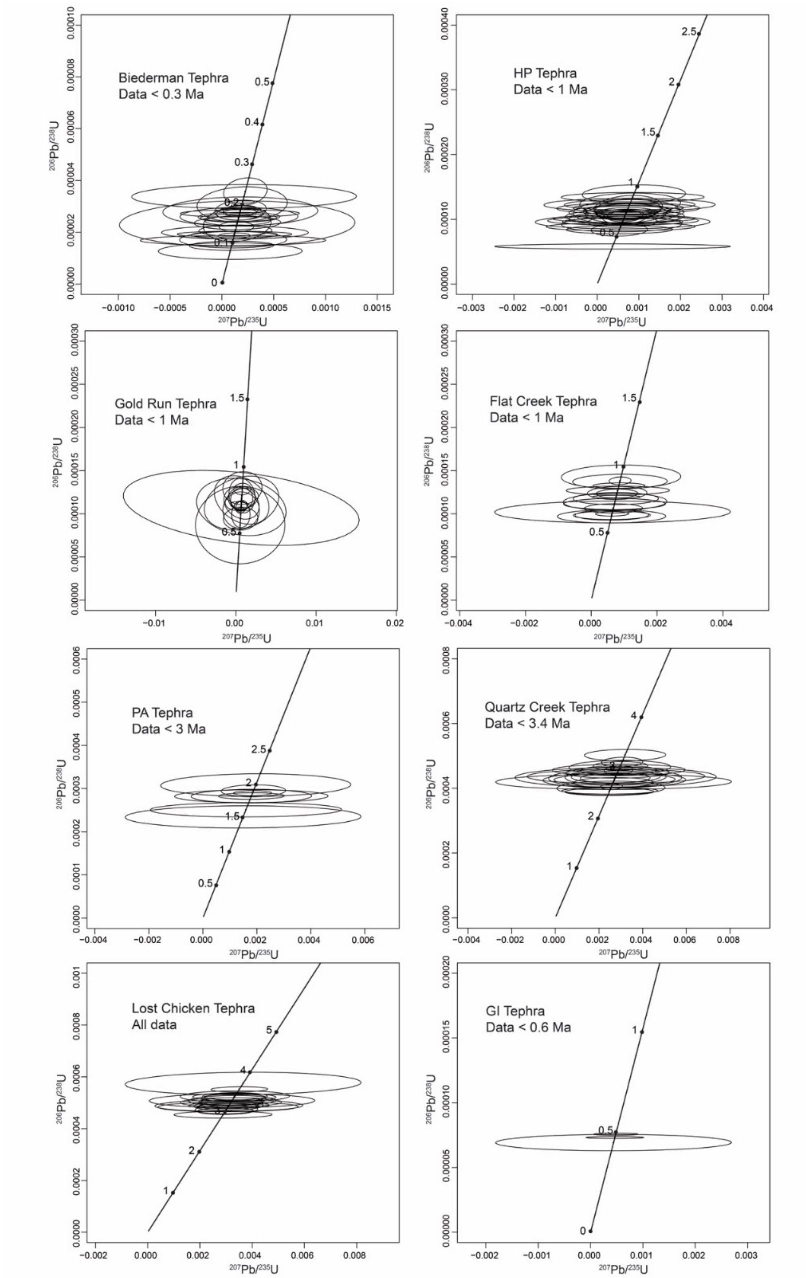

Figure A.1: *Common-Pb-corrected (Williams, 1998) zircon U-Pb Concordia plots for filtered data. Plotted data are deemed to represent the autocrystic zircon population from each tephra sample; all plotted data were used in Bayesian age modeling. Data point ellipses are at 2σ level. Initial $^{207}Pb/^{206}Pb$ value is estimated from Stacey and Kramers (1975) lead evolution model for all tephra except for PA, where $^{207}Pb/^{206}Pb_i$ = 0.981 was used (see text).*

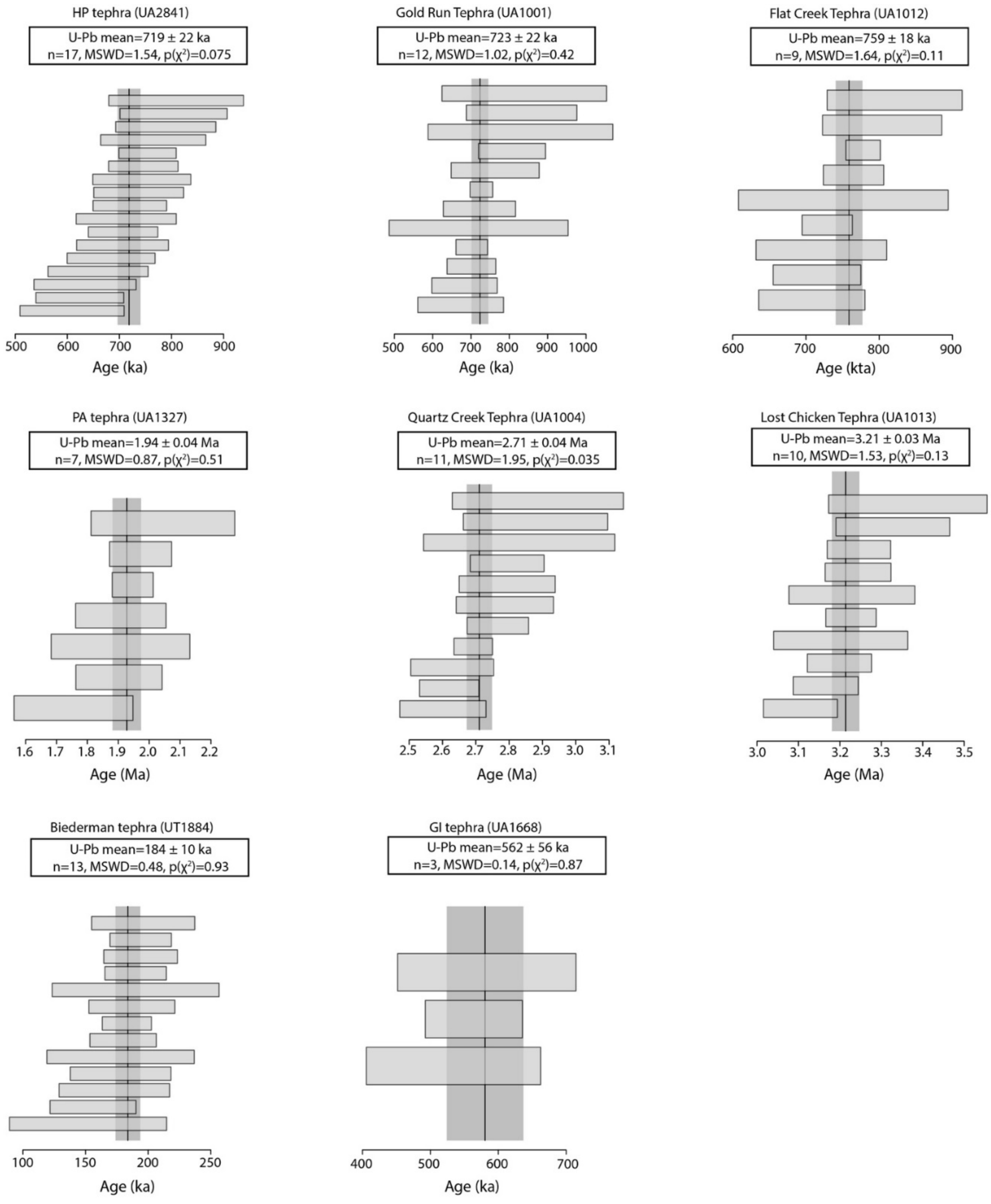

Figure A.2: *Zircon ^{238}U-^{206}Pb weighted mean ages for the tephra analyzed in this study. The weighted mean ages were calculated using IsoplotR v3.8 (Vermeesch, 2018). All uncertainties are at 2σ level.*

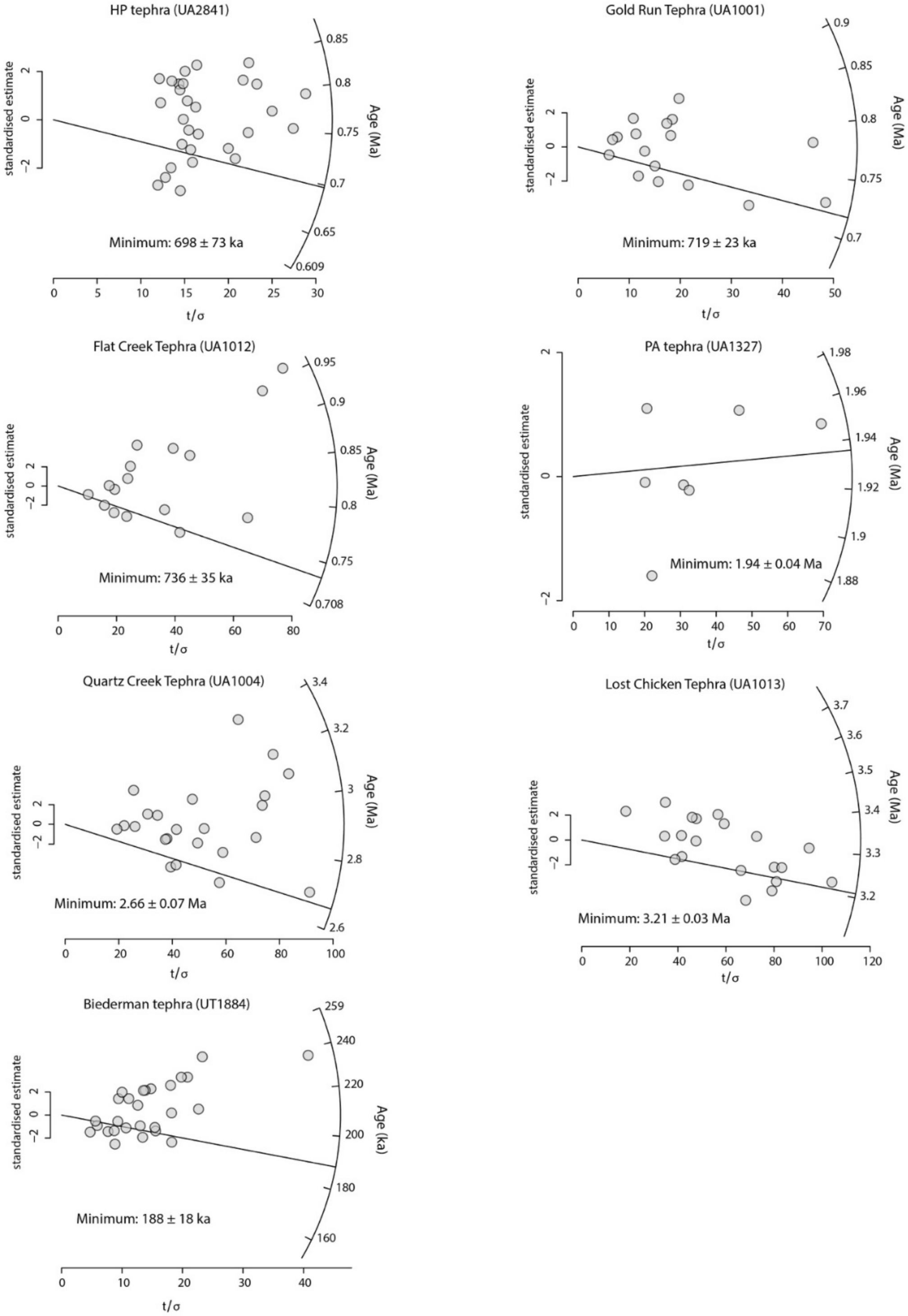

Figure A.3: *Radial plots for maximum likelihood algorithm ages for the tephra analysed in this study. The minimum ages were calculated using IsoplotR v3.8 (Vermeesch, 2018). All uncertainties are at 2σ level.*

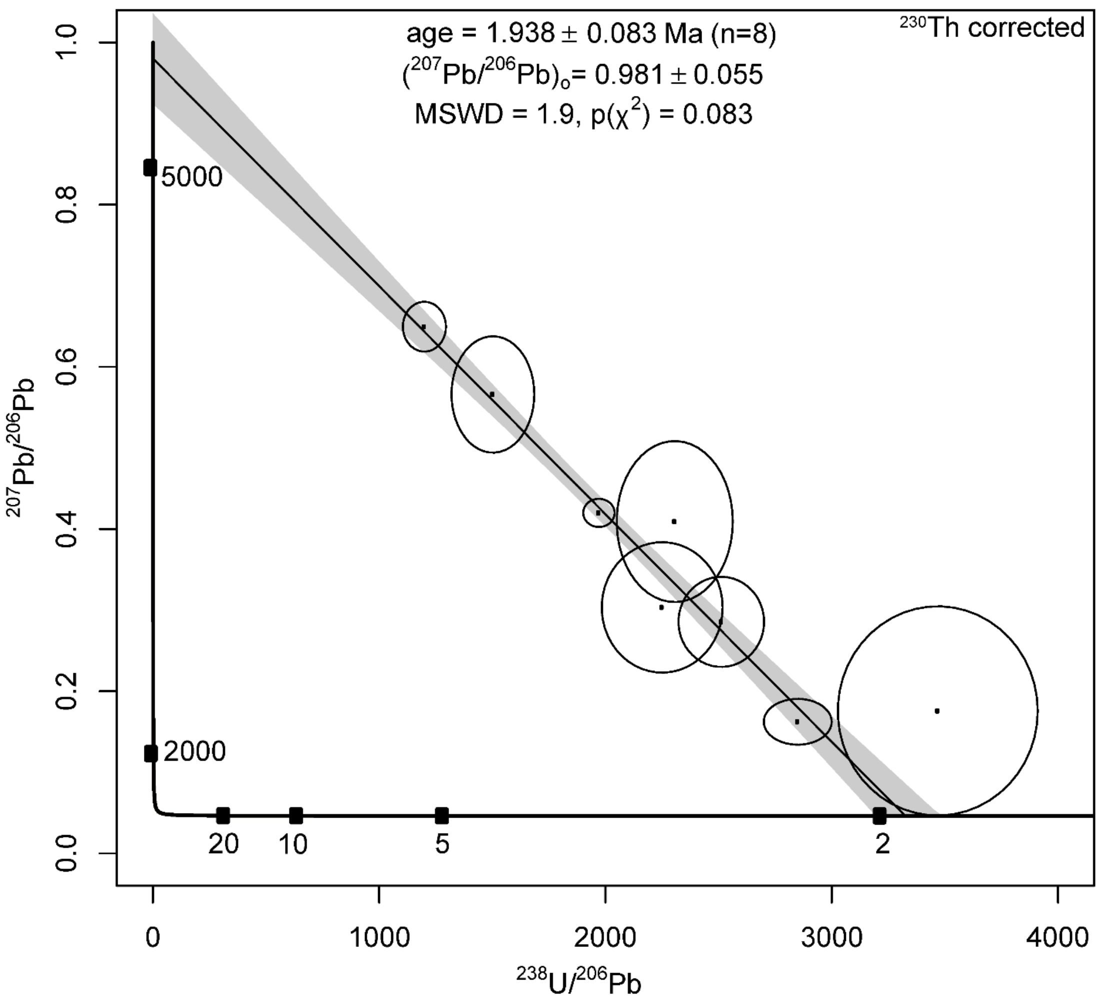

Figure A.4: Terra-Wasserburg Concordia plot at 2σ level for PA tephra zircon U-Pb analyses. Concordia axes are modified to account for initial ^{230}Th disequilibrium in the zircon. An upper intercept ^{207}Pb/^{206}Pb value of 0.981 ± 0.055 was used for common-Pb correction of PA tephra zircon U-Pb analyses.

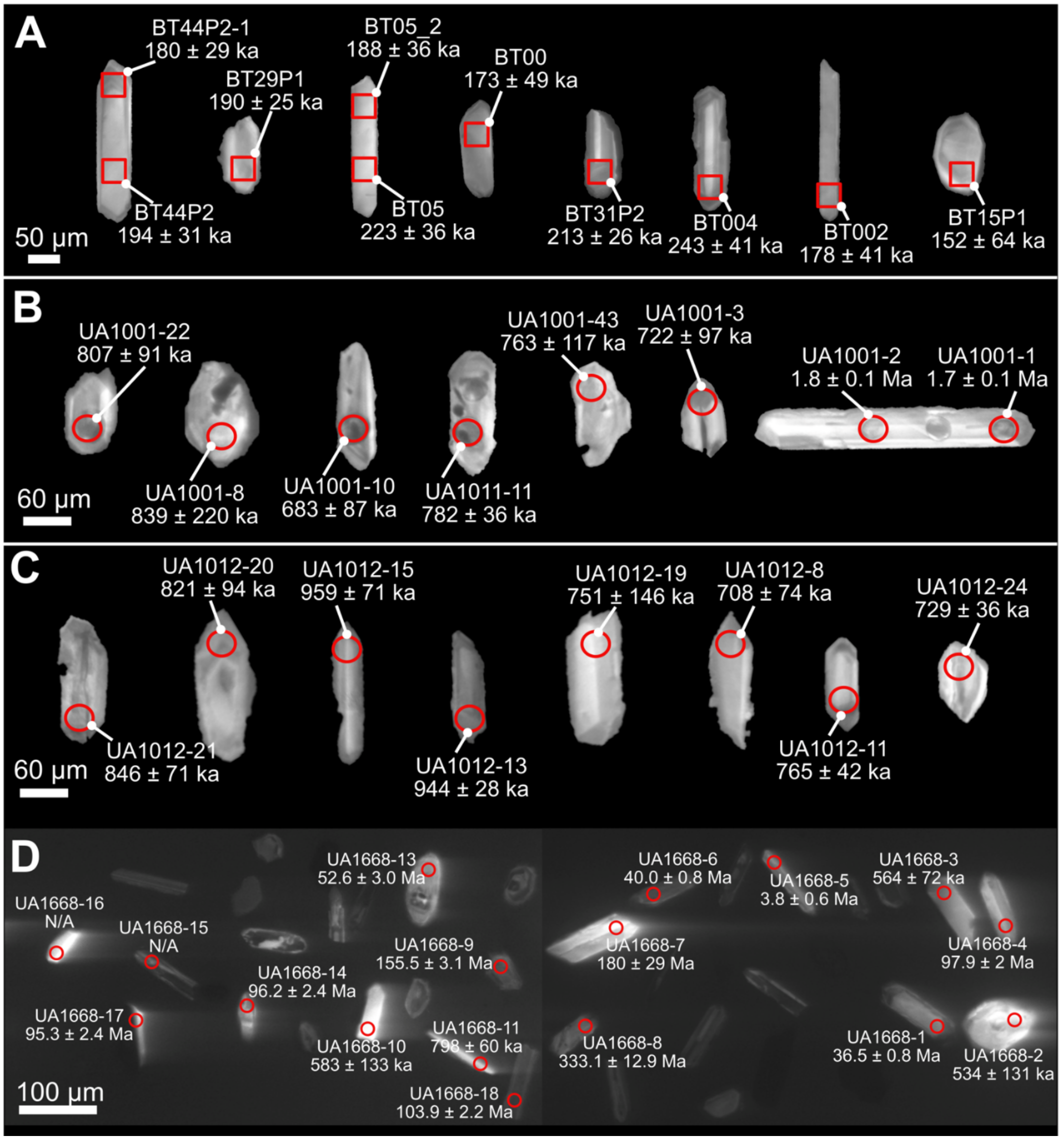

Figure A.5: *Cathodoluminescence imaging micrograph of representative zircons. The LA-ICP-MS U-Pb ablation pits are marked with red circles or squares. A. Representative micrograph of zircon crystals from Biederman tephra sample UT1884. The ablation pit diagonals are ~40 µm. B. Representative micrograph of zircon crystals from Gold Run tephra sample UA1001. The diameter of the ablation pits is ~30-33 µm. C. Representative micrograph of zircon crystals from Flat Creek tephra sample UA1012. The diameter of the ablation pits is ~30-33 µm. D. Representative zircon images from GI tephra sample UA1668. The diameter of the ablation pits is ~30-33 µm.*

2.7. References

Auclair, M., Lamothe, M., Lagroix, F., Banerjee, S.K. 2007. Luminescence investigation of loess and tephra from Halfway House section, Central Alaska. Quaternary Geochronology 2, 34–38. https://doi.org/10.1016/j.quageo.2006.05.009.

Bacon, C.R., Persing, H.M., Wooden, J.L., Ireland, T.R., 2000. Late Pleistocene granodiorite beneath Crater Lake caldera, Oregon, dated by ion microprobe. Geology 28, 467–470. https://doi.org/10.1130/0091-7613(2000)028<0467:LPGBCL>2.3.CO;2

Begét, J., 1990. Middle Wisconsinan climate fluctuations recorded in central Alaskan loess. Géographie Physique et Quaternaire 44, 3–13. https://doi.org/10.7202/032793ar

Begét, J.E., Keskinen, M.J., 2003. Trace-element geochemistry of individual glass shards of the Old Crow tephra and the age of the Delta glaciation, central Alaska. Quaternary Research 60, 63–69. https://doi.org/10.1016/S0033-5894(03)00095-4

Berger, G.W., 1991. The use of glass for dating volcanic ash by thermoluminescence. Journal of Geophysical Research: Solid Earth 96, 19705–19720. https://doi.org/ /10.1029/91JB01899

Berger, G.W., 1987. Thermoluminescence dating of the Pleistocene Old Crow tephra and adjacent loess, near Fairbanks, Alaska. Canadian Journal of Earth Sciences 24, 1975–1984. https://doi.org/10.1139/e87-188

Berger, G.W., Péwé, T.L., Westgate, J.A., Preece, S.J., 1996. Age of Sheep Creek Tephra (Pleistocene) in Central Alaska from thermoluminescence dating of bracketing loess, Quaternary Research 45, 263–270. https://doi.org/10.1006/qres.1996.0027.

Bigazzi, G., Galbraith, R.F., 1999. Point-counting technique for fission-track dating of tephra glass shards, and its relative standard error. Quaternary Research 51,67–73. https://doi.org/10.1006/qres.1998.2019

Bill, N.S., Mix, H.T., Clark, P.U., Reilly, S.P., Jensen, B.J.L., Benowitz, J.A., 2018. A stable isotope record of late Cenozoic surface uplift of southern Alaska. Earth and Planetary Science Letters 482, 300-311. https://doi.org/10.1016/j.epsl.2017.11.029

Biller-Celander, N., Shakun, J.D., McGee, D., Wong, C.I., Reyes, A.V., Hardt, B., Tal, I., Ford, D.C., Lauriol, B., 2021. Increasing Pleistocene permafrost persistence and carbon cycle conundrums inferred from Canadian speleothems. Science Advances 7, eabe5799. https://doi.org/10.1126/sciadv.abe5799

Bond, J.D., 1997. Late Cenozoic history of McQuesten map area, Yukon Territory, with applications to placer gold research. Unpublished M.Sc. thesis, University of Alberta, Edmonton, Alta., Canada. https://doi.org/10.7939/R36Q1SS1N

Brigham-Grette, J., 2001. New perspectives on Beringian Quaternary paleogeography, stratigraphy, and glacial history. Quaternary Science Reviews 20, 15–24. https://doi.org/10.1016/S0277-3791(00)00134-7

Bowring, S.A., Grotzinger, J.P., Isachsen, C.E., Knoll, A.H., Pelechaty, S.M., Kolosov, P., 1993. Calibrating rates of Early Cambrian evolution. Science 261, 1293–1298. https://doi.org/10.1126/science.11539488

Burgess, S.D., Coble, M.A., Vazquez, J.A., Coombs, M.L., Wallace, K.L., 2019. On the eruption age and provenance of the Old Crow tephra. Quaternary Science Reviews 207, 64–79. https://doi.org/10.1016/j.quascirev.2018.12.026

Burgess, S.D., Vazquez, J.A., Waythomas, C.F., Wallace, K.L., 2021. U–Pb zircon eruption age of the Old Crow tephra and review of extant age constraints. Quaternary Geochronology 66, 101168. https://doi.org/10.1016/j.quageo.2021.101168

Chamberlain, K.J., Wilson, C.J.N., Wooden, J.L., Charlier, B.L.A., Ireland, T.R. 2014. New perspectives on the Bishop Tuff from zircon textures, ages and trace elements. Journal of Petrology 55, 395–426. https://10.1093/petrology/egt072.

Chang, Z., Vervoort, J.D., McClelland, W.C., Knaack, C. 2006. U-Pb dating of zircon by LA-ICP-MS. Geochemistry, Geophysics, Geosystems 7, Q05009. https://doi.org/10.1029/2005GC001100.

Charlier, B.L.A., Wilson, C.J.N., Lowenstern, J.B., Blake, S., van Calsteren, P.W., Davidson, J.P., 2005. Magma generation at a large, hyperactive silicic volcano (Taupo, New Zealand) revealed by U-Th and U-Pb systematics in zircons. Journal of Petrology 46, 3–32. https://doi.org/10.1093/petrology/egh060.

Cherniak, D.J., Watson, E.B., 2001. Pb diffusion in zircon. Chemical Geology 172, 5–24. https://doi.org/10.1016/S0009-2541(00)00233-3.

Coble, M.A., Burgess, S.D., Klemetti, E.W., 2017. New zircon (U-Th)/He and U/Pb eruption age for the Rockland tephra, western USA. Quat. Sci. Rev. 172, 109–117. https://doi.org/10.1016/j.quascirev.2017.08.004

Crowley, J.L., Schoene, B., Bowring, S.A., 2007. U-Pb dating of zircon in the Bishop Tuff at the millennial scale. Geology 35, 1123–1126. https://doi.org/10.1130/G24017A.1.

Danišík, M., Schmitt, A.K., Stockli, D.F., Lovera, O.M., Dunkl, I., Evans, N.J., 2017. Application of combined U-Th-disequilibrium/U-Pb and (U-Th)/He zircon dating to tephrochronology. Quat. Geochronol. 40, 23–32. https://doi.org/10.1016/j.quageo.2016.07.005

Dalrymple, G.B., 1969. 40Ar/36Ar analyses of historic lava flows. Earth Planet. Sci. Lett. 6, 47–55. https://doi.org/10.1016/0012-821X(69)90160-5

Davies, L.J., Jensen, B.J.L., Froese, D.G., Wallace, K.L., 2016. Late Pleistocene and Holocene tephrostratigraphy of interior Alaska and Yukon: Key beds and chronologies over the past 30,000 years. Quaternary Science Reviews 146, 28–53. https://doi.org/ 10.1016/j.quascirev.2016.05.026

Deino, A.L., Sier, M.J., Garello, D.I., Keller, C.B., Kingston, J.D., Scott, J.J., Dupont-Nivet, G., and Cohen, A.S. 2021. Chronostratigraphy of the Baringo-Tugen Hills-Barsemoi (HSPDP-BTB13-1A) core – $^{40}Ar/^{39}Ar$ dating, magnetostratigraphy, tephrostratigraphy, sequence stratigraphy and Bayesian age modeling. Palaeogeography, Palaeoclimatology, Palaeoecology, 570: 109519. https://doi.org/10.1016/j.palaeo.2019.109519.

Dickinson, W.R., Gehrels, G.E. 2009. Use of U–Pb ages of detrital zircons to infer maximum depositional ages of strata: A test against a Colorado Plateau Mesozoic database. Earth and Planetary Science Letters 288, 115–125. https://doi.org/10.1016/j.epsl.2009.09.013.

di Vincenzo, G., Skála, R., 2009. 40Ar–39Ar laser dating of tektites from the Cheb Basin (Czech Republic): Evidence for coevality with moldavites and influence of the dating standard on the age of the Ries impact. Geochimica et Cosmochimica Acta 73, 493–513. https://doi.org/10.1016/j.gca.2008.10.002

Edwards, M.E., McDowell, P.F., 1991. Interglacial deposits at Birch Creek, northeast interior Alaska. Quaternary Research 35, 41-52. https://doi.org/10.1016/0033-5894(91)90093-K.

Evans, M.E., Jensen, B.J., Kravchinsky, V.A., Froese, D.G., 2011. The Kamikatsura event in the gold Hill loess, Alaska. Geophysical Research Letters 38, L13302. https://doi.org/10.1029/2011GL047793.

Farley, K.A., 2000. Helium diffusion from apatite: General behavior as illustrated by Durango fluorapatite. Journal of Geophysical Research: Solid Earth 105, 2903–2914. https://doi.org/10.1029/1999JB900348

Froese, D., Stiller, M., Heintzman, P.D., Reyes, A.V., Zazula, G.D., Soares, A.E.R., Meyer, M., Hall, E., Jensen, B.J.L., Arnold, L.J., MacPhee, R.D.E., Shapiro, B., 2017. Fossil and genomic evidence constrains the timing of bison arrival in North America. Proceedings of the National Academy of Sciences of the United States of America 114, 3457–3462. https://doi.org/10.1073/pnas.1620754114

Froese, D.G., 2001. Eastern Beringian paleoclimate from fluvial and eolian deposits, Plio-Pleistocene middle Yukon River, central Yukon and Alaska. Unpublished Ph.D. Thesis, University of Calgary, Alta., Canada. https://doi.org/10.11575/PRISM/14916

Froese, D.G., Smith, D.G., Westgate, J.A., Ager, T.A., Preece, S.J., Sandhu, A., Enkin, R.J., Weber, F., 2003. Recurring middle Pleistocene outburst floods in east-central Alaska. Quaternary Research 60, 50–62. https://doi.org/10.1016/S0033-5894(03)00090-5

Froese, D.G., Enkin, R.J., Smith, D.G., 2001. Placer depositional settings and their ages along Dominion Creek, Klondike area, Yukon. In: Emond, D.S., Weston, L.H. (Eds.), Yukon Exploration and Geology 2000. Exploration and Geological Services Division, Yukon Region, Indian and Northern Affairs, Canada, pp. 159–169

Froese, D.G., Zazula, G.D., Westgate, J.A., Preece, S.J., Sanborn, P.T., Reyes, A. V., Pearce, N.J.G., 2009. The Klondike goldfields and Pleistocene environments of Beringia. GSA

Today 19, 4–10. https://doi.org/10.1130/GSATG54A.1

Froese, D.G., Westgate, J.A., Reyes, A.V., Enkin, R.J., Preece, S.J., 2008. Ancient permafrost and a future, warmer arctic. Science 321, 1648. https://doi.org/10.1126/science.1157525

Gentner, W., Kleinmann, B., Wagner, G.A., 1967. New K-Ar and fission track ages of impact glasses and tektites. Earth and Planetary Science Letters 2, 83–86. https://doi.org/10.1016/0012-821X(67)90104-5

Guillong, M., von Quadt, A., Sakata, S., Peytcheva, I., Bachmann, O., 2014. LA-ICP-MS Pb-U dating of young zircons from the Kos-Nisyros volcanic centre, SE Aegean arc. Journal of Analytical Atomic Spectrometry 29, 963–970. https://doi.org/10.1039/c4ja00009a

Hamilton, T.D., Brigham-Grette, J., 1991. The last interglaciation in Alaska: Stratigraphy and paleoecology of potential sites. Quaternary International 10, 49-71. https://doi.org/10.1016/1040-6182(91)90040-U

Hidy, A.J., Gosse, J.C., Sanborn, P., Froese, D.G., 2018. Age-erosion constraints on an Early Pleistocene paleosol in Yukon, Canada, with profiles of ^{10}Be and ^{26}Al: Evidence for a significant loess cover effect on cosmogenic nuclide production rates. Catena 165, 260-271. https://doi.org/10.1016/j.catena.2018.02.009

Hopkins, D.M., Matthews, J. V., Wolfe, J.A., Silberman, M.L., 1971. A Pliocene flora and insect fauna from the Bering Strait region. Palaeogeography. Palaeoclimatology, Palaeoecology 9, 211–231. https://doi.org/10.1016/0031-0182(71)90032-0

Horn, I., Guillong, M., Günther, D., 2001. Wavelength dependant ablation rates for metals and silicate glasses using homogenized laser beam profiles — implications for LA-ICP-MS. Applied Surface Science 182, 91–102. https://doi.org/10.1016/S0169-4332(01)00465-2.

Hultén, E., 1937. Outline of the history of arctic and boreal biota during the Quaternary period. Bokfoerlags Aktiebolaget Thule, Stockholm, Sweden.

Hurford, A.J., Green, P.F., 1983. The zeta age calibration of fission-track dating. Chemical Geology 41, 285–317 https://doi.org/10.1016/S0009-2541(83)80026-6

Ickert, R.B., Mundil, R., Magee, C.W., Mulcahy, S.R., 2015. The U-Th-Pb systematics of zircon from the Bishop Tuff: A case study in challenges to high-precision Pb/U geochronology at the millennial scale. Geochimica et Cosmochimica Acta 168, 88–110. https://doi.org/10.1016/j.gca.2015.07.018.

Ito, H., Tamura, A., Morishita, T., Arai, S., Arai, F., Kato, O., 2013. Quaternary plutonic magma activities in the southern Hachimantai geothermal area (Japan) inferred from zircon LA-ICP-MS U-Th-Pb dating method. Journal of Volcanology and Geothermal Research 265, 1–8. https://doi.org/10.1016/j.jvolgeores.2013.08.014

Ito, H., 2014. Zircon U–Th–Pb dating using LA-ICP-MS: Simultaneous U–Pb and U–Th dating on the 0.1 Ma Toya Tephra, Japan. Journal of Volcanology and Geothermal Research 289, 210–223. https://doi.org/10.1016/j.jvolgeores.2014.11.002.

Ito, H., 2020. Magmatic history of the Oldest Toba Tuff inferred from zircon U–Pb geochronology. Sci. Rep. 10, 17506. https://doi.org/10.1038/s41598-020-74512-z

Jackson, S.E., Pearson, N.J., Griffin, W.L., Belousova, E.A., 2004. The application of laser ablation-inductively coupled plasma-mass spectrometry to in situ U–Pb zircon geochronology. Chemical Geology 211, 47–69. https://doi.org/10.1016/j.chemgeo.2004.06.017.

Jensen, B.J.L., Evans, M.E., Froese, D.G., Kravchinsky, V.A., 2016. 150,000 years of loess accumulation in central Alaska. Quaternary Science Reviews 135, 1–23. https://doi.org/10.1016/j.quascirev.2016.01.001

Jensen, B.J.L., Froese, D.G., Preece, S.J., Westgate, J.A., Stachel, T., 2008. An extensive middle to late Pleistocene tephrochronologic record from east-central Alaska. Quaternary Science Reviews 27, 411–427. /10.1016/j.quascirev.2007.10.010

Jensen, B.J.L., Froese, D.G., 2009. Biederman tephra: a potential Marine Isotope Stage 7 marker horizon in eastern Beringia. Canadian Quaternary Association Biennial Meeting, May 3-8, Simon Fraser University, BC, Canada. Programme and Abstracts, vol. 101.

Jensen, B.J.L., Reyes, A.V., Froese, D.G., Stone, D.B., 2013. The Palisades is a key reference site for the middle Pleistocene of eastern Beringia: New evidence from paleomagnetics and regional tephrostratigraphy. Quaternary Science Reviews 63, 91–108. https://doi.org/10.1016/j.quascirev.2012.11.035

Keller, C.B., Schoene, B., Samperton, K.M., 2018. A stochastic sampling approach to zircon eruption age interpretation. Geochemical Perspectives Letters 8, 31–35. https://doi.org /10.7185/geochemlet.1826.

Kirkland, C.L., Danišík, M., Marsden, R., Piilonen, P., Barham, M., Sutherland, L., 2020. Dating young zircon: A case study from Southeast Asian megacrysts. Geochimica et Cosmochimica Acta 274, 1–19. https://doi.org/10.1016/j.gca.2020.01.013

Krautz, J., Hofmann, M., Gärtner, A., Linnemann, U., Kleber, A., 2018. Capability of U–Pb dating of zircons from Quaternary tephra: Jemez Mountains, NM, and La Sal Mountains, UT, USA. E&G Quat. Sci. J. 67, 7–16. https://doi.org/10.5194/egqsj-67-7-2018

Kunk, M.J., 1995. $^{40}Ar/^{39}Ar$ age-spectrum data for hornblende, plagioclase and biotite from tephra collected at Dan Creek and McCallum Creek, Alaska and in the Klondike Placer district near Dawson, Yukon Territory, Canada. USGS Open-File Report 95-217, 52 p. https://doi.org/10.3133/ofr95217A

Lamothe, M., Forget Brisson, L., Hardy, F., 2020. Circumvention of anomalous fading in feldspar luminescence dating using Post-Isothermal IRSL. Quaternary Geochronology 57, 101062. https://doi.org/10.1016/j.quageo.2020.101062

Laurenzi, M.A., Balestrieri, M.L., Bigazzi, G., Hadler Neto, J.C., Iunes, P.J., Norelli, P., Oddone, M., Osorio Araya, A.M., Viramonte, J.G., 2007. New constraints on ages of glasses proposed as reference materials for fission-track dating. Geostandards and Geoanalytical Research 31, 105–124. https://doi.org/10.1111/j.1751-908X.2007.00844.x

Lee, J.-Y., Marti, K., Severinghaus, J.P., Kawamura, K., Yoo, H.-S., Lee, J.B., Kim, J.S., 2006. A redetermination of the isotopic abundances of atmospheric Ar. Geochim. Cosmochim. Acta 70, 4507–4512. https://doi.org/10.1016/j.gca.2006.06.1563

Lindsey, D.A., Naeser, C.W., Shawe, D.R., 1975. Age of volcanism, intrusion, and mineralization in the Thomas Range, Keg Mountain, and Desert Mountain, western Utah. USGS Journal of Research 3, 597-604.

Ludwig, K.R., 1977. Effect of initial radioactive-daughter disequilibrium on U-Pb isotope apparent ages of young minerals. USGS Journal of Research 5, 663-667.

Ludwig, K. R., 2012. User's Manual for Isoplot 3.75: A geochronological toolkit for Microsoft Excel. Berkeley Geochronology Center Special Publication 5, 75 p.

Mahon, K.I., 1996. The new “York” regression: application of an improved statistical method to geochemistry. International Geology Review 38, 293–303. https://doi.org/10.1080/00206819709465336

Mankinen, E.A., Dalrymple, G.B., 1979. Revised geomagnetic polarity time scale for the interval 0–5 m.y. B.P. Journal of Geophysical Research: Solid Earth 84, 615–626. https://doi.org/10.1029/JB084iB02p00615

Marillo-Sialer, E., Woodhead, J., Hergt, J., Greig, A., Guillong, M., Gleadow, A., Evans, N., Paton, C., 2014. The zircon ‘matrix effect’: evidence for an ablation rate control on the accuracy of U–Pb age determinations by LA-ICP-MS. Journal of Analytical Atomic Spectrometry 29, 981–989. https://doi.org/10.1039/C4JA00008K

Matheus, P., Begét, J., Mason, O., Gelvin-Reymiller, C., 2003. Late Pliocene to late Pleistocene environments preserved at the Palisades site, central Yukon River, Alaska. Quaternary Research 60, 33–43, https://doi.org/10.1016/S0033-5894(03)00091-7.

Matthews, J. V., Westgate, J.A., Ovenden, L., Carter, L.D., Fouch, T., 2003. Stratigraphy, fossils, and age of sediments at the upper pit of the Lost Chicken gold mine: New information on the late Pliocene environment of east central Alaska. Quaternary Research 60, 9–18. https://doi.org/10.1016/S0033-5894(03)00087-5

Matthews, N.E., Vazquez, J.A., Calvert, A.T., 2015. Age of the Lava Creek supereruption and magma chamber assembly at Yellowstone based on 40Ar/39Ar and U-Pb dating of sanidine and zircon crystals. Geochemistry, Geophys. Geosystems 16, 2508–2528. https://doi.org/10.1002/2015GC005881

Matsu’ura, S., Kondo, M., Danhara, T., Sakata, S., Iwano, H., Hirata, T., Kurniawan, I., Setiyabudi, E., Takeshita, Y., Hyodo, M. and Kitaba, I., 2020. Age control of the first appearance datum for Javanese Homo erectus in the Sangiran area. Science, 367(6474), pp.210-214. https://doi.org/10.1126/science.aau8556

McDougall, I., Harrison, T.M., 1999. Geochronology and Thermochronology by the 40Ar/39Ar Method. Oxford University Press, New York. McIntyre,

Mercer, C.M., Hodges, K. V, 2016. ArAR — A software tool to promote the robust comparison of K–Ar and 40Ar/39Ar dates published using different decay, isotopic, and monitor-age parameters. Chem. Geol. 440, 148–163. https://doi.org/10.1016/j.chemgeo.2016.06.020

Naeser, N.D., Naeser, C.W., 1984. Fission-Track Dating, in: Mahaney, W.C. (Ed.), Developments in Palaeontology and Stratigraphy. Elsevier, pp. 87–100. https://doi.org/ 10.1016/S0920-5446(08)70066-9

Ogg, J.G., 2020. Chapter 5 - Geomagnetic Polarity Time Scale, in: Gradstein, F.M., Ogg, James G, Schmitz, M.D., Ogg, G.M.B.T.-G.T.S. 2020 (Eds.), Elsevier, pp. 159–192. https://doi.org/10.1016/B978-0-12-824360-2.00005-X

Orlando, L., Ginolhac, A., Zhang, G., Froese, D., Albrechtsen, A., Stiller, M., Schubert, M., Cappellini, E., Petersen, B., Moltke, I., Johnson, P.L.F., Fumagalli, M., Vilstrup, J.T., Raghavan, M., Korneliussen, T., Malaspinas, A.-S., Vogt, J., Szklarczyk, D., Kelstrup, C.D., Vinther, J., Dolocan, A., Stenderup, J., Velazquez, A.M. V, Cahill, J., Rasmussen, M., Wang, X., Min, J., Zazula, G.D., Seguin-Orlando, A., Mortensen, C., Magnussen, K., Thompson, J.F., Weinstock, J., Gregersen, K., Røed, K.H., Eisenmann, V., Rubin, C.J., Miller, D.C., Antczak, D.F., Bertelsen, M.F., Brunak, S., Al-Rasheid, K.A.S., Ryder, O., Andersson, L., Mundy, J., Krogh, A., Gilbert, M.T.P., Kjær, K., Sicheritz-Ponten, T., Jensen, L.J., Olsen, J. V, Hofreiter, M., Nielsen, R., Shapiro, B., Wang, J., Willerslev, E., 2013. Recalibrating Equus evolution using the genome sequence of an early Middle

Pleistocene horse. Nature 499, 74–78. https://doi.org/10.1038/nature12323

Otiniano, G.A., Porter, T.J., Benowitz, J.A., Bindeman, I.N., Froese, D.G., Jensen, B.J.L., Davies, L.J., Phillips, M.A., 2020. A late Miocene to late Pleistocene reconstruction of precipitation isotopes and climate from hydrated volcanic glass shards and biomarkers in Central Alaska and Yukon. Paleoceanography and Paleoclimatology 35, e2019PA003791. https://doi.org/10.1029/2019PA003791

Paton, C., Woodhead, J.D., Hellstrom, J.C., Hergt, J.M., Greig, A., Maas, R., 2010. Improved laser ablation U-Pb zircon geochronology through robust downhole fractionation correction. Geochemistry, Geophysics, Geosystems 11, Q0AA06. https://doi.org/10.1029/2009GC002618.

Paton, C., Hellstrom, J., Paul, B., Woodhead, J., Hergt, J., 2011. Iolite: Freeware for the visualisation and processing of mass spectrometric data. Journal of Analytical Atomic Spectrometry 26, 2508–2518. https://doi.org/10.1039/C1JA10172B.

Petrus, J.A., Kamber, B.S., 2012. VizualAge: A novel approach to laser ablation ICP-MS U-Pb geochronology data reduction. Geostandards and Geoanalytical Research 36, 247–270. https://doi.org/10.1111/j.1751-908X.2012.00158.x.

Péwé, T.L., 1975. Quaternary stratigraphic nomenclature in unglaciated central Alaska, USGS Professional Paper 835, 1-145. https://doi.org/10.3133/pp862

Péwé, T.L., Westgate, J.A., Preece, S.J., Brown, P.M., Leavitt, S.W., 2009. Late Pliocene Dawson Cut forest bed and new tephrochronological findings in the Gold Hill Loess, east-central Alaska. Geological Society of America Bulletin 121, 294–320. https://doi.org/10.1130/B26323.1

Popa, R.G., Guillong, M., Bachmann, O., Szymanowski, D., Ellis, B., 2020. U-Th zircon dating reveals a correlation between eruptive styles and repose periods at the Nisyros-Yali volcanic area, Greece. Chemical Geology 555, 119830. https://doi.org /10.1016/j.chemgeo.2020.119830

Preece, S.J., Westgate, J.A., Froese, D.G., Pearce, N.J.G., Perkins, W.T., 2011. A catalogue of late Cenozoic tephra beds in the Klondike goldfields and adjacent areas, Yukon Territory. Canadian Journal of Earth Sciences 48, 1386–1418. https://doi.org/10.1139/e10-110

Preece, S.J., Westgate, J.A., Stemper, B.A., Péwé, T.L., 1999. Tephrochronology of late Cenozoic loess at Fairbanks, central Alaska. Geological Society of America Bulletin 111, 71–90. https://doi.org/10.1130/0016-7606(1999)111<0071:TOLCLA>2.3.CO;2

Renne, P.R., Cassata, W.S., Morgan, L.E., 2009. The isotopic composition of atmospheric argon and 40Ar/39Ar geochronology: Time for a change? Quat. Geochronol. 4, 288–298. https://doi.org/10.1016/j.quageo.2009.02.015

Renne, P.R., Mundil, R., Balco, G., Min, K., Ludwig, K.R., 2010. Joint determination of 40K decay constants and 40Ar∗/40K for the Fish Canyon sanidine standard, and improved accuracy for 40Ar/39Ar geochronology. Geochim. Cosmochim. Acta 74, 5349–5367. https://doi.org/10.1016/j.gca.2010.06.017

Renne, P., Balco, G., Ludwig, K., Mundil, R., Min, K., 2011. Response to the comment by W.H. Schwarz et al. on “Joint determination of 40K decay constants and 40Ar∗/40K for the Fish Canyon sanidine standard, and improved accuracy for 40Ar/39Ar geochronology” by P.R. Renne et al. (2010). Geochim. Cosmochim. Acta - Geochim COSMOCHIM ACTA 75, 5097–5100. https://doi.org/10.1016/j.gca.2011.06.021

Reyes, A.V, Froese, D.G., Jensen, B.J.L., 2010a. Permafrost response to last interglacial warming: field evidence from non-glaciated Yukon and Alaska. Quaternary Science Reviews 29, 3256–3274. https://doi.org/10.1016/j.quascirev.2010.07.013

Reyes, A.V., Jensen, B.J.L., Zazula, G.D., Ager, T.A., Kuzmina, S., La Farge, C., Froese, D.G., 2010b. A late-Middle Pleistocene (Marine Isotope Stage 6) vegetated surface buried by Old Crow tephra at the Palisades, interior Alaska. Quaternary Science Reviews 29, 801–811. https://doi.org/10.1016/j.quascirev.2009.12.003

Sakata, S., Hirakawa, S., Iwano, H., Danhara, T., Hirata, T., 2013. Correction of initial disequilibrium on U-Th-Pb system for dating of young zircons. Mineralogical Magazine 77, 2116. https://doi.org/10.1180/minmag.2013.077.5.19

Sakata, S., 2018. A practical method for calculating the U-Pb age of Quaternary zircon: Correction for common Pb and initial disequilibria. Geochemical Journal 52, 281–286. https://doi.org/10.2343/geochemj.2.0508

Sandhu, A.S., Westgate, J.A., Preece, S.J., and Froese, D.G., 2001. Glass-fission-track ages of late Cenozoic distal tephra beds in the Klondike district, Yukon Territory; In, Yukon Exploration and Geology 2000, D.S. Emond and L.H. Weston (eds.), Exploration and Geological Services Division, Yukon, Indian and Northern Affairs Canada, pp. 247-256.

Sandhu, A.S., Westgate, J.A., 1995. The correlation between reduction in fission-track diameter and areal track density in volcanic glass shards and its application in dating tephra beds. Earth and Planetary Science Letters 131, 289–299. https://doi.org/10.1016/0012-821X(95)00022-5

Schaen, A.J., Jicha, B.R., Hodges, K. V, Vermeesch, P., Stelten, M.E., Mercer, C.M., Phillips, D., Rivera, T.A., Jourdan, F., Matchan, E.L., Hemming, S.R., Morgan, L.E., Kelley, S.P., Cassata, W.S., Heizler, M.T., Vasconcelos, P.M., Benowitz, J.A., Koppers, A.A.P., Mark, D.F., Niespolo, E.M., Sprain, C.J., Hames, W.E., Kuiper, K.F., Turrin, B.D., Renne, P.R., Ross, J., Nomade, S., Guillou, H., Webb, L.E., Cohen, B.A., Calvert, A.T., Joyce, N., Ganerød, M., Wijbrans, J., Ishizuka, O., He, H., Ramirez, A., Pfänder, J.A., Lopez-Martínez, M., Qiu, H., Singer, B.S., 2020. Interpreting and reporting 40Ar/39Ar geochronologic data. GSA Bull. 133, 461–487. https://doi.org/10.1130/B35560.1

Schärer, U., 1984. The effect of initial 230Th disequilibrium on young UPb ages: the Makalu case, Himalaya. Earth and Planetary Science Letters 67, 191–204. https://doi.org/10.1016/0012-821X(84)90114-6

Schmieder, M., Kennedy, T., Jourdan, F., Buchner, E., Reimold, W., 2018. A high-precision 40Ar/39Ar age for the Nördlinger Ries impact crater, Germany, and implications for the accurate dating of terrestrial impact events. Geochimica et Cosmochimica Acta 220, 146–157. https://doi.org/10.1016/j.gca.2017.09.036

Schweger, C., Froese, D., White, J.M., Westgate, J.A., 2011. Pre-glacial and interglacial pollen records over the last 3 Ma from northwest Canada: Why do Holocene forests differ from those of previous interglaciations? Quaternary Science Reviews 30, 2124–2133. https://doi.org/10.1016/j.quascirev.2011.01.020

Sharman, G.R., Sharman, J.P., Sylvester, Z., 2018. detritalPy: A Python-based toolset for visualizing and analysing detrital geo-thermochronologic data. The Depositional Record 4, 202–215. https://doi.org/10.1002/dep2.45

Simon, J.I., Renne, P.R., Mundil, R., 2008. Implications of pre-eruptive magmatic histories of zircons for U–Pb geochronology of silicic extrusions. Earth Planet. Sci. Lett. 266, 182–194. https://doi.org/10.1016/j.epsl.2007.11.014

Simonetti, A., Heaman, L.M., Hartlaub, R.P., Creaser, R.A., MacHattie, T.G., Böhm, C., 2005. U–Pb zircon dating by laser ablation-MC-ICP-MS using a new multiple ion counting Faraday collector array. Journal of Analytical Atomic Spectrometry 20, 677–686. The Royal Society of Chemistry. https://doi.org/10.1039/B504465K

Sisson, T.W., Schmitt, A.K., Danišík, M., Calvert, A.T., Pempena, N., Huang, C.-Y., Shen, C.-C., 2019. Age of the dacite of Sunset Amphitheater, a voluminous Pleistocene tephra from Mount Rainier (USA), and implications for Cascade glacial stratigraphy. J. Volcanol. Geotherm. Res. 376, 27–43. https://doi.org/10.1016/j.jvolgeores.2019.03.003

Sláma, J., Košler, J., Condon, D.J., Crowley, J.L., Gerdes, A., Hanchar, J.M., Horstwood, M.S.A., Morris, G.A., Nasdala, L., Norberg, N., Schaltegger, U., Schoene, B., Tubrett, M.N., Whitehouse, M.J. 2008. Plešovice zircon — A new natural reference material for U–Pb and Hf isotopic microanalysis. Chemical Geology 249, 1–35. https://doi.org/10.1016/j.chemgeo.2007.11.005

Sliwinski, J.T., Guillong, M., Liebske, C., Dunkl, I., von Quadt, A., Bachmann, O., 2017. Improved accuracy of LA-ICP-MS U-Pb ages of Cenozoic zircons by alpha dose correction. Chemical Geology 472, 8–21. https://doi.org/10.1016/j.chemgeo.2017.09.014.

Smith, C.A.S., Tarnocai, C., Hughes, O.L., 1986. Pedological investigation of Pleistocene glacial drift surfaces in the central Yukon. Géographie Physique et Quaternaire 40, 29-37. https://doi.org/10.7202/032620ar

Stacey, J.S., Kramers, J.D., 1975. Approximation of terrestrial lead isotope evolution by a two-stage model. Earth and Planetary Science Letters 26, 207–221. https://doi.org/10.1016/0012-821X(75)90088-6

Staudacher, T., Jessberger, E.K., Dominik, B., Kirsten, T., Schaefferh, O.A., 1982. ^{40}Ar-^{39}Ar ages of rocks and glasses from the Nordlinger Ries crater and the temperature history of impact breccias. Journal of Geophysics 51, 1–11. https://doi.org/10.1016/j.gca.2017.09.036

Stelten, M.E., Cooper, K.M., Vazquez, J.A., Calvert, A.T., Glessner, J.J.G., 2015. Mechanisms and Timescales of Generating Eruptible Rhyolitic Magmas at Yellowstone Caldera from Zircon and Sanidine Geochronology and Geochemistry. J. Petrol. 56, 1607–1642. https://doi.org/10.1093/petrology/egv047

Strong, T.R., Driscoll, R.L., 2016. A process for reducing rocks and concentrating heavy minerals. USGS Open-File Report 2016–1022, 16 p., https://doi.org/10.3133/ofr20161022.

Tera, F., Wasserburg, G.J., 1972. U-Th-Pb systematics in three Apollo 14 basalts and the problem of initial Pb in lunar rocks. Earth and Planetary Science Letters 14, 281–304. https://doi.org/10.1016/0012-821X(72)90128-8.

Till, C.B., Vazquez, J.A., Stelten, M.E., Shamloo, H.I., Shaffer, J.S., 2019. Coexisting Discrete Bodies of Rhyolite and Punctuated Volcanism Characterize Yellowstone's Post-Lava Creek Tuff Caldera Evolution. Geochemistry, Geophys. Geosystems 20, 3861–3881. https://doi.org/10.1029/2019GC008321

Vermeesch, P., 2021. Maximum depositional age estimation revisited. Geoscience Frontiers 12, 843–850. https://doi.org/10.1016/j.gsf.2020.08.008

Vermeesch, P., 2018. IsoplotR: A free and open toolbox for geochronology. Geoscience Frontiers 9, 1479–1493. https://doi.org/10.1016/j.gsf.2018.04.001

von Quadt, A., Gallhofer, D., Guillong, M., Peytcheva, I., Waelle, M., Sakata, S., 2014. U-Pb dating of CA/non-CA treated zircons obtained by LA-ICP-MS and CA-TIMS techniques: Impact for their geological interpretation. J. Anal. At. Spectrom. 29, 1618–1629. https://doi.org/10.1039/c4ja00102h

Waythomas, C.F., Lea, P.D., Walter, R.C., 1993. Stratigraphic context of Old Crow tephra, Holitna lowland, interior southwest Alaska. Quaternary Research 40, 20-29. https://doi.org/10.1006/qres.1993.1052

Westgate, J.A., Walter, R.C., Pearce, G.W., Gorton, M.P., 1985. Distribution, stratigraphy, petrochemistry, and palaeomagnetism of the late Pleistocene Old Crow tephra in Alaska and the Yukon. Canadian Journal of Earth Sciences 22, 893–906. https://doi.org/10.1139/e85-093

Westgate, J., 1988. Isothermal plateau fission-track age of the Late Pleistocene Old Crow Tephra, Alaska. Geophysical Research Letters 15, 376–379. https://doi.org/10.1029/GL015i004p00376

Westgate, J.A., 1989. Isothermal plateau fission-track ages of hydrated glass shards from silicic tephra beds. Earth and Planetary Science Letters 95, 226–234. https://doi.org/10.1016/0012-821X(89)90099-X

Westgate, J.A., 2015. Volcanic glass (fission track). In: Rink, W.J., Thompson, J.W. (Eds), Encyclopedia of Scientific Dating Methods. Springer, Dordrecht, Netherlands, pp. 941–946.

https://doi.org/10.1007/978-94-007-6304-3_60

Westgate, J.A., Stemper, B.A., Péwé, T.L., 1990. A 3 m.y. record of Pliocene-Pleistocene loess in interior Alaska. Geology 18, 858–861. https://doi.org/10.1130/0091-

7613(1990)018<0858:AMYROP>2.3.CO;2

Westgate, J.A., Briggs, N.D., 1980. Dating methods of Pleistocene deposits and their problems: V. Tephrochronology and fission-track dating. Geoscience Canada 7, 3-10.

Westgate, J.A., Pearce, G.W., Preece, S.J., Schweger, C.E., Morlan, R.E., Pearce, N.J.G., Perkins, T.W., 2013. Tephrochronology, magnetostratigraphy and mammalian faunas of Middle and Early Pleistocene sediments at two sites on the Old Crow River, northern Yukon Territory, Canada. Quaternary Research 79, 75–85. https://doi.org/10.1016/j.yqres.2012.09.003

Westgate, J.A., Pearce, N.J.G., 2017. Age of some Pleistocene interglacial beds and associated fossils in eastern Beringia defined by fission tracks in glass shards of Chester Bluff tephra. Quaternary Research 88, 152–159. https://doi.org/DOI: 10.1017/qua.2017.30

Westgate, J.A., Preece, S.J., Froese, D.G., Walter, R.C., Sandhu, A.S., Schweger, C.E., 2001. Dating early and middle (Reid) Pleistocene glaciations in Central Yukon by Tephrochronology. Quaternary Research 56, 335–348. https://doi.org/10.1006/qres.2001.2274

Westgate, J.A., Preece, S.J., Jackson, J.E., 2011. Revision of the tephrostratigraphy of the lower Sixtymile River area, Yukon Territory, Canada. Canadian Journal of Earth Sciences 48, 695–701. https://doi.org/10.1139/E10-106

Westgate, J.A., Sandhu, A.S., Preece, S.J., 2003. Age of the gold-bearing White Channel Gravel, Klondike district, Yukon. Yukon Exploration and Geology 2002, 241–250.

White, J.M., Ager, T.A., Adam, D.P., Leopold, E.B., Liu, G., Jetté, H., Schweger, C.E., 1997. An 18 million year record of vegetation and climate change in northwestern Canada and Alaska: Tectonic and global climatic correlates. Palaeogeography, Palaeoclimatology, Palaeoecology 130, 293–306. https://doi.org/10.1016/S0031-0182(96)00146-0

Wiedenbeck, M.A.P.C., Alle, P., Corfu, F.Y., Griffin, W.L., Meier, M., Oberli, F.V., Quadt, A.V., Roddick, J.C., Spiegel, W., 1995. Three natural zircon standards for U-Th-Pb, Lu-Hf, trace element and REE analyses. Geostandards Newsletter 19: 1–23. https://doi.org/10.1111/j.1751-908X.1995.tb00147.x.

Willerslev, E., Davison, J., Moora, M., Zobel, M., Coissac, E., Edwards, M.E., Lorenzen, E.D., Vestergård, M., Gussarova, G., Haile, J., Craine, J., Gielly, L., Boessenkool, S., Epp, L.S., Pearman, P.B., Cheddadi, R., Murray, D., Bråthen, K.A., Yoccoz, N., Binney, H., Cruaud, C., Wincker, P., Goslar, T., Alsos, I.G., Bellemain, E., Brysting, A.K., Elven, R., Sønstebø, J.H., Murton, J., Sher, A., Rasmussen, M., Rønn, R., Mourier, T., Cooper, A., Austin, J., Möller, P., Froese, D., Zazula, G., Pompanon, F., Rioux, D., Niderkorn, V., Tikhonov, A., Savvinov, G., Roberts, R.G., Macphee, R.D.E., Gilbert, M.T.P., Kjær, K.H., Orlando, L., Brochmann, C., Taberlet, P., 2014. Fifty thousand years of Arctic vegetation and megafaunal diet. Nature 506, 47–51. https://doi.org/10.1038/nature1292

Williams, I.S., 1998. U–Th–Pb geochronology by ion microprobe. In: McKibben MA, Shanks III WC, Ridley WI (eds) Applications of microanalytical techniques to understanding mineralizing processes. Reviews in Economic Geology 7, Society of Economic Geologists, Littleton, Special Publication, 1–35. https://doi.org/10.5382/Rev.07.01

Zimmerer, M.J., Lafferty, J., Coble, M.A., 2016. The eruptive and magmatic history of the youngest pulse of volcanism at the Valles caldera: Implications for successfully dating late Quaternary eruptions. J. Volcanol. Geotherm. Res. 310, 50–57. https://doi.org/10.1016/j.jvolgeores.2015.11.021

Chapter 3: Syn-depositional volcanogenic zircons and how to find them: A challenge for detrital zircon geochronology

3.1. Introduction

Uranium-lead (U-Pb) dating of syn-eruptive zircon derived from ash fallout (tephra) has long been used to estimate the timing of deposition in sedimentary successions (e.g., Bitschene and Schmincke, 1990; Ito, 2014; Buryak et al., 2022). One of the fundamental applications of detrital zircon geochronology is to obtain depositional ages for sediments that lack discrete volcanic ash beds and cannot be precisely dated by any other method (e.g. Gebauer et al., 1989; Sylvester et al., 2022). To estimate the time of deposition of sediments lacking discrete tephra layers, detrital zircon geochronology must rely on the assumptions that (i) volcanism and deposition were coeval or near-coeval (ii) the youngest zircon ages represent the timing of eruption and are consistent with other chronological constraints, and (iii) any primary volcanogenic zircons present can be separated from the sediment matrix and dated (Rossignol et al., 2019, Sharman and Malkowski, 2020). When these assumptions are not met, the youngest detrital zircon ages for a stratum can only be considered as a maximum estimate on the timing of deposition and might be much older than the true depositional age.

The potential for sampling of syn-depositional volcanogenic zircon in clastic sediments is controlled by their relative abundance and accurate discrimination of juvenile crystals from the older detrital zircon background. However, little is known about the relationship between zircon size distribution, presence of adhered glass coating around primary volcanogenic grains, and the final zircon age spectrum. Specifically, the presence of adhered glass coating (or devitrified glass/clay for old samples) around zircon is indicative of crystal interaction with the eruptive melt. If the presence of adhered glass around zircon is indicative of volcanogenic origin, then the eruption age zircons can be potentially identified.

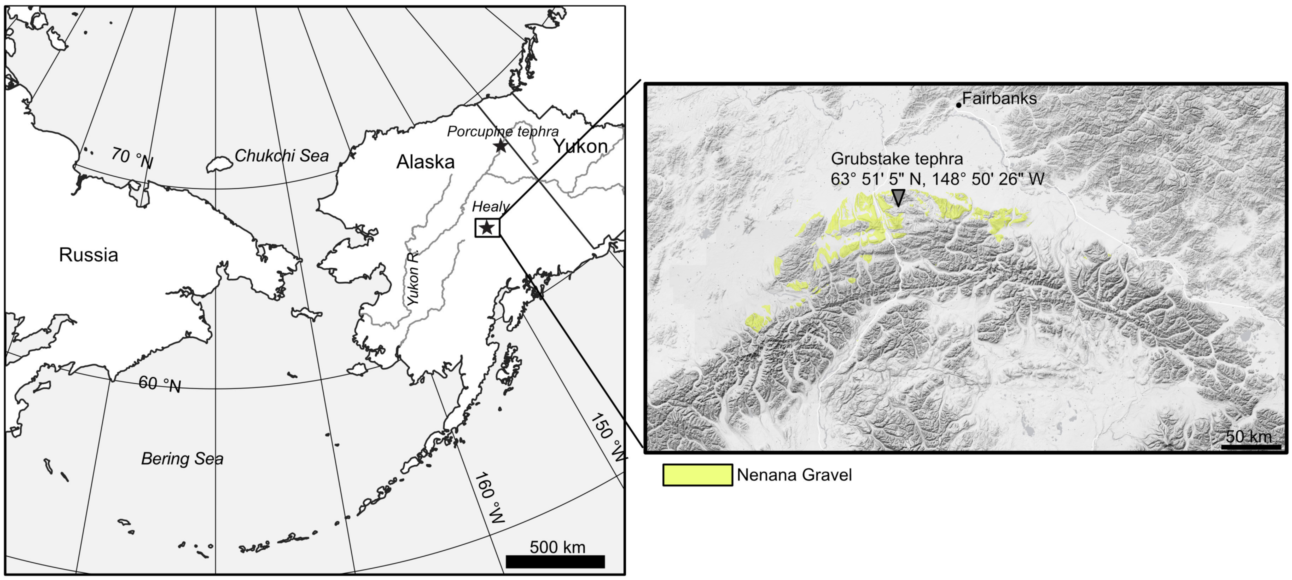

Figure 3.1. *The map of the study area. Star symbols indicate the locations of the Grubstake Formation (Healy area) and Porcupine tephra.*

Here we examine how techniques for recovery of primary volcanogenic zircon from distal fallout ash deposits impart a potential source of bias for depositional age determination from spectra of detrital zircon U-Pb ages. We provide zircon U-Pb ages and grain morphology data for Grubstake tephra, an exceptionally thick Miocene tephra in southern Alaska, and detrital zircon U-Pb ages for stratigraphically and temporally associated Grubstake Formation. We show that volcanogenic zircon size in the detrital record plays an important role for determination of the maximum depositional age that is co-eval with the sedimentation, with implications for regional and global scale detrital studies that rely on the youngest detrital zircon ages to establish sedimentation histories.

3.2. Grubstake Site Background

The Grubstake tephra proximal deposit (6.83 ± 0.11 Ma; $^{40}Ar/^{39}Ar$; revised) is a ~12 m-thick rhyolitic bed at the Tatlanika Creek, Alaska type section (Fig. 3.1.), with glass composition suggesting an Aleutian Arc source during a period of Miocene volcanism (Triplehorn et al., 2000). The Grubstake Formation is the uppermost unit of the Usibelli Group located near Healy, Alaska, and consists of lacustrine deposits interbedded with the Grubstake tephra layer (Fig. 3.1.) (Wahrhaftig, 1987). The Grubstake tephra provides a key maximum age constraint for accelerated erosion of the Alaska Range as recorded by the ~1200 m thick Nenana Gravel that overlies the Grubstake Formation, with erosion and deposition in a foreland basin variously attributed to unroofing of the Alaska Range starting ~6 Ma (Benowitz et al., 2014) or Plio-Pleistocene glacial erosion (Sortor et al., 2021). Grubstake tephra is also an important datum for Miocene paleoclimatic and palynological studies in Alaska (e.g. Leopold and Liu, 1994; Ridgway et al., 2007; Otiniano et al., 2020). Specifically, it provides chronological control on one of the most recent well-documented occurrences of *Metasequoia* fossils in North America found within the Grubstake Formation (Leopold and Liu, 1994).

The revised Grubstake tephra age of 6.83 ± 0.11 Ma is based on a weighted mean of three $^{40}Ar/^{39}Ar$ ages on available data for biotite and plagioclase (Triplehorn et al., 2000). Despite its thickness at its type section, Grubstake tephra has not yet been definitively identified anywhere else in Alaska, though the Porcupine tephra (revised 6.64 ± 0.10 Ma; $^{40}Ar/^{39}Ar$) in northeast Alaska has been proposed as a potentially correlative bed (Fig. 3.1; Kunk et al., 1994; Triplehorn et al., 2000). More curiously, despite the thickness of the tephra, little to no zircon crystals of its age have been found in regional detrital zircon studies (e.g., Brennan and Ridgeway, 2015; Enkelmann et al., 2019).

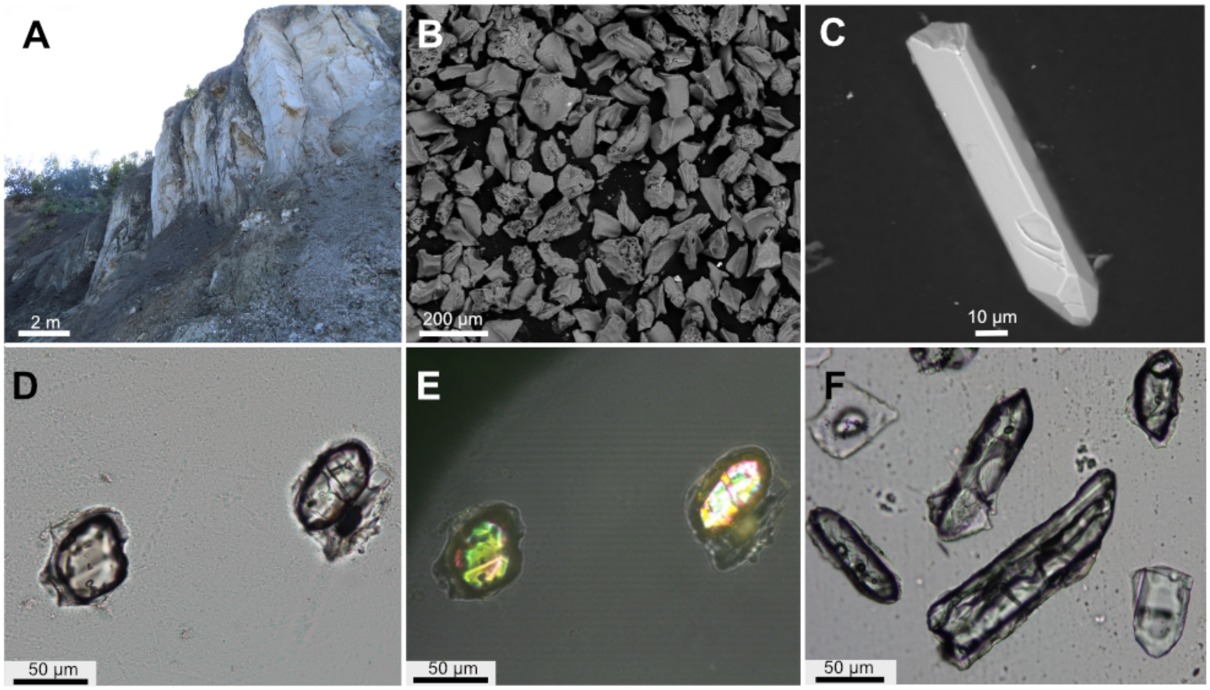

Figure 3.2. *(A) The Grubstake tephra outcrop at Tatlanika Creek, Alaska, USA. (B) The backscatter electron (BSE) image of Grubstake tephra glass shards. Note platy, non-pumiceous shard morphologies. (C) BSE image of a juvenile zircon recovered from distal Eocene ash bed in Giraffe kimberlite core, Northwestern Territories, Canada. The ultra-small grain size and absence of adhered glass is not uncommon for zircon in distal tephra layers. (D-E) Representative transmitted- and polarized-light microscope images of Grubstake tephra zircons and adhered glass. Note, the zircon surface was polished removing the adhered glass from the exposed section of the crystal. (F) Representative transmitted-light microscope images of the distal Old Crow tephra zircon from Palisades West, Alaska, USA. Thick zircon glass coating is common in young or well-preserved tephra. Note on variability in zircon sizes and morphologies.*

3.3. Methods

The Grubstake Formation sample was collected for detrital U-Pb zircon analysis from outcrop on Suntrana Creek near Healy, Alaska. The sample was collected approximately 4 meters up from the creek cut. The Grubstake Formation zircon grains were separated and prepared for LA-ICP-MS analysis at the A2Z laboratory in Viola, Idaho (USA) following Donelick et al. (2005) (Supplemental Table B.2). Briefly, the samples were crushed, sieved through 300 µm nylon mesh, and the <300 µm size fraction washed with tap water and allowed to dry at room temperature. Zircon was separated from other mineral species using a combination of lithium metatungstate (density ~2.9 g/cm^3), Frantz magnetic separator, diiodomethane (density ~3.3 g/cm^3), and hand-panning separation procedures.

The Grubstake tephra was sampled at its type locality at Tatlanika Creek (Fig. 3.2A), 5 m above the base of the ~12 m thick tephra bed. Approximately one kg of Grubstake tephra ash was processed to extract zircon crystals. No water table heavy mineral separation or sample homogenization methods were used for the Grubstake tephra sample. We first followed typical mineral-separation protocols of sieving to isolate the <250 µm fraction followed by methylene iodide (MI) heavy liquid separation on ~50 g aliquots. No Frantz magnetic separation was used due to surface iron oxidation of the glass and minerals. For a second separation, ~0.3 kg of bulk material was dispersed ultrasonically in Calgon solution for seven hours. The dried bulk material was then divided into ~20 g aliquots; each aliquot was sequentially processed in a 250 ml separatory funnel using diluted MI (ρ = ~2500 kg/m^3) followed by full density MI (ρ = 3320 kg/m^3).

A total of 29 tephra zircon crystals were hand-picked from the heavy concentrate under stereoscopic microscope and mounted in epoxy for analysis. Zircon crystals were lightly polished to remove any adhered glass. The grains were analyzed for U-Pb isotope composition using a RESOlution ArF Excimer 193 nm laser ablation system coupled to a Thermo Scientific Element XR magnetic sector-field (SF)-ICP-MS at the Arctic Resources Geochemistry Laboratory, University of Alberta. The same instruments were also used to determine single-shard glass trace-element composition. Glass major-element geochemistry was determined by wavelength dispersive spectrometry on a CAMECA SX100 electron microprobe at University of Alberta. Details of zircon U-Pb dating and glass geochemistry methods are reported in Buryak et al. (2022) and described in the Supplemental Material. All grains morphological characteristics were measured using ImageJ software (Schneider et al., 2012). See detailed methods section for more information (3.6. Supplemental detailed methods).

3.4. Results

Zircon grains are rare in the heavy mineral fraction of Grubstake tephra. They are typically clear, ~20–70 µm long (predominantly silt size) and have consistently high circularity values (0.61 ± 0.23; n=29). All grains, except for two older outliers, have distinct adhered glass coatings with glass:zircon areal ratio up to 2:5 (Fig. 3.2. D-E). Of 21 dated grains, eight of the youngest analyses form a coherent cluster with overlapping uncertainties ranging from 6.6 to 7.5 Ma. The Grubstake tephra zircon U and Th concentrations mostly cluster in relatively restricted ranges of 234 ± 52 ppm and 140 ± 48 ppm, respectively (mean ± 1 s.d.; Table B.1). The older tail of the age spectrum contains three older grains at 10.1, 11.6 and 336.9 Ma suggesting a minor presence of xenocrysts or a detrital component. The youngest coherent zircon age cluster of 8 grains was used to calculate a weighted mean age of 6.81 ± 0.07 Ma (MSWD = 1.5), which is indistinguishable from the revised $^{40}Ar/^{39}Ar$ age of 6.83 ± 0.11 Ma (Fig. 3.3.; Table B.1).

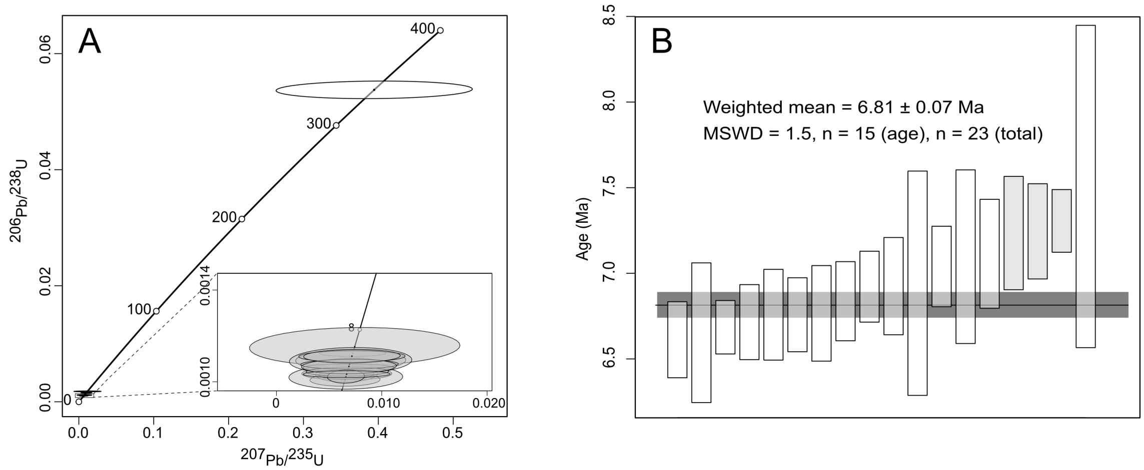

Figure 3.3. *A. The Concordia diagram of all Grubstake tephra zircon U-Pb analyses. Enlarged inset of the youngest U-Pb zircon analyses. marked by box in A. Data is common-Pb corrected using initial lead composition estimated from Stacey and Kramers (1975) lead evolution model. B. The weighted mean U-Pb age for the Grubstake tephra. Analyses in gray are outliers and not used in the weighted mean calculation.*

The Grubstake Formation sediment sample from Suntana Creek, Alaska yielded older grains (n=100) with ages spanning ~10–1000 Ma (Fig. 3.4.). The age peak fitting was done using the algorithms of Galbraith and Green (1990) implemented in IsoplotR software with "auto" setting using Bayes Information Criterion to pick a parsimonious number of components (Vermeesch, 2018). Most Grubstake Formation zircon grains date to the Cretaceous and Paleocene, with modes at ~138 Ma (41%) and ~63 Ma (36%) (Fig. 3.4A). Less pronounced peaks are found at ~10 Ma (2%), ~334 Ma (16%), and ~1080 Ma (Mesoproterozoic, 5%). No grains younger than 10 Ma were present. Zircon crystals recovered form Grubstake Formation sediments have average diameter of 85 ± 21 µm (predominantly fine sand size; n=100) and high circularity value of 0.69 ± 11 (Fig. 3.4B). Very few silt sized grains (<5%) are present.

Glass shards from Grubstake and Porcupine tephra samples (UA4024 and UA1143) are relatively homogenous high-silica rhyolites ranging from ~77.6-79.0 SiO_2 wt%. The tephra beds share some geochemical similarities, including high alkalis (K_2O+Na_2O = ~7-8 wt%) and low FeO_{total} (~0.85–0.64 wt%). However, they can be distinguished based on distinct CaO wt% and trace element compositions (Fig. 3.6.).

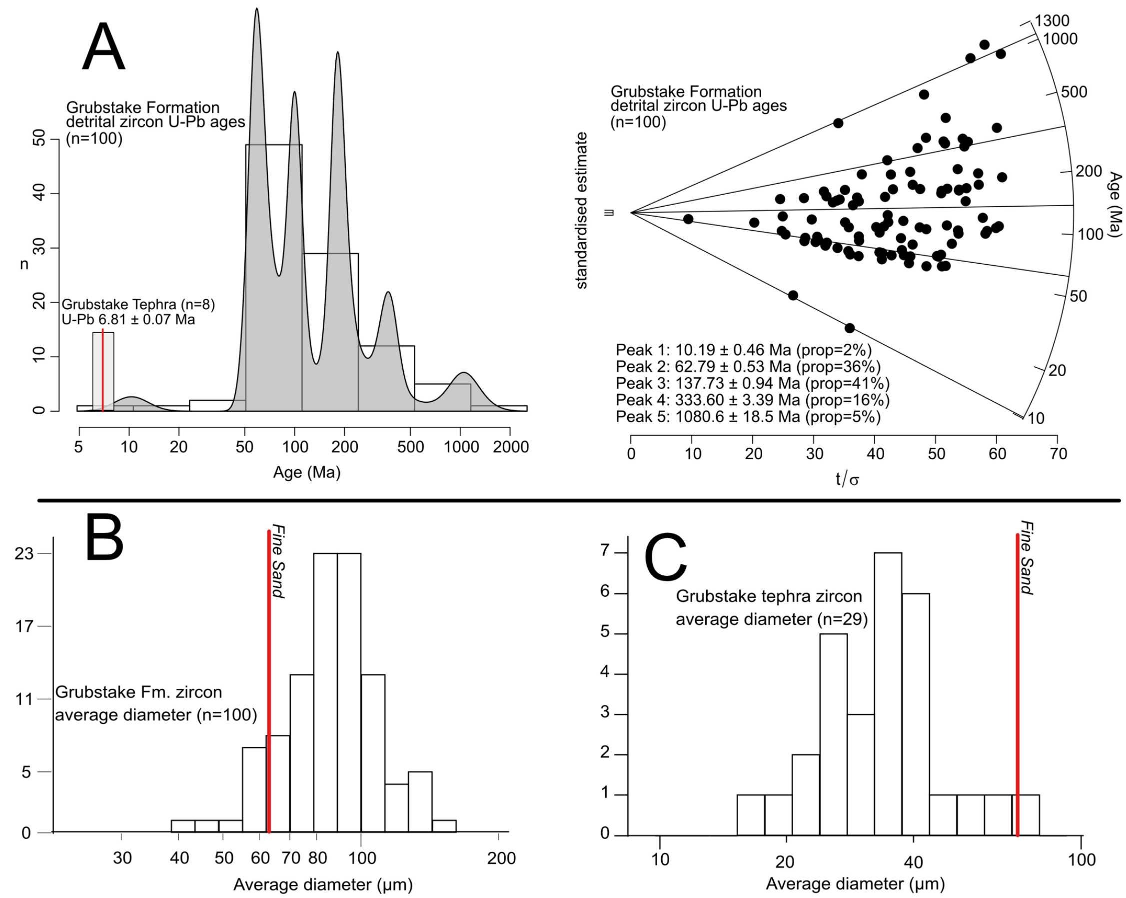

Figure 3.4. *(A) Grubstake Formation detrital zircon ages probability density function and radial plot. Calculation and peak fitting with IsoplotR (Vermeesch, 2018). (B) Mean grain diameter for Grubstake Formation zircon crystals. (C) Mean grain diameter for Grubstake tephra zircon crystals.*

3.5. Discussion

The lack of late Miocene zircon grains in the regional detrital zircon record in south-eastern Alaska can be reflective of limited syn-depositional magmatic sources. However, Grubstake tephra is one of the thickest (~12 meters) and most prominent tephra beds preserved in both Yukon and Alaska. Although Grubstake tephra occurrence appears to be restricted to its type section at Tatlanika Creek, with no known correlative beds in the region, lack of 6-7 Myr syn- or near-depositional magmatic grains separated out at the most proximal sediments is difficult to explain. Though Grubstake tephra is not geochemically correlative to Porcupine tephra, the age and glass geochemistry of the two tephra are similar and likely from the same source region, indicating that active volcanism was present during the late Miocene in the region.

A late Miocene detrital zircon U-Pb age peak at 6-7 Ma is notably absent in the Nenana Gravel which overlays the Grubstake Formation in the northern foothills of the central Alaska Range (Brennan and Ridgeway, 2015) and in Pliocene-Miocene sediments of the Cook Inlet Basin in southern Alaska (Enkelmann et al., 2019). Furthermore, late Miocene zircon is exceedingly rare in fluvial sediments from major river systems in Yukon, with <4% in Yukon River (n=107) and 1% in the lower Tanana River (n=101) of the detrital zircon grains dating between 6 and 7 Myr (i.e. the U-Pb and $^{40}Ar/^{39}Ar$ ages for Grubstake and Porcupine tephra) (Nadin et al., 2022). It is unclear if these ca. 7 Ma zircon ages originated directly from the Grubstake or Porcupine eruptions or were incorporated during tephra admixing with surrounding sediment; regardless, late Miocene ages are very uncommon in the detrital sedimentary record in Alaska and Yukon. Similarly, the Grubstake Formation does not appear to contain syn-depositional zircon ages overlapping with the ~6.8 Ma age of the Grubstake tephra, despite the proximity (within ~40 km) of the sampled outcrops to the tephra exposures. Similarly, despite the abundance of Plio-Pleistocene tephra deposits across the Yukon and Alaska, the detrital volcanogenic signature from these eruptions is also nearly absent in both fluvial and terrestrial detrital zircon records (e.g., Buryak et al., 2022; Nadin et al., 2022).

It is possible syn-depositional magmatic zircon grains might not be present in the detrital zircon component of the sediment due to biases associated sedimentary reworking and transport processes. However, another possibility is that syn-depositional magmatic zircon are present in the detrital component of sediment, but that most of these grains are lost during zircon recovery and concentration, thus biasing the final age distributions towards an older maximum depositional age. Indeed, the efficient and complete recovery of syn-depositional volcanogenic zircon is a major challenge for detrital zircon geochronology (e.g. Sharman et al., 2020). Most studies have focused on sandstones and quartzite, assuming that the sand-sized zircon grains might contain a syn-depositional volcanogenic zircon component. The silt-sized particles, which are the main constituents of mudstones, are much more difficult to separate and date, but might have more potential to contain distal volcanic eruption airfall zircon populations that represent the time of deposition of these rocks (e.g., Sylvester et al., 2022; Sundell et al., 2024).

The autocrystic zircon abundance in the volcanic plume is the main control for the potential of these crystals being recovered from coeval sediments. However, even if these crystals are abundant, the separation efficiency of volcanogenic zircon can be affected by targeting a coarser size fraction for mineral separation. Silt size zircon grains are dominant in Grubstake tephra (median 34 µm), making their recovery challenging from detrital materials using conventional separation methods that typically isolate the sand size fraction for zircon picking (e.g., Donelick et al., 2005). The grain size variation of primary volcanogenic zircon is likely dependent on the zircon sorting during atmospheric dispersion of fine tephra and pre-eruptive zircon growth conditions.

The adhered glass coating around the grains or the products of glass alteration are not uncommon for volcanogenic crystals. Stokes' law settling times in methylene iodide for zircon particles (ρ = 4650 kg/m^3) with 40% of volume being glass (ρ = 2300 kg/m^3) have a 41% lower settling velocity than zircon without adhered glass. Thus, thick glass coating around small zircon grains might lead to "loss" of some or all of the grains during heavy liquid separation when the adhered glass/zircon ratio is large by being pulled upward with more rapidly ascending glass. Similarly, the devitrified glass/clay coating can lead to inefficiencies in heavy liquid flotation methods or, in case of iron oxidation of clays, loss of grains during magnetic separation. Adhered glass is a potential useful marker in determining grains that were in contact with recent melt but is not always preserved around the grains in heavily reworked or weathered samples and does not aid in discrimination between autocrystic, antecrystic or xenocrystic origin of the zircon. The usefulness of adhered glass as a marker to identify juvenile grains is especially complicated for volcanic samples that incorporate zircon cargo released from melting of fully solidified portion of the reservoir or incorporation of xenocrystic minerals from the host and cover rocks during the eruption. Notably, the zircon grains that have distinct adhered glass may yield compatible crystallization (U-Pb, U-Th) and cooling ages ((U-Th)/He) that are much older than the eruption (dubbed *vetucrysts*) because of incomplete resetting or older surficial grain incorporation during the eruption. Morphology, the degree of surface abrasion, and the color of the zircon grains are not always a useful characteristic when determining origin of the grain and often do not allow for clear discrimination of the detrital grains using this criterion (e.g., Burgess et al., 2019; Buryak et al., 2022; Schmitt et al., 2023). However, in Yukon and Alaskan tephra, presence of zircon surface abrasion is often more characteristic of the detrital origin in a group of idiomorphic grains. Taken together, these factors might be the source of bias when estimating the presence of syn-depositional magmatic grains and might account, at least in part, for the rarity of the 6-7 million grains in detrital zircon studies in the region.

Other factors that might influence the accuracy of analyses of tiny syn-depositional zircon grains include instrumental challenges, requiring a small ion or laser beam for U-Pb analyses by LA-ICP-MS or SIMS to produce sufficiently precise and accurate ages and is especially challenging for Miocene-Pleistocene age zircons. Furthermore, chemical abrasion has been shown to reduce or eliminate the effects of Pb-loss in zircon U-Pb geochronology but will also remove any potentially preserved adhered glass coating around grains or dissolve very small zircon grains (e.g., Donaghy et al., 2023). The spatial distribution and the potential capture mechanisms of volcanic ash fall can have a direct effect on the preservation of volcanogenic zircon signal in otherwise tephra devoid sediments. For example, sediments with a longer exposure time (e.g., paleosols) might be a better target for zircon extraction than dynamic fluvial or eolian deposits (e.g., Sitek et al., 2017).

Taken together, the recovery of syn-depositional volcanogenic zircon crystals from detrital materials is challenging due to the typically small size of the distal crystals and low volcanogenic zircon abundance. Additionally, the analytical challenges associated with dating of small zircon crystals can further complicate accurate determination of their ages. Further investigations into relationship between size, morphology, age of volcanogenic zircon crystals and distance from eruptive source will aid with their identification, and prompt more effective recovery of syn-depositional age zircon grains from a suite of pre-depositional detrital grains.

3.6. Supplemental detailed methods

Grubstake tephra SF-ICP-MS zircon U-Pb methods

The zircon U-Pb analyses were performed at University of Alberta in the Arctic Resources Geochemistry Laboratory using a RESOlution ArF 193 nm laser ablation system coupled to a Thermo Scientific Element XR magnetic sector-field (SF)-ICP-MS. Zircon crystals were ablated using 23 µm beam for 35 seconds with the laser configured to a repetition rate of 5 Hz and energy density of ~ 3 J/cm^2. Data were collected for ^{202}Hg, ^{204}Pb, ^{206}Pb, ^{207}Pb, ^{208}Pb, ^{235}U using the ion counting modes of the SEM detector, for ^{232}Th using triple detection mode, and for Pb using analog mode. Dwell times were 10 ms (masses 202, 204), 20 ms (masses 208, 232, 235, 238), 40 ms (mass 206) and 50 ms (mass 207). The primary standard reference sample 91500 (1062.4 ± 0.4 Ma; Wiedenbeck et al., 1995) and secondary zircon reference materials GJ-1 (608.5 ± 0.4 Ma; Jackson et al., 2004), Plešovice (337.1 ± 0.4 Ma; Sláma et al., 2008) and Bishop Tuff (0.767 ± 0.001 Ma; Crowley et al., 2007; Chamberlain et al., 2014; Ickert et al., 2015) were analyzed before and after each set of 10–20 unknowns to monitor U–Pb fractionation, reproducibility, and instrument drift. The 91500, GJ-1, Plešovice, and Bishop Tuff yielded weighted mean ^{206}Pb-^{238}U ages of 1062.2 ± 2.4 Ma (MSWD = 0.5, n = 15), 600.3 ± 3.2 Ma (MSWD = 0.28, n =6), 338.4 ± 1.35 Ma (MSWD = 1.2, n = 9), and 0.756 ± 0.010 Ma (MSWD = 0.44, n = 8) respectively (Table 3.1.).

The ^{206}Pb/^{238}U external reproducibility for these standards is ~1% (2rsd), with MSWD values for the entire suite of analyses within the permissible range at 95% confidence level for the single population of replicated analyses (Mahon, 1996). All zircon analyses were corrected for common-Pb following the "^{207}Pb-method" (Williams, 1998), with initial-Pb composition estimated from the Stacey and Kramers (1975) lead evolution model. The ages are reported with

2σ uncertainties (standard error at 95% confidence level). The deposition age was calculated using the weighted mean of the youngest ages overlapping at 95% confidence level.

Table 3.1. Grubstake tephra LA-ICP-MS operating conditions and methodology.

Laboratory name and Samples	
Laboratory name	Arctic Resources Geochemistry Laboratory, University of Alberta, Canada
Sample type/mineral	Zircon
Analysis	U-Pb
Samples	Grubstake Tephra
Sample preparation	Polished mount (2-5 um)
Reference material location	Separate mount
Imaging	Petrographic microscope
Laser Ablation System	
Make, Model & type	RESOlution ArF 193 nm
Ablation cell & volume	Laurin Technic S-155
Laser wavelength (nm)	193
Pulse width (ns)	20
Fluence (J/cm^2)	~3
Repetition rate (Hz)	5
Ablation duration (s)	35
Ablation pit depth (μm)	~10
Spot size (μm)	23
Sampling mode / pattern	Static spot
Carrier gas	He with Ar and N_2 added after the cell
Cell carrier gas flow (l/min)	1.2
ICP-MS Instrument	
Make, Model & type	ThermoScientific Element XR (SF)-ICP-MS.
Sample introduction	Ablation aerosol
RF power (W)	1200
Make-up gas flow (l/min)	Ar = ~0.85, N_2 = 0.02
Detection system	Single electron multiplier ion counter
Masses measured	202,204, 206, 207, 208, 232, 235, 238
IC Dead time (ns)	16
Data Processing	
Gas blank	Baseline measured 15 seconds prior to each analysis
Calibration strategy	91500 used as primary reference material, Plesovice, GJ-1 and Bishop Tuff used as secondary validation.
Data processing package used / Correction for LIEF	Iolite (Paton et al., 2011) for mass bias correction, data normalization, integration time selection
Mass discrimination	Normalization to primary reference material
Uncertainty level & propagation	Analytical uncertainties are reported as absolute 2S.E (95% confidence level) propagated by quadratic addition. Reproducibility of reference material uncertainty is propagated.

Grubstake Formation LA-ICP-MS zircon U-Pb methods

Grubstake formation zircon grains were isolated and prepared for LA-ICP-MS analysis using standard procedures combined with specific customized procedures described by Donelick et al. (2005). Samples were crushed, sieved through 300 µm nylon mesh, and the <300 µm size fraction washed with tap water and allowed to dry at room temperature. Zircon was separated from other mineral species using a combination of lithium metatungstate (density ~2.9 g/cm^3), Frantz magnetic separator, diiodomethane (density ~3.3 g/cm^3), and hand-panning separation procedures. Epoxy wafers (~1 cm x 1 cm) containing zircon grains for LA-ICP-MS were polished manually using 3.0 µm and 0.3 µm Al_2O_3 slurries to expose internal zircon grain surfaces. The polished zircon grain surfaces were washed in 5.5 M HNO_3 for 20 s at 21° C prior to introduction into the laser system sample cell.

LA-ICP-MS data collection was performed at the A2Z laboratory in Viola, Idaho. Individual zircon grains were targeted for data collection using a Resonetics RESOlution M-50 193 nm solid-state laser ablation system using a 30 µm diameter laser spot size, 5 Hz laser firing rate, and ultra-high purity He as the carrier gas. Isotopic analyses of the ablated zircon material were performed using an Agilent 7700x quadrapole mass spectrometer using high purity Ar as the plasma gas. The following masses (in amu) were monitored for 0.005 s each in pulse detection mode: 202, 204, 206, 207, 208, 232, 235, and 238. At time = 0.0 s, the mass spectrometer began monitoring signal intensities; at time = 6.0 s, the laser began ablating zircon material; at time = 20.0 s, the laser was turned off and the mass spectrometer stopped monitoring signal intensities. A total of 30 data scans were collected for each zircon spot analyzed, comprising approximately four background scans, approximately four transition scans between background and background + signal, and approximately 22 background + signal scans. Detrital zircon U-Pb data for Grubstake Formation is summarized in Supplemental Table B.2.

$^{40}Ar/^{39}Ar$ methods

We recalculated the previously published $^{40}Ar/^{39}Ar$ ages for the Grubstake tephra bed (Triplehorn et al., 2000) studied here using an age for Bern4B biotite (17.33 ± 0.2 Ma; Hall et al., 1984) and updated K decay constants (Renne et al., 2010) using the University of Alaska, Fairbanks (UAF) geochronology inhouse software (e.g., Benowitz et al., 2014) (Supplemental Table B.3-B.4). A note in the UAF archives indicates isotopic data for 7 of the 3 analyses used to calculate an age for Triplehorn et al. (2000) were lost during a hardware failure before the 2000 publication. Hence, we were only able to recalculate the three (two biotite and one plagioclase) analyses that had complete results. All reported $^{40}Ar/^{39}Ar$ ages in this paper are reported with 2σ uncertainty. We do not account for changes in the mass discrimination correction that would result from changes in the accepted Ar isotopic abundance values. However, these corrections, if made, would not affect the age determination significantly (Renne et al., 2009). Following expected reporting requirements (Schaen et al., 2021), Triplehorn et al. (2000) applied a $^{40}Ar/^{39}Ar$ atmospheric ratio of 295.5 ± 0 Ma (Dalrymple, 1969; Steigerand Jäger, 1977) during age determination.

We also recalculated the previously published $^{40}Ar/^{39}Ar$ ages (two biotite and one plagioclase) for the Porcupine Creek River tephra bed (Kunk and Cortesini, 1992) using the currently accepted age for Fish Canyon Tuff (28.294 ± 0.036 Ma; Renne et al., 2011) and updated K decay constants (Renne et al., 2010) using the recalculation software ArAR (Mercer and Hodges, 2016) (Supplemental Table B.3-B.4). All reported $^{40}Ar/^{39}Ar$ ages in this paper are reported with 2σ uncertainty. We do not account for changes in the mass discrimination correction that would result from changes in the accepted Ar isotopic abundance values given there is no practical way to revise legacy data for changes in mass discrimination correction (Mercer and Hodges, 2016). However, as noted above, these corrections would not affect the age determination significantly (Renne et al., 2009). Following expected reporting requirements (Schaen et al., 2020), Kunk and Cortesini (1992) applied a $^{40}Ar/^{39}Ar$ atmospheric ratio of 295.5 ± 0 Ma (Dalrymple, 1969; Steigerand Jäger, 1977) during age determination. We use Isoplot (Ludwig, 2012) to calculate weighted average ages for the three $^{40}Ar/^{39}Ar$ ages from the Porcupine Creek River tephra bed and the Grubstake tephra beds (Fig. 3.5.).

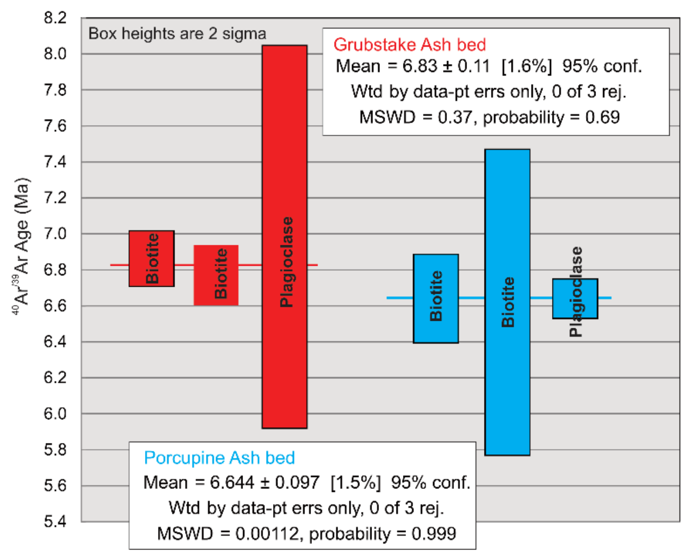

Figure 3.5. *The revised weighted mean* $^{40}Ar/^{39}Ar$ *ages for Grubstake and Porcupine tephra beds.*

Volcanic glass geochemistry

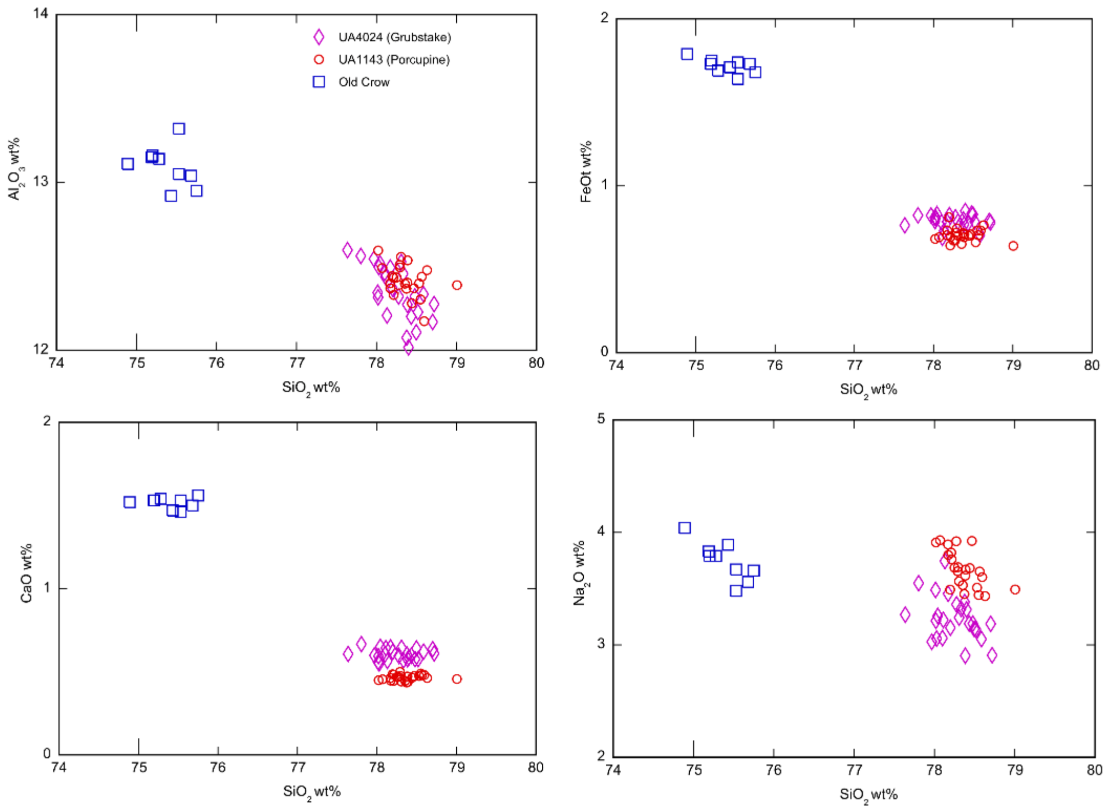

Figure 3.6. *Major element geochemistry for Grubstake, Porcupine and Old Crow tephra.*

Single shard glass major-element geochemistry was determined by wavelength dispersive spectrometry on a JEOL 8900 electron microprobe at University of Alberta using 15 keV accelerating voltage, 6 nA beam current, and 5 µm beam diameter. The software Probe for EPMA (Donovan et al., 2015) was used to correct for any potential Na-loss using time-dependent intensity corrections (e.g., Jensen et al., 2021). Two secondary reference materials, Lipari obsidian (ID 3506) and Old Crow tephra glass (Kuehn et al., 2011), were run concurrently with all samples to assure proper calibration. All data were normalized to 100% on a water-free basis.

Trace-element compositions were determined by LA-ICP-MS using a RESOlution ArF 193 nm excimer laser ablation system coupled to a Thermo Scientific Element XR Sector Field (SF)-ICP-MS at the University of Alberta Arctic Resources Geochemistry Laboratory. Individual glass shards were analyzed with a 10 or 23 µm diameter beam at 2.8 J/cm^2 energy density (measured at the ablation site), 5 Hz repetition rate, and 20 s ablation time. ^{29}Si was used as an internal standard and the instrument was calibrated against NIST SRM 612. NIST SRM 610, ATHO-G were analyzed as secondary standards and reference materials to monitor accuracy and analytical reproducibility. All data is available in Supplemental tables B.6 and B.7.

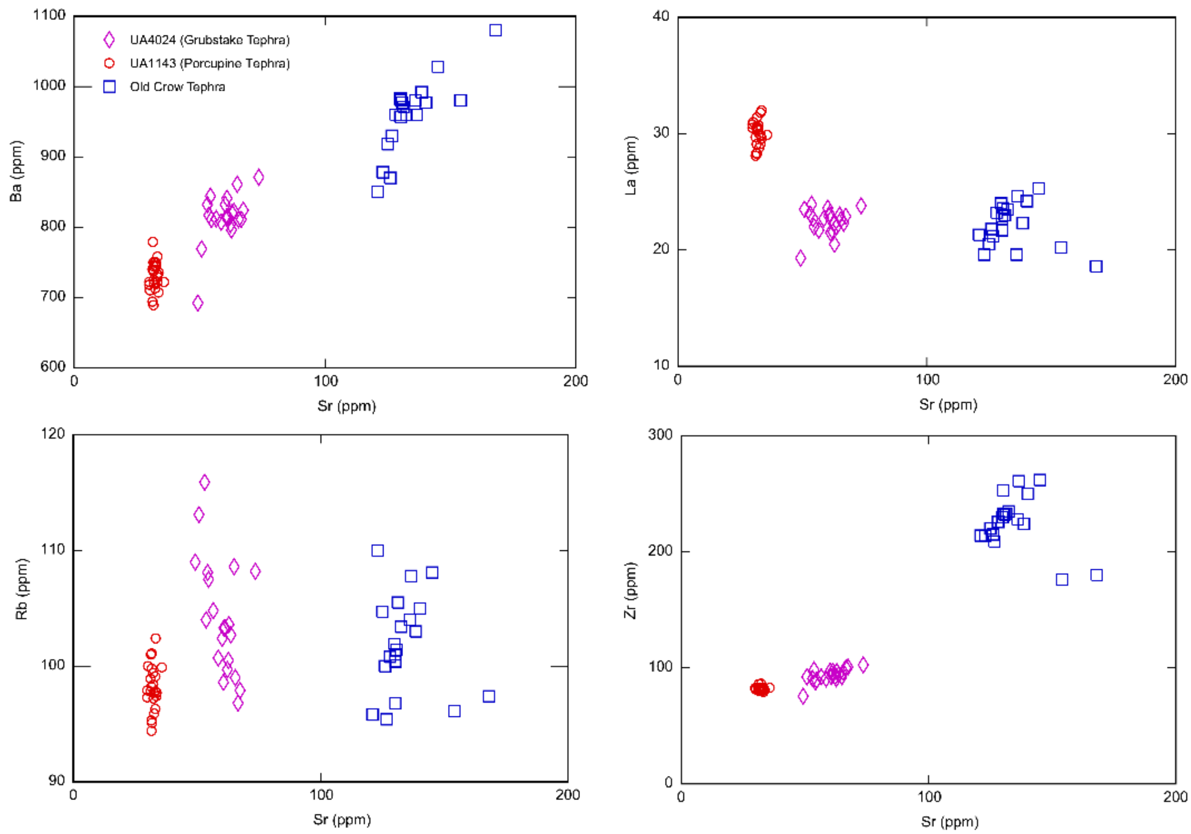

Figure 3.7. *Trace elements geochemistry for Grubstake, Porcupine and Old Crow tephra.*

Grubstake and Porcupine tephra grain size analysis

The tephra grain sizes for Grubstake and Porcupine tephra were completed using the Malvern Mastersizer 3000 integrating the Mie theory to accurately determine particle size distributions (Bohren & Huffman, 1983). Prior to analysis the samples were treated with 0.2% $(NaPO_3)_6$ (Calgon) and mixed gently for 5 minutes before analysis to prevent flocculation of fine-grained particles. After, samples were added to a beaker with 800 mL of deionized water until an obscuration of 14-15% was achieved.

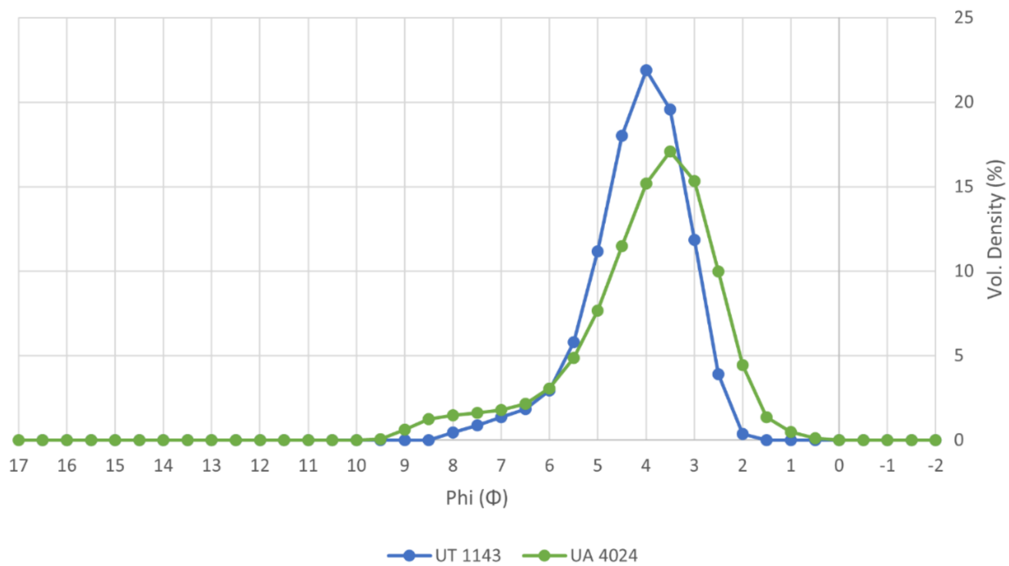

Figure 3.8. *Bulk grain size distributions for Porcupine tephra (UT1143) and Grubstake tephra (UA4024).*

The optical properties used for each analysis were obtained using the Optical Property Optimizer function on the Mastersizer 3000. This process allows the software to scan acquired data and provide refractive and imaginary indices of the best fit based on the intrinsic heterogeneity of tephra deposits coupled with the optical characteristics (Scheidegger et al., 1982; Riehle et al., 2000).

Table 3.2. The optical properties employed during analyses for samples UT1143 and UA4024. The weighted residual indicates the proximity of refractive and absorption indices to the optimal fit. A weighted residual below 1% suggests a good data fit.

	UT1143 (Porcupine tephra)		**UA 4024 (Grubstake tephra)**	
Laser Colour	Refractive Index(n)	Absorption Index (k)	Refractive Index(n)	Absorption Index (k)
Red	1.54	0.001	1.47	0.001
Blue	1.53	0.0003	1.67	0.001
Wtd. Residual		0.21%		0.17%

The median grain sizes for UT1143 (Porcupine tephra) and UA4024 (Grubstake tephra) are 4.13 Φ and 4.33 Φ, respectively, indicating a slightly finer median size for the latter. The statistical parameters further align the two samples. Both UT1143 and UA4024 demonstrate a notably leptokurtic distribution, indicative of heavier tails and more extreme values. Additionally, both UT1143 and UA4024 exhibit a fine skewed distribution. The standard deviation values highlight variations between the two samples. Distinct sorting characteristics are observed, with UT1143 displaying poor sorting and UA4024 showing moderate sorting. The comparative analysis of percentiles reveals differences in particle size distribution. UA4024 encompasses a broader range of particle sizes as indicated by its lower d_{10} and higher d_{90} values compared to UA4024. Despite these differences, the mean grain sizes remain quite similar, with UT1143 at 4.40 Φ and UA4024 at 4.20 Φ.

3.7. References

Benowitz, J.A., Layer, P.W., and Vanlaningham, S., 2014, Persistent long-term (c. 24 Ma) exhumation in the Eastern Alaska Range constrained by stacked thermochronology: Geological Society, London, Special Publications, v. 378, p. 225–243, doi:10.1144/SP378.12.

Bitschene, P.R., and Schmincke, H.-U., 1990, Fallout Tephra Layers: Composition and Significance, in Heling, D., Rothe, P., Förstner, U., and Stoffers, P. eds., Sediments and Environmental Geochemistry: Selected Aspects and Case Histories, Berlin, Heidelberg, Springer, p. 48–82, doi:10.1007/978-3-642-75097-7_4.

Bohren, C.F., and Huffman, D.R., 1983, Absorption and scattering of light by small particles:, https://ui.adsabs.harvard.edu/abs/1983uaz..rept.....B (accessed October 2023).

Brennan, P.R.K., and Ridgway, K.D., 2015, Detrital zircon record of Neogene exhumation of the central Alaska Range: A far-field upper plate response to flat-slab subduction: GSA Bulletin, v. 127, p. 945–961, doi:10.1130/B31164.1.

Burgess, S.D., Coble, M.A., Vazquez, J.A., Coombs, M.L., and Wallace, K.L., 2019, On the eruption age and provenance of the Old Crow tephra: Quaternary Science Reviews, v. 207, p. 64–79, doi:10.1016/j.quascirev.2018.12.026.

Buryak, S.D., Reyes, A.V., Jensen, B.J.L., Davies, J.H.F.L., Westgate, J.A., DuFrane, S.A., Luo, Y., Froese, D.G., Pearson, D.G., and Benowitz, J.A., 2022, Laser-ablation ICP-MS zircon U-Pb ages for key Pliocene-Pleistocene tephra beds in unglaciated Yukon and Alaska: Quaternary Geochronology, p. 101398, doi:10.1016/j.quageo.2022.101398.

Chamberlain, K.J., Wilson, C.J.N., Wooden, J.L., Charlier, B.L.A., and Ireland, T.R., 2014, New Perspectives on the Bishop Tuff from Zircon Textures, Ages and Trace Elements: Journal of Petrology, v. 55, p. 395–426, doi:10.1093/petrology/egt072.

Crowley, J.L., Schoene, B., and Bowring, S.A., 2007, U-Pb dating of zircon in the Bishop Tuff at the millennial scale: Geology, v. 35, p. 1123–1126, doi:10.1130/G24017A.1.

Dalrymple, G.B., 1969, 40Ar/36Ar analyses of historic lava flows: Earth and Planetary Science Letters, v. 6, p. 47–55, doi:10.1016/0012-821X(69)90160-5.

Donaghy, E.E., Eddy, M.P., Moreno, F., and Ibañez-Mejia, M., 2023, Increased accuracy and precision in igneous and detrital zircon geochronology using CA-LA-ICPMS: Geochronological data analysis/statistics/modelling preprint, doi:10.5194/gchron-2023-20.

Donelick, R.A., O'Sullivan, P.B., and Ketcham, R.A., 2005, Apatite Fission-Track Analysis: Reviews in Mineralogy and Geochemistry, v. 58, p. 49–94, doi:10.2138/rmg.2005.58.3.

Donovan, J.J., Kremser, D., Fournelle, J.H. and Goemann, K., 2015, Probe for EPMA: Acquisition, automation and analysis, version 11: Eugene, Oregon, Probe Software. Inc., http://www. probesoftware. com.

Enkelmann, E., Sanchez Lohff, S.K., and Finzel, E.S., 2019, Detrital zircon double-dating of forearc basin strata reveals magmatic, exhumational, and thermal history of sediment source areas: GSA Bulletin, v. 131, p. 1364–1384, doi:10.1130/B35043.1.

Galbraith, R.F., and Green, P.F., 1990, Estimating the component ages in a finite mixture: International Journal of Radiation Applications and Instrumentation. Part D. Nuclear Tracks and Radiation Measurements, v. 17, p. 197–206, doi:10.1016/1359-0189(90)90035-V.

Gebauer, D., Williams, I.S., Compston, W., and Grünenfelder, M., 1989, The development of the Central European continental crust since the Early Archaean based on conventional and ion-microprobe dating of up to 3.84 b.y. old detrital zircons: Tectonophysics, v. 157, p. 81–96, doi:10.1016/0040-1951(89)90342-9.

Hall, C.M., Walter, R.C., Westgate, J.A., and York, D., 1984, Geochronology, stratigraphy and geochemistry of Cindery Tuff in Pliocene hominid-bearing sediments of the Middle Awash, Ethiopia: Nature, v. 308, p. 26–31, doi:10.1038/308026a0.

Ickert, R.B., Mundil, R., Magee, C.W., and Mulcahy, S.R., 2015, The U-Th-Pb systematics of zircon from the Bishop Tuff: A case study in challenges to high-precision Pb/U geochronology at the millennial scale: Geochimica et Cosmochimica Acta, v. 168, p. 88–110, doi:10.1016/j.gca.2015.07.018.

Ito, H., 2014, Zircon U–Th–Pb dating using LA-ICP-MS: Simultaneous U–Pb and U–Th dating on the 0.1Ma Toya Tephra, Japan: Journal of Volcanology and Geothermal Research, v. 289, p. 210–223, doi:10.1016/j.jvolgeores.2014.11.002.

Jackson, S.E., Pearson, N.J., Griffin, W.L., and Belousova, E.A., 2004, The application of laser ablation-inductively coupled plasma-mass spectrometry to in situ U–Pb zircon geochronology: Chemical Geology, v. 211, p. 47–69, doi:10.1016/j.chemgeo.2004.06.017.

Jensen, B.J.L. et al., 2021, A latest Pleistocene and Holocene composite tephrostratigraphic framework for northeastern North America: Quaternary Science Reviews, v. 272, p. 107-242, doi:10.1016/j.quascirev.2021.107242.

Kuehn, S.C., Froese, D.G., and Shane, P.A.R., 2011, The INTAV intercomparison of electron-beam microanalysis of glass by tephrochronology laboratories: Results and recommendations: Quaternary International, v. 246, p. 19–47, doi:10.1016/j.quaint.2011.08.022.

Kunk, M.J., and Cortesini, H., Jr., 1992, 40Ar/39Ar age-spectrum data for whole rock basalts, and plagioclase and biotite from tephra; a traverse down the Porcupine River, east-central Alaska: U.S. Geological Survey Open-File Report 92-701, 81 p.

Kunk, M.J., Rieck, H., Fouch, T.D., and Carter, L.D., 1994, $^{40}Ar/^{39}Ar$ age constraints on neogene sedimentary beds, Upper Ramparts, half-way Pillar and Canyon village sites, Porcupine river, east-central Alaska: Quaternary International, v. 22–23, p. 31–42, doi:10.1016/1040-6182(94)90005-1.

Leopold, E.B., and Liu, G., 1994, A long pollen sequence of Neogene age, Alaska range: Quaternary International, v. 22–23, p. 103–140, doi:10.1016/1040-6182(94)90009-4.

Ludwig, K.R., 2012, User's Manual for Isoplot 3.75: A geochronological toolkit for Microsoft Excel: Berkeley Geochronology Center Special Publication, v. 5, p. 75.

Mahon, K.I., 1996, The New "York" Regression: Application of an Improved Statistical Method to Geochemistry: International Geology Review, v. 38, p. 293–303, doi:10.1080/00206819709465336.

Mercer, C.M., and Hodges, K.V., 2016, ArAR — A software tool to promote the robust comparison of K–Ar and 40Ar/39Ar dates published using different decay, isotopic, and monitor-age parameters: Chemical Geology, v. 440, p. 148–163, doi:10.1016/j.chemgeo.2016.06.020.

Nadin, E., Goddard, S., Benowitz, J., and Sullivan, P.O., 2022, Blowing in the late Cenozoic wind d detrital zircon river contributions to an interior Alaska loess deposit: v. 275, doi:10.1016/j.quascirev.2021.107266.

Otiniano, G.A., Porter, T.J., Benowitz, J.A., Bindeman, I.N., Froese, D.G., Jensen, B.J.L., Davies, L.J., and Phillips, M.A., 2020, A Late Miocene to Late Pleistocene Reconstruction of Precipitation Isotopes and Climate From Hydrated Volcanic Glass Shards and Biomarkers in Central Alaska and Yukon: Paleoceanography and Paleoclimatology, v. 35, p. e2019PA003791, doi:10.1029/2019PA003791.

Renne, P.R., Balco, G., Ludwig, K.R., Mundil, R., and Min, K., 2011, Response to the comment by W.H. Schwarz et al. on "Joint determination of 40K decay constants and 40Ar*/40K for the Fish Canyon sanidine standard, and improved accuracy for 40Ar/39Ar geochronology" by P.R. Renne et al. (2010): Geochimica et Cosmochimica Acta, v. 75, p. 5097–5100, doi:10.1016/j.gca.2011.06.021.

Renne, P.R., Mundil, R., Balco, G., Min, K., and Ludwig, K.R., 2010, Joint determination of 40K decay constants and 40Ar*/40K for the Fish Canyon sanidine standard, and improved accuracy for 40Ar/39Ar geochronology: Geochimica et Cosmochimica Acta, v. 74, p. 5349–5367, doi:10.1016/j.gca.2010.06.017.

Renne, P.R., Cassata, W.S., and Morgan, L.E., 2009, The isotopic composition of atmospheric argon and 40Ar/39Ar geochronology: Time for a change? Quaternary Geochronology, v. 4, p. 288–298, doi:10.1016/j.quageo.2009.02.015.

Riehle, J.R., Dumond, Don.E., Meyer, C.E., and Schaaf, J.M., 2000, Tephrochronology of the Brooks River Archaeological District, Katmai National Park and Preserve, Alaska: what can and cannot be done with tephra deposits: Geological Society, London, Special Publications, v. 171, p. 245–266, doi:10.1144/GSL.SP.2000.171.01.19.

Rossignol, C. et al., 2019, Using volcaniclastic rocks to constrain sedimentation ages: To what extent are volcanism and sedimentation synchronous? Sedimentary Geology, v. 381, p. 46–64, doi:10.1016/j.sedgeo.2018.12.010.

Schneider, C.A., Rasband, W.S., Eliceiri, K.W., 2012. NIH Image to ImageJ: 25 years of image analysis. Nat Methods 9, 671–675. https://doi.org/10.1038/nmeth.2089

Schmitt, A.K., Clementz, M.T., Lovelace, D.M., and Chamberlain, K.R., 2023, Natural Trap Cave tephra correlation to Yellowstone using U-series (230Th/238U) dates and oxygen isotopes of zircon and chemical composition of adherent glass: Quaternary International, v. 647–648, p. 36–41, doi:10.1016/j.quaint.2022.02.017.

Sharman, G.R., and Malkowski, M.A., 2020, Needles in a haystack: Detrital zircon U-Pb ages and the maximum depositional age of modern global sediment: Earth-Science Reviews, v. 203, p. 103109, doi:10.1016/j.earscirev.2020.103109.

Schaen, A.J. et al., 2020, Interpreting and reporting 40Ar/39Ar geochronologic data: GSA Bulletin, v. 133, p. 461–487, doi:10.1130/B35560.1.

Scheidegger, K.F., Federman, A.N., and Tallman, A.M., 1982, Compositional heterogeneity of tephras from the 1980 eruptions of Mount St. Helens: Journal of Geophysical Research: Solid Earth, v. 87, p. 10861–10881, doi:10.1029/JB087iB13p10861

Sitek, B.C., 2017, Analyzing the Cenozoic Depositional History of Western Kansas: A New Approach Using Paleosol Zircon Geochronology [Thesis]: University of Kansas, https://kuscholarworks.ku.edu/handle/1808/25990 (accessed Old Crow tephraober 2023).

Sláma, J. et al., 2008, Plešovice zircon — A new natural reference material for U–Pb and Hf isotopic microanalysis: Chemical Geology, v. 249, p. 1–35, doi:10.1016/j.chemgeo.2007.11.005.

Sortor, R.N., Goehring, B.M., Bemis, S.P., Ruleman, C.A., Caffee, M.W., Ward, D.J., 2021. Early Pleistocene climate-induced erosion of the Alaska Range formed the Nenana Gravel. Geology 49, 1473–1477. https://doi.org/10.1130/G49094.1

Stacey, J.S., and Kramers, J.D., 1975, Approximation of terrestrial lead isotope evolution by a two-stage model: Earth and Planetary Science Letters, v. 26, p. 207–221, doi: /10.1016/0012-821X(75)90088-6.

Steiger, R.H., and Jäger, E., 1977, Subcommission on geochronology: Convention on the use of decay constants in geo- and cosmochronology: Earth and Planetary Science Letters, v. 36, p. 359–362, doi:10.1016/0012-821X(77)90060-7.

Sylvester, P.J., Souders, A.K., and Liu, R., 2022, Significance of U-Pb detrital zircon geochronology for mudstone provenance: Geology, v. 50, p. 670–675, doi:10.1130/G49684.1.

Sundell, K.E., Gehrels, G.E., D. Blum, M., Saylor, J.E., Pecha, M.E., and Hundley, B.P., 2024, An exploratory study of “large-n” detrital zircon geochronology of the Book Cliffs, UT via rapid (3 s/analysis) U–Pb dating: Basin Research, v. 36, p. e12840, doi:10.1111/bre.12840.

Triplehorn, D.M., Drake, Jeff, and Layer, P.W., 2000, Preliminary $^{40}Ar/^{39}Ar$ ages from two units in the Usibelli Group, Healy, Alaska: New light on some old problems, in Pinney, D.S., and Davis, P.K., eds., Short Notes on Alaska Geology 1999: Alaska Division of Geological & Geophysical Surveys Professional Report 119I, p. 117-127. https://doi.org/10.14509/2691

Vermeesch, P., 2018, IsoplotR: A free and open toolbox for geochronology: Geoscience Frontiers, v. 9, p. 1479–1493, doi:10.1016/j.gsf.2018.04.001.

Wahrhaftig, C., 1987, The Cenozoic section at Suntrana, Alaska, in Hill, M.L. ed., Cordilleran Section of the Geological Society of America, Geological Society of America, v. 1, p. 445-450, doi:10.1130/0-8137-5401-1.445.

Wiedenbeck, M., Allé, P., Corfu, F., Griffin, W. l., Meier, M., Oberli, F., Quadt, A.V., Roddick, J. c., and Spiegel, W., 1995, Three Natural Zircon Standards for U-Th-Pb, Lu-Hf, Trace Element and Ree Analyses: Geostandards Newsletter, v. 19, p. 1–23, doi:10.1111/j.1751-908X.1995.tb00147.x.

Williams, I.S., 1998, U-Th-Pb Geochronology by Ion Microprobe: Society of Economic Geologists, v. 7, 0 p., doi:10.5382/Rev.07.01.

Chapter 4: A refined and simplified SF-LA-ICPMS method for combined single-grain U-Th and U-Th-Pb dating of Quaternary zircon

4.1. Introduction

The ^{238}U–^{230}Th disequilibrium dating method provides chronological information derived from the deviation of the $^{230}Th/^{238}U$ from isotopic equilibrium. This disequilibrium can be generated during crystallization/partial melting and is caused by the different zircon/melt partition coefficients of U and Th (Fukuoka, 1974, Fukuoka and Kigoshi, 1974, Reid et al., 1997). Secular equilibrium is achieved in the ^{238}U decay system once the $^{230}Th/^{238}U$ abundance ratio is equal to the ratio of the ^{238}U (1.55125×10^{-10} y^{-1}, Jaffrey et al., 1971) and ^{230}Th (9.1706×10^{-6} y^{-1}) decay constants (1.692×10^{-5}). This dating method can be useful for dating zircon crystals < 350 ka due to the short half-life of ^{230}Th (~75,000 years, Cheng et al., 2000), with a practical range typically between 5 and 200 ka due to an error multiplication effect as the $^{230}Th/^{238}U$ ratio continues to increase and stabilize after ~150 ka. Zircon ^{238}U–^{230}Th dating requires measurements of the (^{230}Th)/(^{232}Th) and (^{238}U)/(^{232}Th) activity ratios (i.e., abundance decay rate; indicated by parenthesis throughout the text). The slope (*m*) of the two-point isochron between the activity ratios from a zircon to the whole rock (or glass) is typically used to calculate the time, *t*, since crystallization:

$$t = -\frac{\ln(m - 1)}{\lambda_{230}}$$

The λ_{230} is 5.9×10^4 larger than λ_{238}, thus requiring the abundance of ^{230}Th to be 5.9×10^4 times smaller than that of ^{238}U for crystals to be in secular equilibrium, (^{230}Th) = (^{238}U), and even smaller for crystals in disequilibrium, (^{230}Th) < (^{238}U). Thus, accurate measurement of the

^{230}Th abundance is challenging for *in-situ* zircon ^{238}U–^{230}Th dating due to the low abundance of the ^{230}Th peak and potential tailing effects from other masses.

Traditionally, *in-situ* ^{238}U–^{230}Th dating is performed by secondary ionisation mass spectrometry (SIMS) (e.g., Reid et al., 1997; Schmitt, 2007; Burgess et al., 2019; Burgess et al., 2021). This method has been successful in obtaining precise and accurate *in-situ* ^{238}U–^{230}Th ages at high spatial resolution, but this approach comes with the drawback of long analysis time per sample (~20 minutes/analysis; Schmitt, 2011), high operational costs and a scarcity of suitable instrumentation. Additionally, because SIMS mass spectra can be complex, the accuracy of the SIMS measurements are dependent on corrections for various mass spectrometric interferences on $^{230}Th^{16}O^+$ and/or requires a complicated correction procedure (e.g., sensitive high resolution ion microprobe; Marsden et al., 2022).

^{238}U–^{230}Th zircon geochronology using laser ablation inductively coupled plasma mass spectrometry (LA-ICP-MS) is a relatively new method with widespread applicability due to the greater abundance of suitable instrumentation versus SIMS. Ito (2014) utilized sector field (SF) LA-ICP-MS in low resolution mode ($M/\Delta M = 300$) to obtain simultaneous ^{238}U–^{230}Th and ^{238}U–^{206}Pb ages from Quaternary zircons. However, the resulting data was likely inaccurate due the effects of the relatively poor abundance sensitivity of the mass spectrometer analyser system for ^{232}Th and because of polyatomic interferences ($^{90}Zr^{92}Zr^{16}O_3^+$) on ^{230}Th (Guillong et al., 2016). The pioneering work by Guillong et al. (2016) provided a correction scheme to mitigate these issues. This correction method involves a correction for polyatomic oxide interferences ($^{90}Zr^{92}Z^{16}O_3^+$) by (1) measuring the abundance of 228 amu and scaling it to subtract the contribution from mass ^{230}Th; and, (2) removing the mass tailing of $^{232}Th^+$ ions on $^{230}Th^+$ by estimating this contribution from the ablation of a high Th/U mineral (monazite). Niki et al.

(2022) utilized a collision/reaction cell quadrupole femtosecond LA-ICP-MS to minimize contributions of polyatomic oxide interferences on mass 230. However, this set up has lower ion transmission efficiency than SF-ICP-MS and requires a combination of a multiple-spot laser ablation system with a dry plasma cone to enhance sensitivity, potentially making the routine application of this method more challenging and suggesting that it requires more testing. In addition, the relatively low fluence of most femtosecond laser systems limits signal compared to higher fluence longer pulse-width excimer systems.

A further challenge is that the above methods require the analysis of minerals with high Th/U to estimate the contribution of ^{232}Th abundance sensitivity on ^{230}Th. The current approach for SF-LA-ICP-MS ^{238}U–^{230}Th zircon dating suggests the analysis of monazite results in a high input of lead into the LA-ICP-MS system (e.g., Kohn and Vervoort, 2008). This makes measurement of lead isotopes in young zircon crystals difficult, decreasing the accuracy of zircon ^{238}U–^{206}Pb chronometer due to elevated lead backgrounds.

The focus of this paper is to evaluate the effective contributions of mass spectrometric interferences and ^{232}Th abundance sensitivity on ^{230}Th and to suggest an improved and simplified correction routine for *in-situ* SF-LA-ICP-MS zircon ^{238}U–^{230}Th dating. In addition, we provide an alternative method to estimate the contributions of abundance sensitivity and polyatomic oxide interferences. Finally, we provide an example of the application of this methodology to simultaneous, single spot ^{238}U–^{206}Pb, ^{232}Th–^{208}Pb and ^{238}U–^{230}Th dating of Quaternary zircon. We achieve this through measurements on four different zircon samples: two widely used zircon reference materials originating from metamorphic rocks – the 91500 (1062.4 ± 0.4 Ma; Wiedenbeck et al., 1995) and Plešovice (337.13 ± 0.37; Sláma et al., 2008) zircon reference materials; and two sets of volcanically derived zircons from the Bishop Tuff (0.767 ± 0.001 Ma;

Crowley et al., 2007; Chamberlain et al., 2014; Ickert et al., 2015) and Breccia Museo facies of the Campanian Ignimbrite (40.9 ± 0.6 ka; Fedele et al., 2008; Gebauer et al., 2014). This refined dating method allows for accuracy verification between different chronometers and is a relatively simple and cost-effective method that allows for the quantification of young zircon ages in samples with multiple age components (e.g., Quaternary detrital zircon).

4.2. Methods

4.2.1. Instrumentation

The 91500, Plešovice, Bishop Tuff and Campanian Ignimbrite zircon crystals were analyzed using a RESOlution ArF Excimer 193 nm laser ablation system coupled to a Thermo Scientific Element XR magnetic sector-field (SF)-ICP-MS, using a Laurin-Technic S-155 cell (Table 4.1.). Samples were spot ablated for 40 seconds using a 40 µm beam at a 5 Hz repetition rate and laser energy, measured at the sample surface was ~3 J/cm^2. The resulting ablation pits are flat-bottomed with near-vertical sides and ~10-15 µm deep. The mass spectrometer was operated in low mass resolution mode (M/ΔM= ~300). An analysis comprised 40 seconds of background gas collection followed by 40 seconds of ablation. Ablated aerosols were entrained in a He cell gas flow (0.350 L/min) with Ar (0.85 L/min) prior to entering the ICP-MS torch. The instrument was optimized by ablating NIST 612 with a 50 µm laser beam diameter, 10 Hz repetition, at 3 µms^{-1} scanning speed and 3.5 J cm^{-2} laser fluence, resulting in a sensitivity of ~ 1.4 Mcps on ^{238}U. Argon and helium gas flow, torch position, and focusing potentials were tuned to achieve optimal signals on Pb and U, and a low ThO/Th at ~0.015%. For U-Th dating, data were collected for 228, 230, 235 amu using the ion counting modes of the SEM detector, for 232 amu using "triple" detection mode, and for 238 amu using analog mode. Dwell times were 20 ms (masses 232, 235, 238), 50 ms (mass 228) and 150 ms (mass 230). For combined ^{238}U–^{230}Th and U-Th-Pb dating, data were collected for 206, 207, 208, 228, 230, 235 amu using the ion counting modes of the SEM detector, for 232 amu using triple detection mode, and for 238 amu using analog mode. Dwell times were 20 ms (masses 232, 235, 238), 40 ms (mass 206, 207, 208, 228) and 150 ms (mass 230). The gas-blank corrected count rates and analytical uncertainties were derived using the Iolite (4.1) data reduction package (Paton et al., 2011), followed by processing using an Excel in-house spreadsheet. The relative sensitivity factor and mass bias corrections were performed using the approach described in Guillong et al. (2016) by normalizing the average $^{238}U/^{232}Th$ ratio in 91500 zircon crystals to the known concentrations of U at 81.2 ppm and Th at 28.6 ppm, resulting in a correction factor of 1.01 ± 0.02. The data accuracy was verified by observing the degree of deviation of the $^{230}Th/^{238}U$ ratio from unity in the 91500, Plešovice and Bishop Tuff reference materials. The U-Pb and Th-Pb ages were calculated and corrected for ^{230}Th disequilibrium and common-Pb using a maximum likelihood algorithm for joint isochron regression of the $^{206}Pb/^{238}U$, $^{207}Pb/^{235}U$, and $^{208}Pb/^{232}Th$ chronometers (Vermeesch, 2020).

Table 4.1. LA-ICP-MS operating conditions and methodology.

Laboratory name and Samples	
Laboratory name	Arctic Resources Geochemistry Laboratory, University of Alberta, Canada
Sample type/mineral	Zircon
Analysis	U-Th
Samples	Bishop Tuff, Campanian Ignimbrite, PAL tephra
Sample preparation	Polished mount (2-5 um)
Reference material location	Separate mount
Imaging	Petrographic microscope. CL, BSE
Laser Ablation System	
Make, Model & type	RESOlution ArF 193 nm
Ablation cell & volume	Laurin Technic S-155
Laser wavelength (nm)	193
Pulse width (ns)	20
Fluence (J/cm^2)	~3
Repetition rate (Hz)	5
Ablation duration (s)	35
Ablation pit depth (μm)	~10
Spot size (μm)	40
Sampling mode / pattern	Static spot
Carrier gas	He with Ar added after the cell
Cell carrier gas flow (l/min)	1.2
ICP-MS Instrument	
Make, Model & type	ThermoScientific Element XR (SF)-ICP-MS.
Sample introduction	Ablation aerosol
RF power (W)	1200
Make-up gas flow (l/min)	Ar = ~0.85
Detection system	Single electron multiplier ion counter
Masses measured	228, 230, 232, 238
IC Dead time (ns)	16
Analyzer vacuum	$\sim 1.5 \times 10^{-7}$ mbar
Data Processing	
Gas blank	Baseline measured 40 seconds prior to each analysis
Calibration strategy	91500 used as primary reference material, Plesovice, and Bishop Tuff used as secondary validation.
Data processing package used / Correction for LIEF	Iolite (Paton et al. 2011) for gas blank corrected abundances. In-house Excel spreadsheet for data processing.
Mass discrimination	Normalization to primary reference material
Uncertainty level & propagation	Analytical uncertainties are reported as absolute 2S.E (95% confidence level) propagated by quadratic addition. Reproducibility of reference material uncertainty is propagated.

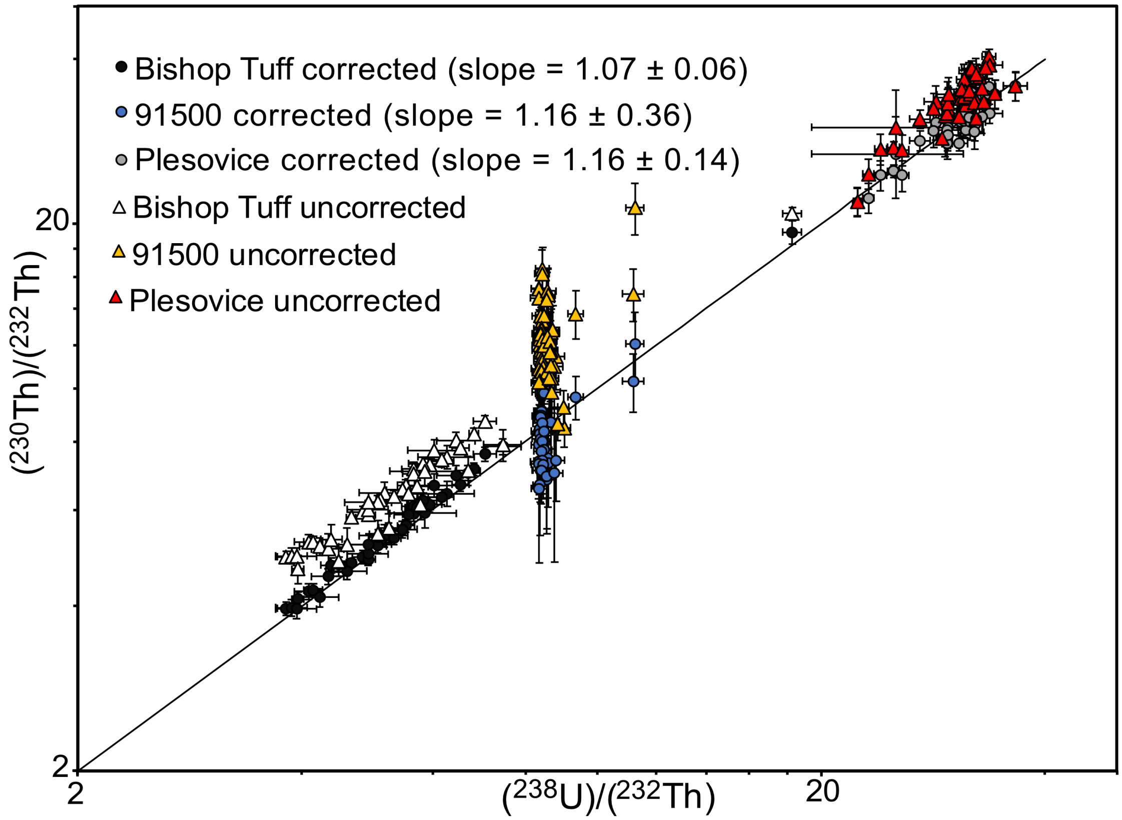

Figure 4.1. *(^{230}Th)/(^{232}Th) vs. (^{238}U)/(^{232}Th) activity ratios for primary reference materials expected to be in secular equilibrium, measured by LA-ICP-MS and corrected for abundance sensitivity, oxide interferences, mass bias and relative sensitivity (see text for details). Note that nearly all reference materials demonstrate secular equilibrium and plot along the equiline. All uncertainties are 2s.*

4.2.2. Corrections applied

Corrections to the measured mass spectra for polyatomic oxide interferences ($Zr_2O_3^+$) and peak tailing were performed using an in-house Excel spreadsheet using the following methods.

1. The degree of deviation of (^{230}Th)/(^{238}U) in zircon in secular equilibrium with high Th and U concentrations (e.g., Bishop Tuff) provides an accurate way to estimate the

combined influence (F_{230}) of abundance sensitivity and polyatomic oxide interference on ^{230}Th:

$$F_{230} = \frac{\left(^{230}\mathrm{Th}_{meas.} - \left[\frac{^{238}\mathrm{U}_{meas.} \times \lambda_{238}}{\lambda_{230}}\right] \times \frac{[^{230}\mathrm{Th}]}{[^{238}\mathrm{U}]} stnd \right)}{^{232}\mathrm{Th}_{meas.}}$$

$^{230}\mathrm{Th}_{meas.}$ = measured ^{230}Th (cps), $^{238}\mathrm{U}_{meas.}$ = measured ^{238}U (cps), $(^{230}\mathrm{Th})/(^{238}\mathrm{U})_{stnd.}$ = known reference material zircon (^{230}Th)/(^{238}U) (~1 for zircon in secular equilibrium). The median F_{230} is used to calculate and subtract the combined abundance sensitivity and polyatomic oxide interference from ^{230}Th. The median contribution of F_{230} in Bishop Tuff was 4.38 ± 0.13 ppm. The variations in F_{230} also provide a time-dependent monitor for the changes in contribution of these interferences on ^{230}Th over the course of analysis.

2. Based on the ablation of a mineral with relatively high Th and U concentrations it is possible to determine the peak tailing of ^{232}Th on ^{230}Th. For this, a mass scan of Ice River perovskite and Bishop Tuff zircon was acquired. The abundance sensitivity of 4.16±0.06 ppm (perovskite = pv) and 4.10±0.07 ppm (zircon; Bishop Tuff = BT_{ms}) were exponentially extrapolated from intensities at half-masses in the vicinity of mass 230 and used to calculate and subtract the abundance sensitivity from ^{230}Th. The median net count rate on mass 228 of all zircon analysis was then used to correct mass 230 for polyatomic oxide interference after applying the scaling factor (0.7142).

To verify the accuracy of the polyatomic oxide interference correction, we calculated $^{90}\mathrm{Zr}^{92}\mathrm{Z}^{16}\mathrm{O}_3^+$ values for Bishop Tuff zircon based on the difference between F_{230} and the abundance sensitivity values obtained from the mass scan interpolation, which yielded similar results, with median values of 5.5 cps and 5.8 cps respectively. This value is also consistent with the estimates obtained from mass 228 measurements, yielding a median value of ~5 cps. To verify this, we also analyzed the MUN-4 reference material, one of a suite of synthetic zircon (Fisher et al., 2011) made to facilitate the correction of rare earth elements on the Hf isotope mass spectrum. Our LA-ICP-MS analysis revealed that these synthetic materials contain very low trace element abundances (U <0.01 ppm, Th <0.01 ppm) because they were not "spiked" with these elements. The ^{230}Th signal combined standard uncertainty was calculated by quadratic addition using counting statistic uncertainties from the gas blank and signal, the oxide and abundance sensitivity corrections. Limits of detection were calculated for each analysis using IUPAC suggestions described by Tanner (2010) and Pettke et al. (2012) for LA-ICP-MS. Analyses below 1.5 × limit of detection were discarded.

For the PAL tephra zircons, we combined age probability distributions of ^{232}Th–^{208}Pb and ^{238}U–^{230}Th individual zircons (following Bayesian rules, Bayes, 1763; Doran and Hodgson, 1975) via the `Combine` function in OxCal (Bronk Ramsey, 1995, 2009). Here, we assume both chronometers represent the timing of zircon crystallization. Thus, the age combination is the product of the two input probability distributions. The `Combine` function directly leverages the probability distributions of the ages, permitting the inclusion of dates from multiple lines of evidence possessing potentially non-Gaussian probability density functions and producing more nuanced (non-Gaussian) posterior age estimates than strictly frequentist methods. Further, while not implemented here, Bayesian combination is well suited for probabilistic outlier analysis, which can pinpoint data points that might deviate from expected values and allow us to make more accurate estimates of the actual chronological age of the samples (Bronk Ramsey, 2009).

4.3. Results and discussion

4.3.1. The effect of the polyatomic $^{91}Zr_2{}^{16}O_3^+$ isotopologue and ^{232}Th abundance sensitivity on corrected ^{230}Th

Reference material analyses that were corrected for oxides, abundance sensitivity and RSF consistently showed (^{230}Th)/(^{238}U) activity ratios at secular equilibrium within uncertainty (two standard error (SE); Fig. 4.1). The (^{230}Th)/(^{238}U) corrected activity ratios for zircon reference materials are consistent between the three correction methods used: 91500 at 0.964 ± 0.04 (F_{230}), 1.05 ± 0.06 (pv), 1.04 ± 0.06 (BT_{ms}); Plešovice at 1.01 ± 0.02 (F_{230}), 1.09 ± 0.03 (pv), 1.01 ± 0.02 (BT_{ms}); Bishop Tuff (1.03 ± 0.01 (F_{230}), 1.05 ± 0.01 (pv), 1.05 ± 0.01 (BT_{ms}) (Fig. 4.2). We recognize that the BT_{ms} abundance sensitivity estimate might be influenced by polyatomic $Zr_2O_3^+$ interferences on the 231 and 232 masses, but the contribution of these interferences is minor and do not affect the final results.

In addition, for the zircon from the Breccia Museo facies of the Campanian Ignimbrite (CI), an isochron ^{238}U–^{230}Th age using 74 measurements yielded compatible results between three corrections methods at the 95% confidence level: 41.7 ± 3.5 ka (F_{230}), 38.0 ± 3.4 ka (pv) and 37.8 ± 3.5 ka (BT_{ms}). The results are similar to the eruption ages obtained by ^{40}Ar/^{39}Ar (40.9 ± 0.6 ka; recalculated by Gebauer et al. (2014) from De Vivo et al. (2001), Ton That et al. (2001) and Fedele et al. (2008)) and a (U-Th)/He age (41.7 ± 1.8 ka) on the Breccia Museo deposit that Gebauer et al. (2014) and others show is likely a facies of the CI formed in the initial stages of the eruption (Fig. 4.3). The zircon age is consistent with the LA-ICP-MS zircon isochron age on the same deposit of 42.1 ± 3.5 ka (Guillong et al., 2016). Model ages of individual zircon grains were calculated using the whole rock values from Arienzo et al. (2011).

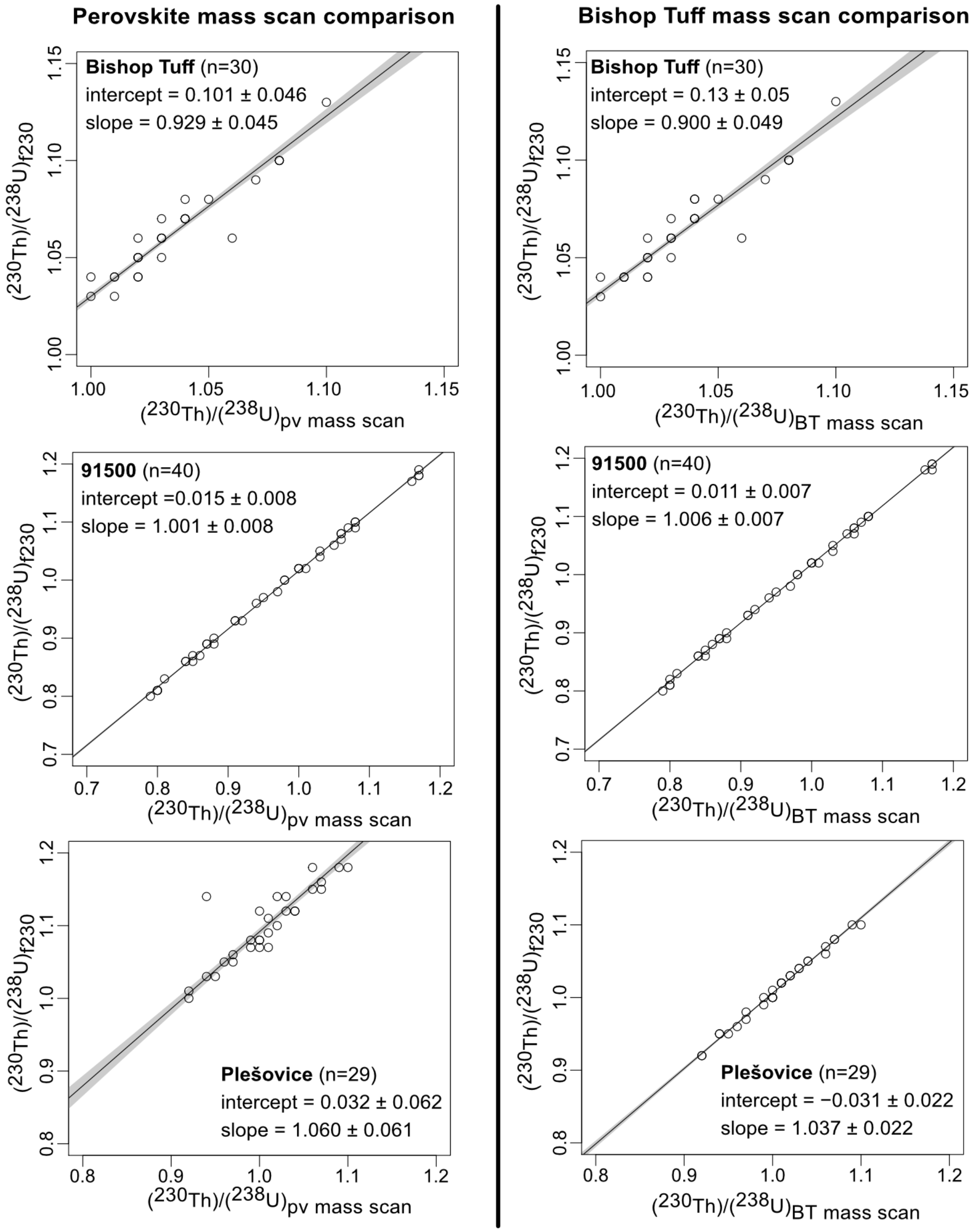

Figure 4.2. *(^{230}Th)/(^{238}U) activity ratios for zircon reference materials in secular equilibrium demonstrating the consistency in these ratios between three corrections methods. (^{230}Th)/(^{238}U)$_{F230}$ = (^{230}Th)/(^{238}U) corrected using F_{230} method; (^{230}Th)/(^{238}U)$_{pv\ mass\ scan}$ = (^{230}Th)/(^{238}U) corrected using Ice River perovskite mass scan; (^{230}Th)/(^{238}U)$_{BT\ mass\ scan}$ = (^{230}Th)/(^{238}U) corrected using Bishop Tuff zircon mass scan. Uncertainties are absolute 2s.*

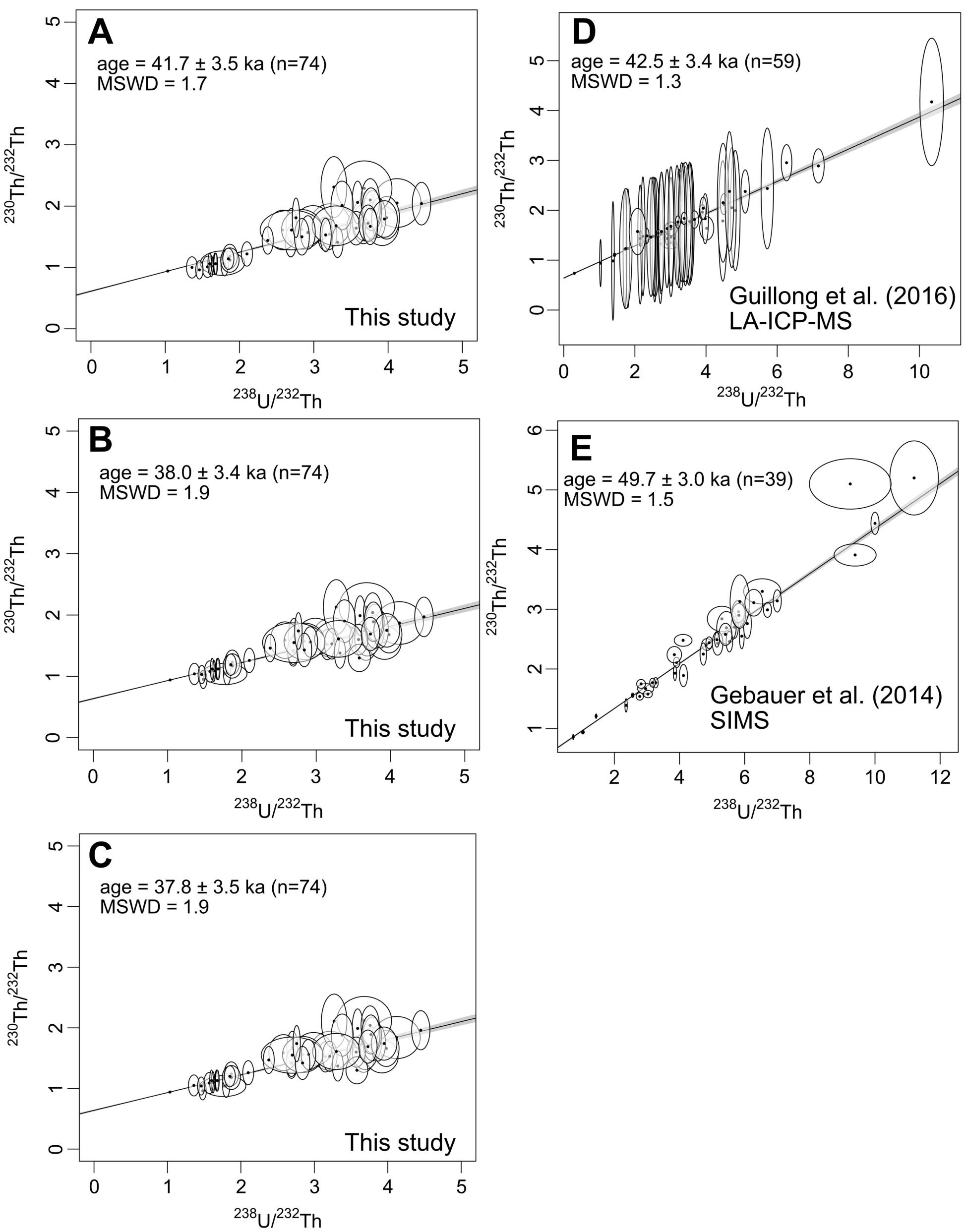

Figure 4.3. *Comparison of ^{238}U–^{230}Th ages obtained by LA-ICP-MS for zircon from syenitic clasts within the phonolitic Campanian Ignimbrite (groundmass value from Arienzo et al. 2011). A. Data corrected using F_{230}, B. Data corrected using perovskite mass scan and measured polyatomic interference, C. Data corrected using Bishop Tuff mass scan and measured polyatomic interference, D. LA-ICP-MS zircon data from Guillong et al. (2016), E. SIMS zircon data from Gebauer et al. (2014). Uncertainties are absolute 2s.*

Of the zircon reference materials measured here, those with the highest U concentrations correlate to the analyses with more precise and accurate (^{230}Th)/(^{238}U) activity ratios; the high Th and U reference material in secular equilibrium (e.g., Bishop Tuff zircons that average ~2700 ppm U and ~ 1700 ppm Th) provide the most reliable data. The contribution of polyatomic $Zr_2O_3^+$ interference to the ^{230}Th peak for zircon crystals with lower Th and U abundances (<500 ppm) is proportionally larger than for grains with higher abundance of those elements, with typically >5% contribution to the total ^{230}Th. In contrast, the abundance sensitivity is a major interfering contribution to the ^{230}Th peak for zircon crystals with higher Th and abundances (>500 ppm), falling between 5 and 10% of the total ^{230}Th (Fig. 4.4.). Thus, the significance of these corrections is inversely correlated with the U and Th abundances of secular equilibrium and disequilibrium zircons analyzed here. In addition, by ablating the synthetic end-member zircon (MUN-4 Zircon) we also explored the presence of polyatomic interferences on mass 230. The gas blank corrected $^{91}Zr_2{}^{16}O_3^+$ abundance of ~5 cps measured in the synthetic zircon using the same ablation parameters (40 µm crater, 5 Hz, 3 J cm^{-2}, scanning with 5 µm s^{-1}) is consistent with the estimates obtained from the measurements on the reference zircons (Fig. 4.5.).

Although the polyatomic contribution to the ^{230}Th peak for zircon with higher Th and U abundances is relatively insignificant (<1% contribution for grains with >2000 ppm U), it becomes increasingly important for grains that have very low ^{230}Th count rates (~10-15% contribution for grains with <100 ppm U). Guillong et al. (2016) proposed peak stripping of a $^{90}Zr_2O_3^+$ signal measured at low mass resolution on mass 228 scaled to the isotopic abundance ratio for $^{90}Zr_2$ and ($^{90}Zr^{92}Zr + {}^{91}Zr_2$) of 0.7142. Although this correction appears to be effective, as shown by consistent zircon reference material (^{230}Th)/(^{238}U) = ~1 activity ratios, it is difficult to quantify $^{90}Zr_2O_3^+$ for individual zircon analyses due a very low mass 228 count rates.

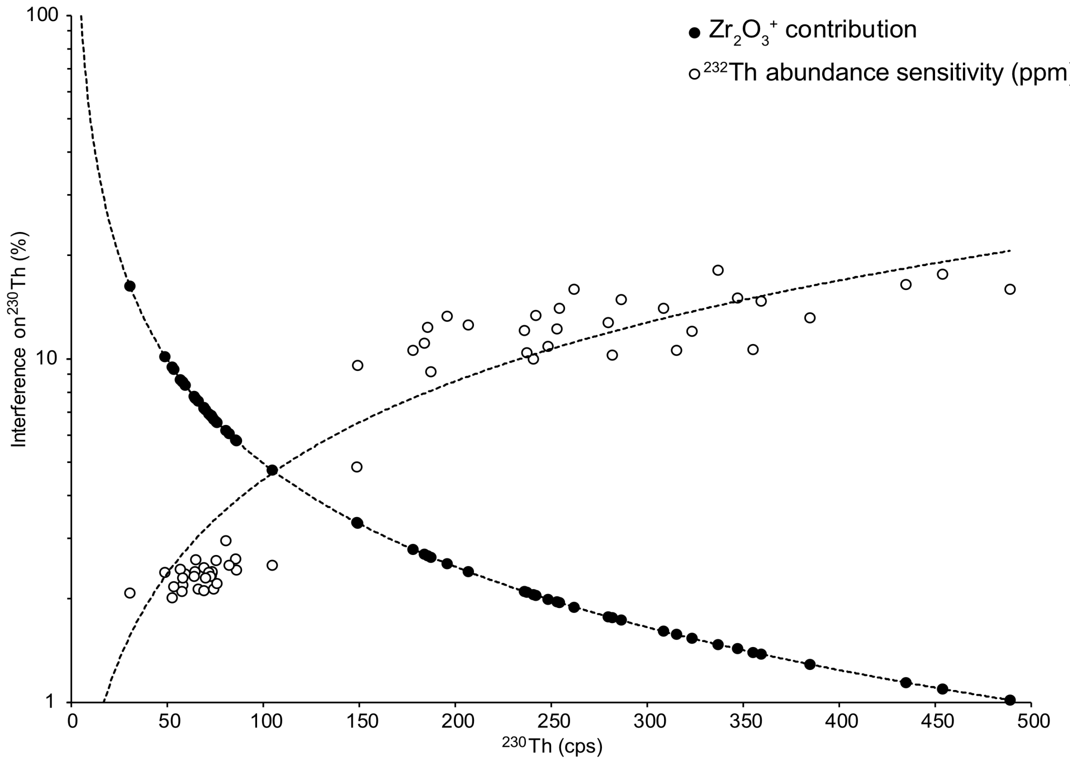

Figure 4.4. *The interference of $Zr_2O_3^+$ and abundance sensitivity on ^{230}Th peak versus the corrected ^{230}Th count rate, in counts per second.*

We estimated a consistent polyatomic interference contribution of ~5-6 cps using the difference between F_{230} and the abundance sensitivity values obtained from the mass scan interpolation, direct measurements at mass 228, and the synthetic zircon mass scan. Similarly, the abundance sensitivity can be accurately estimated by ablating a mineral with high Th and U, with our results being consistent between different methods. These results suggest that polyatomic interferences can be effectively removed from ^{230}Th peak without measuring mass 228, but directly with abundance sensitivity by the estimating degree of deviation of (^{230}Th)/(^{238}U) in a suitable reference zircon that is in secular equilibrium. This approach simplifies the correction methodology, does not require ablation of additional mineral phases that can contribute a high input of non-radiogenic lead to the LA-ICP-MS system, does not dictate measurements of the very small mass 228 signal, and also provides a monitor for time-dependant instrumental drift. Furthermore, this correction routine can be easily combined with the methods suggested by Guillong et al. (2016) to reaffirm the validity of the results. In addition, our ThO/Th ratio of 0.015% is nearly ten times lower than ThO/Th ratio obtained by Guillong et al. 2016, resulting in a correspondingly lower $^{91}Zr_2{}^{16}O_3{}^{+}$ production.

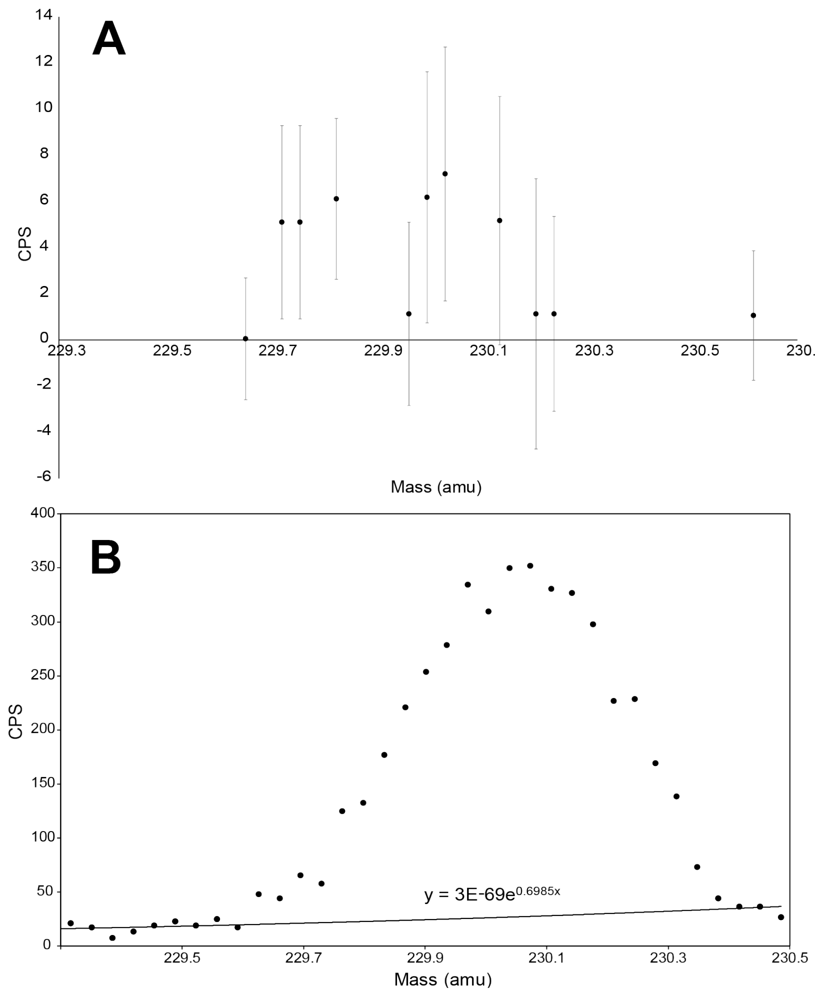

Figure 4.5. *A. Low resolution mass scan from mass 229–230.7 amu during ablation of MUN-4 Zircon (data corrected for gas blank; 40 µm crater, 5 Hz, 3 J cm^{-2}, scanning with 5 µm s^{-1}). B. Low resolution mass scan showing masses 229–230.5 amu while ablating Bishop Tuff.*

4.3.2. Implications for combined U-Th and U-Th-Pb dating of Quaternary zircon

The precise and accurate determination of the crystallization age of Quaternary zircons using U–Th–Pb and/or ^{238}U–^{230}Th methods is a widely used approach to studying magmatic systems (e.g., Bacon et al., 2000; Chamberlain et al., 2014; Schmitt, 2011; Schmitt et al., 2003; Simon and Reid, 2005; Simon et al., 2008; Simon et al., 2014; Guillong et al., 2016; Buryak et al., 2022). However, for U–Pb dating of young zircons, the effect of initial disequilibria associated with intermediate nuclides in the ^{238}U or ^{235}U decay series needs to be quantified and corrected for (Ludwig, 1977; Schärer, 1984; Wendt and Carl, 1985). Without correction for the initial disequilibrium, the resulting ^{238}U–^{206}Pb and ^{235}U–^{207}Pb ages will result in ages that are too young and too old respectively. The ^{238}U–^{230}Th method is also useful for determining crystallization ages of young minerals, but does not work for crystals older than ~350 ka (Fukuoka, 1974; Fukuoka and Kigoshi, 1974; Reid et al., 1997). The ^{232}Th–^{208}Pb dating method is a potential alternative to U–Pb dating as it does not require correction for the initial disequilibrium effect (Harrison et al., 1995; Oberli et al., 2004). However, for in-situ dating methods it is challenging to obtain accurate and precise ^{232}Th–^{208}Pb ages because for zircons <500 ka in age, the $^{208}Pb/^{232}Th$ ratio is <0.00003, making direct measurements difficult.

Here we provide an alternative zircon dating routine that combines ^{238}U–^{206}Pb, ^{232}Th–^{208}Pb and ^{238}U–^{230}Th dating methods to obtain accurate ages from a single spot LA-ICP-MS analyses. This new routine provides the ability to cross-check ^{238}U–^{206}Pb, ^{232}Th–^{208}Pb and ^{238}U–^{230}Th ages in a quick and cost-effective manner. It is particularly useful for young zircon samples with an unclear chronology, or young detrital samples that would otherwise require multi-spot dating to obtain more than one radiometric age.

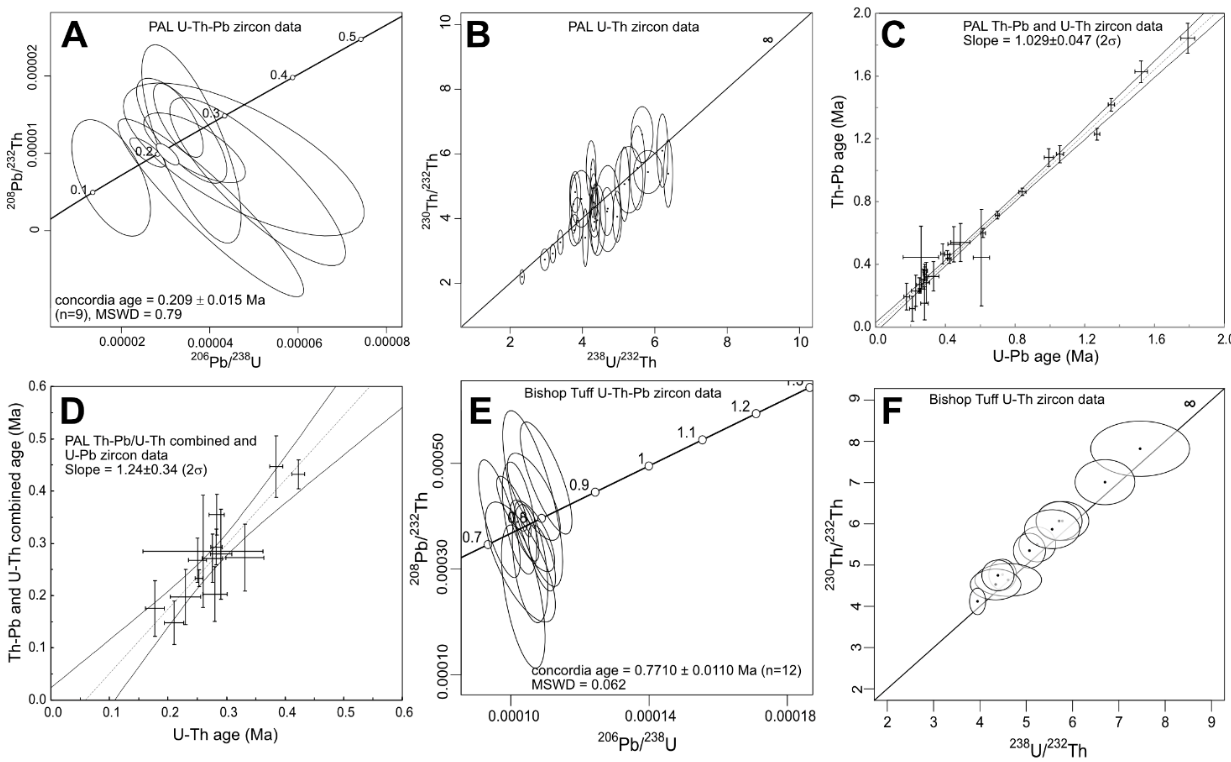

Figure 4.6. *Zircon analyses of (A) U-Th-Pb 3D Concordia age for PAL tephra – youngest cluster of ages only; (B) All PAL tephra zircon U-Th data plotted; (C) Linear regression of PAL tephra U-Th and Th-Pb ages showing total age variation of zircon from this tephra; (D) Linear regression of combined U-Th and Th-Pb ages vs. U-Pb ages; (E) Bishop Tuff U-Th-Pb 3D Concordia age; (F) Bishop Tuff U-Th data indicating secular equilibrium.*

By combining the simplified correction schemes for ^{238}U–^{230}Th dating presented here and combined measurement of U, Th and Pb isotopes we obtained ^{238}U–^{206}Pb, ^{232}Th–^{208}Pb and ^{230}Th-^{238}U data for ~200 ka PAL tephra and Bishop Tuff zircons (Crowley et al., 2007; Jensen et al., 2013). The PAL tephra is a distinct volcanic ash found at the Palisades in central Alaska along the Yukon River (e.g., Matheus et al., 2003). It is Middle Pleistocene in age, thought to be between ~140 and ~500 ka in age (e.g., Jensen et al., 2013), and provides an excellent test for the revised methodologies presented here. PAL tephra zircon crystals are heterotemporal, with ages ranging between ~0.2 to 1.8 Ma and have relatively low U and Th concentrations <200 ppm on average. We calculated the ages for PAL tephra using a maximum likelihood algorithm joint isochron regression of the $^{206}Pb/^{238}U$, $^{207}Pb/^{235}U$, and $^{208}Pb/^{232}Th$ chronometers, combined with the two-stage lead evolution model of Stacey and Kramers (1975) to estimate the common Pb composition. The glass Th/U ratio of 2.8 was used to correct ^{238}U–^{206}Pb for initial Th deficit. The PAL tephra zircon ^{238}U–^{206}Pb and ^{232}Th–^{208}Pb ages are concordant for all the grains analyzed (slope of the regression 1.029 ± 0.047; 2s) and the three-parameter regression age for the youngest cluster of grains yielded an age of 0.209 ± 0.015 Ma (2s; Fig. 4.6A). The zircon grains that yielded ages >350 ka also have (^{230}Th)/(^{238}U) activity ratios ~1 and those grains that are <350 ka yielded ages consistent with the results of obtained by $^{206}Pb/^{238}U$ and $^{208}Pb/^{232}Th$ chronometers (Fig. 4.6C).

Due to the relatively low precision (>20%; 2s) of individual ^{238}U–^{230}Th and ^{232}Th–^{208}Pb analyses, the ages were combined. Combination slightly improves the precision of the age probability distribution product over the two individual chronometers and is especially useful for dating zircon grains that are too small to accommodate multiple ablation spots. The precision for the combined ^{238}U–^{230}Th and ^{232}Th–^{208}Pb dates (3-19%; 2s) is 2 to 8 times improved over the lower precision individual ^{238}U–^{230}Th and ^{232}Th–^{208}Pb dates (6-79%; 2s). The combined ^{238}U–^{230}Th and ^{232}Th–^{208}Pb ages are consistent with the ^{238}U–^{206}Pb ages with a regression slope of 1.24 ± 0.34 (2s; Fig. 4.6D). The addition of the $^{206}Pb/^{238}U$ dates to the combination can further improve the combined age precision but is not necessary since the PAL tephra $^{206}Pb/^{238}U$ dates are more precise (average ~12%; 2s) than dates obtained by ^{238}U–^{230}Th and ^{232}Th–^{208}Pb chronometers. The three-parameter regression age for the youngest cluster of grains provides an alternative age calculation method albeit with slightly lower overall precision (22%; 2s) than the combined $^{238}U–^{230}Th$ and $^{232}Th–^{208}Pb$ dates and requires identification of the youngest cluster of grains. Ultimately, choice of the final age calculation routine (i.e. three-parameter regression or combined two-parameter age) is dependent on the age of the sample, zircon U and Th concentrations, complexity of the zircon age distribution, and the precision of the $^{238}U–^{206}Pb$, $^{232}Th–^{208}Pb$ and $^{238}U-^{230}Th$ zircon data.

Finally, these data provide a first radiometric direct age for the PAL tephra, which was not directly dated previously and suggests tephra deposition during Marine Isotope Stage 7. This first direct age for PAL tephra provides an additional tephrochronological anchor for the depositional timing of the bottom-most sediments at the Palisades site in central Alaska, which has a comprehensive record of permafrost-preserved Quaternary sediments (Matheus et al., 2003; Reyes et al., 2010; Jensen et al., 2013). At multiple exposures at the Palisades site, PAL tephra is located below an assumed unconformity mapped by Matheus et al. (2003) and is overlain by the ca. 160 ka Old Crow tephra (Reyes et al., 2023) and ca. 190 ka Sheep Creek-Fairbanks tephra (Matheus et al., 2003; Jensen et al., 2013). Two thick peat units at the Palisades site are found between Sheep Creek-Fairbanks and PAL tephra beds. Additionally, organic-rich silts and peat are also found below PAL tephra at several outcrops (Jensen et al., 2013). The organic-rich layers are typically associated with interglacial climate, however presence of two peat layers above PAL tephra cannot account for two separate interglacial periods and likely represent periods of regional warming with underlying peat most likely dating to Marine Isotope Stage 7.

4.4. Conclusion

This paper provides an accurate and simplified method for ^{238}U–^{230}Th dating of single Quaternary zircon samples using SF-LA-ICP-MS. The approach is particularly useful for analyzing Quaternary detrital zircons with multiple age components in combination with $^{206}Pb/^{238}U$ and $^{208}Pb/^{232}Th$ chronometers. To summarize, this study:

1. Demonstrated the importance of evaluating mass spectrometric interferences and ^{232}Th mass tailing for accurate ^{230}Th dating using SF-LA-ICP-MS in zircon samples.
2. Introduced an improved and simplified correction routine for enhancing the accuracy of *in-situ* ^{238}U–^{230}Th dating in zircons and provided an alternative method to estimate the contributions of abundance sensitivity and polyatomic oxide interferences, using the mass spectrum measured for a very low U & Th MUN-4 synthetic zircon.
3. Applied the methodology to the simultaneous, single spot (40 µm spot-size) dating of ^{238}U–^{206}Pb, ^{232}Th–^{208}Pb, and ^{238}U–^{230}Th in Quaternary zircon, showcasing its practical utility.
4. Provided a relative low cost and time-efficient approach to obtain ^{238}U–^{230}Th and U-Th-Pb zircon age data using SF-LA-ICP-MS.

4.5. Supplemental Figures

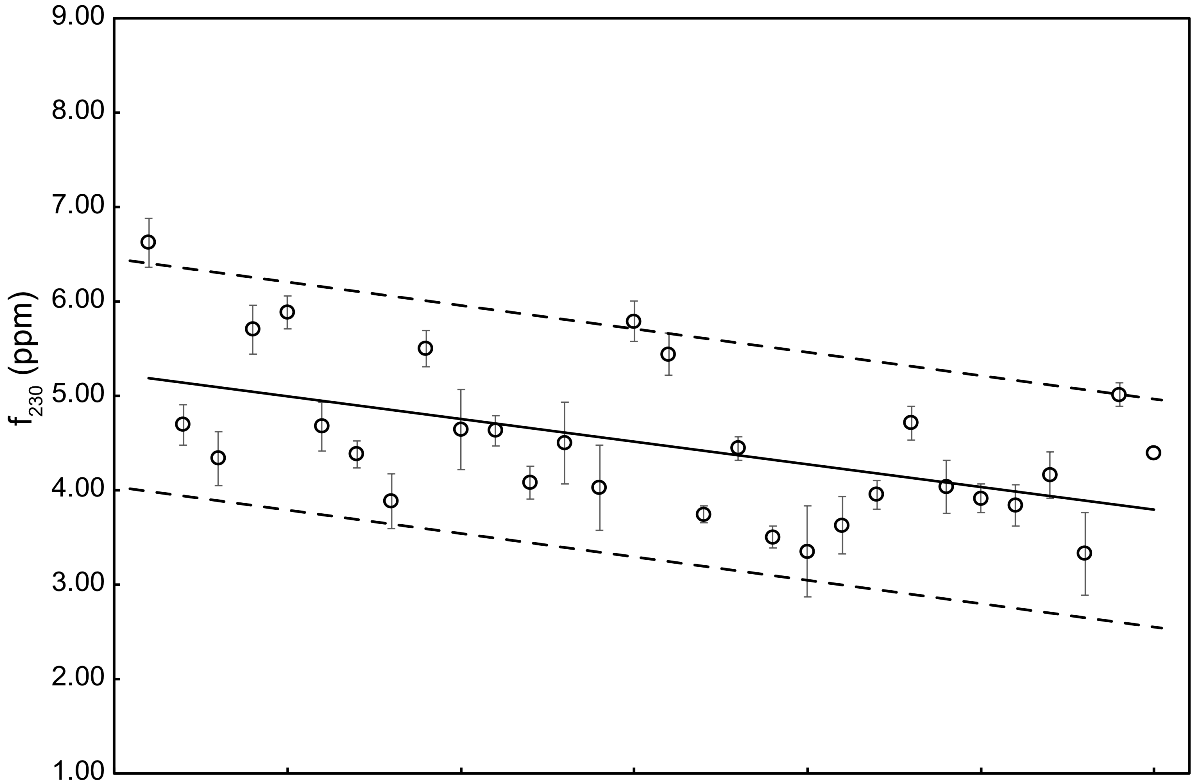

Figure B.1. *The rime dependent variation in F_{230} contribution over the length of analytical session (~7 hours). The error envelope and uncertainties are 1s.*

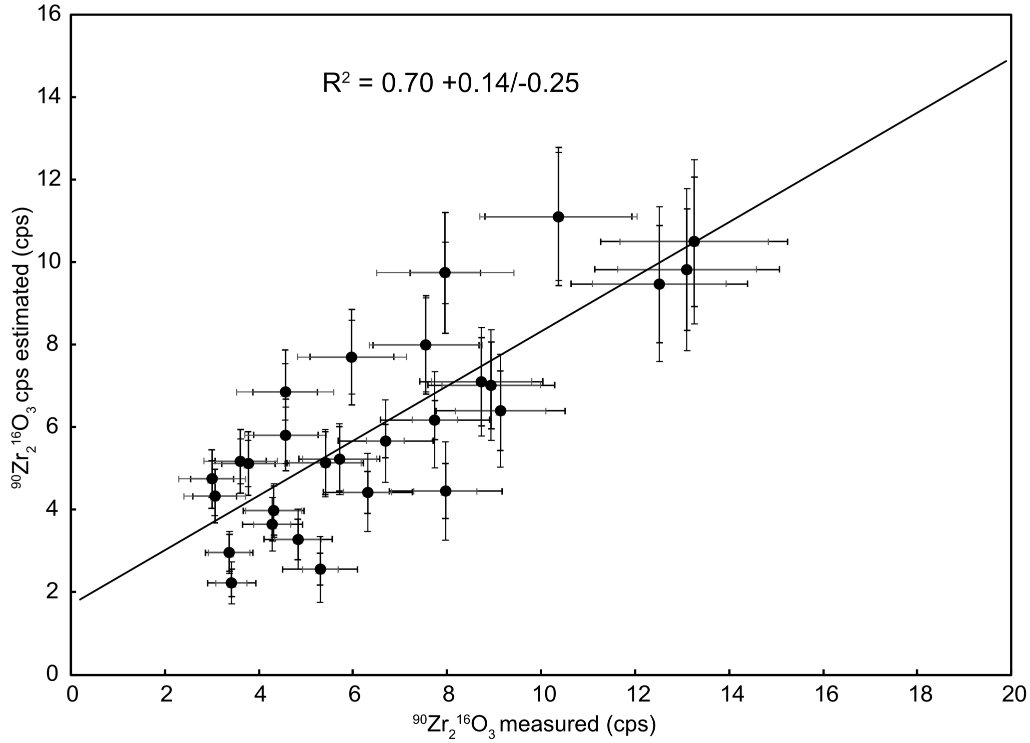

Figure B.2. *Polyatomic $^{91}Zr_2{}^{16}O_3^+$ isotopologue regression using measured $^{91}Zr_2{}^{16}O_3^+$ and counts estimated from Bishop Tuff F_{230} contribution. Uncertainties are 2s.*

4.6. References

Arienzo, I., Heumann, A., Wörner, G., Civetta, L., Orsi, G., 2011. Processes and timescales of magma evolution prior to the Campanian Ignimbrite eruption (Campi Flegrei, Italy). Earth and Planetary Science Letters 306, 217–228. https://doi.org/10.1016/j.epsl.2011.04.002

Bacon, C.R., Persing, H.M., Wooden, J.L., Ireland, T.R., 2000. Late Pleistocene granodiorite beneath Crater Lake caldera, Oregon, dated by ion microprobe. Geology 28, 467–470. https://doi.org/10.1130/0091-7613(2000)028<0467:LPGBCL>2.3.CO;2

Bayes T.R., 1763. An essay towards solving a problem in the doctrine of chances. Philosophical Transactions of the Royal Society 53, 370-418.

Bronk Ramsey, C., 1995. Radiocarbon Calibration and Analysis of Stratigraphy: The OxCal Program. Radiocarbon 37, 425–430. https://doi.org/10.1017/S0033822200030903

Bronk Ramsey, C., 2009. Bayesian Analysis of Radiocarbon Dates. Radiocarbon 51, 337–360. https://doi.org/10.1017/S0033822200033865

Burgess, S.D., Coble, M.A., Vazquez, J.A., Coombs, M.L., Wallace, K.L., 2019. On the eruption age and provenance of the Old Crow tephra. Quaternary Science Reviews 207, 64–79. https://doi.org/10.1016/j.quascirev.2018.12.026

Burgess, S.D.D., Vazquez, J.A.A., Waythomas, C.F.F., Wallace, K.L.L., 2021. U–Pb zircon eruption age of the Old Crow tephra and review of extant age constraints. Quaternary Geochronology 101168. https://doi.org/10.1016/j.quageo.2021.101168

Buryak, S.D., Reyes, A.V., Jensen, B.J.L., Davies, J.H.F.L., Westgate, J.A., DuFrane, S.A., Luo, Y., Froese, D.G., Pearson, D.G., Benowitz, J.A., 2022. Laser-ablation ICP-MS zircon U-

Pb ages for key Pliocene-Pleistocene tephra beds in unglaciated Yukon and Alaska. Quaternary Geochronology 101398. https://doi.org/10.1016/j.quageo.2022.101398

Chamberlain, K.J., Wilson, C.J.N., Wooden, J.L., Charlier, B.L.A., Ireland, T.R., 2014. New Perspectives on the Bishop Tuff from Zircon Textures, Ages and Trace Elements. Journal of Petrology 55, 395–426. https://doi.org/10.1093/petrology/egt072

Cheng, H., Adkins, J., Edwards, R.L., Boyle, E.A., 2000. U-Th dating of deep-sea corals. Geochimica et Cosmochimica Acta 64, 2401–2416. https://doi.org/10.1016/S0016-7037(99)00422-6

Crowley, J.L., Schoene, B., Bowring, S.A., 2007. U-Pb dating of zircon in the Bishop Tuff at the millennial scale. Geology 35, 1123–1126. https://doi.org/10.1130/G24017A.1

De Vivo, B., Rolandi, G., Gans, P.B., Calvert, A., Bohrson, W.A., Spera, F.J., Belkin, H.E., 2001. New constraints on the pyroclastic eruptive history of the Campanian volcanic Plain (Italy). Mineralogy and Petrology 73, 47–65. https://doi.org/10.1007/s007100170010

Doran, J.E. and Hodson, F.R., 1975. Mathematics and computers in archaeology. Harvard University Press.

Fedele, L., Tarzia, M., Belkin, H.E., Vivo, B.D., Lima, A., Lowenstern, J.B., 2006. Chapter 7 Magmatic-hydrothermal fluid interaction and mineralization in alkali-syenite nodules from the Breccia Museo pyroclastic deposit, Naples, Italy, in: De Vivo, B. (Ed.), Developments in Volcanology, Volcanism in the Campania Plain. Elsevier, pp. 125–161. https://doi.org/10.1016/S1871-644X(06)80021-5

Fedele, L., Scarpati, C., Lanphere, M., Melluso, L., Morra, V., Perrotta, A., Ricci, G., 2008. The Breccia Museo formation, Campi Flegrei, southern Italy: geochronology, chemostratigraphy and relationship with the Campanian Ignimbrite eruption. Bull Volcanol 70, 1189–1219. https://doi.org/10.1007/s00445-008-0197-y

Fisher, C.M., Hanchar, J.M., Samson, S.D., Dhuime, B., Blichert-Toft, J., Vervoort, J.D., Lam, R., 2011. Synthetic zircon doped with hafnium and rare earth elements: A reference material for in situ hafnium isotope analysis. Chemical Geology 286, 32–47. https://doi.org/10.1016/j.chemgeo.2011.04.013

Fukuoka, T., 1974. Ionium dating of acidic volcanic rocks. Geochemical Journal 8, 109–116. https://doi.org/10.2343/geochemj.8.109

Fukuoka, T., Kigoshi, K., 1974. Discordant Io-ages and the uranium and thorium distribution between zircon and host rocks. Geochemical Journal 8, 117–122. https://doi.org/10.2343/geochemj.8.117

Gebauer, S.K., Schmitt, A.K., Pappalardo, L., Stockli, D.F., Lovera, O.M., 2014. Crystallization and eruption ages of Breccia Museo (Campi Flegrei caldera, Italy) plutonic clasts and their relation to the Campanian ignimbrite. Contrib Mineral Petrol 167, 953. https://doi.org/10.1007/s00410-013-0953-7

Guillong, M., Sliwinski, J.T., Schmitt, A., Forni, F., Bachmann, O., 2016. U-Th Zircon Dating by Laser Ablation Single Collector Inductively Coupled Plasma-Mass Spectrometry (LA-ICP-MS). Geostandards and Geoanalytical Research 40, 377–387. https://doi.org/10.1111/j.1751-908X.2016.00396.x

Harrison, T.M., McKeegan, K.D., LeFort, P., 1995. Detection of inherited monazite in the Manaslu leucogranite by 208Pb232Th ion microprobe dating: Crystallization age and tectonic implications. Earth and Planetary Science Letters 133, 271–282. https://doi.org/10.1016/0012-821X(95)00091-P

Jaffey, A.H., Flynn, K.F., Glendenin, L.E., Bentley, W.C., Essling, A.M., 1971. Precision measurement of half-lives and specific activities of U235 and U238. Physical Review C 4, 1889–1906. https://doi.org/10.1103/PhysRevC.4.1889

Jensen, B.J.L., Reyes, A.V., Froese, D.G., Stone, D.B., 2013. The Palisades is a key reference site for the middle Pleistocene of eastern Beringia: New evidence from paleomagnetics and regional tephrostratigraphy. Quaternary Science Reviews 63, 91–108. https://doi.org/10.1016/j.quascirev.2012.11.035

Ickert, R.B., Mundil, R., Magee, C.W., Mulcahy, S.R., 2015. The U-Th-Pb systematics of zircon from the Bishop Tuff: A case study in challenges to high-precision Pb/U geochronology at the millennial scale. Geochimica et Cosmochimica Acta 168, 88–110. https://doi.org/10.1016/j.gca.2015.07.018

Ito, H., 2014. Zircon U–Th–Pb dating using LA-ICP-MS: Simultaneous U–Pb and U–Th dating on the 0.1Ma Toya Tephra, Japan. Journal of Volcanology and Geothermal Research 289, 210–223. https://doi.org/10.1016/j.jvolgeores.2014.11.002

Kohn, M.J., Vervoort, J.D., 2008. U-Th-Pb dating of monazite by single-collector ICP-MS: Pitfalls and potential. Geochemistry, Geophysics, Geosystems 9. https://doi.org/10.1029/2007GC001899

Ludwig, K.R., 1977. Effect of initial radioactive-daughter disequilibrium on U-Pb isotope apparent ages of young minerals. Journal of Research of the U.S. Geological Survey 5, 663–667.

Marsden, R.C., Kirkland, C.L., Danišík, M., Daggitt, M.L., Ahn, U.-S., Friedrichs, B., Evans, N.J., 2022. A new approach to SHRIMP II zircon U-Th disequilibrium dating. Comput. Geosci. 158. https://doi.org/10.1016/j.cageo.2021.104947

Matheus, P., Begét, J., Mason, O., Gelvin-Reymiller, C., 2003. Late Pliocene to late Pleistocene environments preserved at the Palisades site, central Yukon River, Alaska. Quaternary Research 60, 33–43, https://doi.org/10.1016/S0033-5894(03)00091-7.

Niki, S., Kosugi, S., Iwano, H., Danhara, T., Hirata, T., 2022. Development of an In Situ U-Th Disequilibrium Dating Method Utilising Multiple-Spot Femtosecond Laser Ablation-CRC-ICP-MS. Geostandards and Geoanalytical Research 46, 589–602. https://doi.org/10.1111/ggr.12458

Oberli, F., Meier, M., Berger, A., Rosenberg, C.L., GierÉ, R., 2004. U-Th-Pb and 230Th/238U disequilibrium isotope systematics: Precise accessory mineral chronology and melt evolution tracing in the Alpine Bergell intrusion. Geochimica et Cosmochimica Acta 68, 2543–2560. https://doi.org/10.1016/j.gca.2003.10.017

Paton, C., Hellstrom, J., Paul, B., Woodhead, J., Hergt, J., 2011. Iolite: Freeware for the visualisation and processing of mass spectrometric data. Journal of Analytical Atomic Spectrometry 26, 2508–2518. https://doi.org/10.1039/C1JA10172B

Pettke, T., Oberli, F., Audétat, A., Guillong, M., Simon, A.C., Hanley, J.J., Klemm, L.M., 2012. Recent developments in element concentration and isotope ratio analysis of individual fluid inclusions by laser ablation single and multiple collector ICP-MS. Ore Geology Reviews 44, 10–38. https://doi.org/10.1016/j.oregeorev.2011.11.001

Reid, M.R., Coath, C.D., Mark Harrison, T., McKeegan, K.D., 1997. Prolonged residence times for the youngest rhyolites associated with Long Valley Caldera:230Th—238U ion microprobe dating of young zircons. Earth and Planetary Science Letters 150, 27–39. https://doi.org/10.1016/S0012-821X(97)00077-0

Reyes, A.V., Jensen, B.J.L., Zazula, G.D., Ager, T.A., Kuzmina, S., La Farge, C., Froese, D.G., 2010. A late-Middle Pleistocene (Marine Isotope Stage 6) vegetated surface buried by Old Crow tephra at the Palisades, interior Alaska. Quaternary Science Reviews 29, 801–811. https://doi.org/10.1016/j.quascirev.2009.12.003

Reyes, A.V., Jensen, B.J.L., Woudstra, S.H., Bolton, M.S.M., Buryak, S.D., Cook, M.S., Harvey, J., Westgate, J.A., 2023. Detrital glass in a Bering Sea sediment core yields a ca . 160 ka Marine Isotope Stage 6 age for Old Crow tephra XX, 1–5.

Schmitt, A.K., Sliwinski, J., Caricchi, L., Bachmann, O., Riel, N., Kaus, B.J.P., Cisneros de Léon, A., Cornet, J., Friedrichs, B., Lovera, O., Sheldrake, T., Weber, G., 2023. Zircon age spectra to quantify magma evolution. Geosphere 19, 1006–1031. https://doi.org/10.1130/GES02563.1

Schmitt, A.K., 2007. Ion microprobe analysis of (231Pa)/(235U) and an appraisal of protactinium partitioning in igneous zircon. American Mineralogist 92, 691–694. https://doi.org/10.2138/am.2007.2449

Schmitt, A.K., 2011. Uranium Series Accessory Crystal Dating of Magmatic Processes. Annu. Rev. Earth Planet. Sci. 39, 321–349. https://doi.org/10.1146/annurev-earth-040610-133330

Schärer, U., 1984. The effect of initial230Th disequilibrium on young UPb ages: the Makalu case, Himalaya. Earth and Planetary Science Letters 67, 191–204. https://doi.org/10.1016/0012-821X(84)90114-6

Simon, J.I., Reid, M.R., 2005. The pace of rhyolite differentiation and storage in an ‘archetypical’ silicic magma system, Long Valley, California. Earth and Planetary Science Letters 235, 123–140. https://doi.org/10.1016/j.epsl.2005.03.013

Simon, J.I., Renne, P.R., Mundil, R., 2008. Implications of pre-eruptive magmatic histories of zircons for U–Pb geochronology of silicic extrusions. Earth and Planetary Science Letters 266, 182–194. https://doi.org/10.1016/j.epsl.2007.11.014

Simon, J.I., Weis, D., DePaolo, D.J., Renne, P.R., Mundil, R., Schmitt, A.K., 2014. Assimilation of preexisting Pleistocene intrusions at Long Valley by periodic magma recharge accelerates rhyolite generation: rethinking the remelting model. Contrib Mineral Petrol 167, 955. https://doi.org/10.1007/s00410-013-0955-5

Sláma, J., Košler, J., Condon, D.J., Crowley, J.L., Gerdes, A., Hanchar, J.M., Horstwood, M.S.A., Morris, G.A., Nasdala, L., Norberg, N., Schaltegger, U., Schoene, B., Tubrett, M.N., Whitehouse, M.J., 2008. Plešovice zircon — A new natural reference material for U–Pb and Hf isotopic microanalysis. Chemical Geology 249, 1–35. https://doi.org/10.1016/j.chemgeo.2007.11.005

Stacey, J.S., Kramers, J.D., 1975. Approximation of terrestrial lead isotope evolution by a two-stage model. Earth and Planetary Science Letters 26, 207–221. https://doi.org/10.1016/0012-821X(75)90088-6

Tanner, M., 2010. Shorter signals for improved signal to noise ratio, the influence of Poisson distribution. J. Anal. At. Spectrom. 25, 405. https://doi.org/10.1039/b921077f

Ton-That, T., Singer, B., Paterne, M., 2001. 40Ar/39Ar dating of latest Pleistocene (41 ka) marine tephra in the Mediterranean Sea: implications for global climate records. Earth and Planetary Science Letters 184, 645–658. https://doi.org/10.1016/S0012-821X(00)00358-7

Vermeesch, P., 2020. Unifying the U–Pb and Th–Pb methods: joint isochron regression and common Pb correction. Geochronology 2, 119–131. https://doi.org/10.5194/gchron-2-119-2020

Wendt, I., Carl, C., 1985. U/Pb dating of discordant 0.1 Ma old secondary U minerals. Earth and Planetary Science Letters 73, 278–284. https://doi.org/10.1016/0012-821X(85)90076-

Wiedenbeck, M., Allé, P., Corfu, F., Griffin, W. l., Meier, M., Oberli, F., Quadt, A.V., Roddick, J. c., Spiegel, W., 1995. Three Natural Zircon Standards for U-Th-Pb, Lu-Hf, Trace Element and Ree Analyses. Geostandards Newsletter 19, 1–23. https://doi.org/10.1111/j.1751-908X.1995.tb00147.x

Chapter 5: Refining Marine Isotope Stage 5 to 7 tephrochronology in eastern Beringia: an integrated zircon geochronology, tephra geochemistry and stratigraphy approach

5.1. Introduction

The sedimentological and paleoenvironmental history of eastern Beringia is intricately linked with global glacial and interglacial cycles during the Quaternary, with the sedimentary record preserving climatic variations over the last 3 million years (Ma; Westgate et al., 1990; Preece et al., 1999, 2000; Jensen et al., 2013, 2016). Although loess deposition goes back to around 3 Ma, records of that age are limited and very fragmentary. Most studied sites in both Alaska and Yukon are middle Pleistocene in age, often younger than 780,000 years (e.g., Preece et al., 2000; Jensen et al., 2016). A major research focus has been on the last interglacial (MIS 5e), and this work has shown that eastern Beringia may contain multiple sites with relatively intact MIS 8 (290-250 ka) to Holocene sites (e.g., Jensen et al., 2013, 2016) that may provide a much more complete picture of terrestrial paleoenvironmental change over the last several interglacial-glacial cycles—a rare perspective, especially for sites adjacent to major ice-sheets. Numerous tephra deposits found in eastern Beringian sedimentary deposits, were indispensable for correlating and dating these unique records.

Tephrochronology has been critical to developing our understanding of broad glacial-interglacial sedimentary records in eastern Beringia. Successful dating of tephra layers in this region has been accomplished using multiple techniques: fission-track dating (e.g. Westgate et al., 1990; Péwé et al., 2009), ^{40}Ar-^{39}Ar dating (Kunk, 1995), luminescence dating (Berger, 1987; Auclair et al., 2007; Lamothe et al., 2020), and more recently using U-based dating methods

(Burgess et al., 2019; Burgess et al., 2021; Buryak et al., 2022). Until recently, distal tephra beds in eastern Beringia >50 ka were predominantly dated by fission-track method (Westgate et al., 1990; Preece et al., 1999, 2000; Sandhu et al., 2001). Ages for various tephra beds obtained through this technique span from <100 ka to 3.5 Ma (Westgate et al., 1990, 2008; Sandhu and Westgate, 1995; Preece et al., 1999; Sandhu et al., 2001). Playing a pivotal role, these ages have contributed to determining crucial geological and paleoenvironmental events, such as the initiation of loess deposition in interior Alaska and the first advance of the Cordilleran ice sheet into the Yukon Territory (Preece et al., 1999; Westgate et al., 2005). However, the relatively low precision of fission-track dates (often >20% at 95 % confidence level) and the dating material requirements (e.g., non-pumiceous glass; defect-free zircon/apatite) often restrict its application.

Luminescence dating has also been used to construct chronological constraints on eastern Beringian tephra deposits dating mainly between 50 to 250 ka (Berger et al., 1992, 1996; Berger and Péwé, 2001; Auclair et al., 2007; Roberts, 2012; Lamothe et al., 2020). Thermoluminescence or infrared stimulated luminescence are the main techniques applied to either coarse-grain feldspar crystals or polymineral fine grained aliquots. Potential drawbacks for the utility of luminescence dating to Beringian studies include under-correction of the data for anomalous fading resulting in age underestimation (e.g., Huntley and Lamothe, 2001, Lamothe et al., 2020) and inability of multi-aliquot protocols to resolve the degree of partial bleaching in a sample leading to significant age overestimation (e.g., Zhang and Li, 2020).

Potassium-argon and argon-argon dating of volcanogenic deposits are established techniques in other settings, yielding high-resolution eruption ages. However, both techniques are typically unsuitable for dating distal tephra layers in eastern Beringia, which are characterized by fine grain sizes, low crystal content, and low potassium concentrations (Shane, 2000; Alloway et al., 2007).

As a result of these limitations in established dating techniques for distal tephra, dating many Pleistocene-aged tephra beds in eastern Beringia—especially the typically low to medium K calc-alkaline dacitic to rhyolitic tephra—has long been a challenge. Tephra beds recovered from MIS 5–7 sediments are too old for indirect dating by radiocarbon and typically lack suitable mineral phases for $^{40}Ar/^{39}Ar$ dating. Continuous improvements in the sensitivity of inductively coupled plasma mass spectrometry and geochronological methodology have led to recent major advances in applying U-Th and U-Pb dating to these problematic tephra beds (and others containing the appropriate mineral phases). As a result, U-based dating, including U-Pb, U-Th disequilibrium, and (U-Th)/He methods, has increasingly been used to date young volcanic deposits (e.g., Österle et al., 2020; Burgess et al., 2021; Prentice et al., 2022; Buryak et al., 2022). The utility of these dating methods to tephrochronometry (determination of the numerical age of the tephra) is critical to elucidation of depositional history and stratigraphy in eastern Beringia and elsewhere.

The importance of accurate and precise tephrochronometry is acute in the context of the last interglaciation (MIS 5; 130,000–71,000 years ago) and both the preceding and proceeding glaciations in eastern Beringia. Abundant sedimentary sections covering this interval are preserved across Yukon and Alaska, and these exposures have long been of interest due to their potential to preserve paleoenvironmental, paleoclimatic, paleobiological, and paleogenomic information. The environmental reconstructions of this period mainly draw from exposures associated with the ~160 ka Old Crow tephra (Hamilton and Brigham-Grette, 1991; Reyes et al., 2023), revealing complex environmental dynamics during MIS 5. Alaskan coastal evidence from

MIS 5e (130-118 ka) depicts submergence of the Bering land bridge (Brigham-Grette, 2001) and sea levels higher than today, with the Bering Sea remaining ice-free (Brigham-Grette and Hopkins, 1995). Fossil records indicate warmer summer temperatures, with the boreal forest extending kilometers north of the present tree line in the Yukon Territory and northwest Alaska (Matthews et al., 1990). Central Alaska experienced widespread thawing and erosion of permafrost during this period (Péwé et al., 1997). The knowledge of the preceding interglacial (MIS 7) remains limited due to the scarcity of major studies. Broad climatic reconstructions, based on variations in climatic controls such as insolation, suggest fluctuations similar to MIS 5a-d but not reaching the ice volume minima observed in MIS 5e (Bartlein et al., 1991). Many tephra beds are found in sediments likely dating to this broad MIS 5–7 interval, but difficulties establishing direct ages of these tephra has hindered detailed correlations of MIS 5 exposures. Indeed, chronological uncertainty even for key beds such as Old Crow tephra has led to fundamental problems in the chronostratigraphic framework for the late-Middle and early-Late Pleistocene in this broad region.

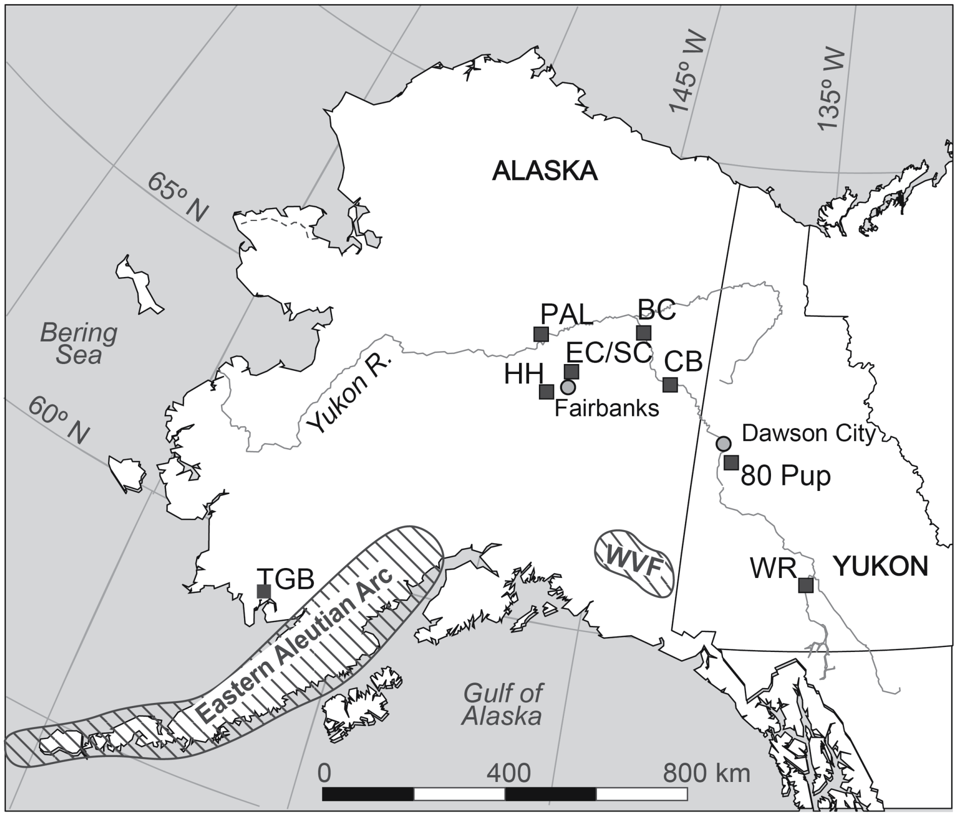

Figure 5.1. *Map of Yukon and Alaska with the locations of the sampling sites for the tephra analyzed in this study and major volcano source regions (WA, Wrangell Arc). PAL (Palisades): PAL tephra, Old Crow tephra; EC/SC (Eva Creek/Sheep Creek Valley): Sheep Creek-Fairbanks tephra; TGB (Togiak Bay): Old Crow tephra; 80 Pup: 80 Pup tephra; WR (White River) Woodchopper Creek tephra, Snag tephra. HH (Halfway House), CB (Chester Bluff), BC (Birch Creek)*

The objective of this paper is to contribute towards resolution of these chronological uncertainties. We combine new techniques in zircon dating (e.g., Buryak et al., 2022) with published and unpublished stratigraphic and geochemical data from key sites across eastern Beringia. Our improved chronostratigraphic framework for MIS 5–7 sedimentary archives in Yukon and Alaska is underpinned by new U-Pb and/or U-Th zircon ages for Snag, Woodchopper

Creek, Old Crow, Sheep Creek-Fairbanks, Biederman, PAL, and 80 Pup—seven important regional marker tephra deposits collected at various sites in Yukon and Alaska (Preece et al., 2000; Preece et al., 2011; Matthews et al., 2003; Jensen et al., 2008; Jensen et al., 2013, Jensen et al., 2016; Fig 5.1.; Table 5.1.). Additionally, we provide (U-Th)/He zircon ages for Biederman tephra and Woodchopper Creek tephra and revised glass fission-track ages for Dominion Creek and VT tephra. In turn, we use the new tephra zircon ages to add additional age control to multiple undated tephra found in association with the dated units. We evaluate our new geochronological framework using stratigraphic and tephra geochemical information from sites across Yukon and Alaska. This new framework will provide a refined MIS 5–7 tephrochronological foundation for paleoenvironmental, palaeoclimatological, paleogenomic and paleobiological studies in the region.

Table 5.1. Tephra collection accession ID numbers and sampling locations for dated tephra beds.

Tephra	ID	Sample Location	Coordinates
Biederman	UT1884	II Bluff, Yukon River	65° 22' 48" N 142° 40' 12" W
Woodchopper Creek	UA1582	White River	62° 34 '41" N 139° 59 '47" W
Snag	UA1589	White River	62° 34 '41" N 139° 59 '47" W
Old Crow	UA1422, UT1434, UT1577	Palasides West (UA1422) Togiak Bay (UT1434, UT1577)	65° 6' 45" N 153° 25' 49" W (UA1422) 58° 42' 18" N 161° 02' 12" W (UT1577) 58° 47' 23" N 161° 10' 45" W (UT1434)
Sheep Creek-Fairbanks	UA207, UT734	Eva Creek (UA207) Sheep Creek Valley (UT734)	64° 47' 60" N 147° 59' 60" W (UA207) 64° 54' 0" N 147° 53' 60" W (UT734)
PAL	UA1305	Palisades	65° 5' 60" N 153° 11' 60" W
80 Pup	UT14	Dawson City	64° 0' 18" N 139° 5' 10" W

Note: UT = University of Toronto collection, UA = University of Alberta collection. Both collections are located at Earth and Atmospheric Sciences Department, University of Alberta, Alberta, Canada.

5.2. Methods

Zircon crystals were extracted from bulk tephra samples from the University of Alberta Tephra Collection (Table 5.1), which were collected at localities across Yukon and Alaska (Fig 5.1). The samples were sieved to isolate the <250 μm fraction and zircon crystals were separated using standard heavy-liquid density separation methods (e.g., Strong and Driscoll, 2016). Zircon crystals were hand-picked from the heavy concentrate under a stereoscopic microscope and mounted in epoxy for analysis. All grains were inspected for inherited cores, inclusions, physical defects, and zonation patterns using cathodoluminescence, backscatter electron imaging, and reflected and transmitted light microscopy. The zircon U-Pb and U-Th analyses were performed at Arctic Resources Geochemistry Laboratory over several analytical sessions.

5.2.1. Sector-field (SF)-ICP-MS U-Pb dating

Zircon crystals from Snag, Woodchopper Creek, Old Crow, Sheep Creek-Fairbanks, Biederman, PAL, 80 Pup, Boneyard, Dominion Ash Bed and P14 tephra were analyzed for U-Pb dating using a RESOlution ArF Excimer 193 nm laser ablation system coupled to a Thermo Scientific Element XR magnetic sector-field (SF)-ICP-MS, using a Laurin-Technic S-155 cell. Samples were spot ablated for 40 seconds using a 40 μm beam or 50 μm beam (Woodchopper Creek and PAL tephra only) at a 5 Hz repetition rate and laser energy at the sample surface ~3 J/cm^2. The resulting ablation pits are flat-bottomed with near-vertical sides and ~10-15 μm deep. The mass spectrometer was operated in low mass resolution mode (M/ΔM= ~300). An analysis comprised 30 seconds of background gas collection followed by 40 seconds of ablation. Ablated aerosols were entrained in a He cell gas flow (0.35 L/min) and subsequently mixed with Ar (0.85 L/min) prior to entering the ICP-MS torch. The instrument was optimized by ablating NIST 612. Argon and helium gas flow, torch position, and focusing potentials were tuned to achieve optimal signals on Pb and U, and ThO/Th < 0.2%. Data were collected for ^{202}Hg, ^{204}Pb, ^{206}Pb, ^{207}Pb, ^{208}Pb, and ^{235}U using the ion counting modes of the SEM detector; for ^{232}Th using triple detection mode; and for ^{238}U using analog mode. Dwell times were 10 ms (masses 202, 204), 20 ms (masses 208, 232, 235, 238), 40 ms (mass 206) and 50 ms (mass 207). The primary standard reference sample 91500 (1062.4 ± 0.4 Ma; Wiedenbeck et al., 1995) and secondary zircon reference materials GJ-1 (608.5 ± 0.4 Ma; Jackson et al., 2004), Plešovice (337.1 ± 0.4 Ma; Sláma et al., 2008), Bishop Tuff (0.767 ± 0.001 Ma; Crowley et al., 2007; Chamberlain et al., 2014; Ickert et al., 2015), and Fish Canyon Tuff (28.402 ± 0.023 Ma; Schmitz and Bowring, 2001) were analyzed before and after each set of 10–20 unknowns to monitor U-Pb fractionation, reproducibility, and instrument drift. The ^{206}Pb-^{238}U ages for reference materials (Supplemental Table D.2) are within 2σ uncertainty of the literature values: values for the entire suite of analyses within the permissible range at 95% confidence level for the single population of replicated analyses (Mahon, 1996). The ^{206}Pb/^{238}U average precision of secondary reference materials is ~1.6% (2σ) for individual spot analyses. Data were reduced off-line using Iolite software (v.4.1) following the method described by Paton et al. (2010, 2011) for subtraction of gas blanks and U-Pb downhole fractionation correction. The uncertainties of measured isotopic ratios are a quadratic combination of the standard error of the measured isotope ratio and reproducibility of the reference material. Zircon U-Pb data is summarized in the Supplemental Table D.1.

5.2.2. Sector-field (SF)-ICP-MS U-Th dating

Zircon crystals from Woodchopper Creek, Snag, Old Crow, Biederman and PAL tephra were analyzed for U-Th dating using a RESOlution ArF Excimer 193 nm laser ablation system coupled to a Thermo Scientific Element XR magnetic sector-field (SF)-ICP-MS, using a Laurin-

Technic S-155 cell. Samples were spot ablated for 40 seconds using a 50 µm beam at a 5 Hz repetition rate and laser energy at the sample surface ~3 J/cm^2. The resulting ablation pits are flat-bottomed with near-vertical sides and ~10-15 µm deep. The mass spectrometer was operated in low mass resolution mode (M/ΔM= ~300). An analysis comprised 30 seconds of background gas collection followed by 40 seconds of ablation. Ablated aerosols were entrained in a He cell gas flow (0.35 L/min) with Ar (0.85 L/min) prior to entering the ICP-MS torch. The instrument was optimized by ablating NIST 612 with a 50 µm beam diameter, 10 Hz repetition, at 3 µm/s scanning speed and 3.5 J/cm^2 laser fluence, resulting in a sensitivity of ~ 1.4 Mcps on ^{238}U. Argon and helium gas flow, torch position, and focusing potentials were tuned to achieve optimal signals on Pb and U, and ThO/Th ~0.015%. Data were collected for 228, 230, 235 amu using the ion counting modes of the SEM detector, for 232 amu using triple detection mode, and for 238 amu using analog mode. Dwell times were 20 ms (^{232}Th, ^{235}U, ^{238}U), 50 ms (mass 228) and 150 ms (^{230}Th). The gas blank corrected count rates and analytical uncertainties were derived using Iolite (4.1) and after processed using Excel in-house spreadsheet.

The relative sensitivity factor and mass bias corrections were performed using approach described in Guillong et al. (2016) by normalizing average ^{238}U/^{232}Th ratio in 91500 zircon crystals to the known concentrations of U = 81.2 ppm and Th = 28.6 ppm resulting in a correction factor ~ 1.01 ± 0.02. The data accuracy was verified by observing the degree of deviation of ^{230}Th/^{238}U in 91500, Plešovice and Bishop Tuff ratio from unity.

The procedure consists of correcting for: (1) interferences on ^{230}Th caused by polyatomic zirconium oxides generated during ablation, (2) the abundance sensitivity effect of ^{232}Th on ^{230}Th, which is estimated using monazite measurements, and (3) the relative sensitivity factor using zircon 91500 as reference material. Zircon U-Th data is summarized in Table D.3.

5.2.3. (U-Th)/He dating

Individual zircon crystals from the Biederman and Woodchopper Creek tephra were selected under a stereo-zoom microscope based on crystal morphology, size, and clarity. The (U-Th)/He analyses for Biederman tephra were performed at Arizona Radiogenic Helium Dating Laboratory, University of Arizona. The alpha-ejection (FT) correction (Ketcham et al., 2011) was calculated using crystal dimensions measured from digital images. Individual zircon crystals were placed inside niobium (Nb) tubes that were sealed on both ends. The Nb packets were then heated using an Nd-YAG laser system to 1065 ˚C for 180 seconds. Extracted radiogenic He was spiked with ^{3}He and further purified using cryogenic and gettering techniques. The He isotope analyses were performed using quadruple mass spectrometer. After the zircon crystals were dissolved in HF at 90 ˚C for 24 hours. ^{233}U-^{229}Th and ^{147}Sm spikes were used to measure the U, Th, Sm concentrations in zircon by isotope solution and dilution using an Thermo Scientific Element 2 ICP-MS.

The Woodchopper Creek tephra (U-Th)/He analyses were performed at UTChron Laboratory, University of Texas at Austin. For Woodchopper Creek tephra zircon crystals were individually packed into platinum (Pt) foil packets. The packets were heated and degassed under ultra-high vacuum; total He concentration was measured on a quadrupole mass spectrometer. Completely degassed grains were removed from Pt packets and dissolved with a combination of HF and HNO_3. Dissolved samples were analyzed on a Thermo Scientific Element 2 ICP-MS for absolute U, Th, and Sm concentrations. Fish Canyon Tuff zircons were run with unknown grains to monitor data quality (Reiners, 2005). 15% standard error was applied to all measurements.

All methods followed here were described in detail by Reiners et al. (2004) and Reiners (2005). The (U-Th-Sm)/He dating results presented in Table D.4.

5.2.4. Tephra glass geochemistry

Single shard glass major-element geochemistry was determined by wavelength dispersive spectrometry on a JEOL 8900 or CAMECA SX100 electron microprobe at University of Alberta using 15 keV accelerating voltage, 6 nA beam current, and 10 µm beam diameter. Some analyses used a 5 µm beam and the software Probe for EPMA (Donovan et al., 2015) to correct for any potential Na-loss using time-dependent intensity corrections (e.g., Jensen et al., 2021). Two secondary reference materials, Lipari obsidian (ID 3506) and Old Crow tephra glass (Kuehn et al., 2011), were run concurrently with all samples to assure proper calibration. All data were normalized to 100% on a water-free basis.

Trace-element compositions were determined by LA-ICP-MS using a RESOlution ArF 193 nm excimer laser ablation system coupled to a Thermo Scientific Element XR Sector Field (SF)-ICP-MS at the University of Alberta Arctic Resources Geochemistry Laboratory. Individual glass shards were analyzed with a 10 or 23 µm diameter beam at 2.8 J/cm^2 and 4.5 J/cm^2 respectively energy density (measured at the ablation site), 5 Hz repetition rate, and 20 s ablation time. ^{29}Si was used as an internal standard and the instrument was calibrated against NIST SRM 612. We analyzed NIST SRM 610, ATHO-G and Walcott tuff as secondary standards and reference materials to monitor accuracy and analytical reproducibility. All major/minor oxide, trace element and reference material are listed in Supplementary Tables D.7-8.

5.2.5. Glass fission track methods

We recalculated previously published glass fission-track ages for the Dominion Creek and VT tephra using the most recent and precise Moldavite tektite age of 14.808 ± 0.021 Ma ($^{40}Ar/^{39}Ar$, Schmieder et al., 2018). The fission-track method used to determine the eruption age of natural glasses is the zeta calibration method (Hurford and Green, 1983), with the Moldavite tektite as the reference material. There have been multiple previous age determinations for the Moldavite tektite: 15.1 ± 0.7 Ma (K-Ar, Gentner et al., 1967); 15.21 ± 0.15 Ma ($^{40}Ar/^{39}Ar$, Staudacher' et al., 1982); 14.34 ± 0.08 Ma ($^{40}Ar/^{39}Ar$, Laurenzi et al., 2007); and 14.68 ± 0.055 Ma ($^{40}Ar/^{39}Ar$, Di Vincenzo and Skála, 2009). More detailed descriptions of glass fission-track age calculation are available in Westgate (1989) and Sandhu and Westgate (1995). Individual recalculated glass fission-track age determinations for a given tephra were combined as inverse-variance weighted means (Supplemental Table D.5.). The averaging of age determinations on different field tephra samples, either at the same site or at different sites, is justified by tephra correlations based on glass geochemistry supplemented by mineralogy, morphology, and stratigraphy. All reported glass fission-track ages in this paper are reported with 2σ uncertainty.

5.3. Site Descriptions

5.3.1. Halfway House

The Halfway House locality (64° 42' 29" N, 148° 30' 11" W) is an important loess deposit located approximately 47 km west of Fairbanks, Alaska (Fig. 5.1.; Fig. 5.2.). Despite poor chronological controls, the Halfway House site is one of the most extensively studied loess deposits in Alaska, providing important tephrochronological and paleoenvironmental insights (e.g., Westgate et al., 1983, 1985; Begét and Hawkins, 1989; Begét, 1990; Begét et al, 1990; Preece et al., 1999; Vlag et al., 1999; Berger, 2003; Muhs et al., 2003, 2008; Jensen et al., 2016).

The Halfway House section is a ~15-meter-thick mid-slope loess exposure with two distinct paleosols and multiple tephra beds found across the section. The lowest tephra in the section is correlated to the undated Boneyard tephra, which is also found at the Palisades and

Gold Hill Loess sites and is located approximately 1 meter below the prominent Old Crow tephra bed (159 ± 8 ka; Reyes et al., 2023) (Muhs et al., 2003, 2008; Jensen et al., 2016). At the Halfway House site, the Old Crow tephra is located stratigraphically below the lower paleosol layer, which thus likely represents MIS 5. Furthermore, the WRUN 5, Snag, Halfway House, and VT (130 ± 59 ka; revised glass fission-track) tephra beds are found stratigraphically above the Old Crow tephra (Preece et al., 1999; Jensen et al., 2016). Additionally, the Snag and WRUN5 tephra have been found in the same stratigraphic sequence at exposures on the White River, Yukon (Turner et al., 2013). At the top of the Halfway House section, the Sheep Creek-Klondike and Dominion Creek (80 ± 18 ka; revised glass fission-track) tephras overlie the upper distinct paleosol unit, which was likely deposited during MIS 3.

5.3.2. Palisades

The Palisades (65° 5' 60" N, 153° 11' 60" W; "The Boneyard") in central Alaska is a 8-km-long bluff featuring gully and face exposures of perennially frozen loess, peat, forest beds, large ice bodies, and tephra beds (Fig 5.1.; Fig. 5.2.). Building on the work of Begét et al. (1991) and Matheus et al. (2003), Reyes et al. (2010a, 2010b) documented relict ice wedges at the Palisades that persisted through MIS 5e and described an *in-situ* tundra surface buried by Old Crow tephra. Jensen et al. (2013) provided a chronostratigraphic revision of Palisades East based on detailed tephrostratigraphic and paleomagnetic sampling.

The chronological framework at this site relies primarily on tephrochronology, including Old Crow tephra (158 ± 8 ka; Reyes et al., 2023), Sheep Creek-Fairbanks tephra (190 ± 40 ka; Berger et al., 1996), and previously undated PAL tephra (Matheus et al., 2003; Jensen et al., 2013). The geochemical similarity between PAL tephra and the older ca. 2 Ma PA tephra initially suggested that the two beds could be comagmatic and of similar age (Matheus et al., 2003). However, based on stratigraphic association between PAL and underlying beds, the normal polarity of the host sediments, and the presence of overlying Sheep Creek-Fairbanks tephra, PAL might be older than ca. 200 ka but younger than ca. 500 ka.

Furthermore, PAL tephra underlies an organic-rich bed with undated P8, PAU, P9, and P10 tephra beds (Jensen et al., 2013). A second stratigraphically higher organic-rich layer is in turn found between P10 tephra and Sheep Creek-Fairbanks tephra, with Boneyard and Old Crow tephra beds stratigraphically above the Sheep Creek-Fairbanks tephra. Finally, Old Crow tephra is overlain by another organic-rich unit, likely indicating deposition during MIS 5, with P14 tephra deposited within it and Halfway House tephra stratigraphically above.

5.3.3. Birch Creek

The Birch Creek site (65° 49' 19” N, 144° 17' 38" W) exposes ~45 m of loess, reworked loess, and paleosols ~200 km northeast of Fairbanks (Fig. 5.1.; Fig. 5.2.). At this site, the Old Crow tephra was deposited above an organic-rich layer that is interpreted as forest duff and is overlain by about 1 m of bedded, organic-rich, redeposited silt (Edwards and McDowell, 1991).

The Biederman tephra (178 ± 17 ka; Buryak et al., 2022) is found stratigraphically below the ca. 160 ka Old Crow tephra and is cryoturbated within the upper contact of a peaty organic-rich silt bed. The Sheep Creek-Fairbanks tephra (190 ± 40 ka; Berger et al., 1996) is also present between the Old Crow and Biederman tephra beds at Birch Creek (McDowell and Edwards, 2001). The peaty organic-rich silt associated with Biederman tephra at Birch Creek is rich in *Picea* macrofossils, including well-preserved logs. Pollen samples from the equivalent unit at Chester Bluff contain up to 38% *Picea* pollen, suggesting this organic silt/peat unit represents an interglacial with a minimum age of MIS 7. Furthermore, at the Birch Creek site, the 80 Pup tephra (Preece et al., 2000) is the lowest tephra, overlain by the BC1 and BC2 tephra beds below the Biederman tephra and the overlying organic-rich silt.

5.3.4. Largent Mine

The Largent Mine (64° 50’ 56” N 148° 2’ 20” W), located 16 km west of Fairbanks, is a placer mining site that exposes middle-Pleistocene loess, paleosols, forest beds, and multiple tephra layers (Fig. 5.1.; Fig. 5.2.).

At this site, the 80 Pup tephra is found beneath the BC1 tephra, following the same stratigraphic sequence as observed at the Birch Creek site, with both tephra deposits lying below an unconformable surface. Above this unconformity, the Boneyard tephra lies below the ca. 160 ka Old Crow tephra, located beneath an organic-rich bed that possibly represents a substage during the last interglacial period (likely MIS 5e). Stratigraphically above this organic-rich bed, the SD, Halfway House, and VT (130 ± 59 ka; revised glass fission-track) tephra underlie another organic-rich horizon, likely representing a warming period during the last interglacial (Woudstra et al., 2020).

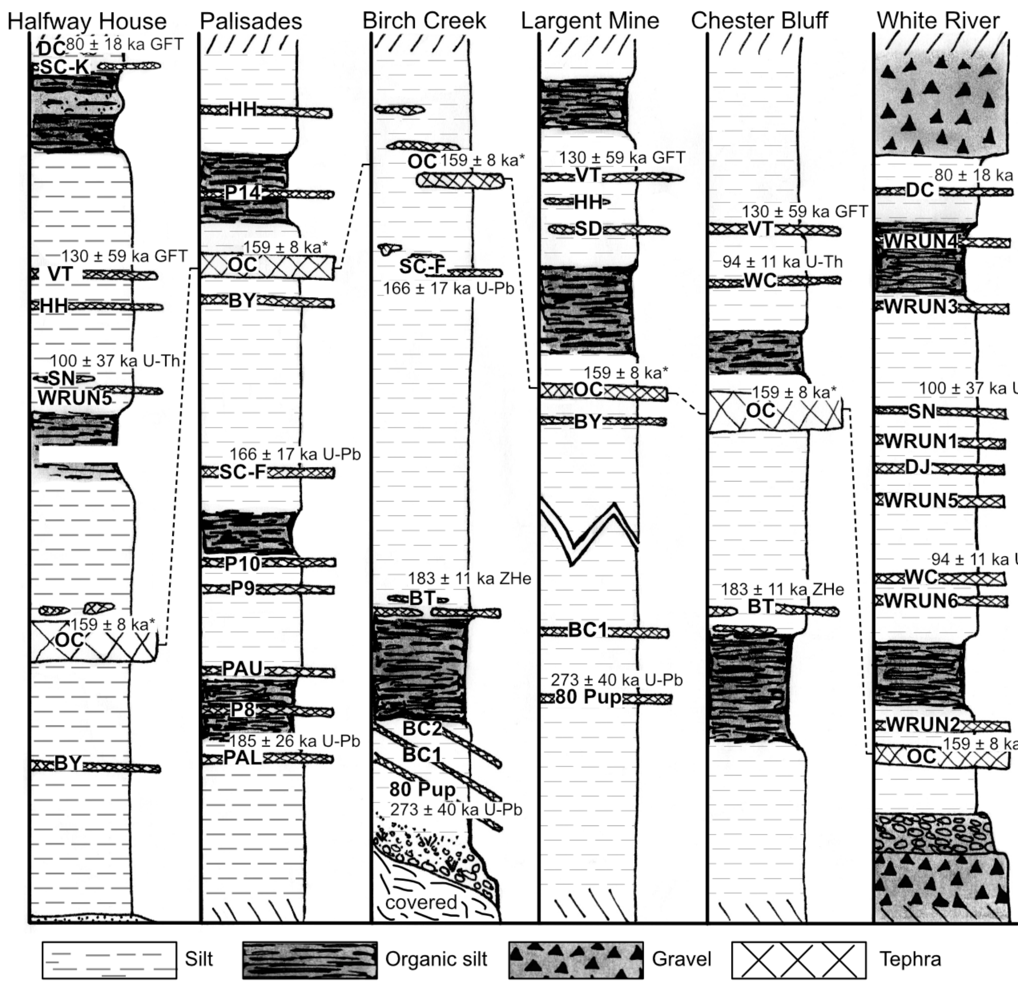

Figure 5.2. *Schematic stratigraphic contexts of the tephra beds in this study. All quoted ages are new data presented in this chapter, with the exception of the Old Crow tephra age estimated from marine sediments (asterisk; Reyes et al., 2023). All locations are composite stratigraphic columns. DC = Dominion Creek tephra; HH = Halfway House tephra; WRUN = White River Unknown; DJ= Donjek tephra; WC = Woodchopper Creek tephra; OC = Old Crow tephra; SN = Snag tephra; SC-F = Sheep Creek-Fairbanks tephra; BT = Biederman tephra; BC = Birch Creek tephra. GFT = glass fission-track. ZHe = zircon (U-Th)/He dating.*

5.3.5. Chester Bluff

Chester Bluff (65° 20' 16.8" N; 142° 43' 30" W) is a site located on the Yukon River in east-central Alaska (Fig. 5.1.; Fig. 5.2.). The upper 15-20 m of loess at Chester Bluff contains previously described tephra beds from MIS 5–7, as well as at least two organic horizons that could potentially represent individual interglacial deposits (e.g., Jensen et al., 2008; Westgate et al., 2013; Westgate and Pearce, 2017). However, there are a number of unconformities present in these sequences, and not all of the sections contain the same tephra sequences. In some instances, the loess, tephra, and organic beds are faulted and overturned, and relatively few of the horizons indicate primary deposition (Jensen et al., 2008). At the Chester Bluff site, the Biederman tephra (178 ± 17 ka; Buryak et al., 2022) is found directly above a 50-cm thick organic bed which contains *Picea* needles and ice wedge casts, likely representing MIS 7. The Old Crow tephra is in turn overlain by an organic-rich horizon (MIS 5), with the VT tephra and Woodchopper Creek tephra above it. Although the Old Crow tephra does not occur together with the Biederman tephra, it does occur at an elevation that is higher than the Biederman tephra.

5.3.6. White River

The White River sections (62° 34'41" N 139° 59'47" W; Fig. 5.1; Fig. 5.2.) provide a record of glacial limits and paleoenvironmental changes during the middle to late Pleistocene in southwest Yukon and southeast Alaska. The exposures contain glacial and non-glacial deposits with multiple tephra beds, extending the record beyond the limit of radiocarbon dating (Turner et al., 2013).

The MIS 5–7 chronostratigraphic framework is based on discrete rhyolitic to rhyodacitic tephra beds (Old Crow, Woodchopper Creek, Donjek, Snag, Dominion Creek). At the White

River, the Old Crow tephra, widely identified below the last interglacial forest beds (MIS 5e), serves as an informal marker bed for latest MIS 6. The Woodchopper Creek tephra, positioned within the early to mid-MIS 5 age range, is found stratigraphically above the Old Crow tephra and is overlain by MIS 4 till deposits. Additionally, the Woodchopper Creek tephra is found above the MIS 5e forest bed deposits and is overlain by WRUN5, Donjek, WRUN1, Snag, WRUN 3, and WRUN4, and ca. 80 ka Dominion Creek tephra beds (Turner et al., 2013).

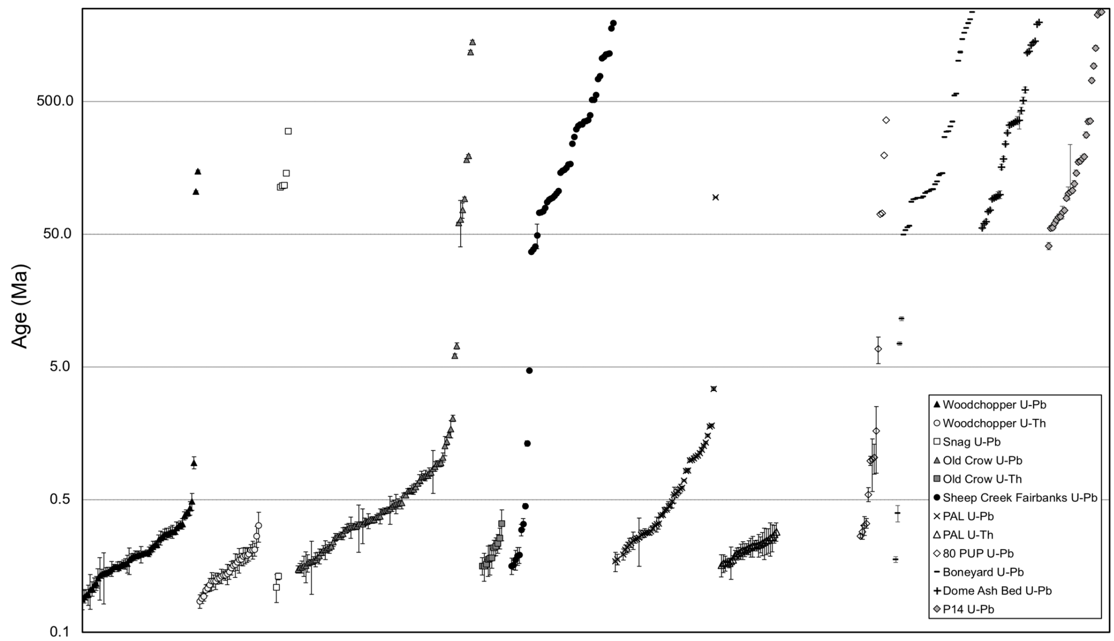

Figure 5.3. *U-Pb and U-Th zircon age rank-order plot for all samples. Note the logarithmic y-axis scale. Uncertainties are displayed at 2σ level.*

5.4. Results

5.4.1. Geochronology Results

The zircon age spectra for all analyzed samples are complex and heterotemporal, suggesting prolonged crystallization and/or post-depositional re-working (Fig. 5.3.). The presence of multiple zircon age populations makes interpretation of the age data challenging for both U-Pb and U-Th zircon dating methods. The challenges for U-Pb zircon dating for Alaska and Yukon tephra were detailed in Buryak et al. (2022).

U-Th disequilibrium data for all analyzed zircon crystals show a variable degree of U-excess, allowing us to calculate model ages (Fig. 5.4.). U-Th data for Woodchopper Creek, Biederman, Old Crow, and Snag tephra do not describe an isochron; instead, they plot as sphenochrons or wedges (Chen et al., 1996). This distribution of the U-Th age data suggests prolonged crystallization of zircon in the magma chamber, resulting in multiple zircon age populations and potentially the presence of older xenocrystic or detrital zircon that are in secular equilibrium (Schmitt, 2011). For our U-Th dataset, ages obtained by identifying peaks in the summed probability distribution of Gaussian uncertainties around all model ages (Lowenstern et al., 2000) would likely overestimate the "true" age of the deposit due to the presence of antecrystic zircon analysis. Here, to estimate the ages of individual crystals, we calculate two-point zircon-melt (glass) isochrons (e.g., Harangi et al., 2015). We use groundmass glass Th and U concentrations to estimate the initial isotopic composition of the melt at the time of zircon crystallization. In addition, we calculate U-Th model ages using the routine proposed by Bohenke et al. (2016) with $Th/U_{zircon/melt} = 0.14 \pm 0.08$. This approach yields ages that are similar to those obtained by two-point isochrons. For consistency, we rely on two-point zircon-melt isochron ages.

Table 5.2. Comparison of maximum deposition age methods used in this study. MLA: maximum likelihood algorithm; YSG: youngest single grain. All ages reported at 2σ uncertainties. Ages in bold are preferred.

U-Pb ages

Tephra	Bayesian Age	Weighted Mean	MLA	YSG	(U-Th)/He
Woodchopper Creek	**92 ± 15 ka**	103 ± 9 ka	98 ± 18 ka	90 ± 29 ka	**114 ± 13 ka**
Snag	-	**131 ± 15 ka**	-	110 ± 52 ka	-
Old Crow	**151 ± 14 ka**	166 ± 8 ka	165 ± 10 ka	150 ± 18 ka	-
Sheep Creek-Fairbanks	163 ± 16 ka	166 ± 16 ka	**166 ± 17 ka**	159 ± 44 ka	-
PAL	**185 ± 26 ka**	207 ± 15 ka	192 ± 56 ka	176 ± 56 ka	-
80 Pup	**273 ± 40 ka**	297 ± 23 ka	300 ± 24 ka	267 ± 36 ka	

U-Th ages

Tephra	Bayesian Age	Weighted Mean	MLA	YSG	(U-Th)/He
Woodchopper Creek	**94 ± 11 ka**	106 ± 9 ka	99 ± 15 ka	86 ± 21 ka	-
Snag	-	**100 ± 37 ka**	-	94 ± 44 ka	-
Old Crow	**164 ± 29 ka**	181 ± 17 ka	170 ± 41 ka	159 ± 47 ka	-
PAL	**173 ± 17 ka**	192 ± 25 ka	180 ± 26 ka	161 ± 60 ka	-
Biederman	**164 ± 21 ka**	171 ± 11 ka	173 ± 12 ka	139 ± 34 ka	183 ± 11 ka

To determine the potential eruptive U-Pb and U-Th ages, we used the age calculation routine discussed in Buryak et al. (2022). We used four methods to estimate the age for each tephra from complex U-Pb and U-Th zircon data: (1) the youngest zircon grain method, (2) Bayesian modeling (Keller et al., 2018), (3) the weighted mean age of the youngest zircon ages that have overlap at 2σ uncertainties (Sharman et al., 2018), (4) the maximum likelihood algorithm (Vermeesch, 2021) (Table 5.2.). We calculate Bayesian eruption age estimates assuming uniform and triangular zircon age distributions, and zircon crystallization distribution based on kinetic and (MELTS) thermodynamic models (Keller et al., 2018). The results are insensitive to the assumed distribution.

5.4.2. Woodchopper Creek tephra

Of the 94 U-Pb dated zircon grains for Woodchopper Creek tephra, 60 grains satisfied the <85% common-Pb threshold (Buryak et al., 2022). The filtered U-Pb ages ranged from 90 ka to

150 Ma, with 57% of analyses being < 200 ka, suggesting only a moderate presence of xenocrysts and/or antecrysts in the zircon population (Fig. 5.3.). The Woodchopper Creek tephra grains < 200 ka are characterized by variable U and Th concentrations ranging between 87-1242 ppm and 34-1513 ppm, respectively, with the majority of analyses < 250 ppm (Supplemental Table D.1.). Most of the zircon interiors have U-Pb ages between 135 ka and 486 ka and are indistinguishable within uncertainty from the rim zircon ages for grains that had rim-core pair analyses. Several analyses (e.g., WCT1582_32, WCT1582_60; Supplemental Table D.1.) have zircon core ages >100 ky older than a rim age. The weighted mean Woodchopper Creek tephra U-Pb age of 103 ± 9 ka (MSWD = 0.67) is slightly older than the maximum depositional ages produced by the youngest grain (90 ± 29 ka), maximum likelihood algorithm (98 ± 18 ka) methods, and the Bayesian model (92 ± 14 ka) (Fig. 5.4; Table 5.2.).

The U-Th zircon data for Woodchopper tephra do not describe a clear isochron but rather plot as a sphenochron ("time wedge") (Fig. 5.5.), and like the U-Pb age spectrum, display multiple zircon age populations. The ages for grains that are not in secular equilibrium range from 86 to 300 ka (n=30), with the majority of analyses < 200 ka (Fig. 5.5.). The weighted mean Woodchopper Creek tephra U-Th age of 106 ± 9 ka (MSWD = 1.9) is slightly older than the maximum depositional ages produced by the youngest grain (86 ± 21 ka), maximum likelihood algorithm (99 ± 15 ka) methods, and the Bayesian model (94 ± 11 ka).

Of the 19 Woodchopper Creek tephra zircons dated by the (U-Th)/He method, 16 crystals produced meaningful ages (Supplemental Table D.4.). The disequilibrium corrected eruptive ages calculated via Monte-Carlo simulations with 100,000 trials per sample show a goodness-of-fit parameter > 10^{-4}, indicating a uniform age population. The pre-eruptive zircon residence time was constrained by U-Pb ages using the weighted mean ages of the youngest interior spot (165 ±

13 ka) analyses. The MCHeCalc (Schmitt et al., 2010) eruption age of 114 ± 13 ka (n=17; goodness of fit = 0.0178) for the Woodchopper Creek tephra is consistent within uncertainty with the U-Pb and U-Th dating results (Fig. 5.4.).

5.4.3. Snag tephra

Few zircon crystals were separated from the Snag tephra sample, and only two out of seven U-Pb dated zircon grains were <150 ka, dating to 133 ± 15 ka (Snag1589_223) and 110 ± 51 ka (Snag1589_225). The zircon weighted mean U-Pb age of 131 ± 15 ka (MSWD=0.71) was calculated for the two youngest grains.

The U-Th results for these two crystals yielded similar glass-zircon model ages at 106 ± 36 ka (Snag1589_223) and 118 ± 46 ka (Snag1589_225). The weighted mean U-Th age of 111 ± 28 ka (MSWD = 0.17) is consistent within uncertainty with the U-Th isochron age of 101 ± 47 ka (MSWD = 0.17) and the U-Pb results (Fig. 5.4.).

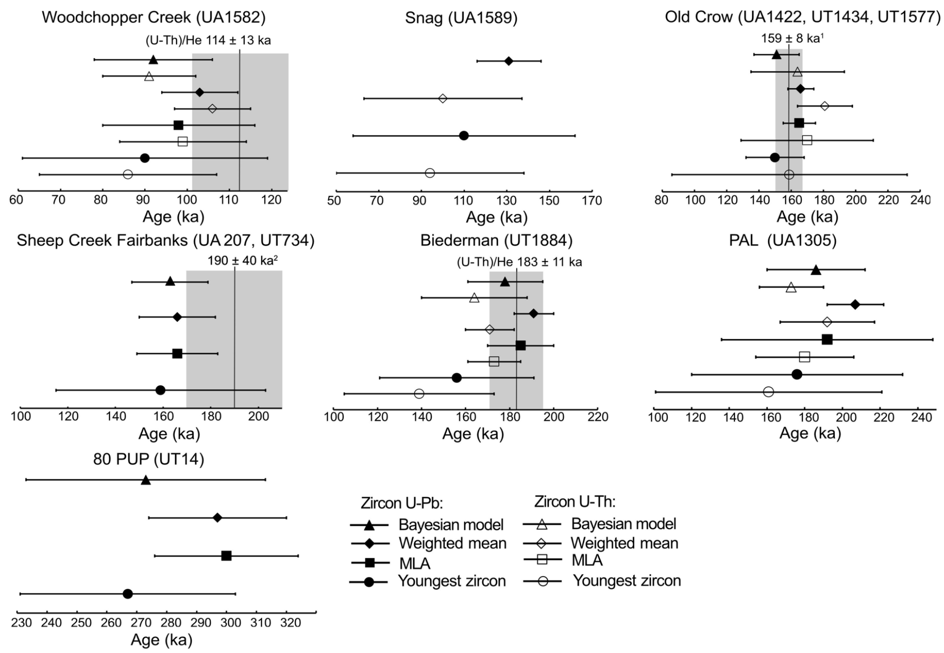

Figure 5.4. *Comparison of tephra maximum depositional age estimates for U-Th and U-Pb age data. Uncertainties are displayed at* 2σ *level.* [1]*159 ± 8 ka stratigraphic age for Old Crow tephra (Reyes et al., 2023).* [2]*190 ± 40 ka TL age for Sheep Creek Fairbanks tephra (*Berger et al., 1996).

5.4.4. Old Crow tephra

The full Old Crow tephra U-Pb dataset (n =148 dated grains) is heterotemporal, with ages ranging from approximately 150 ka to around 1.4 Ga, suggesting either a high proportion of xenocrysts and/or antecrysts in the tephra zircon population or a detrital component (Fig. 5.3.). The Old Crow tephra grains < 250 ka have variable U and Th concentrations ranging from 151 ppm to 762 ppm and from 45 ppm to 777 ppm, respectively (Supplemental Table D.1.). The weighted mean Old Crow tephra U-Pb age of 166 ± 8 ka (MSWD = 0.8) is identical to the maximum depositional age produced by maximum likelihood algorithm methods (165 ± 10 ka) and is slightly older than the youngest grain (150 ± 18 ka), and the Bayesian model (151 ± 14 ka) estimates (Fig. 5.4).

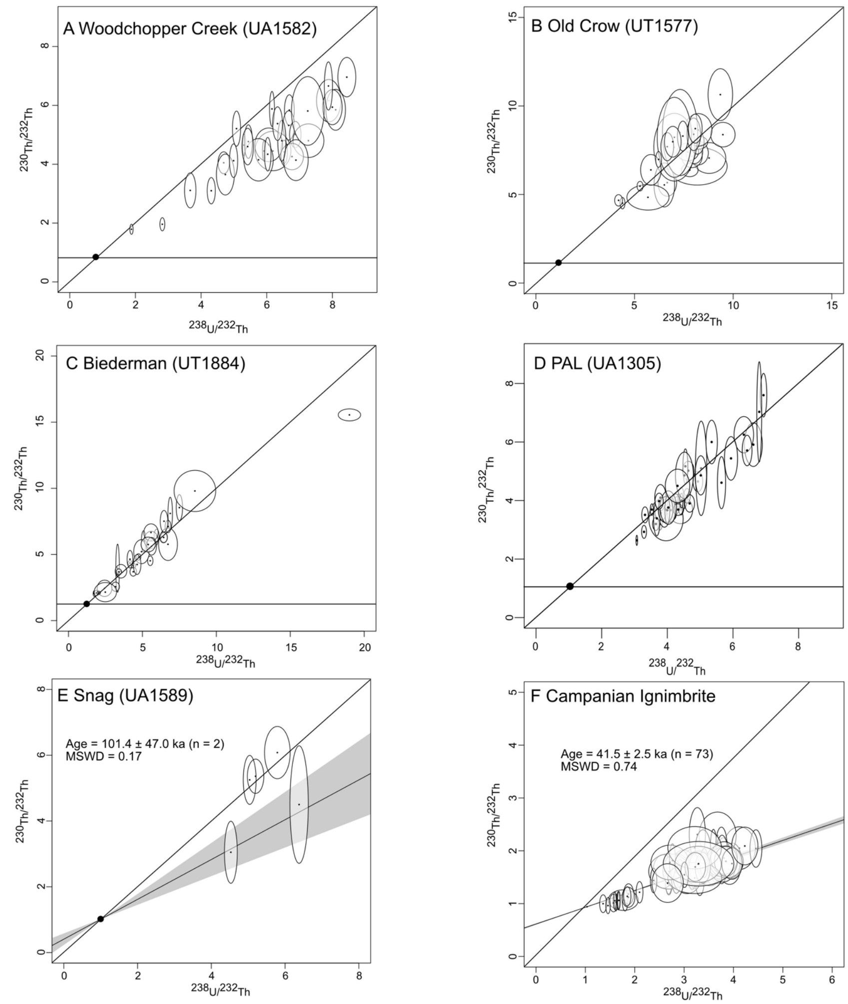

Figure 5.5. *Activity ratio diagrams for $^{238}U/^{232}Th$ and $^{230}Th/^{232}Th$. Uncertainties are displayed at 2σ level. The black circle marks the isotopic activity ratios of the groundmass glasses.*

The U-Th zircon data for Old Crow tephra plot as a sphenochron with ages ranging from 159 ka to 332 ka. Of 28 grains dated, only 11 are in secular disequilibrium, with the majority of the grains being > 350 ka (Fig. 5.5). The weighted mean Old Crow tephra U-Th age yielded is 181 ± 17 ka (MSWD = 1.2) and is slightly older than the maximum depositional ages produced by the youngest grain (159 ± 47 ka), maximum likelihood algorithm (170 ± 41 ka) methods, and the Bayesian model (164 ± 29 ka) (Fig. 5.4).

We note that the calculated U-Pb and U-Th ages are substantially younger than those obtained by Burgess et al. (2019, 2021), and discuss these differences in section 5.6.4.

5.4.5. Sheep Creek-Fairbanks tephra

The two Sheep Creek-Fairbanks tephra samples, UA207 and UT734, contained a large proportion of xenocrystic and potentially detrital zircon crystals substantially older than 0.5 Ma (Fig. 5.3.). The full U-Pb dataset is heterotemporal with ages ranging from 159 ka to 1.9 Ga. Out of 59 zircon grains analyzed only five grains were <200 ka, yielding a weighted mean age of 166 ± 16 ka (MSWD = 0.49), a Bayesian model age of 163 ± 16 ka, and a youngest grain age of 159 ± 44 ka (Fig. 5.4). Zircon U-Th data was not collected for Sheep Creek-Fairbanks tephra due to the small size of grains and high proportion of xenocrystic and/or detrital grains in the analyzed samples.

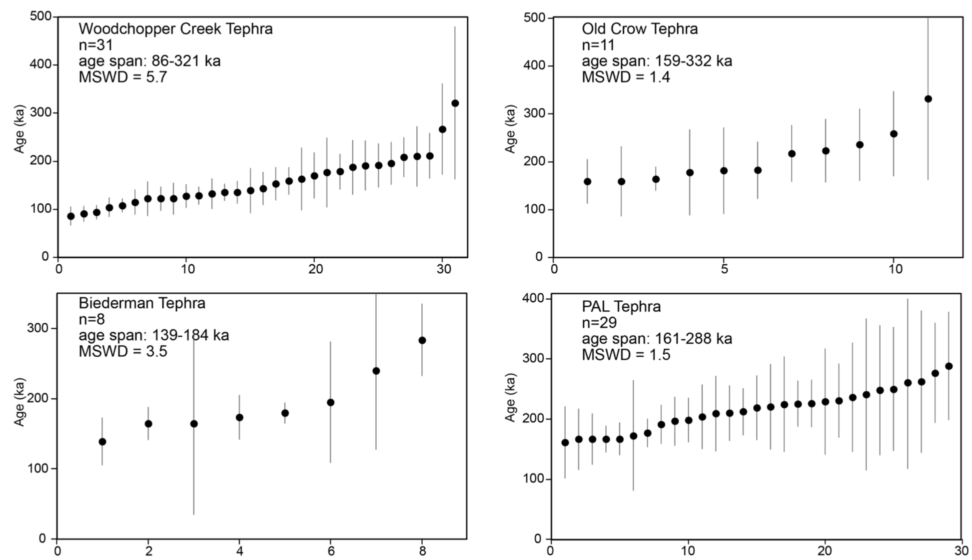

Figure 5.6. *Overview of crystallization timescales for Woodchopper Creek, Old Crow, Biederman and PAL tephra based on rank-order plots of calculated model U-Th ages (2σ error bars plotted). The text indicates the number of crystals analyzed (n), the total age span recorded, and the global MSWD of each dataset.*

5.4.6. PAL tephra

Of the 50 grains dated for PAL tephra, 34 zircon crystals satisfied the common-Pb thresholds. The PAL tephra filtered zircon ages range from 172 ka to 95 Ma, with 56% of the grains being > 300 ka and 21% of the grains being > 1 Ma, suggesting a xenocrystic, antecrystic, and/or detrital zircon component in the tephra (Fig. 5.3.). The analyses with ages < 300 ka are characterized by relatively low U and Th concentrations at 160 ± 82 ppm (1 s.d.) and 129 ± 95 ppm (1 s.d.), respectively. All five methods of calculating the maximum depositional age for PAL tephra overlap within 2σ uncertainty: the Bayesian model age of 185 ± 26 ka overlaps with the weighted mean (207 ± 15 ka, MSWD = 1.3), maximum likelihood algorithm (192 ± 56 ka), and the youngest zircon (176 ± 56 ka) age estimates (Fig. 5.4.).

The U-Th zircon data for PAL tephra display multiple zircon age populations and plot as a sphenochron (Fig. 5.5.). Of the 43 U-Th dated grains, 11 are in secular equilibrium, and the ages for grains that are < 350 ka range from 161 to 288 ka (Fig. 5.6). The weighted mean PAL tephra U-Th age of 192 ± 25 ka (MSWD = 1.9) is consistent with the maximum depositional ages produced by the youngest grain (161 ± 60 ka), maximum likelihood algorithm (180 ± 26 ka) methods, and the Bayesian model (173 ± 117 ka) (Fig. 5.4.).

5.4.7. Biederman tephra

For Biederman tephra, only eight of the 33 U-Th dated grains are not in secular equilibrium, with the age data dominated by grains > 350 ka. The Biederman U-Th model zircon ages range between 139 ka and 284 ka (Fig. 5.3.). The zircon Bayesian model yielded an age of 164 ± 21 ka, which agrees with the maximum likelihood algorithm (173 ± 12 ka), the youngest grain (139 ± 34 ka), and the weighted mean (171 ± 11 ka) methods (Fig. 5.4.).

Of the six Biederman tephra zircons dated by the (U-Th)/He method, three crystals produced ages < 200 ka. The disequilibrium-corrected eruptive ages calculated for these three grains show a goodness-of-fit parameter > 10^{-4}, indicating a uniform age population. The MCHeCalc eruption age of 183 ± 11 ka (n=3; goodness of fit = 0.0644) calculated using the weighted mean of the youngest zircon interior U-Pb ages (245 ± 17 ka) for the Biederman tephra is consistent with the U-Th dating results.

5.4.8. 80 Pup tephra

A total of 14 zircon crystals were separated from the 80 Pup (UT14) tephra sample, and only four dated zircon grains were ≤ 0.5 Ma and satisfied the common-Pb filter. The zircon weighted mean age of 297 ± 23 ka (MSWD = 2) was calculated for the four youngest ages and agrees with the Bayesian model age of 273 ± 40 ka and the maximum likelihood algorithm age of 300 ± 24 ka (Fig. 5.4.). No U-Th ages were collected for 80 Pup tephra.

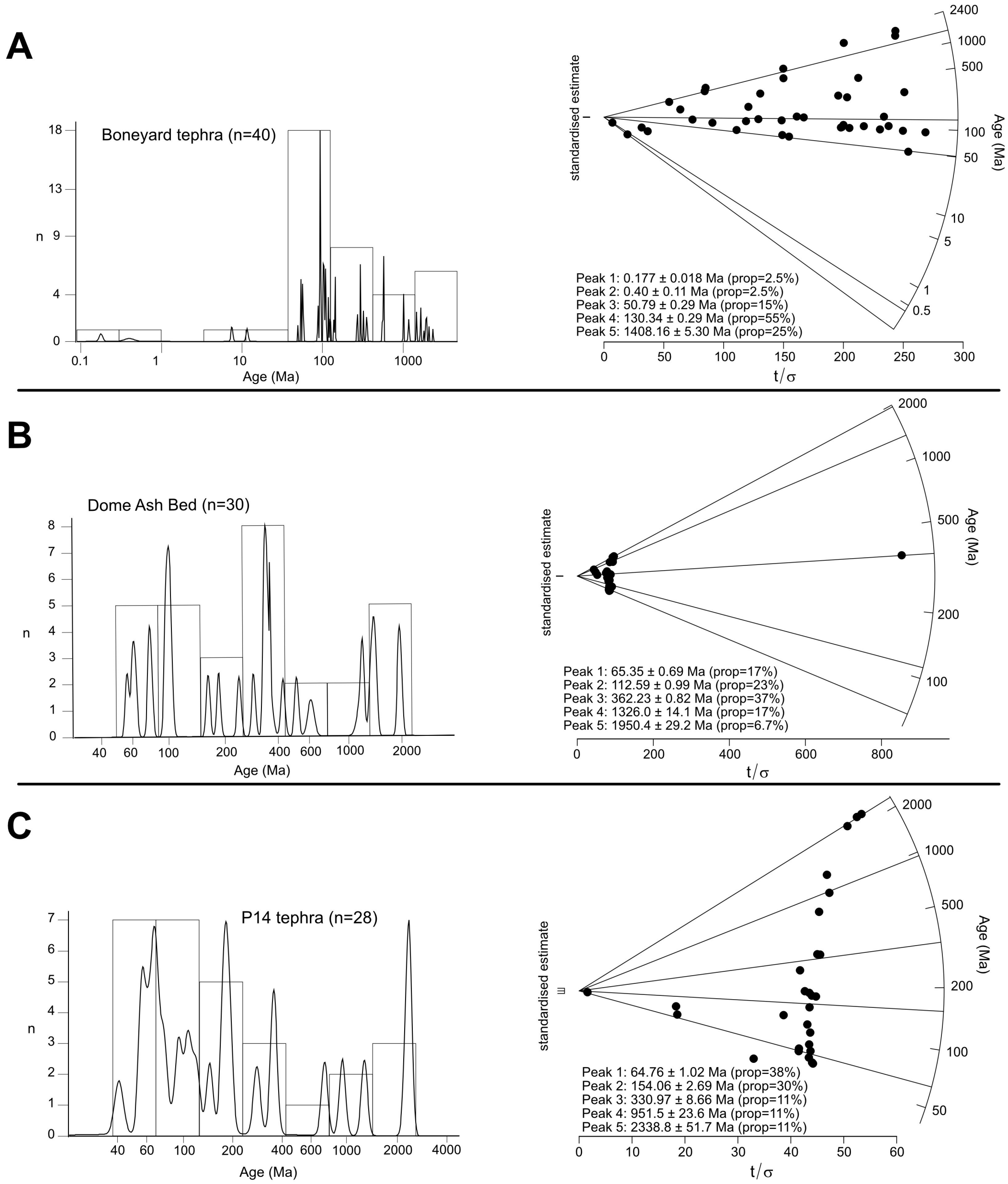

Figure 5.7. *(A) Probability density function and radial plot of Boneyard tephra zircon U-Pb dating results; (B) Probability density function and radial plot of Dome Ash Bed tephra zircon U-Pb dating results; (C) Probability density function and radial plot of P14 tephra zircon U-Pb dating results*

5.4.9. Boneyard tephra, Dome Ash Bed and P14 tephra

The Boneyard tephra yielded grains (n=40) that range in age from 177 ka to >1 Ga. The age peak fitting, performed using the algorithms of Galbraith and Green (1990) implemented in IsoplotR software with the "auto" setting using the Bayes Information Criterion to pick a parsimonious number of components, indicates five distinct age populations. Most of the grains in the Boneyard tephra date to the Cretaceous with a peak at 130.3 ± 0.3 Ma (55%) and the Mesoproterozoic with a peak at 1408.2 ± 5.3 Ma (25%) (Fig. 5.7A). A less pronounced peak is found at 50.8 ± 0.3 Ma (Eocene, 15%). Only two grains have ages <1 Ma at 396 ± 110 ka (BY1609_139) and 177 ± 18 ka (BY1609_143) (Fig. 5.7A).

No juvenile zircon crystals were recovered from Dome Ash Bed tephra. A total of 30 zircon grains were dated with ages ranging from approximately 55 Ma to around 1.9 Ga (Fig. 5.6.B). Most of the grains in the Dome Ash Bed tephra date to the Devonian with a peak at 362.2 ± 0.8 Ma (37%) and the Paleocene with a peak at 65.4 ± 0.7 Ma (23%) (Fig. 5.7B). Less pronounced peaks are found at 112.6 ± 1.0 Ma (Cretaceous, 17%), 1326.0 ± 14.1 Ma (Mesoproterozoic, 17%), and 1950.4 ± 29.2 Ma (Paleoproterozoic, 7%).

A total of 30 zircon grains from P14 tephra were dated with ages ranging from approximately 56 Ma to around 2.4 Ga. Most of the grains in the P14 tephra date to the Paleocene with a peak at 64.8 ± 1.0 Ma (38%) and the Jurassic with a peak at 154.1 ± 2.7 Ma (30%) (Fig. 5.7C). Less pronounced peaks are found at 331.0 ± 8.7 Ma (Carboniferous, 11%), 951.5 ± 23.6 Ma (Neoproterozoic, 11%), and 2338.8 ± 51.7 Ma (Paleoproterozoic, 11%). No grains younger than the Eocene were recovered.

Given the lack of a cluster of juvenile zircon ages for these Pleistocene tephra beds, no depositional ages were calculated.

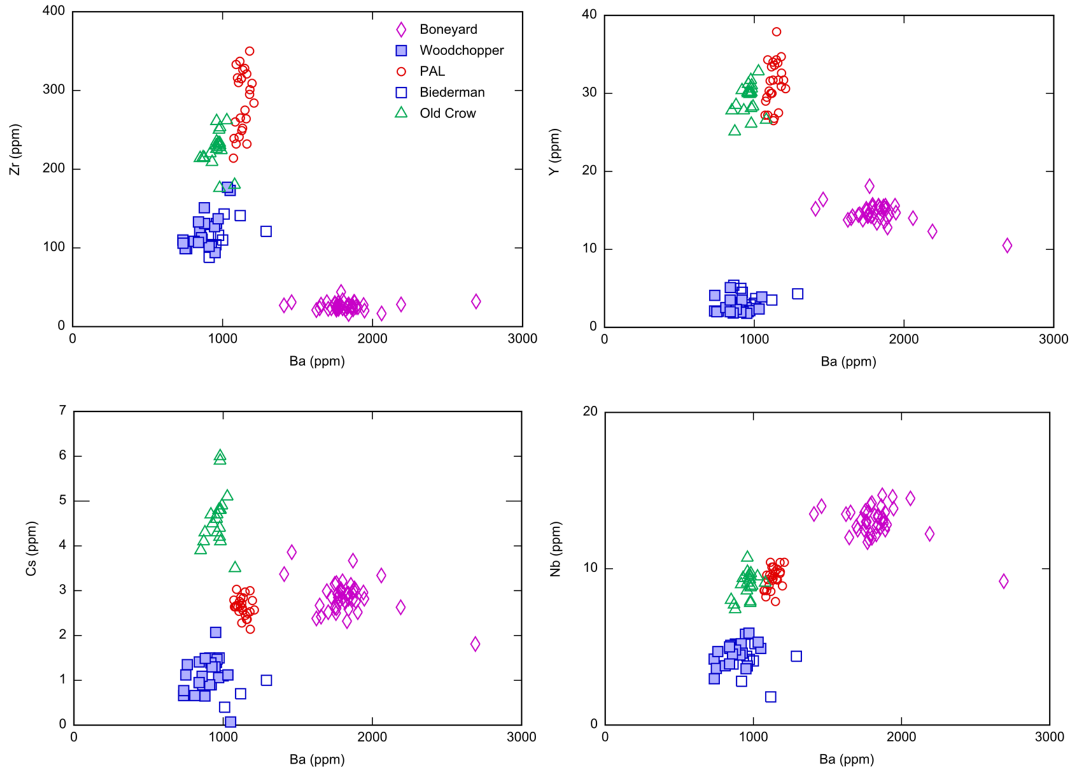

Figure 5.8. *Trace element glass geochemistry for Boneyard, Woodchopper Creek, PAL, Biederman and Old Crow tephra beds.*

5.5. Tephra Glass Geochemistry Results

5.5.1. Previously characterized tephra

Glass major and minor element composition of the tephra beds presented here have been characterized previously. New glass trace element compositions for Boneyard, Woodchopper Creek, Biederman and PAL tephra are summarized as follows.

Boneyard tephra (UA1609 and UA1126) has average trace element values (± 1SD) of 61.9 ± 6.9 ppm Rb, 165.8 ± 22.3 ppm Sr, 17.7 ± 1.0 ppm Y, 25.8 ± 4.8 ppm Zr, 13.1 ± 0.8 ppm Nb, 1808.5 ± 124.4 ppm Ba, and 9.2 ± 1.3 ppm La. The LREE are enriched relative to HREE, with

$La_N/Yb_N = 4.7 \pm 1.5$. PAL tephra (UA1305) has average values (± 1SD) of 107.2 ± 5.7 ppm Rb, 152.5 ± 14.7 ppm Sr, 31.2 ± 2.9 ppm Y, 286.5 ± 39.3 ppm Zr, 9.4 ± 0.7 ppm Nb, 1132.2 ± 38.4 ppm Ba, and 124.5 ± 1.7 ppm La. The PAL tephra glass LREE are slightly more enriched ($La_N/Yb_N = 5.0 \pm 1.0$), compared to the Boneyard tephra (Fig. 5.8.).

The Woodchopper Creek and Biderman tephra glass trace geochemistry is more scattered due to the higher microlite mineral content in the glass shards. Woodchopper Creek tephra (UA1582) has average trace element values (± 1SD) of 61.9 ± 6.9 ppm Rb, 165.8 ± 22.3 ppm Sr, 17.7 ± 1.0 ppm Y, 25.8 ± 4.8 ppm Zr, 13.1 ± 0.8 ppm Nb, 1808.5 ± 124.4 ppm Ba, and 9.2 ± 1.3 ppm La. The LREE are enriched relative to HREE, with $La_N/Yb_N = 4.7 \pm 1.5$.) Biederman tephra (UA1039) has average trace element values (± 1SD) of 61.9 ± 6.9 ppm Rb, 165.8 ± 22.3 ppm Sr, 17.7 ± 1.0 ppm Y, 25.8 ± 4.8 ppm Zr, 13.1 ± 0.8 ppm Nb, 1808.5 ± 124.4 ppm Ba, and 9.2 ± 1.3 ppm La. The LREE are enriched relative to HREE, with $La_N/Yb_N = 4.7 \pm 1.5$.

5.6. Discussion

We prefer the Bayesian modeling age using a triangular prior for tephra that are characterized by predominately auto- and antecrystic zircon component (e.g., Buryak et al., 2022). For tephra that are characterized by predominantly xenocrystic or detrital zircon ages we prefer ages based on the maximum likelihood algorithm. We first discuss the implications of the new tephra zircon ages in the context of existing stratigraphic constraints. We then synthesize our results into a revised tephrostratigraphic framework for the MIS 5–7 interval in eastern Beringia

5.6.1. 80 Pup tephra

The 80 Pup tephra was initially thought to be roughly contemporaneous with the Old Crow tephra based on field observations in the Klondike goldfields of the Yukon Territory (Preece et al., 2000). However, geochemical correlation to a tephra at Birch Creek indicates that 80 Pup (UA 1360) is situated below Biederman tephra (ca. 180 ka; UA 1328) and an organic unit interpreted to represent an interglacial unit (Fig. 5.2.; Buryak et al., 2022). Because Biederman tephra underlies Old Crow tephra at Birch Creek and Chester Bluff, the only sites where the two tephra are found together, 80 Pup tephra must be older than Old Crow tephra.

At Birch Creek, a sharp inclined contact separates 80 Pup tephra and two other closely associated tephra (BC2; UA1358 and BC1; UA1359) from overlying organic-rich sediments with boreal forest pollen (Buryak et al., 2022). These organic-rich sediments and their sharp lower contact with the tephra-bearing silts are thus interpreted as an interglacial unit defined by a substantial thaw unconformity. These correlations and interpretations are supported by observations at the Largent Mine locality near Fairbanks, where 80 Pup tephra is found stratigraphically below BC1 (correlative to LG1 tephra of Woudstra et al. 2000). The 80 Pup tephra U-Pb age of 273 ± 40 ka is consistent with the tephrostratigraphic data from Birch Creek and Largent Mine localities, suggesting an age estimate for 80 Pup tephra, likely during early MIS 8.

5.6.2. PAL tephra

PAL tephra zircon U-Pb dating yielded a Bayesian model age of 185 ± 26 ka, consistent with the U-Th dating Bayesian model age of 173 ± 17 ka. At Palisades East, PAL tephra is overlain by a 1 m thick peat bed (termed “lower peat” by Matheus et al., 2003), while organic-rich silt with large woody macrofossils is present 2 m below the tephra (Fig. 5.2.). As described by Matheus et al. (2003), the lower peat generally lies above PAL ranges from 0–14 m above river level. Where present at river level, the peat is only fully exposed at low river stage and is rich in woody macrofossils. Several tephra samples collected from the peat at river level contained abundant *Picea* needle fragments, suggesting that, like other thick peat beds at the Palisades, it represents an interval of interglacial climate (Matheus et al., 2003; Jensen et al., 2013).

In contrast, Jensen et. (2013) distinguished between the lower and river-level peats using tephrostratigraphy, where unique suites of tephra are associated stratigraphically with the river-level peat and the lower peat. An additional line of evidence in support of unique river-level and lower peats is the presence of a semi-continuous organic unit comprising organic-silt, cryoturbated peat blebs, and large wood fragments between PAL and the river level peat.

Between the lower and middle peat, Matheus et al. (2003) argue that the presence of one, or possibly several, large unconformities is required to reconcile the relatively seamless stratigraphy of alternating peat (interglacial) and massive silt (glacial) units with their identification of the early Pleistocene PA (2.02 ± 0.14 Ma), EC, and MC tephra beds, and interpretation of PAL tephra as similarly aged. However, Jensen et al. (2013) did not identify PA, EC, and MC tephra beds at Palisades, suggesting that large unconformities are not necessary. Our U-Pb and U-Th ages for PAL tephra (185 ± 26 ka and 173 ± 17 ka, respectively) are consistent with this interpretation, suggesting PAL tephra deposition during early MIS 6 or MIS 7.

5.6.3. Sheep Creek-Fairbanks tephra

Zircon U-Pb dating of the Sheep Creek-Fairbanks tephra yielded a maximum likelihood algorithm age of 166 ± 17 ka, suggesting deposition during middle Marine Isotope Stage 6 (MIS 6), which is consistent with the loess thermoluminescence age in the Fairbanks area of 190 ± 40 ka. At its type section, the Sheep Creek-Fairbanks tephra at the Sheep Creek Cut mining exposure, about 15 km northwest of Fairbanks, Alaska, is found within inorganic loess, 1.5 m below the contact of the Gold Hill Loess and the overlying re-transported loess of the late Pleistocene Goldstream Formation (Preece et al., 1999).

At the Upper Eva Creek site in central Alaska, the Sheep Creek-Fairbanks tephra is found approximately 3 and 4.5 m below Old Crow tephra and the Dome Ash Bed, respectively. At several measured sections at the Palisades site in central Alaska, Sheep Creek-Fairbanks tephra is found within inorganic loess about 4–6 m below Old Crow tephra (Reyes et al., 2010a, 2010b; Jensen et al., 2013; Fig 5.3.). Sheep Creek-Fairbanks tephra is present between Old Crow tephra and Biederman tephra (Fig 5.3; 178 ± 17 ka; Buryak et al., 2022) at Birch Creek in east-central Alaska; here, Biederman tephra is cryoturbated within the upper contact of a peaty organic-rich silt bed, possibly representing MIS 7. Thus, stratigraphic evidence at multiple sites in Alaska demonstrates that Sheep Creek-Fairbanks tephra is older than Old Crow tephra, which has a glass fission-track age of 144 ± 14 ka (Buryak et al., 2022) and a stratigraphic age of 159 ± 8 ka (Reyes et al., 2023), and is 22 to 45 ka younger than Biederman tephra.

Table 5.3. All previous chronological constraints for Old Crow tephra.

ID	Location	Method	Type	Age (Ma)	Error (2SE)	Age (ka)	Error (2SE)	Source
UT1	67"28'N 139'54'W	glass fission-track	-	0.04	0.04	40	40	Briggs and Westgate, 1978
UT1	67"28'N 139'54'W	glass fission-track	-	0.12	-	120	-	Neaser et al., 1982
-	Halfway House, Alaska	TL (bulk)	-	0.16	0.025	160	25	Berger, 1987
-	Halfway House, Alaska	TL (glass-rich fraction)	-	0.123	0.02	123	20	Berger, 1987
-	Halfway House, Alaska	TL (glass-rich fraction)	-	0.099	0.015	99	15	Berger, 1987
UT613	Holten, Alaska	glass fission-track	ITP-FT	0.147	0.019	147	19	Westgate, 1988
UT613	Holten, Alaska	glass fission-track	ITP-FT	0.145	0.024	145	24	Westgate, 1988
UT501	Halfway House, Alaska	glass fission-track	ITP-FT	0.118	0.023	118	23	Westgate, 1988
UT501	Halfway House, Alaska	glass fission-track	ITP-FT	0.156	0.026	156	26	Westgate, 1988
-	Imuruk Lake	extrapolation		0.215	0.025	215	25	Beget et al., 1990
UT501	Holten, Alaska	glass fission-track	ITP-FT	0.12	0.02	120	20	Westgate et al., 1990
UT501	Holten, Alaska	glass fission-track	ITP-FT	0.16	0.03	160	30	Westgate et al., 1990
UT613	Halfway House, Alaska	glass fission-track	ITP-FT	0.15	0.02	150	20	Westgate et al., 1990
UT613	Halfway House, Alaska	glass fission-track	ITP-FT	0.16	0.02	160	20	Westgate et al., 1990
UT613	Halfway House, Alaska	glass fission-track	ITP-FT	0.15	0.02	150	20	Westgate et al., 1990
UT613	Halfway House, Alaska	glass fission-track	ITP-FT	0.12	0.02	120	20	Westgate et al., 1990
-	Halfway House, Alaska	TL (glass-rich fraction)	-	0.17	0.027	170	27	Berger, 1991
UT501	Holten, Alaska	glass fission-track	ITP-FT	0.16	0.03	160	30	Sandhu and Westgate, 1995
UT501	Holten, Alaska	glass fission-track	DC-FT	0.14	0.03	140	30	Sandhu and Westgate, 1995
H32	Halfway House, Alaska	IRSL (polymineral fine grain)	-	0.098	0.018	98	18	Auclair et al., 2007
H31	Halfway House, Alaska	IRSL (polymineral fine grain)	-	0.131	0.033	131	33	Auclair et al., 2007
H33	Halfway House, Alaska	IRSL (polymineral fine grain)	-	0.135	0.033	135	33	Auclair et al., 2007
UT1434	Togiak Bay, SW, Alaska	glass fission-track	ITP-FT	0.129	0.014	129	14	Pewe et al., 2009
UT1434	Togiak Bay, SW, Alaska	glass fission-track	ITP-FT	0.122	0.014	122	14	Preece et al., 2011
UT501	Holten, Alaska	glass fission-track	ITP-FT	0.138	0.027	138	27	Preece et al., 2011
UT613	Halfway House, Alaska	glass fission-track	ITP-FT	0.148	0.043	148	43	Preece et al., 2011
UT613	Halfway House, Alaska	glass fission-track	ITP-FT	0.113	0.022	113	22	Preece et al., 2011
HH3A,B	Halfway House, Alaska	zircon U-Pb	-	0.202	0.0055	202	5.5	Burgess et al., 2019
HH3A,B	Halfway House, Alaska	zircon U-series	-	0.205	0.0127	205	12.7	Burgess et al., 2019
HH3A,B	Halfway House, Alaska	zircon (U-Th)/He	-	0.207	0.0173	207	17.3	Burgess et al., 2019
-	Togiak Bay, Alaska	zircon U-Pb	-	0.207	0.0065	207	6.5	Burgess et al., 2021
-	Togiak Bay, Alaska	zircon U-series	-	0.207	0.0065	207	6.5	Burgess et al., 2021
-	Halfway House, Alaska	IRSL	-	0.131	0.001	131	10	Lamothe et al., 2020
UT1434	Togiak Bay, SW, Alaska	glass fission-track	ITP-FT	0.126	0.014	126	14	Buryak et al., 2022
UT1434	Togiak Bay, SW, Alaska	glass fission-track	DC-FT	0.167	0.024	167	24	Buryak et al., 2022
UT1434	Togiak Bay, SW, Alaska	glass fission-track	DC-FT	0.138	0.016	138	16	Buryak et al., 2022
UT1434	Togiak Bay, SW, Alaska	glass fission-track	ITP-FT	0.135	0.026	135	26	Buryak et al., 2022
UT1434	Togiak Bay, SW, Alaska	glass fission-track	ITP-FT	0.149	0.025	149	25	Buryak et al., 2022
UT613	Halfway House, Alaska	glass fission-track	DC-FT	0.17	0.027	170	27	Buryak et al., 2022
UT613	Halfway House, Alaska	glass fission-track	DC-FT	0.183	0.03	183	30	Buryak et al., 2022
UT613	Halfway House, Alaska	glass fission-track	ITP-FT	0.143	0.028	143	28	Buryak et al., 2022
UT501	Holten, Alaska	glass fission-track	ITP-FT	0.153	0.044	153	44	Buryak et al., 2022
UT501	Holten, Alaska	glass fission-track	DC-FT	0.136	0.03	136	30	Buryak et al., 2022
-	IODP U1345	detrital glass	-	0.159	0.08	159	8	Reyes et al., 2023

5.6.4. Old Crow and Biederman tephra

Old Crow tephra is an important chronostratigraphic marker found throughout Alaska and western Yukon, representing the largest known Quaternary eruption in eastern Beringia with ~200 km^3 eruptive volume (Preece et al., 2011). The paleoecology of the sediments hosting Old

Crow tephra indicate deposition in colder conditions, possibly late MIS 6 (e.g., Péwé et al. 2009, Reyes et al. 2010a, Jensen et al. 2016). At multiple sites in Yukon and Alaska the Old Crow tephra has been found below an organic-rich interglacial unit, presumably associated with MIS 5e on the basis of paleoecology, stratigraphy, paleomagnetism, and the nature of the lithostratigraphic contact between tephra-bearing silt and the overlying organic-rich unit. Environmental conditions during deposition of the Old Crow tephra were confirmed by Reyes et al. (2010a) who described a vegetated surface at the Palisades buried by a primary airfall deposit of Old Crow tephra. Plant and insect microfossils and pollen recovered from the vegetated surface indicate tundra-like conditions during tephra deposition, at a location that is presently characterized by boreal forest vegetation.

Despite these stratigraphic and paleoecological constraints, the timing of Old Crow tephra deposition remains uncertain with the most widely cited age of 124 ± 20 ka (2σ) obtained by glass fission-track methods (Preece et al., 2011; Fig. 5.9.), recently updated to 144 ± 14 ka (Buryak et al., 2022) due to more precise ages for the reference material used in the glass fission-track age calculation. Recent attempts at dating Old Crow tephra by U-based techniques (U-Pb, (U-Th)/He, U-Th) have yielded an age of ca. 200 ka, effectively placing deposition of Old Crow tephra during MIS 7 (Burgess et al. 2019, 2021). In contrast, Reyes et al. (2023) obtained a depositional age of 159 ± 8 ka based on the distribution of Old Crow tephra detrital glass shards from samples collected at Integrated Ocean Drilling Program Site U1345 in the Bering Sea and a well-defined sediment core age model from benthic foraminiferal $\delta^{18}O$.

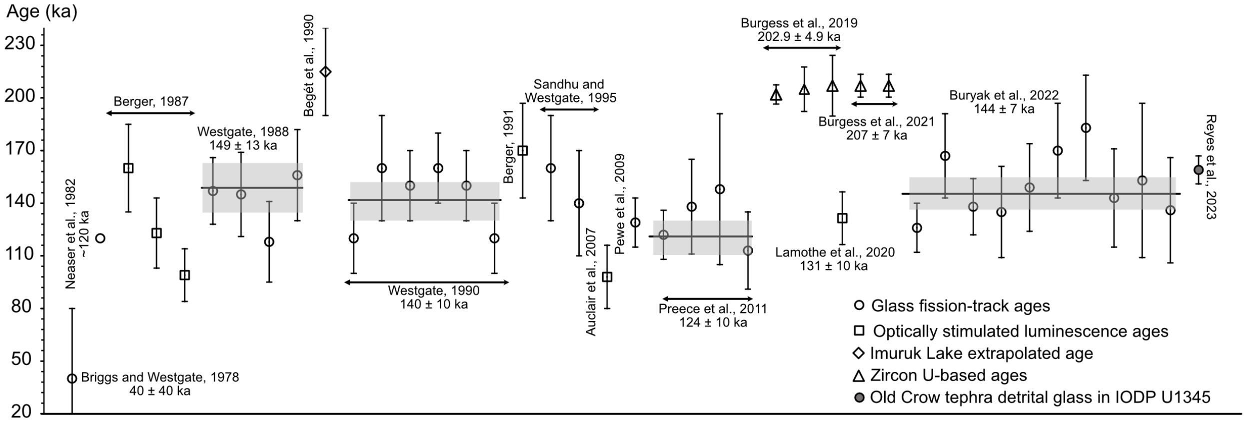

Figure 5.9. *Historical variation in the age of the Old Crow tephra. All uncertainties are at 95% confidence level.*

The *in-situ* U-Pb zircon results from this study provide an additional independent age estimate for Old Crow tephra deposition. The zircon age data yielded a Bayesian model U-Pb (151 ± 14 ka) and U-Th ages (164 ± 29 ka), which are consistent with the glass-fission track age 144 ± 14 ka (Buryak et al., 2022) and depositional age of 159 ± 8 ka (Reyes et al., 2023). The distribution of Old Crow tephra zircon $^{206}Pb/^{238}U$ dates is both heterotemporal (i.e., a long tail of pre-eruptive zircon crystals) and heteroscedastic (i.e., datasets with unequal uncertainties) making age interpretation complicated (Fig. 5.3.). Further complications involve the methods used to synthesize the individual zircon age data into a depositional age. The weighted mean and low-MSWD weighted mean methods presented by Burgess et. al. (2019, 2021) are ideally applicable for zircon populations that reflect instantaneous crystallization with normal analytical uncertainty. However, the Old Crow tephra U-Pb zircon data distribution does not reflect instantaneous crystallization and hence relies on a subjective exclusion of outliers, which can lead to substantial overestimation of the accuracy and precision of a depositional age estimate when the low-MSWD weighted mean method is used. In this case, we consider the Bayesian modeling date as a more accurate estimate for the Old Crow tephra maximum depositional age since it reduces impact of subjectivity in the interpretation and is less likely to underestimate the uncertainty.

In addition, irrespective of the age calculations methodology, different approaches to resolving complexity in U-Pb systematics for relatively young zircons yield critical differences in estimates of depositional age. For young zircon grains <300 ka, the ^{230}Th disequilibrium correction is critical to obtain accurate U-Pb ages and the final ages are sensitive to the choice of the correction scheme. For example, if Old Crow U-Pb data presented here are corrected for ^{230}Th disequilibrium using the method presented by Schärer (1984) and a depositional age is calculated from the youngest set of zircon crystals (by culling older ages to obtain reasonably low MSWD values) we obtain U-Pb age of 191 ± 10 ka (MSWD = 1.68, n = 21) that is similar to the ~200 ka age obtained by Burgess et al. (2019, 2021). However, when the same zircon age data are corrected for ^{230}Th disequilibrium using equations from Sakata et al. (2013), the final calculated ages are ~15-20 % younger.

Multiple other dating methods have been utilized to determine the age of the Old Crow tephra, including radiocarbon, paleomagnetism, luminescence (on the tephra and bracketing sediments) (Fig 5.9). Westgate et al. (1983) provided a summary of radiocarbon ages obtained from organics above Old Crow tephra at various sites across Yukon and Alaska. These dating attempts consistently produced non-finite ages, suggesting tephra deposition > 55,000 ^{14}C a BP. Over the past several decades a substantial Old Crow tephra and bracketing sediment age data was collected through luminescence dating techniques. Direct dating of tephra thermoluminescence (TL) yielded a range of dates between 99 ka to 170 ka (Berger 1987, 1991), while infrared-stimulated luminescence (IRSL) yielded an age 98 +23/-13 ka (Auclair et al.

2007). Both TL and IRSL dates on loess bracketing Old Crow tephra produced ages that are broadly consistent with the glass-fission track age of 144 ± 14 ka (e.g., Lamothe et al. 2020). At the Halfway House locality Old Crow tephra is found in association with underlying Sheep Creek-Fairbanks tephra dated at 190 ± 40 ka (TL, Berger et al. (1996)) and overlying Variegated tephra (VT) dated to 106 ± 20 ka (TL, Jensen et al. (2011)) (Fig. 5.2.; Table 5.3.). If these ages are accurate, they constrain the timing of Old Crow tephra deposition to MIS 5/6. Another line of evidence stems from paleomagnetic studies that were used to support the chronological framework of Old Crow tephra. Paleomagnetic excursions were observed above and below the Old Crow tephra and were initially interpreted as MIS 5 post-Blake and Blake excursions respectively (e.g., Westgate et al., 1985; Beget et al., 1990; Jensen et al., 2016). As noted by Burgess et al. (2021), presence of these excursions alone does not necessarily allow for independent verification of the Old Crow tephra age due to poor replication of magnetostratigraphy between different sites in eastern Beringia. Absent detailed examination of prospective geomagnetic excursions, for example by precise measurements that facilitate mapping of virtual geomagnetic poles, the paleomagnetic data also suffer from uncertain assignment of events to specific excursions. Finally, paleontological and paleogenomic investigations of bison remains in stratigraphic association between Old Crow tephra and an overlying interglacial organic-rich silt at Ch'ijee's Bluff, in northern Yukon, were used to determine the timing of the first arrival and dispersal of bison into the North America. The molecular clock age suggests that the first bison dispersal occurred 195 – 135 ka which is consistent with the deposition of Old Crow tephra during late MIS 6 (Froese et al., 2017).

The wide range of ages attributed to the timing of Old Crow tephra deposition (Fig. 5.9.) calls for further examination of the stratigraphy and chronology for this key marker bed.

Paleoecological and paleoenvironmental evidence clearly argues that Old Crow tephra deposition occurred prior to or during a transition between glacial and interglacial states. Hence, the widely-cited glass-fission track age of 124 ± 20 ka (MIS 5) likely underestimates the age of Old Crow tephra deposition and Burgess et al. (2019, 2021) U-based age of ~200 ka is likely to overestimate it. Similarly, at various locations across Yukon and Alaska the stratigraphic context of Old Crow tephra in relation to Biederman tephra, now dated by U-Pb, U-Th, and (U-Th)/He methods, provides key constraints on the age of Old Crow tephra. If the Biederman tephra U-based age estimates of 178 ± 17 ka (U-Pb; Buryak et al., 2022), 164 ± 21 ka (U-Th), 183 ± 11 ka ((U-Th)/He) are accurate, the organic-rich bed directly underlying Biederman tephra should date to MIS 7. In turn, this would mandate that the stratigraphically higher Old Crow tephra had to be deposited during middle to late MIS 6, which would be consistent with our U-Pb and U-Th zircon ages of 151 ± 14 ka and 164 ± 29 ka respectively. If Old Crow tephra deposition occurred ca. 200 ka (MIS 7) would suggest that Biederman tephra had to be deposited during MIS 8 which contradicts our results.

5.6.5. Snag and Woodchopper Creek tephra

Woodchopper Creek tephra zircon U-Pb dating produced a Bayesian model age of 92 ± 14 ka, aligning with the U-Th dating Bayesian model age of 91 ± 11 ka and the (U-Th)/He eruption age of 114 ± 13 ka at the 2σ level. The agreement between the U-Pb, U-Th, and (U-Th)/He chronometers implies that zircon crystallization likely occurred during or shortly before the eruption.

The Woodchopper Creek tephra was discovered directly above a buried peat with abundant white spruce macrofossils at a site along the White River in southwest Yukon, attributed to 5e (Fig. 5.2.). In this White River location, the Woodchopper Creek tephra is in stratigraphic sequence between Dominion Creek tephra (80 ± 18 ka; revised glass fission-track age) and Old Crow tephra (159 ± 8 ka; Reyes et al., 2023, and see above). Additionally, at the same site, the Woodchopper Creek tephra is associated with the Snag and Donjek tephra found stratigraphically above. At Chester Bluff site in east-central Alaska, the Woodchopper Creek tephra is bracketed (Fig. 5.2.) by the underlying Old Crow tephra and overlying VT tephra (106 ± 20 ka, TL; 130 ± 59 ka, revised glass fission-track, Jensen et al., 2008). Taken together, the existing age constraints for Woodchopper Creek tephra align with the radiometric zircon ages, indicating likely deposition during MIS 5d. This estimate is further supported by the presence of a till above Woodchopper Creek tephra but below Dominion Creek tephra at White River (Turner et al., 2013), which was presumably deposited by glacial advance during a cold substage of MIS 5.

At the White River type section, Snag tephra is situated below a forest bed likely deposited during MIS 5a and both are bracketed by Dominion Creek tephra above and Woodchopper Creek tephra below (Fig. 5.2.; Turner et al., 2013). In this location, Snag tephra is closely associated with the underlying Donjek tephra. Similarly, at the Halfway House locality, central Alaska, Snag tephra is overlain by VT and Halfway House tephra. Although the Snag tephra U-Pb age of 131 ± 15 ka and U-Th age of 100 ± 37 ka are not inconsistent with the existing chronological constraints, the low precision, attributed to a poor recovery of juvenile zircon (n = 2), reduces our confidence in the accuracy of the results and precludes more definitive deployment of Snag tephra in the regional tephrochronostratigraphy. Though Snag tephra is useful for providing stratigraphic correlations and constraints, additional dating is necessary to establish a more robust absolute chronology.

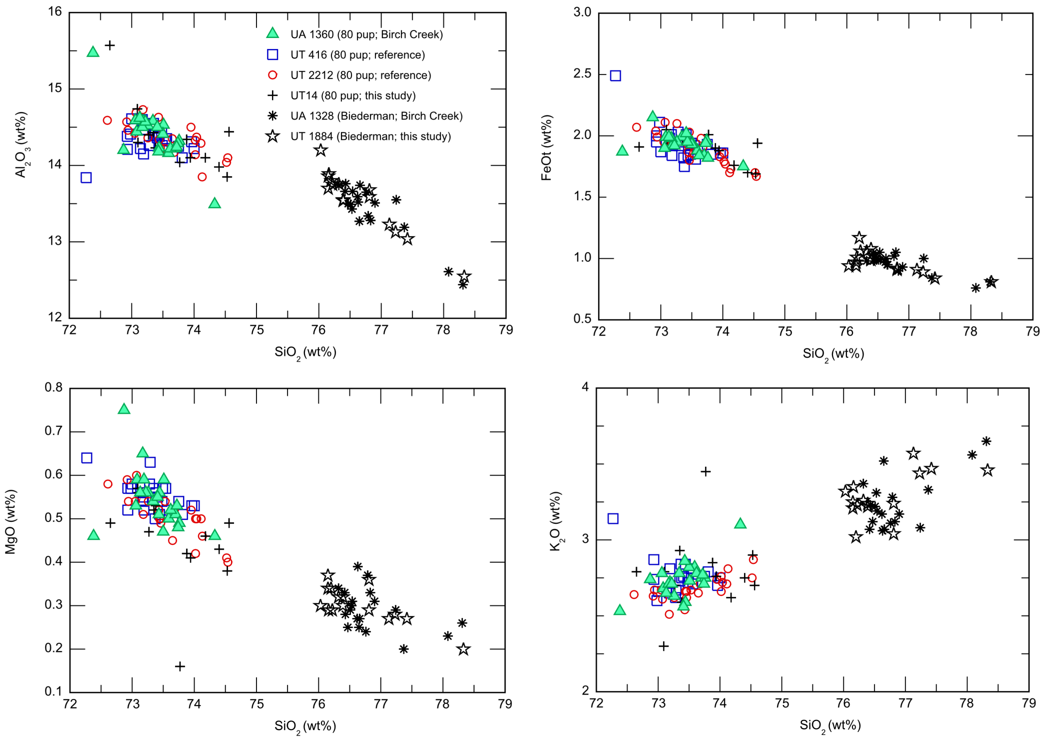

Figure 5.10. *Bivariate plots detailing the major and minor element compositions of 80 Pup and Biederman tephra samples.*

5.6.6. Composite tephrostratigraphy

The tephrostratigraphic framework for eastern Beringia spans the last 3 million years, which is critical for reconstructing the region's geological and paleoenvironmental history. We integrated multiple dating methods and stratigraphic correlations from various sites to construct a coherent framework for one of the most-complete intervals of that record, between MIS 5 to MIS 7, focusing on tephra layers with direct age constraints and established correlations between sites, including (from oldest to youngest): 80 Pup, PAL, Sheep Creek-Fairbanks, Old Crow, Biederman, Snag, and Woodchopper Creek tephra.

The 80 Pup tephra, initially believed to be contemporaneous with the Old Crow tephra based on field observations in the Klondike goldfields (Preece et al., 2000; Preece et al., 2011), has been re-evaluated through geochemical correlation to a tephra at Birch Creek and Largent Mine sites (Fig. 5.2.; Fig. 5.10.). At the Birch Creek site, the 80 Pup tephra, stratigraphically below the ca. 180 ka Biederman tephra and an interglacial organic unit, has a U-Pb age of 273 ± 40 ka, suggesting deposition during early MIS 8. At the same site, 80 Pup tephra, along with overlying BC2 and BC1 tephra, are found below the thaw unconformity that underlies the ca. 160 ka Old Crow tephra and interglacial organic-rich deposits above it (Buryak et al., 2022). At the Largent Mine locality near Fairbanks, the 80 Pup tephra is found stratigraphically below BC1 (=LG1 tephra), suggesting that BC1 tephra likely dates to early MIS 8 or earlier (Fig. 5.11.).

The PAL tephra has been dated using U-Pb and U-Th methods, yielding ages of 185 ± 26 ka and 173 ± 17 ka, respectively. These ages suggest deposition during late MIS 6 or MIS 7. At Palisades East, PAL tephra is overlain by a one-meter-thick peat bed and underlain by organic-rich silt containing large woody macrofossils, indicative of an interglacial climate (Fig. 5.2.; Matheus et al., 2003; Jensen et al., 2013). The PAL tephra's association with interglacial conditions and age suggest deposition during late MIS 6 or MIS 7. The presence of organic-rich silt above the PAL tephra indicates a warm, interglacial environment following its deposition, likely dating to MIS 7 or an intermittent period of warming that does not necessarily correspond to a marine isotope stage.

The Biederman tephra, dated to 178 ± 17 ka (U-Pb), 164 ± 21 ka (U-Th), and 183 ± 11 ka ((U-Th)/He), is found directly above or with an organic-rich silt bed at Birch Creek and Chester Bluff sites, indicative of deposition during MIS 7 (Buryak et al., 2022). Its stratigraphic position above the 80 Pup tephra and below the Sheep Creek-Fairbanks and Old Crow tephra also supports this chronology (Fig. 5.2.). The Old Crow tephra, a crucial chronostratigraphic marker across Alaska and Yukon, has been dated using multiple methods, including U-Pb zircon dating suggesting 151 ± 14 ka, U-Th dating 164 ± 29 ka, and glass fission-track dating 144 ± 14 ka, with a depositional age of 159 ± 8 ka (Buryak et al., 2022; Reyes et al., 2023). These dates align with deposition during late MIS 6. We recognize that this age interpretation contrasts with the ca. 200 ka age for the Old Crow tephra by Burgess et al. (2019, 2021), which is most likely due to the difficulties associated with Quaternary zircon in-situ data collection and corrections, and interpretational challenges leading to a slight, but significant, age overestimation.

The Sheep Creek-Fairbanks tephra, dated to 166 ± 17 ka using zircon U-Pb, aligns with loess thermoluminescence ages of 190 ± 40 ka in the Fairbanks area, suggesting deposition during middle MIS 6 (Berger et al., 1996; Preece et al., 1999). At the Palisades, Sheep Creek-Fairbanks is found within organic-poor loess above PAL tephra and its closely associated organic-rich beds. Furthermore, Sheep Creek-Fairbanks tephra lies stratigraphically below the Old Crow and Dome Ash Bed tephra at various sites, including Upper Eva Creek and the Palisades, confirming the age to be older than MIS 5. At Palisades, the P10, P9, PAU, and P8 tephra beds are collectively bracketed by Sheep-Creek Fairbanks (stratigraphically highest) and PAL (stratigraphically lowest) tephras (Jensen et al., 2013), indicating a sequence of tephra layers likely deposited in a relatively short timeframe during MIS 6 to MIS 7. The exact stratigraphic order of P10, P9, and PAU tephra is unknown and relies on interpolation based on fragmented stratigraphic correlation (Fig. 5.11.).

At multiple sites in eastern Beringia, the Old Crow tephra is commonly found below (or reworked into) interglacial units and thaw unconformities that likely date to MIS 5e based on stratigraphic and paleoecological considerations, indicating deposition during MIS 6 prior to the glacial-interglacial transition (e.g. Reyes et al., 2010b; Preece et al., 2011). Furthermore, the ca. 160 ka age for the Old Crow tephra is anchored by independent age constraints from underlying ca. 170 ka Sheep Creek-Fairbanks and ca. 180 ka Biederman tephra. At Palisades and Largent Mine, the Old Crow tephra is found in close stratigraphic association with the underlying Boneyard tephra, likely deposited shortly before the Old Crow tephra and after the ca. 170 ka Sheep Creek-Fairbanks tephra (Fig. 5.2.).

At the Chester Bluff and White River sections, the Old Crow tephra is found below the Woodchopper Creek tephra, which is dated using zircon U-Pb (92 ± 14 ka), U-Th (91 ± 11 ka), and (U-Th)/He (114 ± 13 ka) and was likely deposited during MIS 5d. At the White River site, it is found above a white spruce-rich peat bed and between the ca. 80 ka Dominion Creek (overlying) and the Old Crow tephra (underlying; Turner et al., 2013). Here, the WRUN2 tephra layer is located above the Old Crow tephra layer, and below the organic-rich unit, which is also beneath the WRUN6 and Woodchopper Creek tephra layers. This stratigraphic correlation suggests that WRUN2 tephra was likely deposited during late MIS 6 and WRUN6 tephra during MIS 5d (Fig. 5.11). At the Chester Bluff site, Woodchopper Creek tephra is bracketed by Old Crow tephra below and ca. 100 ka VT tephra above, indicating stratigraphic and chronological consistency for these tephra (Fig. 5.2.).

Additionally, the Snag tephra, with U-Pb (131 ± 15 ka) and U-Th (100 ± 37 ka) ages, is situated below a forest bed likely deposited during MIS 5a. At the Halfway House and White River locations, it is closely associated with the underlying WRUN1, WRUN5, and Donjek tephra (likely of similar age) and ca. 100 ka Woodchopper Creek tephra. Furthermore, at the White River site, WRUN4 and WRUN3 tephra are found within and below an organic-rich unit, respectively (Fig. 5.2.). These tephra are sandwiched between the ca. 80 ka Dominion Creek tephra and overlying MIS 4 till and ca. 100 ka Snag tephra, suggesting deposition likely during MIS 5d. At the Halfway House locality, the VT and Halfway House tephra are sandwiched between two organic-rich units. The uppermost organic unit is found below ca. 80 ka Dominion Creek and Sheep Creek-Klondike and the lowermost found between ca. 100 ka Snag and ca. 160 ka Old Crow tephra, suggesting that VT and Halfway House tephra were likely deposited during early MIS 5, possibly MIS 5d (Fig. 5.11; Jensen et al., 2011).

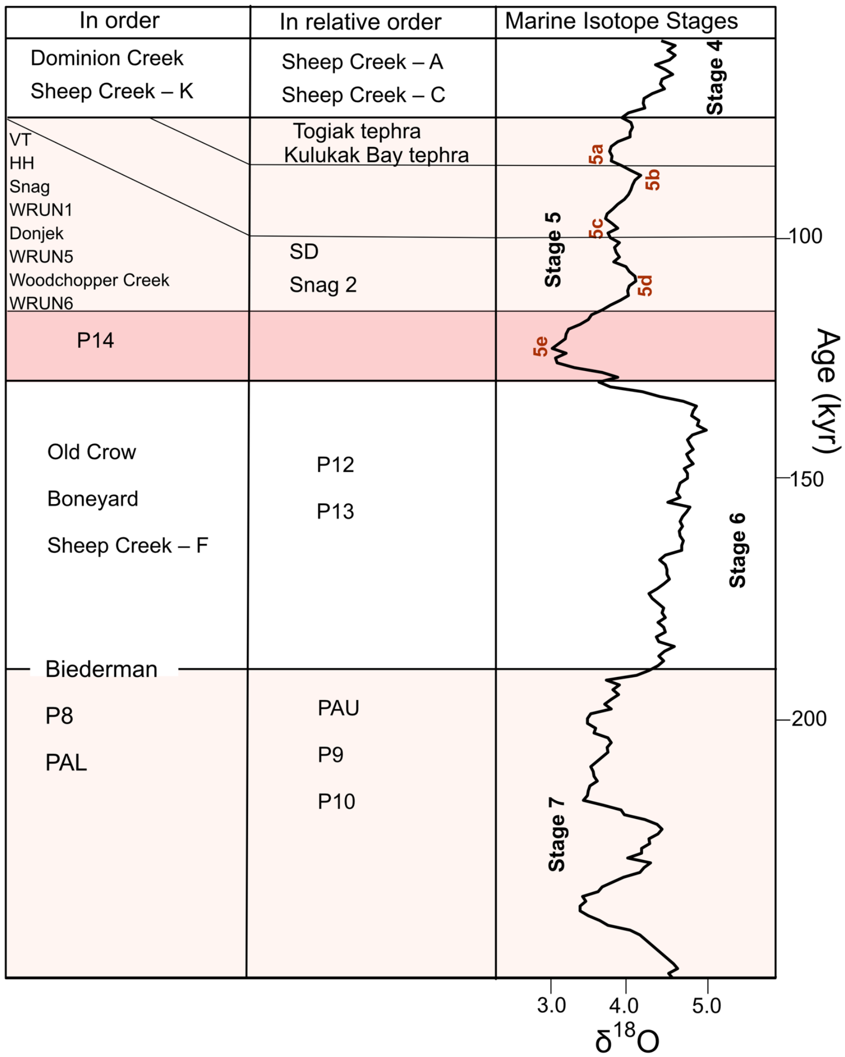

Figure 5.11. *Eastern Beringian MIS 4-7 tephra beds positioned in a stratigraphic order (column 1) and relative order (column 2; exact stratigraphic order is unknown).*

5.7. Implications for juvenile zircon recovery from reworked tephra samples and tephra depositional age determination

The preservation of a tephra bed as a discrete stratigraphic layer is dependent on the environmental controls affecting its preservation potential, morphology, and the level of detrital material contamination (e.g., Cutler et al., 2016; Blong et al., 2017). In terrestrial environments, factors that can impact the preservation of tephra beds include:

(1) The surface topography, including the slope (the critical angle of repose) and variations in the burial rates. Tephra deposited on a slope above its critical angle of repose will result in the movement of material downslope with the finer material remaining on the top of slope and coarser material being accumulated at the base. In turn, increased burial rate at toes of steep slopes will tend to preserve a greater proportion of the original fallout volume in locally over-thickened reworked tephra beds.

(2) The type and structure of vegetation cover can influence the retentiveness of the initial tephra fallout. For example, woodlands and heaths will retain more direct air-fallout tephra but may have areas where material is absent around tree trunks or stems, and grasses might maintain or lose material depending on plant heights and density of the stem coverage.

(3) The tephra layer preservation, thickness, and morphology can also be impacted by surface and sub-surface processes, such as solifluction, cryoturbation, soil movement and/or erosion. Cryoturbation and solifluction are particularly important processes in gemomorphically dynamic, high-latitude environments with permafrost and seasonal frost. For example, Sanborn et al. (2006) demonstrated that cryoturbation and soil reworking due to increasingly drier conditions led to morphological changes of the Sheep Creek-Klondike tephra layer. Solifluction and freeze-thaw conditions can cause material

movement and folding disrupting and convoluting tephra layers at the subsurface in the process. Completely folded tephra layers are not uncommon in the loess deposits across the Yukon and Alaska suggesting material movement post tephra layer deposition.

Thus, a given tephra layer's characteristics and morphology need be considered when assessing its potential as a tephrochronological marker and a target for direct dating (e.g. through zircon dating or glass fission-track dating). However, another aspect that is rarely considered, but is heavily influenced by the above-mentioned factors, is tephrochronometry. The disturbance of the tephra layer might lead to admixing of detrital minerals (and possibly glass) into the initial fallout material. The fine-grained and often re-worked tephra layers at distal sites in Yukon and Alaska often contain detrital silt and clay-sized grains derived from surrounding sediments. The degree of contamination by these detrital grains is variable both spatially and temporally and most likely depends on the location specific syn- and pos-depositional alternations of the initial deposit. Because radiometric dating methods (^{40}Ar-^{39}Ar; U-based chronometer; fission track) commonly rely on the presence of juvenile (autocrystic) minerals to establish the eruption/deposition age of a tephra layer, presence or absence of truly autocrystic minerals with direct temporal association to the volcanic eruption can be obscured in heavily reworked samples and/or lead to overestimation of a tephra's depositional age.

Accordingly, U-Pb, U-Th and (U-Th)/He zircon dating of young Yukon and Alaskan tephra is particularly challenging because many of the distal tephra layers contain abundant detrital crystals (millions to billions of years old) that mirror the zircon age spectra of surrounding sediments, in these cases, juvenile autocrystic zircon crystals are completely overwhelmed by the detrital signal. Only a few of the processed tephra samples we have analyzed contain little to no discernible detrital zircon signal (e.g., Lost Chicken tephra, Quartz Creek tephra; Buryak et al., 2022) or contained no zircon at all (e.g. VT tephra; Halfway House tephra). However, in the majority of the dated tephra samples the detrital signal varied from 100% (only detrital grains; e.g. Boneyard tephra, Dome Ash Bed) to several percent (e.g., Woodchopper Creek tephra; PAL tephra). Furthermore, zircon age distribution in many Yukon and Alaskan tephra are further complicated by antecrystic and xenocrystic zircon crystals that pre-date the eruption by 10s to 100s of thousands of years. For example, Woodchopper Creek tephra and Old Crow tephra U-Pb age are heterotemporal, containing both detrital zircon and a broad spectrum of antecrystic ages pre-dating the youngest, coherent group of grains by 100s of thousands of years.

The zircon characteristics that are commonly used to determine juvenile zircon grains include zircon morphology, the degree of surface abrasion, and presence of adhered glass mantling the grains. The shape of the zircon crystals is not always a useful characteristic when determining origin of the grain and often does not allow for clear discrimination of the detrital grains using this criterion alone. However, in Yukon and Alaskan tephra, presence of zircon surface abrasion is often more characteristic of a detrital origin in a group of idiomorphic grains. Adhered glass is a more useful marker in determining grains that were in contact with the melt (e.g., Schmitt et al., 2023), but mantling glass is not always preserved around grains in heavily reworked or weathered samples, nor does the presence of mantling glass discriminate between autocrystic, antecrystic, or xenocrystic origin of the zircon. The usefulness of adhered glass as a marker to identify juvenile grains is especially complicated for volcanic samples that incorporate zircon cargo released from melting of fully solidified portion of the reservoir or incorporation of xenocrystic minerals from the host and cover rocks during the eruption.

The dynamic environmental changes in Yukon and Alaska over the last three million years are an important factor impacting tephra preservation and suitability of a given tephra as a useful chronologic marker. Thus, it is necessary to access all available information when attempting to interpret the timing of deposition of the tephra from geochronological data, including:

(1) Stratigraphic context: Tephra U-based zircon age spectra may contain co-eruptive population or alternatively only indicate the timing of magmatic crystallization prior to the eruption. We consider zircon U-Pb and U-Th ages, *ipso facto*, to be maximum depositional ages. Geochemical correlation of tephra layers between different, often spatially distant, localities is a useful tool to determine stratigraphic position of different tephra layers. Geochronological data must satisfy the constraints imposed by stratigraphic relations among tephra layers.

(2) Paleoecology: Paleoenvironmental information can provide climatic, environmental, and ecological context for the prevailing conditions during the initial tephra fallout. *In situ* tephra layers cannot have depositional ages that contradict the paleobiological or paleoenvironmental characteristics of intact host sediment. For example, a contradiction can occur when a tephra layer associated with sediments indicating warming (interglacial) conditions has a zircon U-Pb age suggesting deposition during cooling (glacial) conditions.

(3) Multiple chronometer: In some cases multiple dating techniques, such as mineral or glass fission track, $^{40}Ar/^{39}Ar$, or ^{14}C dating methods, can be used to cross-check the validity of the potentially equivocal chronometric data. However, often it might not be possible to incorporate more than one direct dating method (for example, due to absence of suitable mineral phases or method timespan limitation).

If any of the above factors are not consistent the chronological information or vice versa – the age data, stratigraphic/paleoenvironmental context or both may be inaccurate and need to be re-evaluated to minimize the possibility of the *ad hoc* explanation for otherwise geologically inconsistent facts.

Additionally, methodological and analytical challenges and sampling bias can lead to under- or over-estimation of the sample age and analytical associated errors. In the case of tephra zircon dating, this can lead to inaccurate excess scatter in the zircon age spectra. Potential biases affecting analytical reliability of *in situ* LA-ICP-MS zircon dating include uncertainty in fractionation corrections that depend on the depth of the ablation crater or structural heterogeneities within zircon (Buryak et al., 2022; Schmitt et al., 2023). Another potential source of bias is the choice of the statistical technique to calculate the timing of eruption/deposition from heterotemporal series of zircon dates. For example, the weighted mean is a common method used in geochronology for a series of ages. For this method, ages with large uncertainties are given less weight in the mean than ages with smaller uncertainties. The caveat here is that analytical uncertainties are assumed to have a normal (i.e., gaussian) distribution about the mean. However, this assumption often cannot be made for heteroscedastic series of ages that are determined near the limits of instrumental resolution (e.g., U-Pb dating of zircon <500 ka), which usually show a log-normal distribution around the mean. In such instances, the weighted mean will tend to skew the mean towards older (or more precise) ages and underestimate the uncertainty associated with the depositional age calculation for the tephra bed.

5.8. Conclusion

We performed U-Pb and U-Th LA-ICP-MS dating on zircon crystals from seven major tephra deposits in Yukon and Alaska to establish a detailed chronological framework for MIS 5 to MIS 7 sediments in eastern Beringia. By integrating U-Pb and U-Th data with zircon (U-Th)/He ages and revised glass fission-track ages—together with published geochronological, stratigraphic, and paleoecological data—we provide new maximum deposition ages for these tephra layers. The zircon U-based ages were consistent with the available stratigraphic and tephrostratigraphic information, except for the 80 Pup tephra, which yielded a U-Pb age (273 ± 40 ka) much older than previously thought.

Our study highlights the importance of considering the depositional environment, preservation conditions, and zircon characteristics when determining direct ages for tephra beds. Based on our analysis, we recommend the following U-based ages as the most reliable estimates:

1. Woodchopper Creek tephra: 92 ± 15 ka (U-Pb) | 94 ± 11 ka (U-Th) | 114 ± 13 ka ((U-Th)/He): MIS 5d
2. Snag tephra:131 ± 15 ka (U-Pb) | 100 ± 37 ka (U-Th): MIS 5d
3. Old Crow tephra: 151 ± 14 ka (U-Pb) | 164 ± 29 ka (U-Th): MIS 6
4. Sheep Creek-Fairbanks tephra: 166 ± 17 ka (U-Pb): MIS 6
5. PAL tephra: 185 ± 26 ka (U-Pb) | 173 ± 17 ka (U-Th): MIS 7
6. Biederman tephra: 164 ± 21 ka (U-Th) | 183 ± 11 ka ((U-Th)/He): MIS 7
7. 80 Pup tephra: 273 ± 40 ka (U-Pb): MIS 8

For the undated tephra layers, we provide likely marine isotope stages based on their stratigraphic context: the Boneyard tephra, which is stratigraphically associated with the Old Crow tephra, was likely deposited during MIS 6. PAU, P9, P10, P12 and P13 tephra layers positioned between the PAL and Sheep Creek-Fairbanks tephra, are likely from MIS 7 to 6. The Donjek tephra, closely associated with the WRUN1 tephra, and WRUN5 tephra are likely from MIS 5d. The Halfway House tephra, found between the Snag and Old Crow tephra, and the VT tephra, located above the Old Crow tephra, are likely from MIS 5d. The WRUN2 tephra, found below the WRUN6 tephra was likely deposited during the late MIS 6. The WRUN3 tephra, positioned below the WRUN4 tephra, is likely from MIS 5d.

These refined chronological estimates enhance our understanding of MIS 5 to MIS 7 depositional histories in eastern Beringia. Moreover, the U-based zircon dating techniques offer a robust method for dating Quaternary tephra deposits in Yukon and Alaska, which were previously undatable by other methods.

5..9. Supplemental Figures

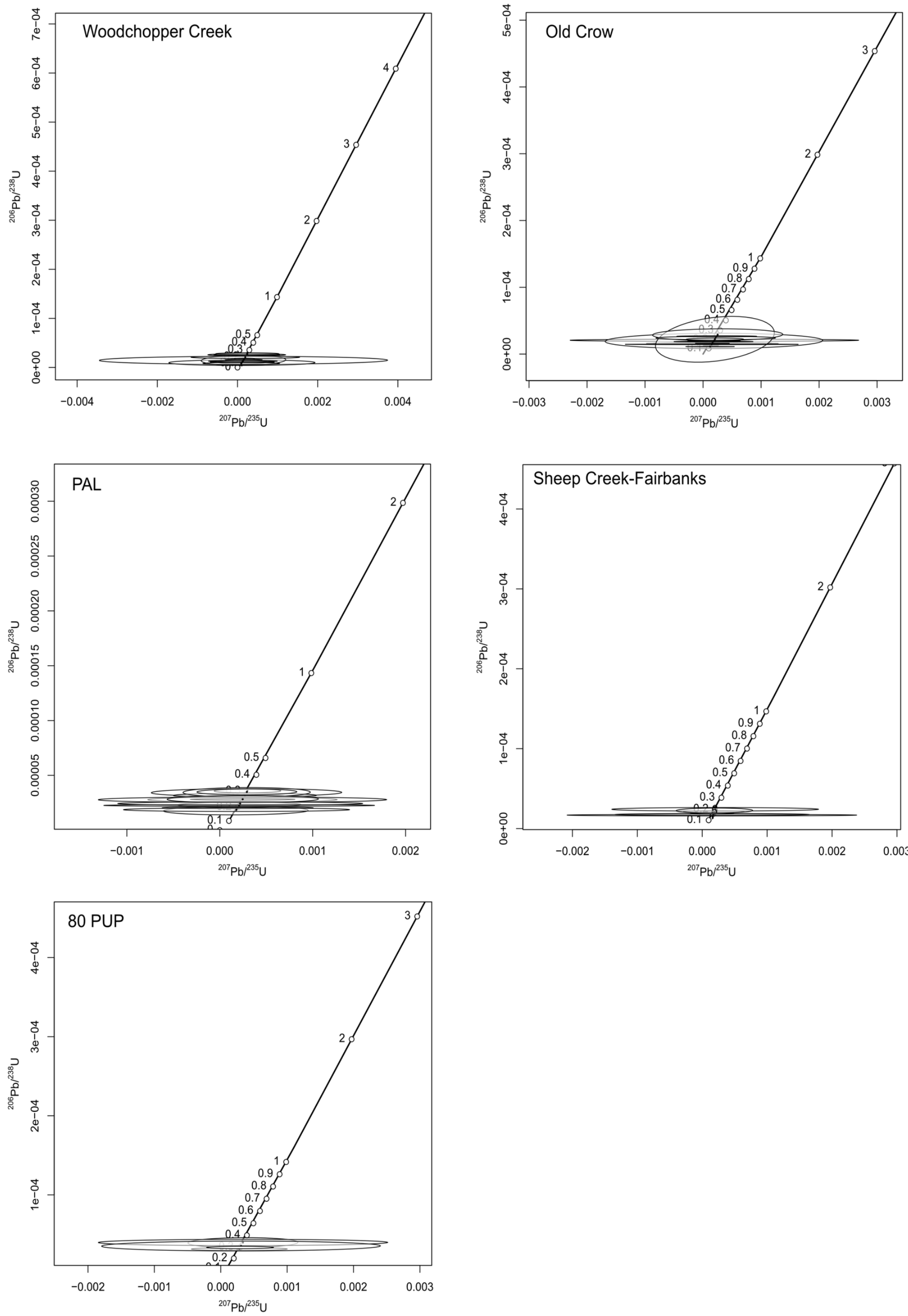

Figure C.1: *Common-Pb-corrected (Williams, 1998) zircon U-Pb Concordia plots for filtered data. Plotted data are deemed to represent the autocrystic zircon population from each tephra sample. Data point ellipses are at 2σ level. Initial $^{207}Pb/^{206}Pb$ value is estimated from Stacey and Kramers (1975) lead evolution model.*

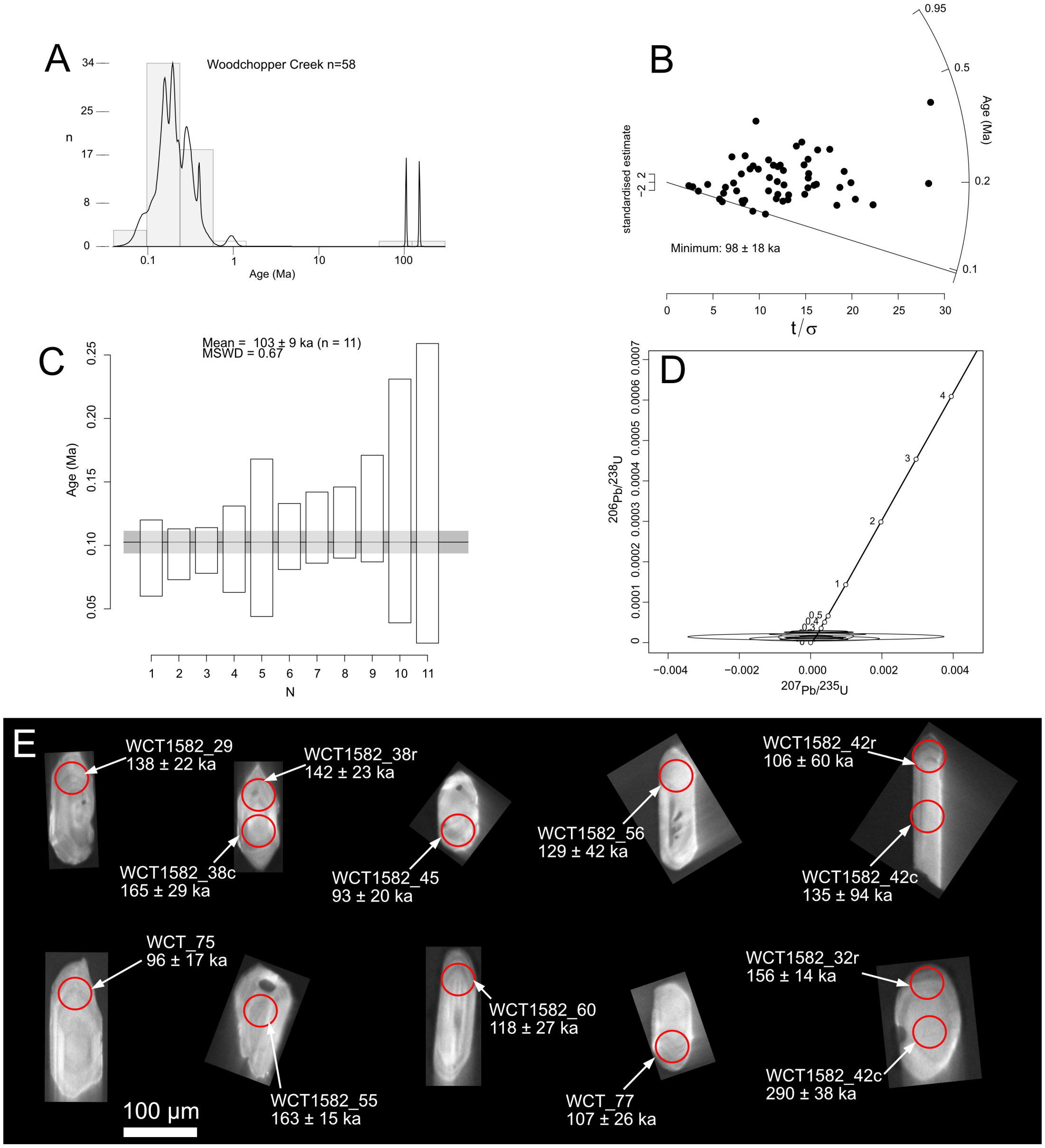

Figure C.2: *(A***)** *Probability density function for all Woodchopper Creek tephra U-Pb zircon analyses. (B) Radial plot and maximum likelihood age calculator for the same tephra. (C) The weighted mean of the youngest most coherent cluster of zircon U-Pb ages with overlapping uncertainties. (D) Common-Pb corrected Concordia diagram of the same zircon analyses as in (C). (E) Micrograph of the representative zircon cathodoluminescence images with the position of the laser beam spot indicated by the red circle.*

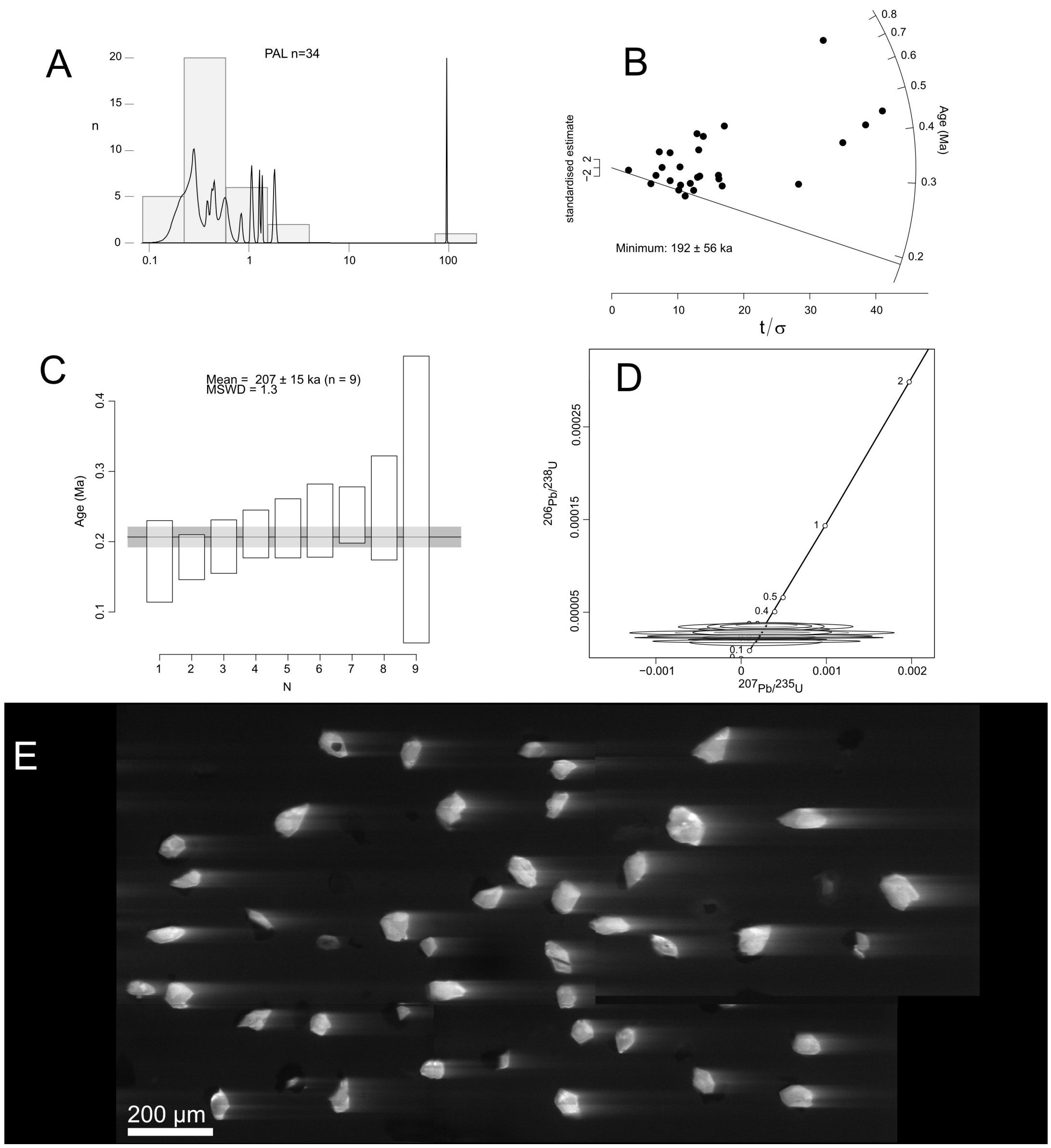

Figure C.3: *(A**)** Probability density function for all PAL tephra U-Pb zircon analyses. (B) Radial plot and maximum likelihood age calculator for the same tephra. (C) The weighted mean of the youngest most coherent cluster of zircon U-Pb ages with overlapping uncertainties. (D) Common-Pb corrected Concordia diagram of the same zircon analyses as in (C). (E) Micrograph of the representative zircon cathodoluminescence images.*

5.10. References

Alloway, B.V., Lowe, D.J., Larsen, G., Shane, P.A.R., Westgate, J.A., 2013. QUATERNARY STRATIGRAPHY | Tephrochronology, in: Encyclopedia of Quaternary Science. Elsevier, pp. 277–304. https://doi.org/10.1016/B978-0-444-53643-3.00058-3

Auclair, M., Lamothe, M., Lagroix, F., Banerjee, S.K. 2007. Luminescence investigation of loess and tephra from Halfway House section, Central Alaska. Quaternary Geochronology 2, 34–38. https://doi.org/10.1016/j.quageo.2006.05.009.

Bartlein, P.J., Anderson, P.M., Edwards, M.E., McDowell, P.F., 1991. A framework for interpreting paleoclimatic variations in Eastern Beringia. Quaternary International, The Climate and Environment of the Last Integlacial in the Arctic and Subarctic 10–12, 73–83. https://doi.org/10.1016/1040-6182(91)90041-L

Begét, J.E., Hawkins, D.B., 1989. Influence of orbital parameters on Pleistocene loess deposition in central Alaska. Nature 337, 151–153. https://doi.org/10.1038/337151a0

Begét, J., 1990. Middle Wisconsinan climate fluctuations recorded in central Alaskan loess. Géographie Physique et Quaternaire 44, 3–13. https://doi.org/10.7202/032793ar

Begét, J., Edwards, M., Hopkins, D., Keskinen, M., Kukla, G., 1991. Old Crow tephra found at the Palisades of the Yukon, Alaska. Quaternary Research 35, 291–297. https://doi.org/10.1016/0033-5894(91)90074-F

Berger, G.W., Péwé, T.L., Westgate, J.A., Preece, S.J., 1996. Age of Sheep Creek Tephra (Pleistocene) in Central Alaska from Thermoluminescence Dating of Bracketing Loess. Quaternary Research 45, 263–270. https://doi.org/10.1006/qres.1996.0027

Berger, G.W., 1987. Thermoluminescence dating of the Pleistocene Old Crow tephra and adjacent loess, near Fairbanks, Alaska. Canadian Journal of Earth Sciences 24, 1975–1984. https://doi.org/10.1139/e87-188

Berger, G.W., 1988. TL dating studies of tephra, loess and lacustrine sediments. Quaternary Science Reviews 7, 295–303.

Berger, G.W., 1991. The use of glass for dating volcanic ash by thermoluminescence. Journal of Geophysical Research 96, 19705–19720.

Berger G.W. 2003. Luminescence chronology of late Pleistocene loess-paleosol and tephra sequences near Fairbanks, Alaska. Quaternary Research 60, 70–83.

Berger, G.W., Pillans, B.J., Palmer, A.S., 1992. Dating loess up to 800 ka by thermoluminescence. Geology 20, 403–406.

Berger, G.W., Péwé, T.L., Westgate, A.G., Preece, S.J., 1996. Age of Sheep Creek tephra (Pleistocene) in central Alaska from thermoluminescence dating of bracketing loess. Quaternary Research 45, 263–270.

Brigham-Grette, J., Hopkins, D.M., 1995. Emergent Marine Record and Paleoclimate of the Last Interglaciation along the Northwest Alaskan Coast. Quaternary Research 43, 159–173. https://doi.org/10.1006/qres.1995.1017

Brigham-Grette, J., 2001. New perspectives on Beringian Quaternary paleogeography, stratigraphy, and glacial history. Quaternary Science Reviews 20, 15–24.

Briggs, N. D., Westgate, J. A., 1978. A contribution to the Pleistocene geochronology of Alaska and the Yukon Territory: fission-track age of distal tephra units: in Short papers of the fourth international conference, geochronology, cosmochronology, isotope geology, 1978, U.S. Geological Survey Open-File Report 78-0701, p. 49-52.

Blong, R., Enright, N., Grasso, P., 2017. Preservation of thin tephra. J Appl. Volcanol. 6, 10. https://doi.org/10.1186/s13617-017-0059-4

Boehnke, P., Barboni, M., Bell, E.A., 2016. Zircon U/Th model ages in the presence of melt heterogeneity. Quaternary Geochronology 34, 69–74. https://doi.org/10.1016/j.quageo.2016.03.005

Burgess, S.D., Coble, M.A., Vazquez, J.A., Coombs, M.L., Wallace, K.L., 2019. On the eruption age and provenance of the Old Crow tephra. Quaternary Science Reviews 207, 64–79. https://doi.org/10.1016/j.quascirev.2018.12.026

Burgess, S.D.D., Vazquez, J.A.A., Waythomas, C.F.F., Wallace, K.L.L., 2021. U–Pb zircon eruption age of the Old Crow tephra and review of extant age constraints. Quaternary Geochronology 101168. https://doi.org/10.1016/j.quageo.2021.101168

Buryak, S.D., Reyes, A.V., Jensen, B.J.L., Davies, J.H.F.L., Westgate, J.A., DuFrane, S.A., Luo, Y., Froese, D.G., Pearson, D.G., Benowitz, J.A., 2022. Laser-ablation ICP-MS zircon U-Pb ages for key Pliocene-Pleistocene tephra beds in unglaciated Yukon and Alaska. Quaternary Geochronology 101398. https://doi.org/10.1016/j.quageo.2022.101398

Chen, Y., Smith, P.E., Evensen, N.M., York, D., Lajoie, K.R., 1996. The Edge of Time: Dating Young Volcanic Ash Layers with the 40Ar-39Ar Laser Probe. Science 274, 1176–1178. https://doi.org/10.1126/science.274.5290.1176

Crowley, J.L., Schoene, B., Bowring, S.A., 2007. U-Pb dating of zircon in the Bishop Tuff at the millennial scale. Geology 35, 1123–1126. https://doi.org/10.1130/G24017A.1

Chamberlain, K.J., Wilson, C.J.N., Wooden, J.L., Charlier, B.L.A., Ireland, T.R., 2014. New Perspectives on the Bishop Tuff from Zircon Textures, Ages and Trace Elements. Journal of Petrology 55, 395–426. https://doi.org/10.1093/petrology/egt072

Cutler, N.A., Shears, O.M., Streeter, R.T., Dugmore, A.J., 2016. Impact of small-scale vegetation structure on tephra layer preservation. Sci Rep 6, 37260. https://doi.org/10.1038/srep37260

Di Vincenzo, G., Skála, R., 2009. 40Ar–39Ar laser dating of tektites from the Cheb Basin (Czech Republic): Evidence for coevality with moldavites and influence of the dating standard on the age of the Ries impact. Geochimica et Cosmochimica Acta 73, 493–513. https://doi.org/10.1016/j.gca.2008.10.002

Donovan, J.J., Kremser, D., Fournelle, J.H. and Goemann, K., 2015, Probe for EPMA: Acquisition, automation and analysis, version 11: Eugene, Oregon, Probe Software. Inc., http://www. probesoftware. com.

Edwards, M.E., McDowell, P.F., 1991. Interglacial deposits at Birch Creek, northeast interior Alaska. Quaternary Research 35, 41-52. https://doi.org/10.1016/0033-5894(91)90093-K.

Froese, D., Stiller, M., Heintzman, P.D., Reyes, A.V., Zazula, G.D., Soares, A.E.R., Meyer, M., Hall, E., Jensen, B.J.L., Arnold, L.J., MacPhee, R.D.E., Shapiro, B., 2017. Fossil and genomic evidence constrains the timing of bison arrival in North America. Proceedings of the National Academy of Sciences of the United States of America 114, 3457–3462. https://doi.org/10.1073/pnas.1620754114

Galbraith, R.F., Green, P.F., 1990. Estimating the component ages in a finite mixture. International Journal of Radiation Applications and Instrumentation. Part D. Nuclear Tracks and Radiation Measurements 17, 197–206. https://doi.org/10.1016/1359-0189(90)90035-V

Gebauer, S.K., Schmitt, A.K., Pappalardo, L., Stockli, D.F., Lovera, O.M., 2014. Crystallization and eruption ages of Breccia Museo (Campi Flegrei caldera, Italy) plutonic clasts and their relation to the Campanian ignimbrite. Contrib Mineral Petrol 167, 953. https://doi.org/10.1007/s00410-013-0953-7

Gentner, W., Kleinmann, B., Wagner, G.A., 1967. New K-Ar and fission track ages of impact glasses and tektites. Earth and Planetary Science Letters 2, 83–86. https://doi.org/10.1016/0012-821X(67)90104-5

Guillong, M., Sliwinski, J.T., Schmitt, A., Forni, F., Bachmann, O., 2016. U-Th Zircon Dating by Laser Ablation Single Collector Inductively Coupled Plasma-Mass Spectrometry (LA-ICP-MS). Geostandards and Geoanalytical Research 40, 377–387. https://doi.org/10.1111/j.1751-908X.2016.00396.x

Harangi, S., Lukács, R., Schmitt, A.K., Dunkl, I., Molnár, K., Kiss, B., Seghedi, I., Novothny, Á., Molnár, M., 2015. Constraints on the timing of Quaternary volcanism and duration of magma residence at Ciomadul volcano, east–central Europe, from combined U–Th/He and U–Th zircon geochronology. Journal of Volcanology and Geothermal Research 301, 66–80. https://doi.org/10.1016/j.jvolgeores.2015.05.002

Hamilton, T.D., Brigham-Grette, J., 1991. The last interglaciation in Alaska: Stratigraphy and paleoecology of potential sites. Quaternary International 10–12, 49–71. https://doi.org/10.1016/1040-6182(91)90040-U

Huntley, D.J., Lamothe, M., 2001. Ubiquity of anomalous fading in K-feldspars and the measurement and correction for it in optical dating. Can. J. Earth Sci. 38, 1093–1106. https://doi.org/10.1139/e01-013

Hurford, A.J., Green, P.F., 1983. The zeta age calibration of fission-track dating. Chemical Geology 41, 285–317. https://doi.org/10.1016/S0009-2541(83)80026-6

Ickert, R.B., Mundil, R., Magee, C.W., Mulcahy, S.R., 2015. The U-Th-Pb systematics of zircon from the Bishop Tuff: A case study in challenges to high-precision Pb/U geochronology at the millennial scale. Geochimica et Cosmochimica Acta 168, 88–110. https://doi.org/10.1016/j.gca.2015.07.018

Jackson, S.E., Pearson, N.J., Griffin, W.L., Belousova, E.A., 2004. The application of laser ablation-inductively coupled plasma-mass spectrometry to in situ U–Pb zircon geochronology. Chemical Geology 211, 47–69. https://doi.org/10.1016/j.chemgeo.2004.06.017

Jensen, B.J.L., Froese, D.G., Preece, S.J., Westgate, J.A., Stachel, T., 2008. An extensive middle to late Pleistocene tephrochronologic record from east-central Alaska. Quaternary Science Reviews 27, 411–427. https://doi.org/10.1016/j.quascirev.2007.10.010

Jensen, B.J.L., Reyes, A.V., Froese, D.G., Stone, D.B., 2013. The Palisades is a key reference site for the middle Pleistocene of eastern Beringia: New evidence from paleomagnetics and regional tephrostratigraphy. Quaternary Science Reviews 63, 91–108. https://doi.org/10.1016/j.quascirev.2012.11.035

Jensen, B.J.L., Evans, M.E., Froese, D.G., Kravchinsky, V.A., 2016. 150,000 years of loess accumulation in central Alaska. Quaternary Science Reviews 135, 1–23. https://doi.org/10.1016/j.quascirev.2016.01.001

Jensen, B.J.L. et al., 2021, A latest Pleistocene and Holocene composite tephrostratigraphic framework for northeastern North America: Quaternary Science Reviews, v. 272, p. 107-242, doi:10.1016/j.quascirev.2021.107242.

Keller, C.B., Schoene, B., Samperton, K.M., 2018. A stochastic sampling approach to zircon eruption age interpretation. Geochemical Perspectives Letters 8, 31–35. http://dx.doi.org/10.7185/geochemlet.1826

Ketcham, R.A., Gautheron, C., Tassan-Got, L., 2011. Accounting for long alpha-particle stopping distances in (U–Th–Sm)/He geochronology: Refinement of the baseline case. Geochimica et Cosmochimica Acta 75, 7779–7791. https://doi.org/10.1016/j.gca.2011.10.011

Kuehn, S.C., Froese, D.G., Shane, P.A.R., 2011. The INTAV intercomparison of electron-beam microanalysis of glass by tephrochronology laboratories: Results and recommendations. Quaternary International 246, 19–47. https://doi.org/10.1016/j.quaint.2011.08.022

Kunk, M.J., 1995. 40Ar/39Ar age-spectrum data for hornblende, plagioclase and biotite from tephra collected at Dan Creek and McCallum Creek, Alaska and in the Klondike Placer district near Dawson, Yukon Territory, Canada. USGS Open-File Report 95-217, 52 p. https://doi.org/10.3133/ofr95217A

Lamothe, M., Forget Brisson, L., Hardy, F., 2020. Circumvention of anomalous fading in feldspar luminescence dating using Post-Isothermal IRSL. Quaternary Geochronology 57, 101062. https://doi.org/10.1016/j.quageo.2020.101062

Laurenzi, M.A., Balestrieri, M.L., Bigazzi, G., Hadler Neto, J.C., Iunes, P.J., Norelli, P., Oddone, M., Osorio Araya, A.M., Viramonte, J.G., 2007. New Constraints on Ages of Glasses Proposed as Reference Materials for Fission-Track Dating. Geostandards and Geoanalytical Research 31, 105–124. https://doi.org/10.1111/j.1751-908X.2007.00844.x

Lowenstern, J.B., Persing, H.M., Wooden, J.L., Lanphere, M., Donnelly-Nolan, J., Grove, T.L., 2000. U–Th dating of single zircons from young granitoid xenoliths: new tools for understanding volcanic processes. Earth and Planetary Science Letters 183, 291–302. https://doi.org/10.1016/S0012-821X(00)00273-9

Mahon, K.I., 1996. The New “York” Regression: Application of an Improved Statistical Method to Geochemistry. International Geology Review 38, 293–303. https://doi.org/10.1080/00206819709465336

Matheus, P., Begét, J., Mason, O., Gelvin-Reymiller, C., 2003. Late Pliocene to late Pleistocene environments preserved at the Palisades Site, central Yukon River, Alaska. Quaternary Research 60, 33–43. https://doi.org/10.1016/S0033-5894(03)00091-7

Matthews, J.V., Ovenden, L.E., 1990. Late Tertiary Plant Macrofossils from Localities in Arctic/Subarctic North America: A Review of the Data. Arctic 43, 364–392.

McDowell, P.F., Edwards, M.E., 2001. Evidence of Quaternary climatic variations in a sequence of loess and related deposits at Birch Creek, Alaska: implications for the Stage 5 climatic chronology. Quaternary Science Reviews, Beringian Paleoenvironments - Festschrift in Honour of D.M. Hopkins 20, 63–76. https://doi.org/10.1016/S0277-3791(00)00131-1

Muhs, D., 2003. Stratigraphy and palaeoclimatic significance of Late Quaternary loess–palaeosol sequences of the Last Interglacial–Glacial cycle in central Alaska. Quaternary Science Reviews 22, 1947–1986. https://doi.org/10.1016/S0277-3791(03)00167-7

Muhs, D.R., Bettis, E.A., Aleinikoff, J.N., McGeehin, J.P., Beann, J., Skipp, G., Marshall, B.D., Roberts, H.M., Johnson, W.C., Benton, R., 2008. Origin and paleoclimatic significance of late Quaternary loess in Nebraska: Evidence from stratigraphy, chronology, sedimentology, and geochemistry. Geological Society of America Bulletin 120, 1378–1407. https://doi.org/10.1130/B26221.1

Naeser, N.D., Westgate, J.A., Hughes, O.L., Péwé, T.L., 1982. Fission-track ages of late Cenozoic distal tephra beds in the Yukon Territory and Alaska. Can. J. Earth Sci. 19, 2167–2178. https://doi.org/10.1139/e82-191

Österle, J.E., Stockli, D.F., Seward, D., Little, T.A., 2020. Dating of young (<1 Ma) tephras: Using U-Pb (zircon) and (U-Th[-Sm])/He (zircon, apatite, magnetite) chronometers to unravel the eruption age of a tephra in the Woodlark Rift of Papua New Guinea. Terra Nova 32, 345–354. https://doi.org/10.1111/ter.12464

Paton, C., Woodhead, J.D., Hellstrom, J.C., Hergt, J.M., Greig, A., Maas, R., 2010. Improved laser ablation U-Pb zircon geochronology through robust downhole fractionation correction. Geochemistry, Geophysics, Geosystems 11. https://doi.org/10.1029/2009GC002618

Paton, C., Hellstrom, J., Paul, B., Woodhead, J., Hergt, J., 2011. Iolite: Freeware for the visualisation and processing of mass spectrometric data. Journal of Analytical Atomic Spectrometry 26, 2508–2518. https://doi.org/10.1039/C1JA10172B

Pettke, T., Oberli, F., Audétat, A., Guillong, M., Simon, A.C., Hanley, J.J., Klemm, L.M., 2012. Recent developments in element concentration and isotope ratio analysis of individual fluid inclusions by laser ablation single and multiple collector ICP-MS. Ore Geology Reviews 44, 10–38. https://doi.org/10.1016/j.oregeorev.2011.11.001

Péwé, T.L., Berger, G.W., Westgate, J.A., Brown, P.M., Leavitt, S.W., 1997. Eva interglaciation forest bed, unglaciated East-Central Alaska: global warming 125,000 years ago. Geological Society of America. https://doi.org/10.1130/SPE319

Péwé, T.L., Westgate, J.A., Preece, S.J., Brown, P.M., Leavitt, S.W., 2009. Late Pliocene dawson cut forest bed and new tephrochronological findings in the Gold Hill Loess, east-central Alaska. Bulletin of the Geological Society of America 121, 294–320. https://doi.org/10.1130/B26323.1

Preece, S.J., Westgate, J.A., Stemper, B.A., Péwé, T.L., 1999. Tephrochronology of late Cenozoic loess at Fairbanks, central Alaska. \Geological Society of America Bulletin 111, 71–90. https://doi.org/10.1130/0016-7606(1999)111<0071:TOLCLA>2.3.CO;2

Preece, S.J., Westgate, J.A., Alloway, B.V., Milner, M.W., 2000. Characterization, identity, distribution, and source of late Cenozoic tephra beds in the Klondike district of the Yukon, Canada. Canadian Journal of Earth Sciences 37, 983–996. https://doi.org/10.1139/e00-011

Preece, S.J., Westgate, J.A., Froese, D.G., Pearce, N.J.G., Perkins, W.T., 2011. A catalogue of late Cenozoic tephra beds in the Klondike goldfields and adjacent areas, Yukon Territory. Canadian Journal of Earth Sciences 48, 1386–1418. https://doi.org/10.1139/e10-110

Preece, S.J., Pearce, N.J.G., Westgate, J.A., Froese, D.G., Jensen, B.J.L., Perkins, W.T., 2011. Old Crow tephra across eastern Beringia: a single cataclysmic eruption at the close of Marine Isotope Stage 6. Quaternary Science Reviews 30, 2069–2090. https://doi.org/10.1016/j.quascirev.2010.04.020

Prentice, M., Pittari, A., Lowe, D.J., Kilgour, G., Kamp, P.J.J., Namaliu, M., 2022. Linking proximal ignimbrites and coeval distal tephra deposits to establish a record of voluminous Early Quaternary (2.4–1.9 Ma) volcanism of the Tauranga Volcanic Centre, New Zealand. Journal of Volcanology and Geothermal Research 429, 107595. https://doi.org/10.1016/j.jvolgeores.2022.107595

Reiners, P.W., Spell, T.L., Nicolescu, S., Zanetti, K.A., 2004. Zircon (U-Th)/He thermochronometry: He diffusion and comparisons with 40Ar/39Ar dating. Geochimica et Cosmochimica Acta 68, 1857–1887. https://doi.org/10.1016/j.gca.2003.10.021

Reiners, P.W., 2005. Zircon (U-Th)/He Thermochronometry. Reviews in Mineralogy and Geochemistry 58, 151–179. https://doi.org/10.2138/rmg.2005.58.6

Reyes, A.V., Jensen, B.J.L., Zazula, G.D., Ager, T.A., Kuzmina, S., La Farge, C., Froese, D.G., 2010a. A late-Middle Pleistocene (Marine Isotope Stage 6) vegetated surface buried by Old Crow tephra at the Palisades, interior Alaska. Quaternary Science Reviews 29, 801–811. https://doi.org/10.1016/j.quascirev.2009.12.003

Reyes, A.V., Froese, D.G., Jensen, B.J.L., 2010b. Permafrost response to last interglacial warming: field evidence from non-glaciated Yukon and Alaska. Quaternary Science Reviews 29, 3256–3274. https://doi.org/10.1016/j.quascirev.2010.07.013

Reyes, A.V., Jensen, B.J.L., Woudstra, S.H., Bolton, M.S.M., Buryak, S.D., Cook, M.S., Harvey, J., Westgate, J.A., 2023. Detrital glass in a Bering Sea sediment core yields a ca . 160 ka Marine Isotope Stage 6 age for Old Crow tephra XX, 1–5.

Roberts, H.M., 2012. Testing Post-IR IRSL protocols for minimising fading in feldspars, using Alaskan loess with independent chronological control. Radiation Measurements 47, 716–724. https://doi.org/10.1016/j.radmeas.2012.03.022

Sanborn, P.T., Smith, C.A.S., Froese, D.G., Zazula, G.D., Westgate, J.A., 2006. Full-glacial paleosols in perennially frozen loess sequences, Klondike goldfields, Yukon Territory, Canada. Quaternary Research 66, 147–157. https://doi.org/10.1016/j.yqres.2006.02.008

Sandhu, A.S., Westgate, J.A., 1995. The correlation between reduction in fission-track diameter and areal track density in volcanic glass shards and its application in dating tephra beds.

Earth and Planetary Science Letters 131, 289–299. https://doi.org/10.1016/0012-821X(95)00022-5

Sandhu, A.S., Westgate, J.A., Preece, S.J., and Froese, D.G., 2001. Glass-fission-track ages of late Cenozoic distal tephra beds in the Klondike district, Yukon Territory; In, Yukon Exploration and Geology 2000, D.S. Emond and L.H. Weston (eds.), Exploration and Geological Services Division, Yukon, Indian and Northern Affairs Canada, pp. 247-256

Schmitt, A.K., Stockli, D.F., Niedermann, S., Lovera, O.M., Hausback, B.P., 2010. Eruption ages of Las Tres Vírgenes volcano (Baja California): A tale of two helium isotopes. Quaternary Geochronology 5, 503–511. https://doi.org/10.1016/j.quageo.2010.02.004

Schmitt, A.K., 2011. Uranium Series Accessory Crystal Dating of Magmatic Processes. Annu. Rev. Earth Planet. Sci. 39, 321–349. https://doi.org/10.1146/annurev-earth-040610-133330

Schmitz, M.D., Bowring, S.A., 2001. U-Pb zircon and titanite systematics of the Fish Canyon Tuff: an assessment of high-precision U-Pb geochronology and its application to young volcanic rocks. Geochimica et Cosmochimica Acta 65, 2571–2587. https://doi.org/10.1016/S0016-7037(01)00616-0

Schmieder, M., Kennedy, T., Jourdan, F., Buchner, E., Reimold, W., 2018. A high-precision 40Ar/39Ar age for the Nördlinger Ries impact crater, Germany, and implications for the accurate dating of terrestrial impact events. Geochimica et Cosmochimica Acta 220, 146–157. https://doi.org/10.1016/j.gca.2017.09.036

Sharman, G.R., Malkowski, M.A., 2020. Needles in a haystack: Detrital zircon U[sbnd]Pb ages and the maximum depositional age of modern global sediment. Earth-Science Reviews 203, 103109. https://doi.org/10.1016/j.earscirev.2020.103109

Shane, P., 2000. Tephrochronology: a New Zealand case study. Earth-Science Reviews 49, 223–259.

Sláma, J., Košler, J., Condon, D.J., Crowley, J.L., Gerdes, A., Hanchar, J.M., Horstwood, M.S.A., Morris, G.A., Nasdala, L., Norberg, N., Schaltegger, U., Schoene, B., Tubrett, M.N., Whitehouse, M.J., 2008. Plešovice zircon — A new natural reference material for U–Pb and Hf isotopic microanalysis. Chemical Geology 249, 1–35. https://doi.org/10.1016/j.chemgeo.2007.11.005

Staudacher', T., Jessberger, E.K., Dominik, B., Kirsten, T., Schaefferh, O.A., 1982. Journal of Geophysics 40 Ar-39 Ar Ages of Rocks and Glasses from the Nordlinger Ries Crater and the Temperature History of Impact Breccias.

Strong, T.R., Driscoll, R.L., 2016. A process for reducing rocks and concentrating heavy minerals. USGS Open-File Report 2016–1022, 16 p., https://doi.org/10.3133/ofr20161022

Turner, D.G., Ward, B.C., Bond, J.D., Jensen, B.J.L., Froese, D.G., Telka, A.M., Zazula, G.D., Bigelow, N.H., 2013. Middle to Late Pleistocene ice extents, tephrochronology and paleoenvironments of the White River area, southwest Yukon. Quaternary Science Reviews 75, 59–77. https://doi.org/10.1016/j.quascirev.2013.05.011

Vermeesch, P., 2021. Maximum depositional age estimation revisited. Geoscience Frontiers 12, 843–850. https://doi.org/10.1016/j.gsf.2020.08.008

Vlag, P.A., Oches, E.A., Banerjee, S.K., Solheid, P.A., 1999. The paleoenvironmental-magnetic record of the Gold Hill Steps loess section in central Alaska. Physics and Chemistry of the Earth, Part A: Solid Earth and Geodesy 24, 779–783. https://doi.org/10.1016/S1464-1895(99)00114-3

Westgate, J.A., 1988. Isothermal plateau fission-track age of the late Pleistocene Old Crow tephra, Alaska. Geophysical Research Letters 15, 376–379.

Westgate, J.A., Briggs, N.D., Stalker, A.M. and Churcher, C.S., 1978. Fission-track age of glass from tephra beds associated with Quaternary Vertebrate Assemblages in the southern Canadian plains. In Geological Society of America Abstracts with Programs (Vol. 10, No. 7, pp. 514-515).

Westgate, J.A., Hamilton, T.D., Gorton, M.P., 1983. Old Crow tephra: a new late Pleistocene stratigraphic marker across north-central Alaska and western Yukon Territory. Quaternary Research 19, 38–54.

Westgate, J.A., Walter, R.C., Pearce, G.W., Gorton, M.P., 1985. Distribution, stratigraphy, petrochemistry, and palaeomagnetism of the late Pleistocene Old Crow tephra in Alaska and the Yukon. Canadian Journal of Earth Sciences 22, 893–906.

Westgate, J.A., Stemper, B.A., Péwé, T.L., 1990. A 3 m.y. record of Pliocene-Pleistocene loess in, interior Alaska. Geology 18, 858–861.

Westgate, J.A., Preece, S.J., Kotler, E., Hall, S., 2000. Dawson tephra: a prominent stratigraphic marker of Late Wisconsinan age in west-central Yukon, Canada. Canadian Journal of Earth Sciences 37, 621–627.

Westgate, J.A., Preece, S.J., Froese, D.G., Pearce, N., Alloway, B., 2005. Late Cenozoic tephrochronology of the Klondike area. In: Froese, D.G., Westgate, J.A., Alloway, B.V. (Eds.), Field Trip Guide for International Field Conference and Workshop on Tephrochronology and Volcanism: Dawson City, Yukon Territory, Canada July 31st – August 8th, 2005 Institute of Geological & Nuclear Sciences science report 2005/26, pp. 43–51

Westgate, J.A., Preece, S.J., Froese, D.G., Pearce, N.J.G., Roberts, R.G., Demuro, M., Hart, W.K., Perkins, W., 2008. Changing ideas on the identity and stratigraphic significance of the Sheep Creek tephra beds in Alaska and the Yukon Territory, northwestern North America. Quaternary International 178, 183–209

Westgate, J.A., Preece, S.J., Froese, D.G., Telka, A.M., Storer, J.E., Pearce, N.J.G., Enkin, R.J., Jackson, L.E., Lebarge, W., Perkins, W.T., 2009. Gold run tephra: A middle pleistocene stratigraphic and paleoenvironmental marker across west-central Yukon Territory, Canada. Canadian Journal of Earth Sciences 46, 465–478.

Westgate, J.A., 1989. Isothermal plateau fission-track ages of hydrated glass shards from silicic tephra beds. Earth and Planetary Science Letters 95, 226–234. https://doi.org/10.1016/0012-821X(89)90099-X

Westgate, J.A., Pearce, G.W., Preece, S.J., Schweger, C.E., Morlan, R.E., Pearce, N.J.G., Perkins, T.W., 2013. Tephrochronology, magnetostratigraphy and mammalian faunas of Middle and Early Pleistocene sediments at two sites on the Old Crow River, northern Yukon Territory, Canada. Quaternary Research 79, 75–85. https://doi.org/10.1016/j.yqres.2012.09.003

Westgate, J.A., Pearce, N.J.G., 2017. Age of some Pleistocene interglacial beds and associated fossils in eastern Beringia defined by fission tracks in glass shards of Chester Bluff tephra. Quaternary Research 88, 152–159. https://doi.org/DOI: 10.1017/qua.2017.30

Wiedenbeck, M., Allé, P., Corfu, F., Griffin, W. l., Meier, M., Oberli, F., Quadt, A.V., Roddick, J. c., Spiegel, W., 1995. Three Natural Zircon Standards for U-Th-Pb, Lu-Hf, Trace Element and Ree Analyses. Geostandards Newsletter 19, 1–23. https://doi.org/10.1111/j.1751-908X.1995.tb00147.x

Wotzlaw, J.-F.F., Schaltegger, U., Frick, D.A., Dungan, M.A., Gerdes, A.G., Günther, D., 2013. Tracking the evolution of large-volume silicic magma reservoirs from assembly to supereruption. Geology 41, 867–870. https://doi.org/10.1130/G34366.1

Woudstra, S., Jensen, B., Thomas, E., Froese, D.G., 2020. MIDDLE PLEISTOCENE LOESS AND TEPHRA DEPOSITS IN THE FAIRBANKS REGION. Presented at the GSA 2020 Connects Online, GSA.

Zhang, J., Li, S.-H., 2020. Review of the Post-IR IRSL Dating Protocols of K-Feldspar. Methods Protoc 3, 7. https://doi.org/10.3390/mps3010007

Chapter 6: Conclusion

6.1 Final Remarks and Future Considerations

This dissertation focused on (1) establishing and assessing the use of LA-ICP-MS U-Pb zircon dating for Pliocene-Pleistocene tephrochronometry in eastern Beringia (Chapter 2); (2) dynamics of preservation potential of volcanogenic Quaternary zircon in the detrital zircon record (Chapter 3); (3) refining and simplifying U-Th disequilibrium and U-Th-Pb zircon in-situ LA-ICP-MS dating methodology, especially applicable for samples with heterotemporal zircon age distributions (Chapter 4); and (5) refining the chronological framework for MIS 5 to 7 tephra deposits in Yukon and Alaska using LA-ICP-MS zircon U-Th and U-Pb dating in combination with glass fission-track and zircon (U-Th)/He dating. Each of these contributions are summarized briefly below.

1. A suite of important eastern Beringian Pliocene-Pleistocene tephra beds were dated using LA-ICP-MS zircon U-Pb methods, and the U-Pb ages were compared to previously collected glass fission-track ages. The zircon data were combined with available stratigraphic, paleoecological, palaeomagnetic information to provide an improved eastern Beringian Pliocene-Pleistocene chronological framework. Importantly, we tested five different methods to calculate a tephra maximum depositional age from a suite of individual zircon U-Pb ages: (1) the weighted mean age, (2) the maximum likelihood age, (3) an iterative-MSWD approach, (4) Bayesian age modeling, and (5) using the youngest zircon age as the age of deposition. The following ^{206}Pb-^{238}U Bayesian model ages are the most reliable and precise estimates of tephra age for: Biederman tephra 178 ± 17 ka; HP tephra 688 ± 47 ka; Gold Run tephra 688 ± 44 ka; Flat Creek tephra 708 ± 43 ka; PA tephra 1.92 ± 0.06 Ma; Quartz Creek Tephra 2.62 ± 0.08 Ma; Lost Chicken tephra 3.14 ±

0.07 Ma; and GI tephra 542 ± 64 ka. Fruitful areas for future research include: (1) combining U-Pb zircon data with thermobarometric information to obtain insight on the zircon crystallization dynamics; (2) testing combined *in-situ* zircon and CA-TIMS U-Pb dating for young zircon crystals; and (3) improving Pliocene-Pleistocene tephrostratigraphic correlations.

2. Detrital zircons are an important source of geological information, including for provenance studies and determination of the maximum depositional ages of otherwise undatable sedimentary deposits. To determine a maximum depositional age that approaches the true depositional age of the sediment from a suite of detrital zircon crystals it is critical that a syndepositional (and likely volcanogenic) signal is present. By analyzing zircon ages and morphologies in the Miocene Grubstake tephra and encompassing Grubstake Formation, we show that volcanogenic zircon grain size in the detrital record plays an important role for determination of the maximum depositional age that is co-eval with the sedimentation, with implications for regional and global scale detrital studies that rely on the youngest detrital zircon ages to establish the sedimentation histories. To expand upon this research future studies should focus on linking potential sources of volcanogenic zircons to the areas of interest. Additionally, further research on the zircon grain size distribution in tephra deposits would provide better understanding of distal volcanogenic zircon abundances and morphological characteristics.

3. Zircon dating by ^{238}U–^{230}Th disequilibrium is an important method for understanding the timing and rates of geological processes and can be used to obtain ages for samples younger than ~350 ka. *In-situ* zircon ^{238}U–^{230}Th dating is challenging due to low ^{230}Th

abundance and potential mass spectrometric interferences. We assessed mass spectrometric interferences and ^{232}Th abundance sensitivity on ^{230}Th and proposed a refined and simplified correction routine for *in-situ* sector field (SF)-LA-ICP-MS zircon ^{238}U–^{230}Th dating. Additionally, an alternative method is introduced to estimate contributions of abundance sensitivity and polyatomic oxide interferences. Furthermore, this methodology is applied to combined ^{238}U–^{206}Pb, ^{232}Th–^{208}Pb, and ^{238}U–^{230}Th dating of Quaternary zircon samples, including widely used reference materials and volcanic zircons. Five zircon samples, including reference materials (91500, Plešovice) and volcanic zircons (Bishop Tuff, Breccia Museo facies of the Campanian Ignimbrite, PAL tephra), are analyzed to verify accuracy across different chronometers. This refined dating method facilitates accurate quantification of young zircon ages, especially in samples with multiple age components, providing a cost- and time-effective approach for dating young zircon crystals. The LA-ICP-MS U-Th and U-Th-Pb dating of Quaternary zircon is still a relatively new technique and requires appropriate reference materials to be developed. The best route for future research is to develop a suite of U-Th zircon reference materials. We have collected a number of promising Quaternary volcanic samples that can yield potentially homogeneous and easily accessible zircon crystals that area suitable for reference material usage. This work is ongoing at the time of writing this thesis with seven samples prepared for inter-laboratory analyses.

4. Lastly, we assessed the utility of LA-ICP-MS zircon U-Pb and U-Th techniques for directly dating of late-Middle Pleistocene tephra, focusing on MIS 5–7 tephra deposits in eastern Beringia. We obtained U-Pb and/or U-Th zircon ages for Snag, Woodchopper

Creek, Old Crow, Sheep Creek-Fairbanks, Biederman, PAL, and 80 Pup—seven important regional marker tephra deposits collected at various sites in Yukon and Alaska. Additionally, we provide (U-Th)/He zircon ages for Biederman tephra and Woodchopper Creek tephra and revised glass fission-track ages for Dominion Creek and VT tephra. The zircon age data were compiled into a region tephrostratigraphic framework using stratigraphic and geochemical correlations from sites across Yukon and Alaska: Halfway House, Palisades, Birch Creek, Largent Mine, Chester Bluff and White River. The results of this research provide detailed geochronology for an important interval of the eastern Beringian paleoenvironmental record which previously relied only on handful of tephra age determinations. Future research should focus on developing a detailed age-depth model supported by geochemical fingerprinting of tephra beds from various sites and multi-chronometer tephra direct ages combined with any other chronological information. The fragmentation of eastern Beringian sedimentary record and presence of numerous unconformities requires further examination of stratigraphy at multiple sites to clarify stratigraphic context currently ambiguous tephra horizons that could not be put in clear stratigraphic order. Additionally, detailed examination (either by analyzing visible tephra beds or detrital glass analysis) of the proximal marine core records to link terrestrial tephra record to the well dated marine core records will provide an improved chronological framework for the eastern Beringian tephra record and is especially important for tephra layers that could not be dated directly.

Bibliography

Alloway, B.V., Lowe, D.J., Larsen, G., Shane, P.A.R., Westgate, J.A., 2013. QUATERNARY STRATIGRAPHY | Tephrochronology, in: Encyclopedia of Quaternary Science. Elsevier, pp. 277–304. https://doi.org/10.1016/B978-0-444-53643-3.00058-3

Anderson, P.M., Lozhkin, A.V., 2001. The Stage 3 interstadial complex (Karginskii/middle Wisconsinan interval) of Beringia: variations in paleoenvironments and implications for paleoclimatic interpretations. Quaternary Science Reviews 20, 93–125

Arienzo, I., Heumann, A., Wörner, G., Civetta, L., Orsi, G., 2011. Processes and timescales of magma evolution prior to the Campanian Ignimbrite eruption (Campi Flegrei, Italy). Earth and Planetary Science Letters 306, 217–228. https://doi.org/10.1016/j.epsl.2011.04.002

Auclair, M., Lamothe, M., Lagroix, F., Banerjee, S.K. 2007. Luminescence investigation of loess and tephra from Halfway House section, Central Alaska. Quaternary Geochronology 2, 34–38. https://doi.org/10.1016/j.quageo.2006.05.009.

Bacon, C.R., Persing, H.M., Wooden, J.L., Ireland, T.R., 2000. Late Pleistocene granodiorite beneath Crater Lake caldera, Oregon, dated by ion microprobe. Geology 28, 467–470. https://doi.org/10.1130/0091-7613(2000)028<0467:LPGBCL>2.3.CO;2

Bartlein, P.J., Anderson, P.M., Edwards, M.E., McDowell, P.F., 1991. A framework for interpreting paleoclimatic variations in Eastern Beringia. Quaternary International 10-12, 73–93.

Begét, J., 1990. Middle Wisconsinan climate fluctuations recorded in central Alaskan loess. Géographie Physique et Quaternaire 44, 3–13. https://doi.org/10.7202/032793ar

Begét, J.E., Hawkins, D.B., 1989. Influence of orbital parameters on Pleistocene loess deposition in central Alaska. Nature 337, 151–153. https://doi.org/10.1038/337151a0

Begét, J.E., 2001. Continuous Late Quaternary proxy climate records from loess in Beringia. Quaternary Science Reviews 20, 499–507. https://doi.org/10.1016/S0277-3791(00)00102-5

Berger G.W. 2003. Luminescence chronology of late Pleistocene loess-paleosol and tephra sequences near Fairbanks, Alaska. Quaternary Research 60, 70–83.

Berger, G.W., Pillans, B.J., Palmer, A.S., 1992. Dating loess up to 800 ka by thermoluminescence. Geology 20, 403–406.

Begét, J.E., Keskinen, M.J., 2003. Trace-element geochemistry of individual glass shards of the Old Crow tephra and the age of the Delta glaciation, central Alaska. Quaternary Research 60, 63–69. https://doi.org/10.1016/S0033-5894(03)00095-4

Benowitz, J.A., Layer, P.W., Vanlaningham, S., 2014. Persistent long-term (c. 24 Ma) exhumation in the Eastern Alaska Range constrained by stacked thermochronology. Geological Society, London, Special Publications 378, 225–243. https://doi.org/10.1144/SP378.12

Berger, G.W., 1991. The use of glass for dating volcanic ash by thermoluminescence. Journal of Geophysical Research: Solid Earth 96, 19705–19720. https://doi.org/ /10.1029/91JB01899

Berger, G.W., 1987. Thermoluminescence dating of the Pleistocene Old Crow tephra and adjacent loess, near Fairbanks, Alaska. Canadian Journal of Earth Sciences 24, 1975–1984. https://doi.org/10.1139/e87-188

Berger, G.W., 1988. TL dating studies of tephra, loess and lacustrine sediments. Quaternary Science Reviews 7, 295–303.

Berger, G.W., Péwé, T.L., Westgate, J.A., Preece, S.J., 1996. Age of Sheep Creek Tephra (Pleistocene) in Central Alaska from thermoluminescence dating of bracketing loess, Quaternary Research 45, 263–270. https://doi.org/10.1006/qres.1996.0027.

Bayes T.R., 1763. An essay towards solving a problem in the doctrine of chances. Philosophical Transactions of the Royal Society 53, 370-418.

Bigazzi, G., Galbraith, R.F., 1999. Point-counting technique for fission-track dating of tephra glass shards, and its relative standard error. Quaternary Research 51,67–73. https://doi.org/10.1006/qres.1998.2019

Bill, N.S., Mix, H.T., Clark, P.U., Reilly, S.P., Jensen, B.J.L., Benowitz, J.A., 2018. A stable isotope record of late Cenozoic surface uplift of southern Alaska. Earth and Planetary Science Letters 482, 300-311. https://doi.org/10.1016/j.epsl.2017.11.029

Biller-Celander, N., Shakun, J.D., McGee, D., Wong, C.I., Reyes, A.V., Hardt, B., Tal, I., Ford, D.C., Lauriol, B., 2021. Increasing Pleistocene permafrost persistence and carbon cycle conundrums inferred from Canadian speleothems. Science Advances 7, eabe5799. https://doi.org/10.1126/sciadv.abe5799

Bitschene, P.R., Schmincke, H.-U., 1990. Fallout Tephra Layers: Composition and Significance, in: Heling, D., Rothe, P., Förstner, U., Stoffers, P. (Eds.), Sediments and Environmental Geochemistry: Selected Aspects and Case Histories. Springer, Berlin, Heidelberg, pp. 48–82. https://doi.org/10.1007/978-3-642-75097-7_4

Blong, R., Enright, N., Grasso, P., 2017. Preservation of thin tephra. J Appl. Volcanol. 6, 10. https://doi.org/10.1186/s13617-017-0059-4

Blong, R.J., Gillespie, R., 1978. Fluvially transported charcoal gives erroneous 14C ages for recent deposits. Nature 271, 739–741

Bond, J.D., 1997. Late Cenozoic history of McQuesten map area, Yukon Territory, with applications to placer gold research. Unpublished M.Sc. thesis, University of Alberta, Edmonton, Alta., Canada. https://doi.org/10.7939/R36Q1SS1N

Bohren, C.F., and Huffman, D.R., 1983, Absorption and scattering of light by small particles:, https://ui.adsabs.harvard.edu/abs/1983uaz..rept.....B (accessed October 2023).

Brennan, P.R.K., Ridgway, K.D., 2015. Detrital zircon record of Neogene exhumation of the central Alaska Range: A far-field upper plate response to flat-slab subduction. GSA Bulletin 127, 945–961. https://doi.org/10.1130/B31164.1

Brendryen, J., Haflidason, H., Sejrup, H.P., 2010. Norwegian Sea tephrostratigraphy of marine isotope stages 4 and 5: Prospects and problems for tephrochronology in the North Atlantic region. Quaternary Science Reviews 29, 847–864.

Brigham-Grette, J., Hopkins, D.M., 1995. Emergent marine record and paleoclimate of the last interglaciation along the northwest Alaskan coast. Quaternary Research 43, 159–173.

Brigham-Grette, J., 2001. New perspectives on Beringian Quaternary paleogeography, stratigraphy, and glacial history. Quaternary Science Reviews 20, 15–24. https://doi.org/10.1016/S0277-3791(00)00134-7

Briggs, N. D., Westgate, J. A., 1978. A contribution to the Pleistocene geochronology of Alaska and the Yukon Territory: fission-track age of distal tephra units: in Short papers of the fourth international conference, geochronology, cosmochronology, isotope geology, 1978, U.S. Geological Survey Open-File Report 78-0701, p. 49-52.

Bronk Ramsey, C., 2009. Bayesian Analysis of Radiocarbon Dates. Radiocarbon 51, 337–360. https://doi.org/10.1017/S0033822200033865

Boehnke, P., Barboni, M., Bell, E.A., 2016. Zircon U/Th model ages in the presence of melt heterogeneity. Quaternary Geochronology 34, 69–74. https://doi.org/10.1016/j.quageo.2016.03.005

Bowring, S.A., Grotzinger, J.P., Isachsen, C.E., Knoll, A.H., Pelechaty, S.M., Kolosov, P., 1993. Calibrating rates of Early Cambrian evolution. Science 261, 1293–1298. https://doi.org/10.1126/science.11539488

Burgess, S.D., Coble, M.A., Vazquez, J.A., Coombs, M.L., Wallace, K.L., 2019. On the eruption age and provenance of the Old Crow tephra. Quaternary Science Reviews 207, 64–79. https://doi.org/10.1016/j.quascirev.2018.12.026

Burgess, S.D., Vazquez, J.A., Waythomas, C.F., Wallace, K.L., 2021. U–Pb zircon eruption age of the Old Crow tephra and review of extant age constraints. Quaternary Geochronology 66, 101168. https://doi.org/10.1016/j.quageo.2021.101168

Buryak, S.D., Reyes, A.V., Jensen, B.J.L., Davies, J.H.F.L., Westgate, J.A., DuFrane, S.A., Luo, Y., Froese, D.G., Pearson, D.G., Benowitz, J.A., 2022. Laser-ablation ICP-MS zircon U-Pb ages for key Pliocene-Pleistocene tephra beds in unglaciated Yukon and Alaska. Quaternary Geochronology 101398.

Chamberlain, K.J., Wilson, C.J.N., Wooden, J.L., Charlier, B.L.A., Ireland, T.R. 2014. New perspectives on the Bishop Tuff from zircon textures, ages and trace elements. Journal of Petrology 55, 395–426. https://10.1093/petrology/egt072.

Chang, Z., Vervoort, J.D., McClelland, W.C., Knaack, C. 2006. U-Pb dating of zircon by LA-ICP-MS. Geochemistry, Geophysics, Geosystems 7, Q05009. https://doi.org/10.1029/2005GC001100.

Charlier, B.L.A., Wilson, C.J.N., Lowenstern, J.B., Blake, S., van Calsteren, P.W., Davidson, J.P., 2005. Magma generation at a large, hyperactive silicic volcano (Taupo, New Zealand) revealed by U-Th and U-Pb systematics in zircons. Journal of Petrology 46, 3–32. https://doi.org/10.1093/petrology/egh060.

Chen, Y., Smith, P.E., Evensen, N.M., York, D., Lajoie, K.R., 1996. The Edge of Time: Dating Young Volcanic Ash Layers with the 40Ar-39Ar Laser Probe. Science 274, 1176–1178.

Chen, J., Li, G., Yang, J., Rao, W., Lu, H., Balsam, W., Sun, Y., Ji, J., 2007. Nd and Sr isotopic characteristics of Chinese deserts: Implications for the provenances of Asian dust. Geochimica et Cosmochimica Acta 71, 3904–3914.

Cheng, H., Adkins, J., Edwards, R.L., Boyle, E.A., 2000. U-Th dating of deep-sea corals. Geochimica et Cosmochimica Acta 64, 2401–2416.

Cherniak, D.J., Watson, E.B., 2001. Pb diffusion in zircon. Chemical Geology 172, 5–24. https://doi.org/10.1016/S0009-2541(00)00233-3.

Coble, M.A., Burgess, S.D., Klemetti, E.W., 2017. New zircon (U-Th)/He and U/Pb eruption age for the Rockland tephra, western USA. Quat. Sci. Rev. 172, 109–117. https://doi.org/10.1016/j.quascirev.2017.08.004

Cooper, A., Turney, C., Hughen, K.A., Brook, B.W., McDonald, H.G., Bradshaw, C.J.A., 2015. Abrupt warming events drove Late Pleistocene Holarctic megafaunal turnover. Science 349, 602–606. https://doi.org/10.1126/science.aac4315

Crowley, J.L., Schoene, B., Bowring, S.A., 2007. U-Pb dating of zircon in the Bishop Tuff at the millennial scale. Geology 35, 1123–1126. https://doi.org/10.1130/G24017A.1.

Cutler, N.A., Shears, O.M., Streeter, R.T., Dugmore, A.J., 2016. Impact of small-scale vegetation structure on tephra layer preservation. Sci Rep 6, 37260. https://doi.org/10.1038/srep37260

Dalrymple, G.B., 1969, 40Ar/36Ar analyses of historic lava flows: Earth and Planetary Science Letters, v. 6, p. 47–55, doi:10.1016/0012-821X(69)90160-5.

Danišík, M., Schmitt, A.K., Stockli, D.F., Lovera, O.M., Dunkl, I., Evans, N.J., 2017. Application of combined U-Th-disequilibrium/U-Pb and (U-Th)/He zircon dating to tephrochronology. Quaternary Geochronology 40, 23–32.

Davies, L.J., Jensen, B.J.L., Froese, D.G., Wallace, K.L., 2016. Late Pleistocene and Holocene tephrostratigraphy of interior Alaska and Yukon: Key beds and chronologies over the past 30,000 years. Quaternary Science Reviews 146, 28–53. https://doi.org/ 10.1016/j.quascirev.2016.05.026

Deino, A.L., Sier, M.J., Garello, D.I., Keller, C.B., Kingston, J.D., Scott, J.J., Dupont-Nivet, G., and Cohen, A.S. 2021. Chronostratigraphy of the Baringo-Tugen Hills-Barsemoi (HSPDP-Biederman tephraB13-1A) core – 40Ar/39Ar dating, magnetostratigraphy, tephrostratigraphy, sequence stratigraphy and Bayesian age modeling. Palaeogeography, Palaeoclimatology, Palaeoecology, 570: 109519. https://doi.org/10.1016/j.palaeo.2019.109519.

Demuro, M., Roberts, R.G., Froese, D.G., Arnold, L.J., Brock, F., Bronk Ramsey, C., 2008. Optically stimulated luminescence dating of single and multiple grains of quartz from perennially frozen loess in western Yukon Territory, Canada: comparison with radiocarbon chronologies for the late Pleistocene Dawson tephra. Quaternary Geochronology 3, 346–364.

De Vivo, B., Rolandi, G., Gans, P.B., Calvert, A., Bohrson, W.A., Spera, F.J., Belkin, H.E., 2001. New constraints on the pyroclastic eruptive history of the Campanian volcanic Plain (Italy). Mineralogy and Petrology 73, 47–65. https://doi.org/10.1007/s007100170010

Dickinson, W.R., Gehrels, G.E. 2009. Use of U–Pb ages of detrital zircons to infer maximum depositional ages of strata: A test against a Colorado Plateau Mesozoic database. Earth and Planetary Science Letters 288, 115–125. https://doi.org/10.1016/j.epsl.2009.09.013.

di Vincenzo, G., Skála, R., 2009. 40Ar–39Ar laser dating of tektites from the Cheb Basin (Czech Republic): Evidence for coevality with moldavites and influence of the dating standard on the age of the Ries impact. Geochimica et Cosmochimica Acta 73, 493–513. https://doi.org/10.1016/j.gca.2008.10.002

Donaghy, E.E., Eddy, M.P., Moreno, F., Ibañez-Mejia, M., 2023. Increased accuracy and precision in igneous and detrital zircon geochronology using CA-LA-ICPMS (preprint). Geochronological data analysis/statistics/modelling. https://doi.org/10.5194/gchron-2023-20

Donovan, J.J., Kremser, D., Fournelle, J.H. and Goemann, K., 2015, Probe for EPMA: Acquisition, automation and analysis, version 11: Eugene, Oregon, Probe Software. Inc., http://www. probesoftware. com.

Donelick, R.A., O'Sullivan, P.B., Ketcham, R.A., 2005. Apatite Fission-Track Analysis. Reviews in Mineralogy and Geochemistry 58, 49–94. https://doi.org/10.2138/rmg.2005.58.3

Edwards, M.E., McDowell, P.F., 1991. Interglacial deposits at Birch Creek, northeast interior Alaska. Quaternary Research 35, 41-52. https://doi.org/10.1016/0033-5894(91)90093-K.

Edwards, M.E., Hamilton, T.D., Elias, S.A., Bigelow, N.H., Krumhardt, A.P., 2003. Interglacial extension of the boreal forest limit in the Noatak Valley, northwest Alaska: Evidence from an exhumed river-cut bluff and debris apron. Arctic, Antarctic, and Alpine Research 35, 460–468.

Elias, S.A., 2001. Mutual climatic range reconstructions of seasonal temperatures based on late Pleistocene fossil beetle assemblages in eastern Beringia. Quaternary Science Reviews 20, 77–91.

Elias, S.A., Brigham-Grette, J., 2013. GLACIATIONS | Late Pleistocene Glacial Events in Beringia, in: Encyclopedia of Quaternary Science. Elsevier, pp. 191–201.

Enkelmann, E., Sanchez Lohff, S.K., Finzel, E.S., 2019. Detrital zircon double-dating of forearc basin strata reveals magmatic, exhumational, and thermal history of sediment source areas. GSA Bulletin 131, 1364–1384. https://doi.org/10.1130/B35043.1

Evans, M.E., Jensen, B.J., Kravchinsky, V.A., Froese, D.G., 2011. The Kamikatsura event in the gold Hill loess, Alaska. Geophysical Research Letters 38, L13302. https://doi.org/10.1029/2011GL047793.

Farley, K.A., 2000. Helium diffusion from apatite: General behavior as illustrated by Durango fluorapatite. Journal of Geophysical Research: Solid Earth 105, 2903–2914. https://doi.org/10.1029/1999JB900348

Fedele, L., Tarzia, M., Belkin, H.E., Vivo, B.D., Lima, A., Lowenstern, J.B., 2006. Chapter 7 Magmatic-hydrothermal fluid interaction and mineralization in alkali-syenite nodules from the Breccia Museo pyroclastic deposit, Naples, Italy, in: De Vivo, B. (Ed.), Developments in Volcanology, Volcanism in the Campania Plain. Elsevier, pp. 125–161. https://doi.org/10.1016/S1871-644X(06)80021-5

Fedele, L., Scarpati, C., Lanphere, M., Melluso, L., Morra, V., Perrotta, A., Ricci, G., 2008. The Breccia Museo formation, Campi Flegrei, southern Italy: geochronology, chemostratigraphy and relationship with the Campanian Ignimbrite eruption. Bull Volcanol 70, 1189–1219. https://doi.org/10.1007/s00445-008-0197-y

Fisher, C.M., Hanchar, J.M., Samson, S.D., Dhuime, B., Blichert-Toft, J., Vervoort, J.D., Lam, R., 2011. Synthetic zircon doped with hafnium and rare earth elements: A reference material for in situ hafnium isotope analysis. Chemical Geology 286, 32–47. https://doi.org/10.1016/j.chemgeo.2011.04.013

Froese, D.G., 2001. Eastern Beringian paleoclimate from fluvial and eolian deposits, Plio-Pleistocene middle Yukon River, central Yukon and Alaska. Unpublished Ph.D. Thesis, University of Calgary, Alta., Canada. https://doi.org/10.11575/PRISM/14916

Froese, D.G., Smith, D.G., Westgate, J.A., Ager, T.A., Preece, S.J., Sandhu, A., Enkin, R.J., Weber, F., 2003. Recurring middle Pleistocene outburst floods in east-central Alaska. Quaternary Research 60, 50–62. https://doi.org/10.1016/S0033-5894(03)00090-5

Froese, D.G., Enkin, R.J., Smith, D.G., 2001. Placer depositional settings and their ages along Dominion Creek, Klondike area, Yukon. In: Emond, D.S., Weston, L.H. (Eds.), Yukon Exploration and Geology 2000. Exploration and Geological Services Division, Yukon Region, Indian and Northern Affairs, Canada, pp. 159–169

Froese, D.G., Zazula, G.D., Westgate, J.A., Preece, S.J., Sanborn, P.T., Reyes, A. V., Pearce, N.J.G., 2009. The Klondike goldfields and Pleistocene environments of Beringia. GSA Today 19, 4–10. https://doi.org/10.1130/GSATG54A.1

Froese, D.G., Westgate, J.A., Reyes, A.V., Enkin, R.J., Preece, S.J., 2008. Ancient permafrost and a future, warmer arctic. Science 321, 1648. https://doi.org/10.1126/science.1157525

Froese, D.G., Zazula, G.D., Reyes, A.V., 2006. Seasonality of the late Pleistocene Dawson tephra and exceptional preservation of a buried riparian surface in central Yukon Territory, Canada. Quaternary Science Reviews 25, 1542–1551.

Froese, D., Stiller, M., Heintzman, P.D., Reyes, A.V., Zazula, G.D., Soares, A.E.R., Meyer, M., Hall, E., Jensen, B.J.L., Arnold, L.J., MacPhee, R.D.E., Shapiro, B., 2017. Fossil and genomic evidence constrains the timing of bison arrival in North America. Proceedings of the National Academy of Sciences of the United States of America 114, 3457–3462. https://doi.org/10.1073/pnas.1620754114

Fukuoka, T., Kigoshi, K., 1974. Discordant Io-ages and the uranium and thorium distribution between zircon and host rocks. Geochemical Journal 8, 117–122. https://doi.org/10.2343/geochemj.8.117

Fukuoka, T., 1974. Ionium dating of acidic volcanic rocks. Geochemical Journal 8, 109–116. https://doi.org/10.2343/geochemj.8.109

Galbraith, R.F., Green, P.F., 1990. Estimating the component ages in a finite mixture. International Journal of Radiation Applications and Instrumentation. Part D. Nuclear Tracks and Radiation Measurements 17, 197–206. https://doi.org/10.1016/1359-0189(90)90035-V

Gentner, W., Kleinmann, B., Wagner, G.A., 1967. New K-Ar and fission track ages of impact glasses and tektites. Earth and Planetary Science Letters 2, 83–86. https://doi.org/10.1016/0012-821X(67)90104-5

Gebauer, D., Williams, I.S., Compston, W., Grünenfelder, M., 1989. The development of the Central European continental crust since the Early Archaean based on conventional and ion-microprobe dating of up to 3.84 b.y. old detrital zircons. Tectonophysics, Evolution of the European Continental Crust: Deep Drilling, Geophysics, Geology and Geochemistry 157, 81–96. https://doi.org/10.1016/0040-1951(89)90342-9

Gebauer, S.K., Schmitt, A.K., Pappalardo, L., Stockli, D.F., Lovera, O.M., 2014. Crystallization and eruption ages of Breccia Museo (Campi Flegrei caldera, Italy) plutonic clasts and their relation to the Campanian ignimbrite. Contrib Mineral Petrol 167, 953. https://doi.org/10.1007/s00410-013-0953-7

Goebel, T., Waters, M., O'Rourke, D.H., 2008. The Late Pleistocene dispersal of modern humans in the Americas. Science 319, 1497–1502.

Guillong, M., von Quadt, A., Sakata, S., Peytcheva, I., Bachmann, O., 2014. LA-ICP-MS Pb-U dating of young zircons from the Kos-Nisyros volcanic centre, SE Aegean arc. Journal of Analytical Atomic Spectrometry 29, 963–970. https://doi.org/10.1039/c4ja00009a

Guillong, M., Sliwinski, J.T., Schmitt, A., Forni, F., Bachmann, O., 2016. U-Th Zircon Dating by Laser Ablation Single Collector Inductively Coupled Plasma-Mass Spectrometry (LA-ICP-MS). Geostandards and Geoanalytical Research 40, 377–387. https://doi.org/10.1111/j.1751-908X.2016.00396.x

Guthrie, R.D., 1990. Frozen Fauna of the Mammoth Steppe: The Story of Blue Babe. University of Chicago Press, Chicago, 323 p.

Guthrie, R.D., 2006. New carbon dates link climatic change with human colonization and Pleistocene extinctions. Nature 441, 207–209.

Hall, C.M., Walter, R.C., Westgate, J.A., and York, D., 1984, Geochronology, stratigraphy and geochemistry of Cindery Tuff in Pliocene hominid-bearing sediments of the Middle Awash, Ethiopia: Nature, v. 308, p. 26–31, doi:10.1038/308026a0.

Hamilton, T.D., Brigham-Grette, J., 1991. The last interglaciation in Alaska: Stratigraphy and paleoecology of potential sites. Quaternary International 10, 49-71. https://doi.org/10.1016/1040-6182(91)90040-U

Harangi, S., Lukács, R., Schmitt, A.K., Dunkl, I., Molnár, K., Kiss, B., Seghedi, I., Novothny, Á., Molnár, M., 2015. Constraints on the timing of Quaternary volcanism and duration of magma residence at Ciomadul volcano, east–central Europe, from combined U–Th/He and U–Th zircon geochronology. Journal of Volcanology and Geothermal Research 301, 66–80. https://doi.org/10.1016/j.jvolgeores.2015.05.002

Harrison, T.M., McKeegan, K.D., LeFort, P., 1995. Detection of inherited monazite in the Manaslu leucogranite by 208Pb232Th ion microprobe dating: Crystallization age and tectonic implications. Earth and Planetary Science Letters 133, 271–282. https://doi.org/10.1016/0012-821X(95)00091-P

Hidy, A.J., Gosse, J.C., Sanborn, P., Froese, D.G., 2018. Age-erosion constraints on an Early Pleistocene paleosol in Yukon, Canada, with profiles of 10Be and 26Al: Evidence for a significant loess cover effect on cosmogenic nuclide production rates. Catena 165, 260-271. https://doi.org/10.1016/j.catena.2018.02.009

Holmes, A., 1911. The association of lead with uranium in rock-minerals, and its application to the measurement of geological time. Proceedings of the Royal Society of London. Series A, Containing Papers of a Mathematical and Physical Character 85, 248–256. https://doi.org/10.1098/rspa.1911.0036

Hopkins, D.M., Matthews, J. V., Wolfe, J.A., Silberman, M.L., 1971. A Pliocene flora and insect fauna from the Bering Strait region. Palaeogeography. Palaeoclimatology, Palaeoecology 9, 211–231. https://doi.org/10.1016/0031-0182(71)90032-0

Hopkins, D.M., 1982. Aspects of the paleogeography of Beringia during the late Pleistocene, in: Hopkins, D. M., Matthews, J.V., Schweger, C.E., Young, S.B. (Eds.), Paleoecology of Beringia. Academic Press, pp. 3–28.

Horn, I., Guillong, M., Günther, D., 2001. Wavelength dependant ablation rates for metals and silicate glasses using homogenized laser beam profiles — implications for LA-ICP-MS. Applied Surface Science 182, 91–102. https://doi.org/10.1016/S0169-4332(01)00465-2.

Hultén, E., 1937. Outline of the history of arctic and boreal biota during the Quaternary period. Bokfoerlags Aktiebolaget Thule, Stockholm, Sweden.

Huntley, D.J., Lamothe, M., 2001. Ubiquity of anomalous fading in K-feldspars and the measurement and correction for it in optical dating. Can. J. Earth Sci. 38, 1093–1106. https://doi.org/10.1139/e01-013

Hurford, A.J., Green, P.F., 1983. The zeta age calibration of fission-track dating. Chemical Geology 41, 285–317 https://doi.org/10.1016/S0009-2541(83)80026-6

Ickert, R.B., Mundil, R., Magee, C.W., Mulcahy, S.R., 2015. The U-Th-Pb systematics of zircon from the Bishop Tuff: A case study in challenges to high-precision Pb/U geochronology at the millennial scale. Geochimica et Cosmochimica Acta 168, 88–110. https://doi.org/10.1016/j.gca.2015.07.018.

Ito, H., Tamura, A., Morishita, T., Arai, S., Arai, F., Kato, O., 2013. Quaternary plutonic magma activities in the southern Hachimantai geothermal area (Japan) inferred from zircon LA-

ICP-MS U-Th-Pb dating method. Journal of Volcanology and Geothermal Research 265, 1–8. https://doi.org/10.1016/j.jvolgeores.2013.08.014

Ito, H., 2014. Zircon U–Th–Pb dating using LA-ICP-MS: Simultaneous U–Pb and U–Th dating on the 0.1 Ma Toya Tephra, Japan. Journal of Volcanology and Geothermal Research 289, 210–223. https://doi.org/10.1016/j.jvolgeores.2014.11.002.

Jackson, S.E., Pearson, N.J., Griffin, W.L., Belousova, E.A., 2004. The application of laser ablation-inductively coupled plasma-mass spectrometry to in situ U–Pb zircon geochronology. Chemical Geology 211, 47–69. https://doi.org/10.1016/j.chemgeo.2004.06.017.

Jaffey, A.H., Flynn, K.F., Glendenin, L.E., Bentley, W.C., Essling, A.M., 1971. Precision measurement of half-lives and specific activities of U235 and U238. Physical Review C 4, 1889–1906. https://doi.org/10.1103/PhysRevC.4.1889

Jensen, B.J.L., Evans, M.E., Froese, D.G., Kravchinsky, V.A., 2016. 150,000 years of loess accumulation in central Alaska. Quaternary Science Reviews 135, 1–23. https://doi.org/10.1016/j.quascirev.2016.01.001

Jensen, B.J.L., Froese, D.G., Preece, S.J., Westgate, J.A., Stachel, T., 2008. An extensive middle to late Pleistocene tephrochronologic record from east-central Alaska. Quaternary Science Reviews 27, 411–427. /10.1016/j.quascirev.2007.10.010

Jensen, B.J.L., Froese, D.G., 2009. Biederman tephra: a potential Marine Isotope Stage 7 marker horizon in eastern Beringia. Canadian Quaternary Association Biennial Meeting, May 3-8, Simon Fraser University, BC, Canada. Programme and Abstracts, vol. 101.

Jensen, B.J.L., Preece, S.J., Lamothe, M., Pearce, N.J.G., Froese, D.G., Westgate, J.A., Schaefer, J., Begét, J., 2011. The variegated (VT) tephra: A new regional marker for middle to late marine isotope stage 5 across Yukon and Alaska. Quaternary International 246, 312–323.

Jensen, B.J.L., Reyes, A.V., Froese, D.G., Stone, D.B., 2013. The Palisades is a key reference site for the middle Pleistocene of eastern Beringia: New evidence from paleomagnetics and regional tephrostratigraphy. Quaternary Science Reviews 63, 91–108. https://doi.org/10.1016/j.quascirev.2012.11.035

Jensen, B.J.L. et al., 2021, A latest Pleistocene and Holocene composite tephrostratigraphic framework for northeastern North America: Quaternary Science Reviews, v. 272, p. 107-242, doi:10.1016/j.quascirev.2021.107242.

Jicha, B.R., Kristjánsson, L., Brown, M.C., Singer, B.S., Beard, B.L., Johnson, C.M., 2011. New age for the Skálamælifell excursion and identification of a global geomagnetic event in the late Brunhes chron. Earth and Planetary Science Letters 310, 509–517.

Keller, C.B., Schoene, B., Samperton, K.M., 2018. A stochastic sampling approach to zircon eruption age interpretation. Geochemical Perspectives Letters 8, 31–35. https://doi.org /10.7185/geochemlet.1826.

Ketcham, R.A., Gautheron, C., Tassan-Got, L., 2011. Accounting for long alpha-particle stopping distances in (U–Th–Sm)/He geochronology: Refinement of the baseline case. Geochimica et Cosmochimica Acta 75, 7779–7791. https://doi.org/10.1016/j.gca.2011.10.011

Kirkland, C.L., Danišík, M., Marsden, R., Piilonen, P., Barham, M., Sutherland, L., 2020. Dating young zircon: A case study from Southeast Asian megacrysts. Geochimica et Cosmochimica Acta 274, 1–19. https://doi.org/10.1016/j.gca.2020.01.013

Kohn, M.J., Vervoort, J.D., 2008. U-Th-Pb dating of monazite by single-collector ICP-MS: Pitfalls and potential. Geochemistry, Geophysics, Geosystems 9. https://doi.org/10.1029/2007GC001899

Krautz, J., Hofmann, M., Gärtner, A., Linnemann, U., Kleber, A., 2018. Capability of U–Pb dating of zircons from Quaternary tephra: Jemez Mountains, NM, and La Sal Mountains, UT, USA. E&G Quat. Sci. J. 67, 7–16. https://doi.org/10.5194/egqsj-67-7-2018

Kunk, M.J., and Cortesini, H., Jr., 1992, 40Ar/39Ar age-spectrum data for whole rock basalts, and plagioclase and biotite from tephra; a traverse down the Porcupine River, east-central Alaska: U.S. Geological Survey Open-File Report 92-701, 81 p.

Kunk, M.J., Rieck, H., Fouch, T.D., Carter, L.D., 1994. 40Ar/39Ar age constraints on neogene sedimentary beds, Upper Ramparts, half-way Pillar and Canyon village sites, Porcupine river, east-central Alaska. Quaternary International 22–23, 31–42. https://doi.org/10.1016/1040-6182(94)90005-1

Kunk, M.J., 1995. 40Ar/39Ar age-spectrum data for hornblende, plagioclase and biotite from tephra collected at Dan Creek and McCallum Creek, Alaska and in the Klondike Placer district near Dawson, Yukon Territory, Canada. USGS Open-File Report 95-217, 52 p. https://doi.org/10.3133/ofr95217A

Lamothe, M., Forget Brisson, L., Hardy, F., 2020. Circumvention of anomalous fading in feldspar luminescence dating using Post-Isothermal IRSL. Quaternary Geochronology 57, 101062. https://doi.org/10.1016/j.quageo.2020.101062

Laurenzi, M.A., Balestrieri, M.L., Bigazzi, G., Hadler Neto, J.C., Iunes, P.J., Norelli, P., Oddone, M., Osorio Araya, A.M., Viramonte, J.G., 2007. New constraints on ages of glasses proposed as reference materials for fission-track dating. Geostandards and Geoanalytical Research 31, 105–124. https://doi.org/10.1111/j.1751-908X.2007.00844.x

Leopold, E.B., Liu, G., 1994. A long pollen sequence of Neogene age, Alaska range. Quaternary International 22–23, 103–140. https://doi.org/10.1016/1040-6182(94)90009-4

Lindsey, D.A., Naeser, C.W., Shawe, D.R., 1975. Age of volcanism, intrusion, and mineralization in the Thomas Range, Keg Mountain, and Desert Mountain, western Utah. USGS Journal of Research 3, 597-604.

Lowe, D.J., 2011. Tephrochronology and its application: A review. Quaternary Geochronology 6, 107–153.

Lowenstern, J.B., Persing, H.M., Wooden, J.L., Lanphere, M., Donnelly-Nolan, J., Grove, T.L., 2000. U–Th dating of single zircons from young granitoid xenoliths: new tools for understanding volcanic processes. Earth and Planetary Science Letters 183, 291–302. https://doi.org/10.1016/S0012-821X(00)00273-9

Ludwig, K.R., 1977. Effect of initial radioactive-daughter disequilibrium on U-Pb isotope apparent ages of young minerals. USGS Journal of Research 5, 663-667.

Ludwig, K. R., 2012. User's Manual for Isoplot 3.75: A geochronological toolkit for Microsoft Excel. Berkeley Geochronology Center Special Publication 5, 75 p.

Mahon, K.I., 1996. The new “York” regression: application of an improved statistical method to geochemistry. International Geology Review 38, 293–303. https://doi.org/10.1080/00206819709465336

Mankinen, E.A., Dalrymple, G.B., 1979. Revised geomagnetic polarity time scale for the interval 0–5 m.y. B.P. Journal of Geophysical Research: Solid Earth 84, 615–626. https://doi.org/10.1029/JB084iB02p00615

Marillo-Sialer, E., Woodhead, J., Hergt, J., Greig, A., Guillong, M., Gleadow, A., Evans, N., Paton, C., 2014. The zircon 'matrix effect': evidence for an ablation rate control on the accuracy of U–Pb age determinations by LA-ICP-MS. Journal of Analytical Atomic Spectrometry 29, 981–989. https://doi.org/10.1039/C4JA00008K

Marsden, R.C., Kirkland, C.L., Danišík, M., Daggitt, M.L., Ahn, U.-S., Friedrichs, B., Evans, N.J., 2022. A new approach to SHRIMP II zircon U-Th disequilibrium dating. Comput. Geosci. 158. https://doi.org/10.1016/j.cageo.2021.104947

Marković, S.B., Stevens, T., Kukla, G.J., Hambach, U., Fitzsimmons, K.E., Gibbard, P., Buggle, B., Zech, M., Guo, Z., Hao, Q. and Wu, H., 2015. Danube loess stratigraphy—Towards a pan-European loess stratigraphic model. Earth-Science Reviews, 148, pp.228-258.

Martin, P.S., 2005. Twightlight of the Mammoths: Ice Age Extinctions and the Rewildering of America. University of California Press, California, 250 p.

Matheus, P., Begét, J., Mason, O., Gelvin-Reymiller, C., 2003. Late Pliocene to late Pleistocene environments preserved at the Palisades site, central Yukon River, Alaska. Quaternary Research 60, 33–43, https://doi.org/10.1016/S0033-5894(03)00091-7.

Matthews, J.V., Ovenden, L.E., 1990. Late Tertiary Plant Macrofossils from Localities in Arctic/Subarctic North America: A Review of the Data. Arctic 43, 364–392.

Matthews, J. V., Westgate, J.A., Ovenden, L., Carter, L.D., Fouch, T., 2003. Stratigraphy, fossils, and age of sediments at the upper pit of the Lost Chicken gold mine: New information on the late Pliocene environment of east central Alaska. Quaternary Research 60, 9–18. https://doi.org/10.1016/S0033-5894(03)00087-5

Mercer, C.M., and Hodges, K.V., 2016, ArAR — A software tool to promote the robust comparison of K–Ar and 40Ar/39Ar dates published using different decay, isotopic, and monitor-age parameters: Chemical Geology, v. 440, p. 148–163, doi:10.1016/j.chemgeo.2016.06.020.

Morgan, L.E., Renne, P.R., Taylor, R.E., WoldeGabriel, G., 2009. Archaeological age constraints from extrusion ages of obsidian: Examples from the Middle Awash, Ethiopia. Quaternary Geochronology 4, 193–203.

Morlan, R.E., 2003. Current perspectives on the Pleistocene archaeology of eastern Beringia. Quaternary Research 60, 123–132.

Muhs, D., 2003. Stratigraphy and palaeoclimatic significance of Late Quaternary loess–palaeosol sequences of the Last Interglacial–Glacial cycle in central Alaska. Quaternary Science Reviews 22, 1947–1986. https://doi.org/10.1016/S0277-3791(03)00167-7

Muhs, D.R., Bettis, E.A., Aleinikoff, J.N., McGeehin, J.P., Beann, J., Skipp, G., Marshall, B.D., Roberts, H.M., Johnson, W.C., Benton, R., 2008. Origin and paleoclimatic significance of late Quaternary loess in Nebraska: Evidence from stratigraphy, chronology, sedimentology, and geochemistry. Geological Society of America Bulletin 120, 1378–1407. https://doi.org/10.1130/B26221.1

Nadin, E., Goddard, S., Benowitz, J., Sullivan, P.O., 2022. Blowing in the late Cenozoic wind d detrital zircon river contributions to an interior Alaska loess deposit 275. https://doi.org/10.1016/j.quascirev.2021.107266

Naeser, N.D., Westgate, J.A., Hughes, O.L., Péwé, T.L., 1982. Fission-track ages of late Cenozoic distal tephra beds in the Yukon Territory and Alaska. Can. J. Earth Sci. 19, 2167–2178. https://doi.org/10.1139/e82-191

Naeser, N.D., Naeser, C.W., 1984. Fission-Track Dating, in: Mahaney, W.C. (Ed.), Developments in Palaeontology and Stratigraphy. Elsevier, pp. 87–100.

https://doi.org/ 10.1016/S0920-5446(08)70066-9

Niki, S., Kosugi, S., Iwano, H., Danhara, T., Hirata, T., 2022. Development of an In Situ U-Th Disequilibrium Dating Method Utilising Multiple-Spot Femtosecond Laser Ablation-CRC-ICP-MS. Geostandards and Geoanalytical Research 46, 589–602.

Oberli, F., Meier, M., Berger, A., Rosenberg, C.L., GierÉ, R., 2004. U-Th-Pb and 230Th/238U disequilibrium isotope systematics: Precise accessory mineral chronology and melt evolution tracing in the Alpine Bergell intrusion. Geochimica et Cosmochimica Acta 68, 2543–2560.

Ogg, J.G., 2020. Chapter 5 - Geomagnetic Polarity Time Scale, in: Gradstein, F.M., Ogg, James G, Schmitz, M.D., Ogg, G.M.B.T.-G.T.S. 2020 (Eds.), Elsevier, pp. 159–192.

Orlando, L., Ginolhac, A., Raghavan, M., Vilstrup, J., Rasmussen, M., Magnussen, K., Steinmann, K.E., Kapranov, P., Thompson, J.F., Zazula, G., Froese, D., Moltke, I., Shapiro, B., Hofreiter, M., Al-Rasheid, K.A.S., Gilbert, M.T.P., Willerslev, E., 2011. True single-molecule DNA sequencing of a Pleistocene horse bone. Genome Research 21, 1705–1719.

Orlando, L., Ginolhac, A., Zhang, G., Froese, D., Albrechtsen, A., Stiller, M., Schubert, M., Cappellini, E., Petersen, B., Moltke, I., Johnson, P.L.F., Fumagalli, M., Vilstrup, J.T., Raghavan, M., Korneliussen, T., Malaspinas, A.-S., Vogt, J., Szklarczyk, D., Kelstrup, C.D., Vinther, J., Dolocan, A., Stenderup, J., Velazquez, A.M. V, Cahill, J., Rasmussen, M., Wang, X., Min, J., Zazula, G.D., Seguin-Orlando, A., Mortensen, C., Magnussen, K., Thompson, J.F., Weinstock, J., Gregersen, K., Røed, K.H., Eisenmann, V., Rubin, C.J., Miller, D.C., Antczak, D.F., Bertelsen, M.F., Brunak, S., Al-Rasheid, K.A.S., Ryder, O., Andersson, L., Mundy, J., Krogh, A., Gilbert, M.T.P., Kjær, K., Sicheritz-Ponten, T., Jensen, L.J., Olsen, J. V, Hofreiter, M., Nielsen, R., Shapiro, B., Wang, J., Willerslev, E., 2013. Recalibrating Equus evolution using the genome sequence of an early Middle Pleistocene horse. Nature 499, 74–78.

Österle, J.E., Stockli, D.F., Seward, D., Little, T.A., 2020. Dating of young (<1 Ma) tephras: Using U-Pb (zircon) and (U-Th[-Sm])/He (zircon, apatite, magnetite) chronometers to unravel the eruption age of a tephra in the Woodlark Rift of Papua New Guinea. Terra Nova 32, 345–354. https://doi.org/10.1111/ter.12464

Otiniano, G.A., Porter, T.J., Benowitz, J.A., Bindeman, I.N., Froese, D.G., Jensen, B.J.L., Davies, L.J., Phillips, M.A., 2020. A late Miocene to late Pleistocene reconstruction of precipitation isotopes and climate from hydrated volcanic glass shards and biomarkers in Central Alaska and Yukon. Paleoceanography and Paleoclimatology 35, e2019PA003791. https://doi.org/10.1029/2019PA003791

Paton, C., Woodhead, J.D., Hellstrom, J.C., Hergt, J.M., Greig, A., Maas, R., 2010. Improved laser ablation U-Pb zircon geochronology through robust downhole fractionation correction. Geochemistry, Geophysics, Geosystems 11, Q0AA06. https://doi.org/10.1029/2009GC002618.

Paton, C., Hellstrom, J., Paul, B., Woodhead, J., Hergt, J., 2011. Iolite: Freeware for the visualisation and processing of mass spectrometric data. Journal of Analytical Atomic Spectrometry 26, 2508–2518. https://doi.org/10.1039/C1JA10172B.

Petrus, J.A., Kamber, B.S., 2012. VizualAge: A novel approach to laser ablation ICP-MS U-Pb geochronology data reduction. Geostandards and Geoanalytical Research 36, 247–270. https://doi.org/10.1111/j.1751-908X.2012.00158.x.

Péwé, T.L., 1975. Quaternary stratigraphic nomenclature in unglaciated central Alaska, USGS Professional Paper 835, 1-145. https://doi.org/10.3133/pp862

Péwé, T.L., Berger, G.W., Westgate, J.A., Brown, P.M., Leavitt, S.W., 1997. Eva interglaciation forest bed, unglaciated East-Central Alaska: global warming 125,000 years ago. Geological Society of America. https://doi.org/10.1130/SPE319

Péwé, T.L., Westgate, J.A., Preece, S.J., Brown, P.M., Leavitt, S.W., 2009. Late Pliocene Dawson Cut forest bed and new tephrochronological findings in the Gold Hill Loess, east-central Alaska. Geological Society of America Bulletin 121, 294–320. https://doi.org/10.1130/B26323.1

Pigati, J.S., Quade, J., Wilson, J., Jull, A.J.T., Lifton, N.A., 2007. Development of low-background vacuum extraction and graphitization systems for 14C dating of old (40–60 ka) samples. Quaternary International 166, 4–14.

Popa, R.G., Guillong, M., Bachmann, O., Szymanowski, D., Ellis, B., 2020. U-Th zircon dating reveals a correlation between eruptive styles and repose periods at the Nisyros-Yali volcanic area, Greece. Chemical Geology 555, 119830. https://doi.org /10.1016/j.chemgeo.2020.119830

Preece, S.J., Westgate, J.A., Gorton, M.P., 1992. Compositional variation and provenance of late Cenozoic distal tephra beds, Fairbanks area, Alaska. Quaternary International 13–14, 97–101.

Preece, S.J., Westgate, J.A., Alloway, B.V., Milner, W., 2000. Characterization, identity, distribution, and source of late Cenozoic tephra beds in the Klondike district of the Yukon, Canada. Canadian Journal of Earth Sciences 37, 983–996.

Preece, S.J., Westgate, J.A., Froese, D.G., Pearce, N.J.G., Perkins, W.T., 2011. A catalogue of late Cenozoic tephra beds in the Klondike goldfields and adjacent areas, Yukon Territory. Canadian Journal of Earth Sciences 48, 1386–1418. https://doi.org/10.1139/e10-110

Preece, S.J., Westgate, J.A., Stemper, B.A., Péwé, T.L., 1999. Tephrochronology of late Cenozoic loess at Fairbanks, central Alaska. \Geological Society of America Bulletin 111, 71–90. https://doi.org/10.1130/0016-7606(1999)111<0071:TOLCLA>2.3.CO;2

Preece, S.J., Pearce, N.J.G., Westgate, J.A., Froese, D.G., Jensen, B.J.L., Perkins, W.T., 2011. Old Crow tephra across eastern Beringia: a single cataclysmic eruption at the close of Marine Isotope Stage 6. Quaternary Science Reviews 30, 2069–2090. https://doi.org/10.1016/j.quascirev.2010.04.020

Prentice, M., Pittari, A., Lowe, D.J., Kilgour, G., Kamp, P.J.J., Namaliu, M., 2022. Linking proximal ignimbrites and coeval distal tephra deposits to establish a record of voluminous Early Quaternary (2.4–1.9 Ma) volcanism of the Tauranga Volcanic Centre, New Zealand. Journal of Volcanology and Geothermal Research 429, 107595. https://doi.org/10.1016/j.jvolgeores.2022.107595

Reid, M.R., Coath, C.D., Mark Harrison, T., McKeegan, K.D., 1997. Prolonged residence times for the youngest rhyolites associated with Long Valley Caldera:230Th—238U ion microprobe dating of young zircons. Earth and Planetary Science Letters 150, 27–39. https://doi.org/10.1016/S0012-821X(97)00077-0

Reiners, P.W., Spell, T.L., Nicolescu, S., Zanetti, K.A., 2004. Zircon (U-Th)/He thermochronometry: He diffusion and comparisons with 40Ar/39Ar dating. Geochimica et Cosmochimica Acta 68, 1857–1887. https://doi.org/10.1016/j.gca.2003.10.021

Reiners, P.W., 2005. Zircon (U-Th)/He Thermochronometry. Reviews in Mineralogy and Geochemistry 58, 151–179. https://doi.org/10.2138/rmg.2005.58.6

Renne, P.R., Balco, G., Ludwig, K.R., Mundil, R., and Min, K., 2011, Response to the comment by W.H. Schwarz et al. on "Joint determination of 40K decay constants and 40Ar∗/40K for the Fish Canyon sanidine standard, and improved accuracy for 40Ar/39Ar geochronology" by P.R. Renne et al. (2010): Geochimica et Cosmochimica Acta, v. 75, p. 5097–5100, doi:10.1016/j.gca.2011.06.021.

Renne, P.R., Mundil, R., Balco, G., Min, K., and Ludwig, K.R., 2010, Joint determination of 40K decay constants and 40Ar∗/40K for the Fish Canyon sanidine standard, and improved accuracy for 40Ar/39Ar geochronology: Geochimica et Cosmochimica Acta, v. 74, p. 5349–5367, doi:10.1016/j.gca.2010.06.017.

Renne, P.R., Cassata, W.S., and Morgan, L.E., 2009, The isotopic composition of atmospheric argon and 40Ar/39Ar geochronology: Time for a change? Quaternary Geochronology, v. 4, p. 288–298, doi:10.1016/j.quageo.2009.02.015.

Reyes, A.V, Froese, D.G., Jensen, B.J.L., 2010a. Permafrost response to last interglacial warming: field evidence from non-glaciated Yukon and Alaska. Quaternary Science Reviews 29, 3256–3274. https://doi.org/10.1016/j.quascirev.2010.07.013

Reyes, A.V., Jensen, B.J.L., Zazula, G.D., Ager, T.A., Kuzmina, S., La Farge, C., Froese, D.G., 2010b. A late-Middle Pleistocene (Marine Isotope Stage 6) vegetated surface buried by Old Crow tephra at the Palisades, interior Alaska. Quaternary Science Reviews 29, 801–811. https://doi.org/10.1016/j.quascirev.2009.12.003

Reyes, A.V., Jensen, B.J.L., Woudstra, S.H., Bolton, M.S.M., Buryak, S.D., Cook, M.S., Harvey, J., Westgate, J.A., 2023. Detrital glass in a Bering Sea sediment core yields a ca. 160 ka Marine Isotope Stage 6 age for Old Crow tephra. Geology 51, 106–110.

Riehle, J.R., Dumond, Don.E., Meyer, C.E., and Schaaf, J.M., 2000, Tephrochronology of the Brooks River Archaeological District, Katmai National Park and Preserve, Alaska: what can and cannot be done with tephra deposits: Geological Society, London, Special Publications, v. 171, p. 245–266, doi:10.1144/GSL.SP.2000.171.01.19.

Rossignol, C., Hallot, E., Bourquin, S., Poujol, M., Jolivet, M., Pellenard, P., Ducassou, C., Nalpas, T., Heilbronn, G., Yu, J., Dabard, M.-P., 2019. Using volcaniclastic rocks to constrain sedimentation ages: To what extent are volcanism and sedimentation synchronous? Sedimentary Geology 381, 46–64. https://doi.org/10.1016/j.sedgeo.2018.12.010

Sakata, S., Hirakawa, S., Iwano, H., Danhara, T., Hirata, T., 2013. Correction of initial disequilibrium on U-Th-Pb system for dating of young zircons. Mineralogical Magazine 77, 2116. https://doi.org/10.1180/minmag.2013.077.5.19

Sakata, S., 2018. A practical method for calculating the U-Pb age of Quaternary zircon: Correction for common Pb and initial disequilibria. Geochemical Journal 52, 281–286. https://doi.org/10.2343/geochemj.2.0508

Sanborn, P.T., Smith, C.A.S., Froese, D.G., Zazula, G.D., Westgate, J.A., 2006. Full-glacial paleosols in perennially frozen loess sequences, Klondike goldfields, Yukon Territory, Canada. Quaternary Research 66, 147–157. https://doi.org/10.1016/j.yqres.2006.02.008

Sandhu, A.S., Westgate, J.A., Preece, S.J., and Froese, D.G., 2001. Glass-fission-track ages of late Cenozoic distal tephra beds in the Klondike district, Yukon Territory; In, Yukon

Exploration and Geology 2000, D.S. Emond and L.H. Weston (eds.), Exploration and Geological Services Division, Yukon, Indian and Northern Affairs Canada, pp. 247-256.

Sandhu, A.S., Westgate, J.A., 1995. The correlation between reduction in fission-track diameter and areal track density in volcanic glass shards and its application in dating tephra beds. Earth and Planetary Science Letters 131, 289–299. https://doi.org/10.1016/0012-821X(95)00022-5

Schaen, A.J. et al., 2020, Interpreting and reporting 40Ar/39Ar geochronologic data: GSA Bulletin, v. 133, p. 461–487, doi:10.1130/B35560.1.

Schaltegger, U., Schmitt, A.K., Horstwood, M.S.A., 2015. U–Th–Pb zircon geochronology by ID-TIMS, SIMS, and laser ablation ICP-MS: Recipes, interpretations, and opportunities. Chemical Geology 402, 89–110.

Schärer, U., 1984. The effect of initial 230Th disequilibrium on young UPb ages: the Makalu case, Himalaya. Earth and Planetary Science Letters 67, 191–204. https://doi.org/10.1016/0012-821X(84)90114-6

Schneider, C.A., Rasband, W.S., Eliceiri, K.W., 2012. NIH Image to ImageJ: 25 years of image analysis. Nat Methods 9, 671–675. https://doi.org/10.1038/nmeth.2089

Schmieder, M., Kennedy, T., Jourdan, F., Buchner, E., Reimold, W., 2018. A high-precision 40Ar/39Ar age for the Nördlinger Ries impact crater, Germany, and implications for the accurate dating of terrestrial impact events. Geochimica et Cosmochimica Acta 220, 146–157. https://doi.org/10.1016/j.gca.2017.09.036

Schmitt, A.K., 2007. Ion microprobe analysis of (231Pa)/(235U) and an appraisal of protactinium partitioning in igneous zircon. American Mineralogist 92, 691–694. https://doi.org/10.2138/am.2007.2449

Schmitt, A.K., 2011. Uranium Series Accessory Crystal Dating of Magmatic Processes. Annu. Rev. Earth Planet. Sci. 39, 321–349.

Schmitt, A.K., Stockli, D.F., Niedermann, S., Lovera, O.M., Hausback, B.P., 2010. Eruption ages of Las Tres Vírgenes volcano (Baja California): A tale of two helium isotopes. Quaternary Geochronology 5, 503–511. https://doi.org/10.1016/j.quageo.2010.02.004

Schmitt, A.K., Clementz, M.T., Lovelace, D.M., Chamberlain, K.R., 2023. Natural Trap Cave tephra correlation to Yellowstone using U-series (230Th/238U) dates and oxygen isotopes of zircon and chemical composition of adherent glass. Quaternary International 647–648, 36–41. https://doi.org/10.1016/j.quaint.2022.02.017

Schmitt, A.K., Sliwinski, J., Caricchi, L., Bachmann, O., Riel, N., Kaus, B.J.P., Cisneros de Léon, A., Cornet, J., Friedrichs, B., Lovera, O., Sheldrake, T., Weber, G., 2023. Zircon age spectra to quantify magma evolution. Geosphere 19, 1006–1031. https://doi.org/10.1130/GES02563.1

Schmitz, M.D., Bowring, S.A., 2001. U-Pb zircon and titanite systematics of the Fish Canyon Tuff: an assessment of high-precision U-Pb geochronology and its application to young volcanic rocks. Geochimica et Cosmochimica Acta 65, 2571–2587. https://doi.org/10.1016/S0016-7037(01)00616-0

Schoene, B., 2013. U-Th-Pb Geochronology, Treatise on Geochemistry: Second Edition. https://doi.org/10.1016/B978-0-08-095975–7 .00310-7

Schweger, C., Froese, D., White, J.M., Westgate, J.A., 2011. Pre-glacial and interglacial pollen records over the last 3 Ma from northwest Canada: Why do Holocene forests differ from those of previous interglaciations? Quaternary Science Reviews 30, 2124–2133. https://doi.org/10.1016/j.quascirev.2011.01.020

Shane, P., 2000. Tephrochronology: a New Zealand case study. Earth-Science Reviews 49, 223–259.

Shane, P., Sandiford, A., 2003. Paleovegetation of marine isotope stages 4 and 3 in Northern New Zealand and the age of the widespread Rotoehu tephra. Quaternary Research 59, 420–429.

Sharman, G.R., Sharman, J.P., Sylvester, Z., 2018. detritalPy: A Python-based toolset for visualizing and analysing detrital geo-thermochronologic data. The Depositional Record 4, 202–215. https://doi.org/10.1002/dep2.45

Sher, A., 1999. Traffic lights at the Beringian crossroads. Nature 397, 103–104.

Simon, J.I., Reid, M.R., 2005. The pace of rhyolite differentiation and storage in an 'archetypical' silicic magma system, Long Valley, California. Earth and Planetary Science Letters 235, 123–140. https://doi.org/10.1016/j.epsl.2005.03.013

Simon, J.I., Renne, P.R., Mundil, R., 2008. Implications of pre-eruptive magmatic histories of zircons for U–Pb geochronology of silicic extrusions. Earth and Planetary Science Letters 266, 182–194. https://doi.org/10.1016/j.epsl.2007.11.014

Simon, J.I., Weis, D., DePaolo, D.J., Renne, P.R., Mundil, R., Schmitt, A.K., 2014. Assimilation of preexisting Pleistocene intrusions at Long Valley by periodic magma recharge accelerates rhyolite generation: rethinking the remelting model. Contrib Mineral Petrol 167, 955. https://doi.org/10.1007/s00410-013-0955-5

Simonetti, A., Heaman, L.M., Hartlaub, R.P., Creaser, R.A., MacHattie, T.G., Böhm, C., 2005. U–Pb zircon dating by laser ablation-MC-ICP-MS using a new multiple ion counting Faraday collector array. Journal of Analytical Atomic Spectrometry 20, 677–686. The Royal Society of Chemistry. https://doi.org/10.1039/B504465K

Sisson, T.W., Schmitt, A.K., Danišík, M., Calvert, A.T., Pempena, N., Huang, C.-Y., Shen, C.-C., 2019. Age of the dacite of Sunset Amphitheater, a voluminous Pleistocene tephra from Mount Rainier (USA), and implications for Cascade glacial stratigraphy. J. Volcanol. Geotherm. Res. 376, 27–43. https://doi.org/10.1016/j.jvolgeores.2019.03.003

Sláma, J., Košler, J., Condon, D.J., Crowley, J.L., Gerdes, A., Hanchar, J.M., Horstwood, M.S.A., Morris, G.A., Nasdala, L., Norberg, N., Schaltegger, U., Schoene, B., Tubrett, M.N., Whitehouse, M.J. 2008. Plešovice zircon — A new natural reference material for U–Pb and Hf isotopic microanalysis. Chemical Geology 249, 1–35. https://doi.org/10.1016/j.chemgeo.2007.11.005

Sliwinski, J.T., Guillong, M., Liebske, C., Dunkl, I., von Quadt, A., Bachmann, O., 2017. Improved accuracy of LA-ICP-MS U-Pb ages of Cenozoic zircons by alpha dose correction. Chemical Geology 472, 8–21. https://doi.org/10.1016/j.chemgeo.2017.09.014.

Smith, C.A.S., Tarnocai, C., Hughes, O.L., 1986. Pedological investigation of Pleistocene glacial drift surfaces in the central Yukon. Géographie Physique et Quaternaire 40, 29-37. https://doi.org/10.7202/032620ar

Sortor, R.N., Goehring, B.M., Bemis, S.P., Ruleman, C.A., Caffee, M.W., Ward, D.J., 2021. Early Pleistocene climate-induced erosion of the Alaska Range formed the Nenana Gravel. Geology 49, 1473–1477. https://doi.org/10.1130/G49094.1

Spell, T.L., Smith, E.I., Sanford, A., Zanetti, K.A., 2001. Systematics of xenocrystic contamination: preservation of discrete feldspar populations at McCullough Pass Caldera revealed by 40Ar/39Ar dating. Earth and Planetary Science Letters 190, 153–165. https://doi.org/10.1016/S0012-821X(01)00382-X

Stacey, J.S., Kramers, J.D., 1975. Approximation of terrestrial lead isotope evolution by a two-stage model. Earth and Planetary Science Letters 26, 207–221. https://doi.org/10.1016/0012-821X(75)90088-6

Staudacher, T., Jessberger, E.K., Dominik, B., Kirsten, T., Schaefferh, O.A., 1982. 40Ar-39Ar ages of rocks and glasses from the Nordlinger Ries crater and the temperature history of impact breccias. Journal of Geophysics 51, 1–11. https://doi.org/10.1016/j.gca.2017.09.036

Steiger, R.H., and Jäger, E., 1977, Subcommission on geochronology: Convention on the use of decay constants in geo- and cosmochronology: Earth and Planetary Science Letters, v. 36, p. 359–362, doi:10.1016/0012-821X(77)90060-7.

Stelten, M.E., Cooper, K.M., Vazquez, J.A., Calvert, A.T., Glessner, J.J.G., 2015. Mechanisms and Timescales of Generating Eruptible Rhyolitic Magmas at Yellowstone Caldera from Zircon and Sanidine Geochronology and Geochemistry. J. Petrol. 56, 1607–1642. https://doi.org/10.1093/petrology/egv047

Sitek, B.C., 2017. Analyzing the Cenozoic Depositional History of Western Kansas: A New Approach Using Paleosol Zircon Geochronology (Thesis). University of Kansas.

Strong, T.R., Driscoll, R.L., 2016. A process for reducing rocks and concentrating heavy minerals. USGS Open-File Report 2016–1022, 16 p., https://doi.org/10.3133/ofr20161022.

Sylvester, P.J., Souders, A.K., Liu, R., 2022. Significance of U-Pb detrital zircon geochronology for mudstone provenance. Geology 50, 670–675. https://doi.org/10.1130/G49684.1

Sun, D., Shaw, J., An, Z., Cheng, M. and Yue, L., 1998. Magnetostratigraphy and paleoclimatic interpretation of a continuous 7.2 Ma Late Cenozoic eolian sediments from the Chinese Loess Plateau. Geophysical Research Letters, 25(1), pp.85-88.

Sundell, K.E., Gehrels, G.E., D. Blum, M., Saylor, J.E., Pecha, M.E., Hundley, B.P., 2024. An exploratory study of “large-n” detrital zircon geochronology of the Book Cliffs, UT via rapid (3 s/analysis) U–Pb dating. Basin Research 36, e12840. https://doi.org/10.1111/bre.12840

Tanner, M., 2010. Shorter signals for improved signal to noise ratio, the influence of Poisson distribution. J. Anal. At. Spectrom. 25, 405. https://doi.org/10.1039/b921077f

Tera, F., Wasserburg, G.J., 1972. U-Th-Pb systematics in three Apollo 14 basalts and the problem of initial Pb in lunar rocks. Earth and Planetary Science Letters 14, 281–304. https://doi.org/10.1016/0012-821X(72)90128-8.

Till, C.B., Vazquez, J.A., Stelten, M.E., Shamloo, H.I., Shaffer, J.S., 2019. Coexisting Discrete Bodies of Rhyolite and Punctuated Volcanism Characterize Yellowstone’s Post-Lava Creek Tuff Caldera Evolution. Geochemistry, Geophys. Geosystems 20, 3861–3881. https://doi.org/10.1029/2019GC008321

Ton-That, T., Singer, B., Paterne, M., 2001. 40Ar/39Ar dating of latest Pleistocene (41 ka) marine tephra in the Mediterranean Sea: implications for global climate records. Earth and Planetary Science Letters 184, 645–658. https://doi.org/10.1016/S0012-821X(00)00358-7

Turner, D.G., Ward, B.C., Bond, J.D., Jensen, B.J.L., Froese, D.G., Telka, A.M., Zazula, G.D., Bigelow, N.H., 2013. Middle to Late Pleistocene ice extents, tephrochronology and paleoenvironments of the White River area, southwest Yukon. Quaternary Science Reviews 75, 59–77. https://doi.org/10.1016/j.quascirev.2013.05.011

Triplehorn, D.M., Drake, Jeff, and Layer, P.W., 2000, Preliminary 40Ar/39Ar ages from two units in the Usibelli Group, Healy, Alaska: New light on some old problems, in Pinney, D.S., and Davis, P.K., eds., Short Notes on Alaska Geology 1999: Alaska Division of Geological & Geophysical Surveys Professional Report 119I, p. 117-127. https://doi.org/10.14509/2691

Ulusoy, İ., Çubukçu, H.E., Mouralis, D., Aydar, E., 2019. Nemrut Caldera and Eastern Anatolian Volcanoes: Fire in the Highlands, in: Kuzucuoğlu, C., Çiner, A., Kazancı, N. (Eds.), Landscapes and Landforms of Turkey, World Geomorphological Landscapes. Springer International Publishing, Cham, pp. 589–599.

Vermeesch, P., 2021. Maximum depositional age estimation revisited. Geoscience Frontiers 12, 843–850. https://doi.org/10.1016/j.gsf.2020.08.008

Vermeesch, P., 2020. Unifying the U–Pb and Th–Pb methods: joint isochron regression and common Pb correction. Geochronology 2, 119–131. https://doi.org/10.5194/gchron-2-119-2020

Vermeesch, P., 2018. IsoplotR: A free and open toolbox for geochronology. Geoscience Frontiers 9, 1479–1493. https://doi.org/10.1016/j.gsf.2018.04.001

Vidal, C.M., Lane, C.S., Asrat, A., Barfod, D.N., Mark, D.F., Tomlinson, E.L., Tadesse, A.Z., Yirgu, G., Deino, A., Hutchison, W., Mounier, A., Oppenheimer, C., 2022. Age of the oldest known Homo sapiens from eastern Africa. Nature 601, 579–583. https://doi.org/10.1038/s41586-021-04275-8

Vlag, P.A., Oches, E.A., Banerjee, S.K., Solheid, P.A., 1999. The paleoenvironmental-magnetic record of the Gold Hill Steps loess section in central Alaska. Physics and Chemistry of the Earth, Part A: Solid Earth and Geodesy 24, 779–783. https://doi.org/10.1016/S1464-1895(99)00114-3

Wahrhaftig, C., 1987. The Cenozoic section at Suntrana, Alaska, in: Hill, M.L. (Ed.), Cordilleran Section of the Geological Society of America. Geological Society of America, p. 0. https://doi.org/10.1130/0-8137-5401-1.445

Walker, M., 2005. Quaternary Dating Methods. John Wiley & Sons Ltd, England. 286 p.

Waythomas, C.F., Lea, P.D., Walter, R.C., 1993. Stratigraphic context of Old Crow tephra, Holitna lowland, interior southwest Alaska. Quaternary Research 40, 20-29. https://doi.org/10.1006/qres.1993.1052

Wendt, I., Carl, C., 1985. U/Pb dating of discordant 0.1 Ma old secondary U minerals. Earth and Planetary Science Letters 73, 278–284.

Westgate, J.A., Hamilton, T.D., Gorton, M.P., 1983. Old Crow tephra: a new late Pleistocene stratigraphic marker across north-central Alaska and western Yukon Territory. Quaternary Research 19, 38–54.

Westgate, J.A., Walter, R.C., Pearce, G.W., Gorton, M.P., 1985. Distribution, stratigraphy, petrochemistry, and palaeomagnetism of the late Pleistocene Old Crow tephra in Alaska and the Yukon. Canadian Journal of Earth Sciences 22, 893–906. https://doi.org/10.1139/e85-093

Westgate, J., 1988. Isothermal plateau fission-track age of the Late Pleistocene Old Crow Tephra, Alaska. Geophysical Research Letters 15, 376–379. https://doi.org/10.1029/GL015i004p00376

Westgate, J.A., 1989. Isothermal plateau fission-track ages of hydrated glass shards from silicic tephra beds. Earth and Planetary Science Letters 95, 226–234. https://doi.org/10.1016/0012-821X(89)90099-X

Westgate, J.A., 2015. Volcanic glass (fission track). In: Rink, W.J., Thompson, J.W. (Eds), Encyclopedia of Scientific Dating Methods. Springer, Dordrecht, Netherlands, pp. 941–946.
https://doi.org/10.1007/978-94-007-6304-3_60

Westgate, J.A., Stemper, B.A., Péwé, T.L., 1990. A 3 m.y. record of Pliocene-Pleistocene loess in interior Alaska. Geology 18, 858–861. https://doi.org/10.1130/0091-7613(1990)018<0858:AMYROP>2.3.CO;2

Westgate, J.A., Briggs, N.D., 1980. Dating methods of Pleistocene deposits and their problems: V. Tephrochronology and fission-track dating. Geoscience Canada 7, 3-10.

Westgate, J.A., Pearce, G.W., Preece, S.J., Schweger, C.E., Morlan, R.E., Pearce, N.J.G., Perkins, T.W., 2013. Tephrochronology, magnetostratigraphy and mammalian faunas of Middle and Early Pleistocene sediments at two sites on the Old Crow River, northern Yukon Territory, Canada. Quaternary Research 79, 75–85. https://doi.org/10.1016/j.yqres.2012.09.003

Westgate, J.A., Pearce, N.J.G., 2017. Age of some Pleistocene interglacial beds and associated fossils in eastern Beringia defined by fission tracks in glass shards of Chester Bluff tephra. Quaternary Research 88, 152–159. https://doi.org/DOI: 10.1017/qua.2017.30

Westgate, J.A., Preece, S.J., Froese, D.G., Walter, R.C., Sandhu, A.S., Schweger, C.E., 2001. Dating early and middle (Reid) Pleistocene glaciations in Central Yukon by

Tephrochronology. Quaternary Research 56, 335–348. https://doi.org/10.1006/qres.2001.2274

Westgate, J.A., Preece, S.J., Jackson, J.E., 2011. Revision of the tephrostratigraphy of the lower Sixtymile River area, Yukon Territory, Canada. Canadian Journal of Earth Sciences 48, 695–701. https://doi.org/10.1139/E10-106

Westgate, J.A., Sandhu, A.S., Preece, S.J., 2003. Age of the gold-bearing White Channel Gravel, Klondike district, Yukon. Yukon Exploration and Geology 2002, 241–250.

Wetherill, G.W., 1956. Discordant uranium-lead ages, I. Eos, Transactions American Geophysical Union 37, 320–326. https://doi.org/10.1029/TR037i003p00320

White, J.M., Ager, T.A., Adam, D.P., Leopold, E.B., Liu, G., Jetté, H., Schweger, C.E., 1997. An 18 million year record of vegetation and climate change in northwestern Canada and Alaska: Tectonic and global climatic correlates. Palaeogeography, Palaeoclimatology, Palaeoecology 130, 293–306. https://doi.org/10.1016/S0031-0182(96)00146-0

Wiedenbeck, M.A.P.C., Alle, P., Corfu, F.Y., Griffin, W.L., Meier, M., Oberli, F.V., Quadt, A.V., Roddick, J.C., Spiegel, W., 1995. Three natural zircon standards for U-Th-Pb, Lu-Hf, trace element and REE analyses. Geostandards Newsletter 19: 1–23. https://doi.org/10.1111/j.1751-908X.1995.tb00147.x.

Willerslev, E., Davison, J., Moora, M., Zobel, M., Coissac, E., Edwards, M.E., Lorenzen, E.D., Vestergård, M., Gussarova, G., Haile, J., Craine, J., Gielly, L., Boessenkool, S., Epp, L.S., Pearman, P.B., Cheddadi, R., Murray, D., Bråthen, K.A., Yoccoz, N., Binney, H., Cruaud, C., Wincker, P., Goslar, T., Alsos, I.G., Bellemain, E., Brysting, A.K., Elven, R., Sønstebø, J.H., Murton, J., Sher, A., Rasmussen, M., Rønn, R., Mourier, T., Cooper, A., Austin, J., Möller, P., Froese, D., Zazula, G., Pompanon, F., Rioux, D., Niderkorn, V., Tikhonov, A., Savvinov, G., Roberts, R.G., Macphee, R.D.E., Gilbert, M.T.P., Kjær, K.H., Orlando, L., Brochmann, C., Taberlet, P., 2014. Fifty thousand years of Arctic vegetation and megafaunal diet. Nature 506, 47–51. https://doi.org/10.1038/nature1292

Williams, I.S., 1998. U–Th–Pb geochronology by ion microprobe. In: McKibben MA, Shanks III WC, Ridley WI (eds) Applications of microanalytical techniques to understanding mineralizing processes. Reviews in Economic Geology 7, Society of Economic Geologists, Littleton, Special Publication, 1–35. https://doi.org/10.5382/Rev.07.01

Wotzlaw, J.-F.F., Schaltegger, U., Frick, D.A., Dungan, M.A., Gerdes, A.G., Günther, D., 2013. Tracking the evolution of large-volume silicic magma reservoirs from assembly to supereruption. Geology 41, 867–870. https://doi.org/10.1130/G34366.1

Woudstra, S., Jensen, B., Thomas, E., Froese, D.G., 2020. MIDDLE PLEISTOCENE LOESS AND TEPHRA DEPOSITS IN THE FAIRBANKS REGION. Presented at the GSA 2020 Connects Online, GSA.

Zazula, G.D., Froese, D.G., Elias, S.A., Kuzmina, S., Mathewes, R.W., 2007. Arctic ground squirrels of the mammoth-steppe: paleoecology of Late Pleistocene middens (~24000–29450 14C yr BP), Yukon Territory, Canada. Quaternary Science Reviews 26, 979–1003. https://doi.org/10.1016/j.quascirev.2006.12.006

Zhang, J., Li, S.-H., 2020. Review of the Post-IR IRSL Dating Protocols of K-Feldspar. Methods Protoc 3, 7. https://doi.org/10.3390/mps3010007

Zimmerer, M.J., Lafferty, J., Coble, M.A., 2016. The eruptive and magmatic history of the youngest pulse of volcanism at the Valles caldera: Implications for successfully dating late Quaternary eruptions. J. Volcanol. Geotherm. Res. 310, 50–57. https://doi.org/10.1016/j.jvolgeores.2015.11.021

APPENDICES

APPENDIX A: CHAPTER 2

Table A.1: LA-ICP-MS U-Pb data.

			Total									Age (Ma)[c]	
Sample number	U (ppm)	Th (ppm)	$^{207}Pb/^{206}Pb$	2σ	$^{207}Pb/^{235}U$	2σ	$^{206}Pb/^{238}U$	2σ (%)	ρ	f_{206} (%)[a]	$f_{Th/U}$[b]	$^{206}Pb^{*}/^{238}U$	2σ[d]
HP Tephra													
iCAP-Q-ICP-MS													
UA2841-1	**3790**	**660**	**0.09100**	**0.02400**	**0.00139**	**0.00038**	**0.000111**	**7**	**0.2669**	**6**	**0.27**	**0.75**	**0.06**
UA2841-2	**2429**	**409**	**0.10200**	**0.03000**	**0.00156**	**0.00048**	**0.000111**	**9**	**0.2929**	**7**	**0.26**	**0.75**	**0.07**
UA2841-3	**2378**	**308**	**0.11300**	**0.04000**	**0.00186**	**0.00067**	**0.000120**	**7**	**0.1922**	**8**	**0.20**	**0.79**	**0.06**
UA2841-4	**1939**	**220**	**0.07500**	**0.04100**	**0.00126**	**0.00071**	**0.000122**	**14**	**0.2470**	**4**	**0.18**	**0.85**	**0.12**
UA2841-5	**1748**	**237**	**0.13000**	**0.05300**	**0.00219**	**0.00093**	**0.000122**	**12**	**0.2887**	**11**	**0.21**	**0.79**	**0.10**
UA2841-6	**1132**	**144**	**0.10700**	**0.05500**	**0.00180**	**0.00094**	**0.000122**	**9**	**0.1728**	**8**	**0.19**	**0.81**	**0.07**
UA2841-7	**1587**	**237**	**0.29800**	**0.04800**	**0.00505**	**0.00107**	**0.000123**	**14**	**0.6512**	**32**	**0.23**	**0.62**	**0.09**
UA2841-8	**2056**	**240**	**0.23000**	**0.05200**	**0.00396**	**0.00097**	**0.000125**	**10**	**0.3908**	**23**	**0.18**	**0.71**	**0.07**
UA2841-9	**1072**	**116**	**0.15400**	**0.06800**	**0.00274**	**0.00129**	**0.000129**	**16**	**0.3459**	**14**	**0.17**	**0.81**	**0.13**
UA2841-10	**1876**	**223**	**0.17100**	**0.04000**	**0.00323**	**0.00088**	**0.000137**	**14**	**0.5100**	**16**	**0.18**	**0.83**	**0.12**
UA2841-11	**1712**	**425**	**0.18700**	**0.05800**	**0.00389**	**0.00131**	**0.000151**	**13**	**0.3927**	**18**	**0.32**	**0.87**	**0.12**
UA2841-12	**3104**	**572**	**0.27000**	**0.03900**	**0.00562**	**0.00093**	**0.000151**	**8**	**0.4820**	**28**	**0.29**	**0.78**	**0.06**
UA2841-13	**1563**	**281**	**0.32400**	**0.07700**	**0.00701**	**0.00187**	**0.000157**	**12**	**0.4538**	**35**	**0.25**	**0.74**	**0.09**
UA2841-14	**1367**	**150**	**0.35000**	**0.08100**	**0.00820**	**0.00220**	**0.000170**	**14**	**0.5047**	**38**	**0.17**	**0.76**	**0.10**

UA2841-15	**1123**	**128**	**0.36000**	**0.07400**	**0.00913**	**0.00222**	**0.000184**	**13**	**0.5358**	**40**	**0.18**	**0.80**	**0.11**
UA2841-16	**1197**	**128**	**0.51100**	**0.09000**	**0.01444**	**0.00340**	**0.000205**	**16**	**0.6633**	**59**	**0.17**	**0.63**	**0.10**
UA2841-17	**1612**	**190**	**0.40100**	**0.05500**	**0.01145**	**0.00189**	**0.000207**	**9**	**0.5562**	**45**	**0.18**	**0.82**	**0.08**
UA2841-18	**1166**	**131**	**0.41700**	**0.06700**	**0.01276**	**0.00235**	**0.000222**	**9**	**0.4891**	**47**	**0.17**	**0.85**	**0.08**
UA2841-19	**1148**	**120**	**0.54700**	**0.08900**	**0.01991**	**0.00423**	**0.000264**	**14**	**0.6423**	**63**	**0.17**	**0.71**	**0.10**
UA2841-20	**907**	**103**	**0.48800**	**0.08700**	**0.01790**	**0.00401**	**0.000266**	**14**	**0.6046**	**56**	**0.18**	**0.84**	**0.11**
UA2841-21	**1095**	**115**	**0.54000**	**0.10000**	**0.02010**	**0.00454**	**0.000270**	**13**	**0.5735**	**63**	**0.16**	**0.74**	**0.10**
UA2841-22	1418.00	197.00	0.45	0.07	0.02	0.00	0.00	9	0.47	50.90	0.21	1.01	0.09
UA2841-23	*1053*	*112*	*0.68000*	*0.10000*	*0.03328*	*0.00611*	*0.000355*	*11*	*0.5985*	*80*	*0.17*	*0.54*	*0.06*
UA2841-24	**1430**	**201**	**0.57700**	**0.07600**	**0.02983**	**0.00631**	**0.000375**	**17**	**0.7821**	**67**	**0.20**	**0.88**	**0.15**
UA2841-25	**701**	**489**	**0.60100**	**0.07600**	**0.03754**	**0.00730**	**0.000453**	**15**	**0.7601**	**70**	**1.07**	**0.86**	**0.13**
UA2841-26	*1054*	*144*	*0.71500*	*0.08800*	*0.05580*	*0.00840*	*0.000566*	*9*	*0.5753*	*85*	*0.20*	*0.64*	*0.06*
UA2841-27	**1891**	**223**	**0.27000**	**0.13000**	**0.00499**	**0.00248**	**0.000134**	**13**	**0.2548**	**28**	**0.20**	**0.71**	**0.09**
UA2841-28	*1020*	*121*	*0.64000*	*0.11000*	*0.03327*	*0.00728*	*0.000377*	*14*	*0.6185*	*75*	*0.20*	*0.69*	*0.09*
UA2841-29	**2190**	**248**	**0.38000**	**0.11000**	**0.00891**	**0.00273**	**0.000170**	**10**	**0.3265**	**42**	**0.20**	**0.72**	**0.07**
UA2841-30	**1020**	**119**	**0.40000**	**0.10000**	**0.01224**	**0.00340**	**0.000222**	**12**	**0.4375**	**45**	**0.20**	**0.88**	**0.11**
UA2841-31	*1771*	*310*	*0.66100*	*0.07200*	*0.04174*	*0.00577*	*0.000458*	*9*	*0.6159*	*78*	*0.20*	*0.74*	*0.06*
UA2841-32	65.10	25.70	0.10	0.02	0.39	0.07	0.03	6	0.34	7.34	0.20	161.72	9.32
UA2841-33*	2162.00	244.40	0.18	0.05	0.00	0.00	0.00	10	0.32	16.33	0.20	0.98	0.10
UA2841-34	**1653**	**155**	**0.17700**	**0.09300**	**0.00271**	**0.00146**	**0.000111**	**13**	**0.2334**	**17**	**0.20**	**0.68**	**0.09**
UA2841-35	**1251**	**114**	**0.53000**	**0.12000**	**0.01673**	**0.00453**	**0.000229**	**15**	**0.5484**	**61**	**0.20**	**0.66**	**0.10**
UA2841-36	**1329**	**128**	**0.47000**	**0.29000**	**0.01360**	**0.00728**	**0.000173**	**17**	**0.3129**	**54**	**0.15**	**0.61**	**0.10**
UA2841-37	*4820*	*157*	*0.74500*	*0.08700*	*0.23831*	*0.04386*	*0.002320*	*14*	*0.7729*	*89*	*0.17*	*1.81*	*0.26*
UA2841-38	828.00	264.00	0.07	0.01	0.05	0.01	0.01	3	0.20	2.61	0.66	36.28	1.00
UA2841-39	541.00	143.00	0.06	0.00	0.10	0.01	0.01	2	0.29	1.55	0.49	79.09	1.63

UA2841-40	896.00	70.00	0.07	0.00	0.13	0.01	0.01	2	0.57	2.89	1.72	86.54	2.10
UA2841-41	312.00	259.00	0.05	0.01	0.15	0.02	0.02	2	0.19	0.83	0.55	126.91	3.01
UA2841-42	1579.00	118.00	0.10	0.01	0.29	0.02	0.02	2	0.32	6.53	0.46	126.67	2.78
UA2841-43	604.00	325.00	0.06	0.01	0.21	0.04	0.03	4	0.22	1.76	0.65	158.23	5.93
UA2841-44	388.00	347.00	0.05	0.01	0.19	0.03	0.03	6	0.32	1.06	0.49	160.06	9.33
UA2841-45	899.00	298.00	0.07	0.01	0.25	0.04	0.03	3	0.16	2.90	0.61	160.88	4.09
UA2841-46	957.00	358.00	0.07	0.01	0.26	0.05	0.03	4	0.20	3.16	0.68	164.60	6.69
UA2841-47	*4889*	*125*	*0.78200*	*0.07200*	*2.95433*	*0.44788*	*0.027400*	*12*	*0.7944*	*93*	*1.05*	*11.99*	*1.48*
UA2841-48	1320.00	210.00	0.09	0.01	0.62	0.07	0.05	2	0.15	4.96	0.73	316.08	5.48
UA2841-49	893.00	162.00	0.07	0.01	0.55	0.05	0.06	2	0.19	2.88	0.65	351.23	5.33
UA2841-50	499.00	112.00	0.06	0.00	0.46	0.03	0.06	3	0.44	1.41	0.93	359.07	9.01
UA2841-51	492.00	105.00	0.06	0.00	0.46	0.02	0.06	1	0.29	1.38	0.46	360.72	5.23
UA2841-52	472.00	91.00	0.06	0.00	0.46	0.02	0.06	1	0.30	1.32	0.39	361.67	4.63
UA2841-53	1666.00	83.00	0.10	0.00	0.85	0.04	0.06	2	0.42	7.12	0.44	352.48	7.37
UA2841-54	761.00	107.00	0.06	0.00	0.82	0.05	0.09	3	0.49	2.35	1.57	553.95	15.58
UA2841-55	1740.00	29.00	0.11	0.00	1.42	0.04	0.10	2	0.84	7.65	0.72	553.06	13.10
UA2841-56	1214.00	46.00	0.08	0.00	1.69	0.05	0.15	2	0.60	4.39	1.94	872.49	14.52
UA2841-57	2105.00	21.00	0.13	0.00	3.43	0.09	0.19	2	0.89	10.69	0.28	1012.90	22.11
UA2841-58	2684.00	30.00	0.18	0.00	7.28	0.62	0.29	8	0.98	17.39	0.53	1375.87	102.43
UA2841-59	2006.00	54.00	0.12	0.00	6.08	0.24	0.36	3	0.64	9.79	1.25	1800.51	40.34

<u>Biederman Tephra (UT1884)</u>

<u>SF-ICP-MS</u>

BTRun2019 1	99	45	0.55000	0.48000	0.00895	0.00821	0.000118	28	0.3086	64	0.15	0.35	0.10

BTRun2019 2	*122*	*58*	*0.91900*	*0.07699*	*0.14415*	*0.01666*	*0.001138*	*8*	*0.6890*	*111*	*0.16*	*N/A*	*N/A*
BTRun2019 3	*319*	*224*	*0.66000*	*0.12000*	*0.01001*	*0.00232*	*0.000110*	*14*	*0.6182*	*78*	*0.23*	*0.23*	*0.03*
BTRun2019 4	*110*	*75*	*0.84500*	*0.05001*	*0.33869*	*0.03902*	*0.002907*	*10*	*0.8579*	*101*	*0.23*	*N/A*	*N/A*
BTRun2019 5	*286*	*188*	*0.80200*	*0.03101*	*0.12328*	*0.01098*	*0.001115*	*8*	*0.9009*	*96*	*0.22*	*0.44*	*0.04*
BTRun2019 6	*378*	*450*	*0.75000*	*0.19688*	*0.01272*	*0.00391*	*0.000123*	*16*	*0.5202*	*89*	*0.40*	*0.13*	*0.02*
BTRun2019 7	*158*	*118*	*0.81900*	*0.09248*	*0.05408*	*0.00818*	*0.000479*	*10*	*0.6651*	*98*	*0.25*	*0.15*	*0.02*
BTRun2019 8	*259*	*244*	*0.82000*	*0.10000*	*0.03561*	*0.00517*	*0.000315*	*8*	*0.5424*	*98*	*0.31*	*0.12*	*0.01*
BTRun2019 9	869	236	0.40500	0.04200	0.01156	0.00139	0.000207	6	0.5010	45	0.09	0.80	0.05
BTRun2019 10	*211*	*116*	*0.78300*	*0.08799*	*0.06014*	*0.00823*	*0.000557*	*8*	*0.5702*	*93*	*0.18*	*0.34*	*0.03*
BTRun2019 11	*247*	*146*	*0.77400*	*0.05399*	*0.09818*	*0.00787*	*0.000920*	*4*	*0.4933*	*92*	*0.20*	*0.58*	*0.03*
BTRun2019 12	*221*	*209*	*0.85000*	*0.08900*	*0.03633*	*0.00480*	*0.000310*	*8*	*0.6100*	*102*	*0.32*	*N/A*	*N/A*
BTRun2019 13	*348*	*580*	*0.78200*	*0.05200*	*0.11594*	*0.01040*	*0.001075*	*6*	*0.6712*	*93*	*0.56*	*0.55*	*0.04*
BTRun2019 14	*64*	*38*	*0.85000*	*0.15000*	*0.10549*	*0.02234*	*0.000900*	*12*	*0.5526*	*102*	*0.20*	*N/A*	*N/A*
BTRun2019 15	*293*	*223*	*0.77000*	*0.16000*	*0.01476*	*0.00340*	*0.000139*	*10*	*0.4339*	*90*	*0.25*	*0.14*	*0.02*
BTRun2019 16	*167*	*178*	*0.76300*	*0.07000*	*0.15159*	*0.02285*	*0.001441*	*12*	*0.7934*	*91*	*0.36*	*0.97*	*0.11*
BTRun2019 17	*389*	*347*	*0.71000*	*0.13000*	*0.01292*	*0.00283*	*0.000132*	*12*	*0.5485*	*84*	*0.30*	*0.20*	*0.03*
BTRun2019 18	*86*	*46*	*0.78700*	*0.09900*	*0.24114*	*0.03595*	*0.002222*	*8*	*0.5366*	*94*	*0.18*	*1.05*	*0.08*
BTRun2019 19	*630*	*1364*	*0.74400*	*0.05000*	*0.03950*	*0.00306*	*0.000385*	*4*	*0.4971*	*88*	*0.72*	*0.32*	*0.03*
BTRun2019 20	397	215	0.05600	0.03700	0.00126	0.00084	0.000163	10	0.1488	1	0.18	1.08	0.10
BTRun2019 21	*141*	*141*	*0.70000*	*1.28333*	*0.01100*	*0.02031*	*0.000114*	*22*	*0.1173*	*83*	*0.33*	*0.18*	*0.04*
BTRun2019 22	*908*	*1005*	*0.78200*	*0.04299*	*0.05908*	*0.00402*	*0.000548*	*4*	*0.5884*	*93*	*0.37*	*0.32*	*0.02*
BTRun2019 23	*215*	*208*	*0.80500*	*0.09600*	*0.06814*	*0.00978*	*0.000614*	*8*	*0.5561*	*96*	*0.32*	*0.25*	*0.02*
BTRun2019 24	*166*	*127*	*0.77000*	*0.10000*	*0.07292*	*0.01042*	*0.000687*	*6*	*0.4180*	*92*	*0.25*	*0.47*	*0.03*
BTRun2019 25	*144*	*77*	*0.77100*	*0.05099*	*0.11644*	*0.01042*	*0.001095*	*6*	*0.6734*	*92*	*0.18*	*0.70*	*0.04*
BTRun2019 26	*364*	*275*	*0.67000*	*0.12000*	*0.01118*	*0.00230*	*0.000121*	*10*	*0.4891*	*79*	*0.25*	*0.23*	*0.02*

BTRun2019 27	271	76	0.23800	0.07002	0.00709	0.00220	0.000216	10	0.3199	24	0.09	1.11	0.11
BTRun2019 28	251	169	0.80000	0.18765	0.01974	0.00539	0.000179	14	0.5115	95	0.22	0.12	0.02
BTRun2019 29	107	66	0.92000	0.12000	0.05430	0.00887	0.000428	10	0.6025	111	0.21	N/A	N/A
BTRun2019 30	313	252	0.83500	0.07600	0.04099	0.00492	0.000356	8	0.6523	100	0.27	N/A	N/A
BTRun2019 31	96	84	0.76000	0.11000	0.08895	0.01470	0.000849	8	0.4828	90	0.29	0.62	0.05
BTRun2019 32	117	50	0.88000	0.10000	0.04865	0.00737	0.000401	10	0.6615	106	0.14	N/A	N/A
BTRun2019 33	190	110	0.84100	0.03500	0.17103	0.00985	0.001475	4	0.6914	101	0.19	N/A	N/A
BTRun2019 34	430	687	0.73500	0.08999	0.03000	0.00556	0.000296	14	0.7507	87	0.53	0.30	0.04
BTRun2019 35	163	120	0.83300	0.07200	0.15605	0.01840	0.001359	8	0.6800	100	0.25	0.17	0.02
BTRun2019 36	114	81	0.80000	0.10000	0.08232	0.01231	0.000746	8	0.5489	95	0.24	0.33	0.03
BTRun2019 37	131	72	0.76000	0.03099	0.23601	0.01728	0.002252	6	0.8306	90	0.18	1.53	0.07
BTRun2019 38	2060	477	0.13000	0.03900	0.38966	0.11928	0.021739	6	0.1988	11	0.08	N/A	N/A
BTRun2019 39	129	70	0.71000	0.11000	0.05855	0.01085	0.000598	10	0.5487	84	0.18	0.70	0.07
BTRun2019 40	**378**	**842**	**0.24000**	**0.16000**	**0.00121**	**0.00085**	**0.000037**	**22**	**0.3136**	**25**	**0.74**	**0.20**	**0.05**
BTRun2019 41	123	57	0.80700	0.11000	0.17145	0.03116	0.001541	12	0.6614	96	0.15	0.52	0.06
BTRun2019 42	107	90	0.81000	0.12000	0.09021	0.01597	0.000808	10	0.5475	97	0.28	0.28	0.03
BTRun2019 43	181	95	0.67000	0.46000	0.00471	0.00353	0.000051	30	0.4014	79	0.18	0.13	0.04
BTRun2019 44	90	47	0.85000	0.35999	0.02602	0.01178	0.000222	16	0.3531	102	0.17	N/A	N/A
BTRun2019 45	268	227	0.88700	0.07600	0.09768	0.01144	0.000799	8	0.6819	107	0.28	N/A	N/A
BTRun2019 46	182	116	0.81000	0.17000	0.03183	0.00740	0.000285	10	0.4292	97	0.21	0.13	0.01
BTRun2019 47	51	33	0.18000	0.46001	0.00186	0.00488	0.000075	58	0.2204	17	0.21	0.47	0.27
BTRun2019 49	296	69	0.09300	0.03200	0.00218	0.00077	0.000170	8	0.2262	6	0.08	1.08	0.08
BTRun2019 50	83	56	0.47000	0.28000	0.00888	0.00564	0.000137	22	0.3453	54	0.22	0.48	0.11
BTRun2019 51	588	977	0.39000	0.19000	0.00323	0.00170	0.000060	20	0.3765	44	0.55	0.25	0.05
BTRun2019 52	512	658	0.81200	0.07000	0.05296	0.00697	0.000473	10	0.7553	97	0.43	0.16	0.02

BTRun2019 53	239	266	0.88000	0.12000	0.06492	0.01104	0.000535	10	0.5977	106	0.37	N/A	N/A
BTRun2019 54	1050	1950	0.26900	0.07699	0.00125	0.00038	0.000034	10	0.3331	28	0.62	0.18	0.03
BTRun2019 55	484	751	0.74600	0.05400	0.11303	0.01066	0.001099	6	0.6409	89	0.52	0.88	0.05
BTRun2019 56	84	137	0.13000	0.29000	0.00046	0.00105	0.000026	36	0.1598	11	0.54	0.19	0.07
BTRun2019 57	75	68	0.41000	0.32000	0.00763	0.00637	0.000135	30	0.3557	46	0.30	0.53	0.16
BTRun2019 58	178	105	0.89100	0.08800	0.10491	0.01493	0.000854	10	0.7200	107	0.20	N/A	N/A
BTRun2019 59	242	169	0.78700	0.04900	0.10484	0.00906	0.000966	6	0.6933	94	0.23	0.50	0.03
BTRun2019 60	880	1763	0.69300	0.07100	0.02026	0.00289	0.000212	10	0.6972	82	0.67	0.28	0.03
BT004	743	1680	0.16600	0.03549	0.00095	0.00024	0.000042	14	0.5508	15	0.75	0.24	0.04
BT003	290	178	0.45000	0.16500	0.00184	0.00078	0.000030	22	0.5128	51	0.20	0.16	0.04
BT002	274	136	0.32000	0.18000	0.00113	0.00069	0.000026	22	0.3657	35	0.17	0.18	0.04
BT001	269	382	0.18000	0.08500	0.00091	0.00047	0.000037	22	0.4226	17	0.47	0.24	0.05
BT00	549	1092	0.06960	0.08487	0.00023	0.00028	0.000024	26	0.2099	3	0.66	0.17	0.05
BT01	489	88	0.06990	0.00345	0.00157	0.00010	0.000163	4	0.6362	3	0.06	1.07	0.03
BT02	188	129	0.81000	0.01800	0.42955	0.01908	0.003846	4	0.8659	97	0.23	1.06	0.05
BT03	399	233	0.78800	0.01500	0.22683	0.00998	0.002088	4	0.9016	94	0.19	0.98	0.04
BT04	529	308	0.74900	0.04250	0.03532	0.00404	0.000342	10	0.8680	89	0.19	0.34	0.04
BT05	237	138	0.37000	0.10500	0.00203	0.00066	0.000040	16	0.4883	41	0.19	0.22	0.04
BT05_2	239	163	0.55000	0.13000	0.00392	0.00117	0.000052	18	0.6079	64	0.23	0.19	0.04
BT06	153	77	-0.20000	0.30500	-0.00132	-0.00204	0.000048	20	0.1311	-31	0.17	N/A	N/A
BT07	549	1092	0.78700	0.02049	0.04948	0.00426	0.000456	8	0.9532	94	0.66	0.23	0.03
BT08	207	118	0.75700	0.03700	0.01952	0.00216	0.000187	10	0.8969	90	0.19	0.20	0.02
BT09	133	138	0.75000	0.02800	0.08938	0.01132	0.000864	12	0.9556	89	0.35	0.69	0.08
BT10	330	319	0.79400	0.01750	0.07095	0.00455	0.000648	6	0.9392	95	0.32	0.32	0.02
BT11	895	1668	0.56400	0.02100	0.00713	0.00039	0.000092	4	0.7349	66	0.62	0.24	0.02

BT13	*148*	*86*	*0.84000*	*0.02050*	*0.23930*	*0.01106*	*0.002066*	*4*	*0.8493*	*101*	*0.19*	*N/A*	*N/A*
BT14P1	*256*	*172*	*0.75600*	*0.04900*	*0.01303*	*0.00155*	*0.000125*	*10*	*0.8392*	*90*	*0.22*	*0.15*	*0.02*
BT15P1	**115**	**37**	**0.45000**	**0.32500**	**0.00161**	**0.00134**	**0.000026**	**42**	**0.4991**	**51**	**0.11**	**0.15**	**0.06**
BT16P1	*315*	*187*	*0.66900*	*0.03550*	*0.01513*	*0.00171*	*0.000164*	*10*	*0.8834*	*79*	*0.20*	*0.30*	*0.03*
BT17P1	**464**	**326**	**0.38500**	**0.04450**	**0.00208**	**0.00035**	**0.000039**	**12**	**0.7237**	**43**	**0.23**	**0.21**	**0.02**
BT18P1	*447*	*444*	*0.66000*	*0.05500*	*0.00580*	*0.00085*	*0.000064*	*12*	*0.8236*	*78*	*0.33*	*0.14*	*0.02*
BT19P1	**208**	**125**	**0.49000**	**0.08500**	**0.00402**	**0.00085**	**0.000059**	**12**	**0.5657**	**56**	**0.20**	**0.24**	**0.03**
BT20P1	*143*	*58*	*0.65000*	*0.16300*	*0.00378*	*0.00121*	*0.000042*	*20*	*0.6203*	*89*	*0.14*	*0.13*	*0.03*
BT21P1	**152**	**100**	**0.36000**	**0.13000**	**0.00212**	**0.00086**	**0.000043**	**18**	**0.4456**	**40**	**0.22**	**0.24**	**0.04**
BT22P1	211	109	0.13000	0.05000	0.00058	0.00024	0.000032	14	0.3387	11	0.17	0.26	0.04
BT23P1	149	80	0.61000	0.05000	0.00832	0.00095	0.000099	8	0.6990	71	0.18	0.26	0.02
BT24P1	**204**	**170**	**0.23000**	**0.10000**	**0.00086**	**0.00039**	**0.000027**	**12**	**0.2636**	**23**	**0.28**	**0.19**	**0.03**
BT25P1	**123**	**66**	**0.52000**	**0.09000**	**0.00466**	**0.00105**	**0.000065**	**14**	**0.6369**	**60**	**0.18**	**0.24**	**0.03**
BT26P1	*247*	*240*	*0.64000*	*0.03150*	*0.01174*	*0.00131*	*0.000133*	*10*	*0.8968*	*75*	*0.32*	*0.28*	*0.03*
BT27P1	**34**	**20**	**0.62000**	**0.31500**	**0.00530**	**0.00324**	**0.000062**	**34**	**0.5573**	**73**	**0.20**	**0.18**	**0.06**
BT28P1	*202*	*212*	*0.79400*	*0.02250*	*0.04992*	*0.00328*	*0.000456*	*6*	*0.9022*	*95*	*0.35*	*0.24*	*0.02*
BT29P1	**226**	**141**	**0.49800**	**0.04900**	**0.00304**	**0.00047**	**0.000044**	**12**	**0.7723**	**57**	**0.21**	**0.19**	**0.03**
BT30P1	*48*	*26*	*0.96000*	*0.17000*	*0.03507*	*0.00835*	*0.000265*	*16*	*0.6681*	*116*	*0.18*	*N/A*	*N/A*
BT31P2	**509**	**933**	**0.26200**	**0.03600**	**0.00139**	**0.00022**	**0.000039**	**8**	**0.5071**	**27**	**0.61**	**0.21**	**0.03**
BT32P2	**416**	**325**	**0.52200**	**0.03450**	**0.00494**	**0.00061**	**0.000069**	**10**	**0.8418**	**60**	**0.26**	**0.24**	**0.02**
BT33P2	287	155	0.29000	0.05000	0.00154	0.00031	0.000039	10	0.5031	31	0.18	0.25	0.03
BT34P2	474	396	0.08400	0.00549	0.00186	0.00014	0.000161	4	0.5239	5	0.28	1.02	0.04
BT35P2	*648*	*942*	*0.69600*	*0.02550*	*0.01439*	*0.00126*	*0.000150*	*8*	*0.9082*	*82*	*0.48*	*0.22*	*0.02*
BT37P2	*584*	*597*	*0.65500*	*0.02000*	*0.01616*	*0.00110*	*0.000179*	*6*	*0.8938*	*77*	*0.34*	*0.33*	*0.02*
BT38P2	*301*	*352*	*0.81700*	*0.03150*	*0.05632*	*0.01037*	*0.000500*	*18*	*0.9778*	*98*	*0.39*	*0.15*	*0.03*

BT39P2	464	189	0.09600	0.00950	0.13105	0.01835	0.009901	10	0.7073	6	0.14	N/A	N/A
BT40P2	87	73	0.59000	0.12500	0.00716	0.00182	0.000088	14	0.5535	69	0.28	0.24	0.04
BT41P2	*271*	*166*	*0.71100*	*0.04750*	*0.01549*	*0.00405*	*0.000158*	*25*	*0.9668*	*84*	*0.20*	*0.24*	*0.06*
BT42P2	*271*	*308*	*0.70100*	*0.02749*	*0.01798*	*0.00160*	*0.000186*	*8*	*0.8979*	*83*	*0.38*	*0.27*	*0.02*
BT43P2	*106*	*109*	*0.72000*	*0.06500*	*0.01142*	*0.00154*	*0.000115*	*10*	*0.7424*	*85*	*0.34*	*0.17*	*0.02*
BT44P2	**334**	**262**	**0.37000**	**0.21000**	**0.00175**	**0.00103**	**0.000034**	**16**	**0.2732**	**33**	**0.26**	**0.19**	**0.03**
BT44P2-1	**304**	**296**	**0.56000**	**0.17000**	**0.00435**	**0.00145**	**0.000056**	**14**	**0.4206**	**40**	**0.32**	**0.18**	**0.03**
BT45P2	*29*	*18*	*0.82400*	*0.03599*	*0.17266*	*0.01889*	*0.001520*	*10*	*0.9168*	*99*	*0.21*	*0.30*	*0.03*
BT46P2	*155*	*96*	*0.79700*	*0.01350*	*0.33401*	*0.06017*	*0.003040*	*18*	*0.9956*	*95*	*0.21*	*1.17*	*0.22*
BT47P2	*211*	*148*	*0.81100*	*0.01150*	*0.11934*	*0.00733*	*0.001067*	*6*	*0.9730*	*97*	*0.23*	*0.34*	*0.02*
BT48P2	*368*	*256*	*0.73800*	*0.01450*	*0.02866*	*0.00126*	*0.000282*	*4*	*0.8950*	*88*	*0.23*	*0.31*	*0.01*
BT49P2	247	157	0.48000	0.05500	0.00299	0.00045	0.000045	10	0.6554	55	0.21	0.31	0.03
BT50P2	*772*	*1296*	*0.71800*	*0.01650*	*0.02069*	*0.00134*	*0.000209*	*6*	*0.9350*	*85*	*0.56*	*0.25*	*0.02*
BT51P2	184	138	0.27000	0.16000	0.00196	0.00120	0.000053	16	0.2578	28	0.25	0.31	0.05

Gold Run Tephra

MC-ICP-MS

UA1001-1	-	-	0.26257	0.05675	0.01354	0.00302	0.000374	5	0.2409	27	-	1.75	0.09
UA1001-2	-	-	0.17863	0.07254	0.00759	0.00310	0.000308	5	0.1155	17	-	1.65	0.08
UA1001-3	**407**	**177**	**0.19009**	**0.08430**	**0.00381**	**0.00174**	**0.000145**	**11**	**0.2377**	**18**	**0.24**	**0.85**	**0.09**
UA1001-4	-	-	0.07396	0.00279	0.29670	0.01313	0.029093	2	0.5241	4	-	178.43	4.08
UA1001-5	-	-	0.08354	0.00497	0.28410	0.01786	0.024664	2	0.3207	5	-	149.70	2.98
UA1001-6	-	-	0.04952	0.00099	0.17818	0.00522	0.026096	2	0.7288	0	-	165.35	3.49
UA1001-7	**151**	**62**	**0.23011**	**0.06954**	**0.00485**	**0.00157**	**0.000153**	**12**	**0.3575**	**23**	**0.21**	**0.84**	**0.10**

UA1001-8	**222**	**141**	**0.32284**	**0.11161**	**0.00890**	**0.00349**	**0.000200**	**19**	**0.4723**	**35**	**0.36**	**0.91**	**0.17**
UA1001-9	-	-	0.05324	0.00137	0.19842	0.00658	0.027031	2	0.6277	1	-	170.48	3.50
UA1001-10	**309**	**177**	**0.13913**	**0.13491**	**0.00205**	**0.00201**	**0.000107**	**13**	**0.1296**	**12**	**0.32**	**0.68**	**0.09**
UA1001-11	**590**	**316**	**0.06555**	**0.04582**	**0.00101**	**0.00071**	**0.000112**	**4**	**0.0630**	**2**	**0.29**	**0.78**	**0.04**
UA1001-12	-	-	0.05068	0.00100	0.20423	0.00561	0.029224	2	0.6975	1	-	184.62	3.49
UA1001-13	*225*	*92*	*0.71143*	*0.05471*	*0.07357*	*0.00647*	*0.000750*	*4*	*0.4863*	*84*	*0.22*	*0.85*	*0.04*
UA1001-14	**381**	**254**	**0.50561**	**0.04861**	**0.02145**	**0.00299**	**0.000308**	**10**	**0.7237**	**58**	**0.37**	**0.90**	**0.09**
UA1001-15	-	-	0.50369	0.02639	0.04904	0.00355	0.000706	5	0.6904	58	-	2.02	0.10
UA1001-16	*1125*	*708*	*0.73535*	*0.03227*	*0.10522*	*0.01734*	*0.001038*	*16*	*0.9639*	*87*	*0.35*	*0.92*	*0.15*
UA1001-17	-	-	*0.68645*	*0.03783*	*0.10867*	*0.02541*	*0.001148*	*23*	*0.9718*	*81*	-	*1.40*	*0.32*
UA1001-18	-	-	*0.69073*	*0.02040*	*0.15749*	*0.01335*	*0.001654*	*8*	*0.9373*	*82*	-	*1.96*	*0.16*
UA1001-19	-	-	*0.74200*	*0.01247*	*0.39972*	*0.01564*	*0.003907*	*4*	*0.9030*	*88*	-	*2.99*	*0.11*
UA1001-20	-	-	0.31009	0.01769	0.01712	0.00111	0.000400	3	0.4762	33	-	1.72	0.05
UA1001-21	-	-	*0.74687*	*0.01330*	*0.35482*	*0.02788*	*0.003446*	*8*	*0.9740*	*89*	-	*2.50*	*0.19*
UA1001-22	-	-	0.05779	0.00091	0.22003	0.00618	0.027616	2	0.8291	1	-	173.04	3.98
UA1001-23	80	33	0.73420	0.05610	0.13353	0.01686	0.001319	10	0.7962	87	0.23	1.18	0.12
UA1001-24	437	255	0.64347	0.02018	0.14975	0.02653	0.001688	17	0.9842	76	0.32	2.72	0.47
UA1001-25	**258**	**198**	**0.53675**	**0.02730**	**0.02046**	**0.00134**	**0.000277**	**4**	**0.6270**	**62**	**0.42**	**0.73**	**0.03**
SF-ICPMS													
UA1001-1	*84*	*27*	*0.76200*	*0.05200*	*0.40200*	*0.08700*	*0.003950*	*21*	*0.2785*	*91*	*0.18*	*2.47*	*0.51*
UA1001-2	*276*	*154*	*0.79500*	*0.04200*	*0.08700*	*0.00750*	*0.000791*	*9*	*0.1375*	*95*	*0.31*	*0.34*	*0.03*
UA1001-3	**195**	**85**	**0.08900**	**0.03600**	**0.00130**	**0.00100**	**0.000105**	**13**	**0.0865**	**5**	**0.24**	**0.72**	**0.10**
UA1001-4	*192*	*106*	*0.31000*	*0.08200*	*0.00730*	*0.01800*	*0.000234*	*56*	*0.0833*	*33*	*0.30*	*1.08*	*0.60*
UA1001-5	*103*	*43*	*0.75300*	*0.03500*	*0.36500*	*0.01900*	*0.003550*	*5*	*0.4880*	*90*	*0.21*	*2.48*	*0.13*
UA1001-6	*149*	*57*	*0.84400*	*0.04000*	*0.19200*	*0.01200*	*0.001711*	*7*	*0.0044*	*101*	*0.21*	*0.00*	*0.01*

~~UA1001-7~~	~~119~~	~~42~~	~~0.05310~~	~~0.00280~~	~~0.19700~~	~~0.01000~~	~~0.026940~~	~~1~~	~~0.0666~~	~~1~~	~~0.19~~	~~169.95~~	~~2.43~~
UA1001-8	**451**	**255**	**0.22300**	**0.15000**	**0.00500**	**0.00350**	**0.000153**	**26**	**0.0040**	**22**	**0.33**	**0.84**	**0.22**
UA1001-9	*102*	*26*	*0.73000*	*0.05500*	*0.08700*	*0.02600*	*0.000980*	*28*	*0.1263*	*87*	*0.14*	*0.94*	*0.26*
UA1001-10	*346*	*148*	*0.34000*	*0.07300*	*0.00550*	*0.00750*	*0.000130*	*63*	*0.4208*	*37*	*0.24*	*0.61*	*0.38*
UA1001-11	*417*	*217*	*0.76400*	*0.04000*	*0.08500*	*0.08400*	*0.000800*	*96*	*0.7111*	*91*	*0.28*	*0.55*	*0.53*
UA1001-12	70	20	0.12600	0.00760	0.40500	0.03100	0.023740	2	0.1577	10	0.15	136.19	3.23
UA1001-13	262	98	0.06110	0.00180	0.21000	0.00640	0.024750	1	0.3903	2	0.21	154.73	2.10
UA1001-14	**229**	**82**	**0.16000**	**0.18000**	**0.00088**	**0.00190**	**0.000106**	**17**	**0.0201**	**14**	**0.19**	**0.67**	**0.11**
UA1001-15	*168*	*53*	*0.75500*	*0.04100*	*0.12290*	*0.02000*	*0.001232*	*15*	*-0.0436*	*90*	*0.17*	*0.90*	*0.14*
UA1001-16	*629*	*429*	*0.55400*	*0.04400*	*0.01830*	*0.02800*	*0.000260*	*81*	*0.1676*	*64*	*0.37*	*0.67*	*0.54*
UA1001-17	302	120	0.24900	0.04600	0.01280	0.00850	0.000386	19	0.1741	26	0.22	1.93	0.37
UA1001-18	*298*	*247*	*0.46900*	*0.05300*	*0.01720*	*0.04200*	*0.000300*	*110*	*0.2796*	*54*	*0.44*	*0.96*	*1.06*
UA1001-19	592	225	0.07790	0.00210	0.42900	0.01200	0.039900	2	0.3585	4	0.19	242.32	3.69
UA1001-20	**184**	**87**	**0.21000**	**0.04400**	**0.00470**	**0.00230**	**0.000147**	**18**	**0.0856**	**21**	**0.26**	**0.83**	**0.15**
UA1001-22	**1535**	**1642**	**0.19000**	**0.03300**	**0.00387**	**0.00220**	**0.000144**	**11**	**0.4224**	**18**	**0.58**	**0.81**	**0.09**
UA1001-23	**574**	**529**	**0.54000**	**0.05400**	**0.01900**	**0.00260**	**0.000268**	**9**	**0.2499**	**63**	**0.50**	**0.70**	**0.07**
UA1001-24	240	60	0.05050	0.00200	0.19070	0.00750	0.027570	1	0.3566	1	0.14	174.44	1.93
UA1001-25	*99*	*31*	*0.26500*	*0.35000*	*0.00450*	*0.01000*	*0.000123*	*60*	*-0.2797*	*28*	*0.17*	*0.66*	*0.40*
UA1001-26	333	201	0.05050	0.00170	0.19680	0.00700	0.028280	1	0.2534	1	0.27	178.86	2.49
UA1001-28	**3977**	**6990**	**0.10500**	**0.01900**	**0.00171**	**0.00063**	**0.000117**	**6**	**0.3139**	**7**	**0.97**	**0.70**	**0.04**
UA1001-29	*252*	*85*	*0.65900*	*0.04700*	*0.02910*	*0.02100*	*0.000350*	*60*	*0.3421*	*78*	*0.19*	*0.59*	*0.36*
UA1001-30	*129*	*48*	*0.77000*	*0.05400*	*0.06680*	*0.08800*	*0.000671*	*91*	*0.3649*	*92*	*0.20*	*0.45*	*0.41*
UA1001-31	*202*	*106*	*0.81300*	*0.03800*	*0.18380*	*0.01500*	*0.001695*	*8*	*0.4169*	*97*	*0.29*	*0.39*	*0.03*
UA1001-32	*380*	*231*	*0.70700*	*0.05000*	*0.04170*	*0.03400*	*0.000447*	*67*	*0.2581*	*84*	*0.34*	*0.54*	*0.36*
UA1001-33	**378**	**207**	**0.28000**	**0.06200**	**0.00460**	**0.00590**	**0.000142**	**33**	**0.0376**	**30**	**0.30**	**0.72**	**0.24**

UA1001-34	*293*	*155*	*0.75600*	*0.01400*	*1.06300*	*0.04400*	*0.010230*	*4*	*0.7669*	*90*	*0.29*	*6.73*	*0.29*
UA1001-35	423	210	0.06030	0.00260	0.24800	0.01100	0.029940	1	0.4970	2	0.25	186.87	2.21
UA1001-36	226	54	0.04980	0.00190	0.17620	0.00670	0.025880	1	0.2257	0	0.13	164.04	2.00
UA1001-37	47	19	0.25200	0.01700	0.99200	0.18000	0.028600	7	0.1276	26	0.22	134.95	9.33
UA1001-39	*172*	*109*	*0.73300*	*0.02900*	*0.30800*	*0.01400*	*0.003100*	*4*	*0.5630*	*87*	*0.34*	*2.67*	*0.10*
UA1001-40	207	243	0.08940	0.00420	0.33200	0.01800	0.026510	2	0.6655	5	0.56	159.57	3.45
UA1001-41	1475	1440	0.05570	0.00160	0.19700	0.00340	0.025650	2	0.2475	1	0.54	161.35	2.67
UA1001-42	**668**	**332**	**0.21500**	**0.05500**	**0.00480**	**0.00540**	**0.000148**	**30**	**0.4370**	**21**	**0.27**	**0.83**	**0.25**
UA1001-43	**310**	**120**	**0.23000**	**0.08300**	**0.00260**	**0.00150**	**0.000137**	**15**	**0.0829**	**23**	**0.21**	**0.76**	**0.12**
UA1001-44	130	63	0.11060	0.00120	4.68400	0.05300	0.306500	1	0.2877	8	0.27	1598.74	14.31
UA1001-45	*153*	*75*	*0.73700*	*0.02300*	*1.26000*	*0.22000*	*0.012500*	*18*	*0.9851*	*88*	*0.21*	10.15	1.78
UA1001-46	64	26	0.05250	0.00390	0.17800	0.01300	0.024340	2	0.0528	1	0.23	153.86	2.75
UA1001-47	120	51	0.05280	0.00270	0.19060	0.00970	0.026160	1	0.0664	1	0.24	165.15	2.37
UA1001-48	*155*	*55*	*0.73700*	*0.03300*	*0.25500*	*0.01900*	*0.002520*	*7*	*0.5283*	*88*	*0.18*	2.12	0.15
UA1001-49	445	197	0.05780	0.00140	0.35140	0.00810	0.043930	1	0.0550	1	0.22	273.20	2.86
UA1001-50	100	38	0.05220	0.00280	0.18000	0.01000	0.024880	2	0.2408	1	0.20	157.29	2.81
UA1001-51	*134*	*72*	*0.62000*	*0.06200*	*0.06100*	*0.03600*	*0.000720*	*47*	*0.6662*	*73*	*0.28*	*1.35*	*0.64*
UA1001-52	*260*	*99*	*0.71200*	*0.03400*	*0.11600*	*0.01200*	*0.001190*	*9*	*0.5108*	*84*	*0.21*	1.29	0.12
UA1001-53	*83*	*33*	*0.83400*	*0.04100*	*0.30600*	*0.05100*	*0.002750*	*16*	*0.1749*	*100*	*0.22*	0.12	0.02
UA1001-54	*92*	*29*	*0.79300*	*0.04600*	*0.28500*	*0.02300*	*0.002590*	*6*	*0.6561*	*95*	*0.17*	0.99	0.06
UA1001-55	192	104	0.06700	0.00370	0.26600	0.01600	0.028270	1	0.3936	3	0.30	175.09	2.38
UA1001-56	*116*	*56*	*0.79500*	*0.02100*	*0.41600*	*0.30000*	*0.003840*	*70*	*0.0976*	*95*	*0.27*	*1.36*	*0.95*
UA1001-57	*212*	*102*	*0.76900*	*0.01800*	*0.31700*	*0.06300*	*0.003060*	*19*	*0.8834*	*92*	*0.27*	*1.75*	*0.34*

MC-ICP-MS

Flat Creek Tephra

UA1012-1	920	674	0.08308	0.01425	0.00166	0.00029	0.000145	3	0.1515	5	0.35	0.96	0.03
UA1012-2	358	724	0.51107	0.03621	0.02060	0.00159	0.000292	3	0.4013	59	0.97	0.78	0.03
UA1012-3	287	134	0.57837	0.07074	0.02418	0.00424	0.000303	13	0.7171	67	0.23	0.72	0.09
UA1012-4	390	173	0.48074	0.08254	0.01643	0.00329	0.000248	10	0.5155	55	0.21	0.80	0.08
UA1012-5	299	157	0.67515	0.03770	0.04637	0.00485	0.000498	9	0.8459	80	0.25	0.73	0.07
UA1012-6	211	87	0.73343	0.02538	0.09819	0.01166	0.000971	11	0.9566	87	0.20	0.90	0.10
UA1012-7	238	121	0.22210	0.03061	0.00487	0.00070	0.000159	4	0.3064	22	0.25	0.88	0.04
UA1012-8	182	99	0.35564	0.10058	0.00786	0.00237	0.000160	10	0.3469	39	0.27	0.71	0.07
UA1012-9	301	182	0.36862	0.06708	0.00850	0.00171	0.000167	8	0.4232	41	0.30	0.71	0.06
UA1012-10	-	-	0.74909	0.02152	0.27764	0.01389	0.002688	4	0.8186	89	-	1.90	0.08
UA1012-11	384	192	0.24908	0.04971	0.00490	0.00101	0.000143	5	0.2634	26	0.25	0.76	0.04
UA1012-12	-	-	0.16755	0.01946	0.00904	0.00107	0.000391	2	0.2038	15	-	2.13	0.05
UA1012-13	336	135	0.27194	0.03522	0.00698	0.00093	0.000186	3	0.2188	29	0.20	0.94	0.03
UA1012-14	-	-	0.14815	0.02487	0.00636	0.00111	0.000312	5	0.2601	13	-	1.75	0.08
UA1012-15	308	192	0.27960	0.06215	0.00750	0.00176	0.000195	7	0.3154	30	0.31	0.96	0.07
UA1012-16	152	61	0.69077	0.02713	0.05982	0.00313	0.000628	3	0.6595	82	0.20	0.83	0.03
UA1012-17	359	135	0.24147	0.07539	0.00634	0.00208	0.000190	10	0.3130	25	0.19	1.01	0.10
UA1012-18	191	96	0.69373	0.05385	0.04720	0.00799	0.000493	15	0.8887	82	0.25	0.65	0.10
UA1012-19	137	37	0.42467	0.20865	0.01145	0.00605	0.000196	19	0.3686	48	0.13	0.75	0.15
UA1012-20	202	74	0.33087	0.08225	0.00810	0.00222	0.000178	11	0.4193	36	0.18	0.82	0.09
UA1012-21	650	294	0.39035	0.06523	0.01127	0.00211	0.000209	8	0.4485	44	0.22	0.85	0.07

UA1012-22	**232**	**99**	**0.34459**	**0.04312**	**0.00952**	**0.00142**	**0.000200**	**8**	**0.5444**	**38**	**0.21**	**0.89**	**0.07**
UA1012-23	**205**	**96**	**0.29859**	**0.07309**	**0.00771**	**0.00193**	**0.000187**	**5**	**0.2028**	**32**	**0.23**	**0.91**	**0.05**
UA1012-24	**386**	**215**	**0.47634**	**0.03017**	**0.01445**	**0.00114**	**0.000220**	**5**	**0.6006**	**54**	**0.29**	**0.73**	**0.04**
UA1012-25	-	-	0.05052	0.00106	0.11471	0.00590	0.016467	5	0.9130	1	-	104.70	4.87
MC-ICP-MS												Age (Ma)[c] (assuming $^{207}Pb/^{206}Pbi$ = 0.981)	
PA Tephra												$^{206}Pb^{*}/^{238}U$	2σ
UA1327-1	-	-	*0.04838*	*0.00111*	*0.06530*	*0.00206*	*0.009789*	*100*	*0.6883*	*0*	-	*62.65*	*1.35*
UA1327-2	**70**	**51**	**0.57672**	**0.05965**	**0.05191**	**0.00745**	**0.000653**	**10**	**0.6931**	**57**	**0.25**	**1.92**	**0.19**
UA1327-3	**184**	**105**	**0.31282**	**0.06782**	**0.01858**	**0.00441**	**0.000431**	**10**	**0.4084**	**29**	**0.20**	**2.03**	**0.20**
UA1327-4	**123**	**100**	**0.65876**	**0.02547**	**0.07458**	**0.00563**	**0.000821**	**6**	**0.8589**	**66**	**0.28**	**1.92**	**0.12**
UA1327-5	-	-	0.06217	0.00148	0.27977	0.00864	0.032637	2	0.6396	2	-	203.52	3.95
UA1327-6	-	-	*0.76462*	*0.01121*	*1.42206*	*0.20028*	*0.013489*	*14*	*0.9946*	*77*	-	*20.02*	*2.78*
UA1327-7	**2492**	**1203**	**0.43173**	**0.01458**	**0.02937**	**0.00130**	**0.000493**	**3**	**0.6493**	**41**	**0.18**	**1.95**	**0.06**
UA1327-8	-	-	0.07726	0.00381	0.06915	0.00381	0.006491	2	0.4438	3	-	40.32	0.98
UA1327-9	-	-	0.13368	0.00193	2.03935	0.08383	0.110642	4	0.9361	9	-	615.96	22.46
UA1327-10	**80**	**62**	**0.16815**	**0.02395**	**0.00785**	**0.00117**	**0.000339**	**4**	**0.2897**	**13**	**0.27**	**1.97**	**0.08**
UA1327-11*	90	50	0.18441	0.11072	0.00698	0.00425	0.000275	10	0.1706	15	0.19	1.64	0.17
UA1327-12	**74**	**47**	**0.29550**	**0.04701**	**0.01567**	**0.00267**	**0.000385**	**6**	**0.3613**	**27**	**0.20**	**1.91**	**0.12**
UA1327-13	-	-	*0.77017*	*0.03086*	*0.92531*	*0.27750*	*0.008714*	*30*	*0.9910*	*78*	-	*12.61*	*3.73*
UA1327-14	**65**	**38**	**0.42233**	**0.08375**	**0.02446**	**0.00534**	**0.000420**	**9**	**0.4163**	**40**	**0.20**	**1.79**	**0.16**
UA1327-15	-	-	*0.76992*	*0.01510*	*0.91588*	*0.06664*	*0.008628*	*7*	*0.9630*	*78*	-	*12.50*	*0.87*

MC-ICP-MS

Quartz Creek Tephra

UA1004-1	**171**	**124**	**0.02649**	**0.00419**	**0.00154**	**0.00243**	**0.000421**	**5**	**0.0333**	**0**	**0.27**	**2.79**	**0.15**
UA1004-2	**138**	**102**	**0.07308**	**0.01166**	**0.00502**	**0.00081**	**0.000498**	**3**	**0.1595**	**3**	**0.25**	**3.18**	**0.08**
UA1004-3	**378**	**413**	**0.07065**	**0.01582**	**0.00472**	**0.00106**	**0.000484**	**2**	**0.1071**	**3**	**0.41**	**3.09**	**0.07**
UA1004-4	**326**	**560**	**0.08597**	**0.00850**	**0.00569**	**0.00058**	**0.000480**	**3**	**0.2637**	**5**	**0.61**	**2.98**	**0.08**
UA1004-5	**276**	**255**	**0.10771**	**0.02592**	**0.00673**	**0.00164**	**0.000453**	**3**	**0.1398**	**8**	**0.35**	**2.77**	**0.09**
UA1004-6	**192**	**108**	**0.35042**	**0.03315**	**0.03087**	**0.00311**	**0.000639**	**3**	**0.3441**	**39**	**0.18**	**2.62**	**0.09**
UA1004-7*	86	78	0.05201	0.02182	0.00376	0.00158	0.000524	3	0.0737	1	0.33	3.42	0.11
UA1004-8	**165**	**167**	**0.11167**	**0.02963**	**0.00780**	**0.00210**	**0.000507**	**4**	**0.1568**	**8**	**0.36**	**3.06**	**0.13**
UA1004-9	**244**	**313**	**0.41287**	**0.05517**	**0.04652**	**0.00717**	**0.000817**	**8**	**0.4982**	**46**	**0.46**	**2.88**	**0.22**
UA1004-10	**199**	**203**	**0.09984**	**0.03156**	**0.00641**	**0.00205**	**0.000466**	**5**	**0.1501**	**7**	**0.37**	**2.87**	**0.14**
UA1004-11	**69**	**57**	**0.10768**	**0.02776**	**0.00700**	**0.00182**	**0.000472**	**4**	**0.1478**	**8**	**0.29**	**2.88**	**0.11**
UA1004-12	**253**	**167**	**0.18652**	**0.00733**	**0.01260**	**0.00057**	**0.000492**	**2**	**0.4829**	**18**	**0.24**	**2.69**	**0.06**
UA1004-13	**1221**	**1477**	**0.45066**	**0.03955**	**0.05819**	**0.00635**	**0.000937**	**6**	**0.5948**	**51**	**0.45**	**3.00**	**0.19**
UA1004-14	**50**	**36**	**0.07723**	**0.02274**	**0.00505**	**0.00149**	**0.000474**	**3**	**0.0912**	**4**	**0.26**	**3.02**	**0.08**
UA1004-15	*149*	*52*	*0.75726*	*0.02019*	*0.67192*	*0.23964*	*0.006435*	*36*	*0.9972*	*90*	*0.13*	*4.22*	*1.50*
UA1004-16	**178**	**107**	**0.34632**	**0.06289**	**0.03348**	**0.00680**	**0.000701**	**9**	**0.4473**	**38**	**0.22**	**2.89**	**0.26**
UA1004-17	**83**	**60**	**0.48941**	**0.04548**	**0.06562**	**0.00913**	**0.000972**	**10**	**0.7439**	**56**	**0.26**	**2.83**	**0.29**
UA1004-18	**591**	**960**	**0.16285**	**0.03856**	**0.01124**	**0.00270**	**0.000501**	**4**	**0.1688**	**15**	**0.59**	**2.79**	**0.11**
UA1004-19	**83**	**60**	**0.40665**	**0.03123**	**0.04640**	**0.00446**	**0.000827**	**6**	**0.6020**	**46**	**0.24**	**2.98**	**0.17**

UA1004-20	*139*	*147*	*0.63910*	*0.03376*	*0.14870*	*0.02214*	*0.001687*	*14*	*0.9350*	*75*	*0.38*	*2.78*	*0.39*
UA1004-21	**367**	**378**	**0.07346**	**0.02205**	**0.00453**	**0.00136**	**0.000447**	**3**	**0.0932**	**3**	**0.37**	**2.85**	**0.08**
UA1004-22	**212**	**142**	**0.45460**	**0.03102**	**0.05065**	**0.00431**	**0.000808**	**5**	**0.5978**	**52**	**0.21**	**2.60**	**0.13**
UA1004-23	**111**	**84**	**0.15490**	**0.07621**	**0.01040**	**0.00515**	**0.000487**	**5**	**0.1084**	**14**	**0.27**	**2.79**	**0.15**
UA1004-24	**675**	**1072**	**0.12464**	**0.03669**	**0.00765**	**0.00228**	**0.000445**	**5**	**0.1621**	**10**	**0.59**	**2.63**	**0.13**
UA1004-25	**223**	**227**	**0.54416**	**0.02192**	**0.10245**	**0.00901**	**0.001365**	**8**	**0.8889**	**63**	**0.33**	**3.32**	**0.26**

MC-ICP-MS

Lost Chicken Tephra

UA1013-1	**550**	**253**	**0.07062**	**0.02448**	**0.00564**	**0.00162**	**0.000478**	**3**	**0.0884**	**3**	**0.22**	**3.17**	**0.08**
UA1013-2	**447**	**211**	**0.19704**	**0.01860**	**0.01647**	**0.00161**	**0.000606**	**3**	**0.2564**	**19**	**0.23**	**3.24**	**0.08**
UA1013-3	**434**	**244**	**0.11496**	**0.01446**	**0.00841**	**0.00108**	**0.000530**	**2**	**0.1925**	**9**	**0.27**	**3.20**	**0.08**
UA1013-4	**319**	**194**	**0.08481**	**0.01356**	**0.00575**	**0.00093**	**0.000492**	**2**	**0.1486**	**4**	**0.29**	**3.25**	**0.08**
UA1013-5	**260**	**265**	**0.09483**	**0.01504**	**0.00660**	**0.00106**	**0.000505**	**3**	**0.1810**	**6**	**0.51**	**3.11**	**0.09**
UA1013-6	**608**	**311**	**0.17893**	**0.01454**	**0.01486**	**0.00125**	**0.000602**	**2**	**0.2509**	**17**	**0.25**	**3.31**	**0.07**
UA1013-7	**-**	**-**	**0.31337**	**0.01943**	**0.03324**	**0.00261**	**0.000769**	**5**	**0.6148**	**34**	**0.24**	**3.36**	**0.16**
UA1013-8	**448**	**204**	**0.19248**	**0.01466**	**0.01649**	**0.00133**	**0.000621**	**3**	**0.3378**	**19**	**0.22**	**3.35**	**0.09**
UA1013-9	**436**	**454**	**0.34968**	**0.01406**	**0.04075**	**0.00214**	**0.000845**	**3**	**0.6431**	**38**	**0.50**	**3.41**	**0.12**
UA1013-10	**447**	**338**	**0.11291**	**0.01610**	**0.00830**	**0.00121**	**0.000533**	**3**	**0.2079**	**8**	**0.36**	**3.21**	**0.10**
UA1013-11	**284**	**145**	**0.23662**	**0.03431**	**0.02100**	**0.00321**	**0.000644**	**5**	**0.3149**	**24**	**0.25**	**3.23**	**0.16**
UA1013-12	**344**	**181**	**0.34671**	**0.03278**	**0.03737**	**0.00403**	**0.000782**	**5**	**0.4789**	**38**	**0.25**	**3.20**	**0.17**
UA1013-13	**518**	**192**	**0.30569**	**0.02285**	**0.03155**	**0.00271**	**0.000748**	**4**	**0.4916**	**33**	**0.18**	**3.33**	**0.14**
UA1013-14	**-**	**-**	**0.34968**	**0.01406**	**0.04075**	**0.00214**	**0.00085**	**4**	**0.643**	**38**	**0.20**	**3.46**	**0.12**

UA1013-15	**-**	**-**	**0.62768**	**0.01164**	**0.18051**	**0.01104**	**0.00209**	**6**	**0.953**	**74**	**0.20**	**3.64**	**0.21**
UA1013-16	**420**	**206**	**0.09488**	**0.01387**	**0.00682**	**0.00101**	**0.00052**	**2**	**0.157**	**6**	**0.24**	**3.23**	**0.06**
UA1013-17	**-**	**-**	**0.40127**	**0.01814**	**0.05258**	**0.00308**	**0.00095**	**4**	**0.637**	**45**	**0.20**	**3.46**	**0.15**
UA1013-18	**498**	**305**	**0.38638**	**0.04644**	**0.05378**	**0.00884**	**0.00101**	**11**	**0.682**	**43**	**0.30**	**3.78**	**0.41**
UA1013-19	**-**	**-**	**0.23525**	**0.02371**	**0.02236**	**0.00245**	**0.00069**	**4**	**0.397**	**24**	**0.20**	**3.47**	**0.15**
UA1013-20	**590**	**211**	**0.25481**	**0.03708**	**0.02418**	**0.00375**	**0.00069**	**6**	**0.343**	**26**	**0.15**	**3.36**	**0.19**
MC-ICP-MS													
GI Tephra													
UA1668-1	-	-	0.06072	0.00547	0.04827	0.00447	0.005766	2	0.2301	2	0.20	36.47	0.77
UA1668-2	**-**	**-**	**0.59550**	**0.19289**	**0.01871**	**0.00761**	**0.000228**	**25**	**0.6043**	**70**	**0.20**	**0.53**	**0.13**
UA1668-3	**-**	**-**	**0.78710**	**0.04481**	**0.13037**	**0.01840**	**0.001202**	**13**	**0.9150**	**94**	**0.20**	**0.56**	**0.07**
UA1668-4	-	-	0.12482	0.01198	0.29213	0.02876	0.016974	2	0.2233	10	0.20	97.85	2.13
UA1668-5	-	-	*0.76730*	*0.01178*	*0.70974*	*0.10988*	*0.006709*	*15*	*0.9951*	*91*	*0.20*	*3.83*	*0.59*
UA1668-6	-	-	0.15766	0.00321	0.15740	0.00438	0.007241	2	0.6829	14	0.20	40.04	0.76
UA1668-7	-	-	*0.78757*	*0.01354*	*1.73719*	*0.17140*	*0.015998*	*10*	*0.9847*	*94*	*0.20*	*6.36*	*0.62*
UA1668-8	-	-	0.08427	0.00458	0.64728	0.04359	0.055708	4	0.5913	5	0.20	333.07	12.91
UA1668-9	-	-	0.05033	0.00104	0.16582	0.00484	0.023897	2	0.7066	1	0.20	151.51	3.09
UA1668-10	**-**	**-**	**0.80351**	**0.03316**	**0.20927**	**0.04874**	**0.001890**	**23**	**0.9842**	**96**	**0.20**	**0.58**	**0.13**
UA1668-11	-	-	*0.76580*	*0.08060*	*0.13163*	*0.01707*	*0.001247*	*8*	*0.5840*	*91*	*0.20*	*0.80*	*0.06*
UA1668-12	-	-	0.05867	0.00101	0.44948	0.01169	0.055563	2	0.7521	2	0.20	343.25	6.54
UA1668-13	-	-	0.26455	0.03056	0.41238	0.05323	0.011305	6	0.4459	28	0.20	52.58	3.01
UA1668-14	-	-	0.12024	0.01275	0.27476	0.02992	0.016573	2	0.2272	9	0.20	96.17	2.36
UA1668-15	-	-	*0.83159*	*0.05669*	*0.04201*	*0.01008*	*0.000367*	*23*	*0.9587*	*99*	*0.20*	*N/A*	*N/A*
UA1668-16	-	-	*0.83766*	*0.03781*	*0.10119*	*0.01552*	*0.000876*	*15*	*0.9557*	*100*	*0.20*	*N/A*	*N/A*
UA1668-17	-	-	0.18164	0.00904	0.44974	0.02504	0.017958	2	0.4475	17	0.20	95.27	2.36

UA1668-18	-	-	0.05085	0.00150	0.11447	0.00419	0.016326	2	0.5946	1	0.20	103.85	2.24
UA1668-19	-	-	0.06606	0.00304	0.13393	0.00666	0.014705	2	0.3799	3	0.20	91.82	1.72
iCAP-Q-ICP-MS													
2838-56	-	-	0.28900	0.02700	0.05280	0.00550	0.001325	5	0.4540	31	0.20	6.00	0.29
2838-59	-	-	0.13200	0.02600	0.18420	0.03680	0.010120	3	0.1730	11	0.20	57.96	2.00
2838-62	-	-	0.08230	0.00430	0.25090	0.01360	0.022110	1	0.2750	5	0.20	134.66	1.99
2838-58	-	-	0.06220	0.00650	0.20300	0.02220	0.023670	3	0.2900	2	0.20	147.85	4.63
2838-55	-	-	0.05480	0.00220	0.33580	0.01480	0.044440	2	0.4130	1	0.20	277.34	4.95
2838-57	-	-	0.09420	0.00470	0.96110	0.07760	0.074000	6	0.7860	6	0.20	433.16	26.55
2838-51	-	-	0.14720	0.00420	1.63180	0.16700	0.080400	10	0.9600	13	0.20	436.85	41.37
2838-52	-	-	0.09440	0.00150	3.18630	0.06390	0.244800	1	0.6110	6	0.20	1333.60	14.75
2838-50	-	-	0.10000	0.00170	3.44420	0.06870	0.249800	1	0.5220	7	0.20	1348.90	12.66
2838-61	-	-	0.11590	0.00340	5.04340	0.18450	0.315600	2	0.5980	9	0.20	1630.03	31.41
2838-54	-	-	0.14380	0.00190	6.80070	0.31070	0.343000	4	0.9570	12	0.20	1694.07	64.82
2838-53	-	-	0.16530	0.00620	9.11660	0.42400	0.400000	3	0.5910	15	0.20	1884.79	44.79
2838-60	-	-	0.18190	0.00300	12.74580	0.27390	0.508200	1	0.6410	17	0.20	2264.05	26.24
2838-61	-	-	0.11690	0.00440	4.75300	0.19400	0.294900	2	0.3900	9	0.20	1532.97	21.71
2838-62	-	-	0.11090	0.00430	4.49100	0.20700	0.293700	2	0.5400	8	0.20	1538.76	33.93
2838-63	-	-	0.13800	0.01100	0.32000	0.03400	0.016800	7	0.6670	12	0.20	95.07	6.74
2838-64	-	-	0.05330	0.00380	0.34700	0.02600	0.047200	2	0.2610	1	0.20	294.73	5.55
2838-65	-	-	0.10100	0.00280	1.29000	0.05200	0.092600	3	0.7250	7	0.20	532.85	14.89
										-		-	-

Note* Measured ratio uncertainties are a quadratic combination of the standard error of the measured isotope ratio and reproducibility of the reference material. Preferred data used for Bayesian age calculations are shown in bold (refer to text). Data in italics contains >75% common-Pb contamination and were excluded from age calculations. Data interpreted as detrital or xenocrystic component are highlighted in yellow.

[a] f_{206} (%) denotes an estimate for the amount of common-Pb in measured ^{206}Pb. Correction for common-Pb was made using ^{207}Pb method (Williams, 1998) with contemporaneous common-Pb composition estimated from Stacey-Kramers (1975) model.

[b] $f_{Th/U}$ = $(Th/U)_{zircon}/(Th/U)_{glass}$. $(Th/U)_{glass}$ values used are as follows: HP 0.65 (Preece et al., 1999), Biederman 3.0 (Jensen, unpublished), Gold Run 1.81 (Westgate et al., 2009), Flat Creek 2.10 (Westgate et al., 2009), PA 2.94 (Preece et al., 1999), Quartz Creek 2.75 (Preece et al., 2011), Lost Chicken 2.10 (Westgate and Walter, 1985), GI no glass data is available, constant $f_{Th/U}$ = 0.2 assumed.

[c] $^{206}Pb^{*}/^{238}U$ ages are corrected for common-Pb and initial ^{230}Th disequilibrium. Uncertainty of weighted mean is at 95% confidence level. N/A = no bisection is found.

[d] Combined uncertainty of the standard error of the measured isotope ratio, reproducibility of the reference materials and $f_{Th/U}$.

Table A.2: Recalculated glass-fission-track ages of tephra beds from eastern Beringia using the Schmieder et al. (2018) age for the Moldavite tektite

Sample number	Method for correction of partial track fading	Irradiation date	Spontaneous track density (10^2 t/cm^2)	Corrected spontaneous track density (10^2 t/cm^2)	Induced track density (10^4 t/cm^2)	Track density on muscovite detector over dosimeter glass (10^5 t/cm^2)	Etching conditions HF:temp:time (%: ºC: s)	D_s (µm)	D_i (µm)	D_s/D_i or D_i/D_s[#]	Age ± 1σ
Gold Run tephra											
UT1907	ITPFT	25/06/2004	3.01 ± 0.28 (119)		6.02 ± 0.07 (6780)	4.90 ± 0.04 (15640)	24: 21: 200	6.46 ± 0.18 [94]	6.81 ± 0.09 [398]	0.95 ± 0.03	761 ± 91 ka
UT1791	DCFT	21/01/2002	4.09 ± 0.28 (211)	4.75 ± 0.33 (211)	11.0 ± 0.10 (12976)	5.15 ± 0.04 (19559)	24: 22: 110	5.39 ± 0.10	6.24 ± 0.06	1.16 ± 0.02[#]	693 ± 67 ka
									Weighted mean and error		**717 ± 54 ka**
HP tephra											
UT836	ITPFT	09/10/1992	2.50 28 (28)		8.97 (3513)	6.74 ± 0.04 (23761) (23761)	26: 22: 125	6.02	6.11	0.99	585 ± 153 ka
UT836	DCFT	09/10/1992	4.51 (70)	4.78 (70)	16.18 (7104)	6.74 ± 0.04 (23761) (23761)	26: 23: 108	7.81	8.25	1.06[#]	622 ± 129 ka
UT2207	DCFT	14/03/2008	9.10 ± 0.34 (727)	10.85 ± 0.40 (727)	19.40 ±0.10 (39195)	4.11 ± 0.03 (15786)	24: 23: 95	5.63 ± 0.09 [177]	6.68 ± 0.07 [597]	1.19 ± 0.02[#]	714 ± 47 ka
UT2207	ITPFT	14/03/2008	5.95 ± 0.35 (286)		10.40 ± 0.06 (32541)	4.11 ± 0.03 (15786)	24: 23: 185	7.03 ± 0.16 [103]	6.84 ± 0.10 [397]	1.03 ± 0.02	728 ± 57 ka
									Weighted mean and error		**706 ± 34 ka**
PA tephra											

UT497	ITPFT	30/11/1988	16.27 ± 1.70 (92)		20.30 ± 0.40 (2625)	7.57 ± 0.06 (14081)	26: 24: 75	6.06 ± 1.53 [109]	5.70 ± 1.39 [185]	1.06 ± 0.37	1.89 ± 0.46 Ma
UT497	ITPFT	30/11/1988	10.76 ± 0.87 (153)		11.80 ± 0.18 (4302)	7.57 ± 0.06 (14081)	26: 24: 60	6.06 ± 1.53 [109]	5.70 ± 1.39 [185]	1.06 ± 0.37	2.14 ± 0.40 Ma
UT497	ITPFT	30/11/1988	10.62 ± 1.03 (107)		11.70 ± 0.18 (4250)	7.57 ± 0.06 (14081)	26: 24: 75	6.06 ± 1.53 [109]	5.70 ± 1.39 [185]	1.06 ± 0.37	2.14 ± 0.43 Ma
									Weighted mean and error		**2.07 ± 0.25 Ma**
<u>Lost Chicken tephra</u>											
UA771	ITPFT	17/12/1990	19.09 ± 1.32 (209)		15.60 ± 0.20 (6269)	7.49 ± 0.04 (39148)	26: 26: 100	5.88 ± 1.16 [52]	5.44 ± 1.61 [298]	1.08 ± 0.38	2.84 ± 0.43 Ma
UT86	DCFT	21/01/2002	26.85 ± 0.80 (1133)	30.61 ± 0.91 (1133)	17.60 ± 0.09 (39109)	5.10 ± 0.03 (31171)	24: 23: 195	6.43 ± 0.10 [249]	7.34 ± 0.09 [596]	1.14 ± 0.02#	2.75 ± 0.18 Ma
UT1865	DCFT	25/06/2004	25.13 ± 1.13 (492)	29.40 ± 1.33 (492)	14.10 ± 0.11 (18138)	4.90 ± 0.04 (15640)	24: 21: 90	5.15 ± 0.07 [151]	6.03 ± 0.05 [664]	1.17 ± 0.02#	3.18 ± 0.29 Ma
									Weighted mean and error		**2.87 ± 0.14 Ma**
<u>Quartz Creek tephra</u>											
UT1001	DCFT	31/01/2000	39.30 ± 1.96 (401)	49.75 ± 2.50 (401)	2.69 ± 0.02 (14637)	5.01 ± 0.04 (12744)	24: 22: 110	6.01 ± 0.09	7.61 ± 0.10	1.27 ± 0.02#	**2.88 ± 0.15 Ma**
<u>GI tephra</u>											
UT 802	DCFT	31/01/2000	5.41 ± 0.76 (50)	6.54 ± 0.93 (50)	19.40 ± 0.21 (8519)	4.91 ± 0.04 (12744)	24: 22: 75	5.19 ± 0.12 [50]	6.29 ± 0.09 [467]	1.21 ± 0.04#	514 ± 99 ka
UT802		31/01/2000	5.00 ± 0.78 (41)	6.05 ± 0.95 (41)	15.50 ± 0.22 (4850)	4.91 ± 0.04 (12744)	24: 22: 75	5.19 ± 0.12 [50]	6.29 ± 0.09 [467]	1.21 ± 0.04#	596 ± 127 ka
									Weighted mean and error		**545 ± 78 ka**
<u>Chester Bluff tephra</u>											
UT1875	DCFT	27/06/2012	1.15 ± 0.11 (103)	1.44 ± 0.14 (103)	8.07 ± 0.07 (15402)	4.54 ± 0.03 (17433)	24: 23.5: 80	5.25 ± 0.27 [45]	6.59 ± 0.01 [406]	1.26 ± 0.05#	253 ± 29 ka
UT1875(2)	DCFT	27/06/2012	1.16 ± 0.11 (116)	1.32 ± 0.12 (116)	7.23 ± 0.05 (18686)	4.54 ± 0.03 (17433)	24: 23.5: 80	5.43 ± 0.13 [54]	6.19 ± 0.07 [555]	1.14 ± 0.03#	257 ± 27 ka
									Weighted mean and error		**255 ± 20 ka**

Notes: The population-subtraction method was used (Westgate, 2015). Ages calculated using the zeta approach and $\lambda_D = 1.551 \times 10^{-10}\ yr^{-1}$. Zeta value is 311 ± 4 based on 7 irradiations at the McMaster Nuclear Reactor, Hamilton, Ontario, using the NIST SRM 612 glass dosimeter and the Moldavite tektite glass with an $^{40}Ar/^{39}Ar$ age of 14.808 ± 0.021 Ma (2σ) (Schmieder et al., 2018). Number of tracks counted is given in parentheses; number of tracks measured is given in square brackets. The fluence is obtained by multiplying the muscovite track density by 0.53×10^{10} based on 9 determinations. Age determinations are corrected for partial track fading using the isothermal plateau method (ITPFT) (Westgate, 1989) or the diameter correction (DCFT) method (Sandhu and Westgate 1995).

The uncertainty on individual age determinations was calculated using methods described in Bigazzi and Galbraith (1999) for DCFT method and Lindsey et al. (1975) for ITPFT method.

Ds = mean long-axis of spontaneous tracks; Di = mean long-axis of induced tracks. Area estimated by the points-counting technique (Naeser et al., 1982).

Sample number	Method for correction of partial track fading	Irradiation date	Spontaneous track density (t/cm^2)	Corrected spontaneous track density (t/cm^2)	Induced track density (10^4 t/cm^2)	Track density on muscovite detector over dosimeter glass (10^5 t/cm^2)	Etching conditions HF:temp:time (%: ºC: s)	D_s (μm)	D_i (μm)	D_s/D_i or D_i/D_s#	Age ± 1σ (ka)
<u>Old Crow tephra</u>											
UT1434(1)	ITPFT	11/9/1997	82.72 ± 6.56 (159)		11.44 ± 0.12 (9170)	5.61 ± 0.05 (14352)	25: 22.5: 165	6.63 ± 0.19 [102]	6.65 ± 0.10 [398]	1.00 ± 0.03	126 ± 14
UT1434(2)	DCFT	18/3/2019	194.3 ± 22.7 (73)	230.0 ± 26.9 (73)	31.10 ± 0.20 (24308)	7.27 ± 0.08 (9311)	24: 19: 150	6.54 ± 0.17 [60]	7.74 ± 0.11 [412]	1.18 ± 0.04#	167 ± 24
UT1434(3)	DCFT	18/3/2019	194.3 ± 22.7 (73)	230.0 ± 26.9 (73)	37.70 ± 0.58 (4197)	7.27 ± 0.08 (9311)	24: 19: 150	6.54 ± 0.17 [60]	7.74 ± 0.11 [412]	1.18 ± 0.04#	138 ± 16
UT1434(4)	ITPFT	18/3/2019	96.1 ± 16.2 (35)		15.70 ± 0.14	7.10 ± 0.07 (9082)	24: 19: 250	6.96 ± 0.32 [38]	7.01 ± 0.12 [367]	0.99 ± 0.05	135 ± 26
UT1434(5)	ITPFT	18/3/2019	96.1 ± 16.2 (35)		14.30 ± 0.32 (1949)	7.10 ± 0.07 (9082)	24: 19: 250	6.96 ± 0.32 [38]	7.01 ± 0.12 [367]	0.99 ± 0.05	149 ± 25
UT613(1)	DCFT	9/4/1985	147 ± 18.8 (61)	173.5 ± 22.2 (61)	11.20 ± 0.13 (7000)	3.55 ± 0.05 (6871)	26: nr: 65	nr	nr	1.18 ± 0.04#	170 ± 27
UT613(2)	DCFT	9/4/1985	157.5 ± 17.4	185.9 ± 20.5	11.20 ± 0.18	3.55 ± 0.05	26: 22.5: 95	nr	nr	1.18 ± 0.04#	183 ± 30

			(82)	(82)	(4104)	(6871)					
UT613(3)	ITPFT	9/4/1985	85.43 ± 14.2 (36)		6.62 ± 0.11 (3748)	3.55 ± 0.04 (6871)	24: 23: 82	nr	nr	nr	143 ± 28
UT501(1)	ITPFT	9/4/1985	108.7 ± 24.9 (19)		7.83 ± 0.21 (1450)	3.54 ± 0.04 (6871)	nr	nr	nr	nr	153 ± 44
UT501(2)	DCFT	9/4/1985	125 ± 29.5 (27)	147.5 ± 28.4 (27)	12.0 ± 0.15 (6820)	3.54 ± 0.04 (6871)	nr	nr	nr	1.18 ± 0.04$^{\#}$	136 ± 30
									Weighted mean and error		**144 ± 7 ka**
<u>Age reference standards</u>											
UT2354	DCFT	18/3/2019	17080 ± 534 (1024)	20660 ± 646 (1024)	73.3 ± 0.93 (6287)	7.10 ± 0.07 (9082)	24: 20: 260	7.20 ± 0.03 [253]	8.70 ± 0.11 [561]	1.21 ± 0.02	6.22 ± 0.22 Ma
UTMoldavite	DCFT	9/4/1985	13210 ± 670 (389)		11.09 ± 0.17 (3153)	3.53 ± 0.04 ((6871)	nr	nr	nr	nr	14.84 ± 0.82 Ma

Notes: The population-subtraction method was used (Westgate, 2015). Ages calculated using the zeta approach and $\lambda_D = 1.551 \times 10^{-10}$ yr^{-1}.

Zeta value is 311 ± 4 based on 7 irradiations at the McMaster Nuclear Reactor, Hamilton, Ontario, using the NIST SRM 612 glass dosimeter and the Moldavite tektite glass with an $^{40}Ar/^{39}Ar$ age of 14.808 ± 0.021 Ma (2σ) (Schmieder et al., 2018). Number of tracks counted is given in parentheses; number of tracks measured is given in square brackets. The fluence is obtained by multiplying the muscovite track density by 0.53 x 10^{10} based on 9 determinations. Age determinations are corrected for partial track fading using the isothermal plateau method (ITPFT) (Westgate, 1989) or the diameter correction (DCFT) method (Sandhu and Westgate 1995). Ds = mean long-axis of spontaneous tracks; Di = mean long-axis of induced tracks; nr = not recorded. Walcott Tuff is 6.27 ± 0.04 Ma (2σ) (Morgan and McIntosh, 2005) and the age of Moldavite tektite is given above. The correction factor (Di/Ds) for partial track fading in samples UT613 and UT 501 is taken from UT1434.

The uncertainty on individual age determinations was calculated using methods described in Bigazzi and Galbraith (1999) for DCFT method and Lindsey et al. (1975) for ITPFT method.

Table A.3: LA-ICP-MS reference material data.

	Total									Age (Ma)[b]	
Sample number	$^{207}Pb/^{206}Pb$	2σ	$^{207}Pb/^{235}U$	2σ	$^{206}Pb/^{238}U$	2σ	ρ	$f_{Th/U}$[a]	f_{206} (%)	$^{206}Pb^{*}/^{238}U$	2σ[c]
MC-ICP-MS											
Plesovice											
plesovice-1	0.05292	0.00077	0.39103	0.01040	0.05359	0.00119	0.837	-	1	333.7	7.2
plesovice-2	0.05282	0.00077	0.39593	0.01025	0.05436	0.00116	0.828	-	1	338.4	7.1
plesovice-3	0.05274	0.00078	0.39233	0.01030	0.05395	0.00117	0.829	-	1	336.0	7.1
plesovice-4	0.05280	0.00077	0.39189	0.00996	0.05383	0.00112	0.820	-	1	335.2	6.8
plesovice-5	0.05301	0.00077	0.39478	0.01060	0.05402	0.00122	0.840	-	1	336.3	7.4
plesovice-6	0.05348	0.00080	0.39547	0.00994	0.05363	0.00109	0.805	-	1	333.7	6.6
plesovice-7	0.05308	0.00078	0.39228	0.01056	0.05360	0.00121	0.836	-	1	333.8	7.3
plesovice-8	0.05342	0.00078	0.40015	0.01032	0.05432	0.00115	0.823	-	1	338.0	7.0
plesovice-9	0.05334	0.00078	0.39540	0.01020	0.05376	0.00114	0.821	-	1	334.7	6.9
plesovice-10	0.05349	0.00079	0.39913	0.00993	0.05412	0.00109	0.807	-	1	336.7	6.6

plesovice-11	0.05327	0.00077	0.40048	0.00951	0.05452	0.00103	0.793	-	1	339.3	6.2
plesovice-12	0.05321	0.00078	0.39625	0.00953	0.05401	0.00103	0.795	-	1	336.2	6.3
plesovice-13	0.05325	0.00076	0.39501	0.00956	0.05380	0.00105	0.805	-	1	334.9	6.4
<u>Bishop Tuff</u>											
1704-1	0.07531	0.01088	0.00112	0.00016	0.00011	0.00000	0.166	0.240	4	0.757	0.018
1704-2	0.06379	0.00782	0.00094	0.00012	0.00011	0.00000	0.184	0.240	2	0.759	0.017
1704-3	0.07887	0.00805	0.00119	0.00013	0.00011	0.00000	0.225	0.240	4	0.765	0.018
1704-4	0.05807	0.01089	0.00086	0.00016	0.00011	0.00000	0.114	0.240	2	0.770	0.017
1704-5	0.06889	0.00803	0.00104	0.00012	0.00011	0.00000	0.188	0.240	3	0.770	0.017
1704-6	0.11617	0.00843	0.00190	0.00014	0.00012	0.00000	0.293	0.240	9	0.784	0.017
1704-7	0.08621	0.00660	0.00134	0.00011	0.00011	0.00000	0.312	0.240	5	0.779	0.020
1704-8	0.05565	0.00889	0.00084	0.00014	0.00011	0.00000	0.134	0.240	1	0.785	0.017
1704-9	0.05844	0.00518	0.00085	0.00008	0.00011	0.00000	0.252	0.240	2	0.760	0.018
1704-10	0.09934	0.01226	0.00157	0.00020	0.00011	0.00000	0.186	0.240	7	0.775	0.018
1704-11	0.07993	0.01175	0.00124	0.00019	0.00011	0.00000	0.191	0.240	4	0.781	0.022
1704-12	0.06088	0.00835	0.00094	0.00013	0.00011	0.00000	0.161	0.240	2	0.794	0.018
1704-13	0.06951	0.00964	0.00104	0.00015	0.00011	0.00000	0.170	0.240	3	0.769	0.018

iCAP Q-ICP-MS

<u>Plesovice</u>											
plesovice-1	0.05430	0.00190	0.41627	0.01886	0.05560	0.00160	0.6352	-	0	348.0	9.7
plesovice-2	0.05110	0.00200	0.38047	0.01826	0.05400	0.00150	0.5788	-	0	339.5	9.2

plesovice-3	0.05480	0.00240	0.40801	0.02116	0.05400	0.00150	0.5356	-	0	338.0	9.1
plesovice-4	0.05710	0.00190	0.42514	0.01701	0.05400	0.00120	0.5554	-	1	337.1	7.3
plesovice-5	0.05240	0.00240	0.38942	0.02295	0.05390	0.00200	0.6295	-	0	338.4	12.2
plesovice-1_1	0.05530	0.00200	0.40907	0.01615	0.05365	0.00085	0.4013	-	0	335.7	5.2
plesovice-2_1	0.05220	0.00240	0.38650	0.01864	0.05370	0.00078	0.3012	-	0	337.3	4.8
GJ-1											
gj1-1	0.0613	0.0026	0.836	0.037	0.0989	0.0014	0.317	-	0	605.6	9.4
gj1-2	0.0596	0.0029	0.811	0.044	0.0987	0.0023	0.432	-	0	604.4	14.7
gj1-3	0.0600	0.0046	0.831	0.068	0.1004	0.0028	0.342	-	1	613.8	17.6
gj1-4	0.0608	0.0023	0.831	0.035	0.0991	0.0018	0.433	-	0	606.8	10.6
gj1-1	0.06090	0.00160	0.82120	0.02350	0.09780	0.00110	0.3940	-	0	600.0	7.0
gj1-2	0.05900	0.00200	0.81020	0.02940	0.09960	0.00130	0.3590	-	0	611.0	8.0
gj1-3	0.05950	0.00170	0.81380	0.02560	0.09920	0.00130	0.4170	-	0	609.0	8.0
gj1-4	0.06040	0.00180	0.81450	0.02690	0.09780	0.00140	0.4330	-	0	601.0	8.0
gj1-5	0.06110	0.00220	0.82810	0.03150	0.09830	0.00120	0.3210	-	0	603.0	7.0
gj1-1_1	0.06030	0.00170	0.82310	0.02560	0.09900	0.00130	0.4220	-	0	608.0	8.0
gj1-2_1	0.05990	0.00170	0.81270	0.02480	0.09840	0.00110	0.3660	-	0	606.0	6.0
94-35											
94-35-1	0.08800	0.03100	0.10544	0.03852	0.00869	0.00084	0.2646	-	5	52.9	5.1
94-35-2	0.05500	0.02000	0.06590	0.02431	0.00869	0.00054	0.1684	-	1	55.2	3.4
94-35-3	0.05400	0.02800	0.06507	0.03426	0.00874	0.00080	0.1738	-	1	55.6	5.1
94-35-4	0.06800	0.02000	0.08129	0.02460	0.00867	0.00062	0.2363	-	3	54.2	3.9
94-35-5	0.05000	0.01200	0.05915	0.01469	0.00858	0.00055	0.2580	-	0	54.9	3.5
94-35-6	0.04900	0.01300	0.06094	0.01667	0.00902	0.00060	0.2432	-	0	57.7	3.8

94-35-7	0.05500	0.01300	0.06522	0.01609	0.00860	0.00061	0.2874	-	1	54.7	3.9
94-35-8	0.06500	0.01500	0.07824	0.01914	0.00873	0.00071	0.3324	-	2	54.8	4.4
94-35-9	0.06700	0.01400	0.08019	0.01810	0.00868	0.00074	0.3778	-	3	54.3	4.6
94-35-10	0.06500	0.02200	0.07788	0.02710	0.00869	0.00070	0.2315	-	2	54.5	4.4
94-35-11	0.11500	0.03600	0.13858	0.04567	0.00874	0.00090	0.3125	-	9	51.3	5.3

SF-ICP-MS

91500											
91500-1	0.07430	0.00087	1.84000	0.03500	0.17940	0.00260	0.1034	-	0	1061.6	14.2
91500-2	0.07475	0.00099	1.83700	0.03200	0.17820	0.00250	0.3811	-	0	1054.5	13.6
91500-3	0.07526	0.00095	1.85100	0.03200	0.17820	0.00270	0.3993	-	0	1053.9	14.7
91500-4	0.07511	0.00084	1.83200	0.02900	0.17690	0.00260	0.4326	-	0	1047.0	14.2
91500-5	0.07472	0.00095	1.84900	0.03700	0.17940	0.00280	0.1467	-	0	1061.1	15.3
91500-6	0.07539	0.00086	1.88600	0.03700	0.18000	0.00280	0.1958	-	0	1063.6	15.2
91500-7	0.07504	0.00078	1.84700	0.03600	0.17800	0.00290	0.1979	-	0	1053.1	15.8
91500-8	0.07476	0.00088	1.84700	0.03200	0.17940	0.00270	0.2626	-	0	1061.0	14.7
91500-10	0.07470	0.00089	1.83400	0.03300	0.17830	0.00260	0.2709	-	0	1055.1	14.2
91500-11	0.07488	0.00081	1.86500	0.03400	0.18040	0.00260	0.1836	-	0	1066.4	14.1
91500-12	0.07501	0.00087	1.85900	0.03400	0.17950	0.00230	0.1612	-	0	1061.3	12.5
91500-13	0.07474	0.00093	1.86100	0.03200	0.18060	0.00270	0.2263	-	0	1067.6	14.7
91500-14	0.07510	0.00094	1.85700	0.03500	0.18000	0.00270	0.1599	-	0	1063.9	14.7
91500-16	0.07450	0.00087	1.86300	0.03400	0.18070	0.00240	0.1952	-	0	1068.4	13.1
91500-17	0.07490	0.00087	1.84000	0.03000	0.17840	0.00280	0.4155	-	0	1055.4	15.3

<u>Plesovice</u>											
Plesovice-1	0.05342	0.00044	0.40290	0.00660	0.05457	0.00080	0.3937	-	0	342.5	4.9
Plesovice-2	0.05530	0.00160	0.41410	0.00850	0.05413	0.00099	0.8213	-	0	339.0	6.0
~~Plesovice-3~~	~~0.05337~~	~~0.00075~~	~~0.55900~~	~~0.01300~~	~~0.07600~~	~~0.00160~~	~~0.32363~~	~~-~~	~~0~~	~~472.1~~	~~9.6~~
~~Plesovice-4~~	~~0.05324~~	~~0.00063~~	~~0.46490~~	~~0.00900~~	~~0.06310~~	~~0.00100~~	~~0.27770~~	~~-~~	~~0~~	~~394.5~~	~~6.1~~
Plesovice-5	0.05326	0.00065	0.40870	0.00730	0.05372	0.00096	0.4583	-	0	337.3	5.9
Plesovice-6	0.05337	0.00058	0.40140	0.00650	0.05450	0.00080	0.4830	-	0	342.0	4.9
Plesovice-7	0.05430	0.00130	0.40340	0.00730	0.05420	0.00100	0.8309	-	0	339.8	6.1
Plesovice-8	0.05353	0.00066	0.40210	0.00800	0.05412	0.00099	0.9912	-	0	339.7	6.0
Plesovice-9	0.05376	0.00072	0.40200	0.00700	0.05403	0.00093	0.7569	-	0	339.0	5.7
Plesovice-10	0.05362	0.00077	0.40140	0.00670	0.05409	0.00093	0.9972	-	0	339.4	5.7
Plesovice-11	0.05401	0.00055	0.41820	0.00670	0.05420	0.00081	0.1905	-	0	339.9	4.9
<u>GJ-1</u>											
GJ-1-1	0.05966	0.00070	0.82000	0.01100	0.09955	0.00100	0.3947	-	0	611.9	5.9
GJ-1-2	0.05959	0.00066	0.80970	0.00970	0.09865	0.00100	0.3901	-	0	606.7	5.9
GJ-1-3	0.05976	0.00056	0.81500	0.00820	0.09924	0.00100	0.5049	-	0	610.1	5.9
GJ-1-4	0.05908	0.00062	0.80030	0.00920	0.09838	0.00100	0.5211	-	0	605.5	5.9
GJ-1-5	0.05972	0.00081	0.81100	0.01200	0.09866	0.00110	0.4512	-	0	606.7	6.5
GJ-1-6	0.05942	0.00079	0.81400	0.01100	0.09960	0.00110	0.3822	-	0	612.4	6.4
GJ-1-7	0.05956	0.00073	0.80900	0.01100	0.09924	0.00110	0.5057	-	0	610.2	6.5
GJ-1-8	0.05971	0.00075	0.81500	0.01200	0.09932	0.00120	0.6052	-	0	610.6	7.0
GJ-1-9	0.05988	0.00077	0.82200	0.01100	0.09893	0.00120	0.4867	-	0	608.2	7.0

<u>Bishop Tuff</u>											
1704-1	0.06300	0.01100	0.00088	0.00015	0.000106	0.000004	-0.0757	0.24	2	0.752	0.030
1704-2	0.05540	0.00660	0.00078	0.00009	0.000106	0.000003	0.0586	0.24	1	0.759	0.021
1704-3	0.05700	0.01200	0.00086	0.00017	0.000106	0.000004	0.2816	0.24	1	0.758	0.025
1704-4	0.08300	0.01400	0.00146	0.00039	0.000115	0.000005	0.9535	0.24	5	0.789	0.032
1704-5	0.09200	0.01100	0.00135	0.00016	0.000108	0.000003	0.6206	0.24	6	0.740	0.023
1704-6	0.07140	0.00950	0.00107	0.00015	0.000107	0.000003	0.5852	0.24	3	0.751	0.022

[a] f_{206} (%) denotes an estimate for the amount of common-Pb in measured ^{206}Pb. Correction for common-Pb was made using ^{207}Pb method (Williams, 1998) with contemporaneous common-Pb composition estimated from Stacey-Kramers (1975) model.

[b] ^{206}Pb*/^{238}U ages are corrected for common-Pb (Williams, 1998). For Bishop Tuff initial ^{230}Th disequilibrium correction $f_{Th/U}$ = 0.24 was assumed.

[c] Uncertainties are a quadratic combination of the standard error of the measured isotope ratio and reproducibility of the reference material.

Table A.4: Pollen counts.

Sample number: BJ08-CR2-85, Nov. 24th 2008 processing (heavy liquids, double acetolysis)

Comments: Charley River 2 at Chester Bluff, from paleosol associated with Biederman Tephra. Sample from "middle" of paleosol. Heavy processing has damaged already poorly preserved pollen. However, most unidentifiable pollen tends to be psilate or with little surface texture, thus *Salix* is probably not underrepresented, but others such as Betulaceae, *Alnus*, perhaps Gramineae and Cyperaceae as well, probably are. *Picea* fragments are also extremely common, thus *Picea* counts are also most likely unrepresentative.

Taxa	Indeterminate	*Picea*	*Salix*	*Alnus*	*Betula*	Graminaceae	Cyperaceae	*Sheperdia canadensis*	Ericaceae	Rosaceae type	Chenopo-daceae	Unknown	Total
raw count (# of grains)	110	131	18	22	10	10	11	4	1	1	3	6	327
relative percent	33.64	40.06	5.50	6.73	3.06	3.06	3.36	1.22	0.31	0.31	0.92	1.83	

Sample number: BJ08-CR2-87, Nov. 24th 2008 processing (heavy liquids, double acetolysis)

Comments: Charley River 2 at Chester Bluff, from paleosol associated with Biederman Tephra. Sample from "top" of paleosol at contact. Pollen is relatively abundant compared to 85, and not as badly preserved. *Picea* is often fragmented.

A fair amount of unknowns.

There were 3 anthers of Cyperaceae that were not counted, this sample is probably skewed due to their presence

Taxa	**Indeterminate**	***Picea***	***Salix***	***Alnus***	***Betula***	**Graminaceae**	**Cyperaceae**	**Caryophyllaceae**	***Sphagnum***	**Unknown**	**Total**
raw count (# of grains)	118	13	3	2	18	2	153	1	133	20	463
relative percent	25.49	2.81	0.65	0.43	3.89	0.43	33.05	0.22	28.73	4.32	

Table A.5: Bayesian modeling results.

TRIANGULAR DISTRIBUTION					
Tephra	Age (Ma)	2.5% CI	97.5% CI	sigma	2 sigma
BT	**0.178**	0.160	0.193	0.008	**0.017**
HP	**0.680**	0.631	0.722	0.023	**0.047**
GR	**0.688**	0.640	0.725	0.022	**0.044**
QC	**2.615**	2.530	2.684	0.039	**0.079**
PA	**1.919**	1.846	1.959	0.029	**0.057**
FC	**0.708**	0.659	0.744	0.021	**0.043**
GI	**0.542**	0.464	0.589	0.032	**0.064**
LC	**3.142**	3.073	3.201	0.033	**0.067**
UNIFORM DISTRIBUTION					
Tephra	Age (Ma)	2.5% CI	97.5% CI	sigma	2 sigma
BT	**0.171**	0.150	0.188	0.010	**0.020**
HP	**0.656**	0.599	0.706	0.028	**0.056**
GR	**0.675**	0.614	0.719	0.027	**0.054**
QC	**2.582**	2.461	2.664	0.052	**0.103**
PA	**1.864**	1.701	1.944	0.066	**0.132**
FC	**0.694**	0.629	0.736	0.028	**0.055**
GI	**0.560**	0.479	0.597	0.032	**0.064**
LC	**3.125**	3.043	3.190	0.038	**0.076**
MELTS DISTRIBUTION					
Tephra	Age (Ma)	2.5% CI	97.5% CI	sigma	2 sigma
BT	**0.162**	0.135	0.183	0.012	**0.025**
HP	**0.630**	0.562	0.689	0.032	**0.065**
GR	**0.657**	0.565	0.713	0.038	**0.076**
QC	**2.512**	2.256	2.637	0.100	**0.200**
PA	**1.904**	1.777	1.957	0.048	**0.095**
FC	**0.671**	0.563	0.727	0.043	**0.086**
GI	**0.530**	0.404	0.587	0.052	**0.103**
LC	**3.096**	2.974	3.174	0.051	**0.102**

Note: BT, Biederman tephra; GR, Gold Run tephra; QC, Quartz Creek tephra; FC, Flat Creek tephra; LC, Lost Chicken tephra

Table A.6. LA-ICP-MS instrumentation.

Laboratory and Sample preparation			
Laboratory name	Canadian Center for Isotopic Microanalysis, Dept. of Earth & Atmos.Sci., University of Alberta, Canada	Canadian Center for Isotopic Microanalysis, Dept. of Earth & Atmos.Sci., University of Alberta, Canada	Arctic Resources Geochemistry Laboratory, Dept. of Earth & Atmos.Sci., University of Alberta, Canada
Sample type/mineral	Zircon	Zircon	Zircon
Analysis	U-Pb	U-Pb, U-Th	U-Pb
Samples	Gold Run (UA1001), Flat Creek (UA1012), Quartz Creek (UA1004), PA (UA1327), Lost Chicken (UA1013) and GI (UA1668)	HP (UA2841) and GI (UA2838)	Gold Run (UA1001), Biederman (UT1884)
Sample preparation	Polished mount	Polished mount	Polished mount
Imaging	CL and BSE	CL and BSE	CL and BSE
Laser Ablation System			
Make, Model & Type	ESI/New Wave Research UP213 Nd YAG	ESI/New Wave Research UP213 Nd YAG	RESOlution ArF Excimer193 nm
Ablation cell & volume	New Wave/ESI standard cell, 33cm^3 volume	New Wave/ESI standard cell, 33cm^3 volume	Laurin Technic S-155 two-volume, 2 cm^3 inner cell funnel to 380 cm^3 cell box
Laser wavelength (nm)	213	213	193
Pulse width (ns)	<4	<4	20
Fluence (J/cm^2)	~3	~3	~3
Repetition rate (Hz)	5	5	5
Ablation duration (s)	40	40	40
Ablation pit depth (μm)	~10–15	~10–15	~10–15
Spot size (um)	30	30	33 (Gold Run); 40 (Biederman)
Sampling mode / pattern	Static spot	Static spot	Static spot
Carrier gas	He with Ar make-up gas	He with Ar and N_2 added after the cell	He with Ar and N_2 mixed in the cell
Cell carrier gas flow (l/min)	1	0.5	0.35
Mercury trap used?	Yes	Yes	Yes
ICP-MS Instrument			
Make, Model & Type	Nu Plasma I multi-collector (MC)-ICP-MS	ThermoScientific ICAP-Q quadrupole ICP-MS	ThermoScientific Element XR (SF)-ICP-MS.
Sample introduction	Ablation aerosol combined with co-aspiration of 0.5 ppb Tl solution	Ablation aerosol	Ablation aerosol
RF power (W)	1300	1550	1200
Make-up gas flow (l/min)	DSN 100 desolvating nebulizer, nebuliser pressure ~30 psi Ar	Ar = 0.55, N_2 = 0.004	Ar = 0.85, N_2 = 0.002
Detection system	Mixed faraday (238, 205, 203), discrete dynode secondary electron multipliers (207, 206, 204)	Discrete dynode secondary electron multiplier	Single electron multiplier ion counter
Masses measured	238, 207, 206, 205, 204, 203	238, 235, 232, 208-204	238, 235, 232, 208-202
Dwell times	Static collection	20 ms (232, 238), 30 ms (235, 208-206), 40 ms (204)	10 ms (202, 204), 20 ms (208, 232, 235, 238), 40 ms (206) and 50 ms (207).
IC Dead time (ns)	~7.9, 10.7, and 9.8 ns for IC0, IC1, and IC2 respectively.	40	16
Typical Oxide Rate (ThO/Th)	-	ThO/Th < 0.5%	ThO/Th < 0.2%
Data Processing			
Gas blank	1. 2% HNO_3 + Gas Blank done prior to each sample (Blank 1; 30 seconds) 2. 0.5 ppb Tl Solution + Gas + 2% HNO_3 Blank done prior to unknowns (Blank 2; 30 seconds) 3. every subsequent 10 spot analyses (Blank ≥3; 30 seconds).	25 seconds on peak zero subtraction.	Baseline measured 15 seconds prior to each analysis.
Calibration strategy	GJ-1 used as primary reference material, Plešovice and Bishop Tuff used for quality control.	GJ-1 used as primary reference material, Plešovice and 94-35 used for quality control.	91500 used as primary reference material, GJ-1, Plešovice and Bishop Tuff used for quality control.
Data processing package used	In house excel based spreadsheet.	Iolite "VizualAge" (Petrus and Kamber 2012), U-Pb fractionation and normalization, uncertainty propagation in external spreadsheet.	Iolite (Paton et al., 2010, 2011) for mass bias correction, U-Pb downhole fractionation, data normalisation, integration time selection.
Mass discrimination	Tl tracer solution used for mass bias correction of Pb isotopes, $^{206}Pb/^{238}U$ normalized to primary reference material.	Normalization to primary reference material.	Normalization to primary reference material.
Uncertainty level & propagation	Analytical uncertainties are reported as absolute 2σ (95% confidence level) propagated by quadratic. addition. Reproducibility of reference material uncertainty is propagated.	Analytical uncertainties are reported as absolute 2σ (95% confidence level) propagated by quadratic. addition. Reproducibility of reference material uncertainty is propagated.	Analytical uncertainties are reported as absolute 2σ (95% confidence level) propagated by quadratic. addition. Reproducibility of reference material uncertainty is propagated.
Quality control and validation	Plešovice Wtd. Mean $^{206}Pb/^{238}U$ age: 336.0 ± 1.9 Ma (2σ; MSWD = 0.3; n = 13); Bishop Tuff Wtd. Mean $^{206}Pb/^{238}U$ age: 0.773 ± 0.005 Ma (2σ; MSWD = 1.6; n = 13)	Plešovice Wtd. Mean $^{206}Pb/^{238}U$ age: 338.0 ± 2.6 Ma (2σ; MSWD = 0.88; n = 7); 94-35 Wtd. Mean $^{206}Pb/^{238}U$ age: 54.8 ± 1.2 Ma (2σ; MSWD = 0.49; n = 11)	Plešovice Wtd. Mean $^{206}Pb/^{238}U$ age: 339.6 ± 1.9 Ma (2σ; MSWD = 0.45; n = 9); GJ-1 Wtd. Mean $^{206}Pb/^{238}U$ age: 609.1 ± 2.1 Ma (2σ; MSWD = 0.64; n = 9); Bishop Tuff Wtd. Mean $^{206}Pb/^{238}U$ age: 0.756 ± 0.009 Ma (2σ; MSWD = 1.3; n = 6)
Th disequilibrium correction and uncertainty	$^{206}Pb/^{238}U$ ages of the samples were corrected following Scharer (1984) and Sakata (2018). Uncertainties from ($^{206}Pb/^{238}U$) measured, $f_{Th/U}$ are propagated.	$^{206}Pb/^{238}U$ ages of the samples were corrected following Scharer (1984) and Sakata (2018). Uncertainties from ($^{206}Pb/^{238}U$) measured, $f_{Th/U}$ are propagated.	$^{206}Pb/^{238}U$ ages of the samples were corrected following Scharer (1984) and Sakata (2018). Uncertainties from ($^{206}Pb/^{238}U$) measured, $f_{Th/U}$ are propagated.

Table A.7: Glass Geochemistry for secondary standards (ID3506 and Old Crow tephra) and GI tephra samples (from type section and new, unpublished samples from Gold Hill IV).

Sample	SiO2	TiO2	Al2O3	FeO	MnO	MgO	CaO	Na2O	K2O	Cl	Total	H2Odiff
ID 3506	**74.10**	**0.07**	**13.10**	**1.55**	**0.07**	**0.04**	**0.74**	**4.06**	**5.13**	**0.34**	**99.08**	**0.92**
	0.96	0.03	0.34	0.06	0.03	0.02	0.05	0.28	0.26	0.03		
Old Crow	**75.29**	**0.31**	**13.05**	**1.69**	**0.05**	**0.29**	**1.49**	**3.82**	**3.72**	**0.28**	**100.00**	
	1.40	0.05	0.30	0.12	0.02	0.02	0.05	0.38	0.28	0.05	-	

Sample	SiO2	TiO2	Al2O3	FeO	MnO	MgO	CaO	Na2O	K2O	Cl	Total	H2O diff
ID3506-1	75.44	0.06	13.32	1.49	0.07	0.07	0.74	3.10	5.06	0.44	99.68	
ID3506-2	74.37	0.12	13.09	1.58	0.09	0.05	0.72	4.17	5.08	0.35	99.54	
ID3506-3	74.27	0.11	12.99	1.56	0.08	0.06	0.76	4.15	4.98	0.37	99.23	
ID3506-4	73.81	0.08	13.16	1.48	0.11	0.07	0.76	4.22	4.99	0.37	98.95	
ID3506-5	73.26	0.09	13.01	1.91	0.10	0.07	0.94	4.43	5.02	0.39	99.11	
ID3506-6	73.22	0.07	13.10	1.51	0.01	0.05	0.70	4.27	4.94	0.37	98.16	
ID3506-7	75.30	0.03	13.05	1.49	0.08	0.05	0.70	4.01	4.88	0.44	99.91	
ID3506-8	75.59	0.07	13.34	1.50	0.05	0.06	0.76	4.21	5.01	0.34	100.85	
ID3506-9	74.48	0.14	13.23	1.61	0.06	0.05	0.72	3.98	5.00	0.38	99.56	
ID3506-10	74.34	0.02	13.07	1.53	0.04	0.05	0.71	4.20	5.13	0.38	99.39	
AVERAGE	74.41	0.08	13.13	1.57	0.07	0.06	0.75	4.07	5.01	0.38	99.44	
STDEV	0.84	0.04	0.12	0.13	0.03	0.01	0.07	0.37	0.07	0.03	0.69	
Old Crow-1	75.76	0.27	12.86	1.58	0.06	0.26	1.43	3.63	3.78	0.37	100.00	5.16
Old Crow-2	75.49	0.33	12.96	1.68	0.09	0.30	1.45	3.62	3.75	0.34	100.00	4.37
Old Crow-3	75.67	0.27	12.90	1.48	0.07	0.29	1.53	3.76	3.73	0.30	100.00	4.40
Old Crow-4	75.20	0.26	13.19	1.74	0.07	0.27	1.49	3.74	3.74	0.31	100.00	4.41
Old Crow-5	75.53	0.30	12.98	1.72	0.12	0.26	1.40	3.74	3.64	0.31	100.00	5.42
Old Crow-6	75.46	0.28	13.00	1.72	0.04	0.26	1.49	3.72	3.65	0.38	100.00	5.45
Old Crow-7	75.47	0.30	12.99	1.70	0.05	0.26	1.48	3.80	3.61	0.35	100.00	4.16
Old Crow-8	75.23	0.24	13.12	1.69	0.07	0.28	1.51	3.73	3.80	0.35	100.00	5.59
Old Crow-9	75.40	0.27	13.04	1.71	0.03	0.31	1.59	3.68	3.69	0.29	100.00	4.86
Old Crow-10	75.41	0.26	12.96	1.80	0.06	0.27	1.58	3.95	3.44	0.28	100.00	2.24
AVERAGE	75.46	0.28	13.00	1.68	0.07	0.27	1.50	3.74	3.68	0.33	100.00	4.61
STDEV	0.17	0.03	0.10	0.09	0.03	0.02	0.06	0.09	0.10	0.03	0.00	0.98
UA 1242-11	64.46	0.93	15.50	5.85	0.14	1.46	4.35	4.55	2.65	0.13	100.00	0.60
UA 1242-7	67.09	0.79	15.11	4.68	0.07	1.05	3.21	4.56	3.29	0.15	100.00	1.14
UA 1242-16	69.45	0.61	14.65	3.73	0.11	0.66	2.44	4.51	3.62	0.21	100.00	2.65
UA 1242-14	70.06	0.54	14.55	3.50	0.17	0.55	2.01	4.33	4.05	0.23	100.00	4.96
UA 1242-2	70.08	0.63	14.44	3.46	0.08	0.51	2.01	4.67	3.95	0.18	100.00	3.24
UA 1242-17	70.11	0.62	14.58	3.49	0.12	0.42	2.03	4.49	3.94	0.19	100.00	3.97
UA 1242-6	70.15	0.56	14.51	3.42	0.12	0.55	2.02	4.54	3.94	0.20	100.00	2.70
UA 1242-13	70.21	0.61	14.70	3.79	0.13	0.57	1.99	4.19	3.59	0.22	100.00	8.47
UA 1242-19	70.21	0.59	14.77	3.45	0.05	0.50	1.99	4.40	3.87	0.16	100.00	2.65
UA 1242-5	70.25	0.58	14.48	3.46	0.13	0.53	1.99	4.49	3.96	0.15	100.00	5.54
UA 1242-1	70.27	0.47	14.52	3.66	0.15	0.45	1.94	4.50	3.86	0.19	100.00	4.79
UA 1242-4	70.28	0.61	14.12	3.47	0.11	0.55	2.01	4.62	4.00	0.23	100.00	3.89
UA 1242-10	70.30	0.54	14.35	3.49	0.11	0.47	2.04	4.68	3.82	0.20	100.00	3.84
UA 1242-12	70.32	0.50	14.51	3.39	0.12	0.50	2.01	4.51	3.97	0.18	100.00	4.12
UA 1242-8	70.42	0.57	14.43	3.43	0.11	0.49	1.93	4.42	4.00	0.20	100.00	5.11
UA 1242-3	70.47	0.53	14.22	3.49	0.11	0.49	1.92	4.62	3.97	0.19	100.00	3.94
UA 1242-20	70.53	0.55	14.30	3.45	0.03	0.48	2.06	4.41	3.99	0.20	100.00	4.55
AVERAGE	69.69	0.60	14.57	3.72	0.11	0.60	2.23	4.50	3.79	0.19	100.00	3.89
STDEV	1.56	0.11	0.33	0.63	0.03	0.26	0.63	0.12	0.35	0.03	0.00	1.78
UA 1338-9	65.38	0.79	15.46	5.51	0.18	1.31	3.73	4.43	3.03	0.18	100.00	6.34

UA 1338-6	65.93	0.89	15.15	5.08	0.10	1.08	3.54	4.75	3.27	0.21	100.00	0.37
UA 1338-19	65.98	0.78	15.05	5.11	0.14	1.14	3.65	4.85	3.13	0.18	100.00	0.08
UA 1338-8	65.99	0.91	15.17	5.31	0.18	1.21	3.57	4.60	2.89	0.17	100.00	7.28
UA 1338-12	66.23	0.94	15.31	5.09	0.18	1.19	3.48	4.39	3.10	0.10	100.00	0.90
UA 1338-10	69.49	0.69	14.96	3.95	0.10	0.55	1.83	4.42	3.81	0.21	100.00	12.22
UA 1338-7	69.94	0.56	14.38	3.57	0.15	0.57	1.99	4.57	4.03	0.24	100.00	7.99
UA 1338-16	70.04	0.54	14.32	3.66	0.10	0.54	2.01	4.51	4.03	0.24	100.00	6.21
UA 1338-18	70.20	0.61	14.53	3.70	0.15	0.57	2.08	4.25	3.70	0.21	100.00	5.76
UA 1338-14	70.26	0.49	14.35	3.35	0.14	0.45	2.08	4.63	4.00	0.24	100.00	3.95
UA 1338-1	70.27	0.52	14.39	3.50	0.08	0.44	2.08	4.48	4.08	0.15	100.00	2.93
UA 1338-13	70.30	0.70	14.37	3.39	0.13	0.53	2.02	4.55	3.80	0.21	100.00	4.18
UA 1338-5	70.32	0.55	14.30	3.33	0.11	0.54	1.98	4.53	4.16	0.18	100.00	4.32
UA 1338-15	70.41	0.48	14.29	3.40	0.12	0.48	2.05	4.60	3.99	0.19	100.00	5.23
UA 1338-11	70.49	0.58	14.48	3.51	0.08	0.56	1.96	4.32	3.85	0.16	100.00	11.92
UA 1338-2	70.52	0.51	14.39	3.44	0.00	0.45	1.97	4.46	4.07	0.19	100.00	4.51
UA 1338-3	70.56	0.52	14.27	3.35	0.04	0.45	2.11	4.57	3.95	0.19	100.00	4.39
UA 1338-17	70.62	0.54	14.21	3.60	0.14	0.52	2.05	4.35	3.81	0.18	100.00	4.36
AVERAGE	69.05	0.64	14.63	3.99	0.12	0.70	2.45	4.51	3.70	0.19	100.00	5.16
STDEV	2.03	0.15	0.42	0.80	0.05	0.32	0.73	0.15	0.42	0.04	0.00	3.32
UA 1576-5	65.01	0.84	15.54	5.55	0.16	1.39	4.00	4.53	2.84	0.14	100.00	2.03
UA 1576-17	65.39	0.89	15.12	5.43	0.20	1.18	3.82	4.46	3.32	0.18	100.00	1.24
UA 1576-16	66.02	0.84	15.19	5.45	0.12	1.19	3.59	4.33	3.12	0.17	100.00	2.53
UA 1576-12	66.18	0.90	15.17	5.00	0.07	1.16	3.55	4.68	3.13	0.15	100.00	2.14
UA 1576-18	66.40	0.88	15.49	4.90	0.11	1.11	3.42	4.45	3.12	0.11	100.00	0.55
UA 1576-13	66.71	0.79	15.28	4.78	0.11	0.95	3.22	4.44	3.51	0.21	100.00	3.42
UA 1576-4	69.57	0.56	14.61	3.69	0.15	0.60	2.20	4.77	3.68	0.16	100.00	3.45
UA 1576-3	69.61	0.73	14.31	3.58	0.09	0.59	2.19	4.75	3.94	0.21	100.00	1.87
UA 1576-1	69.98	0.58	14.42	3.65	0.10	0.54	2.02	4.45	4.05	0.21	100.00	0.27
UA 1576-10	70.11	0.56	14.46	3.46	0.13	0.49	2.03	4.56	4.04	0.15	100.00	4.90
UA 1576-14	70.15	0.58	14.37	3.49	0.12	0.54	2.16	4.50	3.87	0.21	100.00	5.00
UA 1576-2	70.23	0.60	14.27	3.54	0.09	0.51	2.12	4.43	4.02	0.18	100.00	5.02
UA 1576-19	70.27	0.57	14.38	3.52	0.02	0.50	2.01	4.71	3.82	0.19	100.00	2.81
UA 1576-20	70.35	0.64	14.33	3.43	0.08	0.47	1.88	4.69	3.94	0.19	100.00	1.46
UA 1576-9	70.37	0.63	14.31	3.65	0.13	0.44	1.90	4.44	3.97	0.16	100.00	4.69
UA 1576-15	70.59	0.56	14.07	3.49	0.07	0.59	1.98	4.57	3.87	0.22	100.00	4.49
UA 1576-6	70.62	0.56	14.51	3.43	0.05	0.47	1.94	4.35	3.87	0.19	100.00	4.69
AVERAGE	68.68	0.69	14.70	4.12	0.11	0.75	2.59	4.54	3.65	0.18	100.00	2.97
STDEV	2.12	0.14	0.48	0.83	0.04	0.33	0.79	0.14	0.40	0.03	0.00	1.62
Old Crow-11	75.25	0.23	13.45	1.70	0.04	0.29	1.56	3.57	3.62	0.29	100.00	4.23
Old Crow-12	75.33	0.25	13.00	1.75	0.06	0.31	1.46	3.84	3.66	0.34	100.00	4.63
Old Crow-13	75.89	0.31	13.11	1.54	0.02	0.26	1.58	3.25	3.75	0.29	100.00	5.96
Old Crow-14	75.14	0.30	13.03	1.70	0.09	0.29	1.50	3.87	3.80	0.28	100.00	4.45
Old Crow-15	75.52	0.24	13.10	1.73	0.05	0.26	1.48	3.68	3.61	0.34	100.00	6.01
Old Crow-16	75.29	0.29	13.26	1.81	0.04	0.33	1.41	3.54	3.71	0.33	100.00	2.92
AVERAGE	75.40	0.27	13.16	1.70	0.05	0.29	1.50	3.63	3.69	0.31	100.00	4.70
STDEV	0.27	0.04	0.17	0.09	0.02	0.03	0.06	0.23	0.08	0.03	0.00	1.16
ID 3506-11	73.85	0.03	13.03	1.51	0.09	0.04	0.72	3.92	5.03	0.43	98.54	
ID 3506-12	74.06	0.05	13.01	1.52	0.09	0.06	0.74	3.83	5.11	0.38	98.77	
ID 3506-13	74.60	0.04	13.18	1.37	0.08	0.06	0.76	4.22	4.87	0.33	99.42	
ID 3506-14	74.43	0.07	13.28	1.53	0.07	0.04	0.79	3.98	5.06	0.35	99.53	
ID 3506-15	74.27	0.10	13.02	1.51	0.06	0.01	0.73	3.86	4.85	0.40	98.72	
ID 3506-16	74.49	0.08	13.14	1.53	0.01	0.07	0.69	3.82	4.92	0.40	99.06	
AVERAGE	74.29	0.06	13.11	1.49	0.07	0.05	0.74	3.94	4.97	0.38	99.01	
STDEV	0.28	0.03	0.11	0.06	0.03	0.02	0.03	0.15	0.11	0.04	0.40	

APPENDIX B: CHAPTER 3

Table B.1. Zircon LA-ICP-MS U-Pb data for Grubstake tephra and reference materials.

Sample	U (ppm)	Th (ppm)	$^{207}Pb/^{206}Pb$	2S.E.	$^{207}Pb/^{235}U$	2S.E	$^{206}Pb/^{238}U$	2S.E.	ρ	F_{206} (%)[a]	$^{206}Pb^{*}/^{238}U$	2σ	
91500	77	29	0.07518	0.00094	1.85135	0.02872	0.17861	0.00164	0.593	0	1058.8	9.0	
91500	86	32	0.07474	0.00085	1.85333	0.02673	0.17986	0.00159	0.613	0	1066.1	8.7	
91500	77	29	0.07470	0.00095	1.84264	0.03027	0.17890	0.00187	0.637	0	1060.9	10.2	
91500	83	31	0.07516	0.00092	1.86011	0.02832	0.17949	0.00161	0.590	0	1063.6	8.8	
91500	77	29	0.07498	0.00099	1.85622	0.02948	0.17956	0.00158	0.556	0	1064.2	8.6	
91500	80	30	0.07460	0.00087	1.83176	0.02991	0.17809	0.00203	0.698	0	1056.6	11.1	
91500	80	30	0.07511	0.00092	1.85986	0.02655	0.17960	0.00132	0.516	0	1064.3	7.2	
91500	80	30	0.07440	0.00083	1.83072	0.02613	0.17846	0.00158	0.620	0	1058.9	8.6	
91500	81	30	0.07484	0.00093	1.84620	0.02832	0.17891	0.00160	0.584	0	1060.8	8.8	
91500	79	30	0.07445	0.00088	1.84525	0.02687	0.17975	0.00153	0.583	0	1065.9	8.3	
91500	81	30	0.07586	0.00088	1.87119	0.02966	0.17890	0.00194	0.684	0	1059.6	10.6	
91500	80	30	0.07515	0.00088	1.84697	0.02972	0.17826	0.00196	0.684	0	1056.9	10.7	
91500	80	30	0.07495	0.00099	1.85813	0.03242	0.17981	0.00206	0.655	0	1065.6	11.2	
91500	80	30	0.07415	0.00094	1.82754	0.02956	0.17875	0.00180	0.624	0	1060.8	9.9	
91500	80	30	0.07505	0.00101	1.86217	0.03313	0.17996	0.00210	0.655	0	1066.4	11.4	
Plesovice	442	51	0.05366	0.00072	0.40213	0.00621	0.05435	0.00041	0.493	0	341.0	5.0	
Plesovice	822	96	0.05399	0.00054	0.40010	0.00500	0.05374	0.00040	0.592	0	337.1	4.8	
Plesovice	734	68	0.05319	0.00053	0.39792	0.00503	0.05426	0.00042	0.609	0	340.7	5.1	
Plesovice	631	75	0.07961	0.00558	0.60363	0.04289	0.05499	0.00065	0.166	3	334.0	7.3	
Plesovice	750	65	0.05360	0.00044	0.40041	0.00382	0.05418	0.00026	0.500	0	340.0	3.2	
Plesovice	878	95	0.05525	0.00049	0.40878	0.00430	0.05366	0.00031	0.549	0	336.1	3.8	
Plesovice	839	93	0.05833	0.00049	0.43377	0.00430	0.05393	0.00028	0.520	1	336.5	3.4	
Plesovice	491	48	0.05343	0.00051	0.40009	0.00440	0.05431	0.00029	0.491	0	340.9	3.5	
Plesovice	476	47	0.05290	0.00055	0.39148	0.00464	0.05368	0.00030	0.468	0	337.2	3.7	
GJ-1	305	9	0.05974	0.00066	0.80974	0.01138	0.09830	0.00086	0.619	0	604.5	9.8	
GJ-2	316	10	0.06003	0.00060	0.81034	0.00986	0.09791	0.00069	0.579	0	602.0	7.9	
GJ-3	313	9	0.05978	0.00063	0.79930	0.01052	0.09698	0.00076	0.595	0	599.8	8.7	
GJ-4	309	9	0.05969	0.00065	0.80353	0.01034	0.09764	0.00066	0.528	0	600.7	7.6	
GJ-5	301	9	0.05916	0.00057	0.79287	0.00911	0.09720	0.00061	0.551	0	598.5	7.1	
GJ-7	280	9	0.05928	0.00060	0.79463	0.00961	0.09723	0.00064	0.542	0	598.6	7.3	
Bishop	1907	1067	0.07961	0.01387	0.00117	0.00021	0.00011	0.00000	0.688	4	0.75	0.03	
Bishop	1346	593	0.11529	0.02059	0.00187	0.00034	0.00012	0.00000	0.758	9	0.77	0.03	
Bishop	2189	1153	0.08842	0.01303	0.00132	0.00020	0.00011	0.00000	0.697	5	0.75	0.02	
Bishop	1863	913	0.11477	0.01735	0.00168	0.00026	0.00011	0.00000	0.682	9	0.75	0.02	
Bishop	1889	959	0.25189	0.01954	0.00513	0.00043	0.00015	0.00001	0.952	26	0.77	0.03	
Bishop	1367	561	0.08650	0.01587	0.00125	0.00023	0.00010	0.00000	0.673	5	0.75	0.03	
Bishop	2314	1401	0.23225	0.01569	0.00440	0.00033	0.00014	0.00000	0.886	24	0.76	0.02	
Bishop	1342	774	0.19841	0.02929	0.00333	0.00052	0.00012	0.00001	0.786	19	0.75	0.03	
Grubstake tephra (UA4024)													Average diameter (μm)
GBS - 2	230	122	0.41680	0.02408	0.11205	0.00783	0.00195	0.00008	0.562	47	6.758	0.265	40.3
GBS - 3	255	138	0.18337	0.01663	0.03166	0.00304	0.00125	0.00004	0.332	17	6.758	0.216	39.7
GBS - 4	166	203	0.46164	0.05051	0.15462	0.02574	0.00243	0.00030	0.754	53	7.507	0.941	28.9
GBS - 5	261	111	0.19510	0.01802	0.03516	0.00355	0.00131	0.00005	0.406	19	6.925	0.284	29.2
GBS - 7	180	91	0.25727	0.02794	0.05277	0.00620	0.00149	0.00007	0.381	27	7.114	0.318	27.5
~~GBS - 8~~	~~54~~	~~42~~	~~0.29129~~	~~0.01419~~	~~3.06632~~	~~0.17915~~	~~0.07635~~	~~0.00246~~	~~0.552~~	~~30~~	~~336.886~~	~~10.573~~	72.0
GBS - 9	271	154	0.45412	0.02768	0.20086	0.01834	0.00321	0.00022	0.744	52	10.089	0.685	34.3
GBS - 13	243	120	0.30094	0.01922	0.06198	0.00447	0.00149	0.00005	0.465	32	6.612	0.222	26.4
GBS - 14	234	116	0.50789	0.01457	0.17470	0.00878	0.00249	0.00010	0.821	58	6.766	0.279	25.1
GBS - 15	409	676	0.31990	0.03089	0.06875	0.00787	0.00156	0.00010	0.536	35	6.653	0.408	33.1
GBS - 17	62	40	0.65284	0.05907	0.69491	0.12136	0.00772	0.00115	0.855	77	11.606	1.732	27.2
GBS - 18	210	101	0.51732	0.01641	0.19803	0.00801	0.00278	0.00007	0.621	60	7.306	0.183	26.8
GBS - 19	302	161	0.36572	0.03107	0.09210	0.01023	0.00183	0.00013	0.644	40	7.097	0.507	22.8

GBS - 20	236	154	0.50622	0.02386	0.17730	0.00990	0.00254	0.00008	0.536	58	6.922	0.207	42.6
GBS - 22	228	142	0.46229	0.02181	0.14107	0.00818	0.00221	0.00007	0.582	53	6.837	0.231	28.2
GBS - 23	723	793	0.13992	0.01003	0.02240	0.00169	0.00116	0.00003	0.310	12	6.685	0.156	38.8
GBS - 24	137	119	0.46591	0.02654	0.15226	0.01046	0.00237	0.00009	0.559	53	7.245	0.278	35.7
GBS - 26	218	111	0.44920	0.02508	0.13643	0.00887	0.00220	0.00007	0.513	51	7.040	0.235	34.0
GBS - 27	260	152	0.62982	0.02458	0.35406	0.03617	0.00408	0.00038	0.924	74	6.942	0.655	40.5
GBS - 28	217	106	0.54748	0.02334	0.21256	0.01141	0.00282	0.00009	0.608	64	6.715	0.219	37.1
GBS - 31	362	287	0.45313	0.02405	0.14294	0.01002	0.00229	0.00010	0.653	52	7.235	0.331	47.0

[a] F_{206} (%) denotes an estimate for the amount of common-Pb in measured ^{206}Pb. Correction for common-Pb was made using ^{207}Pb method (Williams, 1998) with contemporaneous common-Pb composition estimated from Stacey-Kramers (1975) model.

[b] ^{206}Pb*/^{238}U ages are corrected for common-Pb. GBS is corrected for ^{230}Th disequilibrium using $D_{Th/U}$ = 0.14 (Bohenke et al., 2016). Bishop Tuff is corrected for ^{230}Th disequilibrium using Th/U_{glass} = 2.81.

Table B.2. Zircon LA-ICP-MS U-Pb data for Grubstake Formation.

Analysis Name	Uranium and Thorium [U] (ppm)	[Th] (ppm)	206Pb/238U Ratio	2 sigma	207Pb/206Pb Ratio	2 sigma	Error Correlation	Preferred Age Preferred Age (Ma)	2 - sigma	2 +sigma
1342_002_Zrn_a_01_1	327	154	0.08057	0.03370	0.04976	0.02852	0.42	499.55	202.61	199.47
1342_002_Zrn_a_01_2	0	4	0.21263	3.51367	0.61797	2.66993	0.97	4550.84	9101.67	18.33
1342_002_Zrn_a_01_3	1	1	0.13350	0.41832	0.46466	1.77279	0.46	4132.82	8265.65	854.35
1342_002_Zrn_a_01_4	183	69	0.02699	0.00131	0.05207	0.00775	0.03	171.69	8.23	8.22
1342_002_Zrn_a_01_5	1990	641	0.00824	0.00034	0.04825	0.00370	0.16	52.88	2.18	2.18
1342_002_Zrn_a_01_6	502	129	0.00910	0.00044	0.05054	0.00673	0.13	58.41	2.83	2.83
1342_002_Zrn_a_01_7	0	0	0.00000	0.00000	0.00000	0.00000	0.00	0.00	0.00	0.00
1342_002_Zrn_a_01_8	0	0	0.00000	0.00000	0.00000	0.00000	0.00	0.00	0.00	0.00
1342_002_Zrn_a_01_9	154	103	0.17051	0.00606	0.07282	0.00436	0.28	1014.94	33.43	33.34
1342_002_Zrn_a_01_10	203	49	0.00987	0.00069	0.05305	0.01267	0.04	63.28	4.42	4.42
1342_002_Zrn_a_01_11	738	251	0.00805	0.00039	0.04978	0.00488	0.17	51.71	2.51	2.51
1342_002_Zrn_a_01_12	1732	898	0.01549	0.00053	0.04817	0.00229	0.28	99.09	3.39	3.39
1342_002_Zrn_a_01_13	461	234	0.01004	0.00079	0.05147	0.00984	0.17	64.37	5.07	5.07
1342_002_Zrn_a_01_14	2251	270	0.01348	0.00066	0.04789	0.00336	0.33	86.33	4.23	4.22
1342_002_Zrn_a_01_15	0	0	0.00000	0.00000	0.00000	0.00000	0.00	0.00	0.00	0.00
1342_002_Zrn_a_01_16	381	147	0.02555	0.00156	0.05112	0.00553	0.21	162.66	9.81	9.80
1342_002_Zrn_a_01_17	920	540	0.02703	0.00108	0.04926	0.00355	0.21	171.94	6.75	6.75
1342_002_Zrn_a_01_18	1012	402	0.01854	0.00065	0.04909	0.00379	0.15	118.40	4.10	4.09
1342_002_Zrn_a_01_19	216	137	0.06965	0.00297	0.05595	0.00383	0.37	434.03	17.92	17.90
1342_002_Zrn_a_01_20	1164	1202	0.02354	0.00087	0.04835	0.00267	0.33	150.01	5.46	5.45
1342_002_Zrn_a_01_21	520	207	0.01598	0.00092	0.04849	0.00608	0.17	102.17	5.81	5.80
1342_002_Zrn_a_01_22	0	0	0.00000	0.00000	0.00000	0.00000	0.00	0.00	0.00	0.00
1342_002_Zrn_a_01_23	770	641	0.02773	0.00104	0.04977	0.00356	0.25	176.34	6.55	6.55
1342_002_Zrn_a_01_24	1876	571	0.00932	0.00042	0.04985	0.00503	0.14	59.82	2.67	2.67
1342_002_Zrn_a_01_25	382	177	0.01526	0.00074	0.05314	0.00780	0.09	97.61	4.70	4.70
1342_002_Zrn_a_01_26	893	322	0.03828	0.00145	0.05187	0.00306	0.29	242.16	9.03	9.02
1342_002_Zrn_a_01_27	125	41	0.05451	0.00266	0.04962	0.00791	0.10	342.14	16.26	16.25
1342_002_Zrn_a_01_28	274	59	0.03351	0.00194	0.05009	0.00523	0.18	212.49	12.09	12.07
1342_002_Zrn_a_01_29	856	181	0.01028	0.00041	0.04923	0.00397	0.25	65.92	2.59	2.59
1342_002_Zrn_a_01_30	173	61	0.03108	0.00257	0.05179	0.00770	0.22	197.33	16.10	16.08
1342_002_Zrn_a_01_31	682	303	0.00867	0.00051	0.04765	0.00745	0.15	55.63	3.28	3.28
1342_002_Zrn_a_01_32	2181	1790	0.01665	0.00080	0.04890	0.00335	0.34	106.46	5.04	5.04
1342_002_Zrn_a_01_33	471	374	0.02809	0.00112	0.04966	0.00382	0.30	178.55	7.00	7.00
1342_002_Zrn_a_01_34	0	0	0.00000	0.00000	0.00000	0.00000	0.00	0.00	0.00	0.00
1342_002_Zrn_a_01_35	119	32	0.20830	0.00986	0.08645	0.00452	0.50	1267.03	43.66	42.74
1342_002_Zrn_a_01_36	1024	562	0.01553	0.00066	0.04824	0.00306	0.34	99.32	4.19	4.19
1342_002_Zrn_a_01_37	228	106	0.04503	0.00243	0.05371	0.00659	0.19	283.95	14.98	14.96
1342_002_Zrn_a_01_38	1075	290	0.00999	0.00040	0.04962	0.00514	0.11	64.07	2.55	2.55
1342_002_Zrn_a_01_39	435	155	0.06044	0.00264	0.05403	0.00373	0.37	378.32	16.08	16.06
1342_002_Zrn_a_01_40	271	148	0.02716	0.00161	0.05186	0.00457	0.45	172.75	10.08	10.08
1342_002_Zrn_a_01_41	1002	543	0.01901	0.00091	0.05286	0.00485	0.22	121.41	5.76	5.76
1342_002_Zrn_a_01_42	166	83	0.03008	0.00215	0.05098	0.00915	0.20	191.08	13.45	13.44
1342_002_Zrn_a_01_43	103	33	0.01511	0.01086	0.06840	0.16751	0.11	96.70	69.13	68.76
1342_002_Zrn_a_01_44	1728	513	0.00821	0.00036	0.05067	0.00504	0.19	52.72	2.31	2.31
1342_002_Zrn_a_01_45	555	141	0.00897	0.00042	0.04723	0.00743	0.10	57.55	2.69	2.69
1342_002_Zrn_a_01_46	2686	718	0.01458	0.00055	0.04677	0.00257	0.27	93.29	3.47	3.47
1342_002_Zrn_a_01_47	647	331	0.02539	0.00137	0.05307	0.00564	0.25	161.66	8.64	8.63
1342_002_Zrn_a_01_48	107	67	0.03407	0.00219	0.05307	0.00857	0.14	215.96	13.63	13.62
1342_002_Zrn_a_01_49	202	79	0.18251	0.00934	0.08359	0.00514	0.33	1149.98	41.27	40.45
1342_002_Zrn_a_01_50	2870	453	0.01491	0.00052	0.04955	0.00322	0.26	95.43	3.28	3.28
1342_002_Zrn_a_01_51	405	252	0.01147	0.00050	0.04981	0.00569	0.10	73.52	3.18	3.18
1342_002_Zrn_a_01_52	159	69	0.01658	0.00113	0.05027	0.01059	0.08	106.02	7.14	7.14
1342_002_Zrn_a_01_53	68	31	0.04559	0.00704	0.04566	0.01811	0.09	0.00	0.00	0.00
1342_002_Zrn_a_01_54	555	347	0.00786	0.00042	0.04868	0.00693	0.12	50.46	2.70	2.70
1342_002_Zrn_a_01_55	348	91	0.06244	0.00214	0.05982	0.00618	0.13	390.46	13.00	12.98
1342_002_Zrn_a_01_56	717	499	0.00788	0.00044	0.04898	0.00980	0.09	50.59	2.81	2.80
1342_002_Zrn_a_01_57	236	138	0.01770	0.00143	0.05030	0.00805	0.12	113.08	9.07	9.07
1342_002_Zrn_a_01_58	227	85	0.03083	0.00146	0.05146	0.00501	0.21	195.76	9.10	9.10
1342_002_Zrn_a_01_59	3355	4611	0.01662	0.00055	0.04925	0.00272	0.27	106.27	3.52	3.52
1342_002_Zrn_a_01_60	438	167	0.03472	0.00124	0.04974	0.00418	0.16	220.00	7.72	7.71
1342_002_Zrn_a_01_61	327	186	0.00945	0.00059	0.04896	0.01133	0.06	60.65	3.77	3.77
1342_002_Zrn_a_01_62	1465	771	0.02952	0.00105	0.04909	0.00228	0.35	187.55	6.57	6.57
1342_002_Zrn_a_01_63	350	113	0.03234	0.00142	0.05029	0.00410	0.19	205.16	8.87	8.86
1342_002_Zrn_a_01_64	67	17	0.20630	0.04260	0.09650	0.02828	0.44	1340.70	252.63	224.65
1342_002_Zrn_a_01_65	578	357	0.00873	0.00055	0.04726	0.00999	0.06	56.05	3.51	3.51
1342_002_Zrn_a_01_66	743	461	0.00859	0.00034	0.04959	0.00748	0.12	55.14	2.16	2.16
1342_002_Zrn_a_01_67	0	0	0.00000	0.00000	0.00000	0.00000	0.00	0.00	0.00	0.00
1342_002_Zrn_a_01_68	232	109	0.15933	0.01182	0.07952	0.00662	0.49	1026.01	60.26	58.52
1342_002_Zrn_a_01_69	0	0	0.00000	0.00000	0.00000	0.00000	0.00	0.00	0.00	0.00
1342_002_Zrn_a_01_70	0	0	0.00000	0.00000	0.00000	0.00000	0.00	0.00	0.00	0.00
1342_002_Zrn_a_01_71	691	550	0.04081	0.00182	0.05175	0.00361	0.23	257.87	11.25	11.24
1342_002_Zrn_a_01_72	547	144	0.00974	0.00064	0.04991	0.00613	0.19	62.50	4.06	4.06
1342_002_Zrn_a_01_73	666	152	0.00842	0.00047	0.04893	0.00658	0.18	54.08	3.03	3.03
1342_002_Zrn_a_01_74	939	565	0.05612	0.00209	0.05291	0.00217	0.48	352.00	12.73	12.72
1342_002_Zrn_a_01_75	855	339	0.00153	0.00009	0.05280	0.01340	0.03	9.88	0.55	0.55
1342_002_Zrn_a_01_76	847	331	0.01242	0.00047	0.04880	0.00484	0.17	79.55	3.02	3.01

1342_002_Zrn_a_01_77	1791	648	0.00164	0.00012	0.04489	0.01206	0.04	0.00	0.00	0.00
1342_002_Zrn_a_01_78	903	433	0.05971	0.00226	0.05352	0.00250	0.49	373.85	13.73	13.71
1342_002_Zrn_a_01_79	545	897	0.08837	0.00356	0.05874	0.00327	0.42	545.91	21.13	21.09
1342_002_Zrn_a_01_80	1531	782	0.01495	0.00075	0.04911	0.00425	0.34	95.64	4.75	4.75
1342_002_Zrn_a_01_81	1287	669	0.01634	0.00064	0.05130	0.00355	0.35	104.51	4.03	4.03
1342_002_Zrn_a_01_82	591	116	0.02656	0.00159	0.05204	0.00373	0.45	168.97	9.99	9.99
1342_002_Zrn_a_01_83	1912	614	0.01516	0.00063	0.04873	0.00345	0.31	96.98	4.00	4.00
1342_002_Zrn_a_01_84	3195	898	0.00167	0.00012	0.04569	0.01066	0.16	0.00	0.00	0.00
1342_002_Zrn_a_01_85	161	10	0.01159	0.00247	0.07130	0.04426	0.06	74.29	15.73	15.71
1342_002_Zrn_a_01_86	1630	376	0.00897	0.00063	0.04643	0.00816	0.23	57.56	4.04	4.04
1342_002_Zrn_a_01_87	358	190	0.02346	0.00130	0.05223	0.00603	0.10	149.47	8.20	8.19
1342_002_Zrn_a_01_88	201	93	0.07148	0.01258	0.06129	0.01255	0.54	445.06	75.89	75.44
1342_002_Zrn_a_01_89	805	359	0.01718	0.00078	0.04992	0.00562	0.27	109.79	4.91	4.91
1342_002_Zrn_a_01_90	2603	505	0.01347	0.00134	0.05644	0.00954	0.16	86.23	8.51	8.50
1342_002_Zrn_a_01_91	1010	356	0.00992	0.00039	0.04848	0.00485	0.13	63.63	2.52	2.51
1342_002_Zrn_a_01_92	1400	1259	0.01621	0.00055	0.04719	0.00414	0.28	103.67	3.46	3.46
1342_002_Zrn_a_01_93	460	196	0.05293	0.00198	0.05678	0.00326	0.37	332.46	12.15	12.14
1342_002_Zrn_a_01_94	289	71	0.00919	0.00061	0.04933	0.01229	0.06	58.98	3.89	3.89
1342_002_Zrn_a_01_95	804	896	0.00749	0.00146	0.16501	0.04610	0.26	2507.64	512.87	435.27
1342_002_Zrn_a_01_96	472	152	0.01096	0.00059	0.04796	0.00802	0.09	70.25	3.75	3.75
1342_002_Zrn_a_01_97	995	209	0.01016	0.00046	0.04820	0.00527	0.16	65.17	2.93	2.93
1342_002_Zrn_a_01_98	245	116	0.04094	0.00196	0.05074	0.00516	0.24	258.63	12.12	12.11
1342_002_Zrn_a_01_99	912	451	0.01527	0.00057	0.04807	0.00362	0.25	97.72	3.64	3.64
1342_002_Zrn_a_01_100	142	59	0.01061	0.00070	0.05287	0.01163	0.09	68.06	4.45	4.45
1342_002_Zrn_a_01_101	498	140	0.01104	0.00090	0.04658	0.00706	0.14	70.75	5.71	5.71
1342_002_Zrn_a_01_102	597	336	0.02846	0.00105	0.04966	0.00334	0.26	180.91	6.57	6.56
1342_002_Zrn_a_01_103	1480	686	0.00873	0.00034	0.04776	0.00545	0.12	56.06	2.17	2.17
1342_002_Zrn_a_01_104	463	245	0.03178	0.00106	0.04927	0.00329	0.26	201.67	6.62	6.62
1342_002_Zrn_a_01_105	441	181	0.00896	0.00062	0.04416	0.00883	0.10	0.00	0.00	0.00
1342_002_Zrn_a_01_106	1070	641	0.05890	0.00235	0.05489	0.00267	0.51	368.91	14.31	14.29
1342_002_Zrn_a_01_107	281	201	0.02971	0.00127	0.05119	0.00526	0.18	188.72	7.95	7.95
1342_002_Zrn_a_01_108	4028	1989	0.00916	0.00045	0.04706	0.00356	0.37	58.75	2.88	2.88
1342_002_Zrn_a_01_109	237	67	0.03003	0.00190	0.05165	0.00658	0.31	190.73	11.88	11.87
1342_002_Zrn_a_01_110	244	54	0.02765	0.00151	0.04895	0.00806	0.17	175.83	9.47	9.47
1342_002_Zrn_a_01_111	795	349	0.06119	0.00245	0.05123	0.00273	0.45	382.85	14.92	14.90
1342_002_Zrn_a_01_112	575	175	0.01197	0.00064	0.05006	0.00914	0.20	76.71	4.10	4.09
1342_002_Zrn_a_01_113	154	25	0.00787	0.00096	0.06162	0.02231	0.06	50.55	6.16	6.15
1342_002_Zrn_a_01_114	584	318	0.14258	0.00743	0.07184	0.00328	0.68	894.11	37.16	36.49
1342_002_Zrn_a_01_115	835	339	0.02808	0.00106	0.05057	0.00305	0.40	178.55	6.63	6.63
1342_002_Zrn_a_01_116	2257	1331	0.01436	0.00081	0.04863	0.00418	0.31	91.93	5.14	5.13
1342_002_Zrn_a_01_117	1039	412	0.00929	0.00041	0.04971	0.00458	0.14	59.63	2.60	2.60
1342_002_Zrn_a_01_118	1226	338	0.00168	0.00013	0.04745	0.01162	0.11	10.79	0.81	0.81
1342_002_Zrn_a_01_119	494	75	0.02885	0.00113	0.05168	0.00422	0.22	183.32	7.06	7.06
1342_002_Zrn_a_01_120	566	204	0.01256	0.00057	0.05079	0.00597	0.07	80.47	3.63	3.63

Table B.3. Grubstake and Porcupine tephra updated $^{40}Ar/^{39}Ar$ ages.

Grubstake Tephra Bed		Old dates		Updated dates		Porcupine Tephra Bed		Old dates		Updated dates	
Sample name	Mineral Phase	Age (Ma)	Uncertainty (Ma)	Age (Ma)	Uncertainty (Ma)	Sample name	Mineral Phase	Age (Ma)	Uncertainty (Ma)	Age (Ma)	Uncertainty (Ma)
Grubstake BI#L3	biotite	6.900	0.100	6.866	0.154	K-90-8-20A	biotite	6.580	0.246	6.645	0.246
Grubstake BI#L4	biotite	6.800	0.100	6.774	0.167	K-90-8-21A	biotite	6.560	0.84	6.625	0.849
Grubstake PAG#L4	plagioclase	7.000	0.500	6.988	1.063	K-90-8-21A	plagioclase	6.580	0.11	6.645	0.109
	Age (Ma)	Uncertainty (Ma)	MSWD			Age (Ma)	Uncertainty (Ma)	MSWD			
Weighted Average age	6.83	0.11	0.37			6.66	0.10	0.00			
Ages with +/- 2 sigma uncertainty											

References:

Kunk, M.J. and Cortesini, H., 1992. *40Ar/39Ar Age-spectrum Data for Whole Rock Basalts, and Plagioclase and Biotite from Tephra: A Traverse Down the Porcupine River, East-central Alaska* (p. 81). US Department of the Interior, Geological Survey.

Triplehorn, D.M., Drake, J., Layer, P.W., Pinney, D.S. and Davis, P.K., 2000. Preliminary 40Ar/39Ar ages from two units in the Usibelli Group, Healy, Alaska: New light on some old problems. *Short Notes on Alaska Geology*, pp.117-127.

Table B.4. Grubstake and Porcupine tephra $^{40}Ar/^{39}Ar$ isotopic data.

Grubstake Recalculated (Triplehorn et al., 1999)

L=laser

BI= Biotite

PLAG-Plagocalise

Grubstake BI#L3

Weighted average of J from standards = 2.585e-04 ± 6.029e-07 (1-sigma error)

Days since irradiation = 263

Laser Power (mW)	Cumulative 39Ar	40Ar mV	± mV	39Ar mV	± mV	38Ar mV	± mV	37Ar mV	± mV	36Ar mV	± mV	% Atm. 40Ar	±	Ca/K	±	40Ar*/39ArK	±	Age (Ma)	± (Ma)
3	1	1933.9	2.7439	58.352	0.2049	5.1433	0.0706	-2.5	4.6274	3.6217	0.0289	55.4	0.45	-0.08	0.1455	14.768	0.1626	6.866	0.151
Integrated		1933.9	2.7439	58.352	0.2049	5.1433	0.0706	-2.5	4.6274	3.6217	0.0289	55.4	0.45	-0.08	0.1455	14.768	0.1626	6.866	0.151

Grubstake BI#L4

Weighted average of J from standards = 2.585e-04 ± 6.029e-07 (1-sigma error)

Days since irradiation = 263

Laser Power (mW)	Cumulative 39Ar	40Ar mV	± mV	39Ar mV	± mV	38Ar mV	± mV	37Ar mV	± mV	36Ar mV	± mV	% Atm. 40Ar	±	Ca/K	±	40Ar*/39ArK	±	Age (Ma)	± (Ma)
500	0.0305	868.6	0.4454	2.9487	0.0574	0.7771	0.0458	-2	6.3201	2.7522	0.0327	93.66	1.12	-1.249	3.929	18.667	3.3101	8.675	0.3069
1000	0.0782	237.7	0.5292	4.6224	0.1009	0.4645	0.0213	-1.1	6.029	0.5631	0.0199	70.08	2.48	-0.428	2.3924	15.372	1.3279	7.147	1.2323
2000	0.1536	279.94	0.3768	7.3027	0.0478	0.6388	0.0345	-0.5	6.6193	0.5802	0.028	61.31	2.96	-0.135	1.663	14.817	1.1403	6.889	1.0584
7000	0.3022	541.97	0.6058	14.38	0.1043	1.292	0.0271	-3.3	5.0867	1.0434	0.0257	56.99	1.4	-0.416	0.6489	16.196	0.5434	7.529	0.5042
7001	1	1247.2	1.5404	67.575	0.2912	5.3089	0.043	-3.5	5.407	0.8714	0.0245	20.7	0.58	-0.094	0.1468	14.611	0.1266	6.794	0.1175
Integrated		3175.4	1.8331	96.828	0.3339	8.4814	0.0795	-10.4	13.237	5.8105	0.0593	54.15	0.55	-0.196	0.2508	15.022	0.1895	6.984	0.1789

Grubstake PLAG#L4

Weighted average of J from standards = 2.585e-04 ± 6.029e-07 (1-sigma error)

Days since irradiation = 263

Laser Power	Cumulative	40Ar	±	39Ar	±	38Ar	±	37Ar	±	36Ar	±	% Atm.	±	Ca/K	±	40Ar*/39ArK	±	Age	±

(mW)	39Ar	mV	mV	mV	mV	mV	mV	mV	mV	mV	mV	40Ar						(Ma)	(Ma)
500	0.1478	56.29	0.4695	1.8409	0.0575	0.1252	0.0249	4.8	4.1362	0.0874	0.0171	45.22	8.98	4.804	4.1406	16.764	2.8159	7.792	2.6122
1000	0.2457	23.36	0.2901	1.2154	0.0779	0.0317	0.0181	-1.1	3.9872	0.0208	0.0126	26.77	15.98	-1.683	6.0128	14.045	3.2172	6.531	2.9866
2000	0.3689	32.254	0.392	1.5352	0.0431	0.062	0.0187	5.6	5.6139	0.0144	0.0163	11.81	14.94	6.7547	6.7473	18.551	3.2157	8.621	2.9817
3000	0.6723	55.829	0.2314	3.7793	0.06	0.075	0.0211	9.6	4.7822	0.0017	0.0168	-0.52	8.94	4.6685	2.3313	14.847	1.3473	6.903	1.2505
7000	1	68.193	0.4902	4.0801	0.087	0.0927	0.0189	10.2	4.2822	0.0213	0.0168	8.03	7.28	4.5808	1.935	15.371	1.2694	7.146	1.178
Integrated		235.93	0.8672	12.451	0.1497	0.3867	0.0459	29.1	10.282	0.1457	0.0358	17.26	4.49	4.2954	1.5212	15.68	0.8778	7.284	0.8152

Irradiations done at McMaster Nuuclear Reactor: (39Ar/37Ar)Ca = 0.000706, (36Ar/37Ar)Ca = 0.000279, (40Ar/39Ar)K = 0.0297

Atomospheric 40Ar/36Ar= 295.5 (Steigerand Jäger, 1977)

Standard: Bern=4B biotite with an age of 17.3 (Hall et al., 1984)

Ages with +/- 2 sigma uncertainty were calculated using the decay constants of Renne et al, 2010.

Laser (mW): Laser power for each step of the step-heating experiment

40Ar, 39Ar, and 37Ar: Isotopic measurements corrected for system blank and decay of 37Ar and 39Ar

Ca/K: Calcium to potassium ratio as determined from 37Ar produced from 40Ca and 39Ar produced from 39K

Cl/K: chlorine to potassium ratio as determined from 38Ar produced from 37Cl and 39Ar produced from 39K

40Ar*/39ArK: ratio of radiogenic argon 40 to reactor-produced 39Ar from potassium, corrected for reactor interferences

mV: millivolts

Masses are blank and decay corrected

References:

Hall, C.M., Walter, R.C., Westgate, J.A. and York, D., 1984. Geochronology, stratigraphy and geochemistry of Cindery Tuff in Pliocene hominid-bearing sediments of the Middle Awash, Ethiopia. *Nature*, *308*(5954), pp.26-31.

Renne, P.R., Mundil, R., Balco, G., Min, K. and Ludwig, K.R., 2010. Joint determination of 40K decay constants and 40Ar∗/40K for the Fish Canyon sanidine standard, and improved accuracy for 40Ar/39Ar geochronology. *Geochimica et Cosmochimica Acta*, *74*(18), pp.5349-5367.

Steiger, R.H. and Jäger, E., 1977. Subcommission on geochronology: convention on the use of decay constants in geo-and cosmochronology. *Earth and planetary science letters*, *36*(3), pp.359-362.

Triplehorn, D.M., Drake, J., Layer, P.W., Pinney, D.S. and Davis, P.K., 1999. Preliminary 40Ar/39Ar ages from two units in the Usibelli Group, Healy, Alaska: New light on some old problems. *Short Notes on Alaska Geology*, pp.117-127.

Table B.5. Major element glass geochemical data.

Analysed on a JEOL JXA-8900R electron microprobe with 5 WDS spectrometers using a 5 micron beam, 6nA current and 15KeV with Na time dependent intensity corrections
Secondary standard values of ID3506 are non-normalized and uncorrected (excluding TDI). Old Crow standard values are normalized and corrected.
Consistently high Al2O3 values throughout run (see ID3506) were corrected by multiplying Al2O3 with (published ID3506 Al2O3 value/average run Al2O3 value)

Published values of secondary standards (Kuehn et al., 2011) recalucated without P2O5 are as follows:

Old Crow	75.29	0.31	13.05	1.69	0.05	0.29	1.49	3.82	3.72	0.28	100.00
	1.40	0.05	0.30	0.12	0.02	0.02	0.05	0.38	0.28	0.05	-
ID 3506	74.10	0.07	13.10	1.55	0.07	0.04	0.73	4.07	5.11	0.34	99.18
	1.40	0.02	0.05	0.05	0.03	0.02	0.06	0.22	0.27	0.05	-

SAMPLE	SiO2	TiO2	Al2O3	FeO	MnO	MgO	CaO	Na2O	K2O	Cl	TOTAL	H2Odiff	Tephra ID/comments
ID3506 1-6_1	74.28	0.03	13.42	1.58	0.05	0.04	0.76	4.09	5.13	0.29	99.61	0.39	
ID3506 1-6_2	74.14	0.09	13.43	1.64	0.09	0.03	0.78	3.93	5.00	0.31	99.38	0.62	
ID3506 1-6_3	74.08	0.14	13.44	1.63	0.07	0.03	0.72	4.09	4.93	0.33	99.39	0.61	
ID3506 1-6_4	73.95	0.05	13.32	1.58	0.05	0.05	0.71	4.03	5.25	0.34	99.25	0.75	
ID3506 1-6_5	73.80	0.08	13.26	1.58	0.09	0.06	0.79	4.10	5.07	0.31	99.08	0.92	
ID3506 1-6_6	73.57	0.13	13.42	1.65	0.11	0.02	0.76	3.97	5.16	0.35	99.05	0.95	
Mean	73.97	0.09	13.38	1.61	0.08	0.04	0.75	4.03	5.09	0.32	99.29	0.71	
StDev	0.26	0.04	0.07	0.03	0.02	0.02	0.03	0.07	0.12	0.02	0.21	0.21	
Old Crow 1-6_1	75.53	0.30	13.32	1.74	0.06	0.28	1.46	3.48	3.59	0.32	100.00	4.54	
Old Crow 1-6_2	75.53	0.35	13.05	1.64	0.08	0.28	1.53	3.67	3.64	0.29	100.00	3.02	
Old Crow 1-6_3	74.89	0.28	13.11	1.79	0.09	0.31	1.52	4.04	3.73	0.29	100.00	2.59	
Old Crow 1-6_4	75.20	0.34	13.16	1.75	0.10	0.33	1.53	3.79	3.59	0.27	100.00	3.75	
Old Crow 1-6_5	75.43	0.37	12.92	1.71	0.04	0.29	1.47	3.89	3.65	0.28	100.00	4.61	
Mean	75.31	0.33	13.11	1.72	0.07	0.30	1.50	3.78	3.64	0.29	100.00	3.70	
StDev	0.27	0.04	0.14	0.06	0.02	0.02	0.03	0.21	0.06	0.02	0.00	0.90	
UA 4024_16	77.64	0.18	12.60	0.76	0.06	0.10	0.61	3.27	4.74	0.06	100.00	5.76	Grubstake
UA 4024_21	77.80	0.13	12.56	0.82	0.05	0.10	0.67	3.55	4.24	0.10	100.00	5.34	
UA 4024_4	77.97	0.15	12.54	0.82	0.03	0.08	0.60	3.03	4.72	0.08	100.00	5.13	
UA 4024_1	78.01	0.15	12.34	0.81	0.00	0.10	0.56	3.49	4.48	0.07	100.00	4.49	
UA 4024_7	78.02	0.18	12.32	0.79	0.01	0.13	0.59	3.21	4.69	0.08	100.00	4.89	
UA 4024_18	78.03	0.08	12.50	0.81	0.02	0.12	0.55	3.06	4.79	0.06	100.00	5.38	
UA 4024_12	78.04	0.18	12.52	0.83	0.06	0.13	0.65	3.26	4.30	0.05	100.00	5.54	
UA 4024_17	78.10	0.13	12.46	0.78	0.03	0.12	0.60	3.06	4.66	0.07	100.00	5.69	
UA 4024_14	78.11	0.18	12.44	0.69	0.00	0.12	0.64	3.22	4.57	0.04	100.00	6.11	
UA 4024_25	78.13	0.15	12.21	0.73	0.05	0.12	0.56	3.75	4.26	0.06	100.00	5.27	
UA 4024_5	78.17	0.19	12.49	0.79	0.00	0.11	0.65	3.45	4.13	0.03	100.00	5.67	
UA 4024_20	78.20	0.13	12.37	0.82	0.01	0.14	0.62	3.15	4.50	0.06	100.00	5.63	
UA 4024_3	78.28	0.14	12.32	0.81	0.02	0.10	0.60	3.36	4.32	0.08	100.00	4.98	
UA 4024_23	78.31	0.12	12.53	0.79	0.01	0.09	0.64	3.24	4.25	0.04	100.00	5.50	
UA 4024_19	78.33	0.20	12.46	0.76	0.05	0.11	0.57	3.32	4.16	0.05	100.00	5.45	
UA 4024_15	78.38	0.21	12.08	0.80	0.02	0.12	0.60	3.38	4.37	0.07	100.00	5.06	
UA 4024_10	78.38	0.11	12.27	0.77	0.03	0.13	0.57	2.90	4.77	0.09	100.00	4.91	
UA 4024_6	78.40	0.24	12.02	0.85	0.03	0.15	0.58	3.31	4.38	0.06	100.00	4.95	
UA 4024_11	78.43	0.17	12.20	0.77	0.01	0.10	0.60	3.19	4.48	0.07	100.00	4.90	
UA 4024_13	78.48	0.15	12.32	0.83	0.05	0.12	0.58	3.19	4.23	0.08	100.00	5.37	
UA 4024_8	78.50	0.20	12.11	0.83	0.00	0.12	0.64	3.14	4.42	0.06	100.00	4.51	
UA 4024_22	78.52	0.16	12.23	0.79	0.02	0.12	0.58	3.13	4.42	0.05	100.00	5.36	
UA 4024_9	78.59	0.09	12.33	0.71	0.00	0.10	0.62	3.05	4.46	0.07	100.00	5.15	
UA 4024_24	78.70	0.15	12.17	0.79	0.00	0.10	0.64	3.19	4.25	0.03	100.00	4.87	

UA 4024_2	78.72	0.19	12.28	0.78	0.04	0.10	0.61	2.91	4.34	0.04	100.00	5.38	
Mean	78.25	0.16	12.35	0.79	0.02	0.11	0.61	3.23	4.44	0.06	100.00	5.25	
St. Dev	0.27	0.04	0.16	0.04	0.02	0.02	0.03	0.20	0.20	0.02	0.00	0.39	
UT 1143_24	77.85	0.11	12.71	0.70	0.09	0.06	0.47	3.94	4.02	0.08	100.00	4.93	Canyon Village
UT 1143_25	78.02	0.12	12.59	0.68	0.03	0.07	0.45	3.91	4.06	0.08	100.00	4.70	
UT 1143_5	78.07	0.08	12.49	0.69	0.03	0.06	0.45	3.93	4.13	0.07	100.00	4.63	
UT 1143_9	78.17	0.13	12.40	0.70	0.02	0.08	0.46	3.89	4.09	0.07	100.00	4.02	
UT 1143_13	78.17	0.05	12.37	0.73	0.04	0.05	0.45	3.80	4.29	0.06	100.00	4.33	
UT 1143_3	78.20	0.10	12.44	0.81	0.03	0.08	0.49	3.49	4.31	0.07	100.00	4.66	
UT 1143_12	78.21	0.12	12.43	0.64	0.00	0.08	0.45	3.82	4.21	0.06	100.00	4.49	
UT 1143_8	78.21	0.07	12.33	0.69	0.04	0.06	0.48	3.76	4.30	0.07	100.00	3.44	
UT 1143_22	78.25	0.12	12.43	0.67	0.03	0.08	0.47	3.69	4.19	0.08	100.00	5.29	
UT 1143_23	78.27	0.10	12.39	0.67	0.02	0.06	0.47	3.92	4.04	0.07	100.00	6.19	
UT 1143_20	78.29	0.08	12.51	0.72	0.04	0.08	0.50	3.65	4.06	0.08	100.00	4.63	
UT 1143_14	78.29	0.08	12.49	0.75	0.08	0.07	0.48	3.69	4.03	0.05	100.00	5.19	
UT 1143_1	78.31	0.11	12.56	0.70	0.00	0.04	0.44	3.57	4.21	0.08	100.00	5.05	
UT 1143_4	78.35	0.14	12.40	0.65	0.06	0.07	0.45	3.53	4.29	0.08	100.00	4.80	
UT 1143_19	78.37	0.11	12.37	0.72	0.05	0.10	0.43	3.45	4.35	0.06	100.00	3.42	
UT 1143_2	78.38	0.06	12.40	0.69	0.00	0.08	0.47	3.62	4.24	0.08	100.00	3.82	
UT 1143_18	78.39	0.14	12.54	0.71	0.05	0.04	0.44	3.67	3.98	0.07	100.00	4.41	
UT 1143_11	78.44	0.09	12.28	0.70	0.03	0.05	0.46	3.68	4.18	0.11	100.00	4.20	
UT 1143_6	78.47	0.12	12.37	0.71	0.01	0.04	0.47	3.92	3.83	0.07	100.00	4.34	
UT 1143_7	78.53	0.08	12.40	0.66	0.05	0.07	0.47	3.51	4.18	0.06	100.00	4.22	
UT 1143_16	78.55	0.09	12.30	0.73	0.06	0.04	0.49	3.44	4.25	0.04	100.00	4.98	
UT 1143_17	78.56	0.12	12.44	0.70	0.03	0.03	0.48	3.65	3.93	0.07	100.00	4.73	
UT 1143_15	78.60	0.15	12.17	0.73	0.00	0.07	0.48	3.60	4.14	0.07	100.00	4.58	
UT 1143_10	78.63	0.11	12.48	0.76	0.00	0.05	0.46	3.43	4.02	0.06	100.00	5.30	
UT 1143_21	79.01	0.13	12.39	0.64	0.04	0.06	0.46	3.49	3.75	0.05	100.00	6.54	
Mean	78.34	0.11	12.43	0.70	0.03	0.06	0.46	3.68	4.12	0.07	100.00	4.68	
St. Dev	0.23	0.03	0.11	0.04	0.02	0.02	0.02	0.17	0.15	0.01	0.00	0.71	
Old Crow 7-10_1	75.19	0.38	13.15	1.73	0.07	0.30	1.53	3.83	3.62	0.27	100.00	2.35	
Old Crow 7-10_2	75.75	0.34	12.95	1.68	0.02	0.29	1.56	3.66	3.52	0.29	100.00	2.66	
Old Crow 11-14_2	75.68	0.35	13.04	1.73	0.09	0.31	1.50	3.56	3.54	0.27	100.00	3.82	
Old Crow 11-14_3	75.28	0.32	13.14	1.69	0.04	0.29	1.54	3.79	3.70	0.27	100.00	2.40	
Mean	75.47	0.35	13.07	1.71	0.05	0.30	1.53	3.71	3.59	0.27	100.00	2.81	
StDev	0.28	0.02	0.09	0.02	0.03	0.01	0.03	0.12	0.08	0.01	0.00	0.69	
ID3506 7-10_1	73.99	0.06	13.34	1.60	0.06	0.04	0.72	3.96	5.24	0.32	99.27	0.73	
ID3506 7-10_2	74.22	0.09	13.55	1.56	0.04	0.05	0.76	3.94	5.16	0.31	99.62	0.38	
ID3506 7-10_3	73.81	0.11	13.33	1.49	0.03	0.02	0.71	4.13	5.27	0.32	99.15	0.85	
ID3506 7-10_4	74.23	0.08	13.32	1.61	0.09	0.06	0.79	4.18	5.10	0.34	99.71	0.29	
Mean	74.06	0.08	13.39	1.56	0.06	0.04	0.74	4.05	5.19	0.32	99.44	0.56	
StDev	0.20	0.02	0.11	0.06	0.03	0.02	0.04	0.12	0.08	0.01	0.27	0.27	

Table B6. Trace element glass geochemical data.

Trace element data collected on a Resolution ArF 193 nm excimer laser system with a Laurin-technic S155 2-volume ablation cell and sector-field ICPMS Thermo Element XR
Samples were analyzed with a 23 µm spot size, 5 Hz frequency, and 3 J/cm2 fluence.
Calibration was performed using NIST SRM 612 in conjunction with internal standardization using 29Si. The mass content of Si was determined from WDS-EPMA.
All data were reduced offline using Iolite v3 (Paton et al., 2011; https://iolite-software.com/)

	UA4024 (ppm)	UT1143 (ppm)
Ti	951	663
Ga	15	15
Rb	104	98
Sr	60	32
Y	13	20
Zr	94	82
Nb	7	11
Cs	3	2
Ba	815	731
La	22	30
Ce	43	59
Pr	4	6
Nd	15	19
Sm	2	3
Eu	0	0
Gd	2	3
Tb	0	0
Dy	2	3
Ho	0	1
Er	1	2
Tm	0	0
Yb	2	3
Lu	0	0
Hf	3	3
Ta	1	1
Pb	12	14
Th	10	11
U	5	5

APPENDIX C: CHAPTER 4

Table C.1. U-Th zircon data corrected using Bishop Tuff reference material zircon.

Sample ID	Th (ppm)	U (ppm)	Th/U	$(^{238}U)/(^{232}Th)$	±1s	$(^{230}Th)/(^{232}Th)$	±1s	$(^{230}Th)/(^{238}U)$	±1s	f230 (ppm)	±1s
Bishop Tuff used for correction Thabund. = 4.38±0.13 ppm (SE)											
BIshopTuff-1 June 2022	1264	2410	0.5	6.04	0.47	6.65	0.32	1.10	0.10	6.62	0.65
BIshopTuff-1 June 2022	2391	3089	0.7	4.09	0.18	4.25	0.14	1.04	0.06	4.69	0.26
BIshopTuff-1 June 2022	945	1775	0.5	5.95	0.22	6.14	0.19	1.03	0.05	4.34	0.21
BIshopTuff-1 June 2022	1495	2672	0.5	5.66	0.21	6.08	0.19	1.08	0.05	5.70	0.29
BIshopTuff-1 June 2022	883	1968	0.4	7.06	0.25	7.59	0.22	1.08	0.05	5.89	0.26
BIshopTuff-1 June 2022	3428	4128	0.8	3.81	0.10	3.96	0.11	1.04	0.04	4.68	0.17
BIshopTuff-1 June 2022	3275	4012	0.8	3.88	0.19	3.97	0.14	1.02	0.06	4.38	0.26
BIshopTuff-1 June 2022	1389	2423	0.5	5.52	0.15	5.61	0.15	1.02	0.04	3.88	0.14
BIshopTuff-1 June 2022	1298	2392	0.5	5.83	0.25	6.23	0.20	1.07	0.06	5.50	0.29
BIshopTuff-1 June 2022	988	1766	0.5	5.66	0.19	5.89	0.17	1.04	0.05	4.64	0.19
BIshopTuff-1 June 2022	1129	1844	0.6	5.17	0.39	5.38	0.26	1.04	0.09	4.63	0.42
BIshopTuff-1 June 2022	1751	2675	0.6	4.84	0.15	4.92	0.14	1.02	0.04	4.08	0.16
BIshopTuff-1 June 2022	3469	4545	0.7	4.15	0.12	4.28	0.12	1.03	0.04	4.50	0.17
BIshopTuff-1 June 2022	1195	2370	0.5	6.27	0.54	6.42	0.33	1.02	0.10	4.03	0.44
BIshopTuff-1 June 2022	1122	2289	0.5	6.46	0.38	6.94	0.28	1.08	0.08	5.79	0.45
BIshopTuff-1 June 2022	265	1530	0.2	18.28	0.54	19.29	0.94	1.06	0.06	5.44	0.21
BIshopTuff-1 June 2022	2026	3497	0.5	5.46	0.26	5.52	0.19	1.01	0.06	3.74	0.22
BIshopTuff-1 June 2022	2286	3683	0.6	5.10	0.06	5.27	0.13	1.03	0.03	4.44	0.09
BIshopTuff-1 June 2022	1651	2776	0.6	5.32	0.12	5.33	0.14	1.00	0.04	3.50	0.13
BIshopTuff-1 June 2022	1996	3100	0.6	4.92	0.11	4.87	0.13	0.99	0.03	3.35	0.11
BIshopTuff-1 June 2022	786	1456	0.5	5.86	0.60	5.91	0.35	1.01	0.12	3.63	0.48
BIshopTuff-1 June 2022	1564	2428	0.6	4.91	0.31	4.98	0.20	1.01	0.08	3.95	0.30
BIshopTuff-1 June 2022	801	1726	0.4	6.82	0.10	7.12	0.19	1.04	0.03	4.71	0.15
BIshopTuff-1 June 2022	1416	2266	0.6	5.06	0.14	5.15	0.16	1.02	0.04	4.04	0.18
BIshopTuff-1 June 2022	2713	3375	0.8	3.94	0.25	3.95	0.16	1.00	0.07	3.91	0.28
BIshopTuff-1 June 2022	895	1850	0.5	6.54	0.18	6.67	0.19	1.02	0.04	3.84	0.15
BIshopTuff-1 June 2022	1193	2324	0.5	6.17	0.25	6.34	0.20	1.03	0.05	4.16	0.22
BIshopTuff-1 June 2022	2340	3128	0.7	4.23	0.26	4.15	0.16	0.98	0.07	3.33	0.25
BIshopTuff-1 June 2022	2085	3243	0.6	4.92	0.36	5.19	0.23	1.05	0.09	5.01	0.44
BIshopTuff-1 June 2022	1976	2913	0.6	4.67	0.07	4.80	0.08	1.03	0.02	4.39	0.13
										Average	**S.E.**
										4.38	**0.13**
Bishop Tuff used for correction Thabund. = 4.38±0.13 ppm (SE)											
91500 June 2022	30	80	0.4	8.43	0.19	9.09	1.07	1.08	0.10		
91500 June 2022	23	82	0.3	11.23	0.30	12.07	1.71	1.07	0.12		
91500 June 2022	30	81	0.4	8.43	0.18	8.82	1.23	1.05	0.11		
91500 June 2022	31	81	0.4	8.35	0.20	8.35	0.99	1.00	0.09		
91500 June 2022	30	80	0.4	8.35	0.21	7.88	0.81	0.94	0.07		
91500 June 2022	31	81	0.4	8.34	0.21	7.35	1.06	0.88	0.10		
91500 June 2022	29	79	0.3	8.57	0.21	7.47	1.18	0.87	0.10		
91500 June 2022	30	81	0.3	8.58	0.20	7.31	1.25	0.85	0.11		

91500 June 2022	29	78	0.3	8.55	0.20	6.81	1.38	0.80	0.11
91500 June 2022	30	79	0.4	8.40	0.22	9.84	1.02	1.17	0.14
91500 June 2022	31	83	0.4	8.46	0.21	9.88	0.98	1.17	0.15
91500 June 2022	33	88	0.4	8.44	0.19	9.85	1.22	1.17	0.17
91500 June 2022	29	79	0.4	8.47	0.22	9.80	1.10	1.16	0.17
91500 June 2022	27	79	0.3	9.35	0.23	9.65	0.89	1.03	0.14
91500 June 2022	28	75	0.4	8.37	0.14	8.43	1.10	1.01	0.17
91500 June 2022	27	75	0.3	8.67	0.21	8.69	0.93	1.00	0.14
91500 June 2022	27	75	0.3	8.67	0.21	8.67	1.56	1.00	0.21
91500 June 2022	30	79	0.4	8.40	0.18	9.11	1.12	1.08	0.17
91500 June 2022	30	79	0.4	8.40	0.19	9.07	0.89	1.08	0.14
91500 June 2022	30	79	0.4	8.38	0.20	8.25	1.51	0.98	0.21
91500 June 2022	30	80	0.4	8.37	0.19	8.91	0.72	1.06	0.11
91500 June 2022	31	82	0.4	8.40	0.18	8.94	0.89	1.06	0.14
91500 June 2022	30	80	0.4	8.38	0.20	8.85	1.01	1.06	0.15
91500 June 2022	31	81	0.4	8.38	0.20	8.09	1.13	0.97	0.18
91500 June 2022	30	81	0.4	8.43	0.21	8.00	1.01	0.95	0.15
91500 June 2022	31	83	0.4	8.42	0.23	8.64	0.86	1.03	0.12
91500 June 2022	23	81	0.3	11.18	0.37	10.31	1.27	0.92	0.15
91500 June 2022	30	80	0.4	8.48	0.20	7.72	1.03	0.91	0.16
91500 June 2022	31	82	0.4	8.41	0.19	7.68	0.97	0.91	0.16
91500 June 2022	31	84	0.4	8.48	0.21	8.34	1.04	0.98	0.16
91500 June 2022	29	77	0.4	8.43	0.22	7.38	0.95	0.88	0.15
91500 June 2022	32	83	0.4	8.35	0.19	7.28	0.88	0.87	0.15
91500 June 2022	30	81	0.4	8.45	0.19	7.24	0.97	0.86	0.15
91500 June 2022	27	75	0.3	8.81	0.23	7.39	1.18	0.84	0.17
91500 June 2022	31	81	0.4	8.38	0.20	7.08	0.89	0.85	0.14
91500 June 2022	31	82	0.4	8.40	0.22	7.08	0.92	0.84	0.15
91500 June 2022	29	79	0.3	8.55	0.24	6.91	1.37	0.81	0.13
91500 June 2022	28	76	0.3	8.76	0.23	6.99	2.17	0.80	0.20
91500 June 2022	31	81	0.4	8.37	0.18	6.67	1.29	0.80	0.13
91500 June 2022	30	80	0.4	8.35	0.21	6.56	1.77	0.79	0.17

Bishop Tuff used for correction Thabund. = 4.38±0.13 ppm (SE)

plesovice	48	513	0.1	33.64	0.70	35.68	1.21	1.06	0.04
plesovice	29	309	0.1	33.67	1.36	31.80	1.30	0.94	0.05
plesovice	58	599	0.1	32.67	0.61	33.05	1.17	1.01	0.04
plesovice	78	757	0.1	30.89	0.72	31.54	1.01	1.02	0.04
plesovice	77	744	0.1	30.66	0.81	28.06	0.88	0.92	0.04
plesovice	64	659	0.1	32.36	0.80	34.31	1.04	1.06	0.04
plesovice	108	855	0.1	25.02	0.49	24.98	0.68	1.00	0.03
plesovice	78	770	0.1	31.34	0.78	29.71	1.04	0.95	0.04
plesovice	102	879	0.1	27.18	0.84	28.38	1.15	1.04	0.05
plesovice	80	780	0.1	30.96	1.65	30.88	0.98	1.00	0.06
plesovice	72	722	0.1	31.61	0.93	34.73	1.25	1.10	0.05
plesovice	67	670	0.1	31.86	0.94	34.81	1.23	1.09	0.05
plesovice	55	582	0.1	33.28	0.93	34.40	2.41	1.03	0.08
plesovice	71	720	0.1	32.22	0.78	30.40	2.03	0.94	0.07
plesovice	77	756	0.1	31.12	0.73	33.40	2.29	1.07	0.08

plesovice	80	782	0.1	30.80	0.78	30.74	2.06	1.00	0.07
plesovice	78	770	0.1	31.17	0.76	30.83	2.08	0.99	0.07
plesovice	77	761	0.1	31.26	0.82	31.67	2.21	1.01	0.08
plesovice	64	640	0.1	31.76	1.47	30.70	2.25	0.97	0.08
plesovice	96	863	0.1	28.54	1.06	30.61	2.19	1.07	0.09
plesovice	120	1120	0.1	29.63	0.87	30.02	1.98	1.01	0.07
plesovice	53	499	0.1	29.58	0.98	29.64	2.13	1.00	0.08
plesovice	89	827	0.1	29.37	0.60	28.55	1.98	0.97	0.07
plesovice	73	717	0.1	30.90	1.06	31.87	2.22	1.03	0.08
plesovice	53	539	0.1	32.30	1.18	33.09	2.37	1.02	0.08
plesovice	68	679	0.1	31.60	0.75	31.33	2.22	0.99	0.07
plesovice	64	646	0.1	32.17	0.92	29.47	2.04	0.92	0.07
plesovice	94	842	0.1	28.35	0.45	29.60	2.03	1.04	0.07
plesovice	61	635	0.1	32.89	0.81	31.44	2.19	0.96	0.07

Table C.2. U-Th zircon data corrected using Ice River reference material perovskite.

Sample ID	Th (ppm)	U (ppm)	Th/U	(^{238}U)/(^{232}Th)	±1s	(^{230}Th)/(^{232}Th)	±1s	(^{230}Th)/(^{238}U)	±1s
Ice River perovskite used for correction $Th_{abund.}$ = 4.16±0.06 ppm (1SD)									
BIshopTuff-1 June 2022	1264	2410	0.5	6.04	0.47	6.80	0.29	1.13	0.10
BIshopTuff-1 June 2022	2391	3089	0.7	4.09	0.18	4.39	0.11	1.07	0.05
BIshopTuff-1 June 2022	945	1775	0.5	5.95	0.22	6.28	0.14	1.06	0.05
BIshopTuff-1 June 2022	1495	2672	0.5	5.66	0.21	6.23	0.14	1.10	0.05
BIshopTuff-1 June 2022	883	1968	0.4	7.06	0.25	7.73	0.15	1.10	0.04
BIshopTuff-1 June 2022	3428	4128	0.8	3.81	0.10	4.10	0.07	1.08	0.03
BIshopTuff-1 June 2022	3275	4012	0.8	3.88	0.19	4.11	0.11	1.06	0.06
BIshopTuff-1 June 2022	1389	2423	0.5	5.52	0.15	5.75	0.10	1.04	0.03
BIshopTuff-1 June 2022	1298	2392	0.5	5.83	0.25	6.37	0.15	1.09	0.05
BIshopTuff-1 June 2022	988	1766	0.5	5.66	0.19	6.03	0.12	1.07	0.04
BIshopTuff-1 June 2022	1129	1844	0.6	5.17	0.39	5.52	0.24	1.07	0.09
BIshopTuff-1 June 2022	1751	2675	0.6	4.84	0.15	5.06	0.09	1.05	0.04
BIshopTuff-1 June 2022	3469	4545	0.7	4.15	0.12	4.42	0.08	1.07	0.04
BIshopTuff-1 June 2022	1195	2370	0.5	6.27	0.54	6.57	0.31	1.05	0.10
BIshopTuff-1 June 2022	1122	2289	0.5	6.46	0.38	7.08	0.25	1.10	0.08
BIshopTuff-1 June 2022	265	1530	0.2	18.28	0.54	19.44	0.35	1.06	0.04
BIshopTuff-1 June 2022	2026	3497	0.5	5.46	0.26	5.66	0.15	1.04	0.06
BIshopTuff-1 June 2022	2286	3683	0.6	5.10	0.06	5.41	0.05	1.06	0.02
BIshopTuff-1 June 2022	1651	2776	0.6	5.32	0.12	5.47	0.09	1.03	0.03
BIshopTuff-1 June 2022	1996	3100	0.6	4.92	0.11	5.01	0.08	1.02	0.03
BIshopTuff-1 June 2022	786	1456	0.5	5.86	0.60	6.06	0.33	1.03	0.12
BIshopTuff-1 June 2022	1564	2428	0.6	4.91	0.31	5.12	0.17	1.04	0.07
BIshopTuff-1 June 2022	801	1726	0.4	6.82	0.10	7.26	0.12	1.07	0.02
BIshopTuff-1 June 2022	1416	2266	0.6	5.06	0.14	5.30	0.11	1.05	0.04
BIshopTuff-1 June 2022	2713	3375	0.8	3.94	0.25	4.09	0.14	1.04	0.07
BIshopTuff-1 June 2022	895	1850	0.5	6.54	0.18	6.81	0.12	1.04	0.03
BIshopTuff-1 June 2022	1193	2324	0.5	6.17	0.25	6.48	0.15	1.05	0.05
BIshopTuff-1 June 2022	2340	3128	0.7	4.23	0.26	4.29	0.14	1.01	0.07
BIshopTuff-1 June 2022	2085	3243	0.6	4.92	0.36	5.33	0.21	1.08	0.09
BIshopTuff-1 June 2022	1976	2913	0.6	4.67	0.07	4.94	0.07	1.06	0.02
Ice River perovskite used for correction $Th_{abund.}$ = 4.16±0.06 ppm (1SD)									
91500 June 2022	30	80	0.4	8.43	0.19	9.23	1.04	1.09	0.13
91500 June 2022	23	82	0.3	11.23	0.30	12.21	1.67	1.09	0.15
91500 June 2022	30	81	0.4	8.43	0.18	8.97	1.20	1.06	0.14
91500 June 2022	31	81	0.4	8.35	0.20	8.49	0.96	1.02	0.12

91500 June 2022	30	80	0.4	8.35	0.21	8.02	0.78	0.96	0.10
91500 June 2022	31	81	0.4	8.34	0.21	7.49	1.04	0.90	0.13
91500 June 2022	29	79	0.3	8.57	0.21	7.61	1.15	0.89	0.14
91500 June 2022	30	81	0.3	8.58	0.20	7.45	1.23	0.87	0.14
91500 June 2022	29	78	0.3	8.55	0.20	6.95	1.35	0.81	0.16
91500 June 2022	30	79	0.4	8.40	0.22	9.98	1.00	1.19	0.12
91500 June 2022	31	83	0.4	8.46	0.21	10.02	0.95	1.18	0.12
91500 June 2022	33	88	0.4	8.44	0.19	9.99	1.20	1.18	0.14
91500 June 2022	29	79	0.4	8.47	0.22	9.95	1.08	1.17	0.13
91500 June 2022	27	79	0.3	9.35	0.23	9.79	0.86	1.05	0.10
91500 June 2022	28	75	0.4	8.37	0.14	8.57	1.08	1.02	0.13
91500 June 2022	27	75	0.3	8.67	0.21	8.83	0.91	1.02	0.11
91500 June 2022	27	75	0.3	8.67	0.21	8.81	1.54	1.02	0.18
91500 June 2022	30	79	0.4	8.40	0.18	9.25	1.10	1.10	0.13
91500 June 2022	30	79	0.4	8.40	0.19	9.21	0.87	1.10	0.11
91500 June 2022	30	79	0.4	8.38	0.20	8.39	1.49	1.00	0.18
91500 June 2022	30	80	0.4	8.37	0.19	9.05	0.70	1.08	0.09
91500 June 2022	31	82	0.4	8.40	0.18	9.08	0.86	1.08	0.11
91500 June 2022	30	80	0.4	8.38	0.20	8.99	0.98	1.07	0.12
91500 June 2022	31	81	0.4	8.38	0.20	8.23	1.11	0.98	0.13
91500 June 2022	30	81	0.4	8.43	0.21	8.14	0.99	0.97	0.12
91500 June 2022	31	83	0.4	8.42	0.23	8.78	0.83	1.04	0.10
91500 June 2022	23	81	0.3	11.18	0.37	10.45	1.24	0.93	0.12
91500 June 2022	30	80	0.4	8.48	0.20	7.87	1.01	0.93	0.12
91500 June 2022	31	82	0.4	8.41	0.19	7.82	0.95	0.93	0.12
91500 June 2022	31	84	0.4	8.48	0.21	8.49	1.02	1.00	0.12
91500 June 2022	29	77	0.4	8.43	0.22	7.52	0.93	0.89	0.11
91500 June 2022	32	83	0.4	8.35	0.19	7.42	0.86	0.89	0.10
91500 June 2022	30	81	0.4	8.45	0.19	7.38	0.95	0.87	0.11
91500 June 2022	27	75	0.3	8.81	0.23	7.54	1.16	0.86	0.13
91500 June 2022	31	81	0.4	8.38	0.20	7.22	0.87	0.86	0.11
91500 June 2022	31	82	0.4	8.40	0.22	7.22	0.90	0.86	0.11
91500 June 2022	29	79	0.3	8.55	0.24	7.05	0.80	0.83	0.10
91500 June 2022	28	76	0.3	8.76	0.23	7.14	1.36	0.81	0.16
91500 June 2022	31	81	0.4	8.37	0.18	6.81	0.74	0.81	0.09
91500 June 2022	30	80	0.4	8.35	0.21	6.70	1.05	0.80	0.13

Ice River perovskite used for correction Th$_{abund.}$ = 4.16±0.06 ppm (1SD)

plesovice	48	513	0.1	33.64	0.70	39.65	1.05	1.18	0.04
plesovice	29	309	0.1	33.67	1.36	38.30	1.33	1.14	0.06
plesovice	58	599	0.1	32.67	0.61	36.37	1.03	1.11	0.04

plesovice	78	757	0.1	30.89	0.72	34.07	0.82	1.10	0.04
plesovice	77	744	0.1	30.66	0.81	30.61	0.70	1.00	0.03
plesovice	64	659	0.1	32.36	0.80	37.32	0.79	1.15	0.04
plesovice	108	855	0.1	25.02	0.49	26.83	0.45	1.07	0.03
plesovice	78	770	0.1	31.34	0.78	32.23	0.90	1.03	0.04
plesovice	102	879	0.1	27.18	0.84	30.33	1.05	1.12	0.05
plesovice	80	780	0.1	30.96	1.65	33.33	0.77	1.08	0.06
plesovice	72	722	0.1	31.61	0.93	37.43	1.07	1.18	0.05
plesovice	67	670	0.1	31.86	0.94	37.73	1.05	1.18	0.05
plesovice	55	582	0.1	33.28	0.93	37.88	2.52	1.14	0.08
plesovice	71	720	0.1	32.22	0.78	33.16	2.10	1.03	0.07
plesovice	77	756	0.1	31.12	0.73	35.94	2.34	1.16	0.08
plesovice	80	782	0.1	30.80	0.78	33.18	2.11	1.08	0.07
plesovice	78	770	0.1	31.17	0.76	33.34	2.13	1.07	0.07
plesovice	77	761	0.1	31.26	0.82	34.21	2.27	1.09	0.08
plesovice	64	640	0.1	31.76	1.47	33.74	2.36	1.06	0.09
plesovice	96	863	0.1	28.54	1.06	32.69	2.23	1.15	0.09
plesovice	120	1120	0.1	29.63	0.87	31.71	1.98	1.07	0.07
plesovice	53	499	0.1	29.58	0.98	33.24	2.28	1.12	0.09
plesovice	89	827	0.1	29.37	0.60	30.76	2.03	1.05	0.07
plesovice	73	717	0.1	30.90	1.06	34.53	2.28	1.12	0.08
plesovice	53	539	0.1	32.30	1.18	36.74	2.51	1.14	0.09
plesovice	68	679	0.1	31.60	0.75	34.19	2.31	1.08	0.08
plesovice	64	646	0.1	32.17	0.92	32.52	2.14	1.01	0.07
plesovice	94	842	0.1	28.35	0.45	31.71	2.07	1.12	0.08
plesovice	61	635	0.1	32.89	0.81	34.60	2.30	1.05	0.07

Table C.3. U-Th zircon data corrected using Bishop Tuff reference material perovskite mass scan.

Sample ID	Th (ppm)	U (ppm)	Th/U	(^{238}U)/(^{232}Th)	±1s	(^{230}Th)/(^{232}Th)	±1s	(^{230}Th)/(^{238}U)	±1s
Bishop Tuff mass scan used for correction Thabund. = 4.10±0.07 ppm (1SD)									
BIshopTuff-1 June 2022	1264	2410	0.5	6.04	0.47	6.81	0.29	1.13	0.10
BIshopTuff-1 June 2022	2391	3089	0.7	4.09	0.18	4.41	0.11	1.08	0.05
BIshopTuff-1 June 2022	945	1775	0.5	5.95	0.22	6.29	0.14	1.06	0.05
BIshopTuff-1 June 2022	1495	2672	0.5	5.66	0.21	6.24	0.14	1.10	0.05
BIshopTuff-1 June 2022	883	1968	0.4	7.06	0.25	7.74	0.15	1.10	0.04
BIshopTuff-1 June 2022	3428	4128	0.8	3.81	0.10	4.11	0.07	1.08	0.03
BIshopTuff-1 June 2022	3275	4012	0.8	3.88	0.19	4.13	0.11	1.06	0.06
BIshopTuff-1 June 2022	1389	2423	0.5	5.52	0.15	5.76	0.10	1.04	0.03
BIshopTuff-1 June 2022	1298	2392	0.5	5.83	0.25	6.38	0.15	1.09	0.05
BIshopTuff-1 June 2022	988	1766	0.5	5.66	0.19	6.05	0.12	1.07	0.04
BIshopTuff-1 June 2022	1129	1844	0.6	5.17	0.39	5.53	0.24	1.07	0.09
BIshopTuff-1 June 2022	1751	2675	0.6	4.84	0.15	5.07	0.09	1.05	0.04
BIshopTuff-1 June 2022	3469	4545	0.7	4.15	0.12	4.43	0.07	1.07	0.04
BIshopTuff-1 June 2022	1195	2370	0.5	6.27	0.54	6.58	0.31	1.05	0.10
BIshopTuff-1 June 2022	1122	2289	0.5	6.46	0.38	7.10	0.25	1.10	0.08
BIshopTuff-1 June 2022	265	1530	0.2	18.28	0.54	19.45	0.35	1.06	0.04
BIshopTuff-1 June 2022	2026	3497	0.5	5.46	0.26	5.67	0.15	1.04	0.06
BIshopTuff-1 June 2022	2286	3683	0.6	5.10	0.06	5.42	0.05	1.06	0.02
BIshopTuff-1 June 2022	1651	2776	0.6	5.32	0.12	5.48	0.09	1.03	0.03
BIshopTuff-1 June 2022	1996	3100	0.6	4.92	0.11	5.03	0.08	1.02	0.03
BIshopTuff-1 June 2022	786	1456	0.5	5.86	0.60	6.07	0.33	1.04	0.12
BIshopTuff-1 June 2022	1564	2428	0.6	4.91	0.31	5.13	0.17	1.04	0.07
BIshopTuff-1 June 2022	801	1726	0.4	6.82	0.10	7.28	0.11	1.07	0.02
BIshopTuff-1 June 2022	1416	2266	0.6	5.06	0.14	5.31	0.11	1.05	0.04
BIshopTuff-1 June 2022	2713	3375	0.8	3.94	0.25	4.10	0.14	1.04	0.07
BIshopTuff-1 June 2022	895	1850	0.5	6.54	0.18	6.82	0.12	1.04	0.03
BIshopTuff-1 June 2022	1193	2324	0.5	6.17	0.25	6.49	0.15	1.05	0.05
BIshopTuff-1 June 2022	2340	3128	0.7	4.23	0.26	4.30	0.14	1.02	0.07
BIshopTuff-1 June 2022	2085	3243	0.6	4.92	0.36	5.34	0.21	1.08	0.09
BIshopTuff-1 June 2022	1976	2913	0.6	4.67	0.07	4.96	0.07	1.06	0.02
Bishop Tuff mass scan used for correction Thabund. = 4.10±0.07 ppm (1SD)									
91500 June 2022	30	80	0.4	8.43	0.19	9.24	1.04	1.10	0.13
91500 June 2022	23	82	0.3	11.23	0.30	12.22	1.67	1.09	0.15
91500 June 2022	30	81	0.4	8.43	0.18	8.98	1.20	1.07	0.14
91500 June 2022	31	81	0.4	8.35	0.20	8.50	0.96	1.02	0.12
91500 June 2022	30	80	0.4	8.35	0.21	8.03	0.78	0.96	0.10

91500 June 2022	31	81	0.4	8.34	0.21	7.50	1.04	0.90	0.13
91500 June 2022	29	79	0.3	8.57	0.21	7.62	1.15	`0.89	0.14
91500 June 2022	30	81	0.3	8.58	0.20	7.46	1.23	0.87	0.14
91500 June 2022	29	78	0.3	8.55	0.20	6.96	1.35	0.81	0.16
91500 June 2022	30	79	0.4	8.40	0.22	9.99	1.00	1.19	0.12
91500 June 2022	31	83	0.4	8.46	0.21	10.03	0.95	1.19	0.12
91500 June 2022	33	88	0.4	8.44	0.19	10.00	1.20	1.18	0.14
91500 June 2022	29	79	0.4	8.47	0.22	9.96	1.08	1.18	0.13
91500 June 2022	27	79	0.3	9.35	0.23	9.80	0.86	1.05	0.10
91500 June 2022	28	75	0.4	8.37	0.14	8.58	1.08	1.02	0.13
91500 June 2022	27	75	0.3	8.67	0.21	8.84	0.91	1.02	0.11
91500 June 2022	27	75	0.3	8.67	0.21	8.82	1.54	1.02	0.18
91500 June 2022	30	79	0.4	8.40	0.18	9.26	1.10	1.10	0.13
91500 June 2022	30	79	0.4	8.40	0.19	9.22	0.87	1.10	0.11
91500 June 2022	30	79	0.4	8.38	0.20	8.40	1.49	1.00	0.18
91500 June 2022	30	80	0.4	8.37	0.19	9.06	0.70	1.08	0.09
91500 June 2022	31	82	0.4	8.40	0.18	9.09	0.86	1.08	0.11
91500 June 2022	30	80	0.4	8.38	0.20	9.00	0.98	1.07	0.12
91500 June 2022	31	81	0.4	8.38	0.20	8.24	1.11	0.98	0.13
91500 June 2022	30	81	0.4	8.43	0.21	8.15	0.99	0.97	0.12
91500 June 2022	31	83	0.4	8.42	0.23	8.79	0.83	1.04	0.10
91500 June 2022	23	81	0.3	11.18	0.37	10.46	1.24	0.94	0.12
91500 June 2022	30	80	0.4	8.48	0.20	7.88	1.01	0.93	0.12
91500 June 2022	31	82	0.4	8.41	0.19	7.84	0.95	0.93	0.12
91500 June 2022	31	84	0.4	8.48	0.21	8.50	1.02	1.00	0.12
91500 June 2022	29	77	0.4	8.43	0.22	7.53	0.93	0.89	0.11
91500 June 2022	32	83	0.4	8.35	0.19	7.43	0.86	0.89	0.10
91500 June 2022	30	81	0.4	8.45	0.19	7.40	0.95	0.88	0.11
91500 June 2022	27	75	0.3	8.81	0.23	7.55	1.16	0.86	0.13
91500 June 2022	31	81	0.4	8.38	0.20	7.23	0.87	0.86	0.11
91500 June 2022	31	82	0.4	8.40	0.22	7.23	0.90	0.86	0.11
91500 June 2022	29	79	0.3	8.55	0.24	7.07	0.80	0.83	0.10
91500 June 2022	28	76	0.3	8.76	0.23	7.15	1.36	0.82	0.16
91500 June 2022	31	81	0.4	8.37	0.18	6.82	0.74	0.81	0.09
91500 June 2022	30	80	0.4	8.35	0.21	6.71	1.05	0.80	0.13

Bishop Tuff mass scan used for correction Thabund. = 4.10±0.07 ppm (1SD)

plesovice	48	513	0.1	33.64	0.70	35.84	0.94	1.07	0.04
plesovice	29	309	0.1	33.67	1.36	31.95	1.11	0.95	0.05
plesovice	58	599	0.1	32.67	0.61	33.20	0.93	1.02	0.03
plesovice	78	757	0.1	30.89	0.72	31.70	0.75	1.03	0.03
plesovice	77	744	0.1	30.66	0.81	28.22	0.64	0.92	0.03

plesovice	64	659	0.1	32.36	0.80	34.46	0.73	1.06	0.03
plesovice	108	855	0.1	25.02	0.49	25.13	0.42	1.00	0.03
plesovice	78	770	0.1	31.34	0.78	29.86	0.83	0.95	0.04
plesovice	102	879	0.1	27.18	0.84	28.53	0.98	1.05	0.05
plesovice	80	780	0.1	30.96	1.65	31.03	0.72	1.00	0.06
plesovice	72	722	0.1	31.61	0.93	34.89	1.00	1.10	0.05
plesovice	67	670	0.1	31.86	0.94	34.97	0.97	1.10	0.04
plesovice	55	582	0.1	33.28	0.93	34.56	2.30	1.04	0.07
plesovice	71	720	0.1	32.22	0.78	30.56	1.93	0.95	0.06
plesovice	77	756	0.1	31.12	0.73	33.55	2.18	1.08	0.07
plesovice	80	782	0.1	30.80	0.78	30.90	1.96	1.00	0.07
plesovice	78	770	0.1	31.17	0.76	30.99	1.98	0.99	0.07
plesovice	77	761	0.1	31.26	0.82	31.82	2.11	1.02	0.07
plesovice	64	640	0.1	31.76	1.47	30.86	2.16	0.97	0.08
plesovice	96	863	0.1	28.54	1.06	30.77	2.10	1.08	0.08
plesovice	120	1120	0.1	29.63	0.87	30.17	1.88	1.02	0.07
plesovice	53	499	0.1	29.58	0.98	29.80	2.04	1.01	0.08
plesovice	89	827	0.1	29.37	0.60	28.70	1.89	0.98	0.07
plesovice	73	717	0.1	30.90	1.06	32.02	2.12	1.04	0.08
plesovice	53	539	0.1	32.30	1.18	33.25	2.27	1.03	0.08
plesovice	68	679	0.1	31.60	0.75	31.49	2.13	1.00	0.07
plesovice	64	646	0.1	32.17	0.92	29.62	1.95	0.92	0.07
plesovice	94	842	0.1	28.35	0.45	29.76	1.94	1.05	0.07
plesovice	61	635	0.1	32.89	0.81	31.59	2.10	0.96	0.07

Table C.4. U-Th zircon age data for Campanian Ignimbrite corrected using Bishop Tuff reference material zircon.

	Th (ppm)	U (ppm)	Th/U	(^{238}U)/(^{232}Th)	±1s	(^{230}Th)/(^{232}Th)	±1s	(^{230}Th)/(^{238}U)	Model age 2-point ±1s	Age (ka)	±1s
CI June 2022	326	379	0.8	3.67	0.06	1.71	0.13	0.46	0.04	38.03	5.66
CI	363	449	0.8	3.92	0.09	1.68	0.13	0.43	0.03	34.24	5.08
CI	364	429	0.8	3.72	0.04	1.90	0.14	0.51	0.04	45.63	6.45
CI	333	388	0.8	3.69	0.07	1.78	0.14	0.48	0.04	40.99	6.03
CI	600	610	0.9	3.22	0.11	1.69	0.14	0.53	0.05	43.88	7.86
CI	303	395	0.7	4.12	0.13	2.05	0.16	0.50	0.04	46.28	7.09
CI	376	473	0.8	3.98	0.07	1.81	0.14	0.45	0.04	38.56	5.45
CI	388	451	0.8	3.68	0.15	2.29	0.18	0.62	0.05	65.75	10.94
CI	808	805	0.9	3.15	0.04	1.55	0.11	0.49	0.03	37.92	5.30
CI	708	668	1.0	2.99	0.10	1.71	0.12	0.57	0.05	48.96	7.79
CI	1049	892	1.1	2.69	0.03	1.40	0.09	0.52	0.04	36.81	5.35
CI	1099	939	1.1	2.70	0.03	1.69	0.11	0.62	0.04	54.44	7.57
CI	1115	947	1.1	2.69	0.03	1.42	0.10	0.53	0.04	38.18	5.58
CI	995	811	1.2	2.58	0.08	1.61	0.13	0.62	0.05	52.44	9.43
CI	940	1126	0.8	3.79	0.05	1.76	0.12	0.46	0.03	38.84	5.04
CI	759	862	0.8	3.59	0.03	2.06	0.14	0.57	0.04	55.65	7.05
CI	707	995	0.7	4.45	0.05	2.04	0.14	0.46	0.03	41.79	5.19
CI	749	915	0.8	3.87	0.04	1.81	0.13	0.47	0.03	39.99	5.15
CI	905	1085	0.8	3.79	0.05	1.93	0.13	0.51	0.03	45.91	5.72
CI	913	1084	0.8	3.76	0.05	2.10	0.14	0.56	0.04	54.36	6.83
CI	637	571	1.1	2.84	0.11	1.62	0.13	0.57	0.05	47.24	8.47
CI	623	531	1.1	2.70	0.17	1.61	0.13	0.60	0.06	49.51	10.64
CI	613	342	1.7	1.77	0.12	1.07	0.08	0.60	0.06	31.32	8.83
CI	856	1019	0.8	3.77	0.05	1.95	0.14	0.52	0.04	47.07	6.37
CI	884	1103	0.8	3.95	0.07	1.79	0.12	0.45	0.03	37.94	4.90
CI	339	350	0.9	3.27	0.07	2.31	0.20	0.71	0.06	73.98	14.47
CI	782	883	0.8	3.57	0.05	1.64	0.11	0.46	0.03	36.39	4.91
CI	1835	788	2.2	1.36	0.03	1.00	0.07	0.73	0.05	35.03	7.88
CI	766	437	1.7	1.80	0.02	1.06	0.08	0.59	0.04	30.03	6.45
CI	1089	1106	0.9	3.21	0.04	1.54	0.10	0.48	0.03	36.67	5.01
CI	470	502	0.9	3.38	0.06	2.01	0.16	0.59	0.05	57.41	8.79
CI	700	733	0.9	3.32	0.03	1.41	0.10	0.43	0.03	29.55	4.55
CI	619	646	0.9	3.30	0.13	1.68	0.13	0.51	0.04	41.79	7.02
CI	3739	2215	1.6	1.87	0.04	1.18	0.08	0.63	0.04	38.31	6.83
CI	5937	2943	1.9	1.57	0.03	1.01	0.07	0.65	0.05	30.91	6.52
CI	5458	2792	1.8	1.62	0.01	1.02	0.07	0.63	0.04	30.88	5.91
CI	2680	1776	1.4	2.10	0.03	1.22	0.08	0.58	0.04	36.06	6.03
CI	5996	3027	1.9	1.60	0.01	1.06	0.07	0.66	0.04	34.18	6.33
CI	5310	2796	1.8	1.67	0.01	1.06	0.07	0.64	0.04	32.93	6.06
CI	5345	2836	1.8	1.68	0.01	1.06	0.07	0.63	0.04	32.93	6.01
CI	3417	2021	1.6	1.87	0.05	1.12	0.08	0.60	0.04	33.47	6.53
CI	2507	1887	1.3	2.38	0.03	1.44	0.09	0.60	0.04	45.53	6.62
CI	4980	2908	1.6	1.85	0.03	1.14	0.07	0.62	0.04	35.47	6.17
CI	1169	1078	1.0	2.92	0.04	1.57	0.11	0.54	0.04	42.86	5.98
CI	510	458	1.1	2.84	0.04	1.50	0.12	0.53	0.04	40.34	7.01

CI	623	544	1.1	2.76	0.02	1.81	0.13	0.66	0.05	61.31	8.94
CI	944	1112	0.8	3.73	0.05	1.72	0.12	0.46	0.03	37.83	4.98
CI	8032	3702	2.0	1.46	0.02	0.96	0.06	0.66	0.04	28.69	6.12
CI	955	954	0.9	3.16	0.03	1.53	0.11	0.48	0.03	36.90	5.30
CI	898	1067	0.8	3.76	0.04	1.67	0.12	0.44	0.03	35.29	4.69

Table C.5. U-Th zircon age data for Campanian Ignimbrite corrected using Ice River reference material perovskite.

						Model age 2-point		
	$(^{238}U)/(^{232}Th)$	±1s	$(^{230}Th)/(^{232}Th)$	±1s	$(^{230}Th)/(^{238}U)$	±1s	Age (ka)	±1s
CI June 2022	3.67	0.06	1.56	0.12	0.42	0.03	31.48	4.86
CI	3.92	0.09	1.55	0.11	0.40	0.03	28.81	4.19
CI	3.72	0.04	1.76	0.13	0.47	0.03	39.07	5.51
CI	3.69	0.07	1.63	0.12	0.44	0.03	34.07	5.01
CI	3.22	0.11	1.63	0.13	0.51	0.05	40.07	6.92
CI	4.12	0.13	1.87	0.14	0.45	0.04	38.67	5.73
CI	3.98	0.07	1.68	0.12	0.42	0.03	33.03	4.58
CI	3.68	0.15	2.13	0.16	0.58	0.05	56.61	9.06
CI	3.15	0.04	1.52	0.10	0.48	0.03	35.73	4.89
CI	2.99	0.10	1.65	0.12	0.55	0.04	44.96	7.27
CI	2.69	0.03	1.39	0.09	0.52	0.03	35.65	5.13
CI	2.70	0.03	1.67	0.11	0.62	0.04	52.40	7.28
CI	2.69	0.03	1.42	0.09	0.53	0.03	37.35	5.22
CI	2.58	0.08	1.59	0.12	0.62	0.05	50.09	8.68
CI	3.79	0.05	1.73	0.11	0.46	0.03	36.99	4.54
CI	3.59	0.03	1.99	0.13	0.55	0.04	51.44	6.38
CI	4.45	0.05	1.97	0.13	0.44	0.03	38.73	4.61
CI	3.87	0.04	1.76	0.12	0.45	0.03	37.26	4.81
CI	3.79	0.05	1.88	0.12	0.50	0.03	43.22	5.24
CI	3.76	0.05	2.04	0.13	0.54	0.04	50.80	6.14
CI	2.84	0.11	1.57	0.12	0.55	0.05	43.27	7.68
CI	2.70	0.17	1.55	0.13	0.58	0.06	44.83	9.90
CI	1.77	0.12	1.04	0.07	0.59	0.06	27.95	7.91
CI	3.77	0.05	1.89	0.13	0.50	0.04	43.93	5.73
CI	3.95	0.07	1.75	0.11	0.44	0.03	35.98	4.39
CI	3.27	0.07	2.13	0.18	0.65	0.06	66.33	11.38
CI	3.57	0.05	1.60	0.10	0.45	0.03	34.16	4.28
CI	3.58	0.06	1.30	0.09	0.36	0.02	22.23	3.46
CI	1.36	0.03	1.04	0.07	0.77	0.05	38.00	8.37
CI	1.48	0.02	0.95	0.06	0.65	0.04	25.65	5.72
CI	1.80	0.02	1.06	0.08	0.59	0.04	28.99	6.39
CI	3.21	0.04	1.53	0.10	0.48	0.03	35.42	4.79
CI	3.38	0.06	1.90	0.14	0.56	0.04	50.87	7.41
CI	3.32	0.03	1.38	0.10	0.42	0.03	27.51	4.26
CI	3.30	0.13	1.61	0.12	0.49	0.04	37.96	6.35
CI	1.87	0.04	1.23	0.08	0.66	0.04	41.35	7.18
CI	1.57	0.03	1.08	0.07	0.69	0.05	35.88	7.04
CI	1.62	0.01	1.09	0.07	0.67	0.04	35.50	6.56
CI	2.10	0.03	1.26	0.08	0.60	0.04	38.17	6.04

CI	1.60	0.01	1.12	0.07	0.70	0.04	38.91	6.85
CI	1.67	0.01	1.12	0.07	0.67	0.04	36.97	6.44
CI	1.68	0.01	1.12	0.07	0.67	0.04	36.71	6.39
CI	1.87	0.05	1.17	0.08	0.63	0.04	36.36	6.99
CI	2.38	0.03	1.46	0.09	0.61	0.04	46.08	6.42
CI	1.85	0.03	1.19	0.07	0.65	0.04	38.49	6.09
CI	2.92	0.04	1.56	0.10	0.54	0.03	41.28	5.58
CI	2.84	0.04	1.43	0.11	0.50	0.04	35.55	5.95
CI	2.76	0.02	1.74	0.12	0.63	0.04	55.45	7.93
CI	3.73	0.05	1.69	0.11	0.45	0.03	36.06	4.57
CI	1.46	0.02	1.03	0.06	0.71	0.04	33.91	6.28

Table C.6. U-Th zircon age data for Campanian Ignimbrite corrected using Bishop Tuff zircon mass scan.

						Model age 2-point		
	$(^{238}U)/(^{232}Th)$	±1s	$(^{230}Th)/(^{232}Th)$	±1s	$(^{230}Th)/(^{238}U)$	±1s	Age (ka)	±1s
CI June 2022	3.67	0.06	1.54	0.11	0.42	0.03	30.62	4.44
CI	3.92	0.09	1.53	0.11	0.39	0.03	28.03	4.15
CI	3.72	0.04	1.74	0.13	0.47	0.03	38.16	5.46
CI	3.69	0.07	1.61	0.12	0.44	0.03	33.20	4.96
CI	3.22	0.11	1.62	0.13	0.50	0.04	39.50	6.87
CI	4.12	0.13	1.84	0.14	0.45	0.04	37.49	5.66
CI	3.98	0.07	1.66	0.12	0.42	0.03	32.23	4.55
CI	3.68	0.15	2.12	0.16	0.58	0.05	56.03	9.01
CI	3.15	0.04	1.52	0.10	0.48	0.03	35.65	4.89
CI	2.99	0.10	1.65	0.11	0.55	0.04	44.86	6.77
CI	2.69	0.03	1.39	0.09	0.52	0.03	35.56	5.13
CI	2.70	0.03	1.67	0.11	0.62	0.04	52.29	7.28
CI	2.69	0.03	1.42	0.09	0.53	0.03	37.26	5.21
CI	2.58	0.08	1.59	0.12	0.62	0.05	49.98	8.67
CI	3.79	0.05	1.73	0.11	0.46	0.03	36.92	4.53
CI	3.59	0.03	1.99	0.13	0.55	0.04	51.36	6.38
CI	4.45	0.05	1.96	0.13	0.44	0.03	38.32	4.59
CI	3.87	0.04	1.75	0.12	0.45	0.03	36.80	4.79
CI	3.79	0.05	1.88	0.12	0.50	0.03	43.15	5.24
CI	3.76	0.05	2.04	0.13	0.54	0.04	50.72	6.13
CI	2.84	0.11	1.56	0.12	0.55	0.05	42.60	7.62
CI	2.70	0.17	1.55	0.12	0.57	0.06	44.73	9.41
CI	1.77	0.12	1.04	0.07	0.59	0.06	27.82	7.90
CI	3.77	0.05	1.89	0.13	0.50	0.04	43.86	5.73
CI	3.95	0.07	1.74	0.11	0.44	0.03	35.54	4.37
CI	3.27	0.07	2.11	0.18	0.64	0.06	65.01	11.23
CI	3.57	0.05	1.60	0.10	0.45	0.03	34.09	4.28
CI	3.58	0.06	1.30	0.09	0.36	0.02	22.17	3.46
CI	1.36	0.03	1.05	0.07	0.77	0.05	38.95	8.45
CI	1.48	0.02	0.96	0.06	0.65	0.04	26.43	5.76
CI	1.80	0.02	1.05	0.08	0.58	0.04	28.07	6.34
CI	3.21	0.04	1.53	0.10	0.48	0.03	35.34	4.78
CI	3.38	0.06	1.88	0.14	0.56	0.04	49.77	7.33
CI	3.32	0.03	1.37	0.10	0.41	0.03	27.01	4.24
CI	3.30	0.13	1.61	0.12	0.49	0.04	37.88	6.35
CI	1.87	0.04	1.24	0.08	0.66	0.04	42.06	7.23
CI	1.57	0.03	1.09	0.07	0.69	0.05	36.69	7.10
CI	1.62	0.01	1.10	0.07	0.68	0.04	36.28	6.60
CI	2.10	0.03	1.26	0.08	0.60	0.04	38.05	6.04
CI	1.60	0.01	1.13	0.07	0.71	0.04	39.73	6.90
CI	1.67	0.01	1.13	0.07	0.68	0.04	37.74	6.49
CI	1.68	0.01	1.13	0.07	0.67	0.04	37.47	6.44
CI	1.87	0.05	1.18	0.08	0.63	0.04	37.04	7.04

CI	2.38	0.03	1.47	0.09	0.62	0.04	46.66	6.46
CI	1.85	0.03	1.20	0.07	0.65	0.04	39.19	6.13
CI	2.92	0.04	1.56	0.10	0.54	0.03	41.19	5.57
CI	2.84	0.04	1.42	0.11	0.50	0.04	34.94	5.91
CI	2.76	0.02	1.74	0.12	0.63	0.04	55.34	7.92
CI	3.73	0.05	1.69	0.11	0.45	0.03	35.99	4.57
CI	1.46	0.02	1.04	0.06	0.72	0.04	34.76	6.34

Table C.7. U-Th and U-Th-Pb zircon data for Bishop Tuff and PAL tephra corrected using Bishop Tuff reference material zircon.

														Age (Ma)d		Age (Ma)d		^{230}Th-^{238}U	
Sample number	U (ppm)	Th (ppm)	(^{238}U)/(^{232}Th)	1σ	(^{230}Th)/(^{232}Th)	1σ	$^{208}Pb/^{232}Th$	2σ	$^{207}Pb/^{206}Pb$	2σ	$^{206}Pb/^{238}U$	2σ	ρ	$^{206}Pb^{*}/^{238}U$	$1\sigma^{d}$	$^{208}Pb^{*}/^{232}Th$	$1\sigma^{d}$	Model Age (zircon-glass)	$1\sigma^{d}$
PAL tephra (UA1305)																			
PAL1305_180	194	166	3.80	0.10	4.82	0.42	0.002115	0.000087	0.68639	0.02043	0.00106	0.00003	0.66	1.35	0.02	1.42	0.04	∞	∞
PAL1305_181	97	74	4.29	0.05	4.94	0.60	0.002818	0.000231	0.66953	0.03188	0.00128	0.00005	0.66	1.79	0.04	1.84	0.10	∞	∞
PAL1305_182	95	67	4.68	0.12	4.22	0.49	0.000193	0.000088	0.55281	0.17596	0.00011	0.00002	0.51	0.33	0.03	0.32	0.09	0.22	0.09
PAL1305_183	109	83	4.33	0.10	3.90	0.31	0.000031	0.000041	0.37167	0.17569	0.00006	0.00001	0.30	0.28	0.02	0.15	0.11	0.22	0.06
PAL1305_184	107	83	4.31	0.07	4.50	0.59	0.000211	0.000061	0.42940	0.12910	0.00012	0.00002	0.45	0.45	0.03	0.53	0.11	∞	∞
PAL1305_188	182	104	5.81	0.26	5.44	0.44	0.000046	0.000036	0.24119	0.11591	0.00005	0.00001	0.25	0.29	0.02	0.28	0.13	0.28	0.12
PAL1305_190	140	84	5.65	0.20	6.60	0.57	0.004057	0.000197	0.72198	0.01995	0.00127	0.00003	0.64	1.27	0.02	1.23	0.04	∞	∞
PAL1305_191	140	96	4.96	0.08	4.06	0.52	0.000015	0.000046	0.40193	0.16771	0.00004	0.00001	0.35	0.21	0.02	0.12	0.08	0.16	0.05
PAL1305_192	94	62	5.16	0.09	5.07	0.76	0.002770	0.000216	0.71887	0.03421	0.00102	0.00004	0.62	1.06	0.02	1.10	0.05	∞	∞
PAL1305_194	226	201	3.78	0.10	3.64	0.32	0.000570	0.000062	0.68176	0.03681	0.00028	0.00001	0.67	0.42	0.01	0.43	0.03	0.33	0.19
PAL1305_195	350	361	3.18	0.05	2.92	0.19	0.000072	0.000016	0.37306	0.05866	0.00006	0.00000	0.39	0.28	0.01	0.34	0.05	0.23	0.05
PAL1305_197	255	209	3.97	0.20	4.61	0.58	0.004195	0.000268	0.76834	0.03252	0.00159	0.00008	0.78	0.99	0.03	1.08	0.06	∞	∞
PAL1305_198	381	363	3.39	0.05	3.27	0.25	0.000193	0.000045	0.48699	0.07252	0.00011	0.00001	0.35	0.38	0.01	0.47	0.06	0.33	0.16
PAL_1	104	87	3.86	0.11	3.94	0.47	0.009937	0.000539	0.82309	0.02408	0.00405	0.00012	0.71	0.70	0.01	0.71	0.02	∞	∞
PAL_3	113	71	5.28	0.26	5.20	0.68	0.005388	0.000386	0.79926	0.04816	0.00157	0.00006	0.56	0.62	0.01	0.60	0.03	432.67	∞
PAL_7	706	1084	2.33	0.04	2.20	0.15	0.000432	0.000050	0.75887	0.05507	0.00032	0.00001	0.53	0.25	0.01	0.23	0.02	0.25	0.07
PAL_10	111	66	6.21	0.10	6.10	0.75	0.000760	0.000239	0.67296	0.16230	0.00031	0.00007	0.68	0.49	0.05	0.54	0.12	415.93	∞
PAL_12	200	192	3.75	0.07	4.45	0.60	0.003141	0.000239	0.74418	0.04590	0.00132	0.00007	0.62	0.41	0.02	0.46	0.03	∞	∞
PAL_13	300	241	4.35	0.08	4.00	0.71	0.000360	0.000096	0.71105	0.11724	0.00018	0.00002	0.59	0.25	0.02	0.27	0.04	0.24	0.17
PAL_15	125	86	4.41	0.15	3.95	0.72	0.000367	0.000155	0.74060	0.17589	0.00023	0.00018	0.96	0.26	0.10	0.44	0.20	0.22	0.13
PAL_16	83	59	4.24	0.09	5.53	0.58	0.006135	0.000379	0.76204	0.02662	0.00231	0.00011	0.80	1.52	0.04	1.63	0.07	∞	∞
PAL_20	108	84	4.08	0.05	3.41	0.59	0.000094	0.000050	0.54341	0.38014	0.00005	0.00001	0.25	0.18	0.02	0.19	0.09	0.16	0.07
PAL1305_199	143	109	4.35	0.04	4.46	0.28	0.005368	0.000203	0.78350	0.01431	0.00201	0.00007	0.89	0.84	0.02	0.86	0.02	∞	∞
PAL1305_200	58	35	5.52	0.14	5.57	0.86	0.000097	0.000121	0.27628	0.17565	0.00012	0.00002	0.23	0.61	0.05	0.44	0.31	∞	∞
PAL1305_202	70	37	6.37	0.08	5.39	0.69	0.000227	0.000155	0.66007	0.31766	0.00011	0.00002	0.42	0.23	0.03	0.23	0.10	0.18	0.06
PAL1305_206	94	66	4.70	0.23	4.31	0.88	0.002202	0.000388	0.80927	0.09447	0.00079	0.00007	0.59	0.28	0.01	0.36	0.04	0.24	0.20
PAL1305_207	260	291	2.96	0.08	2.73	0.22	0.000078	0.000028	0.43020	0.08954	0.00007	0.00001	0.50	0.28	0.02	0.30	0.06	0.23	0.07
	179	165												1.79		0.18			
Bishop Tuff																		(^{230}Th)/(^{238}U)	1σ
BIshopTuff	683	1506	7.46	0.43	7.82	0.27	0.000046	0.000011	0.07961	0.01387	0.00011	0.00000	0.08	0.78	0.03	0.63	0.18	1.05	0.07
BIshopTuff	1755	2714	5.24	0.16	5.50	0.17	0.000080	0.000022	0.11529	0.02059	0.00012	0.00000	0.10	0.78	0.05	0.88	0.27	1.05	0.05
BIshopTuff	1658	2831	5.78	0.23	6.07	0.19	0.000061	0.000011	0.08842	0.01303	0.00011	0.00000	0.04	0.76	0.03	0.80	0.17	1.05	0.05
BIshopTuff	3320	4399	4.49	0.12	4.77	0.15	0.000064	0.000013	0.11477	0.01735	0.00011	0.00000	0.06	0.72	0.03	0.80	0.18	1.06	0.04
BIshopTuff	1652	2475	5.07	0.14	5.35	0.17	0.000186	0.000024	0.25189	0.01954	0.00015	0.00001	0.50	0.79	0.04	0.88	0.13	1.05	0.04
BIshopTuff	881	1742	6.70	0.26	7.01	0.22	0.000039	0.000016	0.08650	0.01588	0.00010	0.00000	0.01	0.77	0.03	0.50	0.22	1.05	0.05
BIshopTuff	999	1823	5.71	0.20	6.07	0.19	0.000164	0.000021	0.23225	0.01569	0.00014	0.00000	0.51	0.78	0.03	0.73	0.11	1.06	0.05
BIshopTuff	2419	3558	4.61	0.29	4.64	0.16	0.000101	0.000026	0.19841	0.02929	0.00012	0.00001	0.29	0.76	0.05	0.63	0.19	1.01	0.07
BIshopTuff	2449	3397	4.34	0.22	4.53	0.15	0.000117	0.000018	0.17394	0.01515	0.00014	0.00000	0.50	0.81	0.04	0.95	0.17	1.04	0.06
BIshopTuff	1706	3033	5.56	0.24	5.87	0.19	0.000067	0.000009	0.12639	0.01123	0.00012	0.00000	0.02	0.80	0.02	0.65	0.10	1.05	0.06
BIshopTuff	2202	3086	4.39	0.14	4.75	0.15	0.000141	0.000012	0.22852	0.01132	0.00013	0.00000	0.62	0.75	0.02	0.86	0.08	1.08	0.05
BIshopTuff	3500	4420	3.95	0.07	4.12	0.13	0.000052	0.000006	0.09501	0.00827	0.00011	0.00000	0.17	0.77	0.02	0.75	0.09	1.04	0.04

Table C.8. OxCal combine function output for PAL tephra.

Unmodelled (BP)					Modelled (BP)					Indices	
from	to	%	mu	sigma	from	to	%	mu	sigma	Acomb	A
300944	160899	95	230921	35011	318197	224530	95.45	271344	23564		74.2
368536	241097	95	304816	31860	318197	224530	95.45	271344	23564		79.6
318197	224530	95	271344	23564						68.9	
437445	47256	95	242351	97547	395480	314380	95.45	354962	20043		73.1
400885	318967	95	359926	20480	395480	314380	95.45	354962	20043		99.6
395480	314380	95	354962	20043						79.9	
247954	119726	95	183840	32057	252206	143212	95.45	197747	26968		102.4
331187	131654	95	231421	49883	252206	143212	95.45	197747	26968		104.3
252206	143212	95	197747	26968						104.8	
233970	92214	95	163092	35439	230235	119665	95.45	175562	27248		107.8
278827	108362	95	193595	42616	230235	119665	95.45	175562	27248		111.8
230235	119665	95	175562	27248						114.1	
346577	84051	95	215314	65631	388681	174723	95.45	284876	54783		78
643652	245732	95	444692	99480	388681	174723	95.45	284876	54783		46
388681	174723	95	284876	54783						48.4	
412003	77241	95	244623	83690	311459	223774	95.45	267672	21714		132.1
314303	224369	95	269336	22484	311459	223774	95.45	267672	21714		101.6
311459	223774	95	267672	21714						123.1	
322941	183280	95	253110	34915	249341	216984	95.45	233131	8072		118
248596	215409	95	232003	8297	249341	216984	95.45	233131	8072		100.9
249341	216984	95	233131	8072						113.1	
483151	167291	95	325221	78965	507034	387091	95.45	447039	29919		46.7
532117	402799	95	467458	32330	507034	387091	95.45	447039	29919		93.2
507034	387091	95	447039	29919						55.6	
282010	173527	95	227769	27121	328061	257835	95.45	292848	17386		15.5
383562	292948	95	338255	22654	328061	257835	95.45	292848	17386		31.7
328061	257835	95	292848	17386						11.9	
514027	141637	95	327832	93097	460471	404049	95.45	432271	13981		75.6
462962	406399	95	434680	14141	460471	404049	95.45	432271	13981		99.8
460471	404049	95	432271	13981						81.9	
209517	110066	95	159792	24863	187826	105281	95.45	147763	21130		100.7

196670	36290	95	116481	40095	187826	105281	95.45	147763	21130		98.6
187826	105281	95	147763	21130						99.5	
397467	155959	95	276713	60377	362091	190620	95.45	279364	44094		114.1
411490	153297	95	282394	64548	362091	190620	95.45	279364	44094		116.7
362091	190620	95	279364	44094						122.5	
281795	158752	95	220274	30761	256014	149889	95.45	202942	26595		97.7
257488	45781	95	151635	52927	256014	149889	95.45	202942	26595		86.8
256014	149889	95	202942	26595						89	
315685	132473	95	224079	45803	338960	206131	95.45	272603	32822		79.3
417933	229706	95	323820	47057	338960	206131	95.45	272603	32822		77.9
338960	206131	95	272603	32822						71.1	

APPENDIX D: CHAPTER 5

Table D.1: LA-ICP-MS U-Pb data.

						Total						Age (Ma)[d]	
Sample number		U (ppm)	Th (ppm)	$^{207}Pb/^{206}Pb$	2σ	$^{207}Pb/^{235}U$	2σ	$^{206}Pb/^{238}U$	2σ	ρ	F_{206} (%)[a]	$^{206}Pb^{*}/^{238}U$	1σ[d]
Woodchopper Creek (UA1582)													
WCT1582_1	rim	167	115	0.64245	0.11868	0.01309	0.00282	0.00015	0.00002	0.51	75.5	0.317	0.018
WCT1582_2	*rim*	*234*	*201*	*0.77714*	*0.09916*	*0.01031*	*0.00175*	*0.00010*	*0.00001*	*0.66*	*92.6*	*0.104*	*0.007*
WCT1582_3	**rim**	**235**	**163**	**0.58379**	**0.59127**	**0.00094**	**0.00103**	**0.00001**	**0.00000**	**0.39**	**68.1**	**0.090**	**0.015**
WCT1582_4	*N/A*	*215*	*156*	*0.76528*	*0.03373*	*0.10631*	*0.00611*	*0.00101*	*0.00004*	*0.64*	*91.1*	*0.698*	*0.013*
WCT1582_5	*N/A*	*201*	*169*	*0.79190*	*0.01785*	*0.26107*	*0.01057*	*0.00239*	*0.00008*	*0.83*	*94.5*	*1.034*	*0.018*
WCT1582_6	*rim*	*104*	*52*	*0.79615*	*0.04330*	*0.12780*	*0.00847*	*0.00116*	*0.00004*	*0.57*	*95.0*	*0.518*	*0.010*
WCT1582_7	core	173	118	0.36809	0.26302	0.00160	0.00123	0.00003	0.00001	0.36	40.8	0.195	0.027
WCT1582_8	*rim*	*129*	*90*	*0.81364*	*0.02925*	*0.18085*	*0.00962*	*0.00161*	*0.00006*	*0.74*	*97.2*	*0.458*	*0.009*
WCT1582_9	*rim*	*161*	*102*	*0.79755*	*0.02472*	*0.10901*	*0.00435*	*0.00099*	*0.00002*	*0.63*	*95.2*	*0.441*	*0.006*
WCT1582_10	*N/A*	*112*	*70*	*0.79287*	*0.23337*	*0.00879*	*0.00316*	*0.00008*	*0.00002*	*0.57*	*94.6*	*0.081*	*0.009*
WCT1582_11	rim	122	61	0.40820	0.25430	0.00231	0.00150	0.00004	0.00001	0.27	45.9	0.222	0.020
WCT1582_12	*core*	*154*	*132*	*0.77914*	*0.02455*	*0.13563*	*0.00615*	*0.00126*	*0.00004*	*0.72*	*92.8*	*0.709*	*0.012*
WCT1582_13	*N/A*	*80*	*30*	*0.80024*	*0.01709*	*0.35892*	*0.01517*	*0.00325*	*0.00012*	*0.86*	*95.5*	*1.171*	*0.022*
WCT1582_14	rim	403	716	0.75051	0.05522	0.01579	0.00141	0.00015	0.00001	0.57	89.2	0.156	0.007
WCT1582_15	*core*	*135*	*177*	*0.80501*	*0.05956*	*0.37208*	*0.04576*	*0.00335*	*0.00033*	*0.80*	*96.1*	*1.055*	*0.054*
WCT1582_16	*N/A*	*2*	*4*	*0.80618*	*0.01194*	*46.88817*	*1.26503*	*0.42182*	*0.00951*	*0.84*	*96.3*	*100.646*	*1.149*
WCT1582_19	*N/A*	*1*	*0*	*0.82222*	*0.05829*	*15.40648*	*1.89454*	*0.13590*	*0.01365*	*0.82*	*98.3*	*14.955*	*0.766*
WCT1582_20	rim	130	73	0.68302	0.15631	0.00868	0.00227	0.00009	0.00001	0.48	80.7	0.191	0.012
WCT1582_21	*rim*	*158*	*105*	*0.77150*	*0.06463*	*0.04483*	*0.00504*	*0.00042*	*0.00003*	*0.67*	*91.9*	*0.307*	*0.012*
WCT1582_22	*rim*	*285*	*87*	*0.78621*	*0.04744*	*0.04315*	*0.00719*	*0.00040*	*0.00006*	*0.93*	*93.7*	*0.261*	*0.021*
WCT1582_23	core	136	52	0.26822	0.21294	0.00160	0.00130	0.00004	0.00001	0.20	28.1	0.276	0.023
WCT1582_24	*N/A*	*134*	*57*	*0.79086*	*0.02892*	*0.24429*	*0.01235*	*0.00224*	*0.00008*	*0.69*	*94.3*	*0.990*	*0.018*
WCT1582_25	rim	441	1243	0.69134	0.16537	0.01150	0.00309	0.00012	0.00001	0.45	81.7	0.230	0.015

WCT1582_27	*rim*	*324*	*128*	*0.82750*	*0.04047*	*0.06788*	*0.00531*	*0.00059*	*0.00004*	*0.78*	*99.0*	*0.139*	*0.006*
WCT1582_28	rim	193	108	0.50916	0.25446	0.00557	0.00294	0.00008	0.00001	0.33	58.7	0.288	0.025
WCT1582_29	**rim**	**165**	**61**	**0.66460**	**0.21955**	**0.00560**	**0.00205**	**0.00006**	**0.00001**	**0.43**	**78.3**	**0.138**	**0.011**
WCT1582_30	rim	164	74	0.33625	0.25015	0.00224	0.00173	0.00005	0.00001	0.26	36.8	0.277	0.028
WCT1582_31r	rim	144	55	0.44164	1.93269	0.00192	0.00844	0.00003	0.00001	0.10	50.1	0.177	0.040
WCT1582_31c	core	145	56	0.53223	1.94048	0.00270	0.00989	0.00004	0.00001	0.08	61.6	0.165	0.026
WCT1582_32r	rim	178	103	0.76771	0.07069	0.01996	0.00256	0.00019	0.00002	0.70	89.4	0.156	0.007
WCT1582_32c	core	203	124	0.56674	0.09371	0.00747	0.00157	0.00010	0.00001	0.62	65.9	0.290	0.019
WCT1582_33	*N/A*	*116*	*63*	*0.85469*	*0.06053*	*0.09980*	*0.01074*	*0.00085*	*0.00007*	*0.75*	*102.4*	*N/A*	*N/A*
WCT1582_34c	core	123	54	0.47066	0.16193	0.00488	0.00197	0.00008	0.00002	0.53	53.8	0.308	0.033
WCT1582_34r	rim	118	53	0.52586	0.14452	0.00586	0.00205	0.00008	0.00002	0.62	60.8	0.288	0.032
WCT1582_35	N/A	62	24	0.05177	0.00132	0.16929	0.00593	0.02372	0.00057	0.69	0.7	150.133	1.818
WCT1582_36	rim	294	323	0.29189	0.07723	0.00126	0.00035	0.00003	0.00000	0.31	31.1	0.199	0.010
WCT1582_37r	*rim*	*303*	*391*	*0.80021*	*0.02100*	*0.08211*	*0.00948*	*0.00074*	*0.00008*	*0.97*	*95.5*	*0.315*	*0.019*
WCT1582_37c	*core*	*325*	*443*	*0.79296*	*0.03117*	*0.04994*	*0.00274*	*0.00046*	*0.00002*	*0.70*	*94.6*	*0.240*	*0.007*
WCT1582_38r	**rim**	**87**	**48**	**0.67792**	**0.18338**	**0.00599**	**0.00188**	**0.00006**	**0.00001**	**0.51**	**80.0**	**0.142**	**0.012**
WCT1582_38c	core	87	48	0.64395	0.28203	0.00530	0.00249	0.00006	0.00001	0.37	75.7	0.165	0.015
WCT1582_39	rim	100	48	0.53356	0.54888	0.00244	0.00259	0.00003	0.00001	0.24	61.7	0.151	0.020
WCT1582_39g2	N/A	53	35	0.66737	0.11462	0.05860	0.01558	0.00064	0.00013	0.76	78.7	0.954	0.099
WCT1582_40	*core*	*77*	*33*	*0.83247*	*0.01884*	*0.44881*	*0.03954*	*0.00391*	*0.00033*	*0.97*	*99.6*	*0.412*	*0.018*
WCT1582_41	*N/A*	*191*	*98*	*0.81228*	*0.02361*	*0.13622*	*0.01246*	*0.00122*	*0.00011*	*0.95*	*97.0*	*0.380*	*0.017*
WCT1582_42c	**core**	**100**	**69**	**0.42391**	**1.44389**	**0.00129**	**0.00447**	**0.00002**	**0.00002**	**0.20**	**47.9**	**0.135**	**0.048**
WCT1582_42r	**rim**	**120**	**107**	**0.27330**	**1.09025**	**0.00045**	**0.00182**	**0.00001**	**0.00001**	**0.14**	**28.8**	**0.106**	**0.031**
WCT1582_43	*core*	*373*	*330*	*0.76832*	*0.02487*	*0.07463*	*0.00433*	*0.00070*	*0.00003*	*0.83*	*91.5*	*0.490*	*0.013*
WCT1582_44	rim	185	119	0.16655	0.16657	0.00055	0.00056	0.00002	0.00000	0.14	15.3	0.203	0.017
WCT1582_45	**rim**	**178**	**184**	**0.62911**	**0.25843**	**0.00245**	**0.00111**	**0.00003**	**0.00001**	**0.43**	**73.8**	**0.093**	**0.010**
WCT1582_46	N/A	289	232	0.59641	0.10025	0.00599	0.00127	0.00007	0.00001	0.61	69.7	0.214	0.014
WCT1582_47	N/A	179	141	0.37360	0.17742	0.00439	0.00216	0.00009	0.00001	0.27	41.5	0.394	0.027
WCT1582_47	N/A	156	135	-0.32114	0.74489	-0.00085	-0.00201	0.00002	0.00001	0.17	-46.5	N/A	N/A
WCT1582_48	**rim**	**88**	**59**	**0.38302**	**0.41456**	**0.00111**	**0.00151**	**0.00002**	**0.00002**	**0.60**	**42.7**	**0.141**	**0.059**
WCT1582_49	*core*	*321*	*546*	*0.78260*	*0.02013*	*0.09662*	*0.01365*	*0.00090*	*0.00012*	*0.98*	*93.3*	*0.480*	*0.034*
WCT1582_50	N/A	194	94	0.74280	0.04458	0.04473	0.01068	0.00044	0.00010	0.97	88.2	0.432	0.051

WCT1582_50	rim	160	77	0.71424	0.16571	0.00728	0.00199	0.00007	0.00001	0.53	84.6	0.144	0.011
WCT1582_51	N/A	132	84	0.83621	0.03691	0.05220	0.00455	0.00045	0.00003	0.86	100.1	N/A	N/A
WCT1582_51	N/A	120	77	0.87292	0.05514	0.04366	0.00380	0.00036	0.00002	0.69	104.7	N/A	N/A
WCT1582_52	rim	120	98	0.78182	0.04242	0.06602	0.00566	0.00061	0.00004	0.77	93.2	0.373	0.030
WCT1582_53	N/A	174	149	0.59795	0.08294	0.00787	0.00167	0.00010	0.00002	0.76	69.9	0.258	0.032
WCT1582_54	rim	76	74	0.81429	0.02857	0.27729	0.01443	0.00247	0.00009	0.74	97.3	0.513	0.011
WCT1582_55	core	726	853	0.44348	0.05525	0.00204	0.00030	0.00003	0.00000	0.53	50.3	0.163	0.008
WCT1582_55	rim	804	896	0.42282	0.08230	0.00159	0.00035	0.00003	0.00000	0.45	47.7	0.147	0.008
WCT1582_56	rim	171	71	0.29000	0.31966	0.00057	0.00066	0.00001	0.00000	0.28	30.9	0.129	0.021
WCT1582_56	rim	171	71	0.46395	0.67874	0.00086	0.00129	0.00001	0.00000	0.23	52.9	0.097	0.017
WCT1582_57	N/A	150	67	0.79441	0.05168	0.04738	0.00514	0.00043	0.00004	0.80	94.8	0.243	0.011
WCT1582_58	N/A	92	48	0.82636	0.02338	0.23017	0.02028	0.00202	0.00017	0.95	98.8	0.248	0.011
WCT1582_59	core	149	125	0.79407	0.03562	0.04828	0.00818	0.00044	0.00007	0.96	94.7	0.236	0.020
WCT1582_59	rim	153	135	0.78127	0.04093	0.02673	0.00231	0.00025	0.00002	0.79	93.1	0.188	0.007
WCT1582_60	core	118	66	0.73657	0.13283	0.02070	0.00493	0.00020	0.00003	0.65	87.5	0.252	0.020
WCT1582_60	rim	114	75	0.69831	0.38574	0.00497	0.00296	0.00005	0.00001	0.38	82.6	0.118	0.014
WCT1582_61	core	101	59	0.73949	0.06218	0.03038	0.00449	0.00030	0.00004	0.82	87.8	0.326	0.020
WCT1582_61	rim	74	40	0.77445	0.16674	0.01430	0.00370	0.00013	0.00002	0.56	92.3	0.138	0.010
WCT1582_62	N/A	78	47	0.85969	0.15737	0.01736	0.00385	0.00015	0.00002	0.56	103.0	N/A	N/A
WCT1582_63	rim	308	223	0.22532	0.08514	0.00121	0.00049	0.00004	0.00001	0.33	22.7	0.267	0.018
WCT1582_64	N/A	182	118	0.79702	0.03083	0.09872	0.01854	0.00090	0.00017	0.98	95.1	0.407	0.038
WCT1582_65	core	155	81	0.56356	0.08154	0.00531	0.00095	0.00007	0.00001	0.58	65.5	0.230	0.012
WCT1582_65	rim	191	113	0.54216	0.11276	0.00359	0.00083	0.00005	0.00000	0.44	62.8	0.187	0.010
WCT1582_66	N/A	193	167	0.62396	0.13093	0.00628	0.00152	0.00007	0.00001	0.50	73.2	0.194	0.012
WCT1582_67	N/A	92	42	0.83601	1.78965	0.00337	0.00725	0.00003	0.00001	0.09	100.0	N/A	N/A
WCT1582_68	rim	478	211	0.05136	0.00076	0.11672	0.00320	0.01648	0.00038	0.84	0.7	104.777	1.226
WCT1582_69	rim	144	125	0.53113	0.13728	0.00898	0.00264	0.00012	0.00002	0.47	61.4	0.378	0.027
WCT1582_70	rim	200	99	0.81464	0.02977	0.07253	0.00703	0.00065	0.00006	0.93	97.3	0.206	0.010
WCT1582_71	N/A	273	208	0.75102	0.03293	0.04650	0.00366	0.00045	0.00003	0.83	89.3	0.399	0.014
WCT1582_72	rim	148	78	0.80721	0.04740	0.04772	0.00775	0.00043	0.00006	0.93	96.4	0.195	0.015
WCT_73	rim	148	74	0.81099	0.01572	0.25360	0.01257	0.00227	0.00010	0.92	96.9	0.552	0.013
WCT_74	rim	151	81	0.59482	0.19290	0.00422	0.00148	0.00005	0.00001	0.37	69.5	0.164	0.011

WCT_75	**rim**	**107**	**50**	**0.74266**	**0.39497**	**0.00368**	**0.00210**	**0.00004**	**0.00001**	**0.37**	**88.2**	**0.096**	**0.009**
WCT_76	rim	1242	1513	0.01296	0.02384	0.00004	0.00007	0.00002	0.00000	0.03	-4.2	0.198	0.007
WCT_77	*rim*	*316*	*369*	*0.77395*	*0.19274*	*0.00529*	*0.00153*	*0.00005*	*0.00001*	*0.51*	*92.2*	*0.102*	*0.013*
WCT_78	rim	204	96	0.46489	0.11647	0.00230	0.00065	0.00004	0.00000	0.45	53.0	0.183	0.012
WCT_79	core	161	123	0.62043	0.10602	0.00997	0.00233	0.00012	0.00002	0.68	72.7	0.282	0.023
WCT_80	core	191	121	0.08371	0.79906	0.00078	0.00744	0.00007	0.00002	0.03	4.8	0.486	0.069
WCT_74	rim	156	82	0.58453	0.27655	0.00339	0.00170	0.00004	0.00001	0.32	68.2	0.156	0.013
WCT_75	**rim**	**107**	**51**	**0.77125**	**0.42913**	**0.00366**	**0.00220**	**0.00003**	**0.00001**	**0.38**	**89.8**	**0.114**	**0.014**
WCT_76	rim	1236	1505	0.01226	0.02338	0.00004	0.00007	0.00002	0.00000	0.03	-4.3	0.198	0.007
WCT_77	**rim**	**317**	**381**	**0.75347**	**0.17204**	**0.00478**	**0.00139**	**0.00005**	**0.00001**	**0.62**	**89.6**	**0.107**	**0.013**
WCT_78	rim	192	90	0.46622	0.15983	0.00244	0.00092	0.00004	0.00001	0.42	53.2	0.190	0.015
WCT_79	rim	152	112	0.57421	0.10028	0.00937	0.00231	0.00012	0.00002	0.71	66.9	0.330	0.030
WCT_80	rim	214	138	0.44701	0.24278	0.00212	0.00120	0.00003	0.00001	0.27	50.8	0.158	0.012

PAL UA1305

PAL1305_179	**rim**	**89**	**63**	**0.40983**	**0.25512**	**0.00180**	**0.00127**	**0.00003**	**0.00001**	**0.46**	**46.1**	**0.172**	**0.029**
PAL1305_180	rim	194	166	0.68639	0.02043	0.09992	0.00397	0.00106	0.00003	0.66	81.1	1.352	0.018
PAL1305_181	core	97	74	0.66953	0.03188	0.11805	0.00752	0.00128	0.00005	0.66	79.0	1.791	0.039
PAL1305_182	core	95	67	0.55281	0.17596	0.00860	0.00319	0.00011	0.00002	0.51	64.2	0.331	0.032
PAL1305_183	**rim**	**109**	**83**	**0.37167**	**0.17569**	**0.00290**	**0.00144**	**0.00006**	**0.00001**	**0.30**	**41.2**	**0.280**	**0.021**
PAL1305_184	core	107	83	0.42940	0.12910	0.00686	0.00230	0.00012	0.00002	0.45	48.6	0.448	0.034
PAL1305_185	**rim**	**153**	**98**	**0.55614**	**0.14143**	**0.00676**	**0.00200**	**0.00009**	**0.00001**	**0.51**	**64.6**	**0.273**	**0.021**
PAL1305_186	**rim**	**159**	**123**	**0.68791**	**0.23209**	**0.01005**	**0.00388**	**0.00011**	**0.00002**	**0.48**	**81.3**	**0.193**	**0.019**
PAL1305_187	core	145	118	0.75065	0.07284	0.05424	0.00585	0.00052	0.00002	0.44	89.2	0.451	0.011
PAL1305_188	**rim**	**182**	**104**	**0.24119**	**0.11591**	**0.00150**	**0.00074**	**0.00005**	**0.00001**	**0.25**	**24.7**	**0.291**	**0.018**
PAL1305_189	*core*	*91*	*73*	*0.75957*	*0.01596*	*0.54509*	*0.03452*	*0.00520*	*0.00031*	*0.94*	*90.4*	*3.427*	*0.105*
PAL1305_190	core	140	84	0.72198	0.01995	0.12632	0.00455	0.00127	0.00003	0.64	85.6	1.271	0.015
PAL1305_191	**rim**	**140**	**96**	**0.40193**	**0.16771**	**0.00227**	**0.00101**	**0.00004**	**0.00001**	**0.35**	**45.1**	**0.211**	**0.017**
PAL1305_192	core	94	62	0.71887	0.03421	0.10074	0.00610	0.00102	0.00004	0.62	85.2	1.057	0.020
PAL1305_193	rim	84	67	0.75485	0.04956	0.11540	0.01025	0.00111	0.00007	0.67	89.8	0.833	0.026
PAL1305_194	core	226	201	0.68176	0.03681	0.02634	0.00192	0.00028	0.00001	0.67	80.5	0.423	0.011
PAL1305_195	**rim**	**350**	**361**	**0.37306**	**0.05866**	**0.00308**	**0.00053**	**0.00006**	**0.00000**	**0.39**	**41.4**	**0.283**	**0.010**

PAL1305_196	*core*	*104*	*64*	*0.78617*	*0.03826*	*0.23337*	*0.02056*	*0.00215*	*0.00016*	*0.83*	*93.7*	*1.029*	*0.039*
PAL1305_197	*rim*	*255*	*209*	*0.76834*	*0.03252*	*0.16843*	*0.01131*	*0.00159*	*0.00008*	*0.78*	*91.5*	*0.994*	*0.027*
PAL1305_198	rim	381	363	0.48699	0.07252	0.00767	0.00122	0.00011	0.00001	0.35	55.8	0.385	0.011
PAL_1	*rim*	*104*	*87*	*0.82309*	*0.02408*	*0.45964*	*0.01923*	*0.00405*	*0.00012*	*0.71*	*98.4*	*0.699*	*0.011*
PAL_2	rim	77	51	0.59227	0.18020	0.01959	0.00798	0.00024	0.00007	0.67	69.2	0.548	0.076
PAL_3	*rim*	*113*	*71*	*0.79926*	*0.04816*	*0.17349*	*0.01261*	*0.00157*	*0.00006*	*0.56*	*95.4*	*0.616*	*0.013*
PAL_4	**rim**	**167**	**150**	**0.54064**	**0.21381**	**0.00545**	**0.00233**	**0.00007**	**0.00001**	**0.38**	**62.6**	**0.238**	**0.020**
PAL_5	**rim**	**92**	**43**	**0.70901**	**0.37776**	**0.01327**	**0.00748**	**0.00014**	**0.00003**	**0.33**	**84.0**	**0.219**	**0.021**
PAL_6	**core**	**99**	**72**	**0.63977**	**0.32567**	**0.00982**	**0.00576**	**0.00011**	**0.00003**	**0.50**	**75.2**	**0.248**	**0.037**
PAL_7	*rim*	*706*	*1084*	*0.75887*	*0.05507*	*0.03330*	*0.00285*	*0.00032*	*0.00001*	*0.53*	*90.3*	*0.253*	*0.006*
PAL_8	*core*	*168*	*183*	*0.78884*	*0.03923*	*0.29408*	*0.02321*	*0.00270*	*0.00017*	*0.78*	*94.1*	*1.197*	*0.038*
PAL_9	*rim*	*226*	*211*	*0.81569*	*0.02774*	*0.56327*	*0.02895*	*0.00501*	*0.00019*	*0.75*	*97.5*	*1.128*	*0.022*
PAL_10	core	111	66	0.67296	0.16230	0.02833	0.00926	0.00031	0.00007	0.68	79.4	0.486	0.055
PAL_11	*rim*	*104*	*62*	*0.80047*	*0.07191*	*0.11284*	*0.01410*	*0.00102*	*0.00009*	*0.70*	*95.5*	*0.420*	*0.019*
PAL_12	rim	200	192	0.74418	0.04590	0.13528	0.01069	0.00132	0.00007	0.62	88.4	1.078	0.027
PAL_13	**rim**	**300**	**241**	**0.71105**	**0.11724**	**0.01729**	**0.00353**	**0.00018**	**0.00002**	**0.59**	**84.2**	**0.251**	**0.015**
PAL_14	rim	156	125	0.54931	0.09378	0.01592	0.00352	0.00021	0.00003	0.63	63.7	0.555	0.040
PAL_15	**rim**	**125**	**86**	**0.74060**	**0.17589**	**0.02382**	**0.01926**	**0.00023**	**0.00018**	**0.96**	**88.0**	**0.260**	**0.102**
PAL_16	*rim*	*83*	*59*	*0.76204*	*0.02662*	*0.24249*	*0.01408*	*0.00231*	*0.00011*	*0.80*	*90.7*	*1.523*	*0.036*
PAL_17	*rim*	*122*	*98*	*0.81915*	*0.02715*	*0.18755*	*0.00902*	*0.00166*	*0.00006*	*0.72*	*97.9*	*0.382*	*0.007*
PAL_17	*rim*	*55*	*43*	*0.79914*	*0.03721*	*0.24325*	*0.01660*	*0.00221*	*0.00011*	*0.73*	*95.4*	*0.826*	*0.021*
PAL_18	core	48	23	0.73742	0.05069	0.21514	0.01849	0.00212	0.00011	0.60	87.6	1.814	0.048
PAL_19	*rim*	*195*	*160*	*0.82249*	*0.03505*	*0.17756*	*0.01038*	*0.00157*	*0.00006*	*0.68*	*98.3*	*0.321*	*0.007*
PAL_20	**rim**	**108**	**84**	**0.54341**	**0.38014**	**0.00367**	**0.00265**	**0.00005**	**0.00001**	**0.25**	**63.0**	**0.178**	**0.016**
PAL1305_199	*rim*	*143*	*109*	*0.78350*	*0.01431*	*0.21739*	*0.00855*	*0.00201*	*0.00007*	*0.89*	*93.4*	*1.004*	*0.018*
PAL1305_200	core	58	35	0.27628	0.17565	0.00453	0.00296	0.00012	0.00002	0.23	29.2	0.607	0.047
PAL1305_201	rim	109	76	0.18178	0.34331	0.00122	0.00233	0.00005	0.00001	0.13	17.2	0.328	0.043
PAL1305_202	**rim**	**70**	**37**	**0.66007**	**0.31766**	**0.00975**	**0.00516**	**0.00011**	**0.00002**	**0.42**	**77.8**	**0.230**	**0.026**
PAL1305_203	core	120	54	0.05685	0.00220	0.11714	0.00468	0.01495	0.00015	0.25	1.1	95.000	0.472
PAL1305_204	*N/A*	*126*	*66*	*0.80458*	*0.07391*	*0.08283*	*0.00995*	*0.00075*	*0.00006*	*0.64*	*96.1*	*0.305*	*0.012*
PAL1305_205	rim	76	41	0.74854	0.06915	0.06963	0.01034	0.00067	0.00008	0.78	89.0	0.580	0.034
PAL1305_206	*core*	*94*	*66*	*0.80927*	*0.09447*	*0.08865*	*0.01281*	*0.00079*	*0.00007*	*0.59*	*96.7*	*0.283*	*0.013*

PAL1305_207	**rim**	**260**	**291**	**0.43020**	**0.08954**	**0.00399**	**0.00096**	**0.00007**	**0.00001**	**0.50**	**48.7**	**0.276**	**0.017**
Old Crow (UA1422, UT1434, UT1577)													
OCT1577_2	*rim*	*260*	*108*	*0.76363*	*0.05856*	*0.07009*	*0.00787*	*0.00067*	*0.00005*	*0.73*	*90.9*	*0.496*	*0.026*
OCT1577_3	*core*	*130*	*56*	*0.79408*	*0.02194*	*0.34707*	*0.03059*	*0.00317*	*0.00027*	*0.95*	*94.7*	*1.166*	*0.148*
OCT1577_4	N/A	258	292	0.10768	0.00119	3.12914	0.06180	0.21076	0.00345	0.83	4.2	1185.516	25.787
OCT1577_5	rim	422	219	0.06275	0.00188	0.25171	0.00830	0.02909	0.00040	0.42	1.6	182.057	4.209
OCT1577_6	*rim*	*81*	*28*	*0.83017*	*0.02870*	*0.72419*	*0.04759*	*0.00633*	*0.00035*	*0.85*	*99.3*	*0.717*	*0.026*
OCT1577_7	N/A	437	236	0.11436	0.00651	0.24860	0.01533	0.01577	0.00037	0.38	8.4	92.526	2.338
OCT1577_8	core	103	46	0.20735	0.08932	0.00448	0.00202	0.00016	0.00002	0.30	20.4	0.893	0.073
OCT1577_9	**rim**	**433**	**298**	**0.70460**	**0.05843**	**0.00729**	**0.00184**	**0.00008**	**0.00002**	**0.94**	**83.4**	**0.150**	**0.009**
OCT1577_10	*rim*	*117*	*52*	*0.76850*	*0.04334*	*0.35714*	*0.02809*	*0.00337*	*0.00018*	*0.70*	*91.5*	*1.938*	*0.070*
OCT1577_11	*rim*	*328*	*160*	*0.82477*	*0.03696*	*0.19504*	*0.02995*	*0.00172*	*0.00025*	*0.96*	*98.6*	*0.322*	*0.013*
OCT1577_12	rim	228	138	0.08912	0.00354	0.39595	0.01659	0.03222	0.00043	0.32	4.9	194.689	4.488
OCT1577_13	**rim**	**226**	**92**	**0.70598**	**0.05600**	**0.00724**	**0.00191**	**0.00007**	**0.00002**	**0.95**	**83.6**	**0.155**	**0.011**
OCT1577_14	*core*	*146*	*84*	*0.79172*	*0.05248*	*0.20944*	*0.01778*	*0.00192*	*0.00010*	*0.62*	*94.4*	*0.840*	*0.031*
OCT1577_15	*rim*	*687*	*574*	*0.76988*	*0.04378*	*0.06247*	*0.02076*	*0.00059*	*0.00019*	*0.99*	*91.7*	*0.400*	*0.069*
OCT1577_16	*rim*	*104*	*40*	*0.79282*	*0.04283*	*0.50266*	*0.13744*	*0.00460*	*0.00123*	*0.98*	*94.6*	*1.705*	*0.236*
OCT1577_17	*core*	*117*	*52*	*0.81830*	*0.02576*	*0.72195*	*0.03127*	*0.00640*	*0.00019*	*0.69*	*97.8*	*0.993*	*0.027*
OCT1577_18	**rim**	**468**	**299**	**0.35272**	**0.13972**	**0.00146**	**0.00071**	**0.00003**	**0.00001**	**0.57**	**38.8**	**0.177**	**0.021**
OCT1577_19	rim	251	155	0.74548	0.02776	0.27521	0.03028	0.00268	0.00028	0.94	88.6	2.051	0.118
OCT1577_20	*core*	*152*	*62*	*0.81162*	*0.04855*	*0.18527*	*0.03232*	*0.00166*	*0.00027*	*0.94*	*97.0*	*0.489*	*0.043*
OCT1577_21	*core*	*345*	*283*	*0.78341*	*0.03773*	*0.06747*	*0.00450*	*0.00062*	*0.00003*	*0.69*	*93.4*	*0.337*	*0.014*
OCT1577_22	*core*	*90*	*46*	*0.76151*	*0.10034*	*0.12385*	*0.02557*	*0.00118*	*0.00019*	*0.77*	*90.6*	*0.799*	*0.067*
OCT1577_23	*rim*	*156*	*59*	*0.79058*	*0.03676*	*0.14011*	*0.02777*	*0.00129*	*0.00025*	*0.97*	*94.3*	*0.564*	*0.057*
OCT1577_24	*rim*	*336*	*209*	*0.78993*	*0.04290*	*0.12373*	*0.03341*	*0.00114*	*0.00030*	*0.98*	*94.2*	*0.504*	*0.027*
OCT1577_25	core	68	28	0.58031	0.12279	0.03652	0.00933	0.00046	0.00007	0.56	67.7	1.041	0.080
OCT1577_26	core	153	115	0.12536	0.00206	4.45549	0.11439	0.25778	0.00508	0.77	4.8	1414.450	31.052
OCT1577_27	*core*	*350*	*204*	*0.80688*	*0.02146*	*0.13607*	*0.00572*	*0.00122*	*0.00004*	*0.77*	*96.4*	*0.369*	*0.012*
OCT1577_28	*rim*	*79*	*32*	*0.81292*	*0.04618*	*0.54535*	*0.08006*	*0.00487*	*0.00066*	*0.92*	*97.1*	*0.992*	*0.072*
OCT1577_29	*rim*	*228*	*82*	*0.78172*	*0.08749*	*0.02143*	*0.00757*	*0.00020*	*0.00007*	*0.95*	*93.2*	*0.166*	*0.010*

OCT1577_30	**rim**	**508**	**256**	**0.75422**	**0.05869**	**0.01558**	**0.00184**	**0.00015**	**0.00001**	**0.75**	**89.7**	**0.170**	**0.007**
OCT1577_31	*core*	*135*	*42*	*0.78439*	*0.05291*	*0.12318*	*0.01525*	*0.00114*	*0.00012*	*0.84*	*93.5*	*0.571*	*0.033*
OCT01P2	rim	268	166	0.05513	0.00139	0.09120	0.00286	0.01200	0.00022	0.60	0.9	76.235	10.172
OCT02P2	rim	*188*	*65*	*0.76375*	*0.03611*	*0.07851*	*0.00680*	*0.00075*	*0.00005*	*0.84*	*90.9*	*0.530*	*0.138*
OCT03P2	rim	**220**	**87**	**0.56258**	**0.06740**	**0.00325**	**0.00071**	**0.00004**	**0.00001**	**0.84**	**65.4**	**0.160**	**0.042**
OCT04P2	rim	*189*	*75*	*0.77921*	*0.05333*	*0.05065*	*0.00566*	*0.00047*	*0.00004*	*0.79*	*92.9*	*0.317*	*0.042*
OCT06P2	rim	*148*	*54*	*0.79755*	*0.03539*	*0.26718*	*0.04645*	*0.00243*	*0.00041*	*0.97*	*95.2*	*0.847*	*0.114*
OCT07P2	rim	*195*	*77*	*0.77614*	*0.04657*	*0.05424*	*0.00523*	*0.00051*	*0.00004*	*0.78*	*92.5*	*0.337*	*0.050*
OCT08P2	rim	316	163	0.51871	0.07005	0.00672	0.00110	0.00009	0.00001	0.56	59.9	0.328	0.012
OCT10P2	rim	*160*	*66*	*0.80441*	*0.02488*	*0.22494*	*0.02271*	*0.00203*	*0.00019*	*0.95*	*96.0*	*0.606*	*0.055*
OCT11P2	rim	*929*	*539*	*0.75866*	*0.03252*	*0.05558*	*0.00391*	*0.00053*	*0.00003*	*0.79*	*90.3*	*0.416*	*0.028*
OCT12P2	rim	**2547**	**2090**	**0.11308**	**0.02372**	**0.00054**	**0.00012**	**0.00003**	**0.00000**	**0.39**	**8.5**	**0.261**	**0.017**
OCT13P2	rim	*389*	*193*	*0.79157*	*0.04065*	*0.09432*	*0.01166*	*0.00086*	*0.00010*	*0.91*	*94.4*	*0.397*	*0.073*
OCT14P2	rim	*932*	*579*	*0.79661*	*0.03559*	*0.05184*	*0.00405*	*0.00047*	*0.00003*	*0.82*	*95.1*	*0.240*	*0.021*
OCT15P2	rim	*877*	*545*	*0.80078*	*0.02896*	*0.09600*	*0.01200*	*0.00087*	*0.00010*	*0.96*	*95.6*	*0.327*	*0.047*
OCT16P2	rim	1600	1313	0.70033	0.03152	0.03528	0.00357	0.00037	0.00003	0.90	82.9	0.474	0.049
OCT17P2	N/A	239	113	0.71888	0.05129	0.16935	0.03400	0.00171	0.00032	0.93	85.2	1.715	0.253
OCT18P2	rim	*601*	*309*	*0.75903*	*0.02759*	*0.07409*	*0.00374*	*0.00071*	*0.00002*	*0.69*	*90.3*	*0.528*	*0.042*
OCT19P2	rim	417	175	0.75306	0.04884	0.04535	0.00607	0.00044	0.00005	0.87	89.5	0.377	0.050
OCT20P2	rim	210	74	0.18379	0.09963	0.00122	0.00068	0.00005	0.00001	0.22	17.4	0.348	0.045
OCT21P2	rim	*70*	*20*	*0.81038*	*0.05543*	*0.15805*	*0.01451*	*0.00141*	*0.00009*	*0.67*	*96.8*	*0.388*	*0.068*
OCT22P2	rim	*116*	*53*	*0.81329*	*0.01824*	*0.74982*	*0.08826*	*0.00669*	*0.00077*	*0.98*	*97.2*	*1.307*	*0.032*
OCT23P2	rim	*267*	*125*	*0.81839*	*0.02776*	*0.11438*	*0.00843*	*0.00101*	*0.00007*	*0.89*	*97.8*	*0.272*	*0.016*
OCT24P2	rim	*224*	*100*	*0.77215*	*0.03504*	*0.14768*	*0.01061*	*0.00139*	*0.00008*	*0.78*	*92.0*	*0.807*	*0.166*
OCT25P2	rim	*80*	*40*	*0.81408*	*0.03691*	*0.23155*	*0.01537*	*0.00206*	*0.00010*	*0.73*	*97.3*	*0.448*	*0.061*
OCT26P2	rim	111	47	0.74492	0.03377	0.07486	0.00525	0.00073	0.00004	0.76	88.5	0.629	0.036
OCT27P2	rim	*248*	*133*	*0.77811*	*0.04400*	*0.11864*	*0.01305*	*0.00111*	*0.00010*	*0.86*	*92.7*	*0.603*	*0.065*
OCT28P2	rim	350	167	0.75057	0.02457	0.05093	0.00252	0.00049	0.00002	0.75	89.2	0.429	0.103
OCT30P2	rim	247	103	0.72136	0.04590	0.06932	0.00971	0.00070	0.00009	0.89	85.5	0.740	0.081
OCT31P2	rim	*441*	*188*	*0.77179*	*0.04512*	*0.04357*	*0.00363*	*0.00041*	*0.00002*	*0.71*	*91.9*	*0.303*	*0.137*
OCT33P2	rim	*236*	*107*	*0.81653*	*0.01929*	*0.68389*	*0.08463*	*0.00607*	*0.00074*	*0.98*	*97.6*	*1.035*	*0.213*
OCT34P2	rim	*245*	*95*	*0.81741*	*0.03492*	*0.26438*	*0.06640*	*0.00235*	*0.00058*	*0.99*	*97.7*	*0.440*	*0.088*

OCT35P2	rim	*526*	*206*	*0.78062*	*0.03318*	*0.11599*	*0.00885*	*0.00108*	*0.00007*	*0.83*	*93.0*	*0.575*	*0.076*
OCT36P2	rim	*287*	*114*	*0.81661*	*0.02825*	*0.49554*	*0.08246*	*0.00440*	*0.00072*	*0.98*	*97.6*	*0.774*	*0.091*
OCT37P2	rim	*352*	*148*	*0.81225*	*0.02559*	*0.18059*	*0.01143*	*0.00161*	*0.00009*	*0.87*	*97.0*	*0.397*	*0.099*
OCT38P2	rim	*418*	*175*	*0.81057*	*0.03020*	*0.13731*	*0.01159*	*0.00123*	*0.00009*	*0.90*	*96.8*	*0.341*	*0.039*
OCT39P2	rim	*95*	*37*	*0.76294*	*0.02844*	*0.73851*	*0.06755*	*0.00702*	*0.00059*	*0.91*	*90.8*	*4.256*	*1.857*
OCT40P2	rim	*330*	*164*	*0.79211*	*0.02521*	*0.19000*	*0.01943*	*0.00174*	*0.00017*	*0.95*	*94.5*	*0.704*	*0.156*
OCT41P2 (not zircon?)	*N/A*	*1*	*3*	*0.81666*	*0.01563*	#######	*4.89664*	*1.03206*	*0.03874*	*0.89*	*96.0*	*261.662*	*50.509*
OCT42P2	core	472	337	0.65224	0.05334	0.01423	0.00183	0.00016	0.00002	0.77	76.8	0.313	0.057
togiak - 1	core	178	85	0.33851	0.39062	0.00893	0.01055	0.00019	0.00005	0.21	37.0	0.863	0.306
togiak - 2	**rim**	**278**	**139**	**0.67510**	**0.36849**	**0.00717**	**0.00489**	**0.00008**	**0.00003**	**0.60**	**79.7**	**0.167**	**0.025**
togiak - 3	**N/A**	**191**	**72**	**0.72834**	**0.70130**	**0.01509**	**0.01602**	**0.00015**	**0.00007**	**0.42**	**86.4**	**0.211**	**0.034**
togiak - 4	rim	243	105	0.64382	0.22846	0.01366	0.00588	0.00015	0.00004	0.57	75.7	0.330	0.096
togiak - 5	*rim*	*347*	*131*	*0.79289*	*0.20972*	*0.04198*	*0.01442*	*0.00038*	*0.00008*	*0.64*	*94.6*	*0.229*	*0.044*
togiak - 6	**rim?**	**592**	**321**	**0.75109**	**0.41544**	**0.01525**	**0.00877**	**0.00015**	**0.00002**	**0.27**	**89.3**	**0.171**	**0.074**
togiak - 7	core	289	133	0.11660	0.00541	0.17787	0.00930	0.01106	0.00027	0.46	8.8	64.837	24.534
togiak - 8	rim	319	129	0.72557	0.26568	0.02648	0.01056	0.00026	0.00004	0.40	86.1	0.328	0.127
togiak - 9	N/A	756	430	0.65072	0.05150	0.07119	0.00971	0.00079	0.00009	0.81	76.6	1.280	0.210
togiak - 10	*rim*	*234*	*98*	*0.76708*	*0.12361*	*0.14865*	*0.02855*	*0.00141*	*0.00015*	*0.54*	*91.3*	*0.876*	*0.146*
togiak - 11	rim	208	77	0.50303	0.41397	0.00961	0.00861	0.00014	0.00005	0.40	57.9	0.468	0.078
togiak - 12	*rim*	*314*	*181*	*0.78921*	*0.12915*	*0.06433*	*0.01405*	*0.00059*	*0.00009*	*0.66*	*94.1*	*0.306*	*0.008*
togiak - 13	rim	191	74	0.52856	0.28843	0.01437	0.00875	0.00020	0.00005	0.44	61.1	0.585	0.027
togiak - 14	*core*	*229*	*86*	*0.83892*	*0.13617*	*0.06828*	*0.01324*	*0.00059*	*0.00006*	*0.55*	*100.4*	*N/A*	*N/A*
togiak - 15	**rim**	**185**	**62**	**0.50368**	**0.54884**	**0.00322**	**0.00501**	**0.00005**	**0.00005**	**0.71**	**58.0**	**0.200**	**0.011**
togiak - 16	*core*	*118*	*38*	*0.82384*	*0.12841*	*0.20925*	*0.04189*	*0.00184*	*0.00023*	*0.63*	*98.5*	*0.362*	*0.033*
togiak - 17	*core*	*297*	*200*	*0.84736*	*0.06699*	*0.25302*	*0.02799*	*0.00217*	*0.00017*	*0.70*	*101.5*	*N/A*	*N/A*
togiak - 18	core	687	455	0.22708	0.16761	0.00173	0.00134	0.00006	0.00001	0.30	22.9	0.353	0.020
togiak - 19	core	212	99	-0.06360	0.35501	-0.00081	-0.00454	0.00009	0.00003	0.06	-13.9	0.766	0.043
togiak - 20	rim	460	188	0.30573	0.37054	0.00247	0.00316	0.00006	0.00002	0.32	32.9	0.343	0.014
togiak - 21	**rim**	**151**	**45**	**0.09530**	**0.25602**	**0.00031**	**0.00091**	**0.00002**	**0.00003**	**0.42**	**6.2**	**0.217**	**0.013**
togiak - 22	N/A	427	200	0.23582	0.28940	0.00168	0.00216	0.00005	0.00002	0.30	24.0	0.340	0.022
togiak - 23	rim	523	341	0.20523	0.25274	0.00149	0.00188	0.00005	0.00001	0.20	20.2	0.350	0.019
togiak - 24	*N/A*	*236*	*104*	*0.78608*	*0.05647*	*0.19865*	*0.02242*	*0.00183*	*0.00016*	*0.77*	*93.7*	*0.830*	*0.060*

togiak - 25	N/A	153	58	0.74531	0.16713	0.11763	0.03527	0.00114	0.00023	0.66	88.6	0.935	0.053
togiak - 26	N/A	179	78	0.73624	0.35468	0.07713	0.05171	0.00076	0.00035	0.70	87.4	0.705	0.070
togiak - 27	N/A	243	117	0.65310	0.25279	0.01932	0.00842	0.00021	0.00004	0.46	76.9	0.406	0.013
togiak - 28	N/A	88	22	0.48388	0.56026	0.02973	0.04331	0.00045	0.00039	0.61	55.5	1.377	0.092
togiak - 29	N/A	253	115	0.60878	0.57685	0.00976	0.00997	0.00012	0.00004	0.37	71.3	0.303	0.021
togiak - 30	N/A	281	97	0.37871	0.28959	0.00387	0.00330	0.00007	0.00003	0.44	42.1	0.370	0.016
togiak - 31	N/A	498	263	0.52232	0.33958	0.00661	0.00458	0.00009	0.00002	0.34	60.3	0.319	0.021
togiak - 32	N/A	279	121	0.50768	0.36001	0.01722	0.01278	0.00025	0.00005	0.30	58.5	0.748	0.039
togiak - 33	N/A	176	68	0.26562	0.37017	0.00356	0.00525	0.00010	0.00005	0.33	27.8	0.544	0.021
togiak - 34	N/A	366	165	0.39494	0.20628	0.00748	0.00421	0.00014	0.00003	0.37	44.2	0.582	0.022
togiak - 35	N/A	307	125	0.20660	0.29419	0.00126	0.00207	0.00004	0.00004	0.50	20.3	0.317	0.012
togiak - 36	N/A	190	76	0.32007	0.30643	0.00885	0.00928	0.00020	0.00009	0.41	34.7	0.935	0.052
togiak - 37	N/A	657	485	0.68698	0.15186	0.02668	0.01144	0.00028	0.00010	0.86	81.2	0.416	0.014
UA1422 - 1	rim	206	86	0.25564	0.41757	0.00375	0.00626	0.00011	0.00004	0.21	26.5	0.593	0.041
UA1422 - 2	rim	**194**	**80**	**0.29921**	**0.30084**	**0.00188**	**0.00226**	**0.00005**	**0.00003**	**0.55**	**32.1**	**0.274**	**0.012**
UA1422 - 3	rim	213	361	0.60852	0.36732	0.01265	0.00832	0.00015	0.00004	0.40	71.2	0.309	0.021
UA1422 - 4	rim	**664**	**398**	**0.75423**	**0.21185**	**0.01853**	**0.00702**	**0.00018**	**0.00005**	**0.67**	**89.7**	**0.189**	**0.025**
UA1422 - 5	rim	60	30	0.23153	0.27774	0.00465	0.00617	0.00015	0.00008	0.43	23.5	0.805	0.034
UA1422 - 6	rim	471	586	0.12272	0.20928	0.00121	0.00212	0.00007	0.00003	0.21	9.7	0.468	0.041
UA1422 - 7	rim	46	34	0.24549	0.42614	0.00416	0.00802	0.00012	0.00010	0.44	25.3	0.667	0.027
UA1422 - 8	rim	172	87	0.14739	0.29661	0.00097	0.00207	0.00005	0.00003	0.34	12.8	0.353	0.017
UA1422 - 9	rim	**123**	**43**	**0.31850**	**0.41984**	**0.00196**	**0.00293**	**0.00004**	**0.00003**	**0.47**	**34.5**	**0.265**	**0.013**
UA1422 - 10	rim	364	209	0.26628	0.16944	0.00183	0.00129	0.00005	0.00002	0.43	27.9	0.314	0.018
UA1422 - 11	rim	**694**	**777**	**0.17827**	**0.22657**	**0.00083**	**0.00109**	**0.00003**	**0.00001**	**0.22**	**16.7**	**0.223**	**0.007**
UA1422 - 12	rim	139	91	0.19511	0.67446	0.00448	0.01555	0.00017	0.00005	0.09	18.9	0.949	0.059
UA1422_OCt	rim	*48*	*43*	*0.77285*	*0.17510*	*0.10838*	*0.03021*	*0.00102*	*0.00017*	*0.58*	*92.0*	*0.588*	*0.050*
UA1422_OCt	rim	75	35	0.43454	0.39183	0.01291	0.01186	0.00022	0.00004	0.19	49.2	0.793	0.072
UA1422_OCt	rim	**336**	**203**	**0.41095**	**0.24789**	**0.00252**	**0.00158**	**0.00004**	**0.00001**	**0.26**	**46.2**	**0.218**	**0.021**
UA1422_OCt	rim	**762**	**742**	**0.35072**	**0.13056**	**0.00169**	**0.00066**	**0.00004**	**0.00000**	**0.30**	**38.6**	**0.185**	**0.016**
UA1422_OCt	rim	409	160	0.06203	0.00199	0.08302	0.00279	0.00971	0.00010	0.31	1.9	61.207	0.558
UA1422_OCt	rim	*227*	*117*	*0.84075*	*0.06541*	*0.08962*	*0.01208*	*0.00077*	*0.00009*	*0.82*	*100.6*	*N/A*	*N/A*
UT1434_Togiak_Oct	rim	**314**	**142**	**0.73641**	**0.09907**	**0.02285**	**0.00357**	**0.00023**	**0.00002**	**0.51**	**87.4**	**0.265**	**0.013**
UT1434_Togiak_Oct	rim	1002	818	0.63088	0.07881	0.02020	0.00393	0.00023	0.00003	0.77	74.1	0.459	0.036

UT1434_Togiak_Oct	core	147	59	0.61499	0.15623	0.01683	0.00507	0.00020	0.00003	0.54	72.1	0.448	0.038
UT1434_Togiak_Oct	**rim**	**125**	**37**	**0.75271**	**0.17513**	**0.02840**	**0.00861**	**0.00027**	**0.00005**	**0.64**	**89.5**	**0.278**	**0.030**
UT1434_Togiak_Oct	core	87	35	0.60729	0.17024	0.02284	0.00748	0.00027	0.00005	0.52	71.1	0.599	0.052
UT1434_Togiak_Oct	core	272	109	0.65952	0.10259	0.02075	0.00377	0.00023	0.00002	0.52	77.7	0.418	0.021
UT1434_Togiak_Oct	*rim*	*252*	*118*	*0.78560*	*0.08913*	*0.05459*	*0.00866*	*0.00050*	*0.00006*	*0.70*	*93.7*	*0.305*	*0.019*
UT1434_Togiak_Oct	N/A	291	176	0.74712	0.05209	0.06569	0.00602	0.00064	0.00004	0.65	88.8	0.542	0.018
UT1434_Togiak_Oct	*rim*	*146*	*46*	*0.83821*	*0.12971*	*0.04021*	*0.00935*	*0.00035*	*0.00006*	*0.75*	*100.3*	*N/A*	*N/A*
UT1434_Togiak_Oct	*rim*	**438**	**223**	**0.74511**	**0.10573**	**0.01443**	**0.00248**	**0.00014**	**0.00001**	**0.56**	**88.5**	**0.174**	**0.012**
UT1434_Togiak_Oct	*rim*	*237*	*82*	*0.78627*	*0.05127*	*0.07827*	*0.00680*	*0.00072*	*0.00004*	*0.66*	*93.7*	*0.384*	*0.012*
UT1434_Togiak_Oct	*rim*	**175**	**69**	**0.74797**	**0.22010**	**0.01001**	**0.00347**	**0.00010**	**0.00002**	**0.53**	**88.9**	**0.160**	**0.028**
UT1434_Togiak_Oct	*rim*	**708**	**575**	**0.72941**	**0.06009**	**0.02597**	**0.00295**	**0.00026**	**0.00002**	**0.69**	**86.5**	**0.295**	**0.015**
UT1434_Togiak_Oct	*rim*	*189*	*91*	*0.79490*	*0.04245*	*0.14935*	*0.01101*	*0.00136*	*0.00007*	*0.69*	*94.8*	*0.540*	*0.015*
UT1434_Togiak_Oct	*rim*	312	163	0.63926	0.12180	0.01581	0.00345	0.00018	0.00002	0.49	75.1	0.372	0.021
UT1434_Togiak_Oct	*rim*	*326*	*172*	*0.76896*	*0.03226*	*0.18637*	*0.01046*	*0.00176*	*0.00007*	*0.66*	*91.6*	*1.041*	*0.022*
UT1434_Togiak_Oct	*rim*	**371**	**200**	**0.70714**	**0.15128**	**0.01548**	**0.00397**	**0.00016**	**0.00002**	**0.55**	**83.7**	**0.241**	**0.020**
UT1434_Togiak_Oct	*rim*	*250*	*99*	*0.81004*	*0.03017*	*0.22344*	*0.01115*	*0.00200*	*0.00007*	*0.67*	*96.8*	*0.508*	*0.010*
UT1434_Togiak_Oct	*rim*	*209*	*82*	*0.78845*	*0.04918*	*0.17268*	*0.01347*	*0.00159*	*0.00007*	*0.60*	*94.0*	*0.702*	*0.018*
UT1434_Togiak_Oct	*rim*	**184**	**67**	**0.76477**	**0.13344**	**0.02279**	**0.00503**	**0.00022**	**0.00003**	**0.61**	**89.0**	**0.209**	**0.017**
UT1434_Togiak_Oct	*rim*	*144*	*55*	*0.82034*	*0.03443*	*0.19310*	*0.01062*	*0.00171*	*0.00006*	*0.65*	*98.1*	*0.304*	*0.007*
UT1434_Togiak_Oct	*rim*	248	75	0.72862	0.06215	0.04358	0.00470	0.00043	0.00003	0.61	86.4	0.474	0.017
UT1434_Togiak_Oct	*rim*	409	189	0.62059	0.10060	0.01590	0.00297	0.00019	0.00002	0.50	72.8	0.414	0.021
UT1434_Togiak_Oct	*rim*	*224*	*105*	*0.81231*	*0.04113*	*0.16173*	*0.01147*	*0.00144*	*0.00007*	*0.70*	*97.0*	*0.362*	*0.011*
UA1422_OCt	core	715	1262	0.07751	0.07751	0.00127	0.00127	0.00012	0.00001	0.07	4.0	0.761	0.068
UA1422_OCt	rim	590	345	0.05255	0.05255	0.00166	0.00166	0.00023	0.00001	0.05	0.8	1.543	0.054
UA1422_OCt	rim	187	80	0.05843	0.05843	0.00762	0.00762	0.00095	0.00004	0.04	1.6	6.087	0.157
UA1422_OCt	rim	**162**	**68**	**0.70142**	**0.60014**	**0.00780**	**0.00675**	**0.00008**	**0.00001**	**0.15**	**83.0**	**0.156**	**0.017**
UA1422_OCt	rim	101	88	0.07820	0.07820	0.01248	0.01254	0.00116	0.00011	0.10	4.1	7.220	0.397

Sheep Creek Fairbanks (UA207, UT734)

UA207SCf	**rim**	**81**	**46**	**0.71809**	**0.38664**	**0.01096**	**0.00615**	**0.00011**	**0.00002**	**0.28**	**85.1**	**0.161**	**0.014**
UA207SCf_1	*rim*	*192*	*158*	*0.77254*	*0.12020*	*0.30637*	*0.05545*	*0.00288*	*0.00027*	*0.51*	*92.0*	*1.535*	*0.072*
UA207SCf_2	N/A	145	76	0.10165	0.00237	0.84852	0.02112	0.06054	0.00054	0.36	6.1	356.372	1.565

UA207SCf_3	core	389	66	0.11884	0.00167	1.47419	0.03074	0.08997	0.00138	0.74	7.6	514.983	3.879
UA207SCf_4	rim	991	2970	0.11204	0.00387	0.26838	0.00978	0.01737	0.00020	0.32	8.1	102.058	0.605
UA207SCf_5	rim	130	63	0.26279	0.02207	0.56411	0.04805	0.01557	0.00022	0.17	27.2	72.761	0.523
UA207SCf_6	*rim*	*322*	*290*	*0.76449*	*0.08551*	*0.04131*	*0.00777*	*0.00039*	*0.00006*	*0.80*	*91.0*	*0.282*	*0.023*
UA207SCf_7	rim	421	310	0.51298	0.03370	0.12501	0.00999	0.00177	0.00008	0.57	59.1	4.713	0.109
SCF734_2	rim	248	163	0.73535	0.07469	0.03272	0.00668	0.00032	0.00006	0.87	87.3	0.329	0.030
SCF734_1	rim	91	53	0.74753	0.14195	0.03247	0.00886	0.00032	0.00006	0.72	88.8	0.297	0.030
SCF734_3	*rim*	*294*	*170*	*0.77348*	*0.03432*	*0.14835*	*0.01811*	*0.00139*	*0.00016*	*0.93*	*92.1*	*0.815*	*0.047*
SCF734_4	rim	253	125	0.13548	0.00343	2.48266	0.16557	0.13290	0.00820	0.92	8.8	737.212	21.853
SCF734_5	**rim**	**196**	**197**	**0.78097**	**0.06657**	**0.03241**	**0.01102**	**0.00030**	**0.00010**	**0.97**	**89.1**	**0.177**	**0.030**
SCF734_6	**rim**	**222**	**217**	**0.72050**	**0.19373**	**0.01616**	**0.00589**	**0.00016**	**0.00004**	**0.68**	**85.4**	**0.189**	**0.029**
SCF734_7	*core*	*233*	*212*	*0.76841*	*0.11539*	*0.03380*	*0.00719*	*0.00032*	*0.00005*	*0.71*	*91.5*	*0.225*	*0.017*
SCF734_8	**rim**	**185**	**178**	**0.76114**	**0.24789**	**0.01932**	**0.00847**	**0.00018**	**0.00005**	**0.67**	**89.6**	**0.159**	**0.023**
SCF734_9	N/A	818	415	0.06879	0.00185	0.11333	0.00368	0.01195	0.00022	0.56	2.9	74.449	0.689
SCF734_10	N/A	482	345	0.13899	0.00121	4.05879	0.08515	0.21179	0.00404	0.91	8.0	1148.193	10.230
SCF734_11	core	3067	623	0.05585	0.00209	0.05959	0.02490	0.00774	0.00322	1.00	1.1	49.241	10.400
SCF734_12	rim	301	274	0.08205	0.00767	0.50456	0.04842	0.04460	0.00098	0.23	3.9	270.709	2.973
scf734_13	*N/A*	*147*	*167*	*0.77723*	*0.13216*	*0.05018*	*0.01095*	*0.00047*	*0.00006*	*0.63*	*92.6*	*0.267*	*0.020*
scf734_14	rim	353	58	0.09495	0.00088	2.47267	0.07113	0.18888	0.00515	0.95	2.7	1087.845	13.883
scf734_15	rim	309	207	0.73932	0.07333	0.04921	0.00640	0.00048	0.00004	0.65	87.8	0.449	0.019
SC02P1	rim	1123	1023	0.06747	0.00235	0.46748	0.03413	0.05025	0.00322	0.88	1.9	310.314	9.897
SC03P1	rim	351	234	0.38037	0.04955	0.01780	0.00285	0.00034	0.00003	0.58	42.3	1.325	0.063
SC04P1	*rim*	*260*	*245*	*0.76641*	*0.11333*	*1.04853*	*0.98383*	*0.00992*	*0.00919*	*0.99*	*91.2*	*5.650*	*2.669*
SC05P1	core	813	95	0.11670	0.00867	-0.97203	-1.37437	-0.06041	0.08529	-1.00	8.0	NC	NC
SC06P1	core	1619	56	0.06244	0.00298	0.10827	0.00611	0.01258	0.00038	0.53	1.9	79.172	1.209
SC07P1 (not zircon)	N/A	5	6	0.76192	0.01228	56.83649	2.29369	0.54102	0.02002	0.92	88.3	394.203	7.210
SC08P1	core	311	247	0.13487	0.01542	0.30757	2.13161	0.01654	0.11461	1.00	11.0	94.290	315.334
SC09P1	core	1250	587	0.05136	0.00094	0.10165	0.00218	0.01435	0.00016	0.52	0.4	91.549	0.512
SC10P1	rim	667	41	0.13939	0.01277	0.82921	0.22337	0.04315	0.01093	0.94	11.8	240.808	30.409
SC11P1	rim	233	132	0.05890	0.00209	0.47823	0.01765	0.05889	0.00061	0.28	1.6	363.105	1.861
SC12P1	core	1676	639	0.06027	0.00132	0.11533	0.00357	0.01388	0.00031	0.71	1.8	87.347	0.973
SC13P1	rim	196	55	0.12671	0.00383	1.77606	0.08716	0.10166	0.00393	0.79	10.2	563.156	10.622

SC14P1	rim	414	365	0.06211	0.00131	0.46943	0.01136	0.05481	0.00066	0.49	2.0	337.238	2.003
SC15P1	rim	161	81	0.06669	0.00527	0.05645	0.00457	0.00614	0.00011	0.22	2.6	38.501	0.343
SC16P1	rim	1584	966	0.10429	0.00618	0.08898	0.00546	0.00619	0.00010	0.26	7.4	36.911	0.295
SC17P1	rim	161	87	0.10713	0.00792	0.38443	0.02996	0.02603	0.00064	0.32	7.7	153.040	1.903
SC18P1	rim	246	103	0.06004	0.00121	0.45254	0.01118	0.05467	0.00078	0.58	1.8	337.269	2.386
SC19P1	rim	195	84	0.05756	0.00091	0.45408	0.00868	0.05722	0.00062	0.57	1.5	353.668	1.904
SC20P1	rim	115	101	0.18100	0.00133	5.90778	0.17720	0.23672	0.00688	0.97	17.1	1155.246	15.656
SC22P1	rim	98	43	0.08051	0.00374	0.96669	0.04811	0.08709	0.00155	0.36	4.4	515.777	4.508
SC23P1	rim	1986	430	0.10781	0.01458	0.10131	0.01410	0.00682	0.00022	0.24	7.8	40.465	0.676
SC24P1	**midway rim/core**	**514**	**363**	**0.67019**	**0.07782**	**0.00979**	**0.00284**	**0.00011**	**0.00003**	**0.92**	**79.0**	**0.192**	**0.026**
SC25P1	core	1987	480	0.05395	0.00231	0.17157	0.03882	0.02307	0.00513	0.98	1.0	145.644	16.285
SC26P1	core	1808	476	0.05276	0.00168	0.11188	0.00575	0.01538	0.00062	0.78	0.8	97.658	1.993
SC27P1	rim	462	201	0.11367	0.01291	0.40663	0.11176	0.02594	0.00649	0.91	8.6	151.217	19.031
SC28P1	N/A	529	201	0.19220	0.02554	0.80752	1.16449	0.03047	0.04375	1.00	18.5	158.198	112.541
SC29P1	N/A	1781	644	0.08910	0.00673	2.32830	0.82405	0.18953	0.06553	0.98	5.5	1062.664	168.448
SC30P1	N/A	275	164	0.12484	0.01042	3.67497	1.98400	0.21350	0.11388	0.99	10.0	1133.323	271.321
SC31P1	N/A	119	68	0.19630	0.00629	10.63205	2.96928	0.39282	0.10898	0.99	19.0	1780.353	213.141
SC32P1	N/A	1526	684	0.05279	0.00068	0.10648	0.00173	0.01463	0.00015	0.61	0.9	92.903	0.470
SC33P1	N/A	638	520	0.06700	0.00377	3.36501	0.95867	0.36427	0.10173	0.98	2.7	1956.623	232.075
SC34P1	N/A	769	493	0.15334	0.02125	0.64364	0.19036	0.03044	0.00795	0.88	13.6	167.457	21.962
SC35P1	N/A	588	422	0.07507	0.00372	0.56175	0.06794	0.05427	0.00599	0.91	3.7	328.535	17.979
SC36P1	N/A	449	71	0.15501	0.00479	3.17658	0.38815	0.14862	0.01757	0.97	13.8	777.193	43.867
SC37P1	N/A	974	548	0.09294	0.00890	0.22625	0.04162	0.01766	0.00277	0.85	5.9	106.249	8.435
SC38P1	N/A	132	78	0.39320	0.04138	2.57006	0.70530	0.04741	0.01201	0.92	44.0	169.073	21.508
SC39P1	N/A	532	420	0.06850	0.00354	0.11122	0.00586	0.01177	0.00012	0.20	2.8	73.383	0.391
Snag (UA1589)													
Snag1589__222	NA	272	181	0.04923	0.00069	0.12498	0.00204	0.01841	0.00015	0.52	0.2	117.529	0.500
Snag1589__223	**rim**	**223**	**165**	**0.71066**	**0.07878**	**0.00716**	**0.00088**	**0.00007**	**0.00001**	**0.44**	**84.2**	**0.133**	**0.008**
Snag1589__223 (not zircon?)	NA	0	0	0.36939	0.05299	1.91622	0.33102	0.03762	0.00362	0.56	39.8	144.408	7.005
Snag1589__225	**NA**	**277**	**146**	**0.49157**	**0.07393**	**0.00132**	**0.00064**	**0.00002**	**0.00001**	**0.95**	**56.4**	**0.110**	**0.026**
Snag1589__226	NA	437	282	0.05258	0.00030	0.34453	0.00318	0.04752	0.00035	0.79	0.0	299.286	1.086

Snag1589__227	NA	230	77	0.05157	0.00100	0.13015	0.00281	0.01830	0.00018	0.45	0.4	116.498	0.566
Snag1589__228	NA	296	171	0.04856	0.00071	0.11908	0.00202	0.01778	0.00016	0.52	0.1	113.649	0.504
80PUP (UT14)													
80PUP14_207	core	56	38	0.71500	0.07705	0.15648	0.02095	0.00159	0.00013	0.59	84.7	1.651	0.067
80PUP14_208	**rim**	**161**	**87**	**0.12353**	**0.12340**	**0.00072**	**0.00073**	**0.00004**	**0.00001**	**0.14**	**9.8**	**0.321**	**0.023**
80PUP14_209	rim	294	157	0.68078	0.03943	0.06694	0.00599	0.00071	0.00005	0.76	80.4	0.982	0.034
80PUP14_210	rim	138	75	0.05522	0.00627	0.00849	0.00098	0.00111	0.00002	0.19	1.2	6.862	0.078
80PUP14_211	*rim*	*105*	*59*	*0.79446*	*0.02987*	*0.13482*	*0.00642*	*0.00123*	*0.00004*	*0.61*	*94.8*	*0.549*	*0.009*
80PUP14_212	rim	426	140	0.05435	0.00131	0.08372	0.00225	0.01117	0.00013	0.44	1.1	70.968	0.428
80PUP14_213	core	611	261	0.05580	0.00059	0.24092	0.00330	0.03131	0.00027	0.63	1.2	196.444	0.856
80PUP14_214	**N/A**	**168**	**110**	**0.55485**	**0.13463**	**0.00656**	**0.00180**	**0.00009**	**0.00001**	**0.47**	**64.4**	**0.267**	**0.018**
80PUP14_215	**rim**	**95**	**39**	**0.43393**	**0.31923**	**0.00462**	**0.00347**	**0.00008**	**0.00001**	**0.21**	**49.1**	**0.332**	**0.026**
80PUP14_216	core	1247	106	0.05423	0.00026	0.43712	0.00431	0.05846	0.00050	0.87	1.0	362.671	1.550
80PUP14_217	rim	551	203	0.05027	0.00086	0.07811	0.00146	0.01127	0.00008	0.39	0.5	71.944	0.269
80PUP14_218	*rim*	*71*	*44*	*0.78060*	*0.04059*	*0.21454*	*0.01577*	*0.00199*	*0.00010*	*0.71*	*93.0*	*1.045*	*0.028*
80PUP14_219	*rim*	*103*	*72*	*0.75721*	*0.04821*	*0.14552*	*0.01730*	*0.00139*	*0.00014*	*0.84*	*90.1*	*1.005*	*0.052*
80PUP14_220	**rim**	**90**	**75**	**0.37285**	**0.34739**	**0.00303**	**0.00292**	**0.00006**	**0.00001**	**0.25**	**41.4**	**0.287**	**0.036**
80PUP14_221	*core*	*89*	*51*	*0.83919*	*0.12079*	*0.16259*	*0.02733*	*0.00141*	*0.00012*	*0.52*	*100.5*	*N/A*	*N/A*
Boneyard (UA1609)													
BY1609 _99	-	70	89	0.18786	0.00180	10.12341	0.28868	0.39084	0.01050	0.94	9.6	1949.552	22.968
BY1609 _95	-	150	43	0.11274	0.00057	5.03375	0.05292	0.32384	0.00299	0.88	1.0	1792.951	7.371
BY1609 _96	-	823	187	0.06254	0.00347	0.12016	0.00716	0.01393	0.00030	0.37	1.9	87.639	0.967
BY1609 _100	-	1047	295	0.04920	0.00039	0.09964	0.00125	0.01469	0.00014	0.77	0.2	93.902	0.458
BY1609 _101	-	117	85	0.12942	0.00065	6.85546	0.07317	0.38419	0.00362	0.88	0.7	2082.735	8.556
BY1609 _102	-	1533	608	0.05523	0.00150	0.10960	0.00309	0.01439	0.00011	0.26	0.9	91.312	0.340
BY1609 _103	-	695	240	0.05269	0.00065	0.15870	0.00271	0.02184	0.00026	0.69	0.5	138.696	0.831
BY1609 _104	-	352	184	0.05006	0.00075	0.11060	0.00193	0.01602	0.00015	0.52	0.3	102.244	0.471
BY1609 _105	-	345	239	0.13572	0.00090	5.07609	0.13676	0.27126	0.00709	0.97	5.5	1471.279	17.485
BY1609 _109	-	74	37	0.50728	0.05178	0.30058	0.03593	0.00430	0.00027	0.52	58.4	11.564	0.367
BY1609 _110	-	936	203	0.04702	0.00043	0.09465	0.00119	0.01460	0.00013	0.68	-0.1	93.608	0.406

BY1609 _111	-	399	163	0.14428	0.00068	6.12134	0.09543	0.30771	0.00457	0.95	5.3	1648.928	11.009
BY1609 _112	-	78	35	0.08204	0.00104	1.94663	0.03690	0.17210	0.00243	0.75	1.1	1012.884	6.756
BY1609 _113	-	910	270	0.06390	0.00179	0.13484	0.00401	0.01530	0.00015	0.33	2.0	96.017	0.483
BY1609 _116	-	4087	964	0.04871	0.00035	0.05214	0.00055	0.00776	0.00006	0.73	0.2	49.823	0.196
BY1609 _117	-	1268	612	0.05409	0.00079	0.11062	0.00196	0.01483	0.00015	0.56	0.8	94.212	0.476
BY1609 _118	-	104	61	0.18915	0.00105	12.45573	0.16130	0.47760	0.00559	0.90	7.5	2358.065	11.772
BY1609 _119	-	510	326	0.08426	0.00568	0.20654	0.01435	0.01778	0.00030	0.24	4.6	108.468	0.914
BY1609 _120	-	681	291	0.05328	0.00063	0.10703	0.00152	0.01457	0.00012	0.55	0.7	92.648	0.371
BY1609 _121	-	279	60	0.05558	0.00064	0.36586	0.00516	0.04775	0.00038	0.57	0.4	299.559	1.194
BY1609 _122	-	610	147	0.15817	0.00342	0.22867	0.00640	0.01049	0.00019	0.64	14.0	57.940	0.523
BY1609 _124	-	467	297	0.16923	0.00516	5.28997	0.26399	0.22672	0.00895	0.79	11.6	1177.972	21.620
BY1609 _125	-	218	84	0.10403	0.00121	0.85906	0.02895	0.05989	0.00189	0.94	6.1	352.750	5.531
BY1609 _126	-	299	226	0.05224	0.00081	0.11956	0.00211	0.01660	0.00014	0.47	0.5	105.567	0.444
BY1609 _127	-	145	101	0.07002	0.00146	0.90869	0.02084	0.09413	0.00091	0.42	1.2	573.048	2.698
BY1609 _128	-	111	48	0.06926	0.00104	0.86813	0.01885	0.09091	0.00143	0.72	1.1	554.825	4.250
BY1609 _129	-	136	32	0.10201	0.00577	0.13238	0.00769	0.00941	0.00012	0.23	6.9	56.308	0.378
BY1609 _130	-	400	397	0.33922	0.01747	0.08691	0.00646	0.00186	0.00010	0.72	37.1	7.495	0.205
BY1609 _131	-	137	46	0.07972	0.00440	0.22368	0.01282	0.02035	0.00031	0.27	3.9	124.854	0.968
BY1609 _132	-	349	127	0.05673	0.00086	0.14733	0.00297	0.01884	0.00025	0.66	1.1	119.037	0.802
BY1609 _133	-	73	24	0.22940	0.01643	0.70173	0.05364	0.02219	0.00059	0.35	22.8	109.478	1.480
BY1609 _134	-	290	142	0.06332	0.00154	0.45688	0.01207	0.05233	0.00054	0.39	1.4	324.465	1.658
BY1609 _135	-	192	134	0.06556	0.00095	0.20621	0.00346	0.02281	0.00019	0.50	2.1	142.439	0.609
BY1609 _136	-	237	33	0.05613	0.00062	0.36438	0.00542	0.04708	0.00047	0.66	0.5	295.302	1.454
BY1609 _137	-	153	76	0.10788	0.00466	0.36370	0.01632	0.02445	0.00030	0.27	7.4	144.341	0.896
BY1609 _138	-	339	187	0.06059	0.00110	0.36056	0.00888	0.04316	0.00072	0.67	1.2	269.273	2.232
BY1609 _139	-	1704	179	0.70732	0.15985	0.02815	0.01011	0.00029	0.00008	0.78	83.7	0.396	0.056
BY1609 _140	-	83	50	0.42066	0.00569	0.92004	0.01709	0.01586	0.00020	0.69	47.2	53.799	0.348
BY1609_141	-	*110*	*247*	*0.86761*	*0.17224*	*2.35731*	*0.61280*	*0.01971*	*0.00331*	*0.65*	*104.0*	*N/A*	*N/A*
BY1609_142	-	2486	357	0.05530	0.00061	0.12555	0.00186	0.01647	0.00016	0.67	0.9	104.421	0.522
BY1609_143	-	**236**	**160**	**0.75534**	**0.05818**	**0.02667**	**0.00343**	**0.00026**	**0.00003**	**0.80**	**89.8**	**0.177**	**0.009**
DAB (UT745)	-												

DAB745_1	-	780	160	0.07059	0.00387	0.09722	0.00705	0.00999	0.00047	0.65	3.0	62.286	1.501
DAB745_2	-	182	35	0.07596	0.00288	0.57267	0.03437	0.05468	0.00254	0.77	2.8	333.755	7.706
DAB745_3	-	1060	431	0.07760	0.00280	0.16349	0.00966	0.01528	0.00071	0.79	3.8	94.202	2.228
DAB745_4	-	632	53	0.07987	0.00089	2.26750	0.10769	0.20592	0.00951	0.97	0.4	1202.306	25.733
DAB745_5	-	395	223	0.07404	0.00284	0.12571	0.00765	0.01231	0.00058	0.78	3.3	76.360	1.829
DAB745_6	-	32	0	0.11760	0.00188	5.79350	0.29082	0.35730	0.01700	0.95	-0.6	1979.842	41.128
DAB745_7	-	1043	336	0.06319	0.00263	0.13611	0.00818	0.01562	0.00068	0.72	1.9	98.129	2.155
DAB745_8	-	342	56	0.14882	0.00212	1.33472	0.10434	0.06505	0.00500	0.98	11.8	359.579	13.687
DAB745_9	-	289	154	0.08318	0.00353	0.10457	0.00661	0.00912	0.00043	0.74	4.5	55.948	1.332
DAB745_10	-	402	103	0.10889	0.00215	1.31556	0.07353	0.08763	0.00458	0.94	6.4	508.475	13.020
DAB745_11	-	2362	2135	0.05357	0.00110	0.10700	0.00541	0.01449	0.00067	0.91	0.7	92.106	2.153
DAB745_12	-	309	159	0.06684	0.00327	0.10963	0.00737	0.01190	0.00055	0.69	2.4	74.464	1.741
DAB745_13	-	446	440	0.14860	0.00566	2.28990	0.21463	0.11176	0.00957	0.91	10.9	612.315	25.427
DAB745_14	-	336	186	0.06239	0.00140	0.47595	0.02434	0.05533	0.00254	0.90	1.1	343.481	7.836
DAB745_15	-	292	211	0.10619	0.00120	3.70664	0.17962	0.25316	0.01193	0.97	2.0	1428.259	30.654
DAB745_16	-	1177	204	0.07987	0.00241	0.52531	0.02978	0.04770	0.00229	0.85	3.4	290.422	6.951
DAB745_17	-	678	211	0.08352	0.00184	0.45613	0.02521	0.03961	0.00201	0.92	4.0	240.588	6.103
DAB745_18	-	270	225	0.12227	0.00150	4.06934	0.21364	0.24138	0.01232	0.97	4.5	1337.710	31.313
DAB745_19	-	274	225	0.06186	0.00217	0.21888	0.01307	0.02566	0.00124	0.81	1.6	160.856	3.917
DAB745_20	-	261	159	0.08971	0.00141	2.98804	0.14800	0.24157	0.01135	0.95	0.6	1386.953	29.773
DAB745_21	-	643	137	0.05508	0.00103	0.22166	0.01117	0.02919	0.00137	0.93	0.6	184.405	4.336
DAB745_22	-	219	117	0.08060	0.00372	0.78343	0.05549	0.07050	0.00379	0.76	3.1	425.961	11.279
DAB745_23	-	302	185	0.09956	0.00126	2.80057	0.27976	0.20402	0.02022	0.99	2.8	1166.526	53.510
DAB745_24	-	363	381	0.05352	0.00098	0.39807	0.01972	0.05394	0.00248	0.93	0.0	338.615	7.739
DAB745_25	-	616	230	0.05299	0.00210	0.11003	0.00666	0.01506	0.00069	0.76	0.6	95.840	2.223
DAB745_26	-	2501	449	0.04794	0.00092	0.06188	0.00308	0.00936	0.00043	0.92	0.1	60.114	1.403
DAB745_27	-	364	249	0.15872	0.00445	7.91114	0.44709	0.36149	0.01774	0.87	4.1	1919.329	41.307
DAB745_28	-	301	98	0.07443	0.00175	0.59048	0.03069	0.05754	0.00267	0.89	2.6	351.613	8.084
DAB745_29	-	377	183	0.05759	0.00259	0.12475	0.00809	0.01571	0.00073	0.72	1.2	99.373	2.352
DAB745_31	-	330	150	0.09167	0.00429	0.76856	0.05113	0.06080	0.00287	0.71	4.7	363.057	0.851
P14 (UA1197)	-												

P14_7	-	455	183	0.22261	0.01790	0.22261	0.01790	0.01771	0.00083	0.58	5.4	107.051	4.965
P14_9	-	212	84	3.95166	0.21118	3.95166	0.21118	0.22846	0.01079	0.88	5.4	1261.805	53.896
P14_10	-	86	44	0.42665	0.03367	0.42665	0.03367	0.02139	0.00112	0.66	12.1	120.053	6.215
P14_11	-	372	139	0.42187	0.02606	0.42187	0.02606	0.01310	0.00064	0.78	23.5	64.311	3.100
P14_12	-	477	81	0.16673	0.01962	0.16673	0.01962	0.00742	0.00045	0.52	14.7	40.708	2.469
P14_13	-	520	244	0.37178	0.02557	0.37178	0.02557	0.03163	0.00151	0.69	4.4	192.041	9.006
P14_14	-	445	226	0.23881	0.01572	0.23881	0.01572	0.02350	0.00109	0.71	3.1	145.132	6.667
P14_17	-	0	0	5.13752	6.72861	5.13752	6.72861	0.05962	0.07681	0.98	72.7	104.256	131.875
P14_20	-	478	281	0.20312	0.01009	0.20312	0.01009	0.02772	0.00126	0.91	0.4	175.581	7.847
P14_21	-	337	83	0.12774	0.00888	0.12774	0.00888	0.01228	0.00057	0.67	3.5	75.935	3.494
P14_22	-	1063	350	0.08192	0.00555	0.08192	0.00555	0.00898	0.00041	0.67	2.4	56.282	2.557
P14_25	-	169	80	2.45481	0.28277	2.45481	0.28277	0.03617	0.00398	0.96	55.9	101.907	11.129
P14_26	-	553	370	0.24386	0.01194	0.24386	0.01194	0.02840	0.00131	0.94	1.5	177.846	8.090
P14_29	-	326	82	2.11298	0.10560	2.11298	0.10560	0.12759	0.00596	0.94	7.0	722.981	31.891
P14_30	-	726	170	0.16606	0.01525	0.16606	0.01525	0.01136	0.00055	0.53	7.4	67.494	3.250
P14_31	-	126	61	10.74211	0.49725	10.74211	0.49725	0.46891	0.02116	0.98	4.9	2376.920	89.105
P14_32	-	781	346	0.08018	0.00478	0.08018	0.00478	0.00887	0.00040	0.76	2.3	55.584	2.516
P14_33	-	396	54	0.50447	0.02995	0.50447	0.02995	0.05701	0.00258	0.76	1.3	352.777	15.492
P14_34	-	703	123	1.66153	0.07802	1.66153	0.07802	0.15585	0.00710	0.97	0.6	928.682	39.283
P14_36	-	89	54	12.02306	0.58211	12.02306	0.58211	0.45571	0.02146	0.97	7.8	2261.710	89.223
P14_38	-	471	98	0.33510	0.02316	0.33510	0.02316	0.01670	0.00077	0.67	12.3	93.730	4.293
P14_39	-	149	50	0.62010	0.05610	0.62010	0.05610	0.04699	0.00230	0.54	5.4	280.362	13.433
P14_41	-	52	335	2.92983	0.32549	2.92983	0.32549	0.03608	0.00392	0.98	68.2	73.448	7.920
P14_43	-	92	67	12.42673	0.58690	12.42673	0.58690	0.48034	0.02203	0.97	7.4	2373.038	90.433
P14_45	-	275	111	0.67688	0.04410	0.67688	0.04410	0.03340	0.00156	0.72	12.1	186.448	8.573
P14_48	-	371	98	0.16633	0.01004	0.16633	0.01004	0.01146	0.00053	0.76	7.3	68.114	3.116
P14_49	-	310	100	0.47212	0.02292	0.47212	0.02292	0.05740	0.00263	0.94	0.6	357.632	15.892
P14_50	-	4201	742	0.11761	0.00817	0.11761	0.00817	0.00990	0.00046	0.67	4.9	60.381	2.782

Note* Prefered data used for age calcualtions are shown in bold (refer to text). Data in italics contains >90% common-Pb and were excluded from age calcualtions.

[a] F_{206} (%) denotes an estimate for the amount of common-Pb in measured ^{206}Pb. Correction for common-Pb was made using ^{207}Pb method (Williams, 1998)
with contemporaneous common-Pb composition estimated from Stacey-Kramers (1975) model.

[b] $F_{Th/U} = (Th/U)_{zircon}/(Th/U)_{glass}$. $(Th/U)_{glass}$ values used are as follows: Woodchopper Creek = 3.6; PAL = 2.8; Snag =2.9; Preido Hill = 4.8 (Preece at al., 2000); 80 PUP = 3.2 (Preece et al., 2000); Sheep Creek Fairbanks = 1.6 (Westgate et al., 2008); Old Crow tephra = 2.3 (Preece et al., 2011); Stampede = 2.2.

[c] $^{206}Pb^{*}/^{238}U$ ages are corrected for common-Pb and intial ^{230}Th disequiibrium. Uncertainty of weighted mean is at 95% confidence level. N/A = no bisection is found.

Table D.2: LA-ICP-MS U-Pb reference materials data.

			Total								Age (Ma)	
Sample number	U (ppm)	Th (ppm)	$^{207}Pb/^{206}Pb$	2σ	$^{207}Pb/^{235}U$	2σ	$^{206}Pb/^{238}U$	2σ	ρ	F_{206} (%)[a]	$^{206}Pb^{*}/^{238}U$	2σ[b]
50 micron pit												
91500_33	80	30	0.074929	0.001313	1.854122	0.038845	0.179467	0.002061	0.55	0.0	1063.8	11.3
91500	80	30	0.075045	0.001201	1.844754	0.040117	0.178284	0.002625	0.68	0.0	1057.2	14.3
91500	80	30	0.075739	0.001238	1.874206	0.039506	0.179472	0.002388	0.63	0.1	1062.9	13.0
91500	80	30	0.075977	0.001198	1.890047	0.040611	0.180421	0.002633	0.68	0.2	1067.8	14.3
91500	80	30	0.074875	0.001162	1.835675	0.040155	0.177812	0.002742	0.70	0.0	1054.8	15.0
91500	80	30	0.073914	0.001182	1.826741	0.038738	0.179245	0.002497	0.66	-0.1	1063.7	13.6
91500	80	30	0.074176	0.001332	1.829669	0.040671	0.178900	0.002343	0.59	-0.1	1061.6	12.8
91500	80	30	0.073629	0.001335	1.821630	0.040932	0.179435	0.002381	0.59	-0.1	1065.1	13.0
91500	80	30	0.075982	0.001294	1.874639	0.040224	0.178938	0.002336	0.61	0.2	1059.7	12.7
91500	80	30	0.074171	0.001212	1.842746	0.038923	0.180191	0.002413	0.63	-0.1	1068.6	13.2
91500	80	30	0.074923	0.001219	1.839454	0.039944	0.178062	0.002560	0.66	0.0	1056.1	14.0
91500	80	30	0.075534	0.001426	1.863086	0.042412	0.178890	0.002277	0.56	0.1	1059.9	12.4
91500	80	30	0.074332	0.001260	1.849144	0.040138	0.180423	0.002446	0.62	0.0	1069.7	13.3
91500_40	82	31	0.075139	0.001023	1.846409	0.035533	0.178223	0.002424	0.71	0.1	1056.7	13.2
91500	80	30	0.074249	0.000977	1.841108	0.033668	0.179840	0.002285	0.69	-0.1	1066.6	12.5
91500	80	30	0.075059	0.000956	1.854513	0.032404	0.179196	0.002144	0.68	0.0	1062.1	11.7
91500	80	30	0.075412	0.001124	1.862939	0.033623	0.179167	0.001822	0.56	0.1	1061.6	9.9
91500	80	30	0.074266	0.001013	1.834668	0.032224	0.179170	0.001982	0.63	0.0	1062.9	10.8
91500	80	30	0.074647	0.000983	1.844053	0.031662	0.179168	0.001975	0.64	0.0	1062.5	10.8
91500	80	30	0.075014	0.001024	1.853202	0.035367	0.179175	0.002390	0.70	0.0	1062.1	13.0
91500	80	30	0.075143	0.000989	1.856206	0.029997	0.179158	0.001680	0.58	0.1	1061.8	9.2
91500	80	30	0.075155	0.001054	1.856853	0.036577	0.179191	0.002479	0.70	0.1	1062.0	13.5
91500	80	30	0.074876	0.001116	1.850331	0.034679	0.179227	0.002037	0.61	0.0	1062.5	11.1
91500	80	30	0.075537	0.001030	1.865347	0.034317	0.179100	0.002211	0.67	0.1	1061.1	12.1
91500	80	30	0.074503	0.001041	1.839973	0.033894	0.179118	0.002150	0.65	0.0	1062.4	11.7
91500	80	30	0.074715	0.001045	1.846441	0.033612	0.179237	0.002089	0.64	0.0	1062.8	11.4
91500	80	30	0.074845	0.001202	1.844802	0.038287	0.178765	0.002351	0.63	0.0	1060.0	12.8
91500	80	30	0.074552	0.000956	1.845397	0.032614	0.179527	0.002184	0.69	0.0	1064.5	11.9

91500	80	30	0.074560	0.000964	1.841734	0.032594	0.179152	0.002164	0.68	0.0	1062.5	11.8
91500	80	30	0.075196	0.000987	1.856130	0.033930	0.179024	0.002279	0.70	0.1	1061.0	12.4
91500	80	30	0.075148	0.000925	1.857917	0.031771	0.179311	0.002129	0.69	0.1	1062.7	11.6
91500	80	30	0.074991	0.001151	1.850140	0.034732	0.178933	0.001934	0.58	0.0	1060.8	10.6
91500	80	30	0.074919	0.001086	1.856534	0.036886	0.179726	0.002441	0.68	0.0	1065.2	13.3
91500	80	30	0.074819	0.000924	1.846827	0.031618	0.179024	0.002121	0.69	0.0	1061.5	11.6
Z_91500_UPb_1	77	29	0.075340	0.000760	1.896827	0.032258	0.182600	0.002500	0.81	0.1	1080.4	13.6
Z_91500_UPb_2	90	34	0.074250	0.000820	1.806935	0.034092	0.176500	0.002700	0.81	-0.1	1048.3	14.8
Z_91500_UPb_3	81	30	0.075030	0.000700	1.835227	0.029314	0.177400	0.002300	0.81	0.0	1052.4	12.6
Z_91500_UPb_4	78	29	0.074960	0.000840	1.850052	0.036444	0.179000	0.002900	0.82	0.0	1061.2	15.8
Z_91500_UPb_5	79	30	0.074470	0.000820	1.851307	0.032779	0.180300	0.002500	0.78	0.0	1068.9	13.6
Z_91500_UPb_6	86	32	0.075100	0.000870	1.828656	0.038460	0.176600	0.003100	0.83	0.0	1047.9	17.0
Z_91500_UPb_7	78	29	0.075110	0.000870	1.854789	0.035262	0.179100	0.002700	0.79	0.1	1061.6	14.7
Z_91500_UPb_8	79	30	0.074800	0.001100	1.886325	0.041555	0.182900	0.003000	0.74	0.0	1082.7	16.3
Z_91500_UPb_9	81	30	0.074750	0.000780	1.847961	0.033014	0.179300	0.002600	0.81	0.0	1063.1	14.2
Z_91500_UPb_10	77	29	0.074890	0.000820	1.860715	0.035370	0.180200	0.002800	0.82	0.0	1067.8	15.3
Z_91500_UPb_11	85	31	0.074900	0.000780	1.833080	0.032109	0.177500	0.002500	0.80	0.0	1053.1	13.7
Z_91500_UPb_12	81	30	0.074800	0.001400	1.884263	0.051961	0.182700	0.003700	0.73	0.0	1081.6	20.1
Z_91500_UPb_13	84	31	0.074820	0.000890	1.845565	0.040508	0.178900	0.003300	0.84	0.0	1060.8	18.0
Z_91500_UPb_14	77	29	0.074000	0.001000	1.837582	0.034875	0.180100	0.002400	0.70	-0.1	1068.3	13.1
Z_91500_UPb_13	81	30	0.074900	0.001000	1.853735	0.035026	0.179500	0.002400	0.71	0.0	1064.0	13.1
Z_91500_UPb_12	81	30	0.075500	0.001100	1.864420	0.037619	0.179100	0.002500	0.69	0.1	1061.1	13.6
Z_91500_UPb_11	80	30	0.074800	0.001000	1.840946	0.033475	0.178500	0.002200	0.68	0.0	1058.6	12.0
Z_91500_UPb_15	78	29	0.075700	0.001400	1.867272	0.045240	0.178900	0.002800	0.65	0.1	1059.8	15.3
Z_91500_UPb_10	82	31	0.074400	0.001100	1.831102	0.038004	0.178500	0.002600	0.70	0.0	1059.1	14.2
Z_91500_UPb_9	77	29	0.074400	0.001200	1.837257	0.036636	0.179100	0.002100	0.59	0.0	1062.4	11.5
Z_91500_UPb_8	81	31	0.075900	0.001100	1.872205	0.035585	0.178900	0.002200	0.65	0.1	1059.5	12.0
Z_91500_UPb_7	82	31	0.075200	0.001000	1.868417	0.036662	0.180200	0.002600	0.74	0.1	1067.5	14.2
Z_91500_UPb_5	78	29	0.074870	0.000940	1.862283	0.038804	0.180400	0.003000	0.80	0.0	1068.9	16.4
Z_91500_UPb_4	81	31	0.074800	0.001100	1.827539	0.039449	0.177200	0.002800	0.73	0.0	1051.5	15.3
Z_91500_UPb_3	78	30	0.074300	0.001200	1.850154	0.040029	0.180600	0.002600	0.67	0.0	1070.7	14.2
Z_91500_UPb_2	77	29	0.075300	0.001100	1.860520	0.037582	0.179200	0.002500	0.69	0.1	1061.9	13.6
Z_91500_UPb_1	75	28	0.074820	0.000990	1.840407	0.036998	0.178400	0.002700	0.75	0.0	1058.1	14.8

Z_91500_UPb_1	84	32	0.074900	0.001600	1.856833	0.049086	0.179800	0.002800	0.59	0.0	1065.6	15.3
Z_91500_UPb_2	84	32	0.073800	0.001500	1.820405	0.042228	0.178900	0.002000	0.48	-0.1	1062.0	10.9
Z_91500_UPb_3	76	29	0.077000	0.001700	1.912078	0.052882	0.180100	0.003000	0.60	0.3	1064.8	16.3
Z_91500_UPb_4	77	29	0.075400	0.001800	1.856753	0.049410	0.178600	0.002100	0.44	0.1	1058.5	11.5
Z_91500_UPb_5	44	16	0.072800	0.002100	1.813806	0.065345	0.180700	0.003900	0.60	-0.2	1073.0	21.3
Z_91500_UPb_6	41	16	0.074900	0.002400	1.841342	0.069193	0.178300	0.003500	0.52	0.0	1057.4	19.1
Z_91500_UPb_11	73	28	0.073200	0.001900	1.806614	0.054750	0.179000	0.002800	0.52	-0.2	1063.2	15.3
Z_91500_UPb_12	73	28	0.074800	0.001800	1.849197	0.052494	0.179300	0.002700	0.53	0.0	1063.0	14.7
Z_91500_UPb_13	76	29	0.075800	0.001900	1.883325	0.057854	0.180200	0.003200	0.58	0.1	1066.8	17.4
Z_91500_UPb_14	77	29	0.076000	0.001700	1.865241	0.048716	0.178000	0.002400	0.52	0.2	1054.5	13.1
Z_91500_UPb_15	79	30	0.074800	0.001500	1.854354	0.043562	0.179800	0.002200	0.52	0.0	1065.7	12.0
Z_91500_UPb_16	76	28	0.076000	0.001700	1.876767	0.049484	0.179100	0.002500	0.53	0.2	1060.5	13.6
Z_91500_UPb_17	83	32	0.076200	0.001900	1.884858	0.052846	0.179400	0.002300	0.46	0.2	1061.9	12.5
Z_91500_UPb_18	80	30	0.073700	0.001800	1.817938	0.050657	0.178900	0.002400	0.48	-0.1	1062.1	13.1
Z_91500_UPb_19	79	30	0.073200	0.001800	1.819735	0.050883	0.180300	0.002400	0.48	-0.2	1070.4	13.1
Z_91500_UPb_20	78	30	0.075000	0.001800	1.843800	0.049757	0.178300	0.002200	0.46	0.0	1057.3	12.0
91500-1	-	-	0.074300	0.000870	1.840000	0.035000	0.179400	0.002600	0.10	0.0	1061.6	14.2
91500-2	-	-	0.074750	0.000990	1.837000	0.032000	0.178200	0.002500	0.38	0.0	1054.5	13.6
91500-3	-	-	0.075260	0.000950	1.851000	0.032000	0.178200	0.002700	0.40	0.0	1053.9	14.7
91500-4	-	-	0.075110	0.000840	1.832000	0.029000	0.176900	0.002600	0.43	0.0	1047.0	14.2
91500-5	-	-	0.074720	0.000950	1.849000	0.037000	0.179400	0.002800	0.15	0.0	1061.1	15.3
91500-6	-	-	0.075390	0.000860	1.886000	0.037000	0.180000	0.002800	0.20	0.0	1063.6	15.2
91500-7	-	-	0.075040	0.000780	1.847000	0.036000	0.178000	0.002900	0.20	0.0	1053.1	15.8
91500-8	-	-	0.074760	0.000880	1.847000	0.032000	0.179400	0.002700	0.26	0.0	1061.0	14.7
91500-10	-	-	0.074700	0.000890	1.834000	0.033000	0.178300	0.002600	0.27	0.0	1055.1	14.2
91500-11	-	-	0.074880	0.000810	1.865000	0.034000	0.180400	0.002600	0.18	0.0	1066.4	14.1
91500-12	-	-	0.075010	0.000870	1.859000	0.034000	0.179500	0.002300	0.16	0.0	1061.3	12.5
91500-13	-	-	0.074740	0.000930	1.861000	0.032000	0.180600	0.002700	0.23	0.0	1067.6	14.7
91500-14	-	-	0.075100	0.000940	1.857000	0.035000	0.180000	0.002700	0.16	0.0	1063.9	14.7
91500-16	-	-	0.074500	0.000870	1.863000	0.034000	0.180700	0.002400	0.20	0.0	1068.4	13.1
91500-17	-	-	0.074900	0.000870	1.840000	0.030000	0.178400	0.002800	0.42	0.0	1055.4	15.3

40 micron pit

91500_21	80	30	0.075052	0.000553	1.854259	0.018198	0.179187	0.001162	0.66	0.0	1062.1	6.3
91500_20	80	30	0.074656	0.000552	1.845545	0.017855	0.179292	0.001118	0.64	0.0	1063.1	6.1
91500_19	80	30	0.074857	0.000548	1.849703	0.018146	0.179212	0.001171	0.67	0.0	1062.5	6.4
91500_18	80	30	0.074940	0.000512	1.850924	0.016710	0.179132	0.001058	0.65	0.0	1061.9	5.8
91500_13	80	30	0.074810	0.000629	1.850094	0.018900	0.179364	0.001042	0.57	0.0	1063.3	5.7
91500_11	81	30	0.075072	0.000659	1.849063	0.020231	0.178637	0.001168	0.60	0.0	1059.1	6.4
91500_12	79	30	0.074872	0.000548	1.853961	0.018391	0.179589	0.001204	0.68	0.0	1064.5	6.6
91500_10	81	30	0.074712	0.000494	1.845017	0.016755	0.179106	0.001116	0.69	0.0	1062.1	6.1
91500_8	80	30	0.075007	0.000510	1.851227	0.016853	0.179001	0.001085	0.67	0.0	1061.1	5.9
91500_3	80	30	0.074859	0.000588	1.849314	0.016684	0.179169	0.000795	0.49	0.0	1062.2	4.3
91500_5	80	30	0.075099	0.000580	1.856454	0.018084	0.179288	0.001063	0.61	0.0	1062.6	5.8
91500_17	80	30	0.074870	0.000586	1.846624	0.017733	0.178884	0.000994	0.58	0.0	1060.7	5.4
91500_16	80	30	0.074656	0.000562	1.847784	0.018012	0.179509	0.001112	0.64	0.0	1064.3	6.1
91500_15	81	30	0.074725	0.000500	1.844362	0.018055	0.179010	0.001279	0.73	0.0	1061.5	7.0
91500_14	80	30	0.075099	0.000545	1.855323	0.017394	0.179178	0.001063	0.63	0.0	1062.0	5.8
91500_6	80	30	0.074922	0.000509	1.850986	0.016505	0.179182	0.001034	0.65	0.0	1062.2	5.6
91500_1	80	30	0.074710	0.000599	1.845239	0.018343	0.179131	0.001053	0.59	0.0	1062.2	5.8
91500_2	80	30	0.074980	0.000557	1.852550	0.017484	0.179194	0.001042	0.62	0.0	1062.2	5.7
91500	80	30	0.074862	0.000573	1.851624	0.019655	0.179387	0.001320	0.69	0.0	1063.4	7.2
91500	80	30	0.074911	0.000593	1.847141	0.021552	0.178835	0.001532	0.73	0.0	1060.3	8.4
91500	80	30	0.074860	0.000620	1.849721	0.019664	0.179206	0.001193	0.63	0.0	1062.4	6.5
91500	80	30	0.075314	0.002309	1.860234	0.059084	0.179140	0.001489	0.26	0.1	1061.5	8.1
91500	80	30	0.074844	0.000720	1.849368	0.026323	0.179212	0.001881	0.74	0.0	1062.5	10.3
91500	80	30	0.075024	0.000598	1.854373	0.020106	0.179265	0.001319	0.68	0.0	1062.6	7.2
91500	80	30	0.075720	0.003362	1.870676	0.084275	0.179178	0.001361	0.17	0.1	1061.3	7.4
91500	80	30	0.074858	0.000680	1.849249	0.027424	0.179166	0.002100	0.79	0.0	1062.2	11.5
91500	80	30	0.074888	0.000610	1.850040	0.020197	0.179171	0.001303	0.67	0.0	1062.2	7.1
Z_91500_UPb_1	77	29	0.074900	0.001200	1.844440	0.032044	0.178600	0.001200	0.39	0.0	1059.1	6.6
Z_91500_UPb_2	79	30	0.075000	0.001200	1.860346	0.031865	0.179900	0.001100	0.36	0.0	1066.1	6.0
Z_91500_UPb_3	85	32	0.074900	0.001000	1.841342	0.027531	0.178300	0.001200	0.45	0.0	1057.4	6.6
Z_91500_UPb_4	79	30	0.074400	0.001300	1.841360	0.034096	0.179500	0.001100	0.33	0.0	1064.6	6.0
Z_91500_UPb_5	77	29	0.074600	0.001200	1.850424	0.032631	0.179900	0.001300	0.41	0.0	1066.5	7.1
Z_91500_UPb_6	83	31	0.075300	0.001300	1.855328	0.034369	0.178700	0.001200	0.36	0.1	1059.2	6.6

Z_91500_UPb_7	82	30	0.075100	0.001400	1.853507	0.036719	0.179000	0.001200	0.34	0.0	1061.0	6.6
Z_91500_UPb_8	84	31	0.075300	0.001600	1.862596	0.041192	0.179400	0.001100	0.28	0.1	1063.0	6.0
Z_91500_UPb_9	79	29	0.073900	0.001300	1.824909	0.034728	0.179100	0.001300	0.38	-0.1	1063.0	7.1
Z_91500_UPb_10	80	30	0.075300	0.001400	1.860520	0.037131	0.179200	0.001300	0.36	0.1	1061.9	7.1
Z_91500_UPb_11	80	30	0.075400	0.001500	1.862990	0.039449	0.179200	0.001300	0.34	0.1	1061.8	7.1
Z_91500_UPb_12	81	30	0.075100	0.001500	1.844188	0.039217	0.178100	0.001300	0.34	0.0	1056.1	7.1
Z_91500_UPb_13	74	28	0.074600	0.001300	1.854538	0.034975	0.180300	0.001300	0.38	0.0	1068.7	7.1
Z_91500_UPb_14	82	31	0.074900	0.001300	1.849604	0.034412	0.179100	0.001200	0.36	0.0	1061.8	6.6
Z_91500_UPb_1	80	30	0.075200	0.001100	1.852865	0.029405	0.178700	0.001100	0.39	0.1	1059.3	6.0
Z_91500_UPb_2	79	30	0.075300	0.001200	1.863634	0.031820	0.179500	0.001100	0.36	0.1	1063.5	6.0
Z_91500_UPb_3	80	30	0.074900	0.001000	1.850636	0.027194	0.179200	0.001100	0.42	0.0	1062.4	6.0
Z_91500_UPb_4	82	31	0.074500	0.001100	1.843835	0.029098	0.179500	0.001000	0.35	0.0	1064.5	5.5
Z_91500_UPb_5	79	29	0.074900	0.001100	1.846506	0.029401	0.178800	0.001100	0.39	0.0	1060.2	6.0
Z_91500_UPb_6	80	30	0.074600	0.001100	1.840138	0.029398	0.178900	0.001100	0.38	0.0	1061.1	6.0
Z_91500_UPb_7	82	31	0.073830	0.000990	1.829289	0.026964	0.179700	0.001100	0.42	-0.1	1066.3	6.0
Z_91500_UPb_8	79	29	0.075200	0.001300	1.854938	0.034035	0.178900	0.001100	0.34	0.1	1060.4	6.0
Z_91500_UPb_9	81	30	0.075600	0.001200	1.864596	0.031310	0.178880	0.000980	0.33	0.1	1059.8	5.4
Z_91500_UPb_10	79	30	0.074890	0.000880	1.859683	0.024628	0.180100	0.001100	0.46	0.0	1067.3	6.0
Z_91500_UPb_11	79	29	0.074600	0.001100	1.847338	0.029496	0.179600	0.001100	0.38	0.0	1064.9	6.0
Z_91500_UPb_12	81	31	0.075500	0.001100	1.866502	0.029507	0.179300	0.001100	0.39	0.1	1062.2	6.0
Z_91500_UPb_13	79	30	0.075600	0.001100	1.862720	0.029038	0.178700	0.001000	0.36	0.1	1058.8	5.5
Z_91500_UPb_14	81	30	0.074500	0.001100	1.834590	0.029761	0.178600	0.001200	0.41	0.0	1059.5	6.6
Z_91500_UPb_15	80	30	0.074900	0.001200	1.843407	0.032029	0.178500	0.001200	0.39	0.0	1058.5	6.6
Z_91500_UPb_16	79	30	0.074900	0.001200	1.851669	0.031767	0.179300	0.001100	0.36	0.0	1062.9	6.0
Z_91500_UPb_17	82	31	0.075300	0.001100	1.866749	0.029565	0.179800	0.001100	0.39	0.1	1065.2	6.0
Z_91500_UPb_18	78	29	0.074500	0.001200	1.841780	0.032125	0.179300	0.001200	0.38	0.0	1063.4	6.6
Z_91500_UPb_19	78	29	0.074700	0.001200	1.840545	0.032046	0.178700	0.001200	0.39	0.0	1059.8	6.6
Z_91500_UPb_20	80	30	0.074600	0.001200	1.853510	0.032269	0.180200	0.001200	0.38	0.0	1068.2	6.6
Z_91500_UPb_21	82	31	0.074500	0.001200	1.835617	0.031301	0.178700	0.001000	0.33	0.0	1060.1	5.5
Z_91500_UPb_22	79	30	0.074800	0.001100	1.850228	0.029892	0.179400	0.001200	0.41	0.0	1063.6	6.6
Z_91500_UPb_23	81	30	0.074540	0.000950	1.837630	0.025576	0.178800	0.001000	0.40	0.0	1060.6	5.5
Z_91500_UPb_24	80	30	0.074500	0.001100	1.843835	0.029885	0.179500	0.001200	0.41	0.0	1064.5	6.6
Z_91500_UPb_25	79	30	0.076100	0.001200	1.878188	0.032607	0.179000	0.001300	0.42	0.2	1059.9	7.1

GJ-1 40 micron pit

GJ-1	390	12	0.060436	0.001024	0.813679	0.021647	0.097646	0.002003	0.77	0.1	600.2	11.7
GJ-1	367	11	0.059800	0.000930	0.798015	0.018427	0.096784	0.001652	0.74	0.0	595.6	9.7
GJ-1	348	11	0.060002	0.000833	0.805301	0.016288	0.097339	0.001431	0.73	0.0	598.7	8.4
GJ-1	338	10	0.060016	0.001034	0.807780	0.018169	0.097618	0.001412	0.64	0.0	600.4	8.3
GJ-1	340	10	0.060634	0.000837	0.812560	0.015813	0.097193	0.001333	0.70	0.1	597.4	7.8
GJ-1	368	11	0.059738	0.000848	0.805370	0.014866	0.097778	0.001153	0.64	0.0	601.5	6.8
GJ-1	351	11	0.060326	0.000647	0.815759	0.011769	0.098074	0.000946	0.67	0.1	602.8	5.6
GJ-1	346	11	0.060233	0.000769	0.809738	0.014244	0.097500	0.001179	0.69	0.0	599.5	6.9
GJ-1	370	12	0.060064	0.000663	0.814525	0.012335	0.098354	0.001019	0.68	0.0	604.6	6.0
GJ-1	327	10	0.060044	0.000686	0.812101	0.014062	0.098094	0.001276	0.75	0.0	603.1	7.5
GJ-1	353	11	0.060134	0.000704	0.822977	0.014135	0.099258	0.001248	0.73	0.0	609.9	7.3
GJ-1	324	10	0.060700	0.000696	0.819970	0.012997	0.097973	0.001073	0.69	0.1	602.0	6.3
GJ-1	364	11	0.059881	0.000696	0.814137	0.013444	0.098608	0.001157	0.71	0.0	606.3	6.8
GJ-1	322	10	0.060235	0.000661	0.819824	0.012930	0.098712	0.001118	0.72	0.0	606.6	6.6
GJ-1	335	10	0.060079	0.000664	0.809074	0.013761	0.097670	0.001262	0.76	0.0	600.6	7.4
GJ-1	327	10	0.060114	0.000693	0.803231	0.013076	0.096909	0.001113	0.71	0.0	596.1	6.5
GJ-1	338	10	0.060191	0.000655	0.817426	0.012645	0.098495	0.001084	0.71	0.0	605.4	6.4
GJ-1	~~354~~	~~11~~	0.059926	0.000672	0.818741	0.013217	0.099091	0.001150	0.72	~~0.0~~	609.1	6.7
GJ-1	328	10	0.060104	0.000733	0.814237	0.013897	0.098252	0.001174	0.70	0.0	604.0	6.9
GJ-1	302	9	0.060118	0.000711	0.813229	0.013673	0.098109	0.001172	0.71	0.0	603.2	6.9
GJ-1	293	9	0.060231	0.000680	0.807470	0.013753	0.097232	0.001240	0.75	0.0	597.9	7.3
GJ_1_2	379	9	0.060240	0.000640	0.800688	0.015779	0.096400	0.001600	0.84	0.0	593.0	9.4
GJ_1_3	399	10	0.060390	0.000630	0.812674	0.014414	0.097600	0.001400	0.81	0.1	600.0	8.2
GJ_1_4	317	8	0.060070	0.000580	0.813337	0.014004	0.098200	0.001400	0.83	0.0	603.7	8.2
GJ_1_10	279	7	0.062700	0.001100	0.856727	0.033013	0.099100	0.003400	0.89	0.3	607.1	19.8
GJ_1_9	397	10	0.060550	0.000650	0.824010	0.013365	0.098700	0.001200	0.75	0.1	606.3	7.0
GJ_1_5	341	9	0.060280	0.000810	0.834465	0.015572	0.100400	0.001300	0.69	0.0	616.5	7.6
GJ_1_4	374	9	0.060640	0.000630	0.808513	0.013737	0.096700	0.001300	0.79	0.1	594.5	7.6
GJ-1-1	-	-	0.059660	0.000700	0.820000	0.011000	0.099550	0.001000	0.39	0.0	611.9	5.9
GJ-1-2	-	-	0.059590	0.000660	0.809700	0.009700	0.098650	0.001000	0.39	0.0	606.7	5.9

GJ-1-3	-	-	0.059760	0.000560	0.815000	0.008200	0.099240	0.001000	0.50	0.0	610.1	5.9
GJ-1-4	-	-	0.059080	0.000620	0.800300	0.009200	0.098380	0.001000	0.52	-0.1	605.5	5.9
GJ-1-5	-	-	0.059720	0.000810	0.811000	0.012000	0.098660	0.001100	0.45	0.0	606.7	6.5
GJ-1-6	-	-	0.059420	0.000790	0.814000	0.011000	0.099600	0.001100	0.38	-0.1	612.4	6.4
GJ-1-7	-	-	0.059560	0.000730	0.809000	0.011000	0.099240	0.001100	0.51	0.0	610.2	6.5
GJ-1-8	-	-	0.059710	0.000750	0.815000	0.012000	0.099320	0.001200	0.61	0.0	610.6	7.0
GJ-1-9	-	-	0.059880	0.000770	0.822000	0.011000	0.098930	0.001200	0.49	0.0	608.2	7.0
GJ-1 50 micron pit												
Z_GJ1_1	359	11	0.059660	0.000700	0.818890	0.010840	0.099550	0.000610	0.46	0.0	611.9	3.6
Z_GJ1_2	371	11	0.059590	0.000660	0.810535	0.010088	0.098650	0.000560	0.46	0.0	606.7	3.3
Z_GJ1_3	380	11	0.059760	0.000560	0.817709	0.009164	0.099240	0.000610	0.55	0.0	610.1	3.6
Z_GJ1_4	376	11	0.059080	0.000620	0.801399	0.009852	0.098380	0.000630	0.52	-0.1	605.5	3.7
gj-1 - 2	413	10	0.059470	0.000860	0.814233	0.014348	0.099300	0.001000	0.57	-0.1	610.6	5.9
gj-1 - 3	377	9	0.059850	0.000890	0.809533	0.014595	0.098100	0.001000	0.57	0.0	603.3	5.9
gj-1 - 4	400	10	0.059300	0.000880	0.798496	0.014213	0.097660	0.000960	0.55	-0.1	601.1	5.6
gj-1 - 11	379	9	0.060850	0.000870	0.812991	0.014842	0.096900	0.001100	0.62	0.1	595.6	6.5
gj-1 - 13	372	9	0.060410	0.000740	0.818357	0.012468	0.098250	0.000890	0.59	0.1	603.8	5.2
gj-1 - 14	382	9	0.059800	0.001100	0.810258	0.016837	0.098270	0.000950	0.47	0.0	604.3	5.6
gj-1 - 15	394	10	0.059500	0.001200	0.802091	0.018101	0.097770	0.000990	0.45	0.0	601.6	5.8
gj-1 - 16	375	9	0.060320	0.000920	0.827617	0.014468	0.099510	0.000850	0.49	0.1	611.2	5.0
gj-1 - 20	402	10	0.059700	0.001100	0.816476	0.016489	0.099190	0.000820	0.41	0.0	609.8	4.8
Z_GJ1_1	370	11	0.059580	0.000610	0.809249	0.009558	0.098510	0.000580	0.50	0.0	605.9	3.4
Z_GJ1_2	396	11	0.059680	0.000640	0.808715	0.009899	0.098280	0.000580	0.48	0.0	604.5	3.4
Z_GJ1_3	398	11	0.060120	0.000600	0.814594	0.009487	0.098270	0.000590	0.52	0.0	604.1	3.5
Z_GJ1_4	394	11	0.059910	0.000550	0.812244	0.008689	0.098330	0.000540	0.51	0.0	604.6	3.2
Z_GJ1_5	381	11	0.059850	0.000580	0.813494	0.009223	0.098580	0.000580	0.52	0.0	606.1	3.4
Z_GJ1_6	370	11	0.059700	0.000650	0.811702	0.010006	0.098610	0.000570	0.47	0.0	606.4	3.3
Z_GJ1_7	363	11	0.059980	0.000690	0.813441	0.010231	0.098360	0.000500	0.40	0.0	604.7	2.9
Z_GJ1_8	356	11	0.060100	0.000730	0.818632	0.010804	0.098790	0.000510	0.39	0.0	607.2	3.0

Plesovice 40 micron pit

Plesovice_1	834	85	0.053970	0.000610	0.410392	0.008086	0.055150	0.000890	0.82	0.1	345.9	5.4
Plesovice_2	825	87	0.053650	0.000600	0.403891	0.009960	0.054600	0.001200	0.89	0.0	342.6	7.3
Plesovice_3	775	81	0.053660	0.000480	0.408849	0.006832	0.055260	0.000780	0.84	0.0	346.7	4.8
Plesovice_4	946	101	0.052930	0.000580	0.405038	0.009173	0.055500	0.001100	0.88	-0.1	348.4	6.7
Plesovice_5	849	89	0.053760	0.000660	0.405534	0.008503	0.054710	0.000930	0.81	0.0	343.3	5.7
Plesovice_1	715	87	0.071975	0.004576	0.547462	0.036245	0.055166	0.001019	0.28	2.3	338.3	6.1
Plesovice_3	545	89	0.084868	0.004790	0.645748	0.036781	0.055185	0.000425	0.14	3.9	337.0	2.5
Plesovice_4	509	54	0.080906	0.005108	0.620095	0.042221	0.055587	0.001417	0.37	3.2	337.7	8.4
Plesovice-1	-	-	0.053420	0.000440	0.402900	0.006600	0.054570	0.000800	0.39	0.0	342.1	4.9
Plesovice-2	-	-	0.055300	0.001600	0.414100	0.008500	0.055130	0.000990	0.82	0.0	344.7	6.0
Plesovice-5	-	-	0.053260	0.000650	0.408700	0.007300	0.055720	0.000960	0.46	0.0	349.2	5.9
Plesovice-6	-	-	0.053370	0.000580	0.401400	0.006500	0.054500	0.000800	0.48	0.0	341.7	4.9
Plesovice-7	-	-	0.054300	0.001300	0.403400	0.007300	0.054200	0.001000	0.83	0.0	339.4	6.1
Plesovice-8	-	-	0.053530	0.000660	0.402100	0.008000	0.054720	0.000990	0.99	0.0	342.9	6.0
Plesovice-9	-	-	0.053760	0.000720	0.402000	0.007000	0.054030	0.000930	0.76	0.0	338.6	5.7
Plesovice-10	-	-	0.053620	0.000770	0.401400	0.006700	0.054590	0.000930	1.00	0.0	342.1	5.7

Plesovice 50 micron pit

Z_Plesovice	921	126	0.057723	0.001067	0.424122	0.009015	0.053289	0.000560	0.49	0.6	336.8	3.4
Plesovice_16	831	95	0.047054	0.000312	0.341357	0.005844	0.052615	0.000831	0.92	-0.8	337.0	5.1
Plesovice_16	691	83	0.069548	0.002618	0.528328	0.020523	0.055095	0.000529	0.25	2.0	338.9	3.2
Plesovice_11	736	71	0.053180	0.000620	0.405192	0.007194	0.055260	0.000740	0.75	0.0	343.7	4.5
Plesovice_7	725	72	0.053870	0.000670	0.411043	0.007398	0.055340	0.000720	0.72	0.1	343.9	4.4
Plesovice_6	795	81	0.053480	0.000680	0.407772	0.007421	0.055300	0.000720	0.72	0.0	342.9	4.4
Plesovice_3	774	82	0.053360	0.000660	0.403767	0.007946	0.054880	0.000840	0.78	0.0	344.3	5.1
Plesovice_2	865	92	0.053370	0.000600	0.397735	0.005982	0.054050	0.000540	0.66	0.0	339.3	3.3
Plesovice_1	925	95	0.053260	0.000550	0.389278	0.006584	0.053010	0.000710	0.79	0.0	336.9	4.3

Mudtank 40 micron pit

Mudtank	18	9	0.061911	0.002524	0.950470	0.043093	0.111345	0.002208	0.44	-0.5	683.6	12.8
Mudtank	16	9	0.065627	0.002397	1.030344	0.044039	0.113867	0.002526	0.52	0.3	692.9	14.6

Mudtank	15	7	0.063183	0.002781	0.995304	0.047672	0.114249	0.002157	0.39	0.1	697.0	12.5
Mudtank	15	8	0.063551	0.003390	1.014491	0.059147	0.115778	0.002724	0.40	0.1	705.6	15.7
Mudtank	12	6	0.062027	0.002860	1.005831	0.050105	0.117609	0.002220	0.38	-0.1	717.4	12.8
Mudtank	9	5	0.066739	0.002659	1.086487	0.048872	0.118072	0.002465	0.46	0.5	716.2	14.1
Mudtank	18	9	0.064414	0.001870	1.022596	0.034347	0.115139	0.001944	0.50	0.2	701.2	11.2
Mudtank	17	9	0.063057	0.001735	0.992371	0.032027	0.114140	0.001926	0.52	0.0	696.5	11.1
Mudtank	17	9	0.062420	0.002225	0.997054	0.038945	0.115850	0.001852	0.41	0.0	706.9	10.7
Mudtank	16	8	0.063855	0.002336	1.020457	0.041209	0.115904	0.001982	0.42	0.1	706.1	11.4
Mudtank	17	9	0.061487	0.001720	0.993337	0.031967	0.117168	0.001863	0.49	-0.2	715.3	10.8
Mudtank	15	7	0.063573	0.002101	1.012739	0.036923	0.115537	0.001779	0.42	0.1	704.2	10.3
Mudtank	18	10	0.063787	0.002237	1.011107	0.038365	0.114964	0.001665	0.38	0.1	700.7	9.6
Mudtank	15	8	0.061714	0.002057	0.976054	0.036208	0.114706	0.001866	0.44	-0.1	700.9	10.8
Mudtank	16	8	0.062891	0.002020	0.998520	0.035832	0.115151	0.001844	0.45	0.0	702.5	10.6
Mudtank	15	7	0.064357	0.002225	1.004794	0.038694	0.113236	0.001921	0.44	0.2	690.2	11.1
Mudtank 50 micron pit												
Mudtank_1	17	7	0.062843	0.001318	1.038759	0.023701	0.119882	0.001076	0.39	0.0	729.8	6.2
Mudtank_19	18	7	0.063584	0.001227	1.051458	0.022890	0.119934	0.001210	0.46	0.1	729.5	7.0
Mudtank_20	21	9	0.064735	0.001207	1.064316	0.021736	0.119243	0.000993	0.41	0.2	724.6	5.7
Mudtank_17	19	8	0.065031	0.001476	1.060567	0.025577	0.118281	0.000966	0.34	0.3	718.8	5.6
Mudtank_16	19	8	0.064168	0.001292	1.025279	0.022915	0.115884	0.001124	0.43	-1.0	713.5	6.5
Mudtank_15	18	7	0.061575	0.001316	0.998922	0.023225	0.117659	0.001077	0.39	-0.1	718.1	6.2
Mudtank_2	17	8	0.063743	0.001293	1.051768	0.023172	0.119671	0.001028	0.39	0.1	727.8	5.9
Mudtank_3	18	5	0.064488	0.001465	1.046704	0.025691	0.117719	0.001095	0.38	0.2	716.0	6.3
Mudtank_4	19	7	0.063679	0.001390	1.046255	0.024167	0.119163	0.000898	0.33	0.1	725.0	5.2
Mudtank_22	11	4	0.057049	0.002033	0.900703	0.034369	0.114506	0.001565	0.36	-0.7	713.5	9.1
Fish Canyon Tuff 40 micron pit												
fct - 1	358	135	0.047500	0.004900	0.029930	0.003240	0.004570	0.000150	0.30	0.1	29.4	1.0
fct - 2	274	158	0.048300	0.005000	0.029968	0.003302	0.004500	0.000170	0.34	0.2	28.9	1.1
fct - 3	494	198	0.049800	0.004400	0.028839	0.002700	0.004200	0.000130	0.33	0.4	27.9	0.8

fct - 4	366	200	0.056100	0.006100	0.030554	0.003429	0.004350	0.000110	0.25	1.2	27.6	0.7
fct - 7	298	122	0.049400	0.005100	0.030651	0.003347	0.004500	0.000160	0.33	0.4	28.8	1.0
fct - 8	447	309	0.050400	0.004500	0.030507	0.002870	0.004390	0.000130	0.31	0.5	28.1	0.8
fct - 9	406	180	0.049400	0.003700	0.029833	0.002379	0.004380	0.000120	0.34	0.4	28.1	0.8
fct - 10	430	204	0.052100	0.004400	0.032326	0.002863	0.004500	0.000120	0.30	0.7	28.7	0.8
Fish Canyon Tuff 40/50 micron pit												
Bishop_1	2242	1121	0.083000	0.014000	0.001316	0.000228	0.000115	0.000005	0.23	4.7	0.79	0.03
Bishop_2	2495	1148	0.092000	0.011000	0.001373	0.000169	0.000108	0.000003	0.24	5.8	0.74	0.02
Bishop_3	2089	948	0.071400	0.009500	0.001054	0.000143	0.000107	0.000003	0.21	3.2	0.76	0.02
Bishop_1	2574	1338	0.295000	0.031000	0.005873	0.000735	0.000144	0.000010	0.54	31.5	0.72	0.05
Bishop_3	1867	756	0.079700	0.009300	0.001213	0.000146	0.000110	0.000003	0.26	4.3	0.77	0.02
Bishop_5	2393	1217	0.070300	0.008300	0.001019	0.000124	0.000105	0.000003	0.23	3.1	0.74	0.02
Bishop_6	2941	1614	0.068500	0.008000	0.001011	0.000121	0.000107	0.000003	0.21	2.8	0.76	0.02
1704-1	-	-	0.063000	0.011000	0.000880	0.000150	0.000106	0.000004	-0.08	2.1	0.75	0.03
1704-2	-	-	0.055400	0.006600	0.000783	0.000088	0.000106	0.000003	0.06	1.2	0.76	0.02
1704-3	-	-	0.057000	0.012000	0.000860	0.000170	0.000106	0.000004	0.28	1.4	0.76	0.02
1704-4	-	-	0.083000	0.014000	0.001460	0.000390	0.000115	0.000005	0.95	4.7	0.79	0.03
1704-5	-	-	0.092000	0.011000	0.001350	0.000160	0.000108	0.000003	0.62	5.8	0.74	0.02
1704-6	-	-	0.071400	0.009500	0.001070	0.000150	0.000107	0.000003	0.59	3.2	0.75	0.02

Table D.3: LA-ICP-MS U-Th data.

									^{230}Th-^{238}U		Boehnke et al., 2016	
Sample		U (ppm)	Th (ppm)	Th/U	(^{238}U)/(^{232}Th)	1σ	(^{230}Th)/(^{232}Th)	1σ	Model Age (ka; zircon-glass)	1σ	Model Age (ka)	1σ
PAL (UA1305)												
PAL-1305-1	**rim**	**85**	**48**	**0.5**	**4.40**	**0.15**	**3.68**	**0.19**	**167**	**26**	180	29
PAL-1305-2	**core**	**234**	**158**	**0.6**	**3.98**	**0.05**	**3.55**	**0.12**	**210**	**24**	230	24
PAL-1305-3	**rim**	**127**	**91**	**0.7**	**4.47**	**0.05**	**3.98**	**0.11**	**212**	**20**	225	20
PAL-1305-4	**rim**	**143**	**120**	**0.8**	**3.29**	**0.03**	**2.93**	**0.09**	**198**	**19**	225	21
PAL-1305-5	**rim**	**262**	**270**	**1.0**	**3.77**	**0.03**	**3.19**	**0.08**	**167**	**11**	187	16
PAL-1305-6	**core**	**95**	**76**	**0.8**	**3.96**	**0.21**	**3.37**	**0.30**	**173**	**47**	195	45
PAL-1305-7	**rim**	**162**	**119**	**0.7**	**4.21**	**0.03**	**3.69**	**0.13**	**196**	**21**	212	21
PAL-1305-8	**rim**	**138**	**120**	**0.8**	**3.07**	**0.01**	**2.64**	**0.07**	**167**	**22**	197	16
PAL-1305-9	**rim**	**152**	**115**	**0.7**	**4.93**	**0.06**	**4.65**	**0.14**	**288**	**46**	297	25
PAL-1305-10	**rim**	**242**	**233**	**0.9**	**4.42**	**0.04**	**3.98**	**0.19**	**220**	**36**	233	29
PAL-1305-11	**rim**	**167**	**132**	**0.7**	**6.62**	**0.11**	**5.91**	**0.30**	**225**	**41**	225	30
PAL-1305-12	core	128	102	0.8	6.33	0.12	6.25	0.25	466	313	NC	NC
PAL-1305-13	**rim**	**214**	**151**	**0.7**	**4.60**	**0.04**	**4.16**	**0.10**	**226**	**20**	240	19
PAL-1305-14	**rim**	**109**	**54**	**0.5**	**3.91**	**0.07**	**3.56**	**0.19**	**229**	**45**	246	34
PAL-1305-15	**rim**	**110**	**79**	**0.7**	**4.02**	**0.06**	**3.72**	**0.19**	**250**	**53**	266	33
PAL-1305-16	**core**	**83**	**40**	**0.5**	**4.68**	**0.06**	**3.90**	**0.12**	**167**	**14**	180	18
PAL-1305-17	**core**	**131**	**93**	**0.7**	**4.00**	**0.11**	**3.55**	**0.12**	**204**	**27**	222	26
PAL-1305-18	**rim**	**195**	**134**	**0.6**	**3.80**	**0.07**	**3.58**	**0.10**	**277**	**43**	289	25
PAL-1305-19	**core**	**146**	**118**	**0.8**	**4.26**	**0.05**	**3.88**	**0.14**	**231**	**32**	245	25
PAL-1305-20	**rim**	**118**	**88**	**0.7**	**3.65**	**0.04**	**3.20**	**0.09**	**191**	**17**	215	19
PAL-1305-21	**rim**	**95**	**75**	**0.7**	**4.33**	**0.06**	**3.69**	**0.08**	**177**	**12**	191	17
PAL-1305-22	**rim**	**98**	**82**	**0.8**	**4.43**	**0.02**	**4.00**	**0.10**	**226**	**20**	239	20
PAL-1305-23	**rim**	**171**	**110**	**0.6**	**6.43**	**0.06**	**5.71**	**0.21**	**219**	**27**	221	24
PAL-1305-24	rim	134	67	0.5	4.64	0.07	5.02	0.13	∞	∞	NC	NC
PAL-1305-25	core	165	113	0.6	3.53	0.02	3.69	0.08	∞	∞	NC	NC
PAL-1305-26	rim	175	157	0.8	6.93	0.04	7.60	0.30	∞	∞	NC	NC
PAL-1305-27	**core**	**112**	**51**	**0.4**	**5.65**	**0.05**	**4.61**	**0.36**	**161**	**31**	168	34
PAL-1305-28	N/A	43	20	0.4	6.80	0.03	7.03	0.69	∞	∞	NC	NC

PAL-1305-29	rim	78	50	0.6	5.03	0.07	5.10	0.65	∞	∞	NC	NC
PAL-1305-30	**rim**	**188**	**166**	**0.8**	**3.68**	**0.04**	**3.39**	**0.24**	**241**	**65**	254	40
PAL-1305-31	rim	142	121	0.8	3.79	0.07	4.10	0.18	∞	∞	NC	NC
PAL-1305-32	rim	110	79	0.7	4.55	0.03	5.17	0.24	∞	∞	NC	NC
PAL-1305-33	**N/A**	**151**	**119**	**0.7**	**4.11**	**0.05**	**3.67**	**0.17**	**209**	**32**	227	28
PAL-1305-34	**N/A**	**183**	**150**	**0.8**	**3.95**	**0.09**	**3.69**	**0.18**	**263**	**61**	277	34
PAL-1305-35	**N/A**	**165**	**134**	**0.7**	**4.00**	**0.03**	**3.67**	**0.19**	**236**	**46**	250	31
PAL-1305-36	**N/A**	**176**	**96**	**0.5**	**5.94**	**0.08**	**5.44**	**0.30**	**248**	**55**	251	34
PAL-1305-37	**N/A**	**94**	**75**	**0.7**	**4.03**	**0.10**	**3.76**	**0.23**	**261**	**73**	273	38
PAL-1305-38	N/A	131	79	0.6	5.35	0.07	6.00	0.30	∞	∞	NC	NC
PAL-1305-39	N/A	98	63	0.6	5.02	0.07	4.86	0.27	348	149	NC	NC
PAL-1305-40	N/A	67	48	0.7	4.52	0.11	4.86	0.32	∞	∞	NC	NC
PAL-1305-41	N/A	192	165	0.8	3.75	0.05	3.98	0.11	∞	∞	NC	NC
PAL-1305-42	N/A	115	87	0.7	4.31	0.15	4.50	0.23	∞	∞	NC	NC
PAL-1305-43	N/A	288	280	0.9	3.32	0.04	3.51	0.11	∞	∞	NC	NC

Woodchopper (UA1582)

UA1582 Day 1	**rim**	**149**	**60**	**0.35**	**8.44**	**0.11**	**6.96**	**0.27**	**179**	**19**	**173**	**21**
UA1582 Day 1	**core**	**157**	**79**	**0.45**	**6.69**	**0.06**	**5.84**	**0.21**	**211**	**24**	**209**	**22**
UA1582 Day 1	**rim**	**440**	**281**	**0.56**	**5.31**	**0.02**	**4.65**	**0.15**	**209**	**21**	**210**	**20**
UA1582 Day 1	**rim**	**127**	**65**	**0.45**	**6.67**	**0.07**	**5.32**	**0.20**	**159**	**15**	**158**	**18**
UA1582 Day 1	**rim**	**190**	**138**	**0.64**	**4.69**	**0.07**	**4.05**	**0.15**	**196**	**23**	**203**	**21**
UA1582 Day 1	**rim**	**78**	**43**	**0.48**	**6.19**	**0.22**	**4.45**	**0.27**	**122**	**17**	**124**	**24**
UA1582 Day 1	**rim**	**98**	**48**	**0.43**	**6.87**	**0.07**	**5.01**	**0.18**	**128**	**10**	**126**	**15**
UA1582 Day 1	**rim**	**69**	**36**	**0.46**	**6.53**	**0.04**	**4.42**	**0.16**	**108**	**7**	**107**	**13**
UA1582 Day 1	**rim**	316	568	1.59	1.88	0.02	1.79	0.07	267	48	309	29
UA1582 Day 1	**rim**	**88**	**41**	**0.41**	**7.27**	**0.19**	**4.80**	**0.23**	**104**	**10**	**101**	**16**
UA1582 Day 1	**rim**	**90**	**39**	**0.38**	**7.89**	**0.15**	**6.16**	**0.29**	**153**	**18**	**149**	**22**
UA1582 Day 1	**rim**	**78**	**39**	**0.44**	**6.77**	**0.14**	**4.26**	**0.18**	**94**	**8**	**92**	**13**
UA1582 Day 1	**rim**	**114**	**63**	**0.49**	**6.06**	**0.17**	**4.66**	**0.23**	**143**	**18**	**145**	**22**
UA1582 Day 1	**rim**	**194**	**111**	**0.50**	**5.92**	**0.02**	**4.45**	**0.14**	**135**	**9**	**135**	**14**
UA1582 Day 1	**rim**	**97**	**41**	**0.37**	**8.10**	**0.12**	**5.85**	**0.28**	**128**	**13**	**122**	**17**

UA1582 Day 1	**rim**	**161**	**68**	**0.37**	**8.00**	**0.12**	**5.94**	**0.24**	**136**	**12**	**131**	**18**
UA1582 Day 2	**rim**	**133**	**60**	**0.43**	**6.89**	**0.15**	**4.14**	**0.28**	**86**	**10**	**84**	**17**
UA1582 Day 2	**rim**	**149**	**98**	**0.63**	**4.74**	**0.11**	**3.65**	**0.28**	**139**	**24**	**142**	**30**
UA1582 Day 2	**rim**	**239**	**173**	**0.69**	**4.31**	**0.05**	**3.10**	**0.18**	**115**	**13**	**121**	**20**
UA1582 Day 2	**rim**	**132**	**112**	**0.81**	**3.67**	**0.07**	**3.11**	**0.24**	**177**	**37**	**188**	**36**
UA1582 Day 2	**rim**	**141**	**76**	**0.52**	**5.75**	**0.18**	**4.15**	**0.29**	**122**	**18**	**123**	**25**
UA1582 Day 2	**rim**	**242**	**268**	**1.06**	**2.82**	**0.03**	**1.96**	**0.09**	**91**	**8**	**113**	**16**
UA1582 Day 2	**rim**	**110**	**48**	**0.41**	**7.25**	**0.20**	**5.81**	**0.47**	**163**	**33**	**160**	**34**
UA1582 Day 2	**rim**	**144**	**90**	**0.60**	**4.99**	**0.05**	**4.12**	**0.23**	**170**	**24**	**173**	**26**
UA1582 Day 2	**core**	213	108	0.48	6.16	0.03	5.88	0.24	321	81	315	29
UA1582 Day 2	**rim**	**121**	**59**	**0.46**	**6.46**	**0.05**	**4.80**	**0.28**	**133**	**16**	**131**	**22**
UA1582 Day 2	**core**	**233**	**115**	**0.47**	**6.33**	**0.06**	**5.38**	**0.23**	**191**	**23**	**190**	**23**
UA1582 Day 2	**rim**	**183**	**95**	**0.50**	**6.03**	**0.04**	**4.34**	**0.23**	**122**	**13**	**123**	**18**
UA1582 Day 2	**rim**	**202**	**117**	**0.55**	**5.44**	**0.05**	**4.77**	**0.23**	**210**	**32**	**214**	**27**
UA1582 Day 2	**rim**	**185**	**107**	**0.55**	**5.42**	**0.07**	**4.60**	**0.25**	**188**	**29**	**190**	**27**
UA1582 Day 2	**rim**	**163**	**65**	**0.38**	**7.88**	**0.05**	**6.66**	**0.33**	**191**	**27**	**185**	**25**
UA1582 Day 2	**N/A**	231	142	0.59	5.08	0.05	5.21	0.24	∞	∞	∞	∞
Old Crow (UT1577)												
OCT_	N/A	**288**	**70**	**0.24**	**6.66**	**0.19**	**5.67**	**0.31**	**182**	**30**	**191**	**30**
OCT_	N/A	**197**	**39**	**0.20**	**8.18**	**0.61**	**6.60**	**0.43**	**159**	**37**	**167**	**40**
OCT_	N/A	**198**	**37**	**0.19**	**8.78**	**0.34**	**7.06**	**0.35**	**159**	**24**	**161**	**27**
OCT_	N/A	**246**	**51**	**0.21**	**7.80**	**0.17**	**6.38**	**0.15**	**164**	**13**	**168**	**17**
OCT_	N/A	**109**	**27**	**0.25**	**6.51**	**0.21**	**5.54**	**0.49**	**181**	**46**	**188**	**41**
OCT_	N/A	**417**	**119**	**0.29**	**5.68**	**0.42**	**4.84**	**0.30**	**178**	**46**	**192**	**44**
OCT_	N/A	**239**	**41**	**0.17**	**9.48**	**0.25**	**8.38**	**0.28**	**218**	**30**	**218**	**24**
OCT_	N/A	**368**	**73**	**0.20**	**8.22**	**0.21**	**7.34**	**0.27**	**223**	**34**	**225**	**27**
OCT_	N/A	**305**	**63**	**0.21**	**7.91**	**0.21**	**7.16**	**0.26**	**236**	**39**	**242**	**29**
OCT_	N/A	**306**	**62**	**0.20**	**8.03**	**0.17**	**7.41**	**0.27**	**259**	**45**	**260**	**28**
OCT_	N/A	**184**	**39**	**0.21**	**7.70**	**0.22**	**7.40**	**0.20**	**332**	**87**	**326**	**29**
OCT_	N/A	287	57	0.20	8.23	0.19	7.93	0.15	∞	∞	∞	∞
OCT_	N/A	251	50	0.20	8.18	0.14	7.95	0.27	∞	∞	∞	∞
OCT_	N/A	179	35	0.20	8.23	0.28	8.65	0.37	∞	∞	∞	∞
OCT_	N/A	182	42	0.23	7.02	0.42	7.67	0.76	∞	∞	∞	∞

OCT_	N/A	133	30	0.22	7.31	0.36	8.50	0.97	∞	∞	∞	∞
OCT_	N/A	149	35	0.23	7.02	0.36	8.23	0.91	∞	∞	∞	∞
OCT_	N/A	291	59	0.20	8.00	0.14	8.40	0.37	∞	∞	∞	∞
OCT_	N/A	732	271	0.37	4.39	0.05	4.51	0.13	∞	∞	∞	∞
OCT_	N/A	506	141	0.28	5.83	0.21	6.39	0.34	∞	∞	∞	∞
OCT_	N/A	328	101	0.31	5.28	0.06	5.47	0.11	∞	∞	∞	∞
OCT_	N/A	259	52	0.20	8.08	0.14	8.72	0.33	∞	∞	∞	∞
OCT_	N/A	167	29	0.17	9.35	0.25	10.64	0.58	∞	∞	∞	∞
OCT_	N/A	392	85	0.22	7.45	0.11	8.30	0.34	∞	∞	∞	∞
OCT_	N/A	410	107	0.26	6.22	0.06	6.98	0.18	∞	∞	∞	∞
OCT_	N/A	1259	488	0.39	4.19	0.08	4.67	0.13	∞	∞	∞	∞
OCT_	N/A	376	92	0.24	6.66	0.13	7.70	0.32	∞	∞	∞	∞
OCT_	N/A	355	83	0.23	6.94	0.17	7.98	0.35	∞	∞	∞	∞
Biederman (UT1884)												
Biederman (UT1884)												
Biederman_UT1884-1	N/A	**-**	**-**	**-**	**19.00**	**0.50**	**15.55**	**0.30**	**179**	**8**	**169**	**9**
Biederman_UT1884-2	N/A	**-**	**-**	**-**	**6.73**	**0.42**	**5.77**	**0.81**	**195**	**44**	**190**	**29**
Biederman_UT1884-3	N/A	-	-	-	7.50	0.14	8.54	0.65	∞	∞	∞	∞
Biederman_UT1884-4	N/A	-	-	-	5.08	0.10	5.99	0.53	∞	∞	∞	∞
Biederman_UT1884-5	N/A	-	-	-	5.96	0.11	6.41	0.33	∞	∞	∞	∞
Biederman_UT1884-6	N/A	-	-	-	6.88	0.10	8.10	0.81	∞	∞	∞	∞
Biederman_UT1884-7	N/A	-	-	-	1.74	0.05	2.04	0.14	∞	∞	∞	∞
Biederman_UT1884-8	N/A	-	-	-	3.32	0.08	3.96	1.20	∞	∞	∞	∞
Biederman_UT1884-9	N/A	-	-	-	3.55	0.26	3.73	0.34	∞	∞	∞	∞
Biederman_UT1884-10	N/A	-	-	-	4.94	0.35	5.21	0.60	∞	∞	∞	∞
Biederman_UT1884-11	N/A	-	-	-	5.59	0.31	6.10	0.43	∞	∞	∞	∞
Biederman_UT1884-12	N/A	-	-	-	4.73	0.11	4.81	0.16	∞	∞	∞	∞
Biederman_UT1884-13	N/A	-	-	-	3.36	0.08	3.54	0.10	∞	∞	∞	∞
Biederman_UT1884-14	N/A	-	-	-	5.58	0.32	6.66	0.43	∞	∞	∞	∞
Biederman_UT1884-15	N/A	-	-	-	6.73	0.13	7.11	0.31	∞	∞	∞	∞
Biederman_UT1884-16	N/A	-	-	-	6.45	0.15	6.28	0.24	∞	∞	∞	∞
Biederman_UT1884-17	N/A	-	-	-	6.46	0.17	7.51	0.54	∞	∞	∞	∞
Biederman_UT1884-18	N/A	**-**	**-**	**-**	**3.18**	**0.18**	**2.56**	**0.23**	**139**	**17**	**164**	**21**

Biederman_UT1884-19	N/A	**-**	**-**	**-**	**5.53**	**0.12**	**4.52**	**0.24**	**165**	**12**	**167**	**12**
Biederman_UT1884-20	N/A	-	-	-	1.89	0.12	2.08	0.14	∞	∞	∞	∞
Biederman_UT1884-21	N/A	-	-	-	2.44	0.33	2.44	0.41	∞	∞	254	38
Biederman_UT1884-22	N/A	-	-	-	6.43	0.17	6.29	0.27	∞	∞	∞	∞
Biederman_UT1884-23	N/A	-	-	-	4.16	0.10	4.35	0.12	∞	∞	∞	∞
Biederman_UT1884-24	N/A	-	-	-	3.41	0.12	3.68	0.15	∞	∞	∞	∞
Biederman_UT1884-25	N/A	**-**	**-**	**-**	**2.49**	**0.50**	**2.15**	**0.48**	**165**	**66**	**175**	**44**
Biederman_UT1884-26	N/A	-	-	-	8.55	0.93	9.80	1.03	∞	∞	∞	∞
Biederman_UT1884-27	N/A	-	-	-	5.62	0.22	5.62	0.44	∞	∞	∞	∞
Biederman_UT1884-28	N/A	-	-	-	4.39	0.10	4.14	0.12	284	26	293	13
Biederman_UT1884-29	N/A	-	-	-	4.16	0.13	4.64	0.44	∞	∞	493	18
Biederman_UT1884-30	N/A	**-**	**-**	**-**	**4.38**	**0.15**	**3.69**	**0.22**	**173**	**16**	**185**	**17**
Biederman_UT1884-31	N/A	-	-	-	5.39	0.32	5.75	0.37	∞	∞	∞	∞
Biederman_UT1884-32	N/A	-	-	-	2.04	0.08	2.10	0.08	∞	∞	∞	∞
Biederman_UT1884-33	N/A	**-**	**-**	**-**	**4.64**	**0.17**	**4.24**	**0.50**	**240**	**57**	**230**	**29**
Snag (UA1589)												
Snag1589__222	NA	272	181	0.05	5.04	0.07	5.25	0.30	∞	∞	∞	∞
Snag1589__223	**rim**	**244**	**143**	**0.72**	**4.53**	**0.07**	**3.05**	**0.38**	**94**	**22**	**106**	**18**
Snag1589__223	NA	0	0	0.37	16.35	1.97	227.63	360.33	∞	∞	∞	∞
Snag1589__225	**NA**	**267**	**140**	**0.45**	**6.38**	**0.10**	**4.50**	**0.72**	**114**	**35**	**118**	**23**
Snag1589__226	NA	437	282	0.05	5.20	0.09	5.36	0.21	∞	∞	∞	∞
Snag1589__227	NA	230	77	0.05	10.06	0.40	11.00	0.67	∞	∞	∞	∞
Snag1589__228	NA	296	171	0.05	5.79	0.14	6.08	0.32	∞	∞	∞	∞

Uncertainties are 1σ. ∞ = zircon in secular equilibrium (>350 ka)

Decay constants used: λ_{232}: $4.9475 \cdot 10^{-11}$ a^{-1}; λ_{230}: $9.158 \cdot 10^{-6}$ a^{-1}; λ_{238}: $1.55125 \cdot 10^{-10}$ a^{-1}.

Table D.4: (U-Th)/He dating results.

Output from MCHeCalc, modeled using internal surface zircon crystallization age weighted mean 245 +/- 8.5 ka.

Biederman (UT1884) INDIVIDUAL RESULTS

#	He_Age(ka)	sig_He(ka)	Erup_Age(ka)	+sig	-sig	Avg_sig
1,	**164.9**	**5.7**	**191.4**	**9.4**	**7.8**	**8.6**
3,	**144.9**	**7.7**	**164.4**	**9.8**	**10.2**	**10.0**
6,	**164.0**	**7.3**	**192.0**	**11.1**	**10.4**	**10.7**
2,	603.9	10.6	-	-	-	-
4,	289.2	8.6	-	-	-	-
5,	294.7	15.4	-	-	-	-

GENERAL RESULTS

Name	Erup_Age(ka)	+sig	-sig	Avg_sig
Biederman	183.1	5.8	5.3	5.6

Goodness of Fit = 6.441637873649597E-002

Output from MCHeCalc, modeled using internal surface zircon crystallization age weighted mean 165 +/- 7.5 ka.

Woodchopper Creek INDIVIDUAL RESULTS

#	He_Age(ka)	sig_He(ka)	Erup_Age(ka)	+sig	-sig	Avg_sig
1,	**90.5**	**13.6**	**116.5**	**22.7**	**20.4**	**21.6**
2,	**134.2**	**20.1**	**158.2**	**27.2**	**24.8**	**26.0**
3,	**142.5**	**21.4**	**165.6**	**31.2**	**23.9**	**27.6**
4,	**97.0**	**14.6**	**114.8**	**21.2**	**19.5**	**20.4**
5,	**110.3**	**16.5**	**132.0**	**22.6**	**22.5**	**22.5**
6,	**98.7**	**14.8**	**117.3**	**21.3**	**20.1**	**20.7**
7,	**147.1**	**22.1**	**172.5**	**30.9**	**25.3**	**28.1**
8,	**109.0**	**16.4**	**129.5**	**22.9**	**21.8**	**22.4**
9,	**94.8**	**14.2**	**111.9**	**20.9**	**18.7**	**19.8**
10,	**85.5**	**12.8**	**99.7**	**20.3**	**15.9**	**18.1**
11,	**120.6**	**18.1**	**146.3**	**22.3**	**26.3**	**24.3**
12,	**50.8**	**7.6**	**58.7**	**11.3**	**9.9**	**10.6**
13,	**87.4**	**13.1**	**102.5**	**20.6**	**16.8**	**18.7**
14,	**100.1**	**15.0**	**118.5**	**21.9**	**19.9**	**20.9**
15,	**58.8**	**8.8**	**67.7**	**14.4**	**10.7**	**12.6**
16,	**102.6**	**15.4**	**109.9**	**15.4**	**17.8**	**16.6**
17,	**124.3**	**18.6**	**132.8**	**18.9**	**21.3**	**20.1**

GENERAL RESULTS

Name	Erup_Age(ka)	+sig	-sig	Avg_sig
Woodchopper	114.1	6.7	6.3	6.5

Goodness of Fit = 1.890449493657798E-003

Table D.5: Recalculated glass-fission-track ages of tephra beds from eastern Beringia using the Schmieder et al. (2018) age for the Moldavite tektite

Sample number	Method for correction of partial track fading	Irradiation date	Spontaneous track density (10^2 t/cm^2)	Corrected spontaneous track density (10^2 t/cm^2)	Induced track density (10^4 t/cm^2)	Track density on muscovite detector over dosimeter glass (10^5 t/cm^2)	Etching conditions HF:temp:time (%: ºC: s)	D_s (µm)	D_i (µm)	D_s/D_i or D_i/D_s#	Age (ka) ± 1σ
Dominion Creek											
UT1456	DCFT	23/11/2000	1.577 ± 0.13	1.73 ± 0.14	3.78 ± 0.02	5.61 ± 0.01	24: 24: 120	5.93 ± 0.17	6.64 ± 0.07	1.10 ± 0.03	**80 ± 9**
			(148)	(148)	(42319)	(14359)			[77]	[796]	
VT tephra											
UT1637	DCFT	31/1/2000	1.04 ± 0.23	1.20 ± 0.26	1.45 ± 0.02	5.06 ± 0.04	24: 22: 70	5.31 ± 0.23	6.08 ± 0.08	1.15 ± 0.05	**130 ± 30**
			(21)	(21)	(5867)	(12744)					

Notes: The population-subtraction method was used (Westgate, 2015). Ages calculated using the zeta approach and $\lambda_D = 1.551 \times 10^{-10}$ yr^{-1}. Zeta value is 311 ± 4 based on 7 irradiations at the McMaster Nuclear Reactor, Hamilton, Ontario, using the NIST SRM 612 glass dosimeter and the Moldavite tektite glass with an $^{40}Ar/^{39}Ar$ age of 14.808 ± 0.021 Ma (2σ) (Schmieder et al., 2018). Number of tracks counted is given in parentheses; number of tracks measured is given in square brackets.

The fluence is obtained by multiplying the muscovite track density by 0.53 x 10^{10} based on 9 determinations.

Age determinations are corrected for partial track fading using the diameter correction (DCFT) method (Sandhu and Westgate 1995).

The uncertainty on individual age determinations was calculated using methods described in Bigazzi and Galbraith (1999).

Ds = mean long-axis of spontaneous tracks; Di = mean long-axis of induced tracks. Area estimated by the points-counting technique (Naeser et al., 1982).

Table D.6: U-Pb dating Bayesian modeling results.

TRIANGULAR DISTRIBUTION					
Tephra	Age (Ma)	2.5% CI	97.5% CI	sigma	2 sigma
WCT	**0.092**	0.077	0.105	0.007	**0.015**
PAL	**0.185**	0.157	0.209	0.013	**0.026**
OCT	**0.151**	0.136	0.164	0.007	**0.014**
SCF	**0.163**	0.139	0.179	0.010	**0.020**
ST	**0.212**	0.179	0.230	0.014	**0.027**
PRT 80	**0.282**	0.241	0.313	0.018	**0.035**
PUP	**0.273**	0.227	0.306	0.020	**0.040**
UNIFORM DISTRIBUTION					
Tephra	Age (Ma)	2.5% CI	97.5% CI	sigma	2 sigma
WCT	**0.088**	0.069	0.102	0.008	**0.016**
PAL	**0.176**	0.142	0.203	0.015	**0.030**
OCT	**0.147**	0.127	0.162	0.009	**0.017**
SCF	**0.161**	0.130	0.179	0.013	**0.025**
ST	**0.209**	0.159	0.229	0.020	**0.038**
PRT 80	**0.274**	0.217	0.311	0.024	**0.047**
PUP	**0.266**	0.201	0.304	0.028	**0.055**
MELTS DISTRIBUTION					
Tephra	Age (Ma)	2.5% CI	97.5% CI	sigma	2 sigma
WCT	**0.083**	0.055	0.100	0.011	**0.022**
PAL	**0.166**	0.119	0.197	0.019	**0.038**
OCT	**0.142**	0.111	0.159	0.012	**0.024**
SCF	**0.159**	0.122	0.178	0.015	**0.030**
ST	**0.207**	0.147	0.229	0.024	**0.046**
PRT 80	**0.265**	0.180	0.311	0.034	**0.066**
PUP	**0.530**	0.404	0.587	0.052	**0.103**

Table D.7: U-Th dating Bayesian modeling results

TRIANGULAR DISTRIBUTION					
Tephra	Age (ka)	2.5% CI	97.5% CI	sigma	2 sigma
WCT	**94.2**	79.3	101.8	5.8	**11.3**
PAL	**173.5**	156.3	190.8	8.8	**17.2**
OCT	**164.4**	130.4	188.6	15.0	**29.4**
BT	**163.8**	136.1	177.7	10.7	**21.1**
UNIFORM DISTRIBUTION					
Tephra	Age (ka)	2.5% CI	97.5% CI	sigma	2 sigma
WCT	**87.1**	72.5	98.6	6.5	**12.8**
PAL	**169.6**	150.0	188.8	9.7	**19.0**
OCT	**161.3**	120.1	188.3	17.6	**34.6**
BT	**160.7**	125.1	177.2	13.8	**27.1**
MELTS DISTRIBUTION					
Tephra	Age (ka)	2.5% CI	97.5% CI	sigma	2 sigma
WCT	**81.2**	58.3	95.0	9.3	**18.3**
PAL	**164.7**	140.1	187.2	11.6	**22.8**
OCT	**157.4**	103.0	188.2	22.2	**43.5**
BT	**158.3**	114.1	177.0	17.2	**33.6**

Table D.7. Major element glass geochemical data.

Sample	SiO2	TiO2	Al2O3	FeOt	MnO	MgO	CaO	Na2O	K2O	Cl	total	H2Odif
Biederman at Birch Creek												
UA1328-1	76.51	0.21	13.49	0.99	0.05	0.29	1.46	3.74	3.22	0.05	100.00	5.48
UA1328-2	76.62	0.21	13.59	0.97	0.08	0.27	1.49	3.55	3.17	0.05	100.00	7.97
UA1328-3	78.31	0.13	12.44	0.81	0.06	0.26	0.98	3.34	3.65	0.03	100.00	6.36
UA1328-4	77.24	0.17	13.55	1.00	0.02	0.29	1.48	3.14	3.08	0.03	100.00	7.28
UA1328-5	76.47	0.20	13.50	1.00	0.02	0.25	1.46	3.92	3.12	0.06	100.00	6.86
UA1328-6	76.65	0.21	13.27	0.95	0.00	0.25	1.43	3.70	3.52	0.03	100.00	6.75
UA1328-7	76.53	0.15	13.43	1.05	0.03	0.30	1.43	3.70	3.31	0.07	100.00	5.60
UA1328-8	76.79	0.15	13.34	1.05	0.04	0.37	1.44	3.50	3.28	0.03	100.00	5.80
UA1328-9	77.37	0.12	13.19	0.84	0.03	0.20	1.37	3.54	3.33	0.02	100.00	5.68
UA1328-10	76.90	0.20	13.51	0.93	0.03	0.31	1.45	3.48	3.17	0.02	100.00	5.99
UA1328-11	76.54	0.22	13.66	0.99	0.05	0.31	1.49	3.49	3.19	0.05	100.00	6.04
UA1328-12	76.66	0.13	13.74	0.95	0.03	0.27	1.45	3.68	3.07	0.02	100.00	6.30
UA1328-13	76.32	0.18	13.74	0.98	0.08	0.34	1.57	3.41	3.37	0.01	100.00	4.85
UA1328-14	76.43	0.22	13.76	0.98	0.05	0.28	1.52	3.51	3.23	0.04	100.00	6.39
UA1328-15	76.63	0.15	13.52	1.00	0.03	0.39	1.49	3.66	3.06	0.06	100.00	5.80
UA1328-16	76.83	0.18	13.28	0.90	0.05	0.33	1.46	3.79	3.12	0.05	100.00	5.91
UA1328-17	76.76	0.17	13.65	1.02	0.04	0.24	1.50	3.49	3.11	0.04	100.00	5.95
UA1328-18	76.42	0.20	13.66	1.04	0.05	0.33	1.50	3.68	3.07	0.05	100.00	5.63
UA1328-19	78.08	0.12	12.61	0.76	0.01	0.23	1.11	3.48	3.56	0.02	100.00	6.70
Mean	**76.85**	**0.17**	**13.42**	**0.96**	**0.04**	**0.29**	**1.42**	**3.57**	**3.24**	**0.04**	**100.00**	**6.17**
StDev	**0.55**	**0.03**	**0.36**	**0.08**	**0.02**	**0.05**	**0.14**	**0.18**	**0.18**	**0.02**	**0.00**	**0.72**
80 Pup at Birch Creek												
UA 1360-2	72.38	0.46	15.47	1.87	0.04	0.46	2.57	4.17	2.53	0.05	100.00	1.08
UA 1360-3	73.44	0.52	14.23	1.95	0.04	0.56	2.00	4.63	2.59	0.05	100.00	2.99
UA 1360-4	73.59	0.42	14.16	1.88	0.01	0.50	2.15	4.44	2.82	0.04	100.00	4.46
UA 1360-5	73.51	0.39	14.53	1.94	0.04	0.59	2.06	4.19	2.73	0.04	100.00	2.46
UA 1360-6	73.34	0.45	14.58	1.99	0.03	0.54	2.13	4.13	2.78	0.04	100.00	3.78
UA 1360-8	73.08	0.37	14.44	1.99	0.06	0.59	2.15	4.61	2.68	0.04	100.00	0.73
UA 1360-9	73.19	0.44	14.58	1.93	0.03	0.59	2.28	4.20	2.72	0.04	100.00	1.98
UA 1360-10	73.50	0.46	14.41	1.93	0.02	0.47	1.99	4.37	2.82	0.03	100.00	2.25
UA 1360-11	73.70	0.45	14.22	1.84	0.01	0.51	2.04	4.46	2.75	0.03	100.00	3.59
UA 1360-12	73.26	0.42	14.52	1.95	0.02	0.56	2.12	4.49	2.63	0.03	100.00	5.01
UA 1360-13	73.62	0.50	14.22	1.84	0.03	0.52	2.05	4.38	2.78	0.05	100.00	3.06
UA 1360-14	74.33	0.41	13.49	1.75	0.07	0.46	1.59	4.74	3.10	0.06	100.00	5.36
UA 1360-15	73.76	0.44	14.32	1.82	0.07	0.49	2.01	4.31	2.75	0.04	100.00	1.53
UA 1360-16	73.74	0.42	14.29	1.96	0.05	0.48	2.01	4.31	2.71	0.04	100.00	1.53
UA 1360-17	73.17	0.46	14.50	1.98	0.05	0.65	2.13	4.32	2.71	0.03	100.00	2.73
UA 1360-18	72.87	0.43	14.20	2.15	0.00	0.75	2.19	4.65	2.74	0.04	100.00	1.24
UA 1360-19	73.06	0.44	14.59	1.90	0.06	0.53	2.10	4.51	2.78	0.05	100.00	3.87

UA 1360-20	73.22	0.46	14.57	1.92	0.06	0.56	2.14	4.32	2.71	0.06	100.00	3.61
UA 1360-21	73.13	0.49	14.62	1.99	0.05	0.56	2.18	4.31	2.65	0.03	100.00	0.75
UA 1360-22	73.43	0.42	14.18	1.95	0.02	0.51	2.08	4.51	2.86	0.04	100.00	0.90
UA 1360-24	73.41	0.48	14.50	2.02	0.04	0.55	2.14	4.26	2.56	0.05	100.00	3.67
UA 1360-25	73.72	0.46	14.24	1.94	0.06	0.53	2.02	4.23	2.77	0.05	100.00	5.00
Mean	**73.38**	**0.45**	**14.40**	**1.93**	**0.04**	**0.54**	**2.10**	**4.39**	**2.73**	**0.04**	**100.00**	**2.80**
StDev	**0.39**	**0.04**	**0.34**	**0.08**	**0.02**	**0.07**	**0.17**	**0.17**	**0.12**	**0.01**	**0.00**	**1.47**

Table D.7. Trace element glass geochemical data.

All data were obtained using Thermo Scientific Element XR SF-ICP-MS with RESOlution ArF Excimer 193 nm laser ablation system at the University of Alberta, Canada. The instrument is tuned to NIST612, and data is internally standardised to Si. Data are in ppm unless otherwise noted

Sample	Ti49	Rb	Sr	Y	Zr	Nb	Cs	Ba	La	Ce	Pr	Nd	Sm	Eu	Gd	Tb	Dy	Ho	Er	Tm	Yb	Lu	Hf	Ta	Pb	Th	U
NIST612	39	31	77	39	38	38	42	38	36	38	38	36	41	37	36	38	38	40	38	37	38	38	36	40	38	39	40
NIST612_1	45	32	79	38	38	40	43	39	35	40	38	35	38	35	38	38	36	38	38	36	39	36	38	37	39	38	38
NIST612_2	42	31	79	40	38	40	43	40	37	37	38	37	35	36	36	37	36	39	38	37	41	37	38	38	39	38	40
NIST612_3	48	32	78	38	39	39	43	39	35	39	39	36	38	35	41	37	36	38	39	37	40	37	34	37	38	37	37
NIST612_4	42	31	79	38	37	39	43	38	36	37	38	35	36	36	37	40	37	39	38	37	40	37	36	37	39	39	37
NIST612_5	44	31	77	37	36	37	41	42	37	38	38	35	36	35	37	36	33	38	38	36	39	37	36	37	39	36	36
NIST612_6	43	32	78	39	44	38	43	41	35	38	36	34	37	34	35	38	34	36	37	36	35	35	36	37	39	35	37
NIST612_7	46	31	79	39	37	40	44	42	37	38	37	34	39	36	40	37	35	38	38	38	42	37	36	37	39	38	37
NIST612_8	57	32	78	39	39	39	43	39	36	38	38	37	37	35	38	37	35	38	38	37	41	37	38	37	40	37	38
NIST612_9	40	31	79	38	37	39	42	38	36	38	38	36	38	36	36	38	37	38	40	37	37	37	36	38	37	39	37
NIST612_10	45	32	82	39	39	41	43	43	36	39	39	36	40	37	39	39	37	40	38	37	40	37	37	38	39	38	36
NIST612_11	43	31	78	37	37	38	42	37	35	36	35	33	37	34	38	37	34	38	37	37	38	35	38	36	37	37	36
NIST612_12	48	33	80	39	39	39	44	38	37	39	39	35	40	37	37	39	38	40	43	37	39	37	37	38	40	38	38
NIST612_13	44	32	81	39	35	40	43	40	38	39	39	37	36	36	37	38	36	39	40	37	38	37	37	39	38	39	39
NIST612_14	40	32	76	38	36	39	41	39	35	38	37	34	35	37	37	37	34	38	38	37	41	37	37	37	39	37	37
NIST612_15	42	31	78	38	41	40	46	40	36	38	36	36	37	35	36	37	34	37	34	36	40	38	36	37	39	38	38
NIST612_16	43	31	77	38	35	40	43	37	36	39	39	36	38	36	39	38	37	40	37	37	40	38	38	38	37	39	38
NIST612_17	44	31	80	39	39	37	42	41	36	38	38	36	37	35	38	38	36	37	38	37	37	37	39	38	39	39	38
NIST612_18	46	32	79	38	38	39	42	40	37	39	39	35	40	35	36	37	37	39	40	37	40	37	36	38	39	37	37
Average	44	31	79	38	38	39	43	40	36	38	38	35	38	35	37	38	36	38	38	37	39	37	37	38	39	38	38
StDev	4	1	1	1	2	1	1	2	1	1	1	1	2	1	1	1	1	1	2	0	2	1	1	1	1	1	1
NIST610	448	422	502	448	402	468	367	453	424	447	444	418	443	441	417	434	444	448	438	419	459	427	420	452	431	456	470
NIST610_1	438	419	518	454	412	469	369	456	433	460	458	427	456	444	423	439	443	464	428	408	439	441	415	452	433	456	469
NIST610_4	518	429	512	456	468	470	374	437	433	455	441	440	460	447	467	466	437	463	458	437	461	448	425	460	433	467	464
NIST610_5	496	427	507	442	456	477	370	433	436	456	450	432	448	442	468	443	439	458	435	432	448	427	417	449	413	460	461
NIST610_2	484	415	506	450	451	467	380	457	436	454	451	424	445	446	451	442	436	456	441	424	458	440	424	464	436	446	459

NIST610_3	476	416	505	447	434	457	365	443	426	441	439	417	426	421	435	444	433	446	435	412	437	429	420	439	411	450	456
NIST610_6	558	419	497	437	413	463	371	417	422	437	431	424	450	428	455	447	430	437	451	419	433	420	398	435	414	444	470
NIST610_7	532	411	492	435	417	452	354	410	417	430	425	432	429	419	439	433	412	443	443	425	437	418	412	443	417	438	439
NIST610_8	546	407	509	438	402	463	360	428	419	443	430	433	429	427	417	421	412	431	446	421	435	436	418	449	437	450	460
NIST610_9	525	391	491	436	403	457	356	415	411	433	428	424	431	419	414	421	411	430	454	420	423	416	403	436	425	442	452
NIST610_12	500	408	516	451	457	482	376	454	426	450	442	425	432	436	431	426	430	444	457	426	450	440	432	445	412	443	451
NIST610_13	507	412	508	448	447	471	373	443	429	438	433	430	434	432	426	427	420	433	444	418	444	425	407	426	392	437	450
NIST610_10	503	393	486	424	403	460	355	429	410	424	419	426	429	419	411	412	414	425	447	414	430	422	413	437	422	438	448
NIST610_11	543	413	504	441	423	468	366	450	424	441	435	423	426	423	409	416	419	440	456	431	449	421	408	436	418	448	457
NIST610_14	496	431	512	449	428	458	379	446	438	454	430	421	426	444	447	443	432	446	450	430	459	442	428	435	392	455	458
NIST610_15	502	433	507	445	430	478	381	468	440	455	440	433	445	447	455	449	428	447	467	433	448	434	430	452	410	466	467
NIST610_16	495	433	507	449	453	469	376	439	439	454	439	425	424	449	445	445	430	453	445	404	453	439	430	446	430	462	465
NIST610_17	491	438	518	459	447	477	385	453	448	451	447	416	429	440	430	444	428	439	444	417	463	429	428	431	417	453	460
NIST610_18	496	447	544	472	479	497	386	469	447	463	456	441	455	460	447	460	432	466	452	420	449	450	444	462	418	453	460
Average	503	419	507	446	433	469	371	442	429	447	439	427	438	436	436	437	428	446	447	422	446	432	420	445	419	451	459
StDev	31	14	12	10	24	11	10	17	11	11	11	7	12	12	18	14	10	12	9	9	11	10	11	11	13	9	8
ATHO-G	1336	62.6	90.3	86.1	429.0	54.7	1.2	522	51.1	112.7	13.7	51.4	12.4	2.2	12.5	2.3	14.9	3.3	9.7	1.4	8.7	1.4	13.0	3.1	4.7	6.5	2.1
ATHO-G_1	1360	60.0	88.7	86.6	445.0	54.8	1.2	531	51.2	111.9	13.9	57.6	12.9	2.3	13.1	2.4	15.5	3.2	9.5	1.4	10.5	1.3	12.1	3.2	5.2	6.5	2.1
ATHO-G_2	1376	62.7	89.8	88.5	456.0	55.5	1.0	530	50.9	114.6	13.5	55.2	13.2	2.9	12.8	2.2	15.1	2.8	9.2	1.3	9.1	1.4	12.3	3.4	5.1	6.9	2.2
ATHO-G_3	1432	62.6	87.4	86.1	486.0	54.6	1.0	490	50.7	112.9	13.5	54.6	13.0	2.0	11.7	2.4	14.8	3.0	9.6	1.5	9.2	1.5	12.7	3.3	4.8	6.8	2.1
ATHO-G_4	1470	59.2	86.2	84.1	477.0	51.3	1.1	508	51.5	114.8	13.8	56.6	16.1	2.4	13.0	2.0	15.8	3.0	9.6	1.4	8.5	1.4	12.2	3.2	4.4	6.6	2.1
ATHO-G_5	1479	61.9	87.5	83.0	484.0	54.8	1.1	483	49.3	110.7	14.0	59.0	14.0	2.2	13.1	2.5	14.3	3.4	8.7	1.5	9.3	1.5	12.3	3.2	4.9	6.9	2.3
ATHO-G_6	1469	62.5	87.6	84.6	454.0	52.6	1.1	500	49.9	108.3	12.9	54.0	13.1	2.6	14.0	2.3	14.4	2.9	9.6	1.3	8.1	1.5	11.4	3.0	4.5	7.1	2.1
ATHO-G_7	1556	61.5	89.1	84.5	458.0	55.4	1.1	486	49.8	111.5	13.1	56.4	13.9	2.5	15.1	2.2	15.8	3.0	9.1	1.4	11.0	1.4	11.8	3.0	5.3	6.7	2.0
ATHO-G_8	1535	62.6	90.5	85.7	458.0	53.7	1.0	492	50.9	110.1	13.1	56.0	13.1	2.4	14.1	2.5	14.6	3.2	8.4	1.2	9.0	1.3	12.5	3.1	4.7	6.5	2.1
ATHO-G_9	1582	60.7	86.2	81.7	418.0	53.6	1.1	478	48.1	108.6	13.2	55.7	14.1	2.4	13.1	2.2	14.4	3.0	9.3	1.4	9.6	1.6	11.3	3.0	3.4	6.9	2.3
ATHO-G_10	1593	58.4	82.9	81.4	423.0	52.6	1.0	487	47.3	105.7	12.6	53.3	12.4	2.5	12.5	2.2	14.9	2.8	8.6	1.2	8.3	1.2	12.0	2.8	3.9	6.2	2.1
ATHO-G_11	1622	60.7	90.2	83.8	436.0	53.6	1.0	493	51.7	111.0	13.8	55.9	12.7	2.5	12.6	2.3	16.2	3.0	9.7	1.5	8.5	1.5	11.9	2.9	4.7	6.7	2.3
ATHO-G_12	1552	60.5	88.9	84.3	431.0	54.4	1.0	477	47.7	105.1	13.3	52.9	11.2	2.2	12.1	2.4	13.1	3.0	8.7	1.4	9.4	1.4	11.1	2.9	4.4	6.6	1.9
ATHO-G_13	1567	61.2	89.6	81.5	431.0	53.6	1.2	506	50.9	111.1	13.6	57.3	11.5	2.5	11.9	2.1	14.8	2.8	9.2	1.4	10.2	1.3	12.2	2.8	4.0	6.7	2.2
ATHO-G_14	1585	63.5	88.9	85.1	429.0	54.0	1.0	510	50.4	110.3	13.8	56.4	13.7	3.1	12.2	2.1	15.0	3.4	9.9	1.6	8.5	1.3	11.5	3.6	5.0	6.9	2.2
ATHO-G_15	1481	58.1	88.5	83.4	463.0	54.4	1.0	524	51.6	109.7	13.7	53.3	12.4	2.5	13.4	1.9	15.6	3.4	9.2	1.5	9.2	1.3	13.1	3.5	5.0	6.4	2.2
ATHO-G_16	1507	59.8	87.7	84.1	439.0	55.1	1.1	517	50.9	111.5	13.2	57.6	12.5	3.1	13.2	2.1	14.8	3.0	10.0	1.5	8.0	1.5	12.9	3.3	4.6	7.0	2.2
ATHO-G_17	1531	61.1	87.9	84.3	468.0	55.9	1.0	506	51.8	110.5	14.0	55.0	11.7	2.6	12.9	2.3	15.9	3.3	9.5	1.2	9.8	1.4	12.3	3.3	4.4	6.3	2.1
ATHO-G_18	1539	66.2	90.2	87.3	470.0	53.6	1.0	511	51.0	111.6	13.2	56.0	10.7	2.5	15.8	2.1	14.4	3.5	9.7	1.2	10.2	1.5	13.7	3.2	5.0	7.0	2.2
ATHO-G_19	1465	60.6	85.2	83.8	455.0	54.7	0.8	518	51.8	110.3	12.9	56.6	13.6	2.3	13.4	1.9	14.7	3.1	9.5	1.4	9.2	1.3	12.8	3.0	4.6	6.7	2.3
ATHO-G_20	1596	62.6	89.4	85.6	468.0	55.2	0.9	528	52.9	113.5	13.7	56.1	12.2	2.6	13.2	2.3	13.8	3.1	9.6	1.6	8.8	1.5	13.9	3.9	4.7	6.8	2.2
ATHO-G_21	1481	66.2	89.6	85.0	465.0	55.7	1.1	541	51.9	113.8	14.2	50.5	12.3	2.7	12.4	2.4	15.3	3.3	9.6	1.5	11.1	1.4	12.4	3.6	4.5	7.0	2.5
ATHO-G_22	1483	63.7	88.4	85.1	466.0	54.3	1.1	531	50.9	109.7	13.2	54.5	12.3	2.5	12.3	2.3	15.7	3.3	9.6	1.3	8.7	1.6	12.3	4.0	5.0	7.1	2.2

ATHO-G_23	1439	64.1	88.2	84.9	470.0	55.4	1.2	501	50.9	110.0	12.8	57.1	13.6	2.7	11.8	2.5	14.1	3.0	9.0	1.4	9.4	1.4	12.5	3.2	4.6	7.0	1.9
ATHO-G_24	1512	62.4	89.0	85.5	482.0	54.9	1.0	527	51.9	112.8	14.4	56.0	12.9	2.7	13.8	2.4	15.4	3.3	9.4	1.3	8.7	1.3	14.0	3.4	5.6	6.9	2.2
Average	1502	61.8	88.3	84.6	454.4	54.3	1.1	508	50.7	110.9	13.5	55.4	12.9	2.5	13.0	2.3	14.9	3.1	9.4	1.4	9.2	1.4	12.4	3.2	4.7	6.7	2.2
StDev	75	2.0	1.8	1.7	20.1	1.1	0.1	19	1.4	2.4	0.5	2.0	1.1	0.3	1.0	0.2	0.7	0.2	0.4	0.1	0.8	0.1	0.8	0.3	0.5	0.3	0.1
Walcott_3	1279	183.6	20.8	52.2	209.0	46.3	4.4	903	69.8	135.9	15.5	50.4	10.4	1.1	8.0	1.5	10.1	1.9	5.8	1.0	5.9	0.7	6.5	2.6	26.0	26.9	7.8
Walcott_4	1254	175.8	19.6	50.5	201.3	43.2	3.9	840	67.1	133.7	14.1	47.8	9.1	0.7	8.7	1.4	8.5	2.2	5.7	0.8	4.8	0.8	6.4	3.0	26.0	24.9	7.8
Walcott_5	1265	180.3	20.1	51.1	201.0	44.8	4.1	859	67.1	133.4	13.8	51.1	10.5	0.7	10.4	1.7	8.4	2.0	4.3	1.0	5.1	0.8	6.7	2.7	26.1	26.4	7.7
Walcott	1175	181.3	20.4	52.2	191.0	45.1	4.4	924	71.2	134.7	14.7	47.1	10.1	0.8	9.2	1.5	9.9	2.1	4.7	0.9	4.5	0.7	7.0	2.9	24.7	26.7	7.5
Walcott_1	1180	181.5	21.4	54.2	183.0	45.4	4.3	915	70.3	134.7	14.4	51.7	10.5	1.2	9.5	1.4	10.9	2.0	5.1	0.8	5.4	0.8	7.6	2.7	26.5	26.3	7.8
Walcott_2	1185	182.4	21.5	53.9	193.0	46.0	3.9	930	71.7	136.9	14.4	50.2	9.1	0.8	9.5	1.7	9.3	2.1	5.7	0.7	6.0	0.8	7.7	2.8	27.2	26.1	8.4
Walcott_6	1359	178.5	20.4	49.5	199.0	44.1	4.0	829	66.4	132.5	13.9	53.3	10.6	0.9	9.0	1.5	10.2	1.6	5.5	1.0	4.8	0.8	6.9	2.5	25.6	25.8	8.1
Walcott_7	1348	183.3	20.9	52.3	199.9	43.3	3.9	878	71.3	133.0	14.5	52.4	10.3	0.9	9.6	1.4	8.4	2.0	5.3	0.7	4.9	0.8	6.5	3.5	25.3	25.6	7.4
Walcott_8	1328	172.5	20.3	50.6	193.0	45.1	3.7	846	69.6	133.2	13.6	54.8	9.6	1.1	8.7	1.6	10.3	1.9	5.7	1.1	5.2	0.8	6.4	2.6	26.3	25.0	8.1
Walcott_9	1418	182.2	20.3	51.7	190.0	44.2	4.2	868	68.2	133.6	14.2	48.6	9.4	1.0	10.9	1.4	10.1	2.1	5.2	0.8	5.5	0.8	7.2	3.2	26.2	26.1	8.0
Walcott_10	1379	183.0	20.1	51.4	178.0	45.4	3.7	847	67.4	129.4	13.8	50.5	8.9	1.1	8.2	1.3	8.9	1.9	4.5	0.7	5.2	0.8	7.3	2.8	26.5	23.9	7.6
Walcott_11	1328	171.1	19.6	50.5	184.0	44.6	3.9	829	65.3	130.2	14.7	51.2	9.1	0.8	7.9	1.4	9.5	1.8	5.3	0.9	5.1	0.8	6.5	2.8	25.9	24.7	7.9
Walcott_12	1389	181.9	20.8	51.1	193.0	44.4	4.1	868	66.9	136.0	14.8	51.4	9.4	0.7	7.5	1.5	9.0	2.2	5.4	0.7	4.4	0.7	6.9	2.7	27.1	24.2	7.6
Walcott_13	1362	180.0	19.6	53.0	189.0	45.2	4.0	893	68.2	131.9	13.6	56.3	10.0	0.8	8.8	1.2	9.4	2.0	6.5	0.8	6.2	0.7	5.7	2.9	26.0	25.8	8.3
Walcott_14	1366	179.7	20.7	49.8	199.0	46.0	4.0	902	71.8	133.8	14.8	53.1	11.7	1.0	8.2	1.6	8.6	1.8	5.8	1.0	5.8	0.7	7.8	3.0	26.0	25.0	8.1
Walcott_15	1324	178.6	19.8	51.4	196.0	44.3	4.1	902	68.7	133.5	14.8	53.1	8.4	1.1	8.6	1.5	9.2	2.4	5.7	0.7	4.5	0.8	6.7	2.9	26.9	25.6	7.5
Walcott_16	1287	174.0	20.6	51.5	197.0	44.8	4.1	896	70.9	130.8	13.7	50.0	9.9	1.0	9.8	1.4	9.5	1.6	6.0	0.9	6.2	0.8	7.1	2.7	24.9	26.3	7.5
Walcott_17	1305	176.7	20.0	51.3	203.0	46.8	3.8	879	71.6	134.0	14.6	49.5	10.4	1.0	9.6	1.5	9.0	1.8	6.2	0.8	5.5	0.9	6.5	3.0	27.8	27.8	7.8
Walcott_18	1292	175.8	19.7	51.6	202.0	44.9	4.3	861	67.7	132.7	14.3	50.2	10.4	1.0	8.3	1.3	8.9	1.7	5.7	0.9	6.0	0.9	7.0	2.9	25.5	25.6	7.4
Walcott_19	1303	184.4	19.9	51.8	206.0	43.6	4.3	891	69.0	131.6	14.1	53.8	8.5	1.1	7.0	1.5	9.5	2.1	6.2	0.6	6.0	0.9	7.4	3.3	25.1	26.3	7.4
Walcott_20	1375	182.6	21.0	52.6	209.0	45.4	4.0	910	71.2	138.4	15.2	54.2	10.9	1.0	10.5	1.7	9.8	2.2	5.9	1.0	4.7	0.8	6.7	2.7	25.0	25.7	7.6
Walcott_21																											
Walcott_22	1304	187.9	20.2	53.0	200.2	46.4	4.2	901	69.4	136.3	13.6	52.5	8.3	1.1	8.8	1.5	9.5	2.0	5.1	0.7	6.4	0.7	7.1	2.8	26.3	26.6	8.1
Walcott_23	1315	185.7	20.7	52.5	199.0	45.5	4.7	902	70.0	136.6	14.1	49.9	9.7	0.9	8.3	1.6	9.3	1.9	5.0	0.8	5.6	0.9	7.3	3.1	28.4	27.1	7.8
Walcott_24	1280	185.2	19.7	53.3	203.0	43.9	4.0	906	70.9	132.1	13.9	49.2	9.6	1.2	8.2	1.6	10.3	1.7	5.2	0.9	6.5	0.9	7.9	3.1	25.7	26.3	7.4
Average	1308	180.3	20.3	51.8	196.6	44.9	4.1	882	69.2	133.7	14.3	51.3	9.8	1.0	8.9	1.5	9.4	2.0	5.5	0.8	5.4	0.8	6.9	2.9	26.1	25.9	7.8
StDev	65	4.3	0.6	1.2	7.9	1.0	0.2	30	1.9	2.2	0.5	2.3	0.8	0.2	1.0	0.1	0.7	0.2	0.5	0.1	0.6	0.1	0.5	0.2	0.9	0.9	0.3
UA 1126	205	61.7	148.5	14.4	31.1	12.7	3.0	1695	8.8	18.8	1.9	9.7	2.3	0.5	2.1	0.5	2.7	0.4	1.4	0.2	1.6	0.2	1.4	1.1	12.6	2.1	2.7
UA 1126_1	285	61.8	180.0	15.2	29.8	12.5	3.2	1748	8.8	19.0	2.2	10.6	2.7	0.4	2.1	0.4	2.7	0.4	1.3	0.3	0.9	0.2	1.2	1.5	16.4	2.1	3.1
UA 1126_2	203	67.5	144.6	15.6	31.4	13.1	3.0	1876	9.0	19.9	2.3	9.9	1.9	0.6	1.8	0.4	2.1	0.5	1.3	0.2	1.2	0.2	1.4	1.1	15.5	2.2	2.8
UA 1126_3	237	66.1	150.0	15.0	24.9	12.6	3.1	1856	9.7	20.3	2.7	9.9	2.1	0.4	1.6	0.3	2.1	0.3	1.2	0.1	1.5	0.1	1.6	1.5	13.3	2.2	3.1
UA 1126_4	218	60.4	159.2	14.9	28.6	13.6	2.6	1749	9.2	19.9	2.7	7.7	2.2	0.4	2.0	0.4	2.7	0.3	1.6	0.2	1.6	0.1	1.5	1.2	15.7	2.2	2.8

UA 1126_5	780	63.2	161.7	14.8	33.4	14.2	3.2	1800	9.7	19.0	2.2	9.6	2.8	0.4	1.7	0.3	1.9	0.4	1.4	0.2	1.7	0.2	1.5	1.3	11.3	2.4	3.0
UA 1126_6	323	66.6	159.0	15.5	24.1	12.7	2.9	1830	10.1	20.6	3.1	12.0	1.6	0.5	2.2	0.5	1.6	0.5	1.4	0.3	1.4	0.2	2.0	1.5	17.5	2.2	2.7
UA 1126_7	370	65.2	169.3	15.6	27.4	14.6	3.0	1940	9.5	19.9	2.4	11.9	2.0	0.6	3.0	0.5	2.9	0.5	1.5	0.2	1.4	0.2	1.9	1.2	15.9	2.0	2.7
UA 1126_8	224	71.6	196.0	14.3	23.9	13.7	2.5	1756	8.4	18.3	2.3	7.6	2.1	0.6	2.1	0.3	2.1	0.4	1.4	0.3	1.9	0.3	1.3	1.3	16.2	2.1	2.8
UA 1126_9	224	61.3	156.9	14.5	22.6	12.5	2.5	1704	8.5	19.4	2.7	7.9	1.6	0.4	1.6	0.4	2.6	0.6	1.1	0.2	1.6	0.2	1.4	1.3	13.0	2.2	2.8
UA 1126_10	224	65.6	162.8	15.3	28.2	12.8	2.9	1840	9.9	19.7	2.5	10.3	2.4	0.6	2.2	0.3	2.2	0.5	1.0	0.4	1.3	0.3	1.1	1.2	15.6	2.1	2.8
UA 1126_11	230	67.3	162.3	14.1	26.3	13.3	2.8	1840	9.0	20.7	2.4	11.1	3.5	0.7	2.4	0.4	2.1	0.6	0.6	0.2	1.1	0.1	1.6	1.3	14.4	2.1	2.8
UA 1126_12	670	61.7	142.8	14.2	27.9	13.6	2.4	1656	8.8	19.3	2.5	8.6	1.4	0.4	2.5	0.4	2.0	0.5	1.5	0.3	1.2	0.1	1.2	1.3	15.5	2.1	2.6
UA 1126_13	253	66.5	163.0	15.7	26.2	14.1	3.0	1790	9.3	20.2	2.6	11.0	1.6	0.6	2.1	0.5	2.2	0.5	1.2	0.2	1.7	0.2	1.1	1.4	17.2	2.3	2.6
UA 1126_14	260	70.1	173.0	18.1	30.0	11.7	2.9	1770	12.2	20.0	4.2	12.6	2.3	0.9	3.5	0.3	2.6	0.3	1.0	0.2	0.3	0.3	0.1	1.5	16.9	2.2	3.5
UA 1126_15	251	52.6	258.0	12.3	28.2	12.2	2.6	2190	7.1	15.0	1.8	7.2	1.8	0.6	1.8	0.2	2.3	0.3	1.3	0.1	1.5	0.1	1.4	1.1	14.6	1.7	3.0
UA 1126_16	273	58.6	151.9	14.0	23.4	12.0	2.7	1647	7.9	18.8	2.2	9.4	1.8	0.4	1.8	0.4	1.9	0.5	1.1	0.2	1.5	0.2	2.1	1.3	13.5	2.2	2.5
UA 1126_17	231	63.9	155.7	14.9	22.7	13.6	2.7	1773	9.5	19.0	2.1	9.5	2.1	0.4	2.0	0.3	3.2	0.5	1.0	0.2	1.5	0.2	1.7	1.3	13.2	2.0	3.1
UA 1126_18	4000	67.3	210.0	16.4	31.0	14.0	3.9	1460	8.5	15.7	2.0	9.3	3.1	0.4	1.5	0.4	1.8	0.6	2.1	0.2	2.4	0.1	1.6	1.2	24.4	2.0	2.1
UA 1126_19	326	71.7	168.0	15.3	16.0	13.4	2.6	1840	11.3	22.0	2.5	12.7	2.9	0.5	1.5	0.6	0.7	0.4	1.5	0.1	1.2	0.3	1.9	1.9	17.7	1.6	2.6
UA 1126_20	291	45.4	651.0	10.5	32.0	9.2	1.8	2690	8.1	18.2	2.4	6.5	2.1	1.4	1.7	0.5	1.4	0.2	1.8	0.1	1.8	0.1	1.5	1.3	16.6	2.1	1.7
UA 1126_21	480	61.9	172.3	14.2	25.1	11.9	2.9	1780	9.8	19.6	2.6	8.6	2.7	0.5	3.0	0.5	3.1	0.6	1.2	0.1	1.3	0.1	1.4	1.3	15.4	2.1	3.0
UA 1126_22	219	61.9	161.4	13.4	21.5	13.4	2.8	1819	9.1	18.1	2.1	8.0	1.6	0.5	1.7	0.3	1.9	0.5	1.2	0.2	1.5	0.2	1.6	1.2	15.5	2.2	2.5
UA 1126_23	400	65.4	163.0	15.3	25.4	14.7	3.7	1870	15.0	21.9	2.7	10.2	1.5	0.5	1.5	0.5	2.7	0.7	1.2	0.1	1.9	0.2	1.6	1.8	20.2	2.7	2.8
Average	466	63.6	188.4	14.7	26.7	13.0	2.9	1830	9.5	19.3	2.5	9.7	2.2	0.6	2.1	0.4	2.2	0.4	1.3	0.2	1.4	0.2	1.5	1.3	15.8	2.1	2.8
StDev	767	5.7	101.5	1.4	4.0	1.2	0.4	224	1.6	1.6	0.5	1.7	0.5	0.2	0.5	0.1	0.6	0.1	0.3	0.1	0.4	0.1	0.4	0.2	2.7	0.2	0.4
UA 1609	229	59.3	148.4	14.4	26.7	13.0	2.9	1765	8.4	18.6	2.7	8.0	2.7	0.4	2.9	0.3	2.5	0.5	1.4	0.2	1.5	0.2	1.6	1.2	15.2	2.0	3.2
UA 1609_1	241	60.2	178.0	14.0	23.4	12.0	2.8	1800	8.2	18.4	2.3	9.5	2.3	0.4	2.5	0.3	1.8	0.4	2.0	0.2	1.2	0.2	2.2	1.2	16.1	2.0	2.7
UA 1609_2	255	60.2	204.0	14.7	20.3	13.9	2.8	1946	9.3	20.6	2.6	9.9	2.3	0.7	1.8	0.4	3.0	0.4	1.0	0.2	2.1	0.2	1.8	1.6	16.1	2.1	2.6
UA 1609_3	221	59.4	151.0	14.4	24.7	12.8	2.5	1902	8.6	21.2	2.4	9.2	2.1	0.3	2.9	0.4	2.7	0.4	1.1	0.1	1.6	0.2	1.5	1.3	13.6	1.9	2.7
UA 1609_4	220	58.2	187.0	13.8	21.0	13.5	2.4	1625	7.9	17.6	2.2	8.6	2.2	0.5	1.1	0.4	2.3	0.4	1.1	0.2	1.5	0.3	1.4	1.3	16.3	2.2	2.9
UA 1609_6	247	31.1	201.0	14.0	16.7	14.5	3.3	2060	10.0	20.5	2.7	8.7	3.0	0.2	2.8	0.4	3.3	0.7	1.0	0.1	1.8	0.2	1.1	1.2	10.2	2.0	3.5
UA 1609_7	343	53.1	187.0	12.8	25.0	12.5	2.8	1890	8.4	18.4	2.3	10.6	2.7	0.3	1.4	0.2	0.4	0.4	0.7	0.4	1.2	0.2	0.9	0.9	15.9	1.8	2.7
UA 1609_8	230	51.8	158.0	14.3	24.3	12.7	2.6	1760	9.1	19.5	2.3	9.3	2.7	0.6	1.8	0.3	2.8	0.4	1.6	0.2	1.2	0.3	1.6	1.3	11.7	2.0	3.1
UA 1609_9	630	70.4	118.2	15.2	27.0	13.5	3.4	1409	8.4	18.4	2.3	8.4	2.2	0.1	0.8	0.3	2.8	0.5	2.0	0.3	0.8	0.4	1.9	1.2	6.5	2.0	2.9
UA 1609_12	540	70.0	160.6	15.4	44.0	12.2	3.0	1790	10.2	20.5	2.7	7.7	2.6	0.8	2.4	0.4	2.5	0.4	0.7	0.0	2.1	0.2	0.8	1.5	15.2	2.5	2.5
UA 1609_13	223	62.6	158.0	15.5	25.4	14.0	3.0	1863	9.2	19.6	2.6	10.6	2.2	0.3	3.3	0.4	1.8	0.5	1.6	0.2	1.8	0.2	1.0	1.3	15.9	2.2	3.1
UA 1609_15	202	60.9	161.7	14.1	24.9	13.6	3.0	1889	8.7	18.3	2.5	10.1	2.2	0.3	2.3	0.3	2.0	0.5	1.2	0.2	1.7	0.1	1.6	1.3	13.4	1.5	2.8
UA 1609_17	238	61.3	156.3	13.8	23.4	13.1	2.9	1725	8.4	19.3	2.2	8.7	2.4	0.4	1.5	0.5	2.0	0.4	1.1	0.2	1.1	0.3	1.7	1.3	14.8	2.4	2.8
UA 1609_18	218	61.1	156.8	13.6	22.0	13.3	2.8	1870	8.7	19.6	2.3	9.4	1.9	0.5	2.0	0.3	2.5	0.6	1.6	0.2	1.0	0.2	1.6	1.5	13.5	2.1	3.0
UA 1609_19	200	61.6	166.0	15.6	26.1	12.2	2.3	1830	8.2	18.3	2.8	10.7	1.0	0.4	1.8	0.3	2.2	0.4	1.6	0.2	1.4	0.4	1.6	1.2	13.1	1.9	2.8
UA 1609_20	223	60.0	159.1	15.2	30.9	12.9	3.1	1880	8.2	18.7	2.3	8.4	1.9	0.5	1.8	0.4	2.3	0.5	1.2	0.2	1.9	0.2	1.7	1.4	15.2	1.9	2.5
UA 1609_21	315	61.9	155.0	14.3	21.5	13.0	3.2	1759	8.7	18.2	1.9	6.6	2.6	0.1	1.9	0.3	1.9	0.5	1.7	0.2	1.0	0.2	1.0	1.3	13.8	1.8	3.0
Average	308	56.0	161.5	13.7	24.0	12.4	2.7	1721	8.3	18.2	2.3	8.7	2.2	0.4	2.0	0.3	2.2	0.4	1.3	0.2	1.4	0.2	1.4	1.2	13.3	1.9	2.7

StDev	164	15.0	25.2	3.2	7.5	2.9	0.6	398	1.8	4.3	0.5	2.1	0.6	0.2	0.8	0.1	0.7	0.1	0.5	0.1	0.5	0.1	0.5	0.3	3.6	0.5		0.6
PAL tephra																												
UA 1305	1430	109.7	106.9	37.9	275.0	7.9	2.5	1149	29.0	58.0	6.7	28.0	4.1	0.7	4.6	0.9	6.7	1.4	4.0	0.6	1.7	0.5	6.5	0.7	11.4	9.2		2.9
UA 1305_1	2010	126.0	152.0	30.9	295.0	9.7	2.5	1180	24.6	54.3	6.0	28.0	7.3	0.7	2.9	1.3	4.2	1.3	2.9	0.7	3.9	0.5	10.4	0.9	13.7	9.8		3.2
UA 1305_2	2180	108.4	152.7	33.4	337.0	10.4	2.7	1115	26.6	55.4	6.4	28.0	5.1	0.7	4.6	0.9	6.9	1.0	4.5	0.4	3.1	0.6	8.4	0.5	13.6	8.4		2.7
UA 1305_3	2220	111.7	168.0	31.7	309.0	8.9	2.8	1196	25.9	58.0	6.7	30.5	4.6	0.9	7.6	1.3	7.4	1.4	4.3	0.8	4.1	0.8	8.3	0.7	12.8	10.0		2.6
UA 1305_5	2482	101.0	157.1	34.3	333.0	9.6	2.7	1090	25.6	57.0	6.5	30.4	6.4	0.9	6.0	0.8	5.5	1.3	2.7	0.4	4.9	0.6	7.8	0.7	13.8	8.5		3.5
UA 1305_6	2345	102.9	146.9	34.0	315.0	9.5	2.3	1125	25.0	51.9	6.6	27.4	5.0	1.1	6.2	1.0	5.4	1.0	3.8	0.5	3.2	0.6	9.7	0.9	12.6	8.6		3.4
UA 1305_7	2277	110.5	150.4	31.7	321.0	10.0	2.4	1161	25.1	55.0	7.0	26.8	6.8	1.1	5.0	0.9	6.1	1.2	3.4	0.5	3.9	0.7	8.0	0.7	13.6	9.6		3.3
UA 1305_8	1810	111.6	132.0	27.2	232.0	8.6	3.0	1090	21.3	47.5	6.0	23.4	5.6	0.7	3.3	0.6	3.6	0.8	2.8	0.2	2.9	0.4	6.1	0.5	13.8	8.0		2.9
UA 1305_9	2170	106.5	162.7	34.3	328.0	9.8	3.0	1147	26.1	57.4	6.6	29.5	6.3	0.9	6.9	1.0	6.4	1.0	2.5	0.8	3.2	0.6	9.5	0.3	14.3	8.5		3.3
UA 1305_12	2030	102.7	152.4	33.9	264.0	9.4	2.4	1157	24.6	53.3	6.3	28.2	6.5	0.8	5.6	0.9	5.4	1.1	3.1	0.7	4.1	0.5	7.5	0.7	13.6	8.6		3.0
UA 1305_14	2250	102.3	157.1	31.7	315.0	10.1	2.7	1125	23.9	53.2	6.5	26.9	5.1	0.9	4.9	0.8	5.5	1.0	3.4	0.5	3.6	0.6	7.4	0.5	13.6	8.3		3.1
UA 1305_15	2020	100.9	157.0	29.5	260.0	8.2	2.6	1084	23.1	48.4	5.7	25.6	7.1	1.3	4.0	0.8	5.8	0.9	3.5	0.4	3.1	0.6	6.2	0.4	11.7	8.2		2.8
UA 1305_16	2070	102.5	157.3	30.6	284.0	10.4	2.6	1209	25.0	55.1	6.7	29.4	3.4	1.0	5.4	0.8	5.8	0.8	4.3	0.8	3.1	0.5	6.6	0.8	13.5	9.0		3.4
UA 1305_17	1974	105.3	147.2	27.2	214.0	8.6	2.8	1072	21.8	47.0	5.9	22.7	4.3	0.9	5.1	0.7	4.6	0.9	2.6	0.5	3.2	0.4	6.7	0.6	12.5	8.5		3.1
UA 1305_18	2060	107.4	168.3	27.5	232.0	9.3	2.5	1162	22.6	47.9	5.8	23.1	4.4	0.8	4.8	0.9	4.6	1.0	3.0	0.4	2.4	0.5	7.7	0.5	12.2	7.7		2.4
UA 1305_19	2210	104.5	157.9	30.0	265.0	8.6	2.9	1118	22.4	50.1	6.4	22.3	4.8	0.6	4.9	0.7	5.3	0.8	2.8	0.5	3.7	0.4	6.3	0.6	14.8	8.6		3.1
UA 1305_20	2200	110.1	183.0	32.6	301.0	9.8	2.1	1182	24.9	54.0	6.6	27.0	7.6	1.1	4.8	0.8	5.8	1.0	3.8	0.5	3.8	0.6	7.9	0.6	13.6	9.1		3.2
UA 1305_21	1942	99.2	141.3	26.8	252.0	9.4	2.6	1133	23.2	49.4	6.0	23.8	5.7	0.8	5.4	0.6	5.5	0.8	2.8	0.3	3.5	0.5	5.4	0.5	13.5	8.0		2.6
UA 1305_22	1908	104.6	143.2	26.5	249.0	9.3	2.6	1128	25.2	50.6	6.0	23.8	3.7	0.9	4.5	0.6	4.2	0.8	3.4	0.5	3.1	0.5	7.3	0.5	16.2	8.0		3.0
UA 1305_23	2520	116.0	171.4	34.7	350.0	10.4	3.0	1180	25.7	54.6	7.4	30.5	5.3	0.5	7.0	0.9	6.7	0.9	3.4	0.5	3.9	0.8	9.3	0.6	14.1	8.2		2.7
UA 1305_24	2503	102.4	167.0	30.3	316.0	9.3	2.6	1099	24.4	53.2	6.8	25.9	6.5	1.2	3.9	0.8	5.0	1.3	3.8	0.4	3.9	0.7	8.7	1.1	12.3	8.9		2.9
UA 1305_25	1854	107.3	143.3	29.0	239.0	8.6	2.6	1076	22.7	49.3	5.8	25.4	3.8	0.7	5.5	0.8	5.0	1.0	3.7	0.4	2.9	0.5	7.2	0.5	14.2	8.6		3.2
UA 1305_26	2190	110.9	143.7	33.6	326.0	10.1	2.8	1135	25.0	53.8	7.1	27.4	4.9	0.7	6.0	1.0	6.0	1.4	3.6	0.4	4.0	0.6	9.7	0.8	14.7	9.0		2.9
UA 1305_27	2104	107.1	146.0	31.6	310.0	8.9	2.5	1106	24.6	53.2	6.3	23.3	7.6	1.4	6.5	0.7	5.3	1.3	3.7	0.6	4.3	0.6	9.1	0.6	13.8	8.2		3.2
UA 1305_28	1940	107.5	146.7	30.0	241.0	9.6	2.8	1110	23.1	48.7	5.7	22.3	4.4	0.6	3.9	0.7	4.1	0.8	2.8	0.6	3.0	0.5	7.3	0.6	13.6	8.3		2.9
UA 1305_29	2035	134.7	74.5	13.1	105.7	8.4	2.3	1133	18.3	36.5	4.0	13.5	2.3	0.3	1.6	0.4	2.8	0.4	1.2	0.2	1.8	0.2	3.7	0.5	11.6	8.4		4.1
Average	2105	108.2	149.5	30.5	279.6	9.3	2.6	1133	24.2	52.0	6.3	25.9	5.3	0.8	5.0	0.8	5.4	1.0	3.3	0.5	3.4	0.5	7.6	0.6	13.4	8.6		3.0
StDev	235	7.8	21.0	4.6	52.3	0.7	0.2	38	2.0	4.6	0.7	3.7	1.4	0.2	1.3	0.2	1.1	0.2	0.7	0.2	0.7	0.1	1.5	0.2	1.1	0.6		0.3

NIST610	451	428	503	458	426	477	370	469	440	451	453	415	428	446	446	432	425	438	450	448	469	443	437	448	418	446	456
NIST610_1	452	423	521	464	436	457	356	448	441	454	447	440	463	448	454	446	454	464	452	436	437	427	433	445	430	461	468
NIST610_2	494	427	510	461	462	446	368	444	443	452	450	419	465	447	449	430	446	446	446	425	435	450	438	446	437	452	460
NIST610_3	510	426	518	468	456	487	400	480	472	466	454	456	460	456	452	446	449	462	463	448	474	467	468	452	443	459	462

NIST610_4	434	425	515	461	461	468	365	435	417	452	447	416	430	446	448	435	421	437	436	428	439	409	407	444	408	457	461
NIST610_5	369	421	513	457	452	450	358	430	424	451	444	427	439	444	446	437	439	448	456	427	444	418	411	442	425	457	461
NIST610_6	506	427	519	471	432	479	395	480	483	457	452	466	496	455	452	437	451	448	462	449	471	474	471	450	483	460	463
NIST610_7	420	425	516	464	452	447	360	447	430	452	447	427	475	447	453	439	446	446	466	423	420	422	428	445	415	458	464
NIST610_8	408	426	514	460	449	461	358	446	427	454	449	428	440	447	446	435	431	449	456	426	449	415	428	447	413	457	458
NIST610_9	427	420	513	459	438	458	352	441	409	448	444	410	438	444	452	436	441	444	454	437	433	409	415	443	405	455	457
NIST610_10	484	430	519	471	452	473	394	484	473	457	453	479	489	452	445	439	441	450	466	433	461	466	472	451	466	462	465
NIST610_11	468	428	516	462	432	456	369	445	443	452	448	430	453	449	450	438	430	444	444	427	423	426	426	446	416	458	465
NIST610_12	458	424	515	462	497	488	364	441	437	454	447	428	442	445	449	436	450	475	488	452	483	447	429	446	415	456	457
NIST610_13	451	426	515	464	479	483	383	463	469	453	448	437	464	447	442	438	445	451	447	440	456	450	443	446	440	458	463
NIST610_14	503	425	516	460	445	468	380	456	482	453	448	430	471	447	456	436	451	466	461	440	481	473	440	445	448	457	459
NIST610_15	436	425	515	465	429	441	338	417	397	453	446	427	431	446	447	436	421	435	437	410	424	401	414	446	402	457	464
NIST610_16	384	426	516	461	447	473	366	463	417	453	450	418	439	447	451	438	428	442	460	453	461	428	433	447	397	458	460
NIST610_17	479	425	514	463	436	452	373	456	441	453	448	434	461	449	446	434	444	451	453	435	444	441	436	446	430	457	462
NIST610_18	490	427	517	460	433	474	380	470	440	453	448	439	471	446	451	440	439	442	444	438	448	445	449	446	443	457	462
Average	454	425	515	463	448	465	370	453	441	454	449	433	456	448	449	437	440	449	455	436	450	437	436	446	428	457	461
StDev	41	2	4	4	18	14	16	18	25	4	3	18	20	3	4	4	11	11	12	11	20	23	19	2	22	3	3

NIST612	37	28.4	80.2	38.3	50.2	39.7	41.7	44	36.0	39.1	34.6	32.0	36.2	34.2	32.1	36.5	34.6	40.2	41.9	41.5	36.5	40.4	40.5	37.8	41.4	36.7	35.3
NIST612_1	63	29.7	80.0	34.9	40.0	38.2	43.5	47	37.0	39.8	37.4	36.2	36.2	32.2	32.0	35.3	31.1	41.1	35.5	37.0	41.5	40.9	41.0	37.6	41.9	39.8	36.5
NIST612_2	34	28.9	77.0	36.6	47.3	36.3	42.5	41	35.5	37.0	32.4	34.6	38.5	33.6	36.2	38.1	33.5	38.5	39.4	40.1	39.9	35.7	37.5	32.7	38.8	38.0	35.9
NIST612_3	32	34.1	96.8	44.0	49.7	37.5	41.6	39	35.4	44.1	44.0	38.9	41.9	41.6	39.1	41.6	38.1	39.5	37.0	36.6	37.9	37.5	37.4	45.2	38.2	43.4	40.6
NIST612_4	38	34.7	90.0	40.6	43.0	38.5	44.5	42	36.2	51.8	47.9	42.3	37.4	38.5	45.0	41.0	32.1	39.9	38.1	38.2	42.8	38.6	35.8	49.3	40.1	42.6	39.3
NIST612_3	32	34.1	96.8	44.0	49.7	37.5	41.6	39	35.4	44.1	44.0	38.9	41.9	41.6	39.1	41.6	38.1	39.5	37.0	36.6	37.9	37.5	37.4	45.2	38.2	43.4	40.6
NIST612_4	38	34.7	90.0	40.6	43.0	38.5	44.5	42	36.2	51.8	47.9	42.3	37.4	38.5	45.0	41.0	32.1	39.9	38.1	38.2	42.8	38.6	35.8	49.3	40.1	42.6	39.3
NIST612_5	65	26.9	72.3	39.8	50.0	37.7	43.1	41	37.9	35.0	34.7	38.1	42.4	34.5	42.4	38.5	39.6	39.7	40.0	37.1	38.9	39.2	40.5	32.1	41.3	36.8	37.1
NIST612_6	44	25.9	65.0	35.3	37.0	40.6	45.5	40	41.7	33.3	33.3	34.4	50.5	36.1	34.2	36.6	37.7	39.3	37.7	39.4	42.8	40.3	42.3	31.2	41.0	34.4	32.2
NIST612_7	27	34.0	87.1	47.1	38.0	40.2	45.5	43	37.9	42.3	40.8	37.3	43.3	36.5	40.8	40.8	41.2	41.3	37.7	40.4	45.3	39.5	41.9	44.6	40.1	43.4	41.0
NIST612_8	31	37.0	98.1	47.2	41.0	41.2	42.9	44	37.8	45.0	43.1	36.4	34.8	37.7	44.7	40.8	40.1	41.5	42.0	40.6	39.1	38.1	42.3	44.9	38.1	44.1	43.4
NIST612_9	26	28.9	75.9	40.8	52.0	38.1	43.3	42	37.1	33.8	33.8	40.3	40.7	36.3	42.3	40.0	43.5	40.0	41.2	38.8	40.7	37.4	36.2	32.9	39.0	35.5	36.5
NIST612_10	27	29.9	71.9	38.2	52.0	39.6	44.9	51	40.2	36.5	32.9	38.1	48.2	34.0	41.7	38.9	38.0	41.2	44.6	37.8	47.3	40.6	39.3	33.2	43.3	35.5	36.1
NIST612_11	17	38.7	84.4	42.4	42.0	38.6	42.4	35	37.2	41.2	41.6	38.7	36.3	35.6	39.0	38.6	36.5	38.5	37.4	35.3	36.5	36.1	36.3	38.5	43.3	41.7	40.1
NIST612_12	68	37.3	79.2	38.1	29.0	35.7	39.8	41	36.8	38.7	41.1	35.7	36.6	36.1	45.5	36.9	39.2	39.8	38.2	36.9	39.8	35.7	33.3	38.8	37.6	39.0	41.3
NIST612_13	31	24.9	67.9	33.6	44.0	38.4	38.3	37	34.5	33.1	32.7	28.5	28.9	29.5	31.7	33.5	33.3	35.3	39.3	38.3	41.6	36.5	30.8	34.2	36.3	33.0	33.1
NIST612_14	37	28.7	70.5	37.9	38.0	34.9	41.7	37	39.1	34.6	34.4	34.6	33.2	32.0	32.3	36.8	34.5	37.6	37.6	37.8	37.0	40.1	41.1	38.5	39.5	37.0	35.6
NIST612_15	30	30.8	81.4	39.8	31.2	40.0	40.5	40	36.3	43.5	52.2	36.3	36.6	40.5	38.1	42.1	38.8	41.6	41.0	40.0	42.6	39.1	42.3	48.4	41.7	45.2	39.1
NIST612_16	38	38.3	89.4	40.1	41.8	43.1	48.1	47	41.5	50.9	59.3	46.6	41.0	45.2	40.6	43.2	37.2	40.9	39.6	42.6	39.5	39.6	46.8	52.6	47.0	49.0	39.4
NIST612_17	31	30.5	79.0	38.9	33.0	37.7	42.7	43	38.7	39.6	39.1	37.1	40.9	34.7	46.8	38.2	31.2	37.8	37.5	37.1	38.9	38.5	43.3	38.1	41.3	36.0	36.4
NIST612_18	19	30.2	71.1	36.9	49.0	38.6	42.3	45	36.0	36.1	36.1	33.5	36.7	31.3	35.2	35.5	36.2	36.4	39.0	39.4	42.4	38.4	36.5	37.6	35.9	34.8	36.1

Average	36	31.7	81.1	39.8	42.9	38.6	42.9	42	37.4	40.5	40.2	37.2	39.0	36.2	39.2	38.8	36.5	39.5	39.0	38.6	40.6	38.5	39.0	40.1	40.2	39.6	37.9
StDev	14	4.1	9.8	3.6	6.9	1.9	2.2	4	2.0	5.9	7.2	3.9	4.9	3.8	4.9	2.6	3.5	1.7	2.1	1.8	2.8	1.6	3.8	6.5	2.6	4.3	2.9

Walcott	1190	134.7	21.3	43.0	182.0	47.3	4.2	909	71	119.0	11.8	52.1	7.5	1.2	5.2	1.3	10.5	1.6	7.2	0.8	6.6	1.0	6.5	2.4	22.9	23.1	7.6
Walcott_1	1100	152.1	19.8	49.3	210.0	46.4	4.2	896	70	118.1	11.1	54.3	9.4	0.9	6.9	1.3	8.6	1.6	5.0	0.6	3.2	0.8	6.1	2.2	27.8	24.6	7.4
Walcott_2	1213	156.0	21.3	48.7	211.0	47.3	4.9	930	74	132.0	13.0	52.6	9.6	0.9	6.7	1.2	12.9	2.3	6.9	0.4	5.5	0.6	8.4	2.6	29.4	25.1	7.4
Walcott_3	1130	223.0	25.4	60.1	194.0	47.5	2.9	899	68	195.0	19.0	57.1	9.3	0.8	7.9	2.2	9.2	1.7	5.4	0.6	7.0	0.6	4.8	3.9	31.2	33.0	9.6
Walcott_4	1163	205.0	26.1	62.3	183.0	45.2	4.0	839	62	194.0	18.4	48.9	10.2	0.9	10.0	1.6	10.5	1.9	6.5	0.9	5.2	0.8	6.4	4.3	27.5	29.1	8.7
Walcott_5	1150	141.0	15.6	43.2	195.0	49.0	4.9	825	66	97.0	8.8	46.6	8.0	0.5	8.2	1.3	6.8	1.3	4.5	1.0	5.0	0.8	6.7	2.4	27.2	17.2	6.5
Walcott_6	1049	139.0	21.0	49.4	210.0	48.5	5.4	854	63	91.4	9.8	49.9	9.2	0.6	6.6	1.2	11.5	2.2	5.8	0.7	4.2	0.4	6.2	1.9	31.2	19.6	6.2
Walcott_7	1180	221.0	32.6	63.2	241.0	46.9	5.1	928	76	148.1	16.5	53.9	11.1	1.4	12.8	2.2	7.3	2.1	5.1	0.9	5.6	0.9	7.0	3.1	30.2	30.4	9.7
Walcott_8	1160	234.0	29.0	60.1	187.0	47.8	3.8	944	74	166.0	15.1	62.0	7.4	1.3	11.1	1.9	8.2	1.9	5.1	0.7	6.2	0.8	6.4	4.6	30.7	35.8	9.3
Walcott_9	1130	137.7	13.9	43.0	200.0	49.9	4.8	825	65	99.0	9.5	47.1	10.6	1.1	9.5	1.2	6.4	1.7	4.3	1.1	7.3	0.8	6.2	2.1	24.4	17.8	6.6
Walcott_10	1120	133.0	13.8	44.2	199.0	49.5	3.1	810	65	97.0	10.7	44.3	8.1	0.8	8.5	2.1	11.9	1.8	4.6	0.9	4.8	0.5	7.4	1.8	25.0	18.2	6.5
Walcott_11	1090	199.0	19.6	49.4	204.0	50.0	3.9	820	67	126.0	15.7	46.3	8.8	0.9	10.3	1.4	8.0	1.8	4.2	0.4	5.0	0.8	6.1	3.2	24.6	24.8	8.2
Walcott_12																											
Walcott_13	1320	183.0	19.3	55.5	212.0	52.0	4.8	957	74	132.4	15.2	47.7	11.2	0.9	7.3	1.6	8.6	2.2	4.5	0.8	4.7	0.5	8.3	3.6	30.0	27.4	8.3
Walcott_14	1320	178.5	15.5	52.8	213.0	51.7	4.5	914	77	134.0	14.0	51.2	12.1	0.7	5.6	1.5	10.2	2.1	6.3	0.8	4.3	0.6	6.9	3.5	24.2	25.8	8.7
Walcott_15	1150	173.0	22.8	56.0	227.0	46.3	6.1	870	61	125.0	12.1	47.0	5.9	1.0	11.3	1.8	8.1	2.0	6.8	0.8	2.5	0.7	8.8	2.3	30.2	28.1	7.8
Walcott_16	1570	216.0	26.6	71.0	244.0	61.0	5.3	1370	106	219.0	20.5	79.0	18.0	1.2	21.0	2.8	15.0	3.8	11.7	1.2	6.7	1.2	13.4	4.3	38.3	41.0	11.3
Walcott_17	1220	189.0	16.3	50.3	181.0	43.8	3.5	893	63	133.0	15.0	50.2	10.3	0.5	7.5	1.2	7.1	1.8	4.4	0.4	5.1	0.5	7.6	3.2	26.2	24.0	8.3
Average	1191	177.4	21.2	53.0	205.5	48.8	4.4	911	71	136.8	13.9	52.4	9.8	0.9	9.2	1.6	9.5	2.0	5.8	0.8	5.2	0.7	7.2	3.0	28.3	26.2	8.1
StDev	121	34.8	5.4	8.2	18.9	3.8	0.9	127	10	37.1	3.5	8.2	2.6	0.3	3.7	0.5	2.4	0.5	1.8	0.2	1.3	0.2	1.9	0.9	3.8	6.5	1.4

ATHO_G	1353	47.9	74.7	71	444.0	53.1	1.1	468	48.4	91.5	10.2	55.1	10.5	2.1	13.2	1.8	13.4	2.9	8.3	1.4	8.9	0.8	11.3	2.4	5.1	5.8	2.1
ATHO_G_1	1380	47.0	74.8	72	466.0	56.0	1.2	537	53.8	95.1	10.4	54.3	10.1	2.1	10.9	2.4	14.8	2.7	8.3	1.0	10.2	1.2	12.2	2.9	5.2	5.3	1.7
ATHO_G_2	1370	51.6	70.5	68	470.0	54.8	1.2	498	53.0	93.8	10.7	56.0	13.4	2.3	8.8	1.9	12.3	2.9	10.1	1.3	8.7	1.7	11.3	2.3	6.0	5.9	2.0
ATHO_G_3	1430	79.9	114.0	99	475.0	58.4	1.1	539	55.3	208.0	21.2	59.0	12.7	2.9	14.9	2.5	17.3	3.4	9.3	1.1	6.1	1.5	12.7	6.0	5.7	9.6	2.2
ATHO_G_4	1240	75.1	111.0	97	473.0	55.3	1.3	497	46.8	201.0	23.0	59.8	13.6	2.7	14.7	2.3	12.9	2.8	8.8	1.3	9.4	1.5	12.7	5.5	4.9	8.5	2.8
ATHO_G_5	1210	46.1	58.0	64	437.0	50.5	0.9	433	45.5	72.7	8.5	52.6	12.0	1.6	13.9	2.3	12.5	3.0	8.5	1.5	6.9	1.3	11.7	2.0	4.2	4.8	1.4
ATHO_G_6	1290	50.7	62.8	71	430.0	54.8	0.7	517	51.3	86.0	9.8	63.0	11.0	2.0	12.4	2.0	16.5	3.5	10.1	1.2	8.9	1.6	11.5	2.4	4.7	5.3	2.0
ATHO_G_7	1270	80.6	120.7	105	455.0	54.4	1.4	499	48.5	123.9	16.8	56.1	11.4	2.7	14.8	3.1	15.1	2.8	11.8	1.4	8.0	1.5	12.7	5.0	5.3	8.2	2.9
ATHO_G_8	1481	94.1	143.0	120	472.0	55.2	0.8	553	54.0	147.0	18.5	62.4	14.6	3.0	12.1	2.7	13.8	3.3	8.2	1.9	11.1	1.9	13.7	6.4	6.3	10.6	2.9
ATHO_G_9	1400	44.1	63.5	71	464.0	55.0	0.8	515	47.6	79.9	9.9	49.7	12.4	1.9	12.5	2.4	13.1	2.8	8.3	1.3	7.7	1.4	11.9	2.4	4.9	5.2	2.0
ATHO_G_10	1370	46.5	64.7	70	472.0	57.4	1.0	508	54.8	80.8	8.7	55.0	11.2	1.9	14.0	1.9	15.5	3.1	7.4	1.1	8.5	1.4	12.2	2.4	4.5	4.7	1.8
ATHO_G_11	1200	74.2	91.4	82	444.0	54.2	1.2	444	47.4	104.4	13.7	52.8	10.5	2.1	9.3	1.9	16.0	2.8	10.1	1.5	8.5	1.4	13.4	3.5	4.6	6.6	1.8
ATHO_G_12																											
ATHO_G_13	1410	54.1	79.0	77	466.0	54.3	1.2	502	54.0	106.1	13.4	47.2	12.6	2.1	13.9	2.6	12.4	2.9	9.4	1.0	9.0	1.6	12.8	2.9	4.9	6.3	2.5

ATHO_G_14	1300	55.8	73.8	76	406.0	53.4	1.3	458	48.7	98.6	12.9	51.5	14.4	1.6	11.4	1.7	11.6	2.8	9.2	1.5	8.8	1.2	12.2	3.0	6.1	7.0	2.2
ATHO_G_15	1266	64.7	88.8	85	454.0	55.7	1.2	515	50.0	116.6	12.9	53.4	14.9	3.3	13.5	2.0	14.2	3.5	10.2	1.6	8.9	1.5	12.5	2.8	5.1	6.5	2.4
ATHO_G_16	1410	60.7	88.0	81	418.0	58.2	1.0	561	52.0	118.0	15.1	58.0	15.2	2.5	14.8	2.1	17.5	2.9	10.2	2.1	10.4	1.3	13.8	3.4	4.5	6.6	2.1
ATHO_G_17	1390	67.9	98.1	84	449.0	54.7	0.9	570	54.5	119.8	14.2	60.3	15.1	2.2	13.0	2.9	13.4	2.8	9.5	1.4	10.3	1.7	11.8	3.5	5.7	6.8	2.4
Average	1339	61.2	86.9	82	452.6	55.0	1.1	507	50.9	114.3	13.5	55.7	12.7	2.3	12.8	2.3	14.3	3.0	9.3	1.4	8.8	1.4	12.4	3.5	5.2	6.7	2.2
StDev	82	15.1	23.7	15	20.5	1.9	0.2	39	3.2	38.8	4.3	4.4	1.7	0.5	1.9	0.4	1.8	0.3	1.1	0.3	1.3	0.2	0.8	1.4	0.6	1.7	0.4

UA1039_5	860	43.6	790.0	3.5	141.0	1.8	0.7	1117	18.0	20.2	2.0	8.4	-0.4	0.3	2.7	0.0	0.1	-0.1	0.5	0.0	-0.4	0.2	1.4	0.3	16.2	6.0		1.8
UA1039_7	1159	46.3	247.0	2.9	116.0	4.2	1.5	973	15.2	20.6	2.5	9.1	0.2	0.5	0.5	0.0	0.3	0.3	-0.3	-0.1	-0.2	0.1	1.5	0.2	12.6	5.1		1.9
UA1039_8	960	45.9	347.0	2.2	104.0	4.4	1.4	955	13.6	19.2	1.8	7.2	0.3	0.4	-0.6	0.1	0.0	-0.1	0.0	-0.1	0.5	0.1	3.2	0.1	10.5	4.2		2.0
UA1039_9	920	53.5	437.0	3.7	143.0	5.2	0.4	1010	16.2	20.3	2.3	8.6	2.2	0.2	2.6	0.1	0.3	0.1	0.3	0.0	-0.6	0.0	7.2	0.1	10.0	7.3		2.4
UA1039_11	920	48.9	424.0	4.5	117.0	2.8	0.9	920	15.1	18.5	1.9	8.4	0.7	0.5	2.6	0.1	0.4	0.1	0.6	0.6	1.9	-0.1	3.7	0.0	12.7	6.4		2.1
UA1039_25	970	70.6	587.0	5.0	88.0	4.8	1.5	910	12.6	42.5	3.3	7.6	2.3	0.1	-0.3	-0.2	0.8	-0.1	-0.3	0.0	-0.4	0.0	2.1	0.4	14.4	6.6		1.9
UA1039_27	1320	85.8	683.0	4.3	121.0	4.4	1.0	1290	18.5	45.0	2.9	10.1	2.0	0.2	0.1	0.5	1.7	0.0	0.3	-0.1	0.0	0.3	4.1	0.4	20.6	7.1		2.5
UA1039_28	1160	74.0	576.0	3.1	110.0	4.1	1.1	1000	13.2	30.4	3.0	6.9	2.8	0.6	-0.9	-0.1	0.1	-0.1	-0.3	-0.1	-0.5	0.1	2.9	0.1	12.4	7.5		2.1
UA1039_29	1060	68.6	287.0	5.4	111.0	3.9	0.9	863	14.1	29.0	2.2	14.6	1.2	0.6	-0.9	0.4	1.0	0.1	-0.2	0.2	1.8	0.0	3.5	0.4	17.0	6.2		2.2
Average	1037	59.7	486.4	3.8	116.8	4.0	1.0	1004	15.2	27.3	2.4	9.0	1.3	0.4	0.6	0.1	0.5	0.0	0.1	0.0	0.2	0.1	3.3	0.2	14.0	6.3		2.1
StDev	150	15.3	184.3	1.0	17.2	1.0	0.4	129	2.1	10.3	0.5	2.3	1.1	0.2	1.6	0.2	0.6	0.1	0.4	0.2	1.0	0.1	1.7	0.2	3.4	1.1		0.3

UA1582	1220	45.7	370	2	131	3.78	1.47	959	20.2	22.8	2.12	10.6	0.37	0.28	1.6	-0.1	0.34	0.15	-0	0.02	-0.5	0.05	4.1	0.15	15.7	5.2		1.25
UA1582_1	1140	39.9	347	2.53	127	5.81	1.3	946	19.5	21.5	2.23	8.6	0.6	0.34	0	0.05	0.61	0.13	0.8	0.1	0.5	0.08	4.2	0.17	14	4.6		1.2
UA1582_2	1560	43.2	345	2.14	137	5.88	1.06	970	21.9	28	2.6	13.5	0.49	0.38	0.7	0.07	1.11	0.12	0.05	0.18	0.83	0.05	4.6	0.19	14.9	4.64		1.33
UA1582_3	2210	44.5	539	3.9	173	4.9	0.07	1050	23.8	33	3.13	14.3	2.3	0.54	-0.1	0.14	0.74	0.13	0.1	0.04	-0.2	0.13	4.3	0.05	13.1	5		1.36
UA1582_4	1640	43	423	2.8	151	5.18	0.65	878	20.6	27.2	2.57	12.3	1.4	0.43	0.19	-0	0.07	-0	0.01	-0.1	0.36	0.01	2.9	0.1	10.6	4.74		1.46
UA1582_6	1880	46.6	507	2.35	177	5.3	1.12	1032	26.2	33.5	3.36	6.7	2.7	0.43	0.1	0.04	1.05	0.01	0.42	0.09	0.21	0.14	5	0.56	12.2	5.45		1.51
UA1582_9	1017	50	369	3.5	103	5.2	1.39	918	15.9	25.3	2.25	8.1	1.9	0.15	1.1	0.11	0.21	0.11	0.67	0.08	0.07	-0	3	0.16	15	4.86		1.4
UA1582_24	1017	83	630	5.1	107	4.9	1.41	840	16.8	40.2	3.9	8.7	0.31	-0.1	-0.1	0.09	0.2	0.02	0.7	-0.1	0.55	-0.1	3.4	0.84	11.6	6.7		2.07
UA1582_27	970	72.7	492	3.2	121	5.1	0.95	847	16.9	32.4	3.74	7.9	0.53	-0	1.6	-0	-0.2	-0.1	-0.1	0.34	1	-0	4.1	0.25	11.3	6.2		1.84
UA1582_29	1000	63	493	2	102	4.6	1.3	925	18.8	33.9	2.03	9.1	2.4	0.79	-0.4	0.04	0.15	-0	0.18	-0	-0.3	0.12	2.45	0.43	10.6	5.5		1.51
Average	1365	53.2	451.5	3.0	132.9	5.1	1.1	937	20.1	29.8	2.8	10.0	1.3	0.3	0.5	0.0	0.4	0.1	0.3	0.1	0.2	0.0	3.8	0.3	12.9	5.3		1.5
StDev	434	14.6	95.7	1.0	27.1	0.6	0.4	71	3.3	5.8	0.7	2.6	1.0	0.3	0.7	0.1	0.4	0.1	0.3	0.1	0.5	0.1	0.8	0.2	1.9	0.7		0.3

NIST610 - 1 - 1 - 1	446	427	525	476	447	470	356	477	443	460	464	420	458	458	465	448	437	448	451	444	437	443	453	452	420	461	464
NIST610 - 2 - 1 - 1	439	406	501	447	424	443	341	434	419	439	432	421	423	421	432	419	421	436	435	420	436	420	416	433	416	451	448
NIST610 - 3 - 1 - 1	496	422	516	458	442	476	378	474	448	463	453	427	458	452	439	445	446	447	456	445	468	470	457	470	444	460	478
NIST610 - 4 - 1 - 1	465	452	557	486	465	474	391	467	486	509	491	465	469	464	469	440	434	451	445	436	464	455	454	489	456	485	478
NIST610 - 5 - 1 - 1	436	423	512	466	447	459	364	440	438	452	447	419	461	435	432	430	443	449	467	436	449	420	424	446	419	452	461
NIST610 - 6 - 1 - 1	447	430	527	477	461	476	385	447	458	461	465	434	466	444	458	443	435	456	471	442	452	434	431	450	428	455	459
NIST610 - 7 - 1 - 1	472	447	516	471	445	458	382	457	471	486	469	460	470	449	443	430	434	447	458	431	447	443	439	470	431	445	449
NIST610 - 8 - 1 - 1	466	442	544	476	474	475	368	460	446	461	453	452	483	472	462	455	465	468	478	449	471	449	439	451	430	475	485
NIST610 - 9 - 1 - 1	434	417	488	431	430	451	357	445	413	430	424	411	441	424	434	423	425	442	450	423	430	428	428	420	410	448	461
NIST610 - 10 - 1 - 1	459	464	557	491	474	475	384	459	465	482	474	462	470	479	470	461	446	455	477	439	444	442	437	457	436	481	491
NIST610 - 11 - 1 - 1	449	416	511	469	450	465	367	435	437	446	434	424	448	444	443	439	434	455	442	435	459	433	426	430	412	446	449
NIST610 - 12 - 1 - 1	446	407	492	453	433	445	342	456	413	435	430	413	444	434	445	418	426	427	441	428	440	437	434	428	422	445	451
NIST610 - 13 - 1 - 1	456	399	494	447	435	466	340	446	417	431	425	413	438	425	442	427	416	450	433	431	448	441	436	430	416	455	461
NIST610 - 14 - 1 - 1	446	431	538	492	457	463	374	449	462	469	472	454	471	475	464	448	458	445	448	433	458	435	435	460	442	470	476
NIST610 - 15 - 1 - 1	464	438	528	468	470	489	393	458	456	470	454	432	451	450	448	451	445	461	467	446	446	452	436	466	432	455	468
NIST610 - 16 - 1 - 1	442	420	510	467	450	460	368	460	434	444	434	404	436	437	446	429	436	450	462	429	453	432	430	439	414	447	458
NIST610 - 17 - 1 - 1	461	408	497	447	439	463	375	443	437	443	435	417	429	430	438	428	434	448	446	433	450	446	445	442	411	441	456
NIST610 - 18 - 1 - 1	456	408	497	466	444	470	372	443	433	446	435	408	435	433	434	430	436	446	469	433	455	428	436	457	431	456	463
NIST610 - 19 - 1 - 1	451	455	562	510	463	467	375	459	458	477	482	467	499	487	485	462	447	466	463	439	448	442	435	473	450	487	487
NIST610 - 20 - 1 - 1	428	388	473	428	407	442	343	448	418	433	421	399	420	408	408	407	418	425	426	430	439	428	431	430	412	421	430
NIST610 - 21 - 1 - 1	496	445	529	459	444	475	371	455	449	463	446	429	458	445	445	430	447	443	453	436	456	444	438	463	435	457	455
Average	455	426	518	466	448	465	368	453	443	457	450	430	454	446	448	436	437	448	454	435	450	439	436	450	427	457	463
StDev	18	20	24	20	17	12	16	12	20	21	21	21	20	21	17	15	12	11	15	7	11	12	10	18	13	16	15
NIST612 - 1 - 1 - 1	45	32	78	40	37	40	43	41	40	40	40	37	42	37	44	41	36	40	39	41	38	40	40	40	41	40	39
NIST612 - 2 - 1 - 1	50	35	86	43	40	38	43	41	38	42	42	34	41	37	37	40	47	39	40	38	40	38	40	42	43	41	42
NIST612 - 3 - 1 - 1	36	33	78	39	38	38	40	47	35	37	37	34	38	34	35	38	35	39	37	38	40	35	33	38	37	40	39
NIST612 - 4 - 1 - 1	31	33	78	40	39	39	41	39	35	39	38	33	38	35	36	37	35	39	40	38	32	36	40	38	40	38	39
NIST612 - 5 - 1 - 1	26	33	85	42	40	39	40	36	37	38	38	35	42	38	39	35	37	38	38	34	37	37	37	36	37	39	39
NIST612 - 7 - 1 - 1	29	29	79	39	39	36	41	35	35	36	36	34	39	35	41	39	36	40	38	38	38	34	38	38	39	37	39
NIST612 - 8 - 1 - 1	25	29	78	40	34	37	42	48	37	39	40	40	38	36	37	37	35	39	38	36	38	38	39	39	40	38	37
NIST612 - 9 - 1 - 1	36	31	84	44	40	38	46	47	39	43	43	39	44	36	41	38	34	38	39	39	41	43	44	43	42	41	40
NIST612 - 10 - 1 - 1	44	32	78	36	36	36	39	41	37	39	39	34	39	37	39	37	36	37	38	38	41	37	39	40	42	39	37
NIST612 - 11 - 1 - 1	46	34	82	41	41	36	42	41	39	40	40	38	41	38	39	39	37	37	42	38	40	39	36	38	40	41	40
NIST612 - 12 - 1 - 1	56	33	88	43	44	42	43	46	40	43	42	40	42	36	44	40	35	41	41	40	38	44	44	42	44	42	39
NIST612 - 13 - 1 - 1	37	33	90	42	38	41	46	39	38	42	39	41	38	38	39	36	35	40	39	42	37	41	44	40	41	40	41
NIST612 - 14 - 1 - 1	41	29	81	41	39	38	43	41	37	37	37	39	34	36	36	37	38	37	40	37	35	38	39	37	40	38	36
NIST612 - 15 - 1 - 1	21	28	74	38	35	35	40	33	37	40	36	34	38	35	36	35	36	39	40	37	38	36	37	37	38	36	37
NIST612 - 16 - 1 - 1	33	31	78	37	31	34	39	38	34	36	38	35	37	35	39	37	38	37	35	35	36	35	33	38	39	38	37

NIST612 - 17 - 1 - 1	26	31	80	39	34	36	41	38	37	36	37	38	35	37	40	36	35	37	40	34	37	35	38	37	40	40	40
NIST612 - 18 - 1 - 1	43	33	85	42	41	41	46	42	38	41	39	40	41	38	42	38	37	39	44	37	37	37	37	40	42	38	38
NIST612 - 20 - 1 - 1	32	33	76	37	41	38	40	35	35	37	37	34	38	34	31	36	39	40	39	38	42	34	37	36	38	37	37
NIST612 - 21 - 1 - 1	41	32	77	40	40	41	42	42	35	37	35	34	39	35	38	37	37	38	43	39	44	37	33	37	38	36	37
Average	37	32	81	40	38	38	42	40	37	39	38	36	39	36	39	38	37	39	39	38	38	38	38	39	40	39	38
StDev	9	2	4	2	3	2	2	4	2	2	2	3	3	1	3	2	3	1	2	2	3	3	3	2	2	2	2
ATHO-G - 1 - 1	1380	63.5	87	86	447	56.6	0.77	529	52.2	111	12.7	55.4	16.9	3.2	12.1	2.36	12	3	9.6	1.25	11.4	1.28	12.9	2.8	6.5	6.5	2.54
ATHO-G - 2 - 1	1293	64.7	88.4	86.9	454	49.4	0.95	520	50.7	120.3	14.1	61.3	11.3	2.1	13.5	2.43	13.3	3.49	9.7	0.98	6.7	1.2	11.4	3.62	6	6.7	2.43
ATHO-G - 3 - 1	1262	66.4	86.7	82.7	446	53.1	0.77	482	49.1	110.9	11.5	54.2	13	2.73	12.8	2.1	14	2.47	8.1	1.17	7.4	1.2	11.9	3.36	5.3	6.6	2.5
ATHO-G - 4 - 1	1300	59.9	84	85	439	51.4	0.95	509	56.1	120	14	47.1	12.2	2.99	16.3	2.17	11.1	3.13	8.4	1.34	9.1	1.16	14.5	3.93	4.3	7.67	2.33
ATHO-G - 5 - 1	1300	59.1	85.6	79.2	436	52.3	0.95	522	51	109	14.1	56.4	13.7	2.84	11.8	2.46	14.1	2.78	11.3	1.31	10.9	1.21	12	3.39	5	6.3	2.36
ATHO-G - 6 - 1	1340	66.5	84.2	82	446	53.4	1.11	501	53.9	116.1	14.2	54.7	11.6	2.1	12.2	2.06	12.7	2.81	8.6	1.36	8.6	1.11	11.4	3.33	5.1	6.8	2.16
ATHO-G - 7 - 1	1301	68.6	86.2	84.4	450	51.9	0.74	493	52	115.8	14.2	60.4	12.6	2.29	15.1	1.95	13.2	2.92	9.6	1.14	10.1	1.49	14.4	3.93	5.3	6.4	2.32
ATHO-G - 9 - 1	1366	61	84.7	77.7	447	50.2	1.5	549	47.6	104.3	13	52.6	13	1.75	8.4	2.09	16.8	2.96	9	0.88	8.7	1.33	12	3.13	4.5	6.01	2.24
ATHO-G - 10 - 1	1510	63.1	93.3	81	472	61.8	1.06	580	54.5	122	14.4	56.2	13.6	2.08	13.7	2.16	13	2.94	8.2	1.3	11.1	1.51	14.4	3.28	5.5	7.3	2.47
ATHO-G - 11 - 1	1265	62.9	87.1	83.4	463	55.7	1.19	527	47.9	106.9	13.2	54.4	12.7	2	12.6	2.51	15.5	2.93	12	1.47	10.3	1.46	13.2	3.02	4.9	6.47	1.88
ATHO-G - 12 - 1	1460	61.2	80.8	81	422	57.4	1.28	548	51.9	111	13	55	9.2	2.43	13.4	2.76	16.2	2.29	10	1.65	8.2	1.7	13.4	3.39	5.4	6.49	2.19
ATHO-G - 13 - 1	1310	56.9	78.9	78.2	423	54.7	1.2	518	46.8	103.9	12	52.6	14.8	2.81	11.5	2.44	14.6	3.66	8	1.06	7.8	1.09	9.9	2.87	4.88	6.37	2.26
ATHO-G - 14 - 1	1099	60.2	79.3	73.9	425	50.4	0.74	397	43.3	98.5	12.3	52.1	9.7	2.74	15.1	2.27	15.6	3.23	9.8	0.98	8.6	1.24	9.4	3.37	4.1	5.87	1.99
ATHO-G - 16 - 1	1346	69	87.1	87.7	467	57.7	1.57	526	51	112.9	12.9	57.6	13	1.3	15.5	2.62	14.5	2.69	9.7	1.39	7.7	1.37	13.1	3.21	5	8.14	2.7
ATHO-G - 17 - 1	1347	64.9	90.7	83.6	454	55.6	1.78	518	53	114.8	13.2	54.8	11.8	1.79	13.8	2.25	17.9	3.22	7.7	1.37	9	1.37	11.5	3.13	5.8	7.3	2.24
ATHO-G - 18 - 1	1298	59.2	78.5	76.4	428	51.6	1.15	442	45.5	101.5	12	46.2	11.1	1.73	11	1.84	14.5	2.37	7.6	1.61	8	0.91	10.7	2.76	4.18	6.37	2.07
ATHO-G - 19 - 1	1340	57.7	82.6	76.5	441	53.5	0.95	489	48.2	107.9	12.8	49.9	14.5	2.46	13.7	1.74	13.5	2.81	8.6	1.4	9.5	1.71	9.9	3.34	5.6	5.73	2.11
ATHO-G - 20 - 1	1380	58.3	78.4	74.5	434	55.6	1.22	447	45.7	102.7	12.2	48.3	10.6	2.39	10.7	2.12	13.7	3.07	10.7	1.38	7.4	1.34	12.4	3.2	4.73	6.13	1.9
Average	1328	62.4	84.6	81.1	444.1	54.0	1.1	505	50.0	110.5	13.1	53.8	12.5	2.3	13.0	2.2	14.2	2.9	9.3	1.3	8.9	1.3	12.1	3.3	5.1	6.6	2.3
StDev	85	3.7	4.3	4.2	14.7	3.2	0.3	43	3.5	6.8	0.9	4.1	1.9	0.5	1.9	0.3	1.7	0.4	1.2	0.2	1.4	0.2	1.6	0.3	0.6	0.6	0.2
Walcott - 1 - 1	1220	199	22.9	51.2	201	50.1	3.91	949	77.8	143	14.6	50.7	13.1	1.16	9.8	1.28	10.2	2.06	5.7	0.49	4.5	0.68	6.1	2.95	29.5	25.6	8.04
Walcott - 2 - 1	1160	199	18.5	50.4	202	45.4	4.3	855	72.7	146.8	14.2	50.4	10.6	0.08	8.8	1.42	8.9	2.87	5.4	1.13	4.2	0.87	4.5	3.24	27.4	26.1	8.9
Walcott - 3 - 1	1070	186.4	17.9	51	185	46.4	4.12	893	67.4	133.3	14.8	53.2	11	1.45	12.2	1.41	8.7	1.25	6	0.61	5.9	0.99	5.4	3.88	25.1	25.5	7.45
Walcott - 4 - 1	1228	189	21.2	52.3	201	48.5	6.1	944	76.5	137	15.2	57.7	11.3	1.22	7.7	1.11	7	1.58	3.8	0.66	6.5	1.07	8.5	3.02	26.1	26.6	7.71
Walcott - 5 - 1	1170	193	20.2	49.6	197	40.9	4.59	863	67.9	133.5	14.4	48	10.9	1.07	10.6	1.01	9.3	1.92	5.7	1.01	4.9	0.61	8.1	2.05	26	26.1	8.69
Walcott - 6 - 1	1163	201	20.8	53.9	207	45.6	3.67	894	73.3	143	13.4	58.4	11.8	1.2	7.8	1.51	6.7	1.99	6	1.19	5.4	0.56	5.6	3.48	29.7	26.5	7.97
Walcott - 8 - 1	1220	179	18.2	52.7	196	47	3.17	892	65.7	130.7	14	53.1	9	0.71	6.6	1.38	9.7	1.78	6.2	0.47	5	0.71	6.1	2.26	26.9	25.5	8
Walcott - 9 - 1	1100	170	18.5	44.6	177	42	3.86	817	63.9	119.1	11.8	42.4	10.6	1.03	9.7	1.18	8.8	1.91	4.9	0.78	4.5	0.89	6.5	3.31	24.4	23.2	7.5
Walcott - 10 - 1	1280	181	18.8	49.8	186	46.5	3.5	980	69.2	134	13.9	54.3	12.1	0.92	9.7	1.28	7.3	1.62	6.1	1.11	5.4	1.01	7.2	3.08	31.3	25.3	8.5
Walcott - 11 - 1	1470	180	18.9	51	205	50.7	4.5	1010	76.8	139	14.6	53.2	10.5	1.09	12.6	1.58	8.8	1.68	6.1	0.69	6.8	1.25	7	3.05	31.3	24.8	8.3
Walcott - 12 - 1	1210	192	24.2	50.2	212	46.6	4.31	847	70	139.2	14.5	52	7.2	0.7	11.4	0.95	9.8	2.11	5.7	0.74	5.9	0.58	8.8	2.94	28.5	25.4	8.5
Walcott - 14 - 1	1210	192.7	19.6	56.8	195	46.1	4.08	910	69.5	138.5	14.9	49.9	8.7	1.05	6.6	1.02	9.6	1.53	4.8	1.01	7.3	0.67	7.8	3.48	30	24.9	8.87

Walcott - 15 - 1	1051	168.2	17.6	47.4	179	42	2.99	864	63.1	121.4	12.3	45.7	6.3	1.11	6.2	1.19	9.1	1.68	4.3	0.24	3.6	0.73	7	2.76	27.4	23.3	7.52
Walcott - 16 - 1	1207	179	17.9	51.8	195	46.7	4.14	865	64.7	128.5	13.9	56.1	8	0.59	8.8	1.35	7.7	1.19	4.4	0.86	5.5	0.68	7.4	2.83	27	23.4	7.5
Walcott - 17 - 1	1180	178.1	16.7	50.4	176	45.2	3.95	847	65	128.3	14	50.7	11.6	1.15	10.3	0.97	6	1.86	4	0.65	6.6	0.67	5.6	2.65	29.1	23.9	8.69
Walcott - 18 - 1	1230	172	20.1	47.6	183	46.7	3.46	886	67.4	130	13.5	50.6	9.2	1.16	6.7	1.34	9.8	1.51	5.2	0.46	5.3	0.92	6.5	2.99	25	24	7.34
Average	1198	185.0	19.5	50.7	193.6	46.0	4.0	895	69.4	134.1	14.0	51.7	10.1	1.0	9.1	1.2	8.6	1.8	5.3	0.8	5.5	0.8	6.8	3.0	27.8	25.0	8.1
StDev	95	10.6	2.0	2.8	11.2	2.7	0.7	52	4.7	7.7	0.9	4.1	1.9	0.3	2.0	0.2	1.3	0.4	0.8	0.3	1.0	0.2	1.2	0.5	2.2	1.1	0.5

UA1582	1020	45.3	631	2.1	110	4.22	0.66	735	14.2	25.3	2.42	7.3	1.3	0.25	-0.3	0.05	0.39	0.16	-0.2	-0	0.11	-0	3.4	0.34	10.4	4.9	1.41
UA1582_2	1610	49.8	393	2.06	99	4.7	1.35	760	13.8	23.4	2.53	4.1	0.62	0.88	0.32	0.01	-0.1	-0.1	-0.1	-0	-0.3	0.05	2.57	0.47	10.3	4.9	1.7
UA1582_5	1160	72.4	455	1.8	94	3.6	2.07	950	13.2	24.1	1.87	5.6	-0.2	-0.1	-0.5	-0.1	-0.1	-0	0.11	-0	-0.1	-0.1	2	0.51	19.7	4.1	1.6
UA1582_6	1050	62.8	449	1.94	102	4.48	0.9	910	15.5	26.7	2.82	6	0.46	-0.1	0.4	0	-0.2	0.12	-0.2	0.01	0.28	0.01	3	0.38	9.7	5.06	1.73
UA1582_8	980	49.4	378	2	99	3.62	1.12	750	15.2	23.9	2.22	7.1	0.84	0.41	0.9	0.19	0.98	0.14	0.55	-0	-0.3	-0	2.59	0.41	8.9	4.7	1.48
UA1582_9	1490	69.3	525	2.3	131	4.8	1.49	880	17.6	31.1	2.78	6.9	0.4	0.16	-0.6	-0.2	0.17	0.03	0.4	-0.1	-0.1	0.03	3	0.44	13.6	6.38	2.11
UA1582_10	920	58.8	502	4.1	106	2.96	0.77	736	12.4	26.9	1.76	8	1.5	0.25	1.2	0.05	0.74	-0.1	-0.2	-0	-0.1	0.01	1.94	0.26	9.7	4.36	1.48
UA1582_11	1067	50.8	442	1.84	113	4.54	1.09	859	17.3	31.7	2.55	9	0.14	0.44	-0.6	0.23	0.95	0.06	0.23	-0	-0.3	0.03	2.5	0.49	10.4	5.19	1.9
UA1582_18	995	46.4	444	2.54	108.4	3.79	0.66	810	15.5	26.3	2	7.8	1.34	0.45	1.1	0.01	-0.1	0.06	0.12	-0.1	-0.2	0	2.7	0.18	9.6	5.12	1.64
UA1582_19	1540	55.4	643	3.5	133	3.91	0.95	839	18	31.2	3.01	9.2	1.6	0.36	-0.4	0.18	0.43	0	0.26	0.08	0.21	0.07	3.6	0.24	20	6	2.06
UA1582_20	1280	55.1	419	2	107	5	0.95	839	14	25.3	2.43	6	0.57	0.04	-1.2	0.1	-0.5	-0.1	0.23	-0.1	-0.1	-0.1	3	0.34	9.6	4.3	1.84
Average	1192	56.0	480.1	2.4	109.3	4.1	1.1	824	15.2	26.9	2.4	7.0	0.8	0.3	0.0	0.1	0.3	0.0	0.1	0.0	-0.1	0.0	2.8	0.4	12.0	5.0	1.7
StDev	248	9.0	88.3	0.7	12.5	0.6	0.4	73	1.9	3.1	0.4	1.5	0.6	0.3	0.8	0.1	0.5	0.1	0.2	0.1	0.2	0.1	0.5	0.1	4.1	0.7	0.2